

Enhancing CHO cell productivity through the stable depletion of microRNA-23

A thesis submitted for the degree of Ph.D

Dublin City University



By

Paul S Kelly, B.Sc. (Hons)

The research work described in this thesis was performed under the
supervision of

Dr. Niall Barron and Prof. Martin Clynes

National Institute for Cellular Biotechnology

School of Biotechnology

Dublin City University

September 2014

I hereby certify that this material, which I now submit for assessment on the programme of study leading to the award of Ph.D. is entirely my own work, and that I have exercised reasonable care to ensure that the work is original, and does not to the best of my knowledge breach any law of copyright, and has not been taken from the work of others save and to the extent that such work has been cited and acknowledged within the text of my work

Signed: _____ (Candidate) **ID No.:** 55036275

Date: _____

This thesis is dedicated to my loving parents

Bernard & Paula

Acknowledgements

First and foremost, I would like to thank my supervisor Dr. Niall Barron for his guidance and patience over the last 5 years of my Ph.D. From the moment you said “Pull up a pew”, I knew this was the project for me. Thank you for tolerating my constant science puns, you know you love them. It’s a miR-acle you’ve put up with it for this long. For always being available in times of crisis, the dreaded Guava, and for leaving the office door open for any questions that I ever had. Most of all, thank you for reading every page that I put on front of you and helping in the gruelling process of thesis edits, I promise the next one will be shorter. For performance above and beyond the call of duty.

I would like to thank Professor Martin Clynes for pointing me in the direction to selecting the right project for me. For your enthusiasm over the years, lord knows we all need it at times, and the kind words of support. For your light-hearted emails, adding a little spice to those dreaded PhD blues. You’ve done so much for me and so many others in my time in the centre.

To my saviour, my god, the “bioinfor-magician”, Dr. Colin Clarke. Thank you for saving my PhD when my laptop decided to throw in the towel near the end of writing up.

I would like to thank Dr. Clair Gallagher for her help at such a critical point in my project, FACS sorting 2304 CHO clones, and for the long hours spent sitting at the Guava compensating for GFP. Believe me, I am truly in your debt and a great deal of “compensation” is coming your way.

I would like to thank Dr. Laura Breen for all of her help with the OROBOROS. My apologies for unleashing the alternative name for the OROBOROS to the centre and your responsibility of explaining its meaning. It will forever be remembered.

Thanks to Dr. Sinead Aherne for helping me out with my microarray work, even if the results weren’t the Mae West.

To the proteomics crew, Dr. Paula Meleady, Michael Henry, Shane Kelly and Mark Gallagher, a huge thanks for all the help with my label-free work and data analysis. Navigation through the uncharted lands of proteomics was greatly appreciated.

I would also like to thank Dr. Jonathan Bones from NIBRT in UCD for all of the help with glyco-profiling my antibodies and reformatting my graphs for corrections.

To my molecular biology partner in crime, BD-Griff, D.J. Griffindor or Alan “The Lad” Griffith.....lad lad lad. To the chemistry group attempting to slowly infiltrate the molecular biology lab; Zara Molphy, Creina Slator and Andreea Prisecaru, thanks for mixing things up over the last couple of years. Thanks to the rest of the second floor office crew both past and present; Andrew McCann, Deirdre O’Flynn, Damian Pollard, Martin Power and my neighbour Gemma Moore (the spar trips will be missed).

Carol McNamara, Gerladine Chawke, Mairead Callan and Yvonne for all of their support over the years, for fending off the big bad wolves and for keeping us in the monies. I would like to thank Gillian Smith and Joe Carrey for doing all of our prep room work.

I would like to thank everyone else along the way (this covers you) for being the ear or shoulder from time to time and to those who asked the dreaded question “so, when are you finishing up?”.....**Shudder**.

Lastly, I would like to thank my family, especially my parents, Bernard and Paula Kelly (no, I’m not named after my mother) for supporting me throughout my PhD and from well before that. I know for a fact, life would have been so much more stressful without you two behind me. I will never be able to repay your love and kindness but let this be the start of it.

Table of contents

Abstract: Enhancing CHO cell productivity through the stable depletion of microRNA-23.....	1
Abbreviations.....	2
Publications.....	6
Talks and Posters.....	7
1.0 Introduction.....	8
1.1 Chinese hamster ovary (CHO) cells.....	9
1.1.1 Improving CHO cell productivity.....	12
1.1.2 Media supplements and bioprocess regimes.....	15
1.1.3 Waste metabolites.....	16
1.1.4 The genomics era – Unravelling CHO's genetic knots.....	17
1.1.5 Cellular engineering.....	19
1.1.5.1 Engineering CHO cell growth.....	19
1.1.5.2 Anti-apoptosis engineering.....	20
1.1.5.3 Anti-autophagy engineering.....	22
1.1.5.4 Metabolic engineering.....	23
1.1.5.5 Secretion engineering.....	24
1.1.5.6 Chaperone engineering.....	25
1.1.5.7 Unfolded-protein response engineering.....	26
1.1.6 Has the maximum productive capacity of CHO reached its climax?.....	27
1.2 microRNAs: Global regulators of cellular phenotype.....	27
1.2.1 Discovery of microRNA.....	28
1.2.2 miRNA biogenesis and processing.....	29
1.2.3 Genomic organisation of microRNA and nomenclature.....	31
1.2.4 microRNA mode of action.....	34
1.2.5 Target prediction algorithms and online databases/tools.....	35
1.2.6 microRNAs in Chinese hamster ovary cells – A role in the bioprocess.....	37
1.2.6.1 miR-17~92 cluster.....	41
1.2.6.2 miR-23~27~24 cluster.....	43
1.3 microRNAs: Tools for CHO cell engineering.....	45
1.3.1 microRNA identification.....	45
1.3.2 Transient microRNA interference.....	46
1.3.3 Stable microRNA interference.....	48
1.3.4 microRNA sponge technology.....	52

1.4 Glyco-engineering.....	57
1.4.1 Antibody structure and effector function.....	59
1.4.2 Antibody glycoforms.....	62
1.4.3 Glycan-manipulation.....	65
Aims of thesis.....	68
2.0 Materials and Methods.....	69
2.1 General Techniques of Cell Culture.....	70
2.1.1 Ultrapure water.....	70
2.1.2 Glassware.....	70
2.1.3 Cell culture cabinet.....	70
2.1.4 Incubators.....	71
2.2 Subculture of cell lines.....	71
2.2.1 Anchorage-dependent cells (Monolayer).....	72
2.2.2 Suspension cells.....	72
2.2.3 Cell counting and viability determination.....	72
2.2.3.1 Trypan blue exclusion method.....	72
2.2.3.2 Guava ViaCount [®] assay.....	73
2.2.3.2.1 WorkEdit.....	74
2.2.3.2.2 EasyFit Analysis.....	75
2.2.3.3 Cedex XS Analyzer.....	76
2.2.4 Cryopreservation of cells.....	77
2.2.5 Thawing of cryopreserved cells.....	77
2.2.6 Apoptosis analysis.....	78
2.3 Other Cell Culture Techniques.....	78
2.3.1 Reconstitution/Rehydration of lyophilised miRNA.....	78
2.3.2 siRNA/miRNA transfection.....	79
2.3.2.1 siSPORT [™] NeoFX [™] Transfecting Reagent.....	79
2.3.2.2 INTERFERin [™] transfection reagent.....	80
2.3.3 Transfection of plasmid DNA.....	80
2.3.3.1 Lipofectamine 2000.....	80
2.3.3.2 TransIT [®] -2020 Transfection Reagent.....	81
2.3.4 Limited-dilution/FACS-based cloning.....	81
2.4 Molecular Biology Techniques.....	82
2.4.1 DNase treatment of RNA.....	82
2.4.2 High Capacity cDNA reverse transcription.....	82
2.4.3 Polymerase Chain Reaction (PCR).....	83

2.4.4 Fast SYBR® Green Real-time qPCR.....	85
2.4.5 Determination of DNA/RNA quantity and quality.....	86
2.4.5.1 Bioanalyser/RNA.....	86
2.4.5.2 NanoDrop® Spectrophotometer.....	87
2.5.4.3 Gel electrophoresis/RNA.....	88
2.4.6 Total RNA isolation using TRI Reagent™.....	89
2.4.7 PCR based miRNA Taqman® Low Density Arrays (TLDA).....	89
2.4.7.1 Reverse transcription.....	91
2.4.7.2 Pre-amplification.....	92
2.4.7.3 PCR.....	92
2.4.7.4 Data Analysis.....	93
2.4.8 Singleplex qRT-PCR validation: Taqman® microRNA assays.....	94
2.4.8.1 Reverse transcription.....	95
2.4.8.2 PCR.....	96
2.4.9 MessageAmp™ aRNA amplification kit.....	97
2.4.10 CHO-specific oligonucleotide arrays.....	102
2.4.11 Gel and LB media/LB agar preparation.....	102
2.4.11.1 Agarose gel preparation.....	102
2.4.11.2 LB media preparation.....	102
2.4.11.3 LB agar plate preparation.....	103
2.4.12 Restriction Enzyme Digestion.....	103
2.4.13 Enzyme modification of linearized plasmid DNA.....	104
2.4.13.1 Alkaline Phosphatase (AP).....	104
2.4.13.2 Kinase treatment.....	105
2.4.13.3 Klenow treatment.....	105
2.4.14 Gel extraction.....	107
2.4.15 PCR purification.....	108
2.4.16 Ligation.....	109
2.4.17 Transformation.....	111
2.4.18 DNA mini-prep of plasmid DNA.....	112
2.4.19 DNA midi/maxi-prep of plasmid DNA.....	113
2.4.20 Plasmid diagnostics.....	114

2.5 Mitochondrial studies.....115

2.5.1 MitoTracker™ Deep Red.....	115
2.5.2 OROBOROS Oxygraph-2k.....	115
2.5.3 Mitochondrial Isolation.....	116

2.6 Proteomic analysis.....117

2.6.1 Bradford assay.....	117
2.6.2 Western Blot.....	117
2.6.3 2-D clean up kit.....	118
2.6.4 Label-free sample digestion (Trypsin and Lys-c).....	119
2.6.5 C-18 peptide purification.....	120
2.6.6 Label-free Mass Spectrometry.....	120
2.8.6.1 Identification of proteins from mass spectrometry data.....	121

2.8.6.2 Progenesis LCMS.....	121
2.6.7 SEAP assay.....	123
2.6.8 ELISA.....	123
2.6.9 Glutamate assay.....	125
2.6.10 Akta Prime IgG purification.....	125
2.6.11 Glycomic Characterisation of Antibodies.....	126
2.7 Biotinylated miRNA pull-down of mRNA.....	128
2.8 Statistical analysis.....	129
3.0 Results.....	130
3.1 Identification of microRNAs involved in the regulatory control of CHO cell growth rate with subsequent phenotypic characterisation.....	131
3.1.1 Identification of microRNAs involved in the regulation of CHO cell growth rate and phenotypic characterisation.....	132
3.1.1.1 Differential miRNA expression profile of CHO cells with varying growth rates using an integrated miRNA, mRNA and protein expression analysis technique	132
3.1.1.2 Cell culture and sampling.....	133
3.1.1.3 microRNAs associated with growth.....	133
3.1.2 Phenotypic validation through transient microRNA screening.....	134
3.1.2.1 Cell culture and transfection conditions.....	134
3.1.2.2 Summary of transient miRNA screen.....	135
3.2 The potential of miR-34a as an engineering target.....	138
3.2 Exploring the master “tumour suppressor” miR-34a as a potential CHO engineering target.....	139
3.2.1 Transient knockdown of miR-34a potentially enhances CHO cell growth.....	139
3.2.2 Transient inhibition of miR-34a mildly inhibits the induction of apoptosis.....	140
3.2.2.1 Apoptosis assay development.....	141
3.2.2.2 Transient inhibition of miR-34a mildly inhibits apoptosis in CHO cells induced to undergo cell death.....	143
3.2.3 Stable depletion of miR-34 using microRNA sponge technology.....	144
3.2.3.1 miR-34 sponge design and generation.....	145
3.2.3.2 Confirmation of miR-34 sponge binding efficacy.....	150
3.2.3.3 miR-34a overexpression potentially inhibits conserved targets.....	152
3.2.3.4 miR-34 sponge influence on endogenous miR-34a and CCND1.....	154
3.2.4 Evaluation of miR-34 depletion in CHO mixed pool populations.....	156
3.2.4.1 miR-34 depletion in CHO-K1-SEAP cells.....	156

3.2.4.2 miR-34 depletion in IgG-secreting CHO-1.14 cells.....	158
3.2.5 Generation of miR-34 sponge clones.....	159
3.2.5.1 GFP fluorescence across clonal panels.....	159
3.2.5.2 Impact of miR-34 depletion across a CHO-SEAP cell panel.....	160
3.2.5.3 Impact of miR-34 depletion across a CHO-1.14 cell panel.....	165
3.2.6 Phenotypic evaluation of miR-34 depleted clones in a 5 mL volume.....	170
3.2.6.1 Selected miR-34 depleted CHO-SEAP clones.....	170
3.2.6.2 Selected miR-34 depleted CHO-1.14 clones.....	171
3.2.7 miRNA-mediated interference of CHO cell antibody glycoforms.....	175
3.3 Stable depletion of independent microRNA duplex components: miR-23b and miR-23b*.....	180
3.3 CHO cell engineering using miR-23b and miR-23b*.....	181
3.3.1 Selection of miR-23b and miR-23b* for stable knockdown.....	181
3.3.2 miR-sponge vector design and stable CHO cell line generation.....	182
3.3.3 Investigation of GFP fluorescence.....	183
3.3.4 Analysis in mixed population.....	185
3.3.4.1 Impact on bioprocess phenotypes in CHO-K1-SEAP: Batch and Fed-batch.....	185
3.3.4.2 Impact of miR-23 and miR-23b* depletion on Mab producing cells.....	189
3.3.5 Analysis of single cell clones in 24-well plate.....	191
3.3.5.1 GFP fluorescence across clonal panels.....	193
3.3.5.2 Impact on bioprocess phenotypes across CHO-K1-SEAP clonal panels.....	194
3.3.5.3 Impact on bioprocess phenotypes across CHO-1.14 clonal panels.....	205
3.3.6 Investigation of miR-23 and miR-23b* depletion on selected clones in 5 mL Batch, Fed-batch and Fed-batch Temperature shift.....	215
3.3.6.1 miR-23 and miR-23b* sponge CHO-SEAP clones.....	215
3.3.6.2 miR-23 and miR-23b* sponge CHO-1.14 clones.....	226
3.4 Investigation of the molecular impact of miR-23 depletion in CHO-SEAP cells.....	230
3.4.1 miR-23 depletion improves CHO-SEAP specific productivity.....	231
3.4.2 SEAP transcript levels appear elevated in miR-23 sponge clones.....	231
3.4.3 SEAP mRNA stability is not a contributing factor to enhanced productivity.....	233
3.4.4 Cell size is not a contributing factor to clonal differences in productivity.....	235
3.4.5 miR-23 depleted CHO clones exhibited elevated glutamate levels.....	236
3.4.6 miR-23 depletion impacts positively on CHO cell mitochondrial function.....	237
3.4.6.1 Mitochondrial function of intact rCHO cells.....	239

3.4.6.2 Mitochondrial function of permeabilised rCHO cells.....	243
3.4.7 Mitochondrial content.....	247
3.4.8 Assessment of miR-23 target transcript levels.....	248
3.5 miR-23 target identification and pathway analysis.....	253
3.5 microRNA target identification.....	254
3.5.1 Identification of global mRNA targets through Biotinylated miRNA tags.....	254
3.5.1.1 Evaluation of biotin-miRNA workflow.....	256
3.5.1.2 Microarray identification of biotin-labelled miR-23b and miR-23b* using biotin-labelled mimics.....	260
3.5.2 Identification of global protein targets using Label-free mass spectrometry.....	263
3.5.2.1 Differentially expressed proteins in miR-23 depleted clones...	263
3.5.2.2 High priority targets of miR-23.....	270
3.5.2.3 Gene Ontology analysis of differentially expressed proteins....	273
3.5.3 Identification of differential protein expression in isolated mitochondria.....	273
3.5.3.1 Differentially expressed proteins.....	274
3.5.3.2 Gene Ontology analysis.....	275
3.5.3.3 Potential targets of miR-23.....	277
4.0 Discussion.....	282
4.1 CHO cell engineering using miR-23.....	283
4.1.1 Selection of miR-23 for stable depletion.....	285
4.1.2 GFP as an effective reporter for clone selection and sponge efficiency.....	287
4.1.3 Stable depletion of miR-23 improves CHO-SEAP productivity.....	288
4.1.4 miR-23 depletion improves CHO cell growth in a cell type-dependent manner.....	290
4.1.5 Clonal variation and culture conditions impact on CHO cell phenotypes.....	292
4.1.6 miR-23 depletion enhances CHO cell mitochondrial function at Complex I and II.....	297
4.1.7 Summary of miR-23 depletion in CHO cells.....	303
4.2 Biotinylated miRNA mimics as a novel method for mRNA target identification.....	304
4.3 Analysis of the whole cell proteome reveals potential miR-23 regulated process.....	306
4.3.1 LETM1.....	306
4.3.2 14-3-3-eta (YWHAH).....	309
4.3.3 Calcium signalling.....	311
4.3.4 TCA cycle and metabolism.....	313

4.3.5 Combatting oxidative stress.....	319
4.4 Proteomic analysis of enriched mitochondria.....	321
4.4.1 A deeper insight into mitochondrial function.....	322
4.5 Potential bona fide miR-23 targets.....	326
4.6 Integrated “omics” profile of CHO cells with varying growth rates.....	328
4.6.1 Identification of miRNAs associated with cellular growth.....	329
4.6.2 Transient screening of miRNA.....	331
4.6.2.1 miR-23b*.....	332
4.6.2.2 miR-34a/34a*.....	337
4.6.2.3 miR-181d/200a.....	340
4.6.2.4 miR-532-5p.....	341
4.6.2.5 miR-639.....	342
4.6.2.6 miR-206.....	342
4.6.3 Final miRNA screen comments.....	343
4.7 CHO cell engineering using miR-34.....	345
4.7.1 miR-34’s depletion in various CHO cell types.....	345
4.7.2 miRNA-based glycoform engineering of recombinant antibodies.....	349
4.8 CHO cell engineering using miR-23b*.....	352
4.9 miRNAs place in the bioprocess.....	355
Conclusions.....	358
Future work.....	360
Bibliography.....	363
Appendix.....	422

Abstract: Enhancing CHO cell productivity through the stable depletion of microRNA-23

The Chinese hamster ovary cell (CHO) has been the “work horse” of the biopharmaceutical industry for the past 2 decades. Their preeminent position is due to their genetic tractability and capacity to produce high quality recombinant proteins with human-like post-translational modifications. Productivity limitations, however, have stimulated the application of various optimisation strategies to further improve therapeutic product yields. Despite the marked improvements in bioprocess design and media formulation, enhanced CHO cell performance is by no means routine. microRNAs (miRNAs) offer an attractive alternative to genetic engineering using a protein-coding gene due to their ability to regulate multiple molecular networks simultaneously in addition to reducing the cells translational burden.

Our lab identified various miRNAs whose expression was closely correlated with CHO cell growth rate including the oncogenic miR-17~92 cluster and the ribosome-enhancing miR-10a, as well as various growth-associated miRNAs such as miR-30e, miR-206, miR-451 and miR-639. Transient characterisation of a set of these candidates revealed several to negatively regulate growth and apoptosis such as miR-34a/34a* and miR-23b*; positively influence growth including miR-15a-16-1 and miR-532-5p and potentially enhance specific productivity in the case of miR-200a. CHO clones with enhanced growth attributes could achieve high cell densities early in culture prior to the induction of a temperature-shift, a process control strategy commonly used to enhance specific productivity but often at the cost of growth.

A common trade-off for enhanced growth is often the reduction in CHO cell specific productivity. Stable depletion of miR-23, implicated in B-cell differentiation, using a miR-sponge decoy was observed to enhance recombinant protein yield by ~3-fold without influencing CHO-SEAP cell growth in batch culture. Interestingly, these high producing clones also demonstrated a ~30% increase in oxidative metabolism, an energy state previously associated with productivity. The mitochondrial electron transport system components, Complex I and II, were observed to be responsible for this enhanced energy provision. Proteomic analysis identified potential targets of miR-23 involved in the TCA cycle e.g. IDH1 and MDHA/B and related to mitochondrial function e.g. LETM1.

Process adaptation to complement inherent clonal attributes can be exploited to enhance production yields as evident in the case of a miR-23b*-depleted clone achieving a 50% improved SEAP yield in a fed-batch culture with temperature shift (31°C). Exploiting the role of miRNAs in the regulation of bioprocess-related phenotypes (e.g. miR-34a and its role in antibody fucosylation) highlights the versatility of these small molecules for industrial application, a prospect further explored within this thesis.

Abbreviations

ADCC	–	Antibody-dependent cell cytotoxicity
AGO	–	Argonaut
AMPO	–	Aminopeptidase O
AON	–	Antisense oligonucleotide
ASO	–	Antisense Oligonucleotide
Asp	–	Asparagine
AT-III	–	Antithrombin III
ATCC	–	American Tissue Culture Collection
ATF4	–	Activating transcription factor 4
CDK	–	Cyclin-dependent kinase
CDKI	–	Cyclin-dependent kinase inhibitors
ceRNA	–	Competitive endogenous RNA
CERT	–	Ceramide transfer protein
circRNA	–	Circular RNA
CHO	–	Chinese Hamster Ovary
CTGF	–	Connective tissue growth factor
DE	–	Differential Expression
DGCR8	–	DiGeorge syndrome critical region gene 8
DNA	–	Deoxyribonucleic Acid
dsDNA	–	Double-stranded DNA
ELISA	–	Enzyme-Linked immunosorbent assay
EPO	–	Erythropoietin
ER	–	Endoplasmic reticulum
ERAD	–	ER-associated degradation
Exp5	–	Exportin-5
FCCP	–	Trifluorocarbonylcyanide Phenylhydrazone

Fuc	–	Fucose
FUT8	–	α -1,6 fucosyltransferase
GADD34	–	Growth arrest and DNA damage inducible protein 34
Gal	–	Galactose
GlcNAc	–	N-acetylglucosamine
GLS	–	Glutaminase
GU	–	Glucose units
GnTIII	–	β 1,4-N-acetylglucosaminyltransferase III
GSIS	–	Glucose-stimulated insulin secretion
GOI	–	Gene of Interest
GRN	–	Gene regulatory network
HCP	–	Host cell proteome
HIF-1	–	Hypoxia-inducible factor 1
HPLC	–	High performance liquid chromatography
IFN	–	Interferon
IL	–	Interleukin
IRES	–	Internal Ribosome Entry Site
LC/MS	–	Liquid chromatography/Mass spectrometry
LDH	–	Lactate dehydrogenase
LDSCC	–	Limited-dilution single cell cloning
LNA	–	Locked nucleic acid
lncRNA	–	Long non-coding RNA
MBS	–	MicroRNA Binding Site
mRNA	–	Messenger RNA
miRNA	–	microRNA
miRNA*	–	microRNA* or microRNA (star) or microRNA passenger strand
MRE	–	MicroRNA Response Element

NC	–	Negative control
ncRNA	–	Non-coding RNA
NK	–	Natural killer
nt	–	Nucleotide
PAR-CLIP	–	Photoactivatable-Ribonucleoside-Enhanced Crosslinking and Immunoprecipitation
PCD	–	Programmed cell death
PCR	–	Polymerase chain reaction
PDH	–	Pyruvate dehydrogenase
PDI	–	Protein disulfide isomerase
POX	–	Proline Oxidase
Pre-miRNA	–	Preliminary microRNA
Pri-miRNA	–	Primary microRNA
PRODH	–	Proline Dehydrogenase
PTGR	–	Post-transcriptional gene silencing
PVA	–	Polyvinyl Alcohol
qPCR	–	Quantitative Polymerase chain reaction
RBD	–	RNA binding domains
RISC	–	RNA-Induced Silencing Complex
RNA	–	Ribonucleic Acid
RNAi	–	RNA Interference
RNA pol	–	RNA polymerase
ROS	–	Reactive oxygen species
ROX	–	Residual Oxygen
RP	–	Ribosomal protein(Lempiainen, Shore 2009)
rpm	–	Revolutions per minute
RT	–	Reverse transcription

SEAP	–	Secreted Alkaline Phosphatase
shRNA	–	Short Hairpin RNA
SNARE	–	Soluble NSF attachment protein receptor
ssRNA	–	Single-stranded RNA
TAUT	–	Taurine transporter
TCA	–	Tricarboxylic acid cycle
TMB	–	3,3',5,5' – Tetramethylbenzidine
TNFR	–	Tumour necrosis factor receptor
tPA	–	Tissue plasminogen activator
TPO	–	Thrombopoietin
TPS-1	–	Thrombospondin-1
TGE	–	Transient Gene Expression
TRBP	–	TAR RNA binding protein
TU	–	Transcriptional unit
UPR	–	Unfolded protein response
UTR	–	Untranslated region
VCP	–	Vasolin-Containing Protein
XBP	–	X-box binding protein
XIAP	–	X-linked inhibitor of apoptosis

Publications

Kelly PS, Breen L, Mick H, Kelly S, Clynes M and Barron N 2014. Stable miR-23 depletion enhances recombinant protein yield from a Chinese hamster ovary cell line with an impact on mitochondrial function. **Manuscript in preparation.**

Kelly PS, Clarke C, Clynes M and Barron N 2014. Bioprocess engineering: Micro-managing CHO cell phenotypes. *Pharmaceutical Bioprocessing – Future Science*. **Accepted – August 2014 publication.**

Sanchez N, Kelly P, Gallagher C, Lao N, Clarke C, Clynes M and Barron N 2013. Sponge decoy vectors effectively deplete miR-7 activity to boost CHO cell longevity and yield. *Journal of Biotechnology*. 2014 Mar 9(3):396-404.

Clarke C, Meleady P, Doolan P, Henry M, Kelly S, Aherne S, Sanchez N, Kelly P, Kinsella P, Breen L, Madden S, Zhang L, Leonard M, Clynes M and Barron N 2012. Investigation CHO cell growth rate via the application of omics level platforms conducted simultaneously on a range of closely related sister clones with various growth rates. *BMC Genomics* 2012 Nov 21;13(1):656.

Barron N, Sanchez N, Kelly P, Clynes N 2011. MicroRNAs: tiny targets for engineering CHO cell phenotypes? *Biotechnol Lett*. 2011 Jan; 33(1):11-21.

Scientific talks and posters

**IBC's 10th Annual Cell Line Development & Engineering. September 8-10th, 2014.
Double Tree by Hilton Berkeley Marina, Berkeley CA, USA.**

I was invited to present a talk entitled “Enhancing Chinese hamster ovary cell productivity using microRNA-23” in Berkeley California on the current research within our group.

European Society for Animal Cell Technology (ESACT) – 23rd biennial meeting 2013. Lille, France, 23rd-26th of June.

I presented a research poster focusing on an aspect of my work entitled “MicroRNAs: Engineering tools to enhance CHO cell performance – The “Master tumour suppressor” miR-34a” at this prestigious animal cell technology conference with the underlying theme of “better cells for better health”.

European Society for Animal Cell Technology (ESACT) – UK conference, 9th-10th of January 2013.

I presented a research based lecture entitled “**MicroRNAs: Engineering tools to enhance CHO cell performance**” at the European Society for Animal Cell Technology (ESACT) – UK conference, 9th-10th of January 2013 in the Imago Conference Centre, Loughborough University, Leicestershire LE11 3TU, United Kingdom.

Biotechnology in Action: Stem Cells & Tissue Engineering, Biopharmaceutical Production and Cancer Biomarkers, 4th-6th of September 2012.

I presented a research poster entitled “MicroRNA based Chinese hamster ovary cell engineering – miRNA 34a as a potential route towards improving industrial cell culture?”

Chapter 1

Introduction

This introduction has been accepted for publication as a review focusing on the current status of microRNAs in the field of Chinese hamster ovary cell engineering. The review is entitled “Bioprocess engineering: Micro-managing the CHO cell phenotype”, will be published in *FUTURE SCIENCE – Pharmaceutical Bioprocessing* [August 2014] and was significantly contributed to by Dr. Niall Barron and Dr. Colin Clarke.

1.1 Chinese hamster ovary (CHO) cells

The Chinese hamster ovary (CHO) cell is the primary mammalian cell line used in the biopharmaceutical industry for the production of recombinant therapeutic proteins. They are favoured over their microbial counterparts (bacteria, yeast etc.) for their ability to produce high quality proteins with human like post-translational modifications, glycosylation, ensuring high efficacy. Since the first FDA-approved recombinant protein was manufactured in CHO, tissue plasminogen activator (tPA or Activase[®]) (Birch, Arathoon 1990), over 70% of all recombinants are produced in this cell, earning them the status of the “biological workhorse” of the biopharmaceutical industry (Jayapal et al. 2007). Of the 58 approved biopharmaceuticals (**Table 1.1**) between 2006 and 2010, 32 were manufactured in CHO with the 28 currently available antibodies constituting a large fraction of the market (Ho, Tong & Yang 2013).

Optimisation of their performance has been an area of intense research over the last two decades in order to enhance production yields and ultimately meet the global market demand. Since the 1990's, product titres have been improved ~20-fold primarily as a result of expression vector improvements and the ability to isolate high producing clones in addition to tailor-designed media formulations and the implementation of modified bioprocess regimes. Such improvements have boosted the industry standard to 1-5 g/L for monoclonal antibodies (Mabs) (Butler, Meneses-Acosta 2012, De Jesus, Wurm 2011). However, such achievements are by no means routine and the recent emergence of complex therapeutic molecules, such as fusion proteins and antibody fragments, present new manufacturing challenges for the CHO cell platform.

Enhancing CHO cell performance has taken various forms including the implementation of bioprocess regimes such as temperature shift (Butler 2005) and chemical supplementation of sodium butyrate, discussed later (Hendrick et al. 2001b), to enhance specific productivity in addition to genetic engineering strategies to compliment these previous breakthroughs by overcoming side-effects associated with the bioprocess. Single and multi-gene engineering processes have been exploited to target CHO cell phenotypes critical to the bioprocess including cell cycle (Sunley, Butler 2010), apoptosis (Lee et al. 2013), metabolism (Jeon, Yu & Lee 2011) and secretion (Rahimpour et al. 2013).

Table 1.1: List of FDA/EU approved biologics produced in CHO

Selected list of FDA/EU approved biologics produced in CHO (1987-2012)				
Product	Type	Therapeutic use	Manufacturer	Year of approval (FDA/EU)
Lucentis	Anti-VEGF-A mAb	Diabetic macular edema	Genetech	2012
Yevroy	Anti-CTLA-4 mAb	Melanoma	Bristol-Myers-Squibb	2011
Elonva	Modified rh-FSH	Controlled ovarian stimulation	N.V. Organon	2010
Opgenre	rh-BMP-7	Posterolateral lumbar spinal fusion	Howmedica	2009
Recothrom	rh-Thrombin	Control of minor bleeding during surgery	Zymogenetics (Seattle)	2008
Retacrit	rh-EPO	Anemia associated with chronic renal failure	Hospira	2007
Vectibix	Anti-EGFR mAb	Metastatic colorectal cancer	Amgen	2006
Naglazyme	N-acetylgalactosamine-4-sulfatase	Mucopolysaccharidosis VI	Genzyme	2005
Luveris	Luteinizing hormone	Infertility	Serono	2004
Xolair	Anti-IgE mAb	Moderate/Severe Asthma	Genetech	2003
Humira	Anti-TNF α mAb	Rheumatoid arthritis	Abbott	2002
Aranesp	Erythropoietin (engineered)	Anemia	Amgen	2001
ReFacto	Factor VIII	Hemophilia A	Wyeth	2000
Herceptin	Anti-HER2 mAb	Metastatic breast cancer	Genetech	1998
Benefix	Factor IX	Hemophilia B	Wyeth	1997
Avonex	Interferon- β	Relapsing multiple sclerosis	Biogen Idec	1996
Cerezyme	β -glucocerebrosidase	Gaucher's disease	Genzyme	1994
Pulmozyme	Deoxyribonuclease I	Cystic fibrosis	Genetech	1993
Epogen	Erythropoietin	Anemia	Amgen	1989
Activase	Tissue plasminogen activator	Acute myocardial infarction	Genetech	1987

Engineering approaches have diversified to encompass the tailored manipulation of antibody glycoforms for the enhancement of effector functions such as antibody-dependent cell cytotoxicity (ADCC) (Jefferis 2009a), overviewed in greater detail in **section 1.4**. By reducing core fucosylation of the biantennary-glycan on the Fc region of an antibody, therapeutic potency can be heightened as described in the case of the major blockbuster HerceptinTM (Junttila et al. 2010). Process manipulation such as those described, have demonstrated improved volumetric or specific productivity (Q_p) by sustaining a prolonged production phase, manipulating bioenergetics pathways to reduce toxic by-product accumulation, improving post-translational processing or indirectly meeting global demand by decreasing patient dosages.

The emerging prominence of CHO has been marked by the publication of both the Chinese hamster (Lewis et al. 2013) and CHO (Xu et al. 2011) genomes in addition to a wealth of ‘omics data unravelling the molecular fingerprint of CHO cell genetics (Hackl et al. 2011, Becker et al. 2011) and phenotypic characterisation (Clarke et al. 2012, Clarke et al. 2011a). CHO-specific genomic support will focus cell line engineering, allowing for the derivation away from the dependency on conservation with human and mouse sequences. In addition, vast improvements in the development of a plethora of tools and techniques for the manipulation of the expression networks in order to bend the CHO cell to the specific requirements of product molecules. Sequence access has not only gained insight into the variation of bioprocess characteristics in CHO such as post-translational networks and apoptosis (Xu et al. 2011) but will help refine currently implemented vector design such as recombinase-mediated cassette exchange (Hirano et al. 2011), zinc-finger nucleases (Cost et al. 2010), TALENS (Joung, Sander 2013), endogenous CHO promoters (Pontiller et al. 2008) and CRISPR-Cas (Mali, Esvelt & Church 2013).

With over 350 antibodies currently in the pipeline of pre-clinical trial (Reichert 2013, Walsh 2010) development (Reichert 2013), the emphasis on the availability of robust “off-the-shelf” engineering tools encompassing the genetic diversity of parental CHO cell lines and product specificity remains a priority in animal cell technology. Reducing the translational burden (Hackl, Borth & Grillari 2012) associated with single and multi-gene engineering strategies is now being addressed via RNAi (Wu 2009b) with miRNAs offering this advantage in addition to simultaneous pathway manipulation (Jadhav et al. 2013).

1.1.1 Improving CHO cell productivity

Process limitations associated with cell line stability and transcriptional efficiency of the recombinant product has contributed to the low productivity profiles of recombinant CHO (rCHO) cultures, a constraint significantly relieved by advancements in vector constructs (Li et al. 2007). Random integration of the recombinant gene of interest (GOI) gives rise to an unpredictable expression pattern due to positional effects (Zhou et al. 2010) resulting in the extensive screening of large numbers of CHO clones without addressing stability, an attribute influenced by the type of promoter used (Brooks et al. 2004). As only 0.1% of the genome is considered “active” (Little 1993), the frequency of successful transgene insertions into a transcriptional “hot-spot” is low, further abrogating the isolation of high producing clones.

The majority of production platforms utilize mutant strains of CHO cells (**Table 1.2**) that have both alleles of the dihydrofolate reductase (*dhfr*) gene either mutated or deleted. DHFR catalyses the conversion of folic acid to tetrahydrofolate and is necessary for biosynthetic pathways that produce glycine, purines and thymidylic acid (Cacciatore, Chasin & Leonard 2010). To support growth, DHFR-deficient cells would require media supplemented with glycine, hypoxanthine and thymidine. Incorporation of selection markers on transgenes has allowed for the isolation of high producing CHO clones through removal of untransfected subpopulations in addition to successful transfectants whose endogenous expression is low. Gene amplification in *dhfr*-CHO and *gs*-CHO (glutamine synthase) has been applied in the industrial production of recombinant pharmaceuticals (Cacciatore, Chasin & Leonard 2010). By including the DHFR gene on a plasmid with the GOI, cells can be isolated with further stringent selection through the addition of methotrexate (MTX), inhibitor of DHFR, selecting high producers or gene amplified cells through gene duplication.

Table 1.2: Selected list of commercially available CHO cell lines

Cell Line	Description
CHO-DHFR or CHO-DUKX-B11	Dihydrofolate reductase negative clone derived from the parental CHO cell line
CHO-K1	A subclone from the parental CHO cell line
CHO-MT ⁺	A subclone from the parental CHO cell line
Pro-5	Proline auxotrophs and require medium containing 40 mg/L of proline
CHO-SSF	A subclone of CHO-DUKX-B11
CHO-protein free	CHO cells adapted to grow in protein-free medium
SuperCHO	CHO-K1 subclone expressing insulin, transferring and IGF-1
ViggieCHO	DUKX-B11 subclone adapted to grow in absence of exogenous growth factors

Various selection markers are widely available (**Table 1.3**) in addition to the inclusion of reporter genes such as green-fluorescent protein (GFP) used to isolate clones based on fluorescent-activated cell sorting (FACS) achieving reported specific productivities of 38-fold increase when compared to normal selection procedures (Sleiman et al. 2008). FACS has also been employed under various conditions such as MTX-tagging (Yoshikawa et al. 2001) and secretion based on surface protein expression (DeMaria et al. 2008).

Table 1.3: List of selection markers available in mammalian expression vectors

Selectable marker	Selective reagent
Metabolic selectable marker	
Dihydrofolate reductase (DHFR)	Methionine sulfoximine (MSX)
Glutamine synthase (GS)	Methotrexate (MTX)
Antibiotic selectable marker	
Puromycin acetyltransferase	Puromycin
Blasticidin deaminase	Blasticidin
Histidinol dehydrogenase	Histidinol
Hygromycin Phosphotransferase	Hygromycin
Zeocin resistance gene	Zeocin
Bleomycin resistance gene	Bleomycin
Aminoglycoside Phosphotransferase	Neomycin (G418)
The above table was source from an excellent review on cell culture process development (Li et al. 2010).	

Various recombinases such as Cre and Flp, which recognise *loxP* and FRT sequences, respectively, are applied in various fields of (Hirano et al. 2011) biotechnology (Hirano

et al. 2011). The availability of the CHO genomic sequence draft has allowed the identification and pre-tagging of transcriptional “hot-spots” using the FRT/*loxP* system in combination with a weakened promoter (Zhou et al. 2010). This process was expanded on to include multiple site-specific insertions (Kameyama et al. 2010) and the subsequent successful generation of rCHO with a high copy number of antibody genes (Kawabe et al. 2012). Alternative to targeting specific high transcriptionally active genomic locations, transposable elements have been explored for their unbiased selection in genomic insertion, ability to increase copy number and generate stable production cell lines (Ley et al. 2013).

Promoter choice has been a double edge sword for the expression of heterologous genes within mammalian cell factories ensuring high transcriptional activity on one side through the use of viral promoters such as CMV and SV40 (Spenger et al. 2004) while contributing to instability due to silencing via DNA methylation, a common host response to foreign genetic material (Robertson, Jones 2000). The exploration of endogenous CHO promoters has been an area of interest as a means of navigating around this host response (Pontiller et al. 2008). *CHEF-1* was identified to be constitutively expressed in several CHO cell lines (Running Deer, Allison 2004), an ideal quality for driving transgene expression such as house-keeping genes. However, native CHO promoters that are responsive to certain conditions such as temperature shift offer an attractive alternative to inducible systems such as the identified *calcyclin* promoter in CHO (Pontiller et al. 2008).

A vast array of vector modifications can facilitate the selection of high producing CHO clones that circumvents the requirement of screening thousands of clones ensuring that the clones ultimately being selected will demonstrate a stable, constitutive and high producing phenotype once in the bioprocess. However, beyond this assurance, the heterogeneity within CHO cell clones themselves (Porter et al. 2010) allow for various performance phenotypes once introduced into the wide range production platforms in addition to the multitude of insults associated with production runs such as hypoxia, nutrient deprivation, shear stress and toxin build-up.

1.1.2 Media supplements and bioprocess regimes

Both media composition and bioprocess design have contributed the most over the past 2 decades to achieving gram per litre titres (De Jesus, Wurm 2011). Although capable of attached culture, the adaptability to suspension culture has made CHO cells a desirable mammalian cell type for the large-scale production of biopharmaceuticals. Fed-batch is the most commonly employed bioprocess used today and is generally applied to processes that supply material for phase 3 clinical trials and for the market (Wurm 2004). This type of process enhances maximal cell densities, prolongs culture viability and improves product yields, however, cell waste accumulation is the major limiting factor in this process type. Perfusion (Ryll et al. 2000) and continuous culture (Bleckwenn, Shiloach 2004) culture types can be beneficial for producing labile recombinant products in addition to potential toxic proteins as culture media is constantly removed and replenished with cells remaining in the case of perfusion culture.

Low temperature cultivation of recombinant CHO cells has previously been associated with sustained cell viability and increased productivity (Al-Fageeh et al. 2006) with the fundamental addition of maintaining product quality (Yoon, Song & Lee 2003). The reduction in growth rate associated with hypothermic growth has been linked to an accumulation of cells in the G₁ phase of the cell cycle (Hendrick et al. 2001a), a phase previously characterised as highly transcriptionally active (Kumar, Gammell & Clynes 2007). Several studies have been undertaken to explore the molecular mechanisms that are activated upon temperature shift in CHO cells that stimulate this prolonged production phase and enhanced specific productivity including miRNA profiling (Gammell et al. 2007, Barron et al. 2011b) and temperature-sensitive regulatory genes (Kantardjieff et al. 2010).

Artificial induction of high CHO cell specific productivity can also be achieved with the addition of chemical supplements such as sodium butyrate (NaBu) in addition to other chemicals such DMSO (Fiore, Zanier & Degrassi 2002), pentanoic acid (Liu, Chu & Hwang 2001) and growth factors (Zheng et al. 2006). NaBu has been observed to arrest cellular proliferation through the accumulation of cells in the G₁ phase (Hendrick et al. 2001b). Residence of cells in this stage of the cell cycle is associated with a high transcriptional activity in addition to increased metabolism and cell size (Kumar, Gammell & Clynes 2007). The mechanism of action of NaBu has been suggested towards

its ability to act as an inhibitor of histone deacetylation improving genomic accessibility (Jiang, Sharfstein 2008) including its ability to suppress *c-myc* (Mariani et al. 2003) and induce *p21* (Kobayashi, Tan & Fleming 2004). One metabolic state previously affiliated with an increase in specific productivity has been oxidative phosphorylation (Templeton et al. 2013) and has been observed to be induced under exposure to NaBu treatment (Ghorbaniaghdam, Henry & Jolicoeur 2013). A previous study has demonstrated NaBu to stimulate the release of calcium from the endoplasmic reticulum (ER) (Sun et al. 2012a). The association of calcium signalling with energy metabolism through the TCA cycle potentially highlights the driving force of NaBu's influence on CHO cell productivity. (Kaufman, Malhotra 2014) However, multiple side effects are associated with the addition of NaBu including growth inhibition, induction or repression of gene expression and the induction of apoptosis (Davie 2003).

1.1.3 Waste metabolites

All of the aforementioned process modifications including the environment of the bioreactor itself impose a particular set of insults which makes the culture environment undesirable such as oxygen deprivation (hypoxia), nutrient depletion, metabolic waste product build-up (lactate and ammonia) and sheer stress. These stresses ultimately reduce the accumulation of cell density, induce the onset of cell death ultimately reducing the maximum potential yield in addition to interfering with product quality.

Dissolved oxygen (DO) has been demonstrated to effect cell metabolism and the glycosylation patterns of the recombinant product in addition to causing cellular damage through the production of reactive oxygen species (ROS) (Shigenaga, Hagen & Ames 1994). Culture pH has also been demonstrated to elicit adverse effects on cell growth, metabolism, protein production and product quality (Yoon, Song & Lee 2003). This increase in culture pH is due to lactate production (Tsao et al. 2005), however, the addition of alkaline reagents such as Sodium Hydroxide (NaOH) to combat culture pH can be more detrimental by increasing osmolality of the culture resulting in cell death (Chotteau, Lindqvist 2012). Lactate is considered less of a concern compared to ammonia build-up (Kim do et al. 2013) due to its reversed metabolic consumption late in culture (Ma et al. 2009). The build-up of ammonia has been observed to affect the glycosylation patterns of recombinant proteins thus influencing their quality and bioactivity (Donaldson

et al. 1999). Reports have focused on minimising the generation of these byproducts by limiting the availability of the primary nutrient sources of mammalian energy metabolism, glucose and glutamine. Practical systems approaches have included the replacement of glutamine with glutamate (Hong, Cho & Yoon 2010) and glucose with galactose (Altamirano et al. 2004) resulting in the reduced accumulation of toxic byproducts and enhanced production of recombinant products with favourable modifications.

The utility of temperature shift and chemical-based approaches is abrogated by the unfavourable side-effects induced such as apoptosis and growth arrest which ultimately reduce the density of producing cells. Although certain engineering options such as NaBu do not offer a viable application to industrial processes due to its scalability, such strategies do offer a means of identifying phenotype-related genetic switches potentially associated with desirable phenotypes such as high specific productivity (Barron et al. 2011b, De Leon Gatti et al. 2007).

1.1.4 The genomics era - Unravelling CHO genetic knots

Omics-based approaches, such as transcriptomics, proteomics and metabolomics, have been used in the development of rCHO cell lines destined for the production process, reviewed in (Kim, Kim & Lee 2012). Recent advancements in omics tools have allowed for the detection of global changes in DNA/RNA, protein and metabolites giving a better understanding of the mechanism associated with particular CHO phenotypes and/or certain metabolites that correlate adversely/beneficially with CHO cell performance. Omics-based analysis sets the basis for CHO cell engineering drawing on the single or multiple genes derived from these profiles. Recent advances in the area of omics-based bioengineering has presented the researcher with a wealth of insight into the mechanisms that drive cellular processes, reviewed in (Datta, Linhardt & Sharfstein 2013).

Prior to the release of the CHO genomic sequence, non-CHO-derived DNA microarrays for mouse and rat were successfully utilised (De Leon Gatti et al. 2007, Baik et al. 2006). Comparative transcriptomic analysis using DNA micro-array technology has been carried out in rCHO cells that exhibit enhanced cell-specific productivity (q) under induced culture conditions such as low temperature culture (Baik et al. 2006, Yee, Gerdtzen & Hu

2009), high osmotic conditions (Shen et al. 2010) and Sodium Butyrate (NaBu) treatment (De Leon Gatti et al. 2007). Similarly, an additional study sought to predict the cell-specific production capacity of rCHO by identifying genes expressed across a panel of CHO clones with varying levels of q (Clarke et al. 2011b) and growth rate (Clarke et al. 2011a, Doolan et al. 2013).

The global scale analysis of the post-transcriptional gene regulation (PTGR) mechanisms inherent in a cell system has been made possible from genomic and proteomic profiling (Kanitz, Gerber 2010) allowing for the identification of effector protein targets that functionally contribute to a specific cellular phenotype. Several proteomic studies have been carried within rCHO cell culture systems that have been induced either chemically (NaBu) or environmentally (temperature shift) to exhibit enhanced cell specific productivity (Kumar et al. 2008, Yee et al. 2008). In addition, shotgun proteomics was utilised to identify biomarkers that could be used to predict the production capacity of rCHO cells when comparing a high-producing cell line against a low producing (Nissom et al. 2006, Carlage et al. 2009b). An array of proteomic-based profiles have been carried out in order to characterise and identify potential engineering targets involved in apoptosis induction (Wei et al. 2011), hyperosmotic pressure (Lee et al. 2003) and CHO cells cultured in serum-free medium supplemented with hydrolysates (Kim et al. 2011). Several other proteomic-based tools are available for the identification of large-scale changes within the host cell proteome (HCP) increasing the plethora of potential targets for CHO cell optimization. CHO-specific sequence databases have allowed for the high confident identification of CHO-specific proteins (Meleady et al. 2012c) thus adding to the growing wealth of experimentally validated resources.

The power of omics technology has accommodated the exploration of specific markers associated with CHO cell phenotypes allowing for the potential of predicting CHO cell performance within the bioprocess. Clonal variation is a well appreciated and problematic attribute in cell line development resulting in performance differences of a single clone across multiple bioprocesses (Porter et al. 2010). The ability of predicting a cells performance based on an expression pattern of a set of prerequisite candidates will mediate the selection of clones potentially better equipped with various attributes such as specific productivity (Clarke et al. 2011b) or growth (Clarke et al. 2012). Extracellular metabolite profiling will aid in media development and feeding strategies. Such studies include the characterisation of changes in metabolite accumulation over the culture

process (Bradley et al. 2010)(Chong et al. 2009b), profiling of both intracellular and extracellular metabolites in high producing versus low mAb-producing rCHO cells (Chong et al. 2012) and metabolite accumulation correlated with increased caspase activation and the onset of apoptosis (Chong et al. 2011).

The power of omics technology is evident from the above studies and have led to the identification of priority targets whose genetic manipulation will further enhance the CHO cell phenotype, a process that can be utilised to overcome the inherent adverse side-effects of the bioprocess.

1.1.5 Cellular engineering

An additional layer of engineering exists for the improvement of rCHO cell characteristics in relation to cell growth, recombinant protein production, improved cellular longevity and optimal nutrient utilisation and metabolism. Both gene-based, RNA interference (RNAi) based strategies, and a combination of both, have been successfully implemented in the optimisation of CHO cell activity, reviewed in (Kim, Kim & Lee 2012) and (Wu 2009a). However, the reliance on a single component approach depends strongly on the identification of critical targets that have the capacity to markedly influence the cellular functions associated with recombinant protein expression in CHO cells. Engineering of particular cellular processes covering multiple avenues are described below.

1.1.5.1 Engineering CHO cell growth

A common feature of enhanced specific productivity (qP) conditions are perturbations within the cell cycle leading to a G0/G1 phase arrest, resulting in enhanced protein biosynthesis, mediated by physical (low temperature) and/or chemical (NaBu) environmental stimuli (Sunley, Butler 2010). Based on this observation, anti-cell cycle mediators such as $p27^{KIP1}$ and $p21^{CIP1}$ have been used in rCHO cell engineering to obtain a similar effect without altering the culture environment. Fussenegger *et al.* achieved a 4-fold increase in specific productivity in a secreted alkaline phosphatase (SEAP) producing cell line through the transient expression of $p27^{KIP1}$ and $p21^{CIP1}$ under the

transcriptional control of a tetracycline-repressible system (Fussenegger, Mazur & Bailey 1997). Stable overexpression of these cyclin-dependent kinase inhibitors resulted in a significant increase in specific productivity of 5-15 times for recombinant SEAP and soluble intracellular adhesion molecule (sICAM) (Mazur et al. 1998, Meents et al. 2002). A temperature shift-like phenotype was observed upon the transient overexpression of the microRNA, miR-7, in CHO cells resulting in an increase in normalised productivity (Barron et al. 2011b).

Although strategies such as those described above have led to the increase in normalised CHO cell productivity, the inhibition of maximal CHO cell accumulation through the halt of cell cycle progression results in no improvement to a decline in total volumetric titre. Based on this consensus, the inverse relationship between growth rate and productivity (Wang et al. 2006) must be coupled with engineering strategies that increase maximal cell density before entering the “production phase”. Improvements in maximal cell density and growth rate have been mediated by the overexpression of pro-cell cycle genes such as the cyclin-dependent kinase, *cyclin E*, and the transcription factor *E2F-1* (Jaluria et al. 2007, Majors et al. 2008). Another study demonstrated a 70% increase in the maximal cell density achieved through the overexpression of the *c-myc* transcription factor which was observed to increase the cell cycle kinetics by ushering the cells into S-phase at an accelerated rate (Kuystermans, Al-Rubeai 2009). Target identification through omics-based approaches have been carried out to identify and validate several gene targets involved in proliferation such as Vasolin-containing protein (*VCP*) (Doolan et al. 2010) and *requiem* (Lim et al. 2010).

1.1.5.2 Anti-apoptosis engineering

As mentioned above, cell density is correlated with the maximum production capacity during the bioprocess and with this in mind cell death is considered a critical issue to be addressed as it effects the viable cell concentration thus impacting on product quality and volumetric titre (Arden, Betenbaugh 2004). During rCHO cell culture, cell death pathways can be triggered by a variety of stresses previously mentioned such as nutrient depletion, hypoxia, accumulation of toxic metabolic byproducts, increased osmolality and mechanical stress. The prevention of apoptosis has been recognised and established by

the generation of apoptosis-resistant rCHO cells as a beneficial engineering process to enhance CHO cell performance.

It has already been well established that apoptosis in rCHO cells can be significantly abrogated by the overexpression of anti-apoptotic proteins including *Bcl-2*, *Bcl-xL* and *Mcl-1* or the down-regulation of pro-apoptotic proteins such as *Bak* and *Bax* with the observed increase in protein production (Cost et al. 2010, Majors et al. 2008, Majors et al. 2009, Sung, Lee 2005, Chiang, Sisk 2005).

The apoptotic signalling cascade is mediated by a series of downstream proteolytic enzymes composed of initiator and effector caspases that regulate the induction, transduction and amplification of pro-apoptotic signals. Specific inhibition of the initiator caspases, *caspase-8/-9*, through the stable expression of dominant negative (DN) mutants (Yun et al. 2007) and inhibition of the effector caspases, *caspase-3/-7*, through plasmid based expression of small interfering RNA (Kim, Lee 2002, Sung et al. 2007) has demonstrated beneficial effects on cell growth and culture longevity. A further strategy for suppressing caspase activity is through the overexpression of an intracellular caspase inhibitor, X-linked inhibitor of apoptosis (*XIAP*) which has previously been demonstrated in CHO to inhibit the activity of caspase-3, -7 and -9, offering protection against Sindbis virus-induced apoptosis (Sauerwald, Betenbaugh & Oyler 2002a, Sauerwald, Oyler & Betenbaugh 2003). Two independent studies of *XIAP* overexpression demonstrated the contrary nature of its use in apoptosis inhibition and as a viable tool in CHO cell engineering. The first exhibited no change in growth or productivity when CHO cells expressing EPO were exposed to sodium butyrate despite the simultaneous reduced activity of caspase-3, -7 and -9 (Kim, Kim & Lee 2009). The second conferred a significant growth benefit and increased viable state in CHO cells that were serum deprived through the reduced expression of caspase-3 (Liew et al. 2010). These mixed results offer *XIAP* overexpression as a means of eliminating serum from the CHO cell culture process, particularly during clonal development, while not as a combinatorial strategy with chemical additives.

With the realisation that the apoptosis network is comprised of a complex network of genes, several studies focused on the manipulation of simultaneous avenues in a multi-gene approach. The expression of the mitochondrial pathway associated *Bcl-xL* and *Aven* along with the additional expression of *XIAP* demonstrated additive effects in the

protection against cell death in mammalian cell culture (Sauerwald et al. 2006, Figueroa et al. 2004). Apoptosis engineering has proved to be effective; however, there are conflicting reports as to its influence on productivity. Some have reported negative and positive impacts on CHO cell productivity. Nevertheless, combining such strategies with chemical based methods, such as NaBu, have resulted in a significant increase in recombinant therapeutic protein production (Sung et al. 2007) thus supporting the need for the evaluation of the role of apoptosis pathway manipulation and target identification in CHO.

1.1.5.3 Anti-autophagy engineering

Autophagy is a variant of PCD that takes place through a caspase-independent process in response to both normal and stressful environmental conditions. Autophagy is a catabolic process that acts in a homeostatic way by actively turning over cytoplasmic organelles via lysosomal-mediated degradation. It has been observed that an increase in autophagy induction can be triggered under stressful conditions such as nutrient deprivation and accumulation of protein aggregates (Levine, Yuan 2005, Mizushima, Yoshimori & Levine 2010). It is surmised that cell death may occur in the event of a prolonged autophagic state as a result of excessive degradation of mitochondria or other vital cellular constituents (Pattingre et al. 2005). Inhibition of apoptosis does not guarantee the blocking of autophagy-mediated cell death. With the observation that autophagy was induced late into the batch culture process of rCHO upon nutrient exhaustion (Hwang, Lee 2008), the reverse was also noted with the reduction of apoptosis and autophagy upon nutrient supplementation (Han et al. 2011). There are limitations in the online monitoring of the induction of autophagy with the microtubule associated protein 1 light chain (LC3) being the only *bona fide* autophagy marker (Kabeya et al. 2000). Autophagy progression through FACS-based identification of this protein has been achieved (Eng et al. 2010) with the turnover of long lived proteins offering a potential alternative (Klionsky, Cuervo & Seglen 2007). CHO cell engineering to over-express *Bcl-xL* or the active form of *Akt* were observed to delay the onset of apoptosis and autophagy as a result of nutrient depletion (Kim et al. 2009a, Hwang, Lee 2009).

1.1.5.4 Metabolic engineering

Normal cell growth and metabolic turnover of primary energy sources such as glucose and glutamine can result in the accumulation of byproducts including lactate and ammonia which have been characterised as toxic and impede cellular proliferation and product quantity and quality. Although feeding strategies and the availability of primary nutrient sources have been demonstrated to reduce the production and build-up of such byproducts in CHO cell culture, interference on a genetic level has proven to be a viable option.

Continuously cultured rCHO cell lines have the metabolic disadvantage of completely oxidising glucose to CO₂ and H₂O (Neermann, Wagner 1996) resulting in conversion of glucose to pyruvate and ultimately lactate, the “Warburg effect”. Increased acidification due to elevated lactate levels is mediated by the interconversion of pyruvate to lactate by the catalytic enzyme lactate dehydrogenase (LDH). Genetic manipulation of LDH activity has already been demonstrated to reduce the specific production of lactate in both hybridoma and CHO cell lines (Chen et al. 2001, Jeong et al. 2001). siRNA-mediated suppression of LDH-A, the subunit predominantly associated with anaerobic metabolism and pyruvate reduction (Baumgart et al. 1996), yielded a 54-87% reduction in specific glucose consumption along with a 45-79% reduction in lactate production with no impairment in cellular proliferation and hTPO production (Kim, Lee 2007). An additional layer of glucose metabolism is the conversion of pyruvate to acetyl-CoA for further metabolism in the tricarboxylic acid (TCA) cycle. The enzyme, pyruvate dehydrogenase (PDH), is responsible for this interconversion and its activity is regulated by PDH-Kinase (K) and PDH-Phosphatase (P). It is for this reason that pyruvate is considered the branch point that determines whether the consumed carbon source is excreted as lactate or metabolised further in the TCA cycle. Zhou and colleagues explored the use of a dual siRNA-expression vector against LDH-A and PDHK as a means of further reducing lactate production while also maximising energy generation from the TCA cycle. CHO cells exhibiting limited activity of LDH-A and increased activity of PDH showed reduced lactate production (90%) with the addition of both increased cell specific productivity (75%) and volumetric productivity (68%) (Zhou et al. 2011b). Specific glucose and lactate production has been directly correlated with mAb production allowing the potential to assess and predict CHO cell productivity based on metabolic turnover. Additionally, a high level of mitochondrial dehydrogenase activity was observed

confirming that more efficient utilization of carbon sources through energy release from the TCA cycle impacts positively on the biosynthesis capacity of CHO (Chen et al. 2012).

Another method explored was the controlled utilization of an alternative energy source to glucose, fructose. Overexpression of the fructose-specific transporter (*GLUT5*) allowed for the moderate uptake of fructose in high fructose containing environments, avoiding the overflow of excessive carbon and lactate. The same clones cultured in glucose environments demonstrated high sugar consumption and lactate production. The reduced production of lactate in these *GLUT5* clones resulted in an increased final cell concentration but was only observed for clones that exhibited an appropriate expression of this fructose transporter (Wlaschin, Hu 2007). Prolonged culture viability and enhanced productivity was observed in the instance of stable overexpression of the taurine-transporter (*TAUT*). Enhanced consumption of particular amino acids was evident, taurine and β -alanine, which are known to function as organic osmolytes thus inducing apoptosis upon their accumulation (Tabuchi et al. 2010).

To understand the bioprocess more intimately, a metabolomics-based approach was carried out to identify the accumulation or depletion of particular metabolites at specific time points within the culture using HPLC and LC/MS (Chong et al. 2009a). These findings gave rise to the potential of using such a strategy for guiding media design and fed-batch processes. A similar study, focused on the identification of novel metabolites, oxidized glutathione, that potentially induced apoptosis through correlation with elevated caspase activity (Chong et al. 2011). Metabolite characterisation studies such as these will accommodate the controlled manipulation of CHO cell metabolism thus allowing maximum performance.

1.1.5.5 Secretion engineering

Soluble NSF (N-ethylmaleimide-sensitive factor) attachment receptor, SNARE, proteins are anchored to both transport vesicles and their target membrane, trigger membrane fusion and are crucial in the exocytic pathway (Jahn, Scheller 2006). Vesicle trafficking and SNARE-mediated membrane fusion is regulated by the interaction with Sec/Munc18 (SM). Several efforts have enhanced the production capacity of CHO cells by overcoming this bottleneck associated with a saturated secretory pathway. Overexpression of

components related to the secretory network such as SNAREs (SNAP-23 and VAMP8) and the SM proteins (Sly1 and Munc18c) have been exercised with a positive impact on the secretory capacity of rCHO (Peng, Abellan & Fussenegger 2011, Peng, Fussenegger 2009). An alternative strategy implemented to enhance the secretory capacity of tPA-producing rCHO cells was the generation of a mutant CHO cell line that possessed a phosphorylation-resistant copy of ceramide-transfer protein (CERT), which efficiently transfers ceramide from the endoplasmic reticulum (ER) to the Golgi. Specific productivity was observed to be elevated by 35% (Rahimpour et al. 2013).

1.1.5.6 Chaperone engineering

A study identifying the irrelevance of secreted protein levels versus increasing gene copy number/strong promoter led to the understanding that the bottleneck in enhancing specific productivity lies at the translational and/or post-translational level (Mohan et al. 2008a). To relieve the cells of this blockage, engineering of the chaperone machinery networks have been undertaken. Protein disulfide isomerase (PDI) is predominantly located in the ER and has been found to catalyse disulfide bond formation, assisting in the folding of newly synthesised proteins (Freedman, Hirst & Tuite 1994, Gething, Sambrook 1992) and acting as a molecular chaperone associated with miss-folded proteins in the ER (Cai, Wang & Tsou 1994, Quan, Fan & Wang 1995). From an engineering perspective, increased *PDI* activity in bacterial, yeast and insect hosts has been reported to increase the secretion and activity of heterologous proteins containing disulfide bridges (Davis et al. 2000). Overexpression of *PDI* in rCHO was observed to positively influence the production capacity of antibody-producing CHO cells, but not in the case of TPO, IL-15 and tumor necrosis factor receptor:Fc fusion protein (Davis et al. 2000, Borth et al. 2005, Mohan et al. 2007). Although antibody productivity was observed to be increased, intracellular retention and co localisation in the ER was identified to be the contributing factor to the reduction in TNFR:Fc. In a separate study, an isoform of *PDI*, *ERp57*, was over-expressed to increase the levels of TPO secretion by 2.1 fold without any aberrant effects on CHO cell growth (Hwang, Chung & Lee 2003). These reports give a mixed view on the benefits of *PDI* overexpression as an engineering target with cell line, expression system and target therapeutic protein playing a significant part. Simultaneous overexpression of the chaperones *calnexin* and *calreticulin* exhibited a 1.9 fold increase

in specific TPO production with no change in its *in-vivo* biological activity (Chung et al. 2004). One proposed engineering strategy when exploiting the cells own protein chaperone network would be to co-express several chaperones concomitantly in a functionally meaningful ratio (Mohan et al. 2008b).

1.1.5.7 Unfolded-protein response engineering

With the identification of ER-associated chaperones, endoplasmic and PDI, being highly correlated with CHO cell productivity (Smales et al. 2004) in addition to shotgun proteomics revealing a positive correlation in productivity with the expression of the molecular chaperone BiP (Carlage et al. 2009a), it was evident that the ER played a major role in protein processing and the transmission of signals. However, accumulation of unfolded proteins in the ER lumen induces a response named unfolded-protein response (UPR). This response ultimately leads to the transcriptional activation of numerous factors involved in the folding process, such as molecular chaperones, foldases (Travers et al. 2000) and also genes involved in the ER-associated degradation (ERAD) pathway (Casagrande et al. 2000). Prolonged or excessive UPR activation has been observed to induce pancreatic beta cell death (Eizirik, Miani & Cardozo 2013) thus possessing the potential to interfere with the viable nature of CHO along with offering an engineering route to overcome this secretory bottleneck.

Reprogramming the post-translational processing machinery to overcome production bottlenecks was demonstrated by the overexpression, both transient and stable, of X-box binding protein 1 in transgenic CHO-K1 (Tigges, Fussenegger 2006). A spliced variant (*XBP-1s*) was revealed to increase the specific production capacity of various therapeutic proteins over its non-beneficial unspliced counter-part *XBP-1u*. Additionally, a further study confirmed the utility of *XBP-1s* overexpression in CHO whereby a secretory bottleneck had been reached with a 2.5 fold increase in specific productivity being demonstrated for recombinant proteins such as mAb, erythropoietin (EPO) and interferon γ (IFN γ) (Ku et al. 2008). Suspension CHO cell cultures maintained in a fed-batch format exhibited a 40% increase in antibody titre with appropriate bioactivity and post-translational modifications under stable *XBP-1* expression (Becker et al. 2008).

In instances where the overexpression of *XBP-1* failed to enhance the production of recombinant proteins such as antithrombin III (AT-III), the constitutive activation of the transcription factors ATF4 (Activating transcription factor 4) and GADD34 (Growth arrest and DNA damage inducible protein 34) demonstrated improved titre of recombinant AT-III (Ohya et al. 2008a, Omasa et al. 2008).

1.1.6 Has the maximum productive capacity of CHO reached its climax?

With such marked advancements in the area of recombinant CHO cell technology being seen over the past 25 years, will further improvements in specific and volumetric productivity be seen in the near future? Over the past 25-30 years, volumetric yields for recombinant protein production have increased by about 20-fold primarily due to the improvements in media and bioprocess design. It has been suggested (De Jesus, Wurm 2011) that a biological limit has been achieved at about 100 pg/cell/day in the area of specific productivity. However, this is by no means routine and volumetric yields could still be pushed higher, possibly 2-5-fold, by further increasing the maximal cell density achieved within the bioreactor (De Jesus, Wurm 2011). By combining successful bioprocess feeding strategies with that of genetically modified rCHO hosts, breaking the current limitations of the bioprocess is a tangible goal. Focusing on the lesser explored but emerging field of miRNAs, will not only minimise the translational burden associated with gene-based genetic engineering strategies (Hackl, Borth & Grillari 2012) but will fine tune global gene expression edging the CHO cell towards a more favourable phenotype (Clarke et al. 2012). microRNAs (miRNAs) have been suggested as alternative engineering tools in the past (Muller, Katinger & Grillari 2008, Wu 2009, Barron et al. 2011e) and in a short time have come a long way, reviewed in (Jadhav et al. 2013).

1.2 microRNAs: Global regulators of cellular phenotypes

MicroRNAs (miRNAs) are endogenous, small (~22 nt), single-stranded and non-coding RNA (ncRNA) molecules that play an important functional role in the global regulation of gene expression (Bartel 2004). Gene expression is exerted at the post-translational level whereby mature miRNAs target mRNAs for translational inhibition or mRNA cleavage depending on the level of complementarity between the miRNA and the 3'-untranslated

region (UTR). In some instances rapid mRNA decay has been attributed to accelerated deadenylation via miRNA (Wu, Fan & Belasco 2006) with isolated occurrences of enhanced translation of ribosomal proteins through interaction with their 5'UTRs (Orom, Nielsen & Lund 2008).

It is predicted that miRNAs have the potential to target up to ~30% of protein coding genes (Filipowicz, Bhattacharyya & Sonenberg 2008). The ability of a single miRNA to potentially target hundreds of mRNA transcripts contributes to their complex nature (Chi, Hannon & Darnell 2012). Conservation of the “seed” (nucleotides 2-8) sequence dictates target specificity. Multiple miRNA-Recognition Elements (MREs) of a single miRNA can be found within the 3' UTR of several mRNA transcripts or several MREs belonging to different miRNAs can lie within the same UTR giving rise to synergistic miRNAs (Shukla, Singh & Barik 2011).

As of 2014, over 28,645 miRNAs have been discovered and logged in the miRBase database with 1,881 of these being included in the human genome. miRNAs are involved in a wide range of molecular pathways such as cellular proliferation (Dong et al. 2012), apoptosis (Xie et al. 2012), fat metabolism (Flowers, Froelicher & Aouizerat 2012), glucose-induced insulin secretion (Xia et al. 2011) and developmental timing (Carrington, Ambros 2003). The conservation of 3'UTR miRNA seed sites across species (Friedman et al. 2009) implicate these small RNA based gene regulators as prime targets for CHO cell engineering and therapeutic intervention.

1.2.1 Discovery of microRNAs

The very first miRNA, lin-4, was identified in the nematode *Caenorhabditis elegans* in 1993 whilst studying its post-embryonic developmental timing. It was observed that the transcription of lin-4 negatively regulated the levels of the LIN-14 protein at the L1 stage of larval development. Ultimately, non-coding lin-4 transcript encoded for two small mRNAs of 22 and 61 nucleotides that possessed complementary sequences to those found in the 3'UTR of the lin-14 mRNA (Lee, Feinbaum & Ambros 1993). However, the lack of conservation of lin-4 and lin-14 with any species other than nematodes suggested that this was a “nematode specific curiosity” (Ambros 2008, Lee, Feinbaum & Ambros 2004, Ruvkun, Giusto 1989).

A second and historically significant heterochronic gene switch was identified in the same species, *let-7*, which was shown to code for a 21 nt RNA that possessed complementary elements in the 3'UTR of its gene target *lin-41* (Reinhart et al. 2000). Binding similarities of *let-7* to *lin-4* was confirmed with imperfect complementary sequence binding located within the 3'UTR of the *lin-41* mRNA (Vella et al. 2004, Bagga et al. 2005). The conservation of *let-7* across several species such as vertebrate, ascidian, hemichordate, mollusc, annelid and arthropod lead to the characterisation and identification of miRNAs as a unique family of short interfering RNAs involved in species development, homeostasis and disease (Pasquinelli et al. 2000). The multiple mRNA targets of the *lin-4* miRNA (*lin-14* and *lin-28*) coupled with the predicted crossover target of *let-7* with *lin-28* was the first indication that miRNAs could act both synergistically and independently in numerous molecular networks (Reinhart et al. 2000, Moss, Lee & Ambros 1997).

1.2.2 miRNA Biogenesis and Processing

miRNAs are transcribed by RNA polymerase II, or RNA pol III, (**Fig. 1.1 1**) into long primary (pri-) transcripts of several thousand bases, kilo-bases (kbs) (Lee, Feinbaum & Ambros 2004, Steel, Sanghvi 2012). The removal of a shorter (~70 nt) hairpin stem loop structure termed the preliminary miRNA (pre-miRNA) is performed by the Microprocessing complex (Drosha-DGCR8, **Fig. 1.1 2**). Pri-miRNA processing and recognition is mediated by the RNase type III enzyme Drosha and its double-stranded RNA-binding adaptor protein DGCR8 (DiGeorge Syndrome Critical Region 8). Drosha forms an intramolecular dimer whereby its two RNase III domains cut the 3' and 5' strand independently of each other yielding a RNase III characteristic 2 nt-3' overhang (Han et al. 2004). Not only do the two double-stranded RNA binding domains of DGCR8 recognize the single-stranded RNA extensions flanking the base of the stem thereby directing Drosha cleavage ~11 bp into the duplex from the ss-RNA/ds-RNA junction (Zeng, Cullen 2005, Han et al. 2006) but the protein-protein interactions through DGCR8/Drosha in the Microprocessor complex serve to stabilize the Drosha enzyme (Han et al. 2006, Yeom et al. 2006).

Nucleo-cytoplasmic export of these newly processed pre-miRNAs is mediated by the nuclear receptor Exportin-5 (Exp5) in a Ran-GTP dependent manner (Wang et al. 2011b), (**Fig. 1.1 3**). Structural recognition of the pre-miRNAs stem duplex is weakly bound by

Exportin-5 with the identification of the 2 nt 3' overhang being the pre-requisite for the pre-miRNA recognition by Exp5 (Bohnsack, Czapinski & Gorlich 2004, Lee et al. 2011). In addition to the RNase III-specific 3' overhang being the determining factor for miRNA nuclear export, the pre-miRNA/Exportin-5/Ran-GTP complex also inhibits the exonucleolytic degradation of the bound pre-miRNA (Zeng, Cullen 2004) thus stabilizing and shuttling efficiently processed and folded miRNAs for further processing.

Figure 1.1: miRNA Biogenesis and Processing

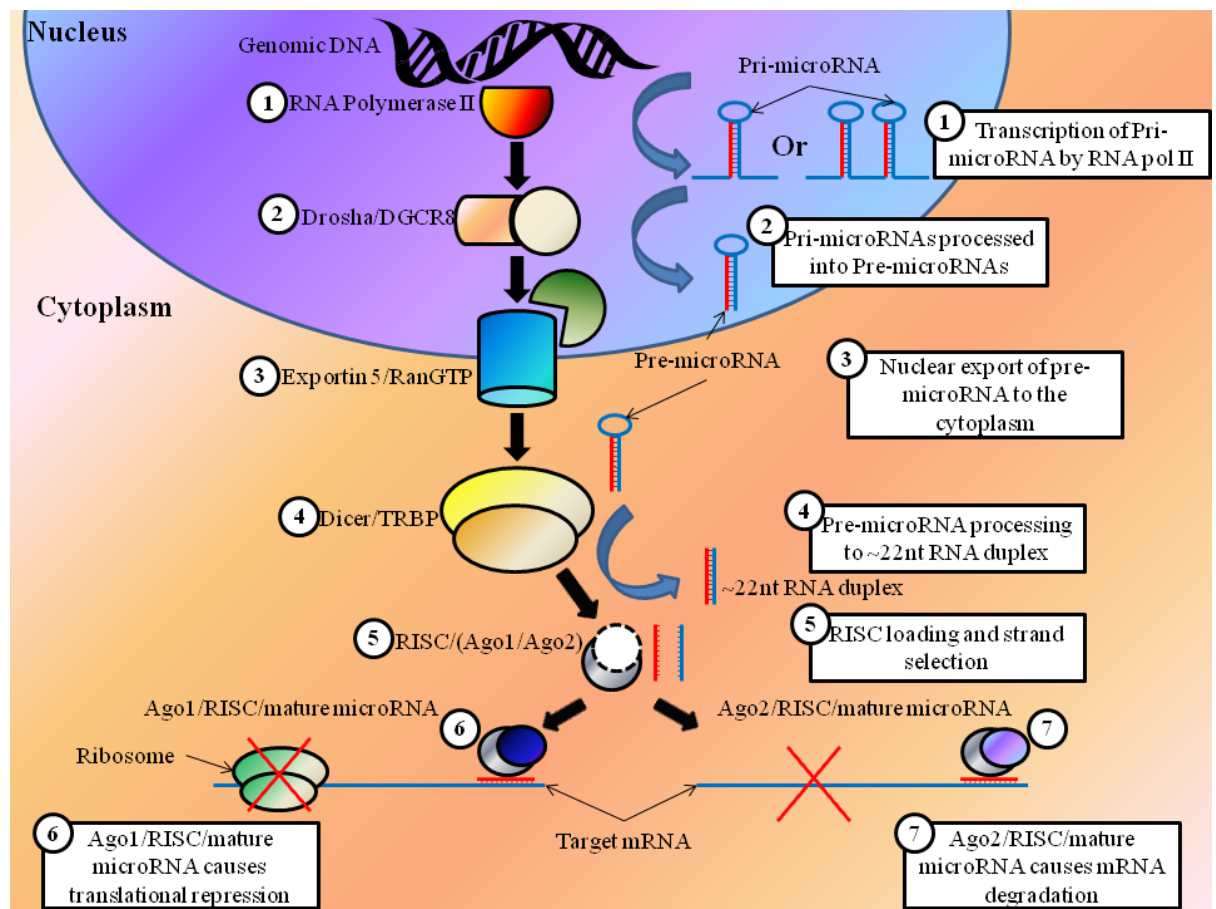


Figure 1.1: 1) miRNA biogenesis begins with the transcriptional initiation by RNA pol II/III yielding a primary miRNA transcript (pri-miRNA). 2) The Microprocessor complex containing Drosha/DGCR8 cleaves the overhanging single stranded RNA liberating a ~70 nt Pre-miRNA hairpin. 3) Nuclear removal of the pre-miRNA is mediated by Exportin-5 in a Ran-GTP dependent fashion. 4) Following export to the cytoplasm, the pre-miRNA is further processed by Dicer removing the hairpin loop and generating a ~22 nt RNA duplex. 5) Strand selection takes place upon RISC loading where the selected guide strand directs RISC mRNA targeting. 6) Translational repression or 7) mRNA degradation takes place based on the level of miRNA: mRNA complementarity and the specific Argonaute loaded in the RISC. Figure sourced from (Barron et al. 2011d).

In order to achieve target gene binding, the pre-miRNA product is further processed by a second RNase III type enzyme, Dicer, which partners with a double-stranded RNA-binding protein TRBP (TAR RNA binding protein) to remove the loop generating a ~22 nt RNA duplex (Koscianska, Starega-Roslan & Krzyzosiak 2011), (**Fig. 1.1 4**). The Dicer-TRBP complex closely associates with a member of the Argonaute family (Ago2) that mediates gene silencing and is intimately involved in the loading of the mature miRNA strand into the (RISC) RNA-Induced Silencing Complex (Chendrimada et al. 2005) (**Fig.1.1 5**). Subsequent to physical association of the miRNA duplex with all Ago proteins, the rate limiting step in miRNA mediated gene inhibition, is in the conversion from inactive RISC complex (Ago associated with RNA duplex) to active RISC complex (Ago associated with ssRNA) with thermodynamic stability of the duplex having the greatest influence (Gu et al. 2011). This thermodynamic stability in the 5' end of the duplex tips the balance of strand selection (Schwarz et al. 2003, Khvorova, Reynolds & Jayasena 2003) with as little a single mismatch in the first four base pairs being enough to favour guide strand selection (Hu et al. 2009). Upon strand selection, the passenger strand (eg. miRNA-34a*) is rapidly degraded. Passenger strand protection from degradation has been observed in species such as *C. elegans* (Chatterjee et al. 2011). The means by which a passenger strand that is not thermodynamically favourable is selected is still an unknown process but is likely dependent on co-factors associated with the RISC complex. Sporadic selection of the passenger strand completely changes the dynamics of miRNA directed gene inhibition by introducing a sequence that will target a separate set of mRNAs.

1.2.3 Genomic Organisation of microRNA and Nomenclature

The transcribed primary (pri) miRNA is between 3 and 4kb, and is structurally equivalent to that of a transcribed mRNA with flanking 5' capped and 3' polyadenylation consensus sequences forming defined boundaries (Cai, Hagedorn & Cullen 2004, Saini, Griffiths-Jones & Enright 2007). Approximately 50% of miRNAs are expressed from the introns of protein coding transcripts while the remaining are located within intergenic regions (**Figure 1.2**). The latter intergenic miRNAs are expressed independently from their own unique upstream promoter often located within flanking genes coding sequences. However, intragenic miRNAs, both intronic and exonic (Olena, Patton 2010), are

commonly co-expressed with their host gene and enter the miRNA processing pathway following intron splicing. The host gene/miRNA co-expression network has implicated these miRNAs in feedback loops with the host gene itself on occasion being the target (Ronchetti et al. 2008, Dill et al. 2012). The miRNA cluster miR-17-92 is an example of an intronic miRNA under the transcriptional control of its own dedicated transcriptional unit (TU) (Ota et al. 2004a).

Figure 1.2: Genomic Organisation of microRNA

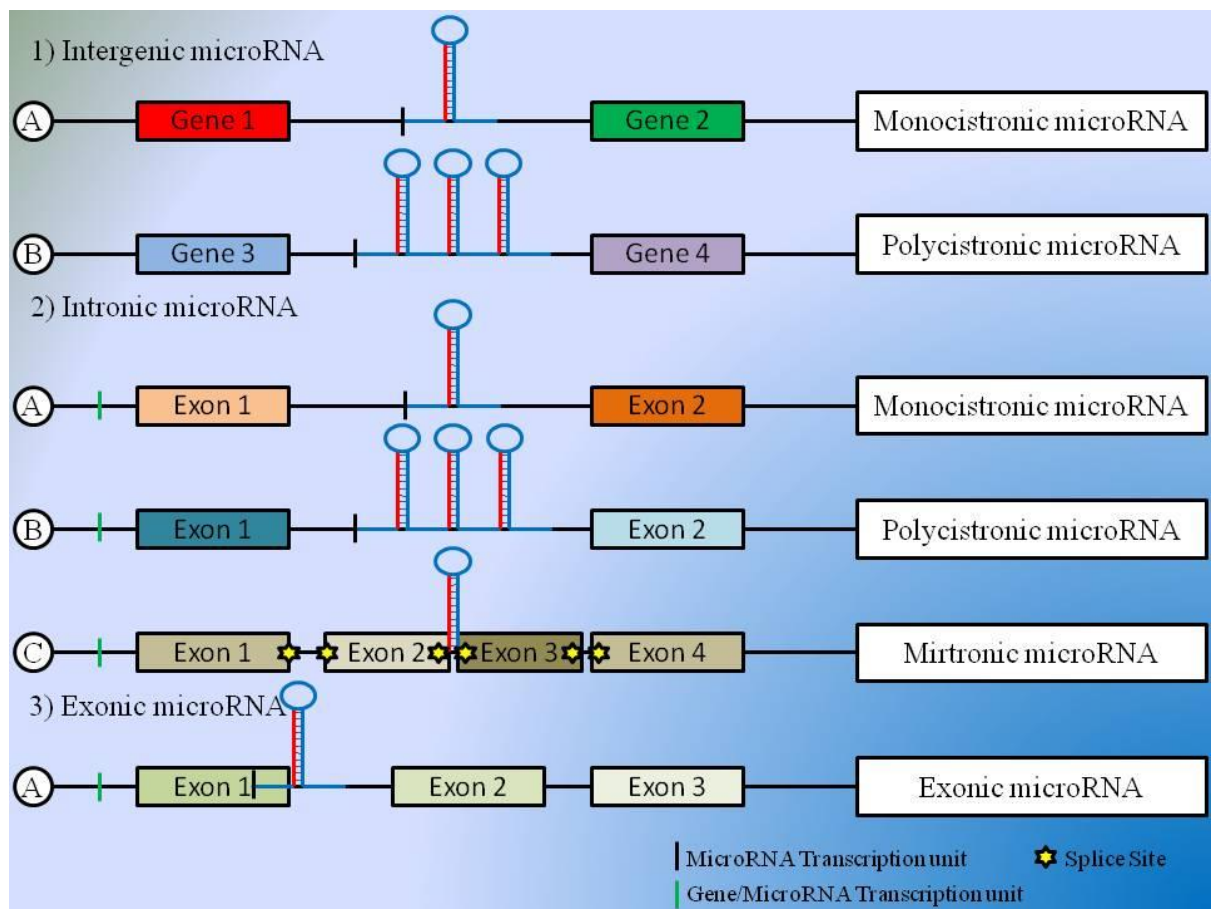


Figure 1.2: Genomic organisation of microRNA. There are four ways in which miRNA can organise within the genome. 1) Intergenic miRNA are located within the non-coding “junk” DNA between coding genes, are under the transcriptional control of their own TU and can be 1a) monocistronic or 1b) polycistronic. 2) Intronic miRNA are processed from the intron of protein coding genes subsequent to intron splicing and can be 2a) monocistronic, 2b) polycistronic and uncommonly 2c) miRtronic whereby the mature pre-miRNA constitutes the entire intron and by-passes cleavage by Drosha/DSCR8 through intronic splicing. All intronic miRNA can be expressed under the control of their own transcription units (TUs) or be co-expressed with their host gene under its own TU. 3) Exonic miRNA are located within the coding exon of a host gene and can be under either its own TU or the host genes TU. This figure was sourced from Kelly and colleagues (Manuscript accepted)

As of 2008 between 36% and 45% of miRNAs were found to be located in clusters in mouse and human (Griffiths-Jones et al. 2008). miRNA clusters are transcribed as a long pri-miRNA transcript and cleaved into several pre-miRNAs by the Microprocessor. miRNA clusters containing homologous and non-homologous miRNAs can result in multiple targeting of a particular mRNA target by several miRNAs (Smith et al. 2012) or the co-suppression of multiple mRNA targets (Kim et al. 2009b). The largest miRNA cluster identified to date is C19MC which consists of 46 pre-miRNAs expressed in tandem from a 100kb primary transcript (Bortolin-Cavaille et al. 2009). An intragenic miRNA of interest is the “mirtron” by which the genomic organisation is unique to any other type of intronic miRNA. In this instance the full mature pre-miRNA constitutes an entire intron between two flanking exons whereby intron splicing serves the role of pre-miRNA cleavage usually filled by DSCR8/Drosha yielding a mature pre-miRNA with the appropriate secondary structure for recognition and removal from the nucleus by Exportin-5 (Okamura et al. 2007, Sibley et al. 2012).

After the discovery of lin-4 and let-7 as a class of small temporal regulatory RNAs, the widespread identification of “microRNAs” in both animals and plants shortly followed with strong homology across species (Lee, Ambros 2001, Lagos-Quintana et al. 2001, Lau et al. 2001). Since the formation of the miRBase database in 2002 over 17,000 mature miRNA sequences in over 140 species have been registered (Griffiths-Jones 2004, Kozomara, Griffiths-Jones 2011). With the high throughput identification of novel miRNAs, it was vital for a nomenclature to be developed that catalogued this diverse family of small RNAs. The first criterion in the miRBase catalogue of miRNA classification is the species affiliation denoted by a three-four letter prefix of the species name. For example, hsa-miR-17 indicates that this miRNA is found in human (*Homo sapiens*) or CHO (*Cricetulus Griceus*). Additionally, “miR” designates the mature form of the miRNA, that being fully processed and RISC loaded, in contrast to “mir” which indicates the pri-miRNA or pre-miRNA sequence. miRNAs can give rise to two individual mature miRNA that are derived from the same pre-miRNA based on thermodynamic stability of the duplex ends, miRNA-17-5p and miRNA-17-3p are selected from the 5' and 3' ends of the hairpin loop respectively. Designation of the mature miRNAs as -5p or -3p over miR/miR* arose from the lack of experimental data indicating which arm of the miRNA duplex was predominantly selected, therefore the miRNA* species could have been originally named -5p or -3p (Ambros et al. 2003).

Considering their small size, a high degree of similarities between unique miRNAs is common and for this reason homologous miRNAs are separated into groups. miRNA-23b and miRNA-23a differ in sequence by a single nucleotide. Given that this nucleotide difference may not necessarily be within the seed region, these miRNAs could target similar genes, placing them in the same “seed family”. As the evolution of miRNA families can be attributed to duplication events (Sun et al. 2012, Ehrenreich, Purugganan 2008) and subsequent mutagenesis (Lee et al. 2011), a system has been devised that infers that two miRNAs are identical, paralogous, but centred in separate chromosomal locations (miR-92a-1 and miR-92a-2). The term “isomiR” refers to the identification of homologous miRNAs from the same sample source that differs purely by the addition of a nucleotide at either end of the mature sequence. This discrepancy in miRNA sequence length can be attributed to the variability in Drosha or Dicer cleavage position during processing of the pre-miR hairpin (Morin et al. 2008). However the Argonaute protein Ago-2 has been hypothesised to be involved in the generation of isomiRs through trimming of the 3'-terminal end of the bound miRNA (Juvvuna et al. 2012).

1.2.4 microRNA mode of action

The catalytic engine driving miRNA-mediated RNA interference is the RISC (RNA-Induced Silencing Complex) which is composed of two vital components, the single-stranded mature miRNA that directs RISC targeting and a member of the Argonaute family of proteins. Mammals encode four Argonaute paralogs referred to as Ago1-4 with characterisation of this family being based on the presence of the N, PAZ, MID and PIWI domains (Boland et al. 2011, Ma, Ye & Patel 2004). Despite the overlapping participation of the four Argonaute paralogs, Ago-2 has been implicated as the main driving force behind miRNA-targeted mRNA cleavage (Liu et al. 2004, Meister et al. 2004) miRNAs regulate the transcription of their target mRNAs through base pairing of the “seed” region situated at 2-8 nt from the 5' end (Chi, Hannon & Darnell 2012). High complementarity between miRNA: mRNA is more commonly associated with target mRNA cleavage, as seen with siRNA, with the more common base-pair mismatching resulting in translational inhibition. As mentioned earlier, through the generation of IsomiRs, this degree of miRNA: mRNA complementarity can hypothetically be optimized in some cases through Ago-2 mediated 3' terminal trimming of the bound mature miRNA (Juvvuna et al. 2012,

Han et al. 2011). Although both the 5' and 3' ends of miRNAs can vary widely depending on the Drosha/Dicer-dependant addition or deletion of 1-2 nt, alterations in the 5' sequence has the potential to alter the seed sequence greatly resulting in changes in miRNA targeting specificity (Krol, Loedige & Filipowicz 2010). Activated RISC complexes degrade target mRNAs or inhibit translation through target binding with complementary/semi complementary sequences within the 3'UTR with binding sites often being found within the 5' UTR and open reading frame (Kloosterman et al. 2004, Lytle, Yario & Steitz 2007). miRNA recognition elements (MREs) within the 3'UTR are further underlined by the observation that these functional target sites appear to be under evolutionary conservation (Kertesz et al. 2007). The RISC complex has also been demonstrated to mediate specific cleavage at the sarcin-ricin loop (SRL) of 28S ribosomal RNA eliciting translational suppression by direct ribosomal interaction (Pichinuk, Broday & Wreschner 2011). Accelerated mRNA decay through miRNA directed de-adenylation has also been observed (Djuranovic, Nahvi & Green 2012, Mishima et al. 2012).

Despite miRNAs being associated with the fine-tuning of gene expression through inhibitory affects, miRNA-10a has been demonstrated to enhance the translation of ribosomal proteins through interactions with their 5' UTR (Orom, Nielsen & Lund 2008).

1.2.5 Target prediction algorithms and online databases/tools

The potential for an individual miRNA to target a large number of protein coding mRNAs has its advantages in relation to cellular homeostasis and as possible targets for genetic manipulation but with this carries disadvantages to the researcher. With the small size of the seed region being of 6-8 nt in length and the minimum of a 6 bp match causing mRNA translational suppression (Brennecke et al. 2005), the challenge of predicting mRNA targets with a high degree confidence poses difficult without experimental validation. PicTar (Krek et al. 2005), miRanda (John et al. 2004) and TargetScan (Lewis et al. 2003) are three algorithms, among others, that utilize the classical method of searching for miRNA targets based on the near complementarity between the 5' miRNA seed region and the target mRNAs 3'UTR; conservation of binding sites across species and binding energy of the miRNA target duplex. Other prediction algorithms expand on the criteria listed above including the incorporation of G: U wobble pairs within the seed region, target site accessibility and local concentration of redundant miRNA patterns with a

degree of flexibility in computer learning. Variation in the binding criterion applied to target prediction across the various databases is shown in **table 1.4**. Although these *in silico* tools can identify real biological targets, the researcher is presented with a substantial list of predicted target genes that must be experimentally verified.

Table 1.4: Summary of the different software algorithms available for miRNA target prediction

Program	Species specificity	Algorithm description	Webserver
miRNA target EMBL	Drosophila	Complementarity with 3'UTR	http://www.russell.embl-heidelberg.de/miRNAs/
miRNAanda	Flies, vertebrates	Complementarity with 3'UTR, thermodynamic stability, duplex species conservation	http://www.microma.org/microma/home.do
RNAhybrid	Any	Complementarity with 3'UTR, thermodynamic stability, binding conservation	http://bibiserv.techfak.uni-bielefeld.de/rnahybrid/
TargetBoost	Worm and fruit fly	miRNA-mRNA binding site characteristics	https://demo1.interagon.com/targetboost/
miTarget	Any	Thermodynamic stability and sequence complementarity	http://cbit.snu.ac.kr/~miTarget/
Pictar	Flies Vertebrates Worm	Perfect and partial complementary sequence with 3'UTR, Thermodynamic stability	http://pictar.mdc-berlin.de/
RNA22	Any	miRNA-mRNA binding sites characteristics, Complementarity with 3'UTR, no cross-species conservation	http://cbcsrv.watson.ibm.com/rna22.html
MicroTar	Any	Complementarity with 3'UTR and thermodynamic stability	http://tiger.dbs.nus.edu.sg/microtar/
EIMMo	Humans, mice, fish, Flies, worms	miRNA binding sites conservation	http://www.mirz.unibas.ch/EIMMo3/
GenMiR++	Any	Sequence complementarity, based on expression data sets	http://www.psi.toronto.edu/genmir/
PITA	Any	Target site accessibility thermodynamic	http://genie.weizmann.ac.il/pubs/mir07/mir07_data.html
NBmiRNATar	Any	Sequence and duplex characteristics, no sequence conservation	http://wotan.wistar.upenn.edu/NBmiRTar/login.php
Sylamer	Any	Based on microarray data to identify 3'UTR sites	http://www.ebi.ac.uk/enright/sylamer/
MiRTarget2	Vertebrates	Based on microarray data to identify 3'UTR sites	http://mirdb.org/miRDB/
TargetScan TargetScan S	Vertebrates	Complementarity with 3'UTR, thermodynamic stability, duplex species conservation	http://www.targetscan.org/
DIANA-microT	Any	Complementarity with 3'UTR, thermodynamic stability, duplex species conservation, combined experimental data sets	http://diana.cslab.ece.ntua.gr/microT/

Table 1.4: The prediction algorithms available and the binding criteria utilised in miRNA target prediction. This table was sourced from a review by Barron *et al* (Barron et al. 2011d) extensively assessing the role of miRNAs as candidates for CHO cell engineering.

Furthermore, most prediction algorithms rely heavily on the central “seed” dogma of miRNA-target binding (all miRNAs contain a 5'-seed region) which is not always the case (Lal et al. 2009a). Reducing the number of false-positives is an essential feature for

novel prediction algorithms. miRGator encompasses the predictive capacity of three well known algorithms (miRanda, PicTar and TargetScanS) providing information on expression, functional annotation, pathway and disease (Nam et al. 2008) with an intimate link to the Tarbase database for experimentally tested miRNAs across 8 organisms (Sethupathy, Corda & Hatzigeorgiou 2006, Vergoulis et al. 2012). Another online database, miRWalk, expands the binding criterion outside that of the 3'UTR encompassing the 5'-UTR promoter region (Lytle, Yario & Steitz 2007) and nucleotide coding sequence (Tay et al. 2008) spanning three species (human, mouse and rat) including both predicted, overlapping with predicted binding sites from 8 other prediction algorithms, and validated miRNA information sourced from the Pubmed online database (Dweep et al. 2011a).

The reliability of combining multiple prediction algorithms appears questionable over one single “accurate” algorithm, reviewed in (Alexiou et al. 2009), however further experimental undertakings will provide insights into mechanism of miRNA:mRNA target interactions. One such algorithm, mirWIP, utilises experimental data in order to define the prediction rules (Hammell et al. 2008) whereas an example of an independent approach establishes an *in silico* prediction model based on an integrative “Omics” study of the mammalian inner ear (Elkan-Miller et al. 2011). Here, while studying both mRNA and protein levels coupled with a differential expression miRNA profile, subsequent crossover with prediction algorithms, including microRNA:Target pathway databases (Jiang et al. 2009, Ruepp et al. 2010), will permit the reduction of false positives allowing a high confident selection of candidate miRNAs and again enhancing the importance of experimental observation in order to better understand the miRNA target binding etiquette.

1.2.6 MicroRNAs in Chinese hamster ovary cells – A role in the bioprocess

The CHO cell is subjected to a number of bio-molecular changes during the bioprocess such as mechanical stress, metabolite accumulation, hypoxia, nutrient limitation, osmolality, etc., which dampen the capacity for optimal protein production. The use of RNA interference (RNAi) technology as an application to improve CHO cell specific productivity and recombinant protein quality ushered in the exploration of miRNAs as an alternative engineering strategy to target multiple genes in a single pathway or several

molecular pathways without impacting on the CHO cells translational machinery, reviewed in (Wu 2009). (Wu 2009) The identification of miRNAs in the pathology of diseases such as cancer through either their deletion or up-regulation implicated them as primary targets for intervention. This stimulated the interest in manipulating the CHO cell phenotype using miRNA.

The pioneering study by (Gammell et al. 2007) explored potential miRNAs involved in growth, increased productivity and sustained viability in CHO-K1 during a temperature shift to 31°C, a commonly exercised protocol in order to extend the CHO production phase (Kumar, Gammell & Clynes 2007) identifying a novel CHO miRNA involved in growth, cgr-miR-21. The exploitation of next-generation sequencing (NGS) technologies has led to the identification of over ~400 conserved mature miRNA sequences with 387 being identified in a single undertaking using small RNAs from 6 biotechnologically relevant CHO cell lines (Hackl et al. 2011) with a similar study identifying a plethora of miR:miR* homologs in CHO across several species using illumine sequencing (Johnson et al. 2011). Upon the release of the CHO-K1 genome sequence (Xu et al. 2011) advancements in CHO genetics such as the identification of the genomic loci for over ~200 miRNA through computational analysis (Hackl et al. 2012) will allow for the identification of novel CHO promoters of miRNAs that are temporally stimulated during the bioprocess or for the site specific overexpression or deletion of endogenous miRNAs. Incorporation of this newly acquired genomic sequence data has been compiled into an online data base (www.CHOgenome.org) (Hammond et al. 2012).

Differential miRNA expression profiles have been carried out on CHO cells in order to better understand the miRNA dynamics involved in numerous industrial process such as engineered CHO cells (Lin et al. 2010) and CHO cells at different time points (Hernandez Bort et al. 2012) including clones with various growth rates (Clarke et al. 2012). A proof-of-concept study based on a temperature shift differential expression profile, implicated the over-expression of the miRNA, miR-7, to have a negative effect on cell growth and a positive effect on cell specific productivity with no influence on apoptosis in a CHO-SEAP cell line (Barron et al. 2011a). Proteomic analysis of miR-7 over-expression demonstrated an overlap in proteins up-regulated or down-regulated with the pathways that were seen to be manipulated (Meleady et al. 2012a).

Some of the cellular processes central to the bioprocess have been shown to be impacted by miRNA regulation in other cell types and turn out to be conserved in CHO, such as the impact of miR-7 deregulation (Barron et al. 2011b), whereas others have not been described elsewhere, as in the case of miR-466h and its role in inhibiting apoptosis in late stage CHO culture (Druz et al. 2013). Stable depletion of miR-7 using a miRNA sponge vector improved peak cell density, prolonged culture longevity and boosted secreted protein yield by almost 2-fold in a fed-batch process (Sanchez et al. 2013b). Similarly, Jadhav and colleagues enhanced the overall yield of an Epo-Fc protein through the stable over-expression of miR-17 (Jadhav et al. 2014). Both studies demonstrate the utility of miRNA-mediated engineering to improve (Lai, Yang & Ng 2013b) CHO cell growth without negatively impacting on specific productivity, a common trade-off for superior growth rates and vice versa (Lai, Yang & Ng 2013b). From a product quality perspective, Strotbek *et al.*, reported that the glycosylation profile of recombinant IgG1 was not compromised in CHO cells engineered to stably co-express miR-557 and miR-1287, while inducing increased specific cellular productivity (Strotbek et al. 2013). Besides the manipulation of individual miRNAs, it has also been shown that tuning global, cellular miRNA levels via the RNAi processing machinery influences bioprocess-relevant phenotypes. Hackl *et al.*, (2011) found that overall miRNA expression in CHO cells cultured in serum-containing medium was elevated (Hackl et al. 2011) and upon further investigation found that Dicer mRNA and protein levels decreased in response to nutrient or serum removal. However, attempts to engineer Dicer expression demonstrated a very sensitive phenotypic response to the levels of Dicer present in the cells. Knockdown below endogenous levels or excessive over-expression both negatively affected growth but mild overexpression was found to be beneficial (Hackl et al. 2014b). For this reason, fine tuning the expression of single or small numbers of individual miRNAs, such as those mentioned previously, is probably a better approach for those interested in targeting a specific cellular function or behaviour. A number of groups have reported on miRNA expression profiling in CHO cells representing different phenotypes, producing different products or grown under different conditions in order to identify potential engineering targets.

Striving to improve the performance of CHO cells in industry has led to the production of hundreds of high quality biopharmaceuticals, sequencing of the CHO genome and now the identification of hundreds of microRNAs that are highly conserved and endogenously

encoded. Efforts to optimise the CHO phenotype using miRNAs are proving promising as an alternative to gene based engineering by achieving the same phenotypic outcome with a lightened dependency on the cells own translational machinery. Some well-known and routinely characterised miRNA families represent a major outlet for CHO cell engineering when considering the conserved nature of their mechanistic actions across numerous species and disease states, such as cancer, with one family in particular, miR-34, representing the first miRNA destined to take part in clinical trials (Bader 2012). Two miRNA clusters are described below that exhibit considerable interest for CHO cell engineering in addition to the wealth of candidates that offer viable engineering targets (see table 1.5)

Table 1.5: Candidate miRNA for CHO cell engineering

Biological process	microRNA	Cluster	Phenotype	Target	Reference
Cell cycle	miR-7 (CHO)	No	Tumour suppressor	Skp2 Psme3	(Sanchez et al. 2013a)
	miR-34a	No	Tumour suppressor	CCND1, CCNE2, CDK4/6	(Sun et al. 2008a, He et al. 2007b)
	miR-24	miR-23a~24-2 miR-23b~24-1	Tumour suppressor	E2F2 MYC	(Lal et al. 2009b)
	miR-17 (CHO)	miR-17~92	Oncogenic	CDKN1a/p21	(Ivanovska et al. 2008)
	miR-31	No	Oncogenic	LATS2 PPP2R2A	(Liu et al. 2010b)
Apoptosis	Mmu-miR-466h (CHO)	mmu-mir-297-669	Pro-apoptotic	Bcl212 Birc6	(Druz et al. 2013)
	miR-34a	No	Pro-apoptotic	Bcl2, surviving	(Bommer et al. 2007, Shen et al. 2012)
	miR-15a/-16	mir-15a~16-1	Pro-apoptotic	PDCD4	(Calin et al. 2008)
	miR-21	No	Pro-apoptotic	HSP60 HSP70	(Itani et al. 2012)
	miR-133	miR-1/-133	Pro-apoptotic	Caspase 9	(Xu et al. 2007)
Culture Stress	miR-126	No	Shear Stress	Bcl2, FOXO3, Irs1	(Zhou et al. 2013)
	miR-31	No	Hypoxia	HIF	(Liu et al. 2010)
	miR-429	miR-200b~429	Osmolarity responsive	OSTF1	(Yan et al. 2012)
	miR-375	No	Lactate production	LDHB	(Kinoshita et al. 2012)

	miR-144	miR-4732~451a	Oxidative stress	NRF2	(Sangokoya, Telen & Chi 2010)
Energy Metabolism	miR-23a	miR-23a~24-1	Glutamine metabolism	GLS	(Gao et al. 2009)
	miR-124	No	Glycolysis	PKM1/2	(Sun et al. 2012b)
	Let-7	Let-7a/d/f	Glucose metabolism	Irs2, INSR	(Frost, Olson 2011)
	miR-23	miR-23a~24-1	Mitochondrial biogenesis	TFAM	(Jiang et al. 2013b)
	miR-122	miR-122~3591	Lipid metabolism	Cholesterol related genes	(Esau et al. 2006b)
Protein Quality	miR-34a	No	Core fucosylation	FUT8	(Bernardi et al. 2013b)
	miR-148b	No	N-Glycosylation	C1GALT1	(Serino et al. 2012)
	miR-30b/d	miR-30b/d	O-Glycosylation	GALNT7	(Gaziel-Sovran, Hernando 2012)
Protein productivity/ secretion	miR-33a/33b	No	GSIS	Irs2	(Davalos et al. 2011)
	miR-30c*	No	UPR	XBP-1	(Byrd, Aragon & Brewer 2012)
	miR-410	mir-323b~656	Protein secretion	?	(Hennessy et al. 2010)
	miR-34a	No	Insulin secretion	VAMP2	(Lovis et al. 2008)
	miR-124	No	Insulin exocytosis	SNAP25 synapsin-1A	(Lovis, Gattesco & Regazzi 2008)
Abbreviations: Bcl2-B-cell lymphoma 2, Birc6-Baculoviral AIP containing repeat 6, C1GALT1- core 1 synthase, glycoprotein-N-acetylgalactosimine 3-beta-galactosyltransferase, 1, CCND1/E2-Cyclin D1/E2, CDK4/6-Cyclin-dependent kinase 4/6, CDKN1a-cyclin-dependent kinase inhibitor 1a, FOXO3-Forkhead box O3, GALNT7- N-acetylgalactosaminyltransferase 7, GLS-Glutaminase, GSIS-Glucose stimulated insulin secretion, Heat-shock protein-60/70, HIF-Hypoxia inducible factor, Irs2-Insulain receptor substrate 1/2, INSR-Insulin receptor, LDHB-Lactate dehydrogenase B, LATS2-Large tumour suppressor 2, NRF2-Nuclear factor erythroid 2-related factor 2, OSTF1-Osteoclast stimulating factor 1, PPP2R2A-PP2A regulatory subunit B alpha isoform, PDCD4-Programmed cell death 4, PKM1/2-Pyruvate kinase 1/2, Psme3-Proteosome activator subunit 3, Skp2-S-phase kinase associated protein 2, SNAP25-synaptosomal-associated protein 25, TFAM-Mitochondrial transcription factor A, UPR-Unfolded protein response, VAMP2-Vesicular associated membrane protein 2, XBP-1-X-box binding protein-1.					

1.2.6.1 miR-17~92 cluster

One of the best characterised oncogenic miRNAs is miR-17~92, a polycistronic miRNA cluster, also known as oncomiR-1, that is among the most potent oncogenic miRNA. The precursor transcript for this miRNA contains 6 stem-loop hairpin structures in tandem that ultimately generate 6 mature miRNAs: miR-17, miR-18a, miR-19a, miR-20a, miR-19b-1 and miR-92-1. Human miR-17~92 is located at 13q31.3, a region of the genome that is frequently amplified in several hematopoietic malignancies and solid tumours, such as diffuse B-cell lymphomas (DLBCLs), follicular lymphomas, Burkitt's lymphomas and lung cancer (Ota et al. 2004b). Studies have revealed that miR-17~92

acts pleiotropically during both normal development and malignant transformation to promote phenotypes such as proliferation, inhibit differentiation, augment angiogenesis and sustain cell survival (**Fig 1.3**). The anti-apoptotic nature of the miR-17~92 cluster is evident in progenitor B-cells whereby c-myc induced apoptosis is suppressed by the transcriptional activation of this cluster (Tagawa, Seto 2005). Furthermore, the oncogenic transcription factor family *E2F* (*E2F1/E2F3*), whose transcription drives the cell through to S phase through the activation of S phase genes such as thymidine kinase, DNA polymerase and *Cyclins E* and *A*, has been demonstrated to be a direct transcriptional activator of miR-17~92 (Sylvestre et al. 2007). Similar to c-myc, the overexpression of *E2F1* in normal and malignant cell types is sufficient to induce *p53*-mediated cell cycle arrest and apoptosis (Hsieh et al. 1997).

Figure 1.3: Pleiotropic functions of miR-17~92

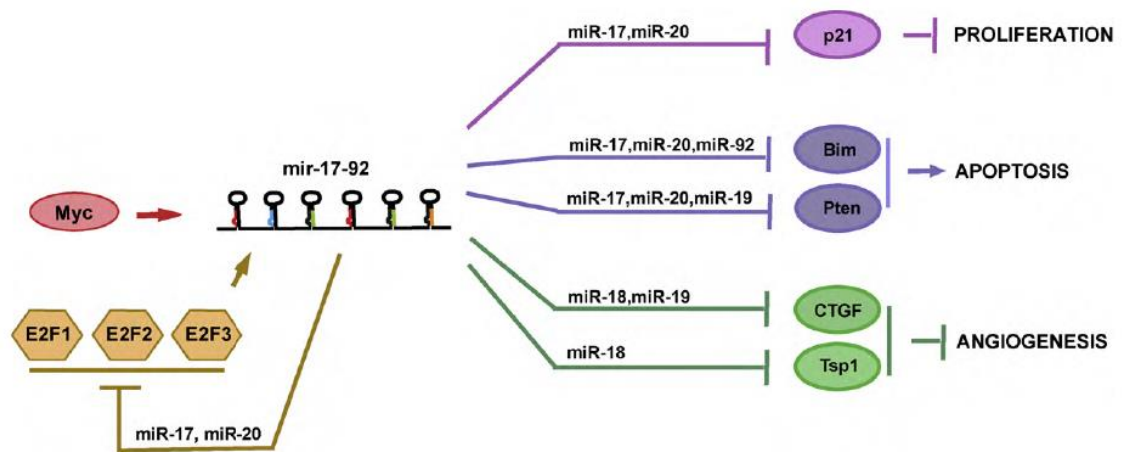


Figure 1.3: Above demonstrates the Pleiotropic functionality of the miR-17~92 cluster and its component members to generate and sustain a more aggressive cancer phenotype. Figure was sourced from the review by V. Olive and colleagues, 2010 (Olive, Jiang & He 2010b).

As *E2F1* acts as a transcription factor for itself it is caught in a perpetual positive feedback loop. However, through transcriptional activation of the miR-17~92 cluster, not only is fine-tuning of its own translation controlled by miR-17-5p (O'Donnell et al. 2005a) but entrance into apoptosis is additionally controlled through the interaction of the miRNA cluster with apoptotic components such as *PTEN* and *Bim* (Ventura et al. 2008). Tumourigenicity and aggressiveness has further been demonstrated by Dews and colleagues in colonocytes through the promotion of angiogenesis by targeting and

repressing anti-angiogenic factors such as thrombospondin-1 (*TPS-1*) and connective tissue growth factor (*CTGF*) by miR-18a and miR-19 respectively (Dews et al. 2006a).

Given the wide characterisation of this miRNA cluster, it is not surprising that it has shown up on the radar in miRNA research in CHO. Two independent studies revealed the potential of the miR-17~92 cluster as an engineering tool for the manipulation of CHO cell growth. In the first instance, next-generation sequencing unveiled the presence of 387 mature miRNA transcripts in CHO with the members of the miR-17~92 cluster being among them. Furthermore, cDNA sequencing of 26 previously validated targets (*E2F1*, *CCND1*, *BCL211*, *MAPK14*, *PTEN*, *RBI* and *VEGFA*) of this cluster demonstrated seed target site conservation suggesting conserved functionality of miR-17~92 in CHO (Hackl et al. 2011). Transient overexpression of miR-17 was carried out by the same group to validate its impact on the proliferation profile of CHO. An increase of 15.4% compared to negative controls was reported for this miRNA suggesting the utility of the entire cluster as an engineering tool as being functionally viable (Jadhav et al. 2012). Secondly, Clarke and colleagues identified the miR-17~92 as being differentially expressed in fast growing CHO cells with each of the cluster members exhibiting a positive correlation in clones with increasing growth rates (Clarke et al. 2012).

1.2.6.2 miR-23~27~24 clusters

In humans, the miR-23a~27a~24-2 cluster is intergenic and localised on chromosome 19p13 while its paralog miR-23b~27b~24-1 is an intronic cluster (*Aminopeptidase O*, *AMPO* (Sikand, Slane & Shukla 2009)) localised to chromosome 9q22 (Chhabra, Dubey & Saini 2010a). The deregulation and aberrant expression of both of these miRNA clusters have been associated with numerous cancerous phenotypes such as miR-23b~27b~24-1 in prostate cancer (Ishteiwy et al. 2012) and miR-23a~27a~24-2 in gastric cancer cells (An et al. 2013). Individually however, each member of these clusters has been associated with numerous cellular phenotypes including cellular proliferation, cell cycle, apoptosis, DNA repair and cellular metabolism. In primary keratinocytes, the overexpression of miR-24 was demonstrated to target the cyclin-dependent kinase inhibitors (*CDKIs*) p27^{Kip1} and p16^{Ink4a} thus promoting cellular proliferation (Giglio et al. 2013). In contradiction to this mechanism of action, the targeting of key nodes of the cell cycle by miR-24 triggered cell cycle arrest in G1 phase through reported gene targets such

as *MYC* and *E2F2*, as well as their downstream targets *CCNBI*, *CDC2* and *CDK4* (Lal et al. 2009a). Furthermore, miR-24 levels were determined to be, in one study, highly expressed in patient breast carcinoma samples compared to benign breast tissues. Ectopic overexpression of miR-24 promoted breast cancer cell invasion and migration while overexpression of its direct targets *PTPN9* and *PTPRF* reversed this observed phenotype (Du et al. 2013).

From a metabolic perspective, recent reports have implicated *c-Myc* to have a role in the catabolism of glutamine through the repression of miR-23a and miR-23b (Gao et al. 2012)(Dang 2010), thereby integrating this transcription factors role in cellular proliferation and metabolism. Altered glucose metabolism, also known as the “Warburg effect”, is a well-studied metabolic phenotype of cancer. This mechanism of “aerobic glycolysis” is characterised by the excessive uptake of glucose and conversion to lactate despite the availability of sufficient oxygen levels (Bensinger, Christofk 2012). C-Myc also collaborates with hypoxia-inducible factor-1 (*HIF-1*) to alter mitochondrial respiration resulting in the increased rate of glycolysis sufficient for tumour cell adaptation to its hypoxic (oxygen deficient) microenvironment, providing a growth advantage through the production of ATP and NADPH via excessive turnover of glucose and glutamine (Dang 2010). The link between glutamine catabolism and the increase in the enzyme glutaminase (*GLS*) has been associated with the repression of miR-23a/b, direct targets of *GLS*, by *c-Myc* in neoplastic cells (Gao et al. 2009).

The third member of these two clusters miR-27a/b has been associated with cellular metabolism through adipogenesis regulation via interference of the key regulator *PPAR γ* (Lin et al. 2009). Overexpression of miR-27a/b was demonstrated to promote endothelial cell sprouting through targeting of the angiogenesis inhibitor semaphoring 6A (*SEMA6A*) (Urbich et al. 2012). Not only has the oncogenic miR-27 been associated as an interfering factor in the G2/M check point of the cell cycle in breast cancer (Mertens-Talcott et al. 2007) but it has additional clinical value as a prognostic marker for breast cancer progression and patient survival with anti-correlated expression with its target *ZBTB10* (Tang et al. 2012).

It can be seen that the component members of the miR-23~27~24 clusters are involved in multiple cellular phenotypes from the opportunistic utilisation of carbon sources to direct activation or inhibition of pro-/anti- cell cycle regulators. Each member has

antagonistic to synergistic functionality, targeting multiple different aspects of cellular homeostasis thereby generating a tailor designed, and thriving cancer cell. The part they play in key cellular processes leading to tumorigenesis could also be potentially translated to CHO cell engineering.

1.3 microRNAs: Tools for CHO cell engineering

Various tools exist for the manipulation of miRNAs suitable for CHO cell engineering, reviewed in (Barron et al. 2011e). Although, upon publication of this review, miRNAs in CHO was still in its infancy, various applications have been published from transient to stable miRNA manipulation on a wealth of recombinant CHO cells with a great degree of success, reviewed in (Jadhav et al. 2013).

1.3.1 microRNA identification

Numerous differential expression profiles have been reported to date in CHO cells under various culture conditions such as temperature shift (Gammell et al. 2007, Barron et al. 2011b), nutrient depletion (Druz et al. 2011), growth rate profiling (Clarke et al. 2012) and culture stage profiling (Hernandez Bort et al. 2012). The conservation of mature miRNAs has allowed the use of human miRNA arrays to be used for the identification global miRNA changes in CHO cells including mouse and rat hybridization. Northern blotting has been used for the identification of pre-miRNA and mature miRNA through the use of short sequence-specific probes (Chen et al. 2004). More recently however, individual miRNAs can be detected based on their mature processed sequence by specifically designed reverse transcription (RT) primers containing a 5'-loop structure. This quantitative RT-PCR (qPCR) method can be SYBR-Green or Taqman based. qPCR based applications can also be used for more "global" large-scale miRNA profiling using 384-well arrays, each containing single miRNA probes, which gives a significant and more comprehensive snapshot of miRNA interaction simultaneously (Weber et al. 2010). The use of hybridisation arrays, miRNA bio-arrays generated with probes against human, rat and mouse miRNAs, have been exploited to identify expression patterns in a similar way to conventional transcriptional profiling methods. This approach identified 26 differentially expressed miRNAs in CHO subject to temperature shift and was the first miRNA profiling study carried out in this cell type (Gammell et al. 2007). With the release

of the CHO-K1 genome and the addition of over 400 mature CHO miRNA sequences to the miRBase database, it is only a matter of time until CHO-specific arrays are developed for the global characterisation of miRNAs intimately involved within different cellular processes of biotechnological interest.

1.3.2 Transient microRNA interference

To verify the utility of predicted miRNAs as engineering tools, phenotypic assessment is performed through the increase or decrease of endogenous miRNA levels. In the case of gain-of-function, mimics take the form of 22 nt dsRNA duplexes that are similar in structure to that of pre-processed or “diced” miRNAs (**Fig. 1.1 4**) (Ford 2006). This introduction of pre-processed miRNAs circumvents the requirement of the utilisation of the primary miRNA processing machinery such as Drosha/DGCR8 and Exportin-5 providing immediate activity with lipid-based delivery remaining the primary method of transient introduction (Tseng, Mozumdar & Huang 2009). These mimics take the form of short-hairpin (sh) RNAs and do not possess the base-pair mismatches associated with natural occurring miRNA duplexes. The benefit of this is that miR* strands can be efficiently overexpressed and analysed, despite their “normal” endogenous structures favouring selection of the guide due to thermodynamic properties (Schwarz et al. 2003). Transient miRNA intervention using mimics has been reported in CHO in the case of miR-7 inducing a temperature-shift like phenotype (Barron et al. 2011b) and the library screen of 879 miRNAs assessing their role in productivity (Strotbek et al. 2013).

With the identification of miRNAs being frequently located at fragile chromosomal locations susceptible to genomic instability resulting in chromosomal deletions or transcriptional attenuation (Lagana et al. 2010) it was important to develop an efficient method to evaluate miRNA loss-of-function phenotypes and this has subsequently been successfully employed through numerous means, reviewed in (Stenvang et al. 2012). Chemically modified antisense oligonucleotides (AON), antimiRs, are a widely employed approach to accomplish miRNA loss-of-function by sequestering the mature target miRNA, by strong hybridisation, inherently in competition with cellular mRNA targets resulting in translational de-repression (Dean 2001). The chemical modification of these small RNAs through various methods has been executed in order to prolong the stability and subsequently their efficacy within the cellular environment, reviewed in

(Stenvang et al. 2012). These modifications include the 2-OH residue of the ribose of the antisense RNA being replaced with 2'-O-methyl (Panzitt et al. 2007), 2'-O-methoxyethyl (Esau et al. 2006a), 2'-Fluoro (Lennox, Behlke 2010) and locked nucleic acid (LNA) (Chan, Krichevsky & Kosik 2005). Modifications confer enhanced benefits such as resistance to nucleases, prolong stability through stable hybridization, increase binding affinity without abrogating specificity and enhance melting temperature (T_m). A modified version of LNAs, termed 8-mer LNA-antimiRs, has been developed to assess the biological functions of entire miRNA seed families (Obad et al. 2011). To reduce off-target effects such as inhibition of entire seed families, RNAi constructs have been designed specific to the primary miRNA sequence allowing a higher degree of specificity (Vaistij et al. 2010). Transient miRNA inhibition is routinely used in CHO cell screening such as in the case of miR-7 (Barron et al. 2011b) and miR-466h (Druz et al. 2011).

The large-scale transfection of miRNAs using non-viral delivery has been demonstrated for mammalian cell cultures such as CHO in complex protein production media (Fischer et al. 2013). This offers new potential for miRNAs to be used in existing approved processes via transfection, having less regulatory implications and ultimately avoiding stable cell line development (**Fig. 1.4**).

Figure 1.4: Transient miRNA intervention within the bioprocess

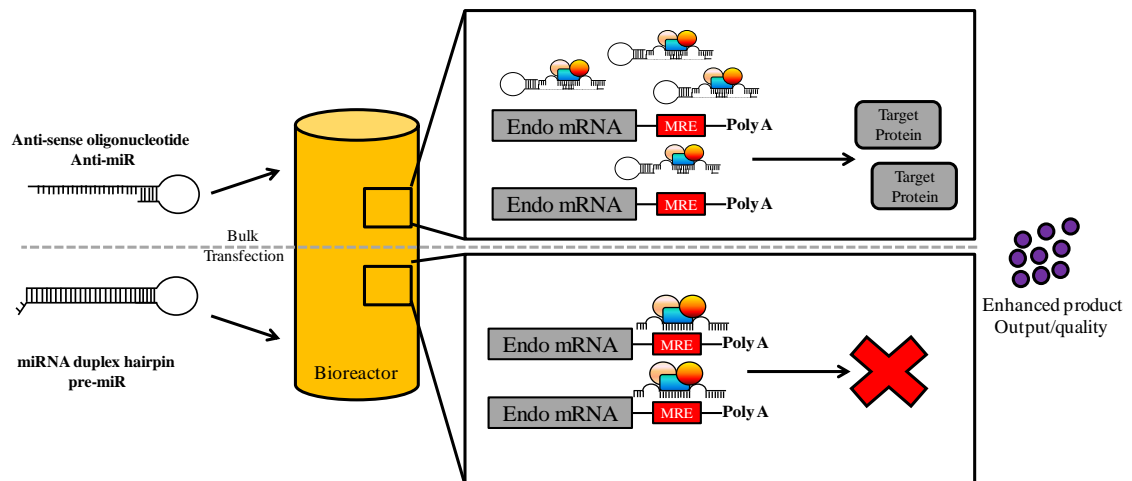


Figure 1.4: Large-scale bulk transfection can be performed transiently by introducing small working concentrations of either mimics or inhibitors at various culture time points in a bioreactor to achieve a multitude of phenotypes such as enhanced quality or yields. This figure was sourced from Kelly *et al.*, 2014 (Manuscript accepted).

Not only does transient overexpression bypass the natural miRNA processing pathways but synthetic miRNA stability does not allow the elucidation of prolonged phenotypic impacts (Thomson, Bracken & Goodall 2011). For this reason and from the perspective of ultimately engineering CHO cell lines for industrial application, stable methods of miRNA intervention are required.

1.3.3 Stable microRNA interference

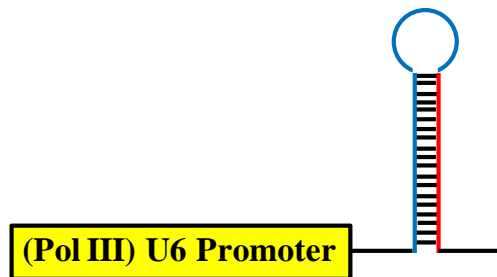
Stable miRNA intervention is required to overcome the inherent pitfalls of transient miRNA assays such as the short half-life of introduced miRNAs, the reduced cytoplasmic payload of miRNAs across daughter cells upon cellular division (Song et al. 2003, Bartlett, Davis 2006), the saturation of miRNA biogenesis machinery and the titrational influence based on the reciprocal relationship between miRNAs and mRNAs (Pasquinelli 2012). In the case of gain-of-function studies, stable overexpression provides a more physiological natural state of miR expression, preventing off-target effects (Grimm et al. 2006). Furthermore, stable miRNA intervention has been reported to induce a phenotype in cases where transient intervention proved unsuccessful such as miR-7 in CHO cells (Barron et al. 2011b, Sanchez et al. 2013b).

The miRNA hairpin structure has been exploited in order to develop short-hairpin (sh) RNA vectors for the validation of gene knockdown studies (Zhu et al. 2007). shRNAs driven by a polymerase (pol) III promoter such as U6 (**Fig. 1.5 A**) are modelled after precursor miRNAs (Rossi 2008) containing a sequence of ~22-25 nt, a short loop region and the reverse complement to the 22-25 nt region whereas other systems such as pol II act more like primary miRNAs in which the shRNA is flanked by natural miRNA sequences (**Fig. 1.5 B**), termed shRNA-miRs (Meerbrey et al. 2011, Du et al. 2006). The natural flanks take the form of miR-30 sequences (125 bases 5' and 3') forming the second generation of shRNAs (Silva et al. 2005) and have been shown to provide a higher knockdown efficiency (Stegmeier et al. 2005) when driven through a pol II promoter. shRNA-miRs transcribed *in vivo* from polymerase II, feed directly into the miRNA biogenesis pathway usurping the entire miRNA processing machinery whereby by shRNAs driven by pol III circumvent nuclear processing by Drosha acting like a less “natural” miRNA system (Lebbink et al. 2011).

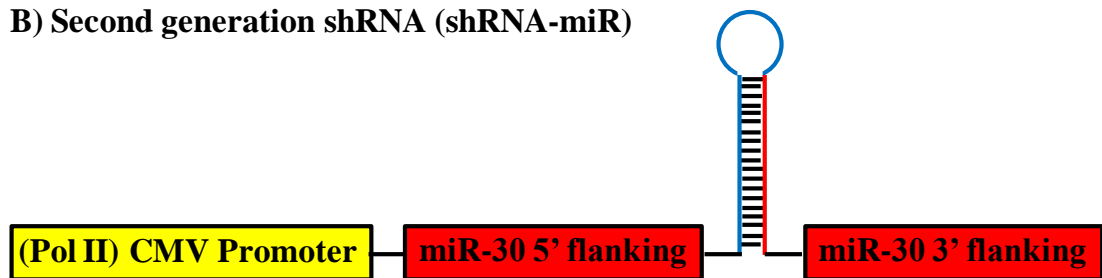
The observation that miR-flanking sequences and pol II promoters enhanced miRNA biogenesis in addition to abrogating it upon sequence mutations (Zeng, Cullen 2003) led to the final evolutionary step of these vectors to directly use the endogenous miRNA sequence itself (**Fig. 1.5 C**). 100 bp 5'- and 3'- flanks were identified to be sufficient to drive miRNA expression in the case of miR-199a (Furukawa et al. 2011). Multi-expression vectors of miRNAs from various genomics locations (miR-34a, -34b and -34c), including 60 bp, flanks have demonstrated the possibility of creating artificial miRNA clusters (Qiu, Friedman & Liang 2011) presenting a flexible system for “off-the-shelf” tailored miR construct design.

Figure 1.5: Construct of siRNA/miRNA expression vectors

A) First generation shRNA



B) Second generation shRNA (shRNA-miR)



C) Complete microRNA expression construct

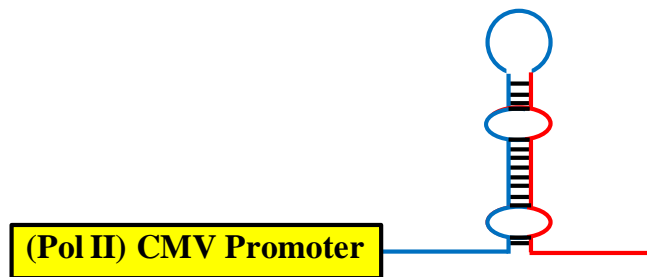


Figure 1.5: A schematic diagram following the evolution of A) first generation shRNA construct transcribed from a pol III promoter as a hairpin that bypasses Drosha nuclear processing. B) Modified shRNA (shRNA-miR) to include endogenous miR-30 flanking sequences (5'- and 3'-) transcribed from pol II to yield a primary miRNA precursor that enters the full biogenesis pathway. C) Complete endogenous miRNA sequence including flanks cloned from genomic DNA and under the control again of a pol II promoter.

Stable miRNA expression constructs have also been generated using the miR-155 flanking motifs and have been successfully employed in CHO cell engineering such as miR-17/-21 (Jadhav et al. 2012) and the miR-17~92 cluster (Jadhav et al. 2014).

Subsequent to the publication of the CHO genome (Xu et al. 2011), pre-miRNA sequences and their respective genomic locations were made available (Hackl et al. 2012). From this, the use of endogenous CHO sequences has been demonstrated to be more efficient when compared to their chimeric counterparts using miR-155 flanks (Klanert et al. 2013). A 3-fold increase in mature miRNA expression was observed in the case of

miR-221/222 and miR-15b/16 clusters when endogenous CHO clusters were stably expressed. The use of endogenous sequences does prove troublesome when attempting to overexpress miR* strands due to the thermodynamic favourability towards the guide strand (Gu et al. 2011). To navigate around this obstacle, shRNA-based designs have been exploited, eliminating natural flanking sequences which contribute a bias in strand selection (Yang et al. 2011) and ensuring almost full complementary of the duplex partner, as reported for miR-146b-3p (Qu et al. 2012).

One method to assess prolonged miRNA inhibition has been the introduction of miRNA-resistant target genes, circumventing miRNA specific deletion, through site-directed mutagenesis of the MRE, rendering the miRNA ineffective (Garcia 2008). Global interference with miRNA expression through genetic deletions of pivotal miRNA biogenesis machinery such as dicer (Ketting et al. 2001) has also been explored. Stable knockdown of miRNA through these means, however, proved itself to be challenging and ineffective as interference with miRNAs during embryonic development has been observed to abrogate the developmental process (Forstemann et al. 2005). The stable expression of shRNAs designed specifically to the mature miRNA sequence has been demonstrated to be effective such as in the case of miR-466h inhibition in CHO cells ultimately extending culture longevity (Druz et al. 2013). To reduce off target effects, RNAi constructs can be designed that target the miRNAs primary transcript which would have a higher degree of uniqueness ultimately allowing for the inhibition of a single miRNA target and not entire seed families (Vaistij et al. 2010). miRNA sponge technology offers an attractive option for stable miRNA inhibition as suggested by Barron and colleagues (Barron et al. 2011e) and has proved its usefulness in the optimisation of pharmaceutical production cells (Sanchez et al. 2013b).

The increased understanding of miRNAs, their regulatory motifs, their biogenesis and processing has allowed for the development of numerous expression constructs allowing the researcher to develop, with minimal understanding, shRNA and miRNA vectors, making these regulatory molecules easily accessible for industrial applications.

1.3.4 microRNA sponge technology

A recent review by Park and colleagues on genetic knockout studies in mice indicated that “genetic ablation of miRNAs may not result in obvious phenotypes” (Park, Choi & McManus 2010). This may be attributed in part to the functional redundancy inherent in the presence of related miRNA seed families as well as paralogs that share endogenous mRNA targets (Bartel 2009). As such, multiple rounds of genetic knockout would potentially be necessary to observe any phenotypic impact. Given the genetic complexity of miRNA organisation, genetic knockouts also pose problematic as the knockout of intronic miRNAs could interfere with host gene transcription or, in the case of clusters, interfere with all components instead of one. A means to navigate around this inherent genetic fortitude has come from observations in nature of the apparent reciprocal relationship between miRNAs and their target genes, reviewed in (Pasquinelli 2012). This lead to the hypothesis that miRNA targets could act as competitive inhibitors, competitive endogenous RNAs (ceRNAs) of miRNA function (Seitz 2009).

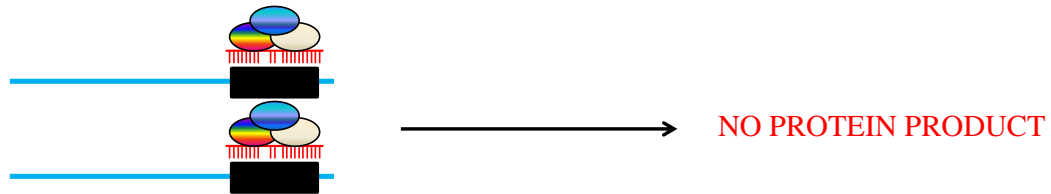
The first observation of an endogenous mRNA impacting on miRNA function was discovered in *Arabidopsis thaliana* and their response to phosphate starvation (Franco-Zorrilla et al. 2007). Upon deprivation of inorganic phosphate, up-regulation of miR-399 resulted in the accumulation, rather than depletion, of its predicted target *PHO2* (putative-conjugating enzyme E2). It was discovered that the expected suppression of *PHO2* was circumvented due to increased expression of the non-coding (nc) gene, *IPS1*. Thus *IPS1* acted as a miRNA decoy, sequestering or titrating miR-399 function away from its endogenous targets. Furthermore, additional mismatches in the duplex formed between miR-399 and *IPS1* prevented Ago2-mediated slicing of the *IPS1* transcript, allowing persistence of this “target mimic” in the cell. The presence of common MREs allow these ceRNAs to mutually regulate each other in a titration-dependent manner, as observed recently for the *ZEB2* transcription factor and the tumour suppressor *PTEN* (Karreth et al. 2011, Salmena et al. 2011). Not only did the observation demonstrate that target mRNA abundance dilutes miRNA activity, but it identified its presence in a mammalian system and in contributing to a disease state (Arvey et al. 2010). Indeed this phenomenon was found to go beyond pairs of protein-encoding genes to include long ncRNAs (lncRNAs) (Ponting, Oliver & Reik 2009). To support the role of *PTEN* as a tumour suppressor, the pseudogene *PTEN1* contains MREs within its 3'UTR similar to that of its

coding counterpart *PTEN*. Expression of this pseudogene transcript retains biological activity as a decoy to sequester and fine tune the translation of the coding *PTEN* through competitive binding. Indeed it's been shown that the *PTEN1* locus is frequently lost in human cancers (Poliseno et al. 2010).

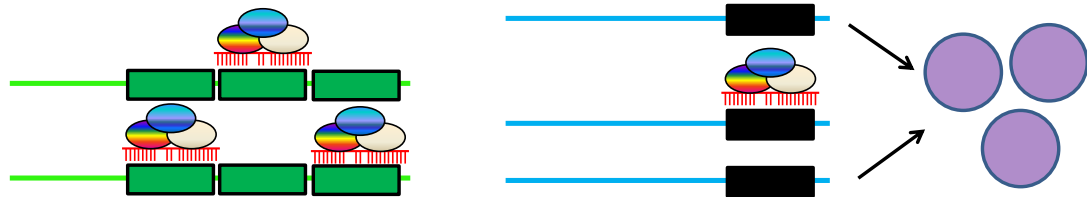
More recently, the phenomenon of head-to-tail splicing of exons has been shown to generate an exciting new class of non-coding RNAs with regulatory potential, known as circular RNAs (circRNAs) (Danan et al. 2012, Burd et al. 2010, Hansen et al. 2011). For example, an antisense transcript from the cerebellar degeneration-related protein 1 (CDR1as) (Memczak et al. 2013) was found to generate a circular decoy that harboured 63 conserved binding sites for the well characterised tumour suppressor miRNA, miR-7 (Zhang et al. 2013). This class of regulatory RNA offers a viable engineering tool due to its superior stability, potentially as a result of its inherent resistance to cytoplasmic debranching enzymes and RNA exonucleases (Jeck et al. 2013).

Figure 1.6: microRNA sponges divert endogenous miRNA activity

A) mRNA translation repression by miRNA



B) miRNA inhibition through target mimicry: “miR-Sponges”



C) miRNA inhibition through reduced sponge expression with increased MBS

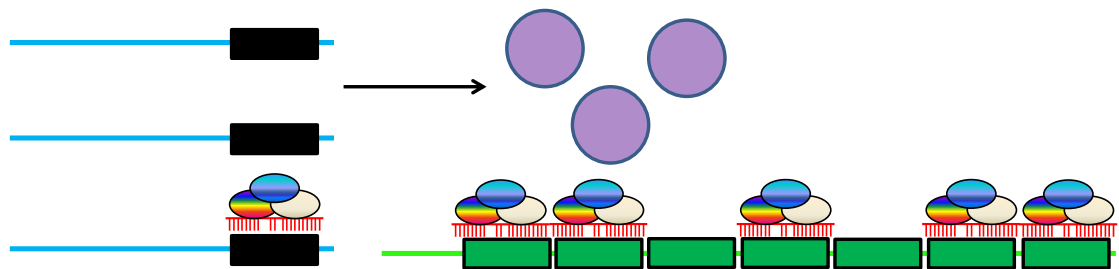


Figure 1.6: microRNA sponges repress microRNA function: A) demonstrates the microRNA mediated translational repression of the target gene through Watson-Crick imperfect base-pairing to the miRNA target sequence (Black box) resulting in no protein expression. B) Translational activation of the endogenous mRNA target through sequestration of the antagonizing miRNA by decoy miR-sponge sequences (Green box) transiently expressed from a plasmid vector. C) Similar level of microRNA sponging achieved by a chromosomally integrated sponge containing more MBS that is expressed at lower levels compared to transient expression from a plasmid in diagram B.

The discovery of these endogenous miRNA decoys led to the development of “microRNA sponge technology” as an experimental tool to evaluate miRNA function (Ebert, Neilson & Sharp 2007). Named for their ability to soak up endogenous miRNAs, miRNA sponges contain multiple sites of complementarity to the miRNA of interest, usually in an artificial 3’UTR placed downstream of a reporter gene such as GFP (**Fig. 1.6**). Drawing from lessons in nature, mismatches or “wobble” are introduced as a means to inhibit miRNA-mediated mRNA cleavage thus prolonging the life-time of the sponge decoy (Kluiver et al. 2012b). Introduction of “wobble” has been demonstrated to be more effective at diverting endogenous miRNA function than perfect antisense MREs due to the prolonged

life-time of the miR-sponge transcript as a result of miRNA/RISC-mediated mRNA cleavage inhibition (Haraguchi, Ozaki & Iba 2009). As seed pairing has been observed to be sufficient to drive miRNA-target interactions, miR-sponges have the potential to sequester entire miRNA seed families as demonstrated in the case of the let-7 family (Yang et al. 2012). Although this can complicate efforts to understand the network of downstream molecular events that accompany multi-miRNA inhibition, research has proven the miR-sponge approach to be a viable tool for industrial rCHO cell line engineering (Sanchez et al. 2013b). In this study, stable diversion of miR-7 through the presence of a sponge decoy resulted in increased peak cell density, prolonged viability and ultimately enhanced yield in a CHO fed-batch culture.

Another potential application of this approach is the use of sponge sequences as a means of controlling the expression of transgenes in a miRNA-dependent manner. For example if there were a situation where overexpression of a particular gene was desirable only at a particular point in the culture but otherwise it should be silent. By identifying an endogenous miRNA whose expression was anti-correlated with the desired transgene expression profile, a sponge for that miRNA placed downstream of the transgene sequence would suppress its expression during the chosen culture phase but become de-repressed later when the miRNA was down-regulated (**Fig. 1.7**). This application is in some ways equivalent to the use of inducible promoters.

Figure 1.7: Mechanism of exploiting a miRNA-dependent transgene

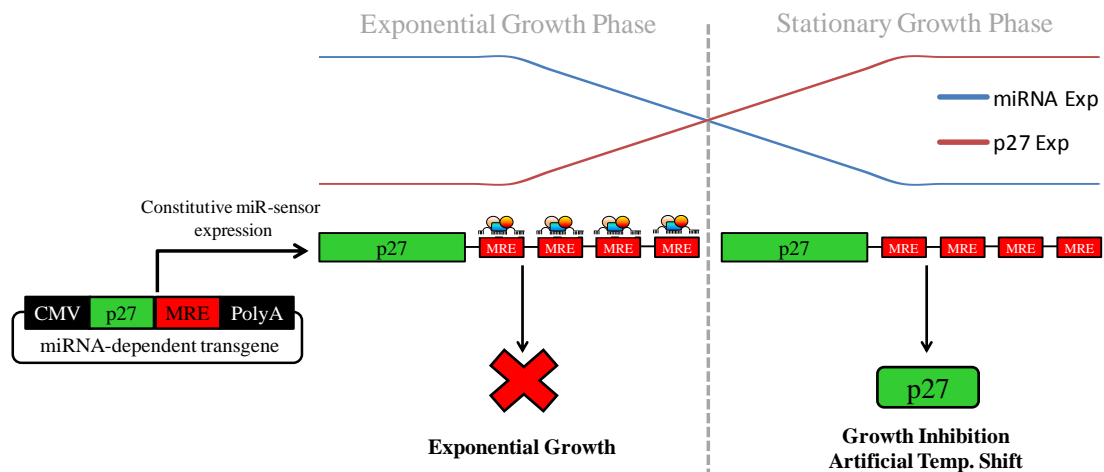


Figure 1.7: The above schematic diagram demonstrates the hypothetical utility of miRNA sponge technology when implemented within a CHO cell system of whose miRNA expression profile across various stages of the culture is known. A plasmid vector expressing the cell cycle inhibitor, *p27*, engineered to contain MREs specific for a given miRNA whose expression profile is known across various phases of CHO cell culture (**blue line**). In early Exponential growth phase *p27* expression (**red line**) is maintained at a low level due to the high abundance of mature miRNA specific for the pre-engineered MREs. Once endogenous miRNA expression is transcriptionally down-regulated, *p27* translation gradually becomes de-repressed ultimately halting the cell cycle mimicking a temperature shift-like phenotype. The above figure was sourced from Kelly and colleagues, 2014 (Manuscript accepted).

1.4 Glyco-engineering

As of 2012, there were 28 FDA approved recombinant therapeutic antibodies which represented 36% of the total market revenue for pharmaceutical biologics (Butler, Meneses-Acosta 2012). The development of chimeric and humanised antibodies marked a major breakthrough in monoclonal antibody (Mabs) therapy as previous therapeutic antibodies were of murine origin thus introducing a foreign, highly immunogenic protein demonstrating suboptimal effector functions with short half-lives (Reichert 2010). The efficiency of Mabs is due to their antigen specificity and their downstream effector functions through the formation and activation of immune complexes. All FDA approved therapeutic Mabs (**Table 1.6**) are of the immunoglobulin G (IgG) class which in itself is composed of four subclasses: IgG1, IgG2, IgG3 and IgG4, defined according to their relative concentrations in normal serum. It has been demonstrated that each subclass elicits a unique profile of effector functions and that selection of each isotype for clinical development is dependent on the desired therapeutic outcome and disease type (Jefferis 2007). The utility of monoclonal antibody therapy is layered and when tailor designed in the right way can achieve several outcomes such as: (i) killing cells or organisms, cancer/bacteria; (ii) neutralisation of soluble molecules such as cytokines in chronic diseases or endotoxins; (iii) act as agonists or antagonists of cellular activity; (iv) induce apoptosis, and (v) delivery of a cytotoxic payload such as a chemotherapeutic drug. The end point clinical efficacy of therapeutic antibodies is dependent on two mechanisms: target-specific binding of the Fab (antigen-binding fragment) domain in addition to the availability of cell surface epitopes and the immune-mediated effector functions orchestrated through the activation of antibody-dependent cell cytotoxicity (ADCC) and/or complement-dependent cytotoxicity (CDC) (Chan et al. 2010, Raju 2008). Immune-mediated effector functions are mediated by interactions between the Fc (Crystallisable fragment) of the Mab and Fc receptors (FcRs) on various cell types (Siberil et al. 2007). Although CHO cells are the primary mammalian cell type for recombinant therapeutic protein production due to their similar posttranslational modifications, it has now emerged that the variable glycoforms produced in CHO can impose limitations on effector functions (Nimmerjahn, Ravetch 2008). Such glycoforms can reduce the potency of ADCC activation, requiring higher therapeutic doses per treatment and ultimately increase global demand thus placing a strain on biopharma companies to boost product titres.

Table 1.6: FDA approved therapeutic antibodies and Fc fusion proteins

Generic name	Format	Target	Disease	MOI	Class	Effector function
Campath	Humanized IgG1 κ	CD52	CLL	Induction of ADCC	I	High
Erbix	Chimeric (murine/human) IgG1 κ	EGFR	Metastatic colorectal cancer/head and neck cancer	Inhibition of EGFR signalling, ADCC	I	High
Arzerra	Human IgG1 κ	CD20	CLL	Induction of CDC and ADCC	I	High
Rituxan	Chimeric (murine/human) IgG1 κ	CD20	Non-hodgkin's lymphoma, RA and CLL	Induction of apoptosis, CDC and ADCC	I	High
Herceptin	Humanized IgG1 κ	HER2	HER2+ breast cancer	Inhibition of HER2 signalling, ADCC	I	High
Humira	Human IgG1 κ	TNF α	RA, JIA, PA, CD, AS and plaque psoriasis	Neutralisation of TNF α activity	II	Moderate
Simulect	Chimeric (murine/human) IgG1 κ	CD25	Acute transplant rejection	Inhibition of IL-2-mediated activation of lymphocytes	II	Moderate
Raptiva	Humanized IgG1 κ	CD11a	Plaque psoriasis	Inhibition of CD11a-associated leukocyte adhesion	II	Moderate
Simponi	Human IgG1 κ	TNF α	RA, PA and AS	Neutralisation of TNF α activity	II	Moderate
Remicade	Chimeric (murine/human) IgG1 α	TNF α	CD, RA, PA, ulcerative colitis, AS and plaque psoriasis	Neutralisation of TNF α activity	II	Moderate
Enbrel	TNFR2 ECD-Fc (IgG1) fusion	TNF α	RA, JIA, PA, AS and plaque psoriasis	Neutralisation of TNF α activity	II	Low
Vectibix	Humanized IgG2 κ	EGFR	Metastatic colorectal carcinoma	Inhibition of EGFR signalling: Induction of apoptosis	II	Low
Avastin	Humanized IgG1 κ	VEGF	Metastatic colorectal cancer	Neutralisation of VEGF activity	III	Low
Xolair	Humanized IgG1 κ	IgE	Allergic Asthma	Inhibit binding of IgE to Fc ϵ RI	III	Low

Table 1.6: Of the list of antibody therapeutics listed, Class refers to the specific mode of action (MOA) specified further in figure 1.9.

1.4.1 Antibody structure and effector functions

Antibodies form an intricate part of the adaptive immune system and are responsible for the recognition of potentially any antigen (epitope) through the three variable regions within both the light and heavy chain that form the complementarity-determining region (CDR) (Sela-Culang, Kunik & Ofran 2013) of the antigen-binding fragment (Fab). The basic structure of a Mab consists of four polypeptide chains: two identical light chains and two identical heavy chains (EDELMAN, BENACERRAF 1962). **Figure 1.8** shows the association that the four polypeptides demonstrate through covalent and non-covalent interactions to form the three independent mature antibody structures. The two Fabs are composed of the light chain and the N-terminal domain of the heavy chain harbouring the variable regions which determines hyper-variability in antigen specificity along with two constant domains (CH1 and CL). Additionally, two domains forming the heavy chains are composed of two constant domains (CH2 and CH3) which constitute the crystallisable fragment (Fc) and contain moieties that interact with ligands on immune cells that elicit effector functions.

Figure 1.8: Structure of the immunoglobulin G (IgG) molecule

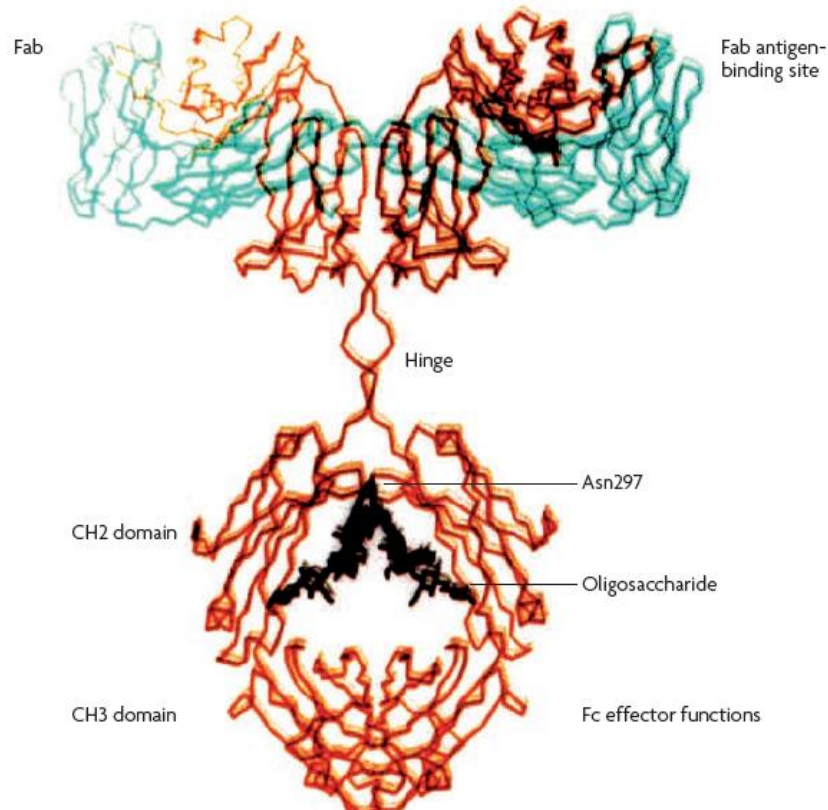


Figure 1.8: Various domains the makes up a mature IgG molecule. The two heavy chains and two light chains are represented as the orange and blue structures, respectively, linked non-covalently by the flexible hinge region. Antigen specificity is dictated by the two antigen-binding fragments (Fab) made up of covalently linked light and heavy chain. Glycosylated sites are located on the conserved Asparagine 297 (Asn297) on each heavy chain CH2 domain.

Fc receptors (FcRs) are glycoproteins belonging to the immunoglobulin superfamily and are composed of the classes Fc α R, Fc γ R and Fc ϵ R of which Fc γ R are mostly expressed on immune cells and are fundamental for therapeutic outcome. Fc γ Rs are divided into three subtypes – Fc γ RI (CD64), Fc γ RII (CD32) and Fc γ RIII (CD16) categorised based on the their affinity for IgG and the downstream signalling pathways that they trigger (Nimmerjahn, Ravetch 2008). As mentioned earlier, antibodies can be exploited to elicit a series of therapeutic outcomes such as neutralisation of a soluble signalling molecule such as TNF α in Rheumatoid arthritis (Class III), opsonisation and clearance through ADCC/CDC via targeting of cell-bound antigens (Class I) and receptor blocking interfering with “normal” aberrant signalling (Class II), **Figure 1.9**.

Figure 1.9: Mechanism of action of therapeutic antibodies.

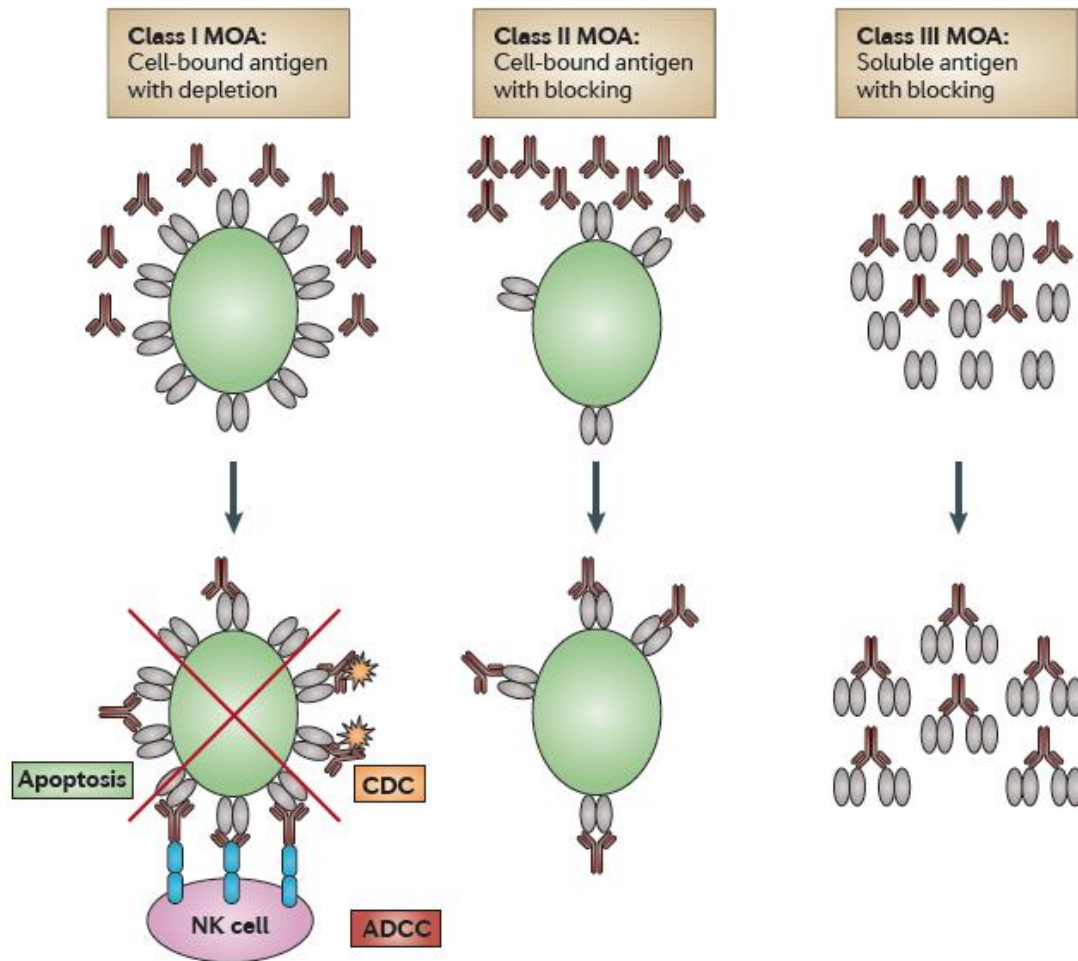


Figure 1.9: Mechanisms of action (MOA) of therapeutic antibodies including targeting and subsequent clearance of cell/molecule via antigen binding and ADCC/CDC activation (Class I), Interference with aberrant signalling through receptor binding and blocking (Class II) and Clearance and deactivation of soluble antigens (Class III). Figure was sourced from (Jiang et al. 2011).

Additionally, better understanding of antibody structure and function have allowed for the development of Fc-fusion proteins, such as Etanercept (Enbrel), which is a Tumour Necrosis factor receptor 2 (TNFR2) fused to the constant Fc-region of an antibody which prolongs its half-life in serum via its interaction with the neonatal Fc receptor and appears to act independently of glycoforms (Roopenian, Akilesh 2007). The predominant subclass of antibody licensed for therapeutic rMab use is the IgG1 isotype (Bruggemann et al. 1987) largely due to its strong association with the Fc γ RIIIa, a ligand responsible for ADCC activation through natural killer (NK) cells (Bruhns et al. 2009). This affinity is

shared by the IgG3 isotype but not with the IgG2 and 4 subclasses. For example, the primary pathway of Rituximab in the treatment of CD20⁺ B lymphocytes in non-Hodgkin's lymphoma appears to be mediated through the activation of ADCC via association with NK cells expressing FcγRIIIa receptors (Congy-Jolivet et al. 2007). It is interesting that a clinically approved EGF-R antibody, panitumumab of the IgG2 isotype, interacts less efficiently with human FcγRs and does not activate the complement cascade (Dechant et al. 2007). It is from these advancements in our understanding of Mab/immune system relationship that derivation away from the predominant IgG1 isotype is a growing field. Long term exposure to such antibodies in the case of chronic inflammatory diseases can, by nature, activate immune cells to release inflammatory cytokines thus contributing to the symptoms being targeted. Development of Mabs or fusion proteins specific for TNFα but with a low affinity for FcγRIIIa receptors could function to sequester and block TNFα signalling without, in this instance, the unwanted immune signalling.

1.4.2 Antibody glycoforms

Despite the CHO cell being the favoured production vessel of recombinant protein therapeutics due to similarities in their post-translational modifications, the recent release of the CHO genome sequence has revealed a number of discrepancies in the genomic and transcriptomic profile of genes associated with glycan synthesis and degradation (Xu et al. 2011). Although only constituting 2-3% of the total antibody mass, glycosylation of the IgG-Fc region has been demonstrated to be essential to the activation of the downstream biological effector functions. This glycosylation is through covalent attachment of an oligosaccharide at the conserved Asparagine 297, Asn297 (**Figure 1.8**). A diantennary type oligosaccharide comprised of a core heptasaccharide and variable addition of fucose, galactose, bisecting N-acetylglucosamine and sialic acid contributes to the glycoforms of Fc modified Mabs (**Fig. 1.10**). With the variation in the addition of sugars to the core heptasaccharide, a total of 32 unique oligosaccharides can be generated from each partner of the heavy chain. Taking into account the duplicity of heavy chains in a single Mab there is the potential of ~500 glycoforms to be generated of mature antibody (Jefferis 2009a).

Figure 1.10: Diantennary-complex oligosaccharide composition of the IgG-Fc

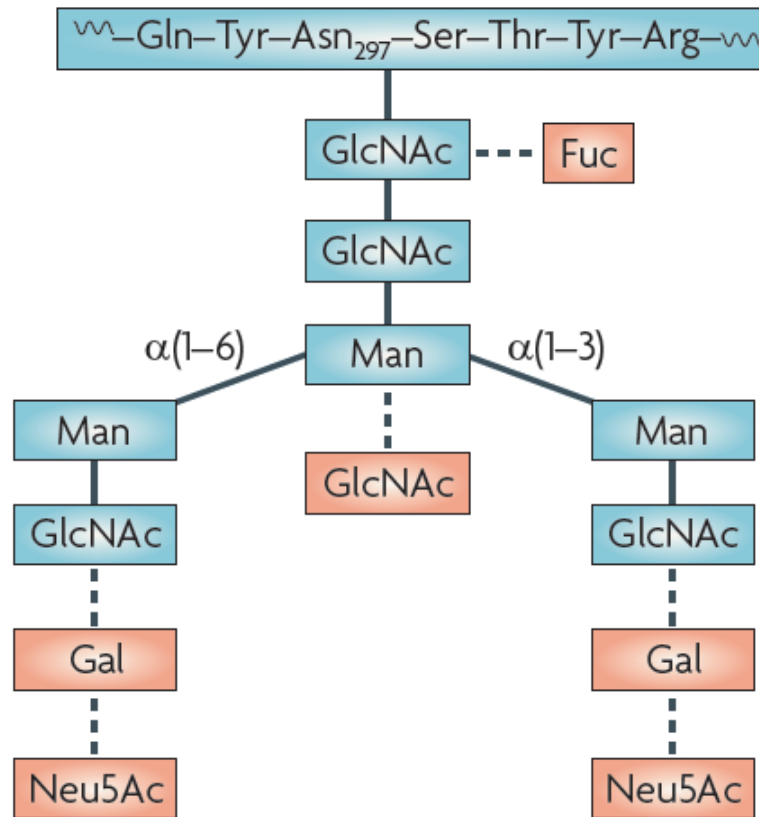


Figure 1.10: A schematic representation of the Diantennary-complex oligosaccharide that is covalently attached to the conserved Asparagine 297 (Asn₂₉₇) on both CH₂ domains of the heavy chains. The oligosaccharide is composed of a core heptasaccharide (sugars in blue) and outer arm sugars (in red) variably attached, Fucose (Fuc), Galactose (Gal), Bisecting N-acetylglucosamine (GlcNAc), sialic acid and N-acetylneuraminic acid (Neu5Ac). This figure was sourced from (Jefferis 2009a).

Nomenclature for naming the various glycoforms can use G₀, G₁ and G₂ for core oligosaccharides bearing zero, one or two galactose residues, respectively. In the event of an addition of fucose (Fuc), the notation G₀F, G₁F and G₂F is used. Finally, with the addition of a bisecting N-acetylglucosamine (GlcNAc) a B is added to the naming system previously described, such as G₀B or G₀BF (**Fig. 1.11**). Less than 10% of oligosaccharides are sialylated so have not been included in the notation description (Mizuochi et al. 1982).

Figure 1.11: Diantennary oligosaccharide structure and nomenclature

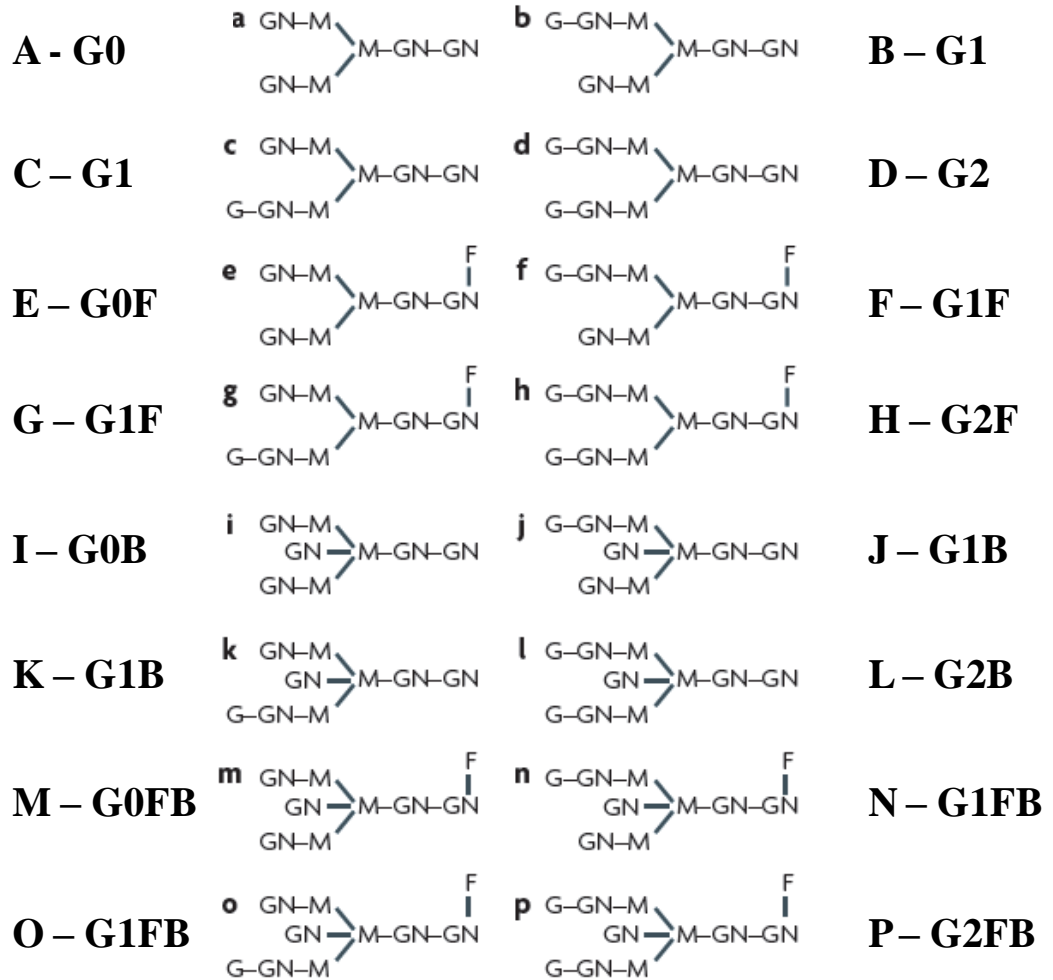


Figure 1.11: The naming system of the variable oligosaccharides that can be generated on each isolated heavy chain and their corresponding glycan structure. Above shows the 16 variants of each core heptasaccharide without including the addition of a sialic acid group. Taking into account the 16 variations on both heavy chains shown above, the total number of unique glycoforms is 128 (16 x 16) which is divided by two because of the symmetry of the molecule. This figure was sourced and modified from (Jefferis 2009a).

It has been observed that the oligosaccharide present on glycoproteins contribute to their stability and solubility (Krapp et al. 2003, Mimura et al. 2000) so it is not surprising that a-glycosylated or de-glycosylated IgG forms result in a compromised or ablated effector mechanism mediated through FcγRI, FcγRII and FcγRIII.(Sinclair, Elliott 2005). CHO cells predominantly produce the top eight glycoforms (a-h) in **figure 1.11**; however, the proportion of galactosylated and non-fucosylated IgG-Fc is relatively low by comparison. CHO cells are unable to add the bisecting N-acetylglucosamine as they do not express the GnTIII gene but do possess a genomic homolog (Xu et al. 2011). In the absence of these

glycan modifications, CHO cells possess the ability to add other sugars that humans do not retain thus contributing to immunogenicity such as the addition of galactose in an $\alpha(1-3)$ linkage. These observations have led to the exploration and development of CHO cells engineered to produce specific glycoforms that mediate enhanced effector functions.

1.4.3 Glycan-manipulation

Present CHO cell production vessels produce rMabs with over 90% fucosylated forms of IgG-Fc. Engineered CHO cells to express the GnTIII gene to add the bisecting N-acetylglucosamine residue on the IgG-Fc bound core heptasaccharide demonstrated a 2-fold increase in ADCC for a rituximab-like product (Davies et al. 2001). Further investigation revealed that this enhanced effector ADCC was mediated through the inhibition of the subsequent addition of Fucose to the primary N-acetylglucosamine residue through the prior addition of the bisecting GlcNAc in the golgi apparatus (Ferrara et al. 2006). Targeting fucosylation of the primary GlcNAc is now emerging as a viable approach for cellular engineering strategies, a process that has been extended to encompass the therapeutic antibody Herceptin with a great deal of success in the laboratory (Suzuki et al. 2007b).

A multitude of strategies have been employed in the engineering of CHO cells that produced non-fucosylated antibodies such as short-hairpin RNA technology or genetic knockouts of the gene responsible for mediating fucosylation, $\alpha 1,6$ -fucosyltransferase (FUT8) generating Mabs with over 100-fold increased potency in ADCC (Mori et al. 2004, Malphettes et al. 2010, Yamane-Ohnuki et al. 2004). Alternative strategies have attempted to hit the fucosylation process from multiple angles including simultaneous knockdown of the enzyme responsible for generating the prerequisite, GDP-fucose, for fucosylation GDP-mannose 4,6-dehydratase (GMD), including the GDP-fucose transporter and FUT8 with great success (Kanda et al. 2007, Imai-Nishiya et al. 2007). An interesting observation was that in the case of GMD-only knockouts, fucosylation was revived in the presence of L-Fucose supplementation through a salvage pathway that bypassed the glucose-derived GMD-mediated generation of GDM-fucose (**Fig. 1.12**).

Figure 1.12: GDP-fucose salvage pathway for FUT8-mediated fucosylation

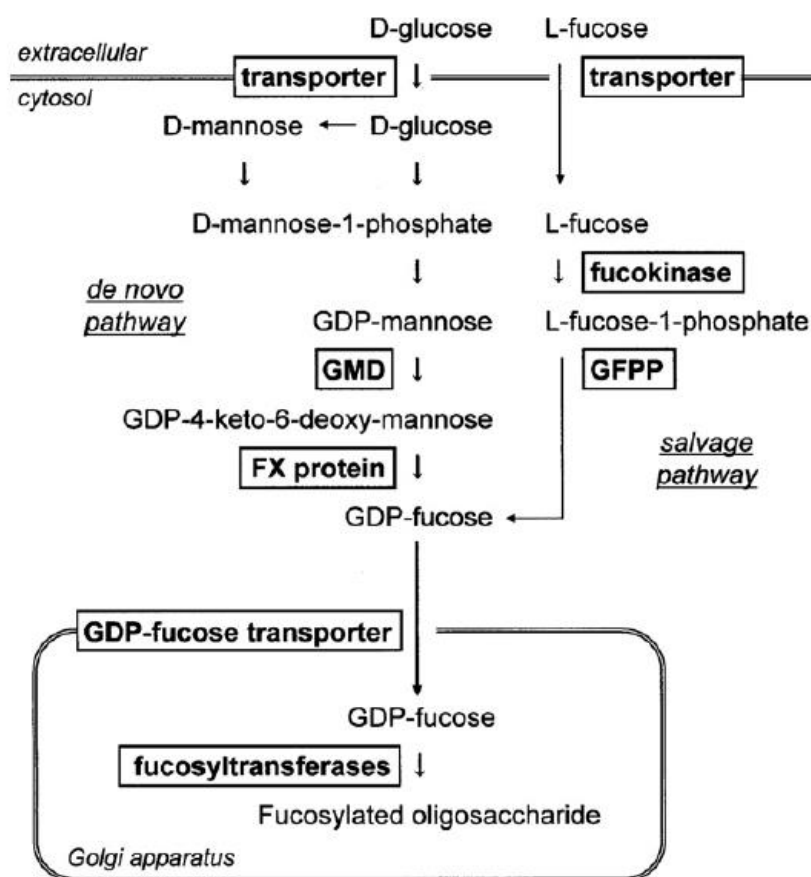


Figure 1.12: Antibody fucosylation can be targeted with the addition of compensatory pathways that exist through the salvage pathway that generates GDP-fucose through the supplementation of L-fucose which compensates for GMD knockout. The schematic diagram above was reported in (Kanda et al. 2007).

The increased affinity of non-fucosylated IgG-Fc for FcγRIIIa may be due to the reduction or absence of steric inhibition at the receptor-ligand interface. The structure of the Fc portion of IgG is flexible and takes the form of a horseshoe-like conformation that forms a binding cleft for FcγR interaction. The oligosaccharides covalently linked to Asn297 are also flexible in nature and move to accommodate the IgG-Fc-FcγR association. Fucosylation has been proposed to reduce the flexibility of the Diantennary glycan thus contributing to this stoichiometric interference.

Despite the advancements in cell line development for the production of tailor designed antibody glycoforms eliciting enhanced effector functions, implementing such technologies to the manufacture of currently available recombinant Mabs such as

Herceptin and Rituxan would be a futile endeavour. The reason for this is that, although the process would ultimately generate a more potent product, the resources and time required to develop the engineered production CHO cell lines would be extensive. Because the glyco-profile of the product being different to its predecessor despite antigen specific remaining unchanged, it would be classified as a “New” product thus requiring clinical trial testing, at high a cost, before FDA approval. All is not lost however, with the patents expiring on many of these blockbuster therapeutics and over 350 novel and competing therapeutic Mabs in early development, CHO cell production factories genetically engineered to produce specific glycoforms can be implemented from the ground up, playing a pivotal part in the generation of “Bio-similar” or hopefully “Bio-Betters” (Reichert 2013).

Aims of thesis

1 Functional screen of a panel of miRNAs identified in a multi-omics profile of CHO cells with varying growth rates

To:

- Determine whether the integration of multiple datasets (miRNA, mRNA and protein) can allow for the identification of high priority miRNA targets.
- Evaluate the role miRNAs play in the regulation of CHO cell growth and other bioprocess relevant phenotypes (Apoptosis and productivity).
- Explore the feasibility of screening combinations of miRNAs.
- Prioritize a short list of mRNA candidates desirable for stable CHO cell development.

2 miR-34a as a potential candidate for CHO cell engineering

To:

- Explore the stable depletion of miR-34 using miRNA sponge technology on the CHO cell phenotype.
- Determine if miR-34 depletion and miR-34a overexpression alters secreted antibody fucosylation profiles.

3 miR-23b* as a potential candidate for CHO cell engineering

To:

- Explore the influence of stable depletion of miR-23b* using miR-sponge technology on the CHO cell phenotype.

4 miR-23 depletion as an attractive tool for industrial application

To:

- Identify the role miR-23 depletion alone plays in CHO-SEAP cells following the observation of enhanced growth/productivity under stable cluster inhibition.
- Determine if miR-23 depletion enhances CHO cell mitochondrial function.
- Determine the mechanism behind the observation of elevated SEAP activity.
- Attempt to identify potential targets of miR-23 through label-free mass spectrometry.
- Carry out label-free mass spectrometry on isolated mitochondria.

Chapter 2

Materials & Methods

2.1 General Techniques of Cell Culture

2.1.1 Ultrapure water

Ultrapure water was used in the preparation of all media and solution when specified. For ultra-purification, the water was initially pre-treated which involved activated carbon, pre-filtration and anti-scaling. This water was then purified by a reverse osmosis system (Elga USF Maxima Water Purification System) to a standard of 12 – 18 MΩ/cm resistance.

2.1.2 Glassware

All glassware and lids were soaked in a 2% (v/v) solution of RBS-25 (VWR International) for at least 1 h (hr). This is a deproteinising agent, which removes proteineous material from the bottles. Glassware was scrubbed and rinsed several times in tap water. The bottles were then washed by machine using Neodisher detergent, an organic, phosphate-based acid detergent. Bottles were then rinsed twice with distilled water, once with ultrapure water and sterilised by autoclaving (121 °C for 20 min under a pressure of 1 bar). The spinner vessels were additionally treated with 1M NaOH solution over night to further ensure the elimination of cell debris from the inner surface and were then washed twice with ultrapure water. Spinners were sealed in autoclave bags (Stericlin, 0775) and autoclaved. Thermo-labile solutions (i.e. 10% DMSO, serum) were filtered through a 0.22 µm sterile filter (Millipore, millex-gv, SLGV-025BS).

2.1.3 Cell culture cabinet

All cell culture work carried out in a class II laminar air-flow (LF) cabinet (Holten). Before use, the laminar was turned on and the air flow was allowed to acclimatize for 10 min. Both before and after use, the laminar flow cabinet was cleaned with 70% industrial methylated spirits (IMS). Any items brought into the LF cabinet were swabbed down with IMS and regular cleaning of gloved hands with IMS was carried out to insure the prevention of contamination. Only a single cell line/clone was used in the LF cabinet at any one time. If a second cell line/clone was being used a period of 15 min clearance was adhered to in order to prevent/minimize cross contamination between cell lines/clones.

Weekly cleaning of the LF cabinet included Virkon, a detergent solution (Virkon, Antec International; TEGO, TH. Goldschmidt Ltd.), followed by water and IMS.

2.1.4 Incubators

Adherent cells were maintained at 37 °C, in an atmosphere of 5% CO₂ and 80% humidity. Cells in suspension were also maintained in these conditions in an ISF1-X (Climo-Shaker) Kuhner incubator with a speed of 130-170 rpm. Weekly cleaning of the incubators was adhered to and followed the same protocol as described for the cell culture cabinet.

2.2 Subculture of cell lines

Cells were maintained as described above (see **2.1.4: Incubators**). Cells were sub-cultured every 3-4 days in order to maintain them in mid-exponential phase of their growth cycle. In the event of temperature shift assays, cells were transferred from ambient 37 °C growth to a 31 °C incubator. All cell lines used and their required culture conditions are tabulated below (**Table 2.1**).

Table 2.1: Cell lines, Culture conditions, Media types and Selection reagents

Cell lines and their associated growth conditions					
Cell line I.D.	Cell Type	Culture Media	Culture Format	Antibiotic Selecting Agent	Antibiotic Concentration (nM/mL)
CHO-K1-SEAP	rCHO	CHO-S-SFMII	Suspension	Geneticin (G418)	1000 µg
CHO-K1	CHO	ATCC +5%FCS	Monolayer	None	None
CHO-1.14	IgG-secreting-rCHO	R5	Suspension	Methorexate (MTX)	450 nM
CHO-5.18F	IgG-secreting-rCHO	AS1	Monolayer	MTX	450 nM
CHO-11.1S	IgG-secreting-rCHO	AS1	Monolayer	MTX	450 nM
CHO-5.22F	IgG-secreting-rCHO	AS1	Monolayer	MTX	450 nM

2.2.1 Anchorage-dependent cells (Monolayer)

Spent media was removed from the flask by pipette and discarded into a sterile waste bottle. The flask was then rinsed with 2-5 mL of autoclaved/sterile PBS in order to remove any residual media. Depending on the size of the culture vessel, 2-5mL of trypsin was added to the flask covering the cells and incubated at 37 °C for approximately 2-5 min until all of the cells have become detached. The level of cell detachment was monitored by microscopic observation. A 5mL volume of serum-containing media was added to the flask once all the cells were detached in order to deactivate the trypsin. The cell suspension was placed into a 30 mL sterile universal container and centrifuged at 1000 rpm for 5 min. The supernatant was discarded from the universal and the pellet was resuspended in fresh complete media. A small aliquot was removed and cell count was performed. Another aliquot of this cell suspension was then removed and used to seed a fresh culture vessel at the required density. Cells were passaged once 90-100% confluency was reached otherwise spent media was removed and fresh media was added to the culture flask.

2.2.2 Suspension cells

Stock cells were maintained in a spinner vessel in a 30-50 mL volume at 37 °C in a Kuhner Climo-shaker at 170 rpm. A small aliquot was sampled for counting by trypan blue exclusion and the required seeding density of 2×10^5 cells/mL was calculated. If the required volume of cells from the working stock exceeds 10% of the culture volume then the amount of cells needed is centrifuged at 1000 rpm for 5 min. Conditioned media is poured off into a sterile waste container and the cell pellet is resuspended in 30-50 mL of media. Some cells lines require the fresh stock flask to be supplemented with 10% conditioned media.

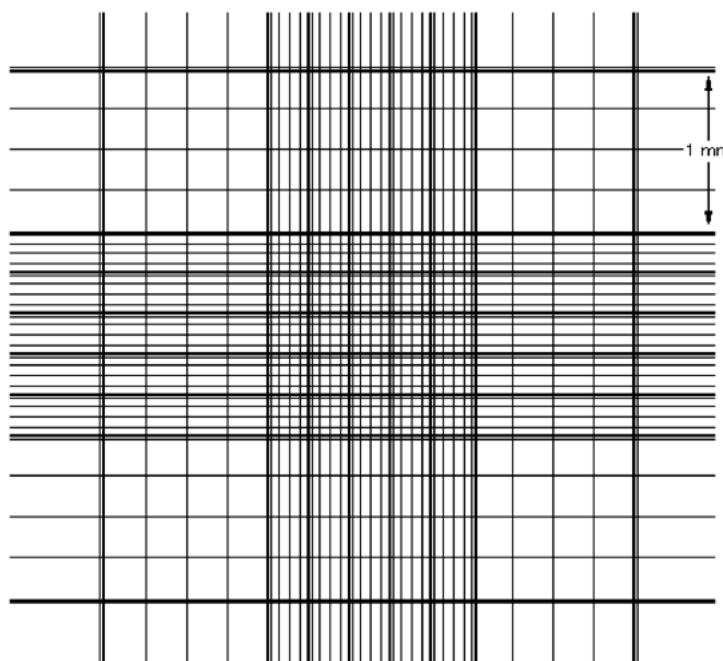
2.2.3 Cell counting and viability determination

2.2.3.1 Trypan blue exclusion method

Prior to cell counting, an aliquot of sample was extracted from either the subculture of adherent cells or a direct sampling from suspension cells as described in (**Subculture**

2.2.2). An aliquot of cell suspension was added to Trypan Blue (GIBCO, 525) at a ratio of 1:1. Prior to the addition of Trypan Blue a dilution can be performed by adding volume of media to the sample. The Trypan Blue/Cell sample mixture was incubated at room temperature for 2-3 min. A small aliquot (10 μ L) was then applied to the chamber of a glass cover-slip enclosed haemocytometer. For each of the four corner grids of the haemocytometer, cells in the 16 squares were counted under a light microscope (**Fig. 2.1**).

Figure 2.1: Haemocytometer Grid Layout



The average of the four grids was multiplied by a factor of 10^4 (Volume of the grid) and the relevant dilution factor to determine the average cell count per mL in the original suspension. Viable cells exclude the Trypan Blue dye as their membranes remain intact and therefore remain unstained while non-viable cells stain blue. The percentage viability of the culture is calculated by counting non-viable cells and viable cells in the sample and dividing the total cell count (viable and non-viable) by the viable cell count.

2.2.3.2 Guava ViaCount® assay

The Guava ViaCount assay is an efficient alternative to Trypan Blue Exclusion for the high throughput determination of cell numbers and viability. The active Guava

ViaCount[®] Reagent (Guava Technologies, 4000-0041) discriminates between viable and non-viable cells based on the permeability of two DNA-binding dyes. One dye is membrane permeable and stains all nucleated cells producing a fluorescent signal that is detected by photomultiplier tube 2 (PM2). The remaining dye penetrates the membrane of non-viable cells of which membrane integrity has been lost producing a detectable fluorescent signal on photomultiplier tube 1 (PM1). Single positive events of viable cells are detected and recorded when the fluorescent signal is accompanied by a signal of forward light scatter (FSC) which is of an appropriate intensity to that produced by a cell above a particular size. An Event with an accompanying low FSC is counted as cellular debris and not included within the live nucleated cell population. Non-viable cells will emit a fluorescent signal from the dead cell stain. The read out format for the Guava ViaCount assay is a 96-well plate and no less than 100 μL should be used per well. It is essential that the cell count present is no less than 10 cells/ μL and no more than 500 cells/ μL which could result in inaccurate reads. Cells were diluted in serum free media as well as taking into account the addition of 100 μL of Guava ViaCount[®] Reagent. Plate set-up and inclusion of dilution factors is described in section (see **2.2.3.2.1**). Guava ViaCount[®] Reagent was allowed to adjust to room temperature. 100 μL of pre-diluted sample was added to 100 μL of Guava ViaCount[®] Reagent and allowed to incubate at room temperature for at least 10 min before using the Guava flow cytometer.

2.2.3.2.1 WorkEdit[™] Software

The WorkEdit[™] software programme allows the acquisition command set-up to be performed for samples in a 96 well Round Bottom microplate (Corning Inc. COSTAR[®], 10308005) in the sample tray. **Figure 2.2** shows the screen layout of the WorkEdit[™] command template. The right hand side of the screen shows the grid template of the 96 well microplate and allows for the selection of sample wells highlighted in green. The left hand side of the screen allows for the selection of the assay type to be performed in this case being Guava ViaCount. Acquisition events and acquisition order allows the selection of the number of viable cell events per sample and the order in which the microplate will be read. Most importantly, entering the dilution factor is necessary for the analysis of each samples cell numbers accurately.

Figure 2.2: WorkEdit™ command screen layout

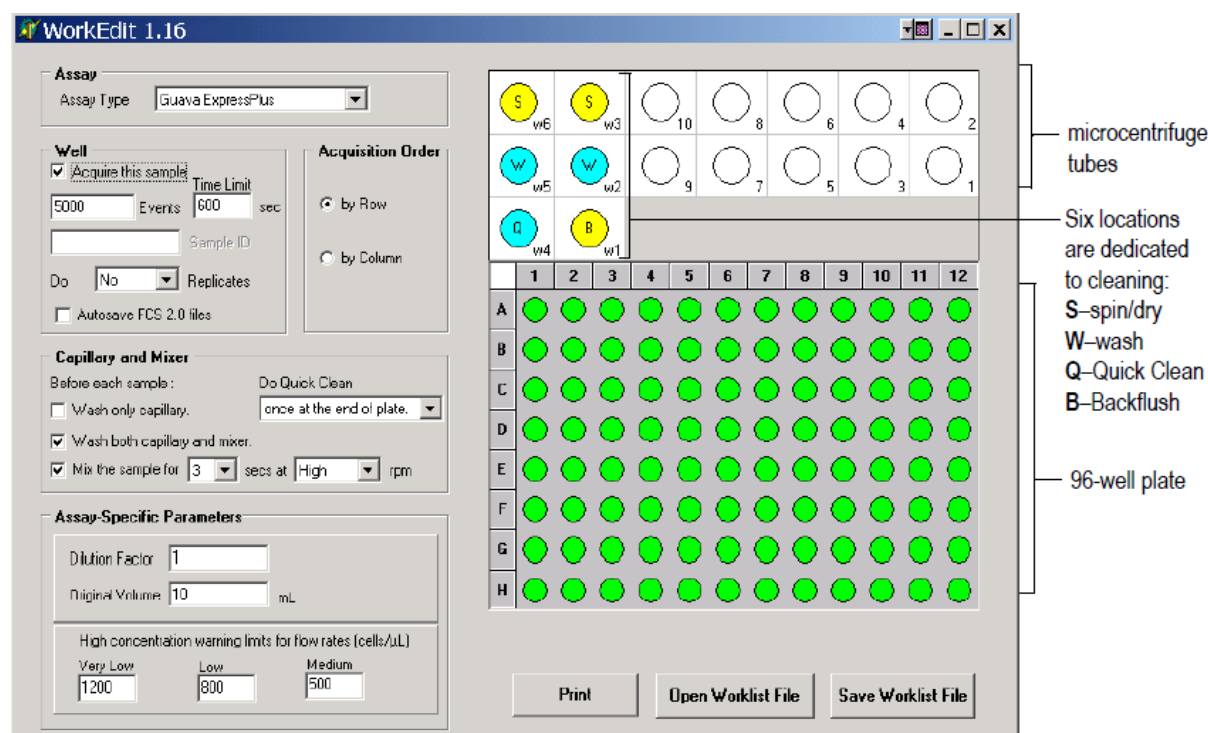


Figure 2.2: WorkEdit™ command screen layout: The right hand side shows the sample well layout and allows selection of the well for analysis (highlighted in green). Above it the layout for 10 microcentrifuge sample tubes along with the 6 well locations required for cleaning. The left hand side of the screen allows the selection of assay type, acquisition event number, acquisition order, auto saving data files, mid run washing steps, and sample dilution factor.

2.2.3.2.2 EasyFit Analysis

EastFit analysis allows the software to calculate the results based on its own methodology. This type of analysis groups all events into three individual population categories – viable cells, dead/apoptotic cells and cellular debris. EasyFit uses its own grouping method that clusters data into populations discriminating between the three population types. A manual method can be executed alongside this where a gate can be imposed upon the “healthy” population by altering the FSC threshold thereby completely discriminating between cellular debris and viable cells.

2.2.3.3 Cedex XS Analyser

The Cedex XS Analyser (Roche Innovatis, Bielefeld, Germany) is a semi-automated image-based cell analyser based on the Trypan Blue Exclusion method providing information about cell concentration and viability. The Cedex XS Smart Slide has eight chambers for testing samples. Four sample chambers (*e.g.* Chambers A1-A4) can be measured without turning the Cedex XS Smart Slide. Cell samples for measurement are pre-diluted (below 1×10^7 cells/mL) using and stained using the appropriate amount of 0.2% Trypan Blue while accounting the addition of Trypan Blue into the dilution factor. This solution is mixed thoroughly by pipetting up and down. Pipette 10 μ L of sample into each chamber of the Cedex Smart Slide for measurement (**Figure 2.3 A**). The slider carrier is pulled out and the Cedex Smart Slide is placed in the slide carrier with the chambers containing the samples going in first. The slide carrier is pushed gently in until a soft click is felt followed by the illumination of a blue light indicating the first chamber is in position, with an additional light for chambers 2, 3 and 4. By clicking on MEASURE from the Cedex XS control centre the measurement dialogue box is accessed where sample information is entered such as sample ID including replicates and dilution factor before taking the final measurement.

Figure 2.3: Cedex Smart Slide & Sample view

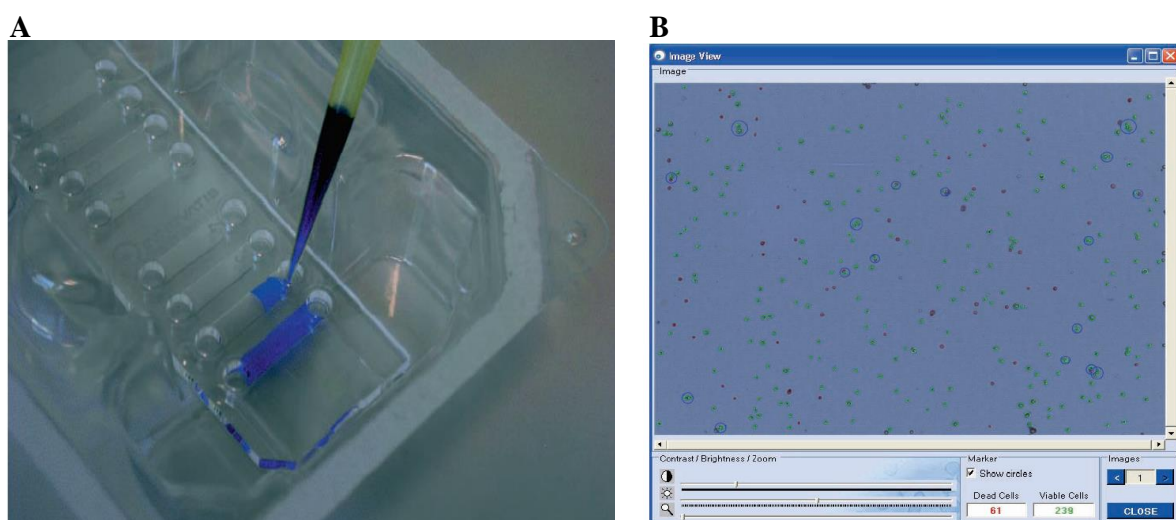


Figure 2.3: Cedex smart slide and Sample view: A) Sample loading of 10 μ L of pre-diluted sample into the chamber of the Cedex Smart Slide. B) Sample view accounting for viable cells circled in green, non-viable cells circled in red and aggregates circled in blue.

Once the sample parameters have been entered the START MEASUREMENT button is clicked. The Cedex XS analyser accounts for information such as cell density by taking the dilution factor into account, cellular viability and others such as cell size ranging from 2-180 μm and aggregates (**Figure 2.3 B**).

2.2.4 Cryopreservation of cells

Cells being preserved were frozen down in a suitable medium supplemented with 5% DMSO (SIGMA-ALDRICH, D5879) and 5% FCS. Given the cytotoxic effects of DMSO at warm temperatures a separate solution of suitable medium supplemented with 10% DMSO/FCS was made up initially and kept on ice until required. This 10% DMSO/FCS solution was filtered using a 0.22 μm bell filter (Gelman, 121-58) before storage on ice. Cells for cryopreservation were harvested during their log phase of the growth cycle. Generally, cells are frozen down at 1×10^6 cells/mL in 1mL of media (supplemented with 5% DMSO/FCS) in a cryovial (Greiner, 201151). After counting and centrifugation, cells are resuspended in half the final volume of pre-warmed suitable media giving a cell density at 2×10^6 cells/mL. Finally, this mixture is made up with 1 volume of the 10% DMSO/FCS supplemented media yielding a final solution of 5% DMSO/FCS at 1×10^6 cells/mL. This suspension was then aliquoted in 1mL volumes to pre-labelled cryovials and immediately placed at -20°C . After 1-2h, cells are transferred to -80°C for 6-12 h and then transferred to the liquid nitrogen tank for long term storage at -196°C .

2.2.5 Thawing of cryopreserved cells

Prior to thawing of cells under liquid nitrogen storage, a 10 mL volume of fresh medium was pre-warmed in a sterile universal. The cryopreserved cells were removed from the liquid nitrogen storage, immediately placed on ice and slightly thawed at 37°C . Cells were transferred from the cryo-vial to the aliquoted medium in the sterile universal using a pastet. Cells were centrifuged at 1000 rpm for 5 min in order to remove the toxic DMSO. The supernatant was decanted and the pellet was resuspended in fresh pre-warmed media. Antibiotic selection agent is omitted in the first passage. Thawed cells were then added to the appropriate culture vessel, i.e. spinner or T-flask, with the appropriate volume of culture medium and allowed to grow at 37°C . In the case of adherent cells, the culture

media was removed and cells were re-fed the next day in order to remove non-viable cells and allow the successful proliferation of attached cells.

2.2.6 Apoptosis analysis

Annexin-V is a calcium-dependent phospholipid binding protein that binds with high affinity to phosphatidylserine (PS), which is normally located on the inner face of the cell membrane. Annexin V-PE is used to detect PS on the external face of the membrane and is a sign of early apoptosis. 7-AAD is also membrane impermeable and is excluded from live, healthy cells and early apoptotic cells.

Non-apoptotic cells: Annexin-V (-) and 7-AAD (-)

Early Apoptosis: Annexin-V (+) and 7-AAD (-)

Late stage apoptosis/Dead: Annexin-V (+) and 7-AAD (+)

Debris: Annexin-V (-) and 7-AAD (+)

Cells were harvested and resuspended in 200 μ L Guava Nexin reagent (Merck-Millipore) at 48 h and 96 h after transfection. Cells were incubated for 20 min at room temperature in the dark before analysis with a Guava EasyCyte96 (Millipore). It was ensured that at least 1% of FCS was added to the cell sample before incubation in cases of serum-free culture.

2.3 Other Cell Culture Techniques

2.3.1 Reconstitution/Rehydration of lyophilized miRNA

miRNAs were ordered from Applied Biosystems and NBS Biologicals and arrived in a lyophilised condition. Reconstitution/Rehydration of miRNA was performed using nuclease-free water (Ambion[®], AM9932) in sterile conditions in the laminar flow hood. miRNAs were resuspended so that their final stock concentration was at 50 μ M. The appropriate volume of nuclease-free water was added by pipette and mixed vigorously by pipetting up and down and vortex. This mixture was allowed to sit at room temperature for 10 min and subsequently centrifuged briefly before storage at -20°C. Stocks were also

subsequently made as low as 5 μ M in the event of transfecting small concentrations of miRNA, allowing for high volumes being used to avoid pipetting error.

2.3.2 siRNA/miRNA transfection

2.3.2.1 siSPORT™ NeoFX™ Transfecting Reagent

Transient transfection of CHO cells was carried out using the AMBION® transfecting reagent siSPORT™ NeoFX™ (AMBION®, AM4510) in accordance with the manufacturer's specifications. The following protocol describes the experimental setup for a single transfection event at a siRNA/miRNA concentration of 50 nM including a 10% excess. Each siRNA/miRNA/NeoFX complex volume of 200 μ L was added to a 2 mL sample of cells at 1×10^5 cells/mL. All sample sets were carried out in triplicate with appropriate experimental controls. Using serum free media (SFM) such as OPTI-MEM® (Life Technologies, 31985-062) or CHO-S-SFM II (GIBCO®, 12052-098), 2.2 μ L of a 50 μ M miRNA/siRNA was added to 110 μ L of SFM previously warmed to 37 °C and incubated at room temperature for 10 min. The siSPORT™ NeoFX™ transfecting reagent was allowed to sit and adjust to room temperature before the addition of 2.2 μ L to 110 μ L of pre-warmed SFM in a separate microcentrifuge tube. Formation of siRNA/miRNA complexes was achieved by adding 112.2 μ L of siSPORT™ NeoFX™ transfecting Reagent/SFM media mixture to the incubated siRNA/miRNA/SFM sample and allowed to complex by incubation for 10 min at room temperature. In order to inoculate the 2 mL (1×10^5 cells/mL) culture with a 50 nM final concentration of siRNA/miRNA 204 μ L of the final complex was added with gentle swirling of the culti-flask disposable bioreactor (Sartorius Stedium Biotech, DF-050MB-SSH). Cells were incubated at 37 °C in a Kuhner Climo-shaker incubator (Kuhner, Climo-Shaker ISF1-X) at 170 rpm. Replacement of the culture media is not necessary as the addition of siSPORT™ NeoFX™ transfecting Reagent does not induce cellular stress that can lead to cytotoxicity.

2.3.2.2 INTERFERin™ transfection reagent

Transfection of CHO cells was carried out using the PolyPlus-transfection™ reagent INTERFERin™ (PolyPlus-Transfection™, PPLU-409-01) as per manufacture's specifications unless otherwise indicated. miRNAs were transfected at a range of 100 nM-20 nM final concentration per 2 mL volume at 1×10^5 cells/mL. Below describes the master mix preparation for one single transfection. Using SFM such as OPTI-MEM® (Life Technologies, 31985-062) or CHO-S-SFM II (GIBCO®, 12052-098) 110 µL of pre-warmed SFM media at 37 °C was aliquoted into a sterile cryovial or Eppendorf. All reagents such as INTERFERin™ and miRNAs were kept on ice until required, however INTERFERin™ was allowed to adjust to room temperature before use. As described in **section 2.3.1.1**, 2.2 µL of the appropriate stock miRNA mimic or inhibitor was added to the aliquot of 110 µL SFM and mixed by pipetting up and down gently. From optimization results shown in **section 3.1.2.4**, 1.1 µL of INTERFERin™ was added to the SFM containing miRNA mixture and allowed to incubate at room temperature for ~15 min. After this incubation period, 100 µL of complexed miRNA was added directly to each 2 mL volume of cells and swirled briefly to mix. Cells were incubated at 37 °C in a Kuhner Climo-shaker incubator (Kuhner, Climo-Shaker ISF1-X) at 170 rpm. Replacement of the culture media is also not necessary as the addition of INTERFERin™ transfecting reagent does not induce cellular stress that can lead to cytotoxicity.

2.3.3 Transfection of plasmid DNA

Plasmid transfection required the use of a separate set of transfection reagents as plasmids are required to reach the nuclear membrane thus having to bypass two membranes.

2.3.3.1 Lipofectamine 2000

Cells were transfected at 5×10^5 attached 24 hs prior to transfection or at $0.5-1 \times 10^6$ cells/mL in suspension culture. DNA to Lipofectamine™ (Invitrogen, Cat. No. 11668-019) was 1:2, respectively. DNA was diluted in 50 µL SFM and mixed gently. Transfection reagent was diluted in a separate 50 µL, mixed and incubated for 5 min at room temperature. After 5 min, both mixtures were combined, mixed and incubated at

RT for 25 min. After 25 min, the 100 μ L mixture was added drop-wise to the cells and gently rocked to mix. This transfection reagent requires a media change after 4-6 hs of incubation.

2.3.3.2 TransIT[®]-2020 Transfection Reagent

Cells were transfected at 5×10^5 attached 24 hs prior to transfection or at $0.5-1 \times 10^6$ cells/mL in suspension culture. Transfection complexes were made up in SFM such as CHO-S-SFMII or Optim-MEM. For a single transfection, 250 μ L of SFM was pre-heated to 37°C in a 1.7 mL Eppendorf. 1 μ L of TransIT-2020 (Mirus, Cat. No. MIR-5400) was used for every 1 μ g of plasmid DNA transfected. DNA was added first using a pipette and mixed followed by the transfection reagent. Contents were mixed and allowed to incubate at room temperature for 20 min. After this time, DNA/transfection reagent complex was added drop-wise to the cells. This transfection reagent does not require a media change.

2.3.4 Limited-dilution/FACS-based cloning

Clonal isolation was carried out using a FACS-Aria based on mid-to-high GFP intensity or limited dilution single cell cloning. The culture process after isolation was the same for both processes. In the case of limited-dilution cloning, a stock solution is made up containing 10 cells/mL so that when 100 μ L is placed into a well, the well contains a single clone. Clones were sorted into 2 separate 96 well plates containing CHO-S-SFM II media supplemented with ~30% conditioned media (media previously cultured CHO cells and harvested containing secreted growth factors) and 5% serum. Conditioned media was harvested 2-3 days into culture with cells removed by centrifugation and filtered through a 0.2 μ m filter. Single clones were allowed to attach and grow at 37 °C for 10-14 days. After this time, cells were assessed for growth and clonality visually using a bench-top microscope. Clonal panels were subsequently adapted to suspension culture in a 24-well suspension plate.

2.4 Molecular Biology Techniques

2.4.1 DNase Treatment of RNA

DNase treatment of RNA samples is useful for the removal of contaminating genomic DNA and for the removal of plasmid DNA from transfection reactions that would have, in its high abundance, carry over during the RNA isolation protocol.

DNase treatment was carried out using the DNase I (RNase-free) kit (M0303S, from New England Biolabs®) as per manufacturer's specifications. Each DNase treatment reaction was made up to a reaction volume of 20 µL. 2 µg of RNA was added to a 0.5 mL PCR tube as well as 2 µL of 10X DNase Buffer (resulting in a 1X DNase Buffer when made up to 20 µL with RNase-free water). 2 Units of DNase I (1 µL) was added to the reaction resulting in a final reaction volume of 20 µL. The reaction mixture was mixed thoroughly and incubated at 37 °C for 10-15 min. 1 µL of 0.5 M EDTA (to a final concentration of 5 mM) was added after this incubation step in order to deactivate the DNase I enzyme with a subsequent heat inactivation step at 75°C for 10 min.

2.4.2 High Capacity cDNA reverse transcription

Reverse transcription of RNA to cDNA was carried out using the High Capacity cDNA reverse transcription kit (Applied Biosystems, 4368814) in accordance with the manufacturer's specifications. A maximum of 2 µg RNA was made up to 10 µL in a 0.5 mL PCR tube using Nuclease-free water. In a separate 0.5 PCR tube reaction vessel, the reverse transcription master mix was prepared in accordance with the following table (single reaction volumes):

Component	Volume/Reaction (µL)	
	Kit with RNase Inhibitor	Kit without RNase Inhibitor
10X RT Buffer	2	2
25X dNTP Mix (100mM)	0.8	0.8
10X RT Random Primers	2	2
Multiscribe™ Reverse Transcriptase	1	1
RNase Inhibitor	1	-
Nuclease-free H ₂ O	3.2	4.2
Total per reaction	10.0	10.0

10 μ L of the RT master mix was added to the 10 μ L RNA sample and mixed using a pipette. The temperature profile for the reverse transcription reaction carried out using a bench top thermocycler G-Storm GS1 PCR machine following the below criteria:

	Step 1	Step 2	Step 3	Step 4
Temperature ($^{\circ}$ C)	25	37	85	4
Time	10 min	120 min	5 min	∞

Reverse transcribed cDNA product is ready to use and is stored at -20° C until further required.

2.4.3 Polymerase Chain Reaction (PCR)

The DreamTaqTM PCR Master Mix kit (Fermentas Life Sciences, #K1071) was the kit used to perform all PCR amplification reactions in accordance with the manufacturer's specification. DreamtaqTM PCR Master Mix was vortexed after thawing and placed on ice until further required. Each PCR reaction was made up to a volume of 50 μ L. Following the component table below, a 25 μ L reaction volume was made up in a thin walled PCR tube using a maximum concentration range of 1-100 ng of genomic DNA or cDNA and 10 pg of forward and reverse PCR primer. Once all components have been added, 25 μ L of the 2X DreamTaqTM PCR Master Mix was added to each sample creating a 50 μ L reaction volume.

Component	Volume/Concentration
DreamTaq TM PCR Master Mix (2X)	25 μ l
Forward Primer	0.1 – 1.0 μ M
Reverse Primer	0.1 – 1.0 μ M
Template DNA	1 – 100 ng
Nuclease-free water	To 50 μ L
Total Volume	50μL

Samples were gently vortexed and quickly spun down. The thermo-cycling conditions are shown in the table below with variation lying within the specific melting temperature (T_m) of each primer set and length of the Amplicon. A bench top PCR machine was used to perform the polymerisation cycle.

Step	Temperature, °C	Time	Number of cycles
Initial Denaturation	95	1-3 min	1
Denaturation	95	30s	25-40
Annealing	T _m – 5	30s	
Extension	72	1min/kb	
Final Extension	72	5-15 min	1
HOLD	4	∞	1

After completion of the PCR reaction, samples were stored at -20°C until further required. Primer sequences for all PCR reactions are shown in **table 2.2**.

Table 2.2: Primer sequences for all genes explored in PCR

Gene ID	Primer For-Rev (5'-3-)	Amplicon (bp)	Tm (°C)	GC%	Ann Temp
E2F3	For- CAGAGGTGCTCAAAGTGCAG	175	59.4	55	56
	Rev- AGCTCGGTCACTTCTTTGGA		57.3	50	
BCL2	For- GGTGGTGGAGGAACTCTTCA	153	59.4	55	56
	Rev- CGGTTCAAGTACTCGGTCAT		59.4	55	
CCND1	For- ACACCAACCTCCTGAACGAC	214	59.4	55	56
	Rev- GACAGGAAACGGTCCAGGTA		59.4	55	
MYCN	For- CAAGAGCGAGGTTTCTCCAC	202	59.4	55	56
	Rev- AGCCTTCTCGTTCTTCACCA		57.3	50	
GLS	For- AAGTGCTTGAATGGGCTGTT	197	59.7	45	56
	Rev- AGCAGTGGGGTGGAGTGTAT		59.4	55	
TFAM	For- ATCTGCTCCGGAAGACTG	190	60.3	57	56
	Rev- GTCTGAGCGTCTCACATTGC		59.5	55	
DICER1	For- GGAGAACTTCAGCAGCCAAC	164	59.4	55	56
	Rev- TCAGGTGGTTCAGGGTTTTC		57.3	50	
FUT8	For- TTCATCCCAGGTCTGTAGGG	200	59.4	55	56
	Rev- TTCCAGCCACACCAATGATA		55.3	45	

CCNE2	For- CGCAGTAGCCGTTTACAAGC	177	59.4	55	
	Rev- AGTCCACGTCTGCATTACCC		59.4	55	
CDK4	For- GGATTGCCCTCAGAAGATGA	179	57.3	50	56
	Rev- AGGGATTGGAAGGCAGAAAT		55.3	45	
CDK6	For- TCAAATGGCCCTTACCTCAG	160	57.3	50	56
	Rev- CACGTCTGAACTTCCACGAA		57.3	50	

2.4.4 Fast SYBR® Green Real-time qPCR

Real-time qPCR was performed using the Applied BioSystems™ Fast SYBR® Green Master Mix (Applied BioSystems™, Cat. No. 4385612) in accordance with the manufacturers' specifications. Quantification of the target gene is based on the binding affinity of SYBR® Green for double-stranded DNA. During PCR amplification by AmpliTaq® Fast DNA Polymerase, the target sequence is amplified creating more double-stranded Amplicon for SYBR® Green to bind to. As the PCR reaction proceeds, the fluorescent intensity is proportional to the increase in double-stranded PCR product. 20 µL reaction mixtures were prepared in a MicroAmp™ Fast Optical 96-well Reaction plate with Barcode (4346906). Both primers and cDNA were placed on ice to thaw with subsequent vortexing and brief centrifugation. The Fast SYBR® Green Master Mix was mixed thoroughly by swirling. Prior to plate setup, a master mix was prepared for all samples and technical replicates including a separate master mix for the endogenous control (β -actin or GAPDH). For a single reaction, 10 µL of Fast SYBR® Green Master Mix (2X) was added to an Eppendorf tube along with 7 µL Nuclease-Free water and 1 µL of the appropriate forward and reverse primers (200 nM of each primer). Subsequent to master mix preparation, 18 µL were added to each well of the MicroAmp™ reaction plate. Using a micro pipette designed for small volumes (<10 µL), 2 µL of cDNA template was added to each reaction well using a fresh filter tip for each aliquot. It is recommended that a maximum of 20 ng of template cDNA be used for each reaction to achieve optimal detection. The reaction plate was then sealed using MicroAmp™ Optical adhesive film (4311971) to avoid loss of reaction volume during the PCR process. The sample plate was read using a 7500 Real-time PCR system. Data analysis was based on the Relative

Quatitation ($2^{-\Delta\Delta C_t}$) where the relative expression of the target gene is compared to the expression of an internal standard, endogenous control.

2.4.5 Determination of DNA/RNA quantity and quality

Numerous methods are available for the determination of the quantity and quality of DNA and RNA.

2.4.5.1 Bioanalyser/RNA

The Agilent 2100 Bio-analyser is a microfluidics-based platform used for the analysis of proteins, DNA and RNA. The miniature chips are made from glass and contain a network of interconnected channels and reservoirs. The RNA 6000 Nano LabChip kit enables analysis of samples containing as little as 5 ng of total RNA. To each well, 1 µl of each sample is loaded along with a fluorescent dye (marker). An RNA ladder is loaded into another sample well for size comparison. When all the wells are loaded, the chip is briefly vortexed and loaded onto the bio-analyser machine. The machine is fully automated and electrophoretically separates the samples by injecting the individual samples contained in the wells into a separation chamber.

Figure 2.4: RNA 6000 Nano chip and RNA Integrity Number graphs

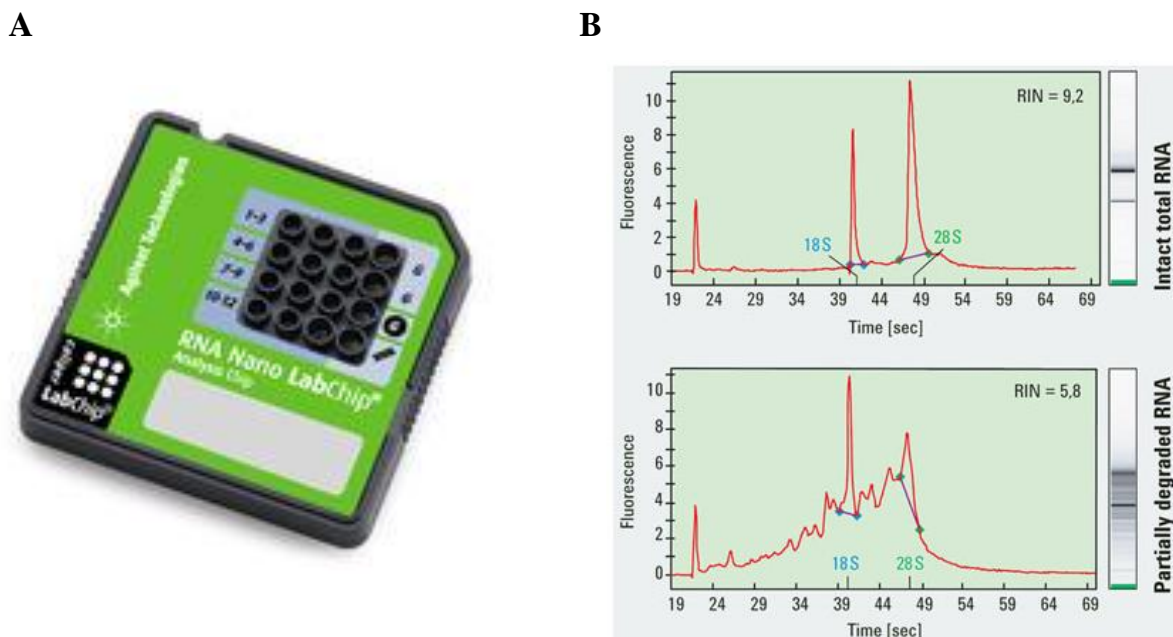


Figure 2.4: RNA 6000 Nano chip and RNA Integrity Number graphs: A) a picture of the front of the RNA Nano chip. B) Upper panel represents the RIN values for high quality RNA while the lower panel displays the RIN values for low quality RNA. Diagrams were sourced from <http://www.agilent.com/chem/labonachip>.

The fluorescence was measured and presented in the form of peaks for 18S and 28S ribosomal RNA peaks. In **figure 2.4 B**, the upper electropherogram and gel-like image show the analysis of high quality total RNA resulting in a RNA Integrity Number (RIN) of 9.2. The lower electropherogram shows the analysis of a partially degraded total RNA sample. Many degradation products appear between the two ribosomal bands and below the 18S band resulting in a RIN of 5.8. As RNA degrades, the 28S RNA peaks decrease and the smaller fragments appear.

2.4.5.2 NanoDrop® Spectrophotometer

Purified RNA/DNA samples were quantified using the Nanodrop® ND-1000 spectrophotometer (NanoDrop Technologies). Before applying the RNA/DNA sample, the pedestal was wiped down using a lint-free tissue dampened with UHP. A volume of 2 µL of UHP was then loaded onto the lower measurement pedestal. The upper arm was then lowered down so as to be in contact with the RNA/DNA containing solution. The

programme “Nucleic acid” and then “RNA-40” or “DNA-50” was selected on the NanoDrop software main screen to read the samples at 260 nm. Upon selection of the appropriate programme (RNA-40, DNA-50) the blank option was chosen, after a straight line appeared on the screen with zero appearing in all measurement fields the “measure” option was selected. Before and after loading each subsequent sample the pedestal was repeatedly wiped with a lint-free wipe. The concentration of RNA/DNA was calculated by software using the following formula:

$$OD_{260nm} \times \text{Dilution factor} \times 40 = \text{ng}/\mu\text{l RNA}$$

A_{260}/A_{280} and A_{260}/A_{230} ratio for each sample was recorded. An A_{260}/A_{280} ratio ~2 and an A_{260}/A_{230} of ~1.8-2.2 is indicative of a pure RNA/DNA sample with an absorbance considerably above or below these values indicating the presence of contaminants such as protein or phenol. However, RNA/DNA ratios of as low as 1.86 and 2.24 for A_{260}/A_{280} and A_{260}/A_{230} respectively have been used in subsequent experiments.

Sample limitation for accurate read outs of RNA/DNA is 2 ng/ μL minimum and 3000 ng/ μL maximum without dilution.

2.4.5.3 Gel Electrophoresis/RNA

Visual determination of RNA integrity can be identified using gel electrophoresis. RNA samples were previously diluted in RNase free water with all agarose gel containers being cleaned and wiped down with RNase Zap. A 1% agarose gel in 50 mL 1 x TAE with 5 μL ethidium bromide (EtBr) added for staining the RNA. A DNA ladder was added to one well of the gel to estimate the location of the RNA bands. The gel was run for a sufficient enough time to ensure clear separation of the RNA bands. Two RNA bands should be visualised, 28S and 18S, with 28S being roughly twice as bright as the 18S band. Bands should appear discrete without any leading smear. No bands should appear between the 28S and 18S bands indicating genomic contamination and/or RNA degradation.

2.4.6 Total RNA isolation using TRI Reagent™

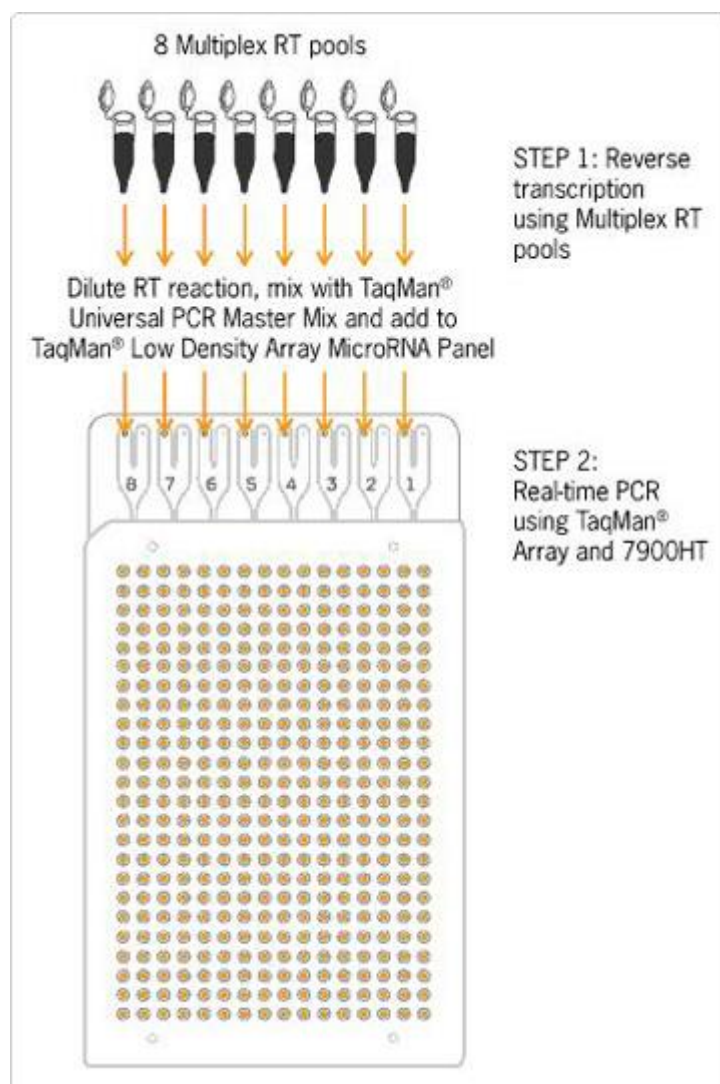
Isolation of total RNA from cell lysates was performed using the TRI Reagent™ mRNA isolation method (SIGMA-ALDRICH®, T9424) in accordance with the manufacturer's specifications. Total RNA was extracted from a maximum of 10×10^6 cells. Suspension cells were harvested by determining the appropriate cell count per mL using Trypan Blue Exclusion (GIBCO®, 15250-061) and spinning the appropriate volume of culture mixture at 2,000 rpm for 5 min. Supernatant was removed from the cell pellet and cells were subsequently lysed with the addition of 1 mL TRI Reagent™, mixed well by pipetting and transferred to a microcentrifuge tube. Cell lysates can be stored in TRI Reagent™ at -70°C for up to one month. Samples were allowed to stand for 5 min at room temperature to allow complete dissociation of nucleoprotein complexes. Phase separation was achieved with the addition of 200 µL of Chloroform (SIGMA-ALDRICH, C2432) to the cell lysate in 1 mL of TRI Reagent™. This mixture was mixed vigorously by vortexing at high speed for 15 seconds and allowed to stand at room temperature for 10 min. Separation of the three distinct phases (red organic phase containing protein, intermediate phase containing DNA and an upper aqueous colourless phase containing RNA), was achieved by centrifugation at 12,000 rpm for 15 min at 4°C. The aqueous phase (upper-clear) was transferred to a fresh microcentrifuge tube and 500 µL isopropanol (SIGMA-ALDRICH, I9516) was added and mixed. This mixture was allowed to stand for 10 min at room temperature and then subsequently centrifuged at 12,000 rpm for 10 min at 4°C. RNA will form a precipitate along the side/bottom of the tube. The supernatant was removed and a wash step was performed using 1 mL of 75% ethanol. Sample was mixed well by vortex and centrifuged at 7,500 rpm for 10 min at 4°C. Decant 75% ethanol as best as possible and air dry the RNA pellet by allowing sitting for 10-15 min. The RNA pellet was not allowed to dry completely before re-suspension in 30-50 µL nuclease-free water.

2.4.7 PCR based miRNA Taqman® Low Density Arrays (TLDA)

Taqman® Low Density Arrays (Applied Biosystems, 4334812) are 384-well micro fluidic cards designed for the analysis of global miRNA expression patterns of up to 8 samples in parallel across a defined set of miRNA targets (**Fig 2.5**). Taqman® Low Density Array

is a real-time PCR-based, highly sensitive and reproducible array that contains specific probes for human miRNA signatures.

Figure 2.5: Schematic representation of a miRNA Taqman® Low Density Array



Given the large number of known human miRNAs, miRNA TLDA cards are split into two cards (A + B) with probes for 380 unique miRNA on each card and 8 endogenous controls. Total RNA was harvested from cells using the TRI Reagent protocol and cDNA was prepared using the Multiplex™ RT Primer kit.

2.4.7.1 Reverse transcription

The Taqman[®] microRNA Reverse Transcription kit and the Megaplex[™] RT Primers Pool A and B (4399966 and 4399968) were used to synthesise single-stranded cDNA from total RNA. The RT-master mix was prepared as described below:

RT Reaction Mix Components	Volume for One Sample (μL)	Volume for Ten Samples (μL) with 12.5% excess
Megaplex [™] RT Primers	0.80	9.00
100mM dNTPs with dTTP	0.20	2.25
Multiscribe [™] Reverse Transcriptase (50 U/μl)	1.5	16.88
10 X RT Buffer	0.80	9.00
MgCl ₂ (25mM)	0.90	10.12
RNase Inhibitor (20 U/μl)	0.10	1.12
Nuclease-Free water	0.20	2.25
Total	4.50	50.62

The above mixture was combined in a 1.5mL Eppendorf tube depending on the number of sample reactions being reverse transcribed. The mixture was mix by inverting the tube and briefly centrifuged. In a 96 well MicroAmp[®] Optical reaction plate (4314320), 4.5 μL of the RT mixture was added into each well as required. 3 μL of total RNA (100 ng) was then added to each reaction well and the plate was sealed using MicroAmp[®] Clear Adhesive Film. The plate was left to incubate on ice for 5 min. Multiplex reverse transcription was performed using the thermocycler under the 9600 Emulation mode with a final reaction volume of 7.5 μL in the HT7900 RT-PCR machine and programmed as follows:

Step Type	Time (min)	Temperature (°C)
HOLD	30	16
HOLD	30	42
HOLD	5	85
HOLD	∞	4

cDNA can be stored at -15 to -20°C for at least one week.

2.4.7.2 Pre-amplification

The Pre-amplification step is required for low concentrations of starting cDNA whereby specific cDNA targets are amplified for further Taqman[®] MicroRNA array analysis. The Megaplex[™] PreAmp Primers (Pool A and B, 4399233 and 4399201) were thawed on ice, mixed by inverting and briefly centrifuged. Master Mix was prepared in a 1.5 mL Eppendorf tube in accordance with the following recipe:

PreAmp Reaction Mix Components	Volume for One sample (μL)	Volume for Ten sample (μL) with excess of 12.5%
Taqman [®] PreAmp Master mix (2X)	12.5	140.62
Megaplex [™] PreAmp Primers (10X)	2.5	28.13
Nuclease-free water	7.5	84.37
Total	22.5	253.12

Invert the master mix six times to mix thoroughly and briefly centrifuge. In a 96-well MicroAmp[®] Optical Reaction Plate place, 22.5 μL of the PreAmp master mix into each appropriate well. Pipette 2.5 μL of the RT reaction product into each appropriate well brings the final reaction volume to 25 μL. The plate was sealed using MicroAmp[®] Clear Adhesive Film and incubated on ice for 5 min. Pre-Amplification parameters were set up in accordance with the following:

Stage	Temp (°C)	Time (min)
Hold	95	10
Hold	55	2
Hold	72	2
Cycle (12 Cycles)	95	15 sec
	60	4
Hold	99.9	10
Hold	4	∞

2.4.7.3 PCR

RT products were diluted using 75 μL nuclease-free water, inverted to mix and spun down briefly by centrifugation. The miRNA PCR reaction was carried out using the Taqman[®]

2X Universal PCR Master Mix (No AmpErase[®] UNG) and in accordance with the below protocol in a 1.5 mL Eppendorf tube:

Component	Volume for One array (μL) with 12.5% excess
Taqman [®] 2X Universal PCR Master Mix (No AmpErase [®] UNG)	450
Diluted PreAmp Product	9
Nuclease-Free Water	441
Total	900

The tube was inverted 6 times to mix and briefly centrifuged. A volume of 100 μL of the PCR reaction mix was loaded into each filling port of the Taqman MicroRNA Array (Figure 2.5).

Taqman microRNA Array	Filling Port 1	Filling Port 2	Filling Port 3	Filling Port 4	Filling Port 5	Filling Port 6	Filling Port 7	Filling Port 8
Multiplex RT Primer Pool	1	2	3	4	5	6	7	8

Plate was centrifuged so that all micro fluidic wells are filled with RT reaction mixture and then subsequently sealed. Arrays were incubated for 10 min on ice and were loaded on HT7900 real time PCR machine and ran under the following protocol:

Step	AmpliTaq Gold [®] Enzyme Activation	PCR	
		CYCLE (40 cycles)	
		Denatured	Anneal/Extend
Time (min)	10	15 sec	60 sec
Temp (°C)	(°C)	95	95

2.4.7.4 Data Analysis

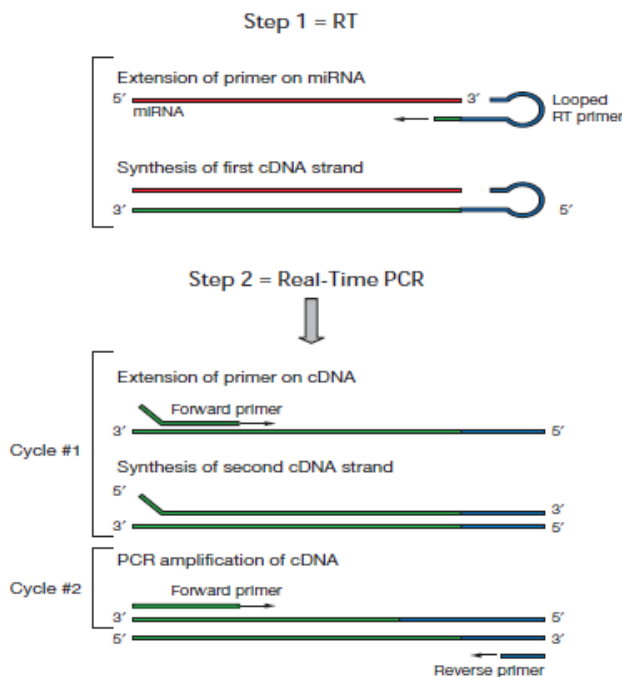
Data was analysed using Real-Time *StatMiner*[™] software form Integromics.

2.4.8 Singleplex qRT-PCR validation: Taqman® microRNA assays

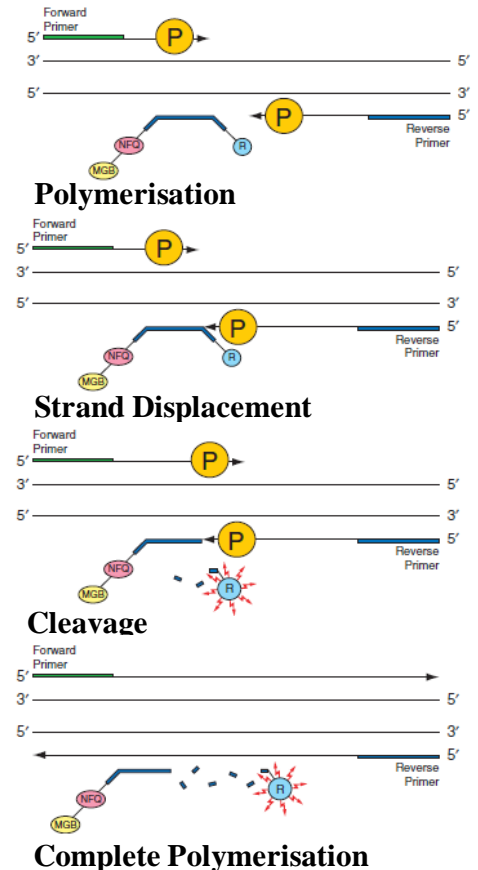
Taqman® microRNA assay kits are pre-formulated primer and probe sets designed to detect and quantify mature miRNAs in real time. This assay can discriminate mature miRNAs from their precursor sequences and quantify small amounts (1-10 ng). Assays range for the majority of content found in the miRBase miRNA sequence repository. Total RNA was reverse transcribed by specific primers within the miRNA RT kit while the PCR reaction is performed using another set of miRNA specific primers together with the Taqman® Universal Master mix (**Figure 2.6 A**). miRNA PCR Amplicon detection is based on a DNA probe containing a fluorescent tag (FAM™) at the 5' end of the probe along with a non-fluorescent quencher (NFQ) at the 3' end of the probe. The Taqman minor groove binding (MGB) probe hybridizes to complementary sequences within the forward and reverse primers. This intact probe prior to DNA binding holds the fluorescent tag in close proximity to the non-fluorescent quencher resulting in no fluorescence (**Fig 2.6 B**).

Figure 2.6: RT/PCR Mechanism and FAM™ – based detection mechanism

A) Two-Step RT/PCR Mechanism



B) Probe Mechanism



During DNA polymerization, the DNA polymerase cleave only probes that are bound to the complementary sequences thus releasing the fluorescent FAMTM tag from the suppressive proximity of the quencher. As the number of PCR cycles increases the level of probe hybridization/cleavage/fluorescence increases.

2.4.8.1 Reverse transcription

RT master mix for each sample was prepared separately using the Taqman microRNA Reverse Transcription kit (ABI, 4366596) from Applied Biosystems.

Component	Master Mix (15 μ L-Single Reaction)
100mM dNTPs (with dTTP)	0.15
MultiScribe TM Reverse Transcriptase, 50 U/ μ L	1.00
10X Reverse Transcriptase Buffer	1.5
5X RT Primer	3
RNase Inhibitor, 20 U/ μ L	0.19
Nuclease-free water	4.16
Total Volume	10

A separate master mix reaction was prepared without MultiScribeTM RT enzyme for each primer set to be used within the assay in order to validate genomic contamination of the primers and reaction components. RT-master mix was mixed gently and centrifuged prior to distribution. An aliquot of 10 μ L of RT-master mix was transferred into a 0.5 mL Eppendorf and placed on ice until RNA was prepared. RNA samples were pre-diluted to a working concentration of 2 ng/ μ L in nuclease-free water. For each 15 μ L reaction, 5 μ L of RNA (1-10 ng/reaction) was added to the 10 μ L master mix, mixed gently and centrifuged. RT was performed using the following parameters in a G-StormTM thermocycler.

Step	Time (min)	Temperature ($^{\circ}$ C)
HOLD	30	16
HOLD	30	42
HOLD	5	85
HOLD	∞	4

cDNA samples were stored at -20°C until further required.

2.4.8.2 PCR

PCR reaction for individual miRNA was performed using the Taqman 2X Universal PCR Master Mix (ABI, 4324018) from Applied Biosystems and was prepared in accordance with the following table.

Component	20 µL (Single reaction)
Taqman MicroRNA Assay (20X)	1.00
Product from RT reaction (Minimum 1:15 Dilution)	1.33
Taqman 2X Universal PCR Master Mix, No AmpErase® UNG	10.00
Nuclease-free water	7.67
Total Volume	20

To each well of a MicroAmp™ optical reaction plate, 16 µL of PCR-master mix, containing appropriate primer, was loaded. From the pre-diluted RT reaction, 5 µL of product was added to each PCR-master mix. The plate was sealed with microAmp™ optical adhesive film (ABI, 4311971) and then incubated for 10 min on ice. PCR was performed using 9600 emulsion mode of thermocycler with reaction volume of 20 µL in a HT7600 real time PCR machine. Conditions for the PCR reaction were as follows:

Step	AmpliTaQ Gold® Enzyme Activation	PCR	
		CYCLE (40 cycles)	
		Denatured	Anneal/Extend
Time (min)	10	15 sec	60 sec
Temp (°C)	(°C)	95	95

The table below represents all miRNA assay kits used over the course of this Ph.D.

Table 2.3: microRNA assay kits (Applied Biosystems)

Applied Biosystems™ microRNA assay kits		
miR	Cat. No	Assay I.D.
U6 snRNA (Endogenous control)	4427975	001973
miR-18a	4427975	002422
miR-23b	4427975	000400
miR-23b*	4427975	002126
miR-34a	4427975	000426

2.4.9 MessageAmp™ II aRNA amplification kit

The MessageAmp™ II aRNA amplification kit is an RNA amplification protocol. The procedure consists of reverse transcription with an oligo(dT) primer bearing a T7 promoter using ArrayScript™ reverse transcriptase (RT), designed to produce high yields of first-strand cDNA. ArrayScript RT mediates the synthesis of virtually full-length cDNA, which is the best way to ensure production of reproducible microarray samples. The cDNA then undergoes second-strand synthesis and clean-up to become the template for in vitro transcription (IVT) with T7 RNA polymerase. To maximise aRNA yield, Ambion MEGAscript® IVT technology is used to generate hundreds to thousands of anti-sense RNA copies of each mRNA in a sample (aRNA is often referred to as cRNA). RNA samples of limited amounts (0.1-100 ng) can be put through two rounds of amplification if required. **Figure 2.7** demonstrates the amplification procedure using MessageAmp™ II aRNA amplification kit.

Figure 2.7: MessageAmp™ II aRNA amplification procedure

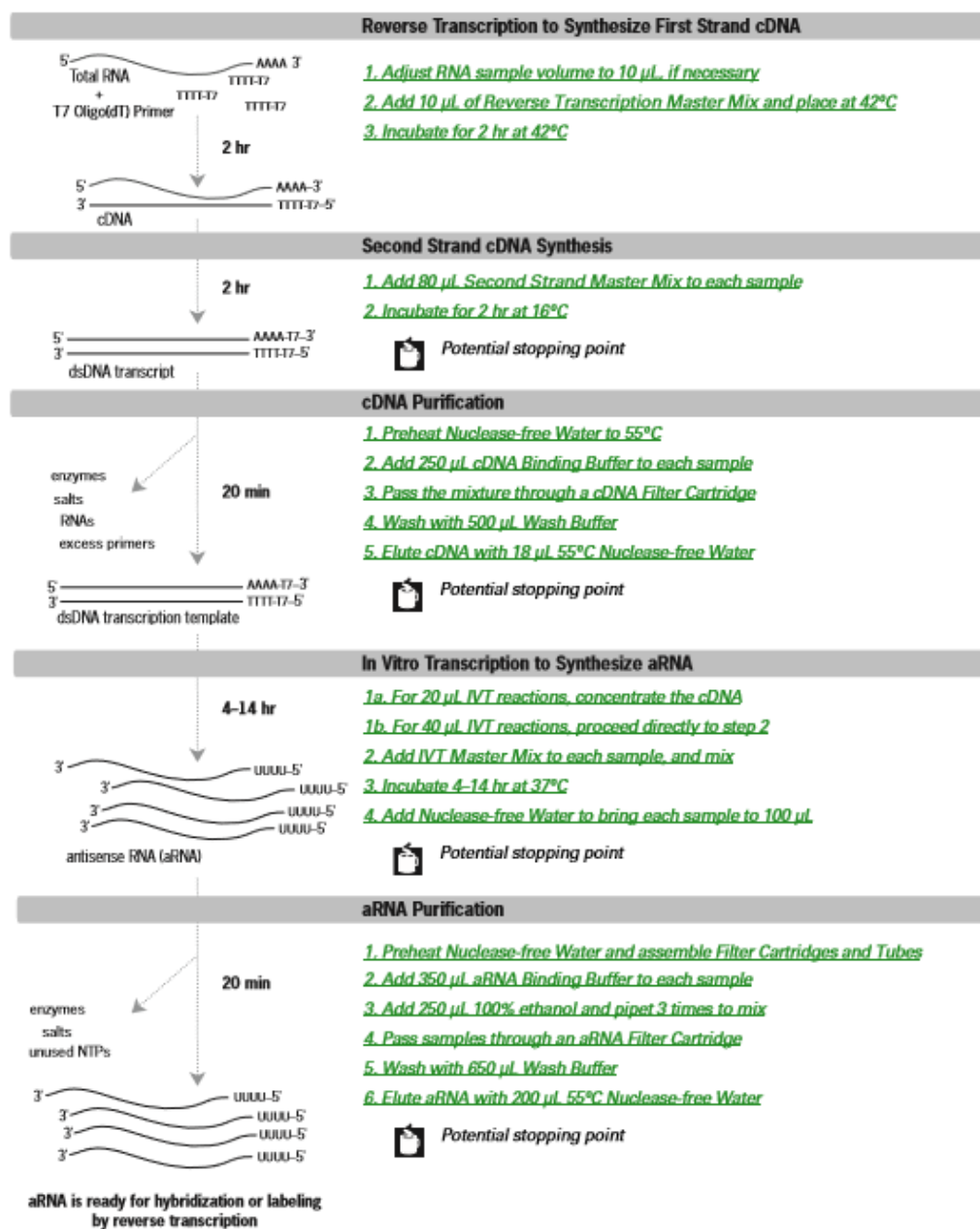


Figure 2.7: A schematic flow diagram of the procedure undertaken to amplify low quantities of RNA in preparation of carrying out microarray studies requiring a high amount RNA per card. This diagram was sourced from http://tools.lifetechnologies.com/content/sfs/manuals/cms_056141.pdf.

Amplification procedure was carried out in accordance with the manufacturer's specification (Life Technologies, #AM1751). First strand cDNA synthesis was carried out on a maximum of 1000 ng of RNA in a maximum volume of 10 μ L topped up with

high quality water. This mixture was vortexed briefly and centrifuged to collect. The reverse transcription master mix was prepared at room temperature in nuclease-free including a 5% excess to cover pipetting errors according to the following cocktail:

Reverse Transcription master mix (for a single 20 μ L reaction)	
Amount (μ L)	Component
1	Nuclease-free water
1	T7 Oligo(dT) primer
2	10X First Strand Buffer
4	dNTP Mix
1	RNase Inhibitor
1	ArrayScript

This mixture was gently vortexed and centrifuged briefly to collect and placed on ice until required. 10 μ L of Reverse Transcription Master Mix was added to each RNA sample forming the final 20 μ L reaction volume. The mixture was pipetted up and down 2-3 times, flicked 3-4 times and briefly centrifuged to collect. Samples were placed in a thermo cycler and subjected to the following conditions:

Temp	Time	Cycles
42°C (50°C lid)	2 h	1
4°C	Store	

Samples were placed on ice immediately after first-strand synthesis.

Second-strand cDNA synthesis was carried out next. On ice, the second-strand Master Mix was prepared in nuclease-free water according to the cocktail below to a final volume of 80 μ L:

Second Strand Master Mix (For a single 100 μ L reaction)	
Amount (μ L)	Component
63	Nuclease-free Water
10	10X Second Strand Buffer
4	dNTP Mix
2	DNA polymerase
1	RNase H

This reaction included a 5% excess to cover pipetting errors. Master Mix was mixed gently by vortexing and centrifuged to collect and placed on ice. 80 μ L of second strand master mix was transferred to each 20 μ L first-strand sample. Mix was pipetted up and

down 2-3 times, then flicked 3-4 times and centrifuged to collect. Samples were placed on a thermo cycler in accordance with the following steps:

Temp	Time	Cycles
16°C (no heated lid)	2 h	1
4°C	hold	

Be sure to deactivate the heated lid and allow thermo cycler to cool to 16°C before incubation as temperatures above this can compromise aRNA yield. Samples can be placed on ice for no more than 1 h or frozen at -20°C.

Double-stranded cDNA was then purified. 250 µL of cDNA binding buffer was added to each sample, mixed thoroughly by pipetting up and down 2-3 times, flicked 3-4 times followed by a quick spin to collect. The entire sample was placed onto the centre of the cDNA filter cartridge. Samples were centrifuged for 1 min at 10,000 g or until mixture was fully through the filter. The flow-through was discarded and the cDNA filter cartridge was replaced into the collection tube. 500 µL of wash buffer was added to each cDNA filter cartridge. Samples were centrifuged for 1 min at 10,000 g. The flow-through was discarded and the cDNA filter cartridge was centrifuged for an additional minute to remove trace amounts. cDNA filter cartridge was transferred to a clean elution tube. 18 µL of nuclease-free water pre-incubated at 50-55°C was added to the centre of each cDNA filter cartridge. This was left to incubate for 2 min and then centrifuged for 1 min at 10,000 g. The remaining ~16 µL contains double-stranded cDNA.

In vitro transcription to synthesise aRNA was carried out using un-modified or biotin-labelled UTP. The 16 µL of double-stranded cDNA prepared previously was transferred to a PCR tube. IVT master mix was prepared for a maximum reaction volume for 40 µL to achieve highest aRNA yield in accordance with the following cocktail:

Un-modified 40 μ L reaction	Component
16 μ L	Double-stranded cDNA: previous step
IVT Master Mix for a single reaction	
4 μ L	T7 ATP
4 μ L	T7 CTP
4 μ L	T7 GTP
4 μ L	T7 UTP
--	Biotin-11-UTP, 75 mM
4 μ L	T7 10X Reaction Buffer
4 μ L	T7 Enzyme Miz

Master Mix was mixed well by vortexing and centrifuged to collect the IVT master mix at the bottom of the tube and placed on ice. Transfer IVT master mix to each sample and thoroughly mix by pipetting 2-3 times, flicking 3-4 times with a brief centrifugation to collect. Once mixed, samples were placed in a thermo cycler and processed at the following conditions:

Temp	Time	Cycles
37°C (100-105°C heated lid)	14 h	1
4°C	hold	

Reaction was stopped by adding Nuclease-free water to each aRNA sample to bring the final volume to 100 μ L, mixed by vortexing and stored at -20°C.

aRNA purification was final carried out to remove enzymes, salts, and unincorporated nucleotides from the aRNA. 200 μ L of nuclease-free water for each samples was pre-heated to 55°C. For each sample, an aRNA filter cartridge was placed into an aRNA collection tube. 350 μ L of aRNA binding buffer was added to the 100 μ L of aRNA. 250 μ L of 100% ethanol was added to each aRNA sample and mixed by pipetting up and down 3 times-**DO NOT VORTEX OR CENTRIFUGE**. Pipet each sample onto the centre of the filter in the aRNA filter cartridge/collection tube. Centrifuge for 1 min at 10,000 g. Discard flow-through and replace the aRNA filter cartridge back into aRNA collection tube. Apply 650 μ L wash buffer to each aRNA filter cartridge. Centrifuge for 1 min at 10,000 g. Discard flow-through and spin aRNA filter cartridge for an additional minute to remove trace amounts of wash buffer. Transfer filter cartridge to a fresh aRNA collection tube. To the centre of the filter, add 200 μ LL pre-heated nuclease-free water and incubate samples on a heat block at 55°C for 10 min. Centrifuge for 1.5 min at 10,000

g and quantify. 33.3 ng/μL of aRNA is required for microarray processing or a second round of amplification can be performed. Samples are stored at -80°C for up to one year.

2.4.10 CHO-specific oligonucleotide arrays

Following from the amplification using the MessageAmp™ aRNA amplification kit (see 2.4.9) of the low quantity RNA generated from the biotin-labelled miRNA pull-down, 100 ng of total RNA from each sample underwent cDNA synthesis, followed by clean-up, overnight IVT amplification and labelling using the GeneChip 3' IVT Express Kit (#901229, Affymetrix) according to manufacturer's specifications. cRNA clean-up was carried out using the GeneChip Sample Clean-up Module (#900371, Affymetrix) according to manufacturer's specifications. The custom CHO oligonucleotide WyeHamster3a microarray (Affymetrix) used in this target identification analysis contains a total of 19,809 CHO-specific transcripts, combining library-derived and publicly-available hamster sequences.

2.4.11 Gel and LB media/LB agar preparation

2.4.11.1 Agarose gel preparation

Depending on the percentage gel desired, agarose (Sigma-Aldrich, A9539) was added to 1X TAE (Thermo, #B49) with 2% (w/v) being considered a high percentage for resolution of small DNA bands (~ 100 bp). The solution was heated to boiling until completely dissolved and cooled under a running cold tap. 0.5 μg/mL of ethidium bromide was added to the gel before pouring. Prior to pouring the gel, gel tray was sealed at both ends using autoclave tape and left to set in the dark upon pouring.

2.4.11.2 LB media preparation

For 1 litre of LB media, 10 grams of Tryptone (Sigma-Aldrich, #T7293), 5 grams of Yeast (Sigma-Aldrich, #92144) and 10 grams of NaCl (Sigma-Aldrich, S9888) was dissolved in 1000 mL of UHP and subsequently autoclaved.

2.4.11.3 LB agar plate preparation

LB agar preparation follows the same ingredients as LB media with the addition of 15 grams of agar select (Sigma-Aldrich, A5306) in 1,000 mL of UHP and subsequently autoclaved. LB agar is then melted in the microwave and allowed to cool at room temperature until bottle is cool enough to handle. It is at this point that antibiotics are to be added to the LB agar media mixed well and poured into petri dishes.

2.4.12 Restriction Enzyme Digestion

Restriction enzymes are enzymes isolated from bacteria that are used as tools in molecular cloning techniques to recognise and cut DNA at specific genetic locations to produce DNA fragments known as restriction fragments. Restriction enzymes are used to create acceptor sites or “sticky ends” within multiple cloning sites (MCS) of plasmid backbones and the recombinant DNA insert.

Digestion reactions were set up in 0.5 mL PCR tubes at a reaction volume of 20 μ L. The reaction volume can vary depending on the amount of DNA required. The following represents the components required for the digestion of 2 μ g of DNA with a single restriction enzyme in a volume of 20 μ L.

Component	Volume (μ L)
Plasmid DNA	2 μ g
NEBuffer 1-4 (10X)	2
BSA (100X)	0.2
Restriction enzyme	1U (0.5-1 μ L)
Nuclease-Free water	To 20 μ L reaction volume

Enzymatic digestions are carried out at a temperature of 37 °C on a hot plate until complete digestion is achieved. 1 Unit of a restriction enzyme is defined as the digestion of 1 μ g of λ DNA in 1 h at a total volume of 50 μ L (see NEB website <https://www.neb.com/>). Double digests can be carried out within the same reaction vessel depending on the compatibility and activity of the respective enzymes in the reaction buffers. Enzymatic activity charts can be found on the New England Biolabs website cited above.

2.4.13 Enzyme modification of linearized plasmid DNA

2.4.13.1 Alkaline Phosphatase (AP)

Alkaline Phosphatase treatment is exploited in molecular cloning as a technique to remove the 5'-phosphate residue from the DNA backbone after the circularised plasmid has been linearized, producing either 3' or 5' overhangs with exposed hydroxyl or phosphate groups, respectively. The phosphate group on C-6 and the hydroxyl (OH) group on C-3 serve as the basis of the chemical reaction of polymerisation of the DNA strand through a process known as condensation.

The purpose and function of CIP treatment in molecular cloning is to remove the 5'-phosphate group of the DNA backbone inhibiting self-re-ligation of the linearized plasmid unless in the presence of DNA ligase. CIP treatment can be used on the linearized plasmid vector whether the exposed termini are incompatible, overhangs are not complementary, or compatible, blunt ends, but is more commonly used in the latter.

Alkaline Phosphatase Protocol

Prior to AP treatment, during the elution step of cleaning up the restriction digest product, elution was carried out using 45 µL of elution buffer (EB). 4.5 µL of AP Buffer (NEBuffer 3 (50 mM Tris-HCl, 100 mM NaCl, 10 mM MgCl₂, 1 mM Dithiothreitol, pH 7.9 @ 25°C). 0.4 µL of Alkaline Phosphatase enzyme (Storage Conditions: 10 mM Tris-HCl, 50 mM KCl, 1 mM MgCl₂, 0.1 mM ZnCl₂, 50% Glycerol, pH 8.2 @ 25°C) was added to the reaction vessel and mixed gently by using a pipette. Reaction was incubated on a hotplate at 37 °C for 1 h. 45 µL of Chloroform (SIGMA) was added to the reaction mixture subsequent to the incubation period and mixed rigorously by vortexing for 1 minute. Centrifugation at 13,000 rpm for 4 min was performed to separate both layers. The top layer was transferred to a fresh clean Eppendorf tube without any contamination from the lower layer. To ensure maximum amount of CIP treated DNA, 10 µL of nuclease-free water was added to the previous tube containing the chloroform and centrifuged again at 13,000 rpm for a further 2 min. Using a lower volume pipette, the top layer was removed again and placed into the tube containing the top layer from the previous centrifugation

step. DNA was cleaned using the PCR clean-up kit (see 2.6.5) and stored at -20°C until further required.

2.4.13.2 Kinase Treatment

T4 PNK catalyses the transfer of the terminal gamma (γ) phosphate group from Adenosine Tri-phosphate (ATP) to the 5'-hydroxyl termini of DNA and RNA (Fig 2.10). This enzyme can be used for the phosphorylation of the 3'-ends of RNA to prevent circularisation, phosphorylate the 5' ends of DNA and RNA in order to provide the necessary phosphate backbone required for ligation processes and label 5'-hydroxyl ends of DNA with [γ -³²P]-ATP (Hui Zhu *et al*, 2007). In some instances, with the presence of an excess of Adenosine Di-Phosphate, the reverse reaction of T4 PNK transfers the 5'-phosphate from DNA/RNA to ADP thereby fulfilling the role of (CIP) Calf Intestinal Phosphatase which prevents linearized plasmids from circularising.

0.5 μ L of both sense and anti-sense strands that were previously annealed were added to a 0.5 mL PCR tube. 2 μ L of 10 x T4 kinase buffer (500 mM Tris-HCl, 100 mM MgCl₂, 1 mM EDTA, 50 mM dithiothreitol, 1 mM spermidine pH 8.2 (at 25°C). 0.4 μ L of 50 mM ATP (pH 7.5) was added to this reaction as the source of phosphate. This reaction was made up to a volume of 20 μ L with the addition of 17 μ L nuclease free water (Ambion® Cat. AM9932). Lastly 0.4 μ L (4U) of Kinase enzyme (ROCHE, storage buffer, 50 mM Tris-HCl, 1 mM dithiothreitol, 0.1 mM EDTA, 1 μ M ATP, 50% glycerol (v/v), pH 7.5 (at 25°C) was added. Using a heating block this reaction was incubated at 37 °C for 30 min. Upon completion of the 30 minute incubation, the kinase treated linearized DNA was ready for ligation and can be used up to one year later and must be stored at -20°C. The T4 PNK supplied by ROCHE must not undergo the 20 minute incubation at 65°C like the SIGMA supplied enzyme.

2.4.13.3 Klenow Treatment

Escherichia Coli DNA Polymerase I: All DNA polymerase enzymes add deoxyribonucleotides to the 3'-hydroxyl terminus of a primed double stranded DNA molecule. Synthesis is strictly in a 5'-3' direction. Many DNA polymerases have a 3'-5'

exonuclease activity associated with the polymerase activity. In the absence of dNTPs, this activity will catalyze the degradation from a **free** 3'hydroxyl end of both single- and double-stranded DNA. In the presence of dNTPs, the exonuclease activity on double-stranded DNA is inhibited by the polymerase activity. Some DNA polymerase enzymes (eg., *E. Coli* DNA polymerase I) have an associated 5'-3' exonuclease activity. This activity degrades double-stranded DNA from a free 5'-hydroxyl end. This allows Nick Translation which degrades in the 5'-3' direction ahead of the polymerizing activity.

Klenow treatment can be used to trim overhangs to make them compatible with other restriction enzymes where combinations are not applicable. Additionally, the klenow treatment can also inhibit self-re-ligation (**Fig. 2.8**).

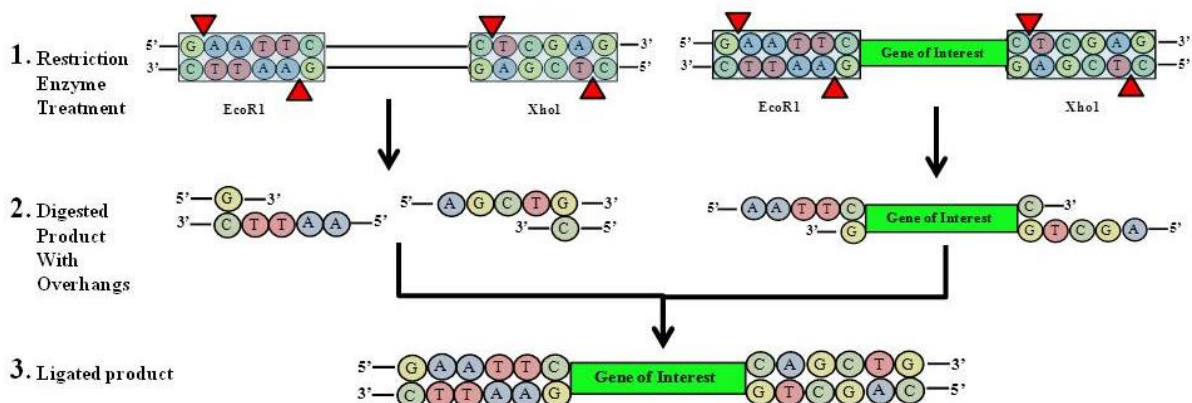
Klenow Protocol

Upon digestion and cleaning of the plasmid/DNA fragment of interest, 1 µg of digested product was loaded into a 0.5 mL PCR tube. For a 20 µL reaction volume, 2 µL of 10X NEBuffer 2 (10 mM Tris-HCl, 50 mM NaCl, 10 mM MgCl₂, 1 mM Dithiothreitol (pH 7.9 at 25°C)) is added to the reaction vessel. See table below for variations according to final reaction volume. dNTPs were added to a final concentration of 33 µM. 1U of Klenow enzyme (Storage Conditions: 25 mM Tris-HCl, 1 mM Dithiothreitol, 0.1 mM EDTA, 50% Glycerol (Ph 7.9 at 25°C)) is added for every 1 µg of DNA in the reaction. Reaction volume is made up using Nuclease-free water. Reaction mixture should be mixed gently using a pipette before placing on a heating block at 25°C for 15 min. Klenow reaction was stopped by the addition of 10mM EDTA and heating at 75°C for 20 min.

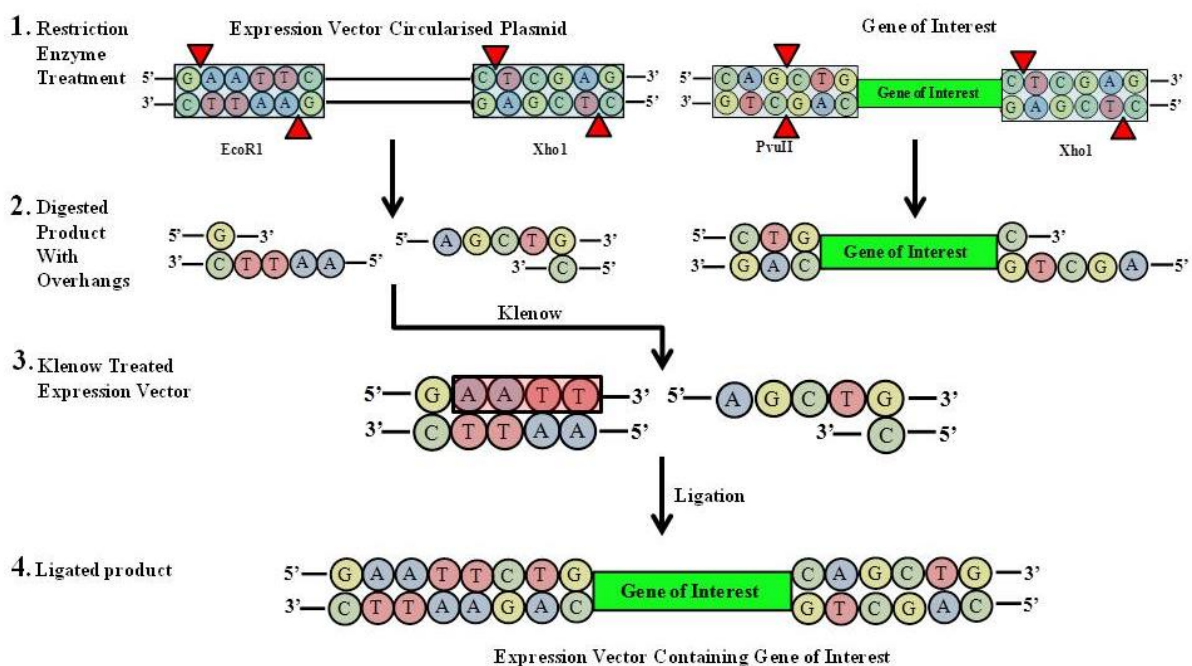
Reaction Vol. (µL)	Template DNA (µg)	1xNEBuffer 2 (µL)	Klenow	dNTPs (33 µM) (µL)	H₂O
20	1 µg	2	0.1-0.5 (1-5U)	0.5	Up to 20 µL
30	1 µg	3	0.1-0.5 (1-5U)	0.5	Up to 30 µL
50	1 µg	5	0.1-0.5 (1-5U)	0.5	Up to 50 µL

Figure 2.8: Cloning process and Klenow treatment

A. Generic Cloning Process



B. Klenow Treatment



2.4.14 Gel extraction

Plasmid DNA fragments of interest containing gene coding sequences were extracted from DNA agarose gels using the QIAGEN® QIAquick Gel Extraction kit (QIAGEN®, 28704). The DNA fragment was excised from a low-melting agarose gel using a clean

scalpel. 400 mg of agarose can be processed by the spin column so it is important to minimize the size of the gel slice by removing extra agarose. The gel slice was finely chopped up and placed into a microcentrifuge tube. The gel slice was then weighed by weighing an empty microcentrifuge tube and the one containing the gel slice. 3 volumes of Buffer QG was added to 1 volume of gel (100 mg ~ 100 μ L). This mixture was incubated at 50°C for 10 min and vortexed every 2-3 min until the gel slice was completely dissolved. Once the gel was dissolved, the mixture colour was yellow. If the mixture was orange or violet then 10 μ L of 3M sodium acetate (Sigma-Aldrich, #W302406) was added allowing efficient adsorption of DNA to the QIAquick membrane. 1 gel volume of isopropanol (Sigma-Aldrich, #190764) was added to the sample and mixed using a pipette. A QIAquick spin column was placed into a 2 mL collection tube. To bind the DNA, the sample mixture was applied to the QIAquick spin column and centrifuged for 1 minute at 13,000 rpm. The flow through was discarded and the QIAquick column was placed back into the collection tube. The remaining traces of agarose were washed from the column by loading 500 μ L of Buffer QG to the QIAquick column and spinning at 13,000 rpm for 1 minute. A second wash step was performed by applying 750 μ L of Buffer PE to the QIAquick column followed by centrifugation at 13,000 rpm for 1 minute. The flow through was discarded and a second spin for 1 minute was performed to dry the column. DNA elution was carried out by placing the QIAquick column into a fresh microcentrifuge tube and adding 30-50 μ L of Buffer EB or water directly onto the QIAquick membrane and left standing for 1 minute at room temperature before centrifugation at 13,000 rpm for 1 minute. Eluted DNA was quantified by measuring the OD_{260nm} using a NanoDrop spectrophotometer. Plasmid was sorted at -20°C for further use.

2.4.15 PCR Purification

All plasmid DNA was purified using the QIAGEN® QIAquick PCR Purification kit (QIAGEN®, 28104) in accordance with the manufacturer's specifications. This clean up kit was necessary for the purification of single-/double-stranded DNA from PCR and all other enzymatic reactions such as Kinase/CIP/Klenow. Into the PCR mix, 5 volumes of Buffer PB was added and mixed by pipetting. The colour of this mix will turn yellow if a pH indicator has been added to Buffer PB. If this solution appears orange or violet then

10 µL of 3M Sodium Acetate is added and mixed. A QIAquick spin column was placed into a 2 mL collection tube. In order to bind the DNA, the sample mix was applied to the QIAquick column and spun by centrifugation at 13,000 rpm for 1 minute. The flow through was discarded and the QIAquick column was placed back into the same 2 mL collection tube. A wash step was performed by adding 750 µL of Buffer PE to the QIAquick column and centrifuged at 13,000 rpm for 1 minute. Flow through was discarded and the QIAquick column was placed back into the collection tube and spun for a further 1 minute at 13,000 rpm to dry the membrane. Before elution of the purified DNA, the QIAquick spin column was placed into a clean microcentrifuge tube. DNA was eluted by adding 30-50 µL of Buffer EB or water directly to the QIAquick membrane and allowing sitting for 1 minute at room temperature followed by spinning at 13,000 rpm for 1 minute. Quantification of DNA was determined using a NanoDrop spectrophotometer and measuring the OD_{260nm}. Purified DNA was stored at -20°C until required.

2.4.16 Ligation

The T4 DNA ligase kit from ROCHE® (Cat. No. 10 481 220 001) was used for all ligation reactions carried out. It is recommended that no more than a total of 1 µg of DNA is to be used in any given ligation reaction and a range of 1-5 Units of T4 DNA ligase enzyme. The online tool LIGATION CALCULATOR (http://www.insilico.uni-duesseldorf.de/Lig_Input.html) was used to determine the optimum ratio in nanograms of insert to vector backbone (**Fig 2.9**). To insure efficient ligation it is important to have a saturation of insert to vector by using the recommended ratios of 1:3 or 1:5.

Figure 2.9: Online LIGATION CALCULATOR tool

The screenshot shows a web-based form titled "LIGATION CALCULATOR" on a blue background. The form asks for the following information: vector size (in bp), vector amount (in ng), insert size (in bp), and a molar ratio of vector to insert. It includes a note about cohesive end ligations and a "do calculation" button.

LIGATION CALCULATOR

Please provide the following information:

.....vector size (in bp):

vector amount (in ng):

.....insert size (in bp):

Please enter the molar vector : insert ratio:

(normally a vector to insert ratio of 1 to 3 is used of cohesive end ligations. higher molar ratios can be used for blunt end ligations)

When pressing the "do calculation" button the tool calculates the required amount of insert DNA (in ng) resulting in the given molar ratio

Figure 2.9: Online LIGATION CALCULATOR tool: All relevant information is to be entered into the above fields including vector backbone size (after restriction enzyme digestion) in base pair (bp), vector amount in nanograms (ng) after clean-up, insert size in bp and finally the ration of insert to vector (1:3 or 1:5).

A range of ~80-150 ng of vector backbone was used in all ligation protocols depending on the yields achieved after the previous two cleaning and CIP treatments beforehand. The concentration of insert used was determined based on the fragment size and the amount/size of vector being used (Ligation Calculator). All reactions were carried out at 20 μ L but scale up as far as 50 μ L can be done if required. 2 μ L of 10x T4 DNA ligase reaction buffer (660 mM Tris-HCl, 50 mM $MgCl_2$, 10 mM ATP, 50 mM EDTA, pH 7.5 at 25°C) was added to the reaction mixture. Nuclease-free water was used to make up the reaction volume to 19 μ L prior to the addition of the T4 DNA ligase enzyme. Finally 1 μ L (1 U) of T4 DNA ligase enzyme (20 mM Tris-HCl, 60 mM KCl, 5 mM Dithioerythritol, 1 mM EDTA, 50% Glycerol, pH 7.5 at 4°C) was added to the reaction mixture creating a reaction volume of 20 μ L. This reaction was incubated overnight on ice water. This allows the ligation reaction to commence over a temperature gradient. Ligated samples were stored at -20°C. It is important to set up an identical reaction containing all components except the fragment to be inserted (no insert control). This accounts for the frequency of self-ligation of the DNA backbone and incomplete digestion of the vector backbone resulting in non-positive colonies.

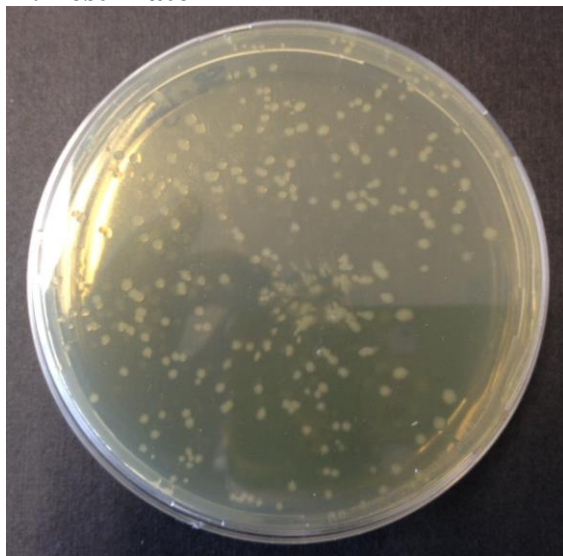
2.4.17 Transformation of competent cells

Two kits supplied by Initrogen™ were used for the transformation of ligated vectors or for the amplification of plasmid vector stocks. These kits were the Subcloning Efficiency™ DH5α™ Competent cells (Sigma-Aldrich, Cat. No.18265-017) and MAX Efficiency® DH5α™ Competent Cells (Sigma-Aldrich, Cat No. 18258-012). The only difference between the two kits above is that the MAX Efficiency® DH5α™ Competent Cells kit has a greater transformation efficiency of 1×10^3 transformants/μg pUC19 DNA.

A 14 mL polypropylene Round-Bottom tube (Falcon®) was placed on ice while the water bath (NICKLE-ELECTRO Ltd., Clifton, 14 Litre Unstirred Thermostatic Bath, series NEI-14) was pre-heated to 42°C. 50 μL of competent cells were transferred into each tube and kept on ice. ~5 μL of DNA (Ligation product, less for stock plasmid) was added to the competent cells and tapped to mix. This mixture was left on ice for ~20 min. The competent cells/DNA was heat-shocked by placing in the water bath at 42°C for 45 seconds. This step serves to cause contraction of the membrane pores resulting in the uptake of DNA from the surrounding environment. Upon heat shock the cells are then immediately placed on ice for a further 3 min which serves to constrict the membrane pore once again. 500 μL of pre-heated (37 °C) S.O.C media (supplied in MAX Efficiency® DH5α™ Competent Cells kit) was added to the transformed competent cells. Cells were incubated for ~1 h at 37 °C on a shaker platform. After an h, the contents were transferred into a 1.7 mL microcentrifuge tube (Costar®, Corning Incorporated, Cat. No. 3620) and centrifuged at 3000 rpm for 4 min. All but 50 μL of SOC media was decanted from the bacterial pellet. The pellet was resuspended using a pipette and transferred onto a LB agar plate containing the appropriate selection antibiotic (**Section 2.4.11**). Using a sterile microbiological spreader (Copan Innovation, Cat. No. 22-091-241), the transformed competent cells were homogenously spread over the LB agar plate containing the appropriate antibiotic selecting agent. These plates were then sealed with Parafilm® M (SPI Supplies®, Cat. No. 01851-AB) and incubated at 37 °C for 16-24 hs.

Figure 2.10: Test and Control plate under Ampicillin selection

A: Test Plate



B: No-Insert control Plate

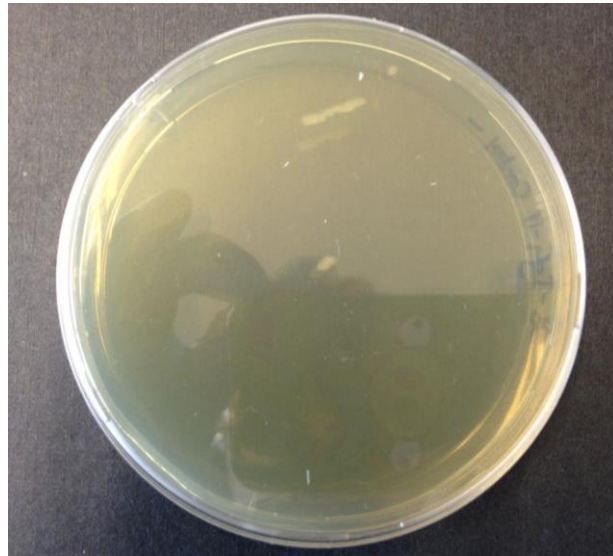


Figure 2.10: The requirement of carrying out a no-insert control during the ligation process is demonstrated. A) Colonies as a result of successful insertion causing circularisation in addition to circularised plasmids with no insert as a result of incomplete digestion. B) Colonies formed only as a result of incomplete digestion giving an indication of colony number without target inserts.

After a time period of 16-24 hs of incubation, competent cells that successfully took up the plasmid will form single round colonies on the agar plates. The presence of the antibiotic selecting agent will select for colonies efficiently expressing the functional circularised plasmid that harbours the antibiotic resistance gene. **Figure 2.10 A and B** shows a test and control plate under ampicillin (Sigma-Aldrich, #A9393) selection after 24 hs of growth. The no-insert control plate was important to account for occurrence of incomplete digestion and random circularisation of the vector backbone not containing the fragment of interest. By counting the number of colonies on the test and control plate, it gives an idea of the number of colonies that is required to be picked and mini-prepped (**Section 2.6.8**) that will contain the plasmid of interest.

2.4.18 DNA mini-prep of plasmid DNA

The QIAGEN QIAprep Spin Miniprep kit (QIAGEN, 27104) was used according to the manufacturer's instructions for the isolation of plasmid DNA from a 5mL culture. This. After incubation, cells were pelleted by centrifugation at 4000 rpm for 10 min. Cell pellets

were resuspended in 250 μ L of buffer P1 and transferred to a microcentrifuge tube. 250 μ L of buffer P2 was added to this solution and mixed gently by inversion. A 350 μ L volume of buffer N3 was subsequently added to this solution and again mixed gently by inversion. This mixture was centrifuged for 10 min at 13,000 rpm. The decanted supernatant was applied to the QIAprep spin column and centrifuged for 60 seconds at 13,000 rpm. This flow through was discarded. The column was washed by adding 500 μ L of Buffer PB and centrifugation for a further 60 seconds at 13,000 rpm. Again, the flow through was discarded. A second wash was performed using 750 μ L of Buffer PE and centrifuging for 60 seconds. The flow through was discarded and the column was dried by an additional centrifugation step for 60 seconds to remove any remaining wash buffer. The spin column was then placed into a clean microcentrifuge tube. The DNA was eluted by adding 30-50 μ L (depending on the desired DNA yield) of Buffer EB or water to the spin column. This was allowed to stand for 1 minute at room temperature (RT) before centrifugation at 13,000 rpm for 1 minute. The eluted DNA was reapplied to the spin column and centrifuged for an additional 60 seconds to collect any remaining plasmid DNA. Quantification of the eluted plasmid DNA was determined using a NanoDrop spectrophotometer by measuring at OD_{260nm}. Plasmid was stored at -20°C until required.

2.4.19 DNA midi/Maxi-prep of plasmid DNA

Stock plasmids were amplified and purified using an Endotoxin-free Plasmid DNA Purification Midi/Maxi kit (Nucleobond® Xtra Midi plus EF, Macherey-Nagel, 740416.50). Typical yield from the Nucleobond® Xtra Midi kit is 250 μ g of plasmid DNA compared to the 1000 μ g from the Nucleobond® Xtra Maxi kit. Both midi and maxi preps were carried out according to the manufacturer's specifications with midi prep being the general route of plasmid amplification. 5 mL of inoculated LB media was added to 100 mL of pre-warmed LB media once again under the selection of antibiotic and incubated over night at 37 °C on a shaker platform. Pellets were harvested by transferring this 100 mL to a 250 mL centrifuge flask and spun at 6,000 g for 10 min at 4°C. Supernatants were discarded completely and pellets were either processed immediately or stored at -20°C until required. The Bacterial pellet was resuspended in 8 mL of Buffer RES-EF by pipetting up and down until no clumps remained and transferred into a 50 mL Falcon tube. Cells were lysed open by adding 8 mL of Buffer LYS-EF and mixed gently by

inverting. This mixture was incubated at room temperature (18-25°C) for 5 min. During this incubation period, the Nucleobond® Xtra Column with the inserted column filter was equilibrated with the addition of 15 mL Buffer EQU-EF around the rim of the inserted column filter. The cell lysate mixture was neutralised with the addition of 8 mL Buffer NEU-EF, inverted 10-15 times and incubated on ice for 5 min. The crude lysate was homogenised by inverting before applying it directly to the equilibrated Nucleobond® Xtra Column Filter and allowed to empty by gravity flow. The first wash consisted of the addition of 5 mL Buffer FIL-EF to the rim of the Nucleobond® Xtra Column Filter and once again left to empty by gravity flow. Once the column was emptied completely, the Nucleobond® Xtra Column Filter was removed and discarded. The second wash step washes the Nucleobond® Xtra Column by adding 35 mL of Buffer ENDO-EF directly into the column and allowing emptying by gravity flow. The third and final wash requires the addition of 15 mL Buffer WASH-EF to the column and emptying by gravity flow. Plasmid DNA was eluted into a 20 mL Universal by adding 5 mL of Buffer-ELU-EF to the column. For elution of DNA using the Nucleobond® Finalizer the DNA was precipitated with the addition of 3.5 mL isopropanol (SIGMA), vortexed well and left to sit for 2 min. The plunger was removed from a 30 mL Syringe and the Nucleobond® Finalizer was attached. The precipitate was loaded into the syringe and the plunger was reinserted into the syringe. Using constant force the precipitate passes through the Nucleobond® Finalizer and the flow though is discarded. The Finalizer was removed before the removal of the plunger and then reattached. Using the same technique a wash step with 2 mL Endotoxin-free 70% EtOH was carried out again discarding the flow though. The filter membrane of the Nucleobond® Finalizer was dried by removing the plunger and reinserting it into the syringe and expelling the air though the filter. This was performed three times. Finally, the plasmid DNA was eluted in 400 µL of Buffer TE-EF or H₂O-EF by using a 1 mL syringe attached to the Nucleobond® Finalizer. The concentration of eluted plasmid DNA was determined using a NanoDrop spectrophotometer by measuring the OD_{260nm}. Plasmid was stored at -20°C until required.

2.4.20 Plasmid diagnostics

Plasmid diagnostics requires a combination of the above listed protocols. Restriction enzymes are selected that will cut the target insert out of the plasmid constructed in

addition to select an enzyme that cuts once at a sequence within the insert. Digestions are then run out on an agarose gel stained with ethidium bromide, including a DNA ladder (Life Technologies, 1 kb Plus DNA Ladder, #10787-018), and compare band sizes to an appropriate plasmid reference map.

2.5 Mitochondrial studies

2.5.1 Mitotracker® Deep Red FM

Mitochondrial content was assessed using the fluorescent dye Mitotracker® Deep Red MTDR) FM (Invitrogen™, M22426). Mitochondrial abundance was determined for 1×10^6 cells stained with a working concentration of 50 ng. Cells were cultured for 72 hs, pelleted and resuspended in a 1 mL volume of culture medium containing the desired concentration of MTDR dye and incubated at 37 °C for 30 min in a shaker incubator. Cells were pelleted and resuspended in fresh culture media and analyzed using a FACS flow cytometer (BD). The MTDR emission wavelength of 665 nm did not interfere with the emission peak of GFP at 509 nm eliminating the need of compensation in the case of stable CHO cell lines expressing the miR-sponge construct.

2.5.2 OROBOROS Oxygraph-2k

The OROBOROS/Oxgraph-2k, a two chambered respirometer equipped with a peltier thermostat and integrated electromagnetic stirrers, was used to determine respirometric measurements. The oxygen concentration was recorded using the software DatLab (OROBOROS instruments) and specific oxygen consumption rates were represented as (pmol O₂/s/10⁶ cells). Measurements were performed using 1×10^6 cells/mL in 2 mL of CHO-S-SFMII for intact cells or in the case of the permeabilised assay, respiration buffer Mir05 (Hirsch et al. 2012) at 37 °C with continuous stirring. The following substrate-uncoupler-inhibitor-titration (SUIT) protocol was applied in both instances.

In the case of intact cells, oxygen consumption was allowed to stabilise upon inoculation and sealing of the chambers which resulted in the acquisition of routine respiration (R). Leak respiration (L) was established upon inhibition of ATP synthase through the

addition of oligomycin (2 µg/mL). Maximum respiratory capacity in an uncoupled state was achieved through addition of FCCP (0.2 µM).

For the more in depth permeabilised protocol, upon initial stabilisation of oxygen consumption, the cell membrane was permeabilised with 3 µL digitonin (30 µg/10⁶ cells). Complex I dependent respiration was driven with the addition of glutamate (10 mM) and malate (0.5 mM). OXPHOS capacity driven by Complex I was achieved by the addition of ADP (1 mM). Cytochrome C (10 µM) was added to test for aberrations in the integrity of the outer mitochondrial membrane. Maximal coupled respiration of Complexes I and II was stimulated by the addition of a Complex II-specific substrate, succinate (10 mM). By uncoupling the mitochondrial membrane and interfering with the proton gradient, maximum capacity of the electron transport system (ETS) was obtained using FCCP (0.2 µM). Inhibition of Complex I with rotenone (0.5 µM) shows the maximal uncoupled respiration via Complex II. Complex II and III were inhibited by the addition of Malonic acid (5 mM) and Antimycin A (2.5 µM) to estimate the residual oxygen consumption. Finally, Complex IV was stimulated by the addition of the artificial electron donor TMPD (0.5 mM) and its reducing agent ascorbate (2 mM) with Complex IV inhibition achieved through the addition of Azide (100 mM).

2.5.3 Mitochondrial Isolation

Intact mitochondria were isolated using a Mitochondrial Isolation kit for cultured cells (Thermo Scientific, #88794) in accordance with the manufacturers' specifications. A maximum of 6 samples were processed at any one time with 2 x 10⁷ cells being the processing limits. Following the reagent-based method, 2 x 10⁷ cells were pelleted by centrifugation ~850 g for 2 min and supernatant was discarded. 800 µL of Mitochondria Isolation Reagent A was added and vortexed at medium speed for 5 seconds followed by a 2 minute incubation on ice. 10 µL of Mitochondria Isolation Reagent B was added and vortexed at maximum for 5 seconds followed by incubation on ice for 5 min with vortexing at maximum every minute. 800 µL of Mitochondria Isolation Reagent C was added followed by inversion of samples. Samples were centrifuged at 700 x g for 10 min at 4°C. Supernatant was transferred to a new 2 mL tube and centrifuged at 12,000 x g for 15 min at 4°C. This contains mitochondria, lysosome and peroxisomes (3,000 x g for 15 min at 4°C to further reduce by >50%). Transfer the supernatant (cytosol fraction) to a

new tube. The pellet contains the isolated mitochondria. 500 μ L Mitochondria Isolation Reagent C was added to the pellet and centrifuged at 12,000 x g for 5 min. The supernatant was discarded. Pellet was maintained on ice until required. Freeze-thawing may compromise mitochondria integrity.

2.6 Proteomic analysis

2.6.1 Bradford assay

A BSA standard was serially diluted using UHP from a 2 mg/mL stock of Quick startTM Bovine Serum albumin Standard (Bio-Rad, #500-0206) starting with 1 mg/mL and spanning 0.5, 0.25, 0.125 and 0 mg/mL. Standards and samples were measured in triplicates at least by pipetting 5 μ L of each into the corner of the base of a well in a 96-well plate. 250 μ L of Quick startTM Bradford 1X Dye Reagent (Bio-Rad, #500-0205) to each well and incubate in the dark for 10-15 min. Absorbance readings are measured on a bench top spectrophotometer at a wavelength of 595 nm.

2.6.2 Western Blot

Proteins for analysis by Western Blotting were resolved using SDS-polyacrylamide gel electrophoresis (SDS-PAGE). Lysis buffer containing urea was added to cell pellet. Cell lysis was carried out over 20 min on ice and following vortex, the lysate was spun at 4°C for 15 min at maximum speed to remove insoluble debris. Protein was quantified the Bradford protocol. Protein samples were diluted in 2X Laemlli buffer (which contains loading dye, Sigma-Aldrich, S#3401) and appropriate volumes of lysis buffer. Before loading into the gel, samples were boiled for 5 min and cooled on ice. 5-20 μ g of protein and the molecular weight marker (New England Biolabs) were loaded onto a 4-12% NuPAGE Bis Tris precast gradient gel (Life Technologies, NP0322BOX). Electrophoretic transfer, blocking and development of western blots was carried out. Membranes were probed with the appropriate antibody of choice diluted in Tris-buffer saline containing 0.1%-20% Tween (TBS-T). An anti-mouse GAPDH monoclonal antibody (Abcam, #ab8245) was used as an internal control.

2.6.3 2-D clean up kit

Lysed protein samples were cleaned up using the ReadyPrep™ 2-D Cleanup Kit (Bio-Rad, #163-2130) as means of removing any contaminating substances like ionic detergents, salts, nucleic acids and lipids as a result of the lysis buffer or residual cellular debris. This will reduce streaking, background staining and other artifacts associated with substances contaminating 2D/IEF samples. A maximum of 500 µg can be cleaned using this kit for any one sample. Sample clean-up volume can be up to a maximum of 100 µL in a 1.5 mL microcentrifuge tube with maintenance on ice unless otherwise indicated. Always place the centrifuge in the same orientation in the centrifuge.

1-500 µg of protein was transferred to a final volume of 100 µL of MS-grade water. 300 µL of precipitating agent 1 was added to the protein sample and mixed by vortexing with a 15 minute incubation ice. A further 300 µL of precipitating agent 2 was added to the mixture and mixed well by vortexing. This was centrifuged at 12,000 g for 5 min to pellet removing tube promptly after spin step. Without disturbing the pellet, supernatant was removed using a pipette and discarded. Tube was centrifuged for an additional 15-30 seconds to collect any residual liquid and carefully removed and discarded. 40 µL of wash reagent 1 was added on top of the pellet and centrifuged at 12,000 g for 5 min, this was subsequently removed and discarded using a pipette. 25 µL of ReadyPrep proteomic grade water of UHP was added on top of the pellet and vortexed for 10-20 seconds. 1 mL of wash reagent 2 (pre-chilled at -20°C for at least 1 h) and 5 µL of wash 2 additive was added and vortexed for 1 min to mix. Samples were incubated at -20°C overnight. After this incubation, tubes were centrifuged at 12,000 g for 5 min to form a tight pellet. Supernatant was removed and discarded with an additional centrifuge for 15-30 seconds to collect remaining wash. Pellet was air dried at room temperature for no more than 5 min until the pellet appears translucent. Pellet was resuspended by adding an appropriate volume of 2-D rehydration/sample buffer and vortexed for at least 30 seconds. Tube was incubated at room temperature for 3-5 min, vortexed again and pipetted up and down a few times to fully resuspend. Sample was centrifuged to collect at 12,000 g for 2-5 min. Protein is ready for subsequent analysis or treatment and stored long term at -80°C.

2.6.4 Label-free sample digestion (Trypsin and Lys-c)

ProteaseMAX™ Sufactant, Trypsin Enhancer (Promega, #V2072) was used to carry out and enhance in-solution digestions in accordance with the manufacturer's specifications. ProteaseMAX™ Sufactant solubilizes proteins including difficult proteins (membrane proteins) and enhances protein digestion by providing a denaturing environment prior to the addition of protease enzymes. ProteaseMAX™ Sufactant degrades over the course of the digestion reaction yielding products that are compatible with downstream processes such as mass spectrometry (MS). 10 µg of protein was used for digestion. 2 µL of 1% ProteaseMAX™ Sufactant: 50 mM NH₄HCO₃ and the final reaction volume was made up to 100 µL of reaction mixture according to the table below:

Component	Volume (µL)
0.1% ProteaseMAX™ Sufactant:50 mM NH ₄ HCO ₃	20
1.0% ProteaseMAX™ Sufactant:50 mM NH ₄ HCO ₃	2
50 mM NH ₄ HCO ₃	58.5
0.5M DTT	1
0.55M iodoacetamide	2.7
Trypsin (1 µg/µL)	1.8
1% ProteaseMAX™ Sufactant	1
Final Volume	100

50 mM NH₄HCO₃ was added to the 10 µg of protein to a final volume of 93.5 µL. 1 µL of 0.5M DTT was additionally added and incubated at 56°C for 20 min. 2.7 µL of 0.55M iodoacetamide was added and incubated in the dark for 15 min. 1 µL of 1% ProteaseMAX™ Sufactant and 0.1 µg of Lys-c (Promega, #V1071) and incubated at 37°C for 6 hs. Lys-c is a protease that hydrolyses the carboxyl side of Lysine (Lys). After this incubation, 1 µg/µL of trypsin (Promega, #V5280) was added to the mixture and incubated at 37°C overnight. Trypsin is a protease that specifically hydrolyses arginine and lysine residues. The condensate from the walls was collected by centrifugation at 12,000 g for 10 seconds. A final concentration of 0.5% TFA was added, mixed and incubated for 5 min and room temperature. Sample is now ready for cleaning or peptide concentration.

2.6.5 C-18 spin column peptide concentration

Peptides were purified using a C-18 spin column (Thermo Scientific, #89870) in accordance with the manufacturer's specifications. Buffer preparation was as follows:

Activation Solution: 50% Methanol

Equilibrium Buffer: 0.5% TFA in 5% CAN

Sample Buffer: 2% TFA in 20% CAN

Wash Solution: 0.5% TFA in 5% CAN

Elution Buffer: 70% CAN

The Column was prepared by tapping until the resin was collected at the bottom. The column was placed into a collection tube. 200 μ L of activation solution was used to rinse the column walls and to wet the resin, centrifuged at 1500 g for 1 minute and flow-through was discarded. This was repeated. Next, 200 μ L of equilibration buffer was added and centrifuged at 1500 g for 1 minute. This step was also repeated. The sample was loaded into the resin bed. The column was placed into a receiver and centrifuged at 1500 g for 1 minute. Flow through was processed again following a repeat step. The column was placed into a receiver and 200 μ L of wash solution was added and centrifuged for 1 minute at 1500 g. The flow through was discarded. This wash step was repeated. The column was placed into a new receiver tube. 20 μ L of elution buffer was placed in top of the resin and centrifuged at 1500 g for 1 minute. This step was repeated with an additional 20 μ L of elution buffer to yield a final volume of 40 μ L of purified peptides. Samples were dried using a vacuum centrifuge until required.

2.6.6 Label-free mass spectrometry

Nano LC–MS/MS analysis was carried out using an Ultimate 3000 nanoLC system (Dionex) coupled to a hybrid linear ion trap/Orbitrap mass spectrometer (LTQ Orbitrap XL; Thermo Fisher Scientific).

A 5 μ L injection of digested sample were picked up using an Ultimate 3000 nanoLC system (Dionex) autosampler using direct injection pickup onto a 20 μ L injection loop.

The sample was loaded onto a C18 trap column (C18 PepMap, 300 μm ID \times 5 mm, 5 μm particle size, 100 Å pore size; Dionex) and desalted for 5 min using a flow rate of 25 $\mu\text{L}/\text{min}$ in loading buffer (0.1% TFA, 2% acetonitrile). The trap column was then switched online with the analytical column (PepMap C18, 75 μm ID \times 500 mm, 3 μm particle and 100 Å pore size; (Dionex)) using a column oven at 35 °C and peptides were eluted with the following binary gradients of:

Mobile phase buffer A (0.1% formic acid in 2% acetonitrile) and mobile phase B (0.08% formic acid in 80% acetonitrile) 0-25% B over 280 min and 25-100% for a further 20 minutes.

Data were acquired with Xcalibur software, version 2.0.7 (Thermo Fisher Scientific).

The Hybrid linear ion trap/Orbitrap mass spectrometer (LTQ Orbitrap XL; Thermo Fisher Scientific) was operated in data-dependent mode and externally calibrated.

Survey MS scans were acquired in the Orbitrap in the 400–1800 m/z range with the resolution set to a value of 30,000 at m/z 400. Up to three of the most intense ions (1+, 2+ and 3+) per scan were CID fragmented in the linear ion trap. A dynamic exclusion was enabled with a repeat count of 1, repeat duration of 30 seconds, exclusion list size of 500 and exclusion duration of 40 seconds. The minimum signal was set to 500. All tandem mass spectra were collected using a normalised collision energy of 35%, an isolation window of 2 m/z , activation Q was set to 0.250 with an activation time of 30.

2.6.6.1 Identification of Proteins from Mass Spectrometry Data

The CHO fasta database was downloaded from:

<ftp://ftp.ncbi.nlm.nih.gov/blast/db/FASTA> consisting of 24,383 predicted genes.

2.6.6.2 Progenesis LCMS

The resulting total ion chromatograms (TIC) of quantitative label-free LC-MS data were subjected to statistical analysis using Progenesis LC-MS software (NonLinear Dynamics). This programme imports all runs in an “ion intensity map” format which

maps the ions discovered in the run, by plotting retention time against the mass/charge ratio. All ion maps may be aligned against one reference run which allows for any shift in retention time between runs. The intensity of each ion may then be compared against that of all other runs, thus generating quantitative data on patterns of differential expression between sample sets which may be analysed with statistical analysis tools such as ANOVA, and principal component analysis.

For all experiments, unless stated otherwise, all peptides, and all proteins demonstrated ANOVA scores of ≤ 0.05 for differential analysis between sample sets.

For all quantitative LC-MS/MS data, Progenesis provides the following information; protein accession number, peptide count, number of peptides matched, confidence score, an ANOVA value, the maximum fold change, and the average normalised abundance. The protein accession number represents the code corresponding to the protein in NCBI-CHO protein database. "Peptide count" refers to the number of peptides identified and "number of peptides matched" refers to the number of peptides which were matched to the protein. The MASCOT score (or ion score) is calculated from the combined scores of how well each peptide matches to the protein sequence. The significance of the differential expression between the two groups is represented by an ANOVA score (p-value). The fold change, or average ratio, illustrates the greatest fold different in protein ion abundance between the two groups. The average normalised abundance is calculated from the sum of all peptide abundances from every run for each protein.

The MASCOT search parameters that were used allowed two missed cleavages, fixed modification of cysteine (carbamidomethyl-cysteine) and variable modification of methionine (oxidised). Peptide tolerance depended on the instrument used to acquire the mass spectrometry data, in this case the Hybrid linear ion trap/Orbitrap mass spectrometer used a peptide tolerance of 20 ppm. The MS/MS tolerance was set at 0.6 Da. On completion of the database search the peptide results were filtered using MASCOT criteria of 95% confidence interval (C.I.) threshold ($p < 0.05$), with a minimum ion score of ≥ 40 . Protein identifications were accepted if they had one matched peptide.

2.6.7 SEAP assay

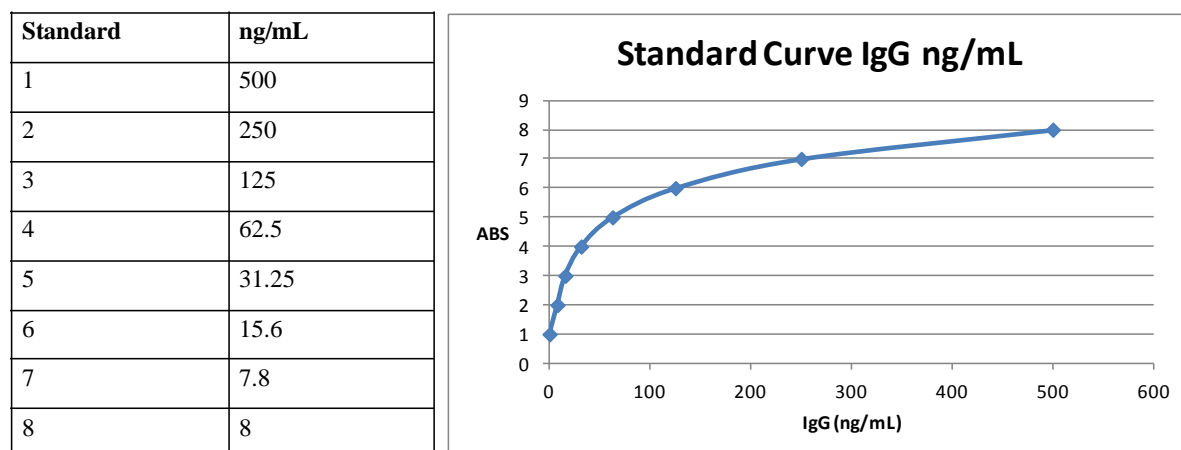
The enzymatic assay for the quantification of SEAP (secreted alkaline phosphatase) was adapted from the method reported by Lipscomb *et al.*, (2005). 50 μ L of supernatant was transferred to a single well on a 96 well flat bottom plate. To each sample, 50 μ L of 2X SEAP reaction buffer (10.5g diethanolamine (100%), 50 μ L of 1M MgCl_2 and 226 mg of L-homoarginine in a total volume of 50 mL) was added. Plates were incubated at 37 °C for 10 min in order to increase enzymatic activity. After this time, 10 μ L of phosphates substrate (158 mg of p-nitrophenolphosphate (SIGMA-ALDRICH®, P4744) in 5 mL of 1 X SEAP reaction buffer, made fresh for each use – adjust to suit number of sample wells) was added to each well. A Kinetic absorbance assay was performed and the change in absorbance per minute ($\text{OD}_{405\text{nm}}/\text{min}$) was considered as an indicator of the amount of SEAP present in the sample. Mean V was taken as the change in the average of the kinetic slope.

2.6.8 Enzyme-linked immunosorbent assay (ELISA)

CHO-secreted IgG was quantified using the Bethyl Laboratories Human IgG ELISA Quantitation Set (Bethyl Laboratories Inc., E80-104) in accordance with the manufacturer's specifications. Initially the amount of samples required including replicate number ($n = 3$), blank samples and standards were calculated to determine the number of plates required to perform an assay. 1 μ L of Affinity Purified Human IgG Coating Antibody (SIGMA-ALDRICH, A80-104A) was diluted in 100 μ L of Coating Buffer (One capsule of Carbonate-Bicarbonate Buffer (SIGMA-ALDRICH, C3041-50CAP) in 100 mL of UHP making a 0.05M Carbonate-Bicarbonate coating buffer solution) for each well to be coated. Add 100 μ L of diluted antibody to each well and incubate at 4°C overnight. Wash plate 3 times using Wash Solution (SIGMA-ALDRICH, Tris Buffered Saline, with Tween®, pH 8.0, T9039-10PAK). In order to prevent non-specific binding, 200 μ L of Blocking Solution (SIGMA-ALDRICH, Tris Buffered Saline, with BSA, pH 8.0, T6789-10PAK) was added to each well after washing and incubated at room temperature for 60 min. During this incubation step, standard and sample preparation was performed. Starting from a pre-diluted (using PBS) IgG stock of 1000 ng/mL, a serial dilution was undertaken creating a range of known IgG concentrations from 500 ng/mL-7.8 ng. A blank control of Diluent only (Blocking Solution with 0.5%

Tween 20) was run alongside the standards (**Fig 2.11**). Samples were diluted using Diluent based on the expected IgG concentration so that the final concentration/mL fell within the range of the standard curve.

Figure 2.11: Standard Curve Dilutions



After incubation, the blocking buffer was removed by washing 3 times as previously described. Into each appropriate well, 100 μ L of standard and sample in triplicate was loaded and incubated at room temperature for 60 min. After, plates were washed 3 times. Prior to addition of the HRP detection antibody (SIGMA-ALDRICH, A80-104P), a 1/50,000 dilution in Diluent was carried out by adding 1 μ L of HRP Detection Antibody to 50 mLs of Diluent. 100 μ L of pre-diluted HRP detection antibody was transferred to each sample/standard well and incubated at room temperature for 60 min. Once again, after incubation, the HRP detection antibody was removed and the plate washed 3 times. 100 μ L of the TMB substrate (SIGMA-ALDRICH, 3,3',5,5'-Tetramethylbenzidine, T8665-100mL) was added to each well and the enzymatic reaction was allowed to develop at room temperature in the dark for 10-15 min yielding a colour change to a blue solution. After 10-15 min, the reaction was stopped with the addition of 100 μ L of 0.18M (H_3PO_4) Phosphoric Acid (SIGMA-ALDRICH, 04102-500G) to the TMB previously added to each well. The solution should yield a colour change from blue to yellow. Within 30 min of stopping the reaction, the enzymatic activity should be evaluated by measuring the absorbance on an ELISA plate reader at 450 nm. Triplicate absorbance values should be within 10% of each other. By plotting a standard curve, the elucidation of IgG content of the unknown samples can be calculated based on the curve and taking the dilution factor into account.

2.6.9 Glutamate assay

The detection of glutamate was carried out using the Glutamate Assay Kit (Sigma-Aldrich, #MAK004) in accordance with the manufacturer's specifications. Absorbance readings were performed on a bench top spectrophotometer at a wavelength of 450 nm. Glutamate standards were prepared by diluting 10 μ L of the 0.1 M Glutamate standard in 990 μ L of the glutamate assay buffer to make a 1 mM standard solution. From this, 0, 2, 4, 6, 8 and 10 μ L into a 96 well plate forming a 0 (blank), 2, 4, 6, 8 and 10 nmole/well. Glutamate assay buffer was added to each well to bring the volume to 50 μ L. Samples were prepared in a similar fashion topping up to 50 μ L using glutamate assay buffer. Assay reaction mixes were made up according to the scheme below:

Reagent	Blank Sample	Samples and Standards
Glutamate Assay Buffer	92 μ L	90 μ L
Glutamate Developer	8 μ L	8 μ L
Glutamate Enzyme Mix	-	2 μ L

100 μ L of the appropriate Reaction Mix was added to each of the wells, mixed using a shaker/pipetting and placed in the dark to incubate for 30 min at 37°C. The plate was measured at 450 nm on a spectrophotometer.

2.6.10 Akta Prime IgG purification

HiTrap Protein A HP column (GE HealthCare-Life Sciences, #17-0402-01) was used for the purification of IgG antibodies in conjunction with using the AktaPrime Plus system (GE Healthcare). The AktaPrime Plus is a chromatography system that performs single purifications of tagged and untagged proteins. The system is compact and comprises of a pump, fraction collector, monitors for UV, conductivity and pH. Valves for buffer selection, sample injection, gradient formation, and flow diversion are also integrated into the system. The AktaPrime was cleaned using 50% ethanol and the system was purged with PBS, including the protein A column, before each sample loading. When setting up the AktaPrime commands, a flow rate of 1 mL/min (1 mL protein A column) with a fraction size of mL and a pressure of 1 MPa. Load position was set to "Pos 1" for

equilibration and washing procedures and “Pos 8” in the case of sample loading/washing and elution. All elutes were sent to “Waste” except in the case of sample loading, if flow-through sample was required to be retained, and elution of IgG in which case were sent to “load”. Finally, 0% gradient was predominantly selected except in the case of elution in which case an 80% gradient of Buffer B (0.5% Acetic Acid) was used. After purging the system with PBS and cleaning the protein A column using PBS (Buffer A), IgG supernatant sample was loaded through “position 8”. The UV detector will detect all secreted proteins as the sample flows through while IgG binds the column prior to UV detection. After all sample has been passed through the column, Buffer A (PBS) was used to wash the system/Column until the UV absorbance returns to baseline. An 80% gradient was then selected for Buffer B (0.5% Acetic Acid) to flow through “position 8” and sent to “load”. This elution was collected in waste until there was a spike in the UV detector indicating the start of IgG elution from the column (This may take a few min – so don’t panic). After the sample was collected, the column was washed with a 100% gradient of Buffer B and then the system and column was washed with Buffer B in preparation for the next sample. If finished, the system was cleaned with MS grade water loading through both “positions 1 and 8” and sending to both “Waste” and “Load” for at least 10 column volumes, followed with the same cleaning procedure using 20% ethanol. Once the column was cleaned with 20% ethanol, it was also stored in 20% ethanol at 4°C. The eluted IgG was buffer exchanged using Amicon Ultra – 4 Ultracal 10kC filters by applying the sample to the filter and centrifuging at 4,000 g for 10 min at 4°. Flow through was discarded and filters were topped up with 4 mL of PBS and centrifuged again following the same conditions. This was repeated about 3-4 times and the remaining ~500 µl of IgG-containing PBS was removed, placed in an eppi and stored at -20°C.

2.6.11 Glycomic Characterisation of Antibodies

Characterisation of antibody glycoforms was determined based on the procedure reported by Mittermayr and Bones *et al.*, (Mittermayr et al. 2011). Clones were cultured in a 20 mL volume spinner flask and cultured for a maximum of 4 days. Cells were removed by centrifugation at 1500 rpm for 5 min with a centrifugation step at 4000 rpm for 10 min to ensure removal of residual cellular debris. IgG was purified using an IgG-protein A column on an AktaPrime™ Plus system (see section 2.6.10 of Materials and Methods).

An in-solution digest was carried out using the PNGase F enzyme to remove any asparagine N-linked glycans in addition to serine or threonine O-linked glycans. 500 µg of total antibody protein was added to a micro-centrifuge tube in sodium bicarbonate (SBC) making up the volume to that of the highest volume sample. As N-glycans usually protrude from the external surface, it was not required to reduce or alkylate antibodies. PNGase F was added to the final digest at 5% of the total volume and incubated at 37°C overnight. A 10 kDa MWCO filter was treated with a 1:1 ethanol water solution and centrifuged at 13,000 rpm for 5 min discarding the flow-through. Digested sample was added to the filter and spun at 13,000 rpm for 10 min. The digestion tube was washed with 200 µL water, added to the filter and spun at 13,000 rpm for 10 min. The filtrate was vacuum dehydrated by centrifugation. Once dry, 20 µL of 1% formic acid was added to the tube, vortexed briefly and reduced to dryness. This ensures complete conversion of glycosamines present back to the reducing aldose. As monosaccharides lack chromophores or fluorophores, it was necessary to label monosaccharides with an absorbing group to increase overall analytical sensitivity. To the dried N-glycans, 5 µL of labelling solution (50 mg 2-AB, 2-aminobenzoic acid, 60 mg sodium cyanoborohydride in 70:30 DMSO acetic acid). Mix by pipetting. An additional 5 µL of 70:30 DMSO acetic acid was added, vortexed and incubated at 65°C for two hs. Following incubation, 90 µL of water was added to the labelling solution, mixed and vortexed. 900 µL of acetonitrile was subsequently added, mixed and vortexed with a brief spin to collect. Unconjugated 2-AB was removed by aspirating the liquid through a 1 mL/10 µL PhyNexus Normal Phase PhyTip preconditioned with 95% v/v acetonitrile. At least 10 in-out cycles were performed. The tip was washed with 10 in out cycles of 95% v/v acetonitrile venting the waste each time. The labelled N-glycans were eluted with 5 x 200 µL washes of water, collected, combined and reduced to dryness in a vacuum centrifuge. Samples were reconstituted in an appropriate volume of water and stored at -20°C. Ultra-Pure liquid chromatography (UPLC)-fluorescence profiling of N-glycans was utilised to the antibody glycoform patterns in antibody samples. Hydrophilic interaction liquid chromatography (HILIC) was used as a suitable separation technique due to the polar nature of oligosaccharides. 2-AB labelled N-glycans were separated by UPLC with fluorescence detection on a Waters Acquity UPLC instrument consisting of a binary solvent manager, sample manager and fluorescence detector under the control of Empower 2 chromatography workstation software (Water, Milford, MA). Separations were performed using Waters BEH glycan columns, 100 x 2.1 mm i.d., 1.7 µm BEH

particles, using a linear gradient of 70-53% acetonitrile at 0.56 mL/min in 16.5 min, 50 mM ammonium formate pH 4.5 was used as buffer A. An injection volume of 20 μ L sample prepared in 80% v/v acetonitrile was used throughout. Samples were maintained at 5°C prior to injection and the separation temperature was 40°C. The fluorescence detection excitation/emission wavelengths were $\lambda_{\text{ex}} = 330$ nm and $\lambda_{\text{em}} = 420$ nm, respectively.

2.7 Biotinylated miRNA pull-down of mRNA

The protocol utilised for the target identification of specific microRNAs including the comparative analysis of protein complexes associated with miRNA guide and passenger strands was based on the method published by Ørum and Lund (Orom, Lund 2007) using Biotinylated synthetic miRNAs. Before carrying out the experimental procedure of miRNA pull-down, 100 μ L of Streptavidin-agarose beads (Sigma-Aldrich, 85881-1ML) was incubated with 10 μ L of a 10 mg/mL stock of tRNA (Sigma-Aldrich, R8508-1ML) and 10 μ L of a 10 mg/mL stock of BSA (Sigma-Aldrich, B2518-10MG) in a 1.7 mL Eppendorf tube on a rotating platform at 4°C for ~3 hs. This served to reduce the level of non-specific binding. These pre-blocked beads were then washed twice in 300 μ L lysis buffer by centrifugation at 12,000 g for 30s and subsequently resuspended in 100 μ L of lysis buffer. This 100 μ L of slurry was sufficient for 4 samples. To avoid separation of bound mRNAs to our biotin-tagged miRNA as well as associated protein complexes, a gentle lysis buffer was prepared in accordance to the recipe below.

In 100 mL of UHP water:

20 mM Tris

200 mM NaCl

2.5 mM MgCl_2 (Sigma-Aldrich, M2670-100G)

0.05% Igepal (Sigma-Aldrich, 13021-50ML)

60U/mL RNase Inhibitor, Superscript 20U/ μ L (Life-technologies, AM-2694)

1 mM DTT

Halt Protease inhibitor cocktail, EDTA-free (100X) (Thermo-fischer scientific, 87785)

The addition of the RNase inhibitor, DTT and Protease inhibitor cocktail was carried out prior to use of the lysis buffer. For each sample, 25 μ L of slurry was transferred to a 1.7

mL Eppendorf tube and washed twice with 500 μ L of lysis buffer and resuspended in 25 μ L of fresh lysis buffer. Cells were harvested 24-48 hs after transfection and washed once with PBS by centrifugation at 1500 g for 5 min. Cells were resuspended in 1 mL lysis buffer in a 1.7 mL Eppendorf and placed on ice. Lysed cells were then vortexed vigorously for 10s and placed on ice for 10 min and vortexed. The lysate was cleared by centrifugation at 12,000 g at 4°C for 15 min in a microcentrifuge. The supernatant was transferred to a new cold tube on ice. At this point, a 50 μ L input sample was removed from the total volume and placed on ice for further analysis. The remaining lysate was then incubated on a rotating platform for 1 h at 4°C with 25 μ L of pre-washed streptavidin-agarose beads. Beads incubated in lysate were collected by centrifugation for 1 minute at 5000 rpm at 4°C. The supernatant was carefully removed and the beads washed in 500 μ L of ice-cold lysis buffer. This washing step was repeated 3 times. After the last wash, 50 μ L of lysis buffer was left on the pellet. This final solution contained Biotinylated-miRNA bound to the streptavidin-agarose beads with associated mRNA/protein complexes ready for further processing such as RNA/Protein isolation.

2.8 Statistical analysis

A paired t-test was utilised in the case of OROBOROS measurements in miR-23 depleted clones (**Section 3.4 of results**) due to the high through-put constraints within the machine itself. Only two samples (test versus control) could be measured at any one time in addition to a large degree of innate variance in data output. To account for this variance, samples were statistically tested as “unequal variance” with each individual test and control being compared individually to each other. Using excel, a paired t-test is a type 1 t-test.

A more stringent statistical method was applied for most data analysis throughout this thesis, except in the case above. This was an unpaired t-test used to assess whether the population means were different. This is a type 2 t-test in excel.

Chapter 3

Results

Section 3.1

Identification of microRNAs involved in the regulatory control of CHO cell growth rate with subsequent phenotypic characterisation

3.1.1 Identification of microRNAs involved in the regulation of CHO cell growth rate and phenotypic characterisation

This section describes the functional assessment of a panel of miRNAs identified in a multi-omics profiling experiment performed in our lab and described in detail in Clarke 2012 (Clarke et al. 2012).

3.1.1.1 Differential miRNA expression profile of CHO cells with varying growth rates using an integrated miRNA, mRNA and protein expression analysis technique

Briefly, a panel of CHO clones were selected exhibiting a range of growth rates (0.011 to 0.044 hr⁻¹) (**Table 3.1**) with a mean productivity of 24 (± 3) pg of protein/cell/day. The selection of sister clones derived from the same transfection pool differing only in growth rate served to remove productivity as a variable within the profile thus enriching for variations inherently associated with cellular proliferation.

Table 3.1: Clonal I.Ds of fast and slow CHO clones

I.D.	Phenotype	Specific Growth rate
X5.13F	F	0.011-0.044 division/hr
X5.16F	F	
X5.18F	F	
X5.22F	F	
X5.2F	F	
X10.2S	S	
X11.1S	S	
X5.11S	S	
X5.1S	S	
X7.7S	S	

Of the clones represented in the table **3.1**, the 10 clones were separated into two groups: 5 “fast” (≥ 0.025 hr⁻¹) and 5 “slow” (≤ 0.023 hr⁻¹) samples.

The incorporation of multiple “omics” disciplines served to facilitate in the identification of non-seed miRNA targets, a problem recurrently encountered when identifying potential targets of specific miRNAs, which is reported in greater detail in (Clarke et al. 2012). Here we focus on only the miRNAs identified within this study and pursue their potential application in CHO cell engineering

3.1.1.2 Cell Culture and sampling

Clonal cell lines were grown in batch shake flask suspension culture in AS1 media (proprietary serum-free media) at a working volume of 60 mL at 37 °C. Cells were inoculated at a starting density of 2×10^5 cells/mL. Each clone was grown in triplicate and samples were collected during mid/late exponential (log) phase (72 h). Samples were separated into three fractions for subsequent analytical profiling of miRNA expression using qRT-PCR based Taqman Low-Density Array (TLDA) technology, mRNA expression using a proprietary CHO-specific WyeHamster3a oligonucleotide microarray and protein expression using label-free LC-MS. The focus of this thesis is the miRNA targets identified as potential engineering tools of CHO cell growth.

3.1.1.3 microRNAs associated with growth

Of the 51 miRNAs found to be DE in this study exhibiting a correlation with CHO cell growth rate, a number have previously been associated with cellular proliferation including miR-451 (Godlewski et al. 2010), miR-206 (Yan et al. 2009a), miR-23b* (Liu et al. 2010a), miR-31 (Laurila et al. 2012) and miR-10a (Tan et al. 2009). Several of the miRNAs found to be up-regulated form the miRNA cluster, miR-17 ~ 92 (miR-17, miR-20a, miR-20b, miR-18a, miR-18b and 106a). This is a well characterised miRNA cluster in respect to cancer (Olive, Jiang & He 2010a), having direct oncogenic transcriptional activators such as c-myc (O'Donnell et al. 2005b) in addition to being previously identified as highly expressed in CHO (Hackl et al. 2011).

To demonstrate the strength of this profiling strategy in reducing the false positive/negative hits generated through utilisation of miRNA: mRNA binding criteria by prediction algorithms (**see section 1.2.6**), the following is an example from the literature in support of our findings. An experimentally validated target of miR-451 is the activator of tumour suppression, Rab14 (Wang et al. 2011a). miR-451 was shown to be down-regulated in fast growing CHO cells while the Rab14 protein was up-regulated in addition to the level of expression of its mRNA remaining constant. In the case of Rab14-miR-451, TargetScan would score Rab14 as a candidate target gene of miR-451 quite poorly given the low degree of conservation of the 3'UTR binding site. As a result, sole dependence on a prediction algorithm would result in the oversight of true molecular

targets but in cases such as this, the availability of datasets generated as described in this current profile can aid in the prioritisation of true mRNA targets of miRNAs and complement the output hits from prediction algorithms.

3.1.2 Phenotypic validation through transient microRNA screening

Phenotypic characterisation of a select subgroup of miRNAs derived from the list determined to be DE in CHO cells with varying growth rates was carried out transiently by the exogenous introduction of an artificial miRNA hairpin or duplex, termed a pre-miR (mimic), or a single-stranded oligonucleotide fully complementary to the mature sequence of the miRNA being targeted, termed an anti-miR/antagomiR or inhibitor (see **section 1.3.2**). To ensure sufficient exogenous levels of a miRNA or adequate knockdown of a highly expressed endogenous miRNA, 50-100 nM of mimic/inhibitor was used during the screening process. The following section summarises the interesting results generated from the primary phenotypic screen of the miRNAs identified from the profile (see **section 3.1.1**) with the inclusion of interesting targets from literature sources/current ongoing work.

3.1.2.1 Cell culture and transfection conditions

All transient transfections were carried out as described in **section 2.3.2** of Materials & Methods using either the transfecting reagent siSPORT™ NeoFX™ transfecting reagent (AMBION®, AM4510) or INTERFERin™ (PolyPlus-Transfection™, PPLU-409-01). Cells were seeded at a starting density of 1×10^5 cells/mL in a 50 mL aerated culti-flask disposable bioreactors (Sartorius Stedium Biotech, DF-050MB-SSH) at a final volume of 2 mL CHO-S-SFM II (GIBCO®, 12052-098) culture media. A list of all miRNA mimics (NBS Biologicals, M-01) and miRNA inhibitors (NBS Biologicals, M-02) used in this transient screen are listed in the appendix (**Appendix Figure A1**). All appropriate controls were included: untreated cells, transfection reagent only, a positive control (siRNA designed against VCP) and a non-specific negative control (NC). Transfection efficiency was based on the transfection of a siRNA designed against the mRNA coding sequence of Vasolin-containing protein (VCP). VCP was initially identified as being highly expressed in CHO cells with increased growth rates with subsequent siRNA-

mediated knockdown resulting in the induction of apoptosis and growth arrest (Doolan et al. 2010). Inclusion of a NC (NBS Biologicals, M-03) for either a miRNA mimic or inhibitor, served to account for the off-target effects on the cells miRNA processing machinery. Data represented includes only the negative control and the miRNA under investigation, however, assays yielding a poor transfection efficiency, based on siVCP, were omitted from analysis.

Combination transfection of particular miRNAs was undertaken with optimisation carried out as a means to determine the concentration to use that would be sufficient to potentially mediate a phenotype without losing potency due to titrational effects. 20 nM of pre/anti-miR was selected with a total of two miRNAs co-transfected at any one time. Each miRNA was transfected individually (20 nM) as a means to compare any potential synergy taking place while, however to account for the total concentration of 40 nM in the case of co-transfected miRNAs, 20 nM of a negative control pre/anti-miR was included for each individual miRNA (Data not shown).

After transfection, cells were cultured for 7 days at 170 rpm in a Kuhner Climo-shaker incubator (Kuhner, Climo-shaker, ISF1-X) at 37 °C and assessed for growth and productivity.

3.1.2.2 Summary of transient miRNA screen

With the focus of this thesis being that of the exploitation of miRNAs as engineering targets to enhance the performance of CHO cells within the bioprocess, this section summarises a subset of the list of 51 miRNAs revealed to be DE (**section 3.1.1**) and their impact on the CHO cell phenotype upon transient evaluation.

From a large panel of miRNAs screened, a small subset of these miRNA was observed to exhibit a consistent impact on CHO cell phenotype. This supports previous observations within the literature of miRNA acting subtly, buffering cellular networks with few miRNAs driving particular phenotypes (Mullokandov et al. 2012). The most interesting miRNAs from the screen and their associated CHO cell phenotypes are presented in **Table 3.1**.

Several high priority miRNAs, based on phenotypic potency, were identified such as the tumour suppressor miR-34a, its passenger strand miR-34a* and the passenger strand of a member of another well-known cancer-associated miRNA cluster, miR-23b*. All three miRNAs were found to impact negatively on CHO cell viability with potent inhibition of cellular proliferation, despite two candidates being demonstrated to be upregulated in fast growing CHO cells. In all three instances, volumetric productivity was observed to be reduced considerably predominantly attributed to the reduced cell numbers in early-mid stage culture, a phenotype recurrent in instances of growth inhibition.

A large portion of the list of miRNAs screened were observed to elicit either an inconsistent or no phenotype across replicates (data not shown). Combinatorial miRNA transfections were explored for these inconsistent miR targets in order to exploit potential synergy. miRNAs that exhibited mild phenotypes (in both a positive or negative direction) or no phenotype at all were co-transfected with a certain degree of success. Numerous miRNAs such as miR-455-3p/5p, miR-409-3p and miR-338-3p were observed to act negatively upon transient knockdown. However, the mild and inconsistent phenotypic shift observed for these miRNAs compared to the potent effects exhibited by miR-34a, -34a* and -23b* over-expression resulted in these latter candidates moving to the next level of validation as potential CHO cell engineering targets. Following experience within our research group with miR-7 (Barron et al. 2011a), stable depletion of miR-34a/-34a*/23b* may offer potential benefits based on their potent negative phenotype upon their over-expression.

Despite not pursuing a small number of candidates due to resource and time constraints, various miRNAs screened present themselves as viable candidates for stable manipulation such as the growth inhibitor miR-206 and miR-639, the growth promoting and potentially apoptotic protective miR-15a/-16-1 and the growth inhibitory with possible productivity boosting attributes, miR-200a.

Table 3.1: Summary of all screening data in CHO-K1-SEAP

Summary of miRNA screening data in CHO		
miRNA	Screening Data	Conclusion/Approach
miR-34a (pre-miR)	Overexpression reduced cellular proliferation, induced cell death. Knockdown improved growth inconsistently.	Transient/stable knockdown for the enhancement of growth and resistance to apoptosis
miR-23b* (pre-miR)	Reduced cellular proliferation, mild induction of apoptosis	Transient/stable knockdown for the enhancement of growth and the resistance of apoptosis
miR-532 (pre-miR)	Overexpression reduces volumetric productivity. Knockdown improves growth rate inconsistently.	Further validation
miR-200a (pre-miR)	Overexpression reduces growth and improves volumetric titre	Stable overexpression under inducible promoter to enhance productivity/Stable inhibition to improve growth
miR-181d (pre-miR)	Inconsistent	Further Validation
miR-639 (pre-miR)	Reduced cell growth	Stable knockdown to improve growth and volumetric titre – Further Validation
miR-455-5p/-455-3p (anti-miR)	Inconsistent with an indication towards inhibitory growth effects	Further Validation
miR-206 (anti-miR)	Mild reduction in cell growth	Further Validation
miR-34a* (pre-miR)	Reduced cellular proliferation, induction of apoptosis	Transient/stable knockdown for the enhancement of growth and resistance to apoptosis
miR-126	Inconsistent	Further Validation
miR-338-3p (anti-miR)	Inconsistent	Further Validation
miR-378 (anti-miR)	Inconsistent	Further Validation
miR-409-3p (anti-miR)	Inconsistent	Further Validation
miR-15a/16-1 (anti-miR)	Inconsistent/Increases growth	Further Validation/Stable knockdown

Section 3.2

The potential of miR-34a as an engineering target

3.2 Exploring the master “tumour suppressor” miR-34a as a potential CHO engineering target

Both miR-34a and miR-34a* were observed to reduce cell growth and induce apoptosis, in CHO-SEAP cells upon their transient overexpression (**section 3.1.2.2.2 and 3.1.2.3.1 of Results**). Despite both miR-34a and miR-34a* dramatically reducing volumetric protein output, miR-34a was observed to enhance specific productivity.

This section explores the potential of miR-34a as a candidate for CHO cell engineering using miR-sponge technology when taking into account its conserved effect on CHO-SEAP upon overexpression and its vast number of validated targets (**Table 4.1 of discussion**).

3.2.1 Transient knockdown of miR-34a potentially enhances CHO cell growth

Given that transient overexpression of miR-34a induced an unfavourable CHO cell phenotype it was anticipated that its transient inhibition may mediate the reverse phenotype, i.e. accelerated growth and apoptosis resistance. However, the phenotype observed upon its transient knockdown using anti-miRs was not as potent as hoped and inconsistent over the course of independent assays.

A mild increase in cell density of ~13% and 30% ($p \leq 0.05$) was observed on day 2 and 4 of culture, respectively (**Fig. 3.1 A**), with no impact on viability. Normalised productivity was reduced by ~13% and ~25% on day 2 and 4, respectively (**Fig. 3.1 B**).

Figure 3.1: Transient miR-34a inhibition in CHO-K1-SEAP cells

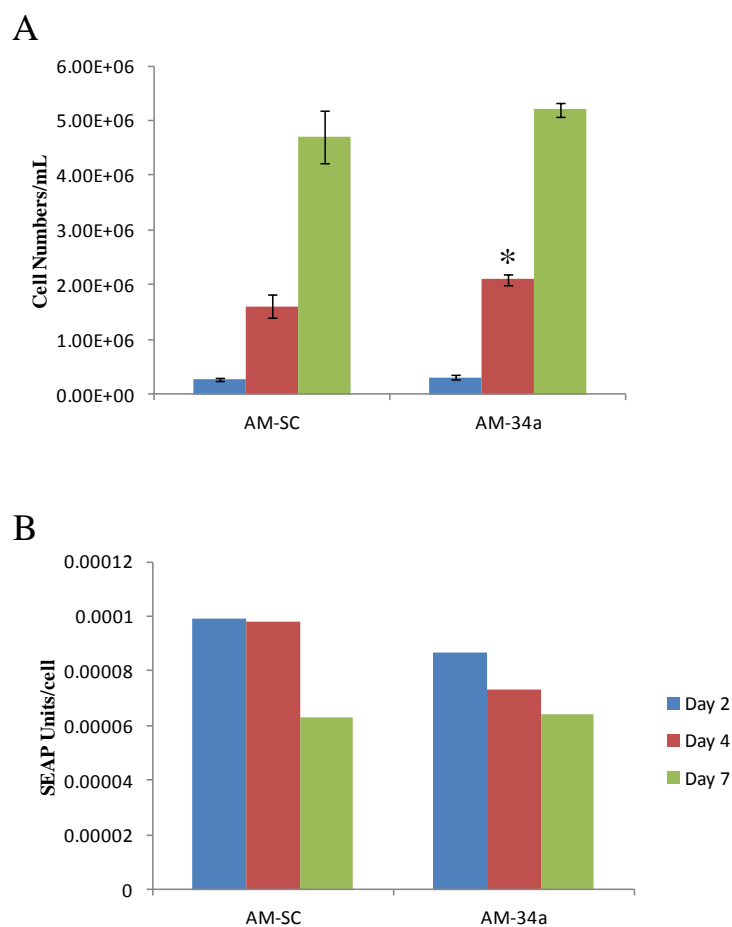


Figure 3.1: Transient miR-34a inhibition was achieved using fully complementary antagonists of the mature miR-34a commercially designed by NBS biologicals. Phenotypes under investigation were A) Cell numbers/mL and B) Normalised productivity. Statistical significance was calculated using a standard student t-test ($p \leq 0.05^*$) with an $n = 3$.

3.2.2 Transient inhibition of miR-34a mildly inhibits the induction of apoptosis

The transient nature of exogenously introduced anti-/pre-miRs impedes the assessment of late stage culture phenotype such as apoptosis. Given miR-34a's mild impact on CHO cell viability, it was anticipated that reversing its function would positively affect viability and prolong cell survival. We sought to induce apoptosis early in culture by mimicking late stage culture conditions so that the transient influence of the miR-34a inhibitors has not worn off.

3.2.2.1 Apoptosis assay development

Cell death can be induced by the supplementation of reagents such as Sodium butyrate (NaBu) (Lee, Lee 2012) or Dimethyl sulfoxide (DMSO). However, we wanted to induce a more realistic onset of apoptosis that would resemble the nutrient starved, hypoxic and toxin-enriched environment of the bioreactor. This method of inducing apoptosis has been previously reported by Druz and colleagues (Druz et al. 2011) which identified a pro-apoptotic miRNA in CHO, miR-466h.

We grew CHO-K1-SEAP parental cells seeded at 1×10^5 cells/mL in suspension for 13 days until cell numbers and viability ceased to decline. By day 13, cultures were 15% viable with a cell density of $\sim 2 \times 10^5$ cells/mL (Fig. 3.2).

Figure 3.2: CHO-K1-SEAP growth curve

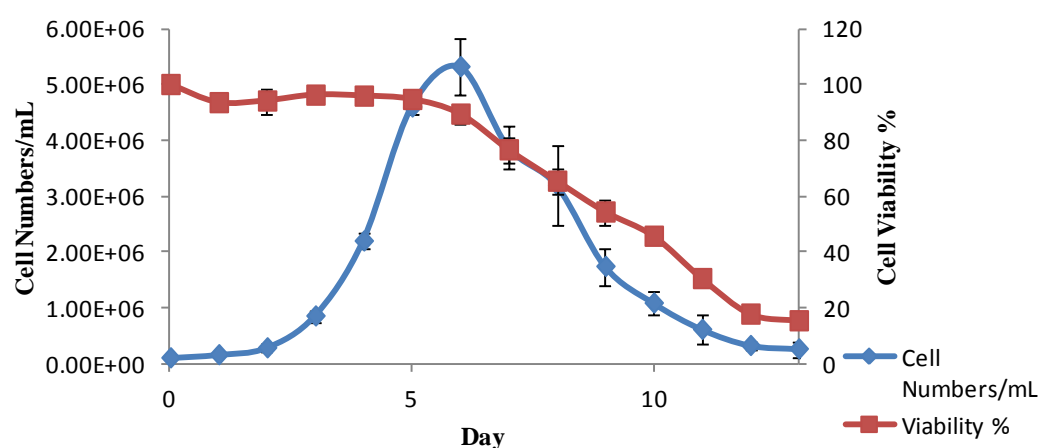


Figure 3.2: The growth profile for parental CHO-K1-SEAP cells as a means of determining the point of culture at which to harvest nutrient depleted (spent) media. Cells were seeded at 1×10^5 cells/mL and cultured until cell viability was poor (less than 20%). Cell numbers are represented in blue on the left axis while viability is shown in red on the right axis.

As the most potent impact of a miRNA was often observed at day 4 of culture, we wanted to establish an assay that would be monitored over the course of 4 days in an attempt to identify the full influence of miR-34a inhibition.

We wanted to monitor the induction of cell death by culturing CHO-K1-SEAP cells seeded at 1×10^5 cells/mL in nutrient depleted media harvested at various time points (Fig. 3.2). Cells were cultured in spent media harvested at days 2, 3 and 4 with a fresh media control included. It was observed that as the quality of media decreased the level

of exponential cell growth diminished (**Fig. 3.3 A**). Another interesting observation was that culture viability in all three media types declined initially but recovered (**Fig. 3.3 A**).

Figure 3.3: Spent medium profiling

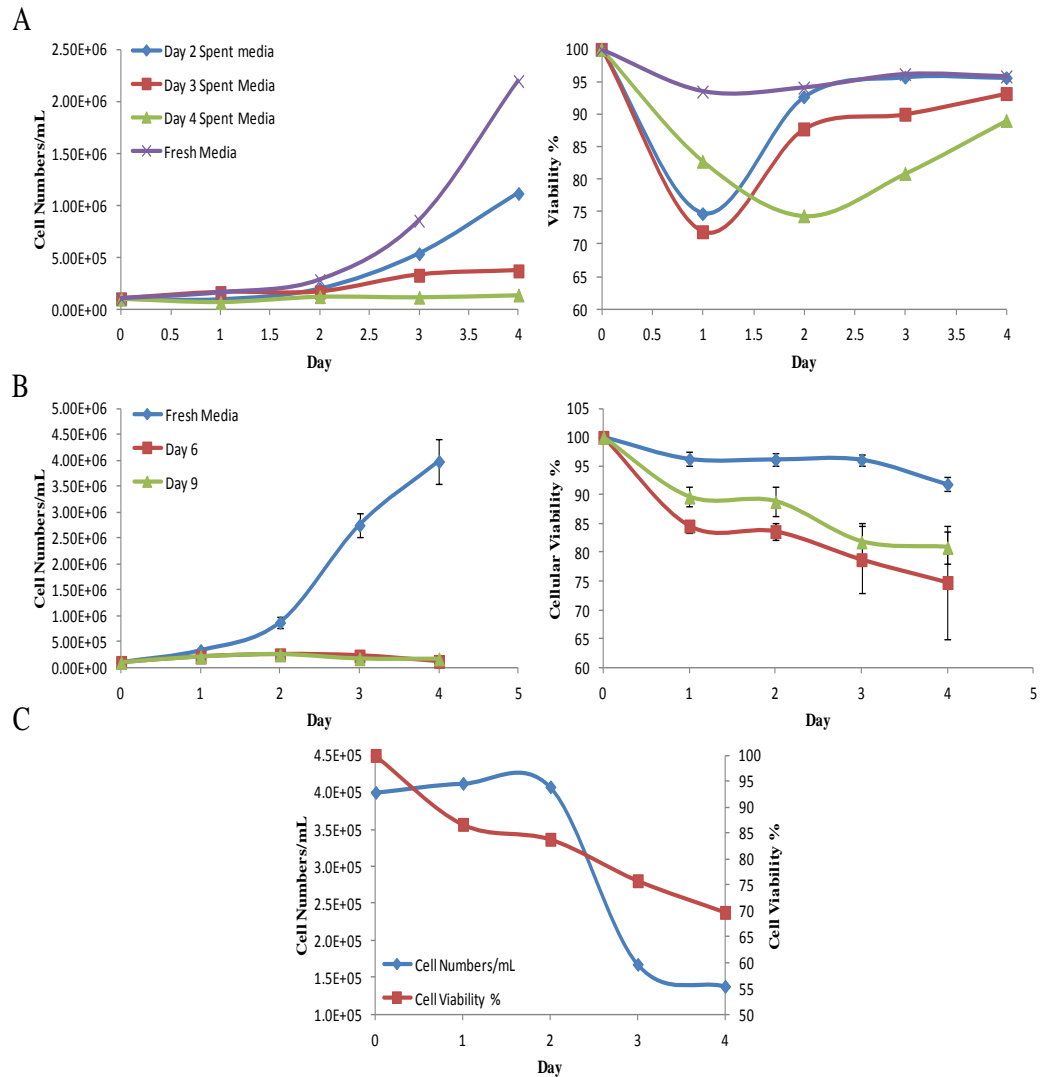


Figure 3.3: Various levels of spent media were evaluated under batch conditions in an attempt to elicit a mild and gradual impact on CHO cell growth and viability. Cells were seeded at 1×10^5 cells/mL and cultured in media harvested at A) days 2, 3 and 4 with a fresh media control B) day 6 and 9 with a fresh media control and C) day 9 media seeded at 4×10^5 cells/mL.

Next, day 6 and day 9 spent media was assessed. In this instance, cellular proliferation was dramatically reduced similar to what was observed for day 4 spent media as well as a gradual decline in cellular viability that did not recover (**Fig. 3.3 B**). Day 9 media demonstrated a more defined drop in viability as far as 70% although inconsistent upon repeat.

Finally, we attempted to increase the initial seeding density to 4×10^5 cell/mL in day 9 spent media. When this was performed there was a nice decrease in viability to a maximum of 70% on day 4 with cell numbers declining to $\sim 1.5 \times 10^5$ cells/mL. Upon repetition, cells cultured in this format were not observed to revive themselves (**Fig. 3.3 C**).

From these results, we decided to seed at 4×10^6 /mL in nutrient depleted media as it gave a more consistent decline in both viability and cell density. However, from previous experience, transfection at high cell density had proven troublesome. Increasing concentrations to 4 μ L of transfection reagent containing a negative control pre-miRNA generated a similar inhibitory growth phenotype as did for siRNA-VCP (**Appendix Fig. A3**). 50 nM of siRNA against VCP complexed with 4 μ L of transfection reagent was the only condition to reduce cell viability below 80% (88%) indicating a very low transfection efficiency.

3.2.2.2 Transient inhibition of miR-34a mildly inhibits apoptosis in CHO cells induced to undergo cell death

Several aspects of this assay were inspired by the work of Druz *et al.*, 2011 who performed viability assays by transfecting cells at high cell density ($\sim 10^6$ cells) using Lipofectamine and transferring cells into nutrient depleted media 24 h after transfection and assayed 24 h later.

In this instance we transfected CHO cells at 1×10^5 cells/mL in 2 mL of fresh culture media including a positive control (siRNA designed against VCP) using INTERFERinTM (**Fig. 3.4**). After 48 h of growth, to allow cell density to build up, cells were pelleted and resuspended in 2 mL of day 9 nutrient depleted media except for siRNA-VCP treated cells in order to gauge transfection efficiency.

Transient inhibition of miR-34a in cells induced to undergo apoptosis appeared to mildly inhibit the onset of apoptosis by 5-10% ($p \leq 0.01$). Interestingly, as previously observed, the inhibition of miR-34a also increased cellular proliferation from 1.35-2-fold ($p \leq 0.001$) over numerous replicates.

Figure 3.4: miR-34a knockdown using a modified apoptosis assay

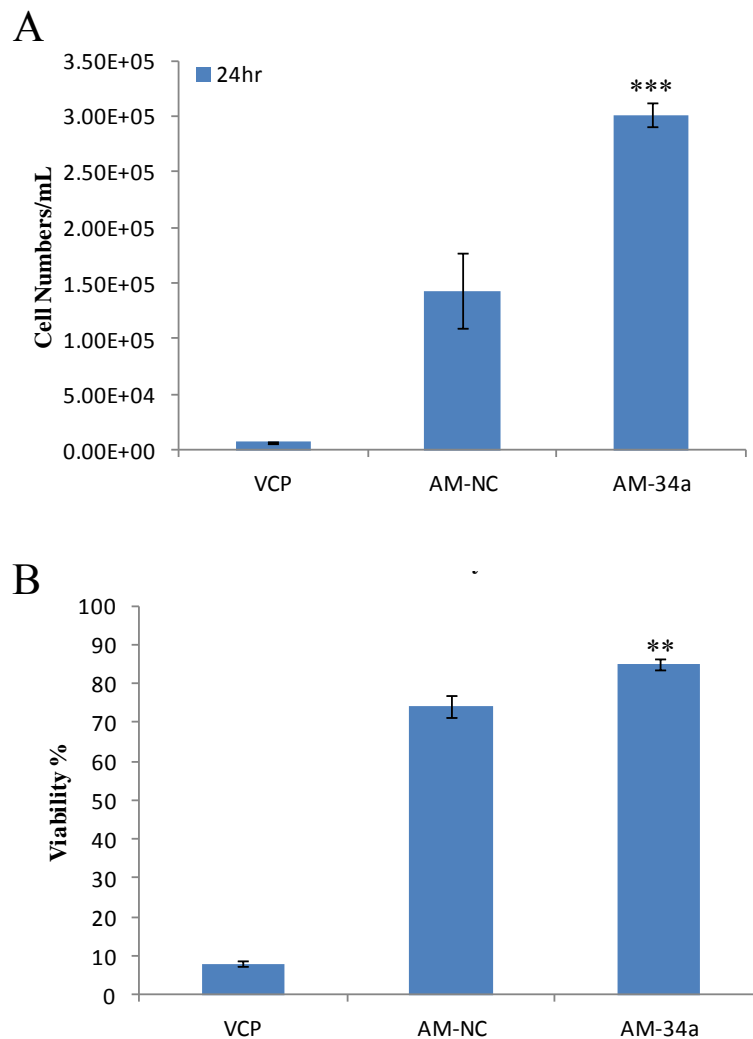


Figure 3.4: CHO grown in spent medium were assessed for A) Cell numbers/mL and B) Viability 24 h subsequent to exposure to spent media, n = 3, t-test were calculated using a standard student t-test.

3.2.3 Stable depletion of miR-34 using a microRNA sponge

With the previous observation that transient inhibition of miR-34a improved CHO cell growth and mildly inhibited apoptosis, we thought it encouraging to explore its stable depletion in both SEAP and IgG-secreting CHO cells. miR-34a has been observed to be expressed at quite low levels in CHO cells (Hackl et al. 2011) using next-generation sequencing while its counterparts miR-34b/c were expressed quite abundantly. With the single nucleotide difference lying outside the seed region, both miR-34b and miR-34c are members of the same seed family as miR-34a thus potentially targeting the same mRNAs

(Bader 2012). Stable depletion of miR-34a using a fully complementary binding sequence downstream of a deGFP sponge reporter will effectively target all three miRNAs, miR-34a/b/c. Hence forth, miR-34a when in reference to its depletion through a sponge decoy will be referred to as miR-34.

3.2.3.1 miR-34 sponge design and generation

The miR-34 miR-sponge sequence was designed to be fully complementary to its specific target miRNA with the exception of base-pair mismatches or “wobble” introduced at nucleotide locations 10-12 and placed downstream of a deGFP reporter (**Fig. 3.5**). This wobble was introduced to reduce miRNA-RISC-mediate mRNA cleavage that has been characterised to occur at nt 9-10 thus prolonging the functional half-life of the sponge construct (Kluiver et al. 2012a).

Figure 3.5: miR-34 sponge construct and miR interaction

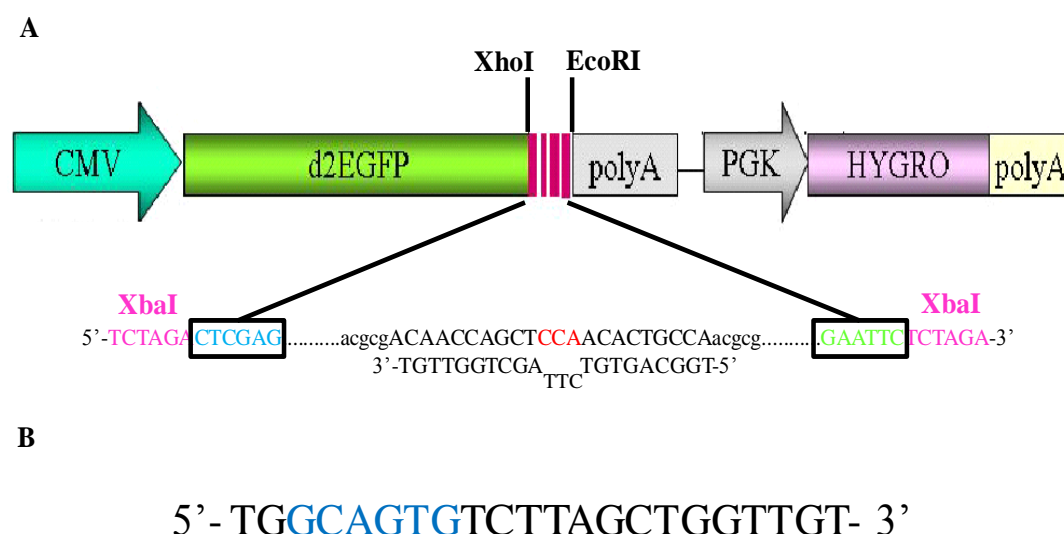


Figure 3.5: The construct that forms the miR-34 sponge, A) a destabilised GFP reporter under the transcriptional activation of a CMV promoter and a downstream polyA tail. Sandwiched between the deGFP coding sequence and polyA tail is the multiple cloning site (MCS) containing XhoI/EcoRI used for insertion of the miR-34 sponge sequence. This sequence contains four concatemeric binding sites for the miR-34 family in tandem with 5 nucleotide spacers and forms an artificial 3'UTR of deGFP. Wobble is introduced into the sponge sequence across nt 10-12 (**highlighted in red**) which serves to prolong the life time of the sponge mRNA as mRNA cleavage should be inhibited. An additional selection gene is incorporated into the sponge construct, Hygromycin resistance (HYGRO or HYG), which is used for the generation of stable CHO populations. B) The mature sequence of miR-34a with the seed sequence highlighted in **blue**.

The sequence of the miR-34 sponge construct including restriction sites is shown in **table 3.2**.

Table 3.2: miRNA sponge sequence design for miR-34

5'-3' microRNA Sponge sequence					
miR Sponge	XbaI Res.	XhoI Res.	Sponge seq.	EcoRI Res.	XbaI Res.
miR- 34a	TCTA GA	CTCG AG	acgcgACAACCAGCT CCCA ACACTGCCAac gcgACAACCAGCT CCCA ACACTGCCAacga gACAACCAGCT CCCA ACACTGCCAatgacgt ACAACCAGCT CCCA ACACTGCCAatcatc	GAA TTC	TCTA GA

The miR-34 sponge sequence pEX-A-miR-34 (**Fig. 3.6 A**) was amplified in DH5α cells to achieve a working concentration suitable for molecular cloning (see **material and**

methods section 2.4.17 for transformation protocol). Removal of the sponge sequence was carried out using the restriction enzymes *XhoI/EcoRI*. Linearization of the pdeGFP plasmid backbone was carried out using the same enzymes to generate “sticky-ends”. Both miR-34 sponge insert and backbone were isolated by gel extraction (**Fig. 3.7 A and B**, see **Materials and methods section 2.4.14**). After ligation of the miR-34 sponge sequence into the pd2EGFP-sponge vector, several colonies were picked upon ampicillin selection and mini-prepped to isolate plasmid DNA. Two restriction sites *NotI* and *XbaI* were selected to diagnose successful miR-34 sponge insertion (**Fig. 3.7 C**). A positive colony (1 or 4 from **Fig. 3.7 C**) was re-amplified to a working stock and diagnosed using the same enzymes (**Fig. 3.7 D**). miR-34 sponge vector was sequenced using the following primer:

EGFP-701-For 5'-GGACGAGCTGTACAAGAAGC-3'

Sequence alignment can be seen in **appendix figure A4**.

The miR-34 sponge and control sponge plasmid was transfected into SEAP and 1.14 secreting cells (see **Materials and Methods section 2.3.3**). 24 h after transfection, cells were selected in the presence of 350 µg/mL Hygromycin for 3 passages generating a mixed pool (MP) population. Stable cells were adapted to suspension culture in the presence of PVA (anti-clumping agent) before characterisation.

Figure 3.6: Plasmid maps for pEX-A (carrying sponge sequences) and microRNA Sponge backbone

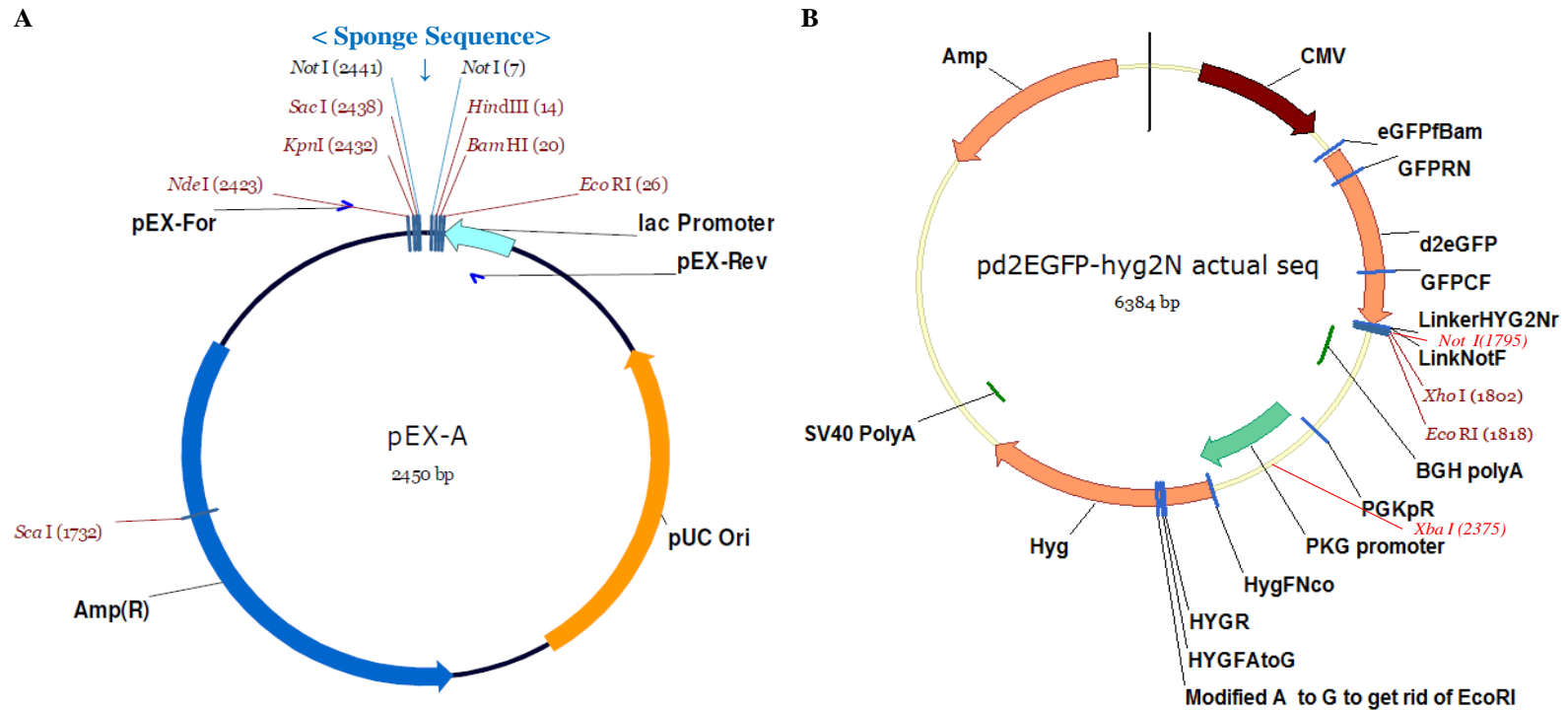


Figure 3.6: Plasmid maps for pEX-A (carrying miR-sponge sequences) and microRNA sponge backbone: A) Bacterial expression vector harbouring the microRNA sponge concatemers with an ampicillin resistance marker (proprietary plasmid from MWG Eurofins) B) microRNA sponge backbone containing multiple cloning site (MCS) with cloning restriction sites, GFP reporter construct and Hygromycin (HYGR) resistance marker.

Figure 3.7: Diagnostic gels for miR-34 sponge vector preparation

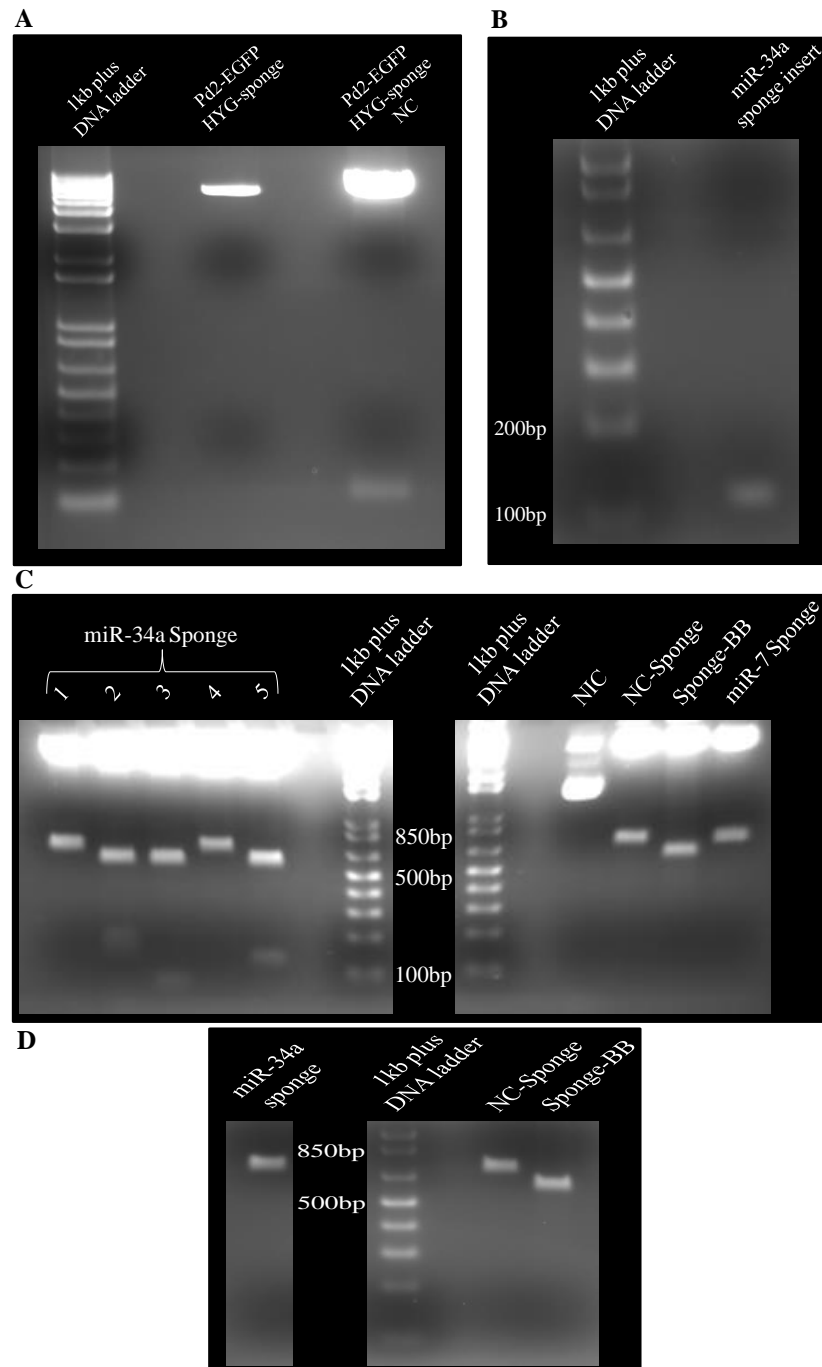


Figure 3.7: Diagnostic gels for miR-sponge preparation A) digests of the sponge backbone and a pre-made sponge negative control using restriction enzymes XhoI/EcoRI B) miR-34 sponge insert extracted using XhoI/EcoRI ran on a 2% agarose gel to confirm is successful extraction C) mini-prep digestion of miR-34 sponge bacterial colonies tested using restriction enzymes XbaI/NotI liberating successful inserts of ~750 bp. Control sponge digestions using the same restriction enzymes were carried out to include no-insert control (NIC), sponge-NC (negative control), raw sponge backbone (BB) with no insert and miR-7 sponge.

3.2.3.2 Confirmation of miR-34 sponge binding efficacy

To assess the binding efficiency of the miR-34 sponge for endogenous miR-34 family members, we transiently introduced mature miR-34a pre-miRNA into both miR-34 and miR-NC sponge mixed pool populations. The varying GFP intensities indicated the generation of mixed populations for both plasmids (Random integration) (**Fig. 3.8 A**). Cells expressing the miR-34 sponge exhibited a lower average GFP expression when assessed flow cytometry when compared to miR-NC spg (**Fig. 3.8 B**). This reduced average GFP expression was potentially due to endogenous miR-34 interacting with and repressing GFP translation. Transient introduction of a pre-miRNA duplex specific for miR-34a resulted in a 90% ($p \leq 0.001$) reduction in GFP fluorescence in the case of the miR-34 sponge mixed pool (**Fig. 3.8 B**). A reduction in GFP expression was also observed in the case of miR-NC sponge upon miR-34a overexpression but not as dramatic as in the case of miR-34 sponge, possible a side-effect of miR-34's known impact on cell growth.

The average reduced GFP expression in miR-34 sponge cells was reflected again when a clonal panel was isolated from both mixed pools potentially due to endogenous miR-34 (**Fig. 3.9**). A range in GFP expression can also be observed for all sponge panels due to random integration. The GFP intensity was observed to be much higher in CHO-1.14 cells stably transfected with miR-34 and miR-NC sponge constructs. This could potentially be due to a reduced transfection efficiency in the case of CHO-SEAP cells. Furthermore, the integration efficiency or transcriptional activity may be higher in the case of CHO-1.14s contributing to this significant GFP expression difference.

Figure 3.8: miR-34 sponge binding efficiency

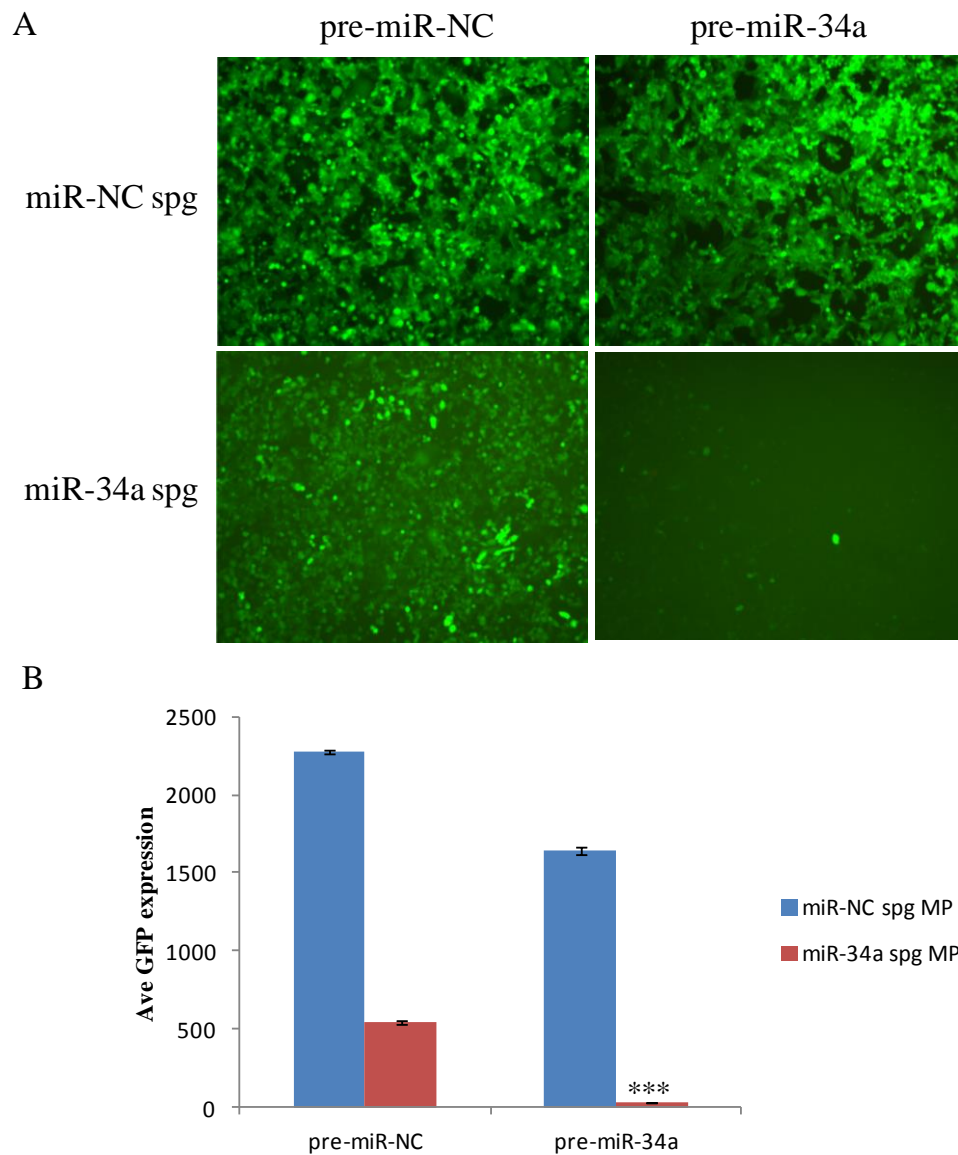


Figure 3.8: The binding efficacy of the miR-34 sponge construct when miR-34a was transiently over expressed. A) Visually demonstrates the intensity of GFP in both mixed populations (miR-34 and miR-NC sponge) transfected with either pre-miR-NC or pre-miR-34a. B) GFP intensity of both mixed pools is further demonstrated using the Guava ExpressPlus programme. Statistical analysis was carried out using a standard student t-test ($p \leq 0.001^{*}$).**

Figure 3.9: GFP profile of miR-34 sponge clonal panels in CHO-SEAP and CHO-1.14 cells

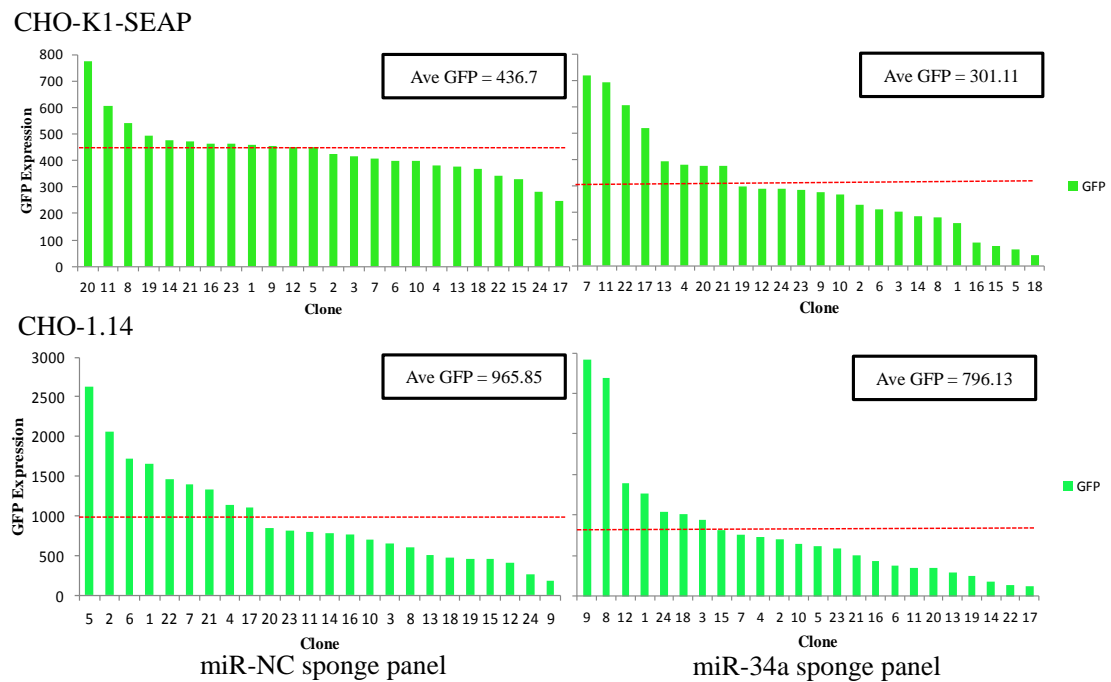


Figure 3.9: The GFP expression of 24 clones isolated from both miR-34 and miR-NC sponge mixed populations using FACS sorting in both CHO-K1-SEAP and CHO-1.14 cells. Average GFP expression calculated across each panel condition is represented as a broken red line.

3.2.3.3 miR-34a overexpression potentially inhibits conserved targets

Prior to miR-34 sponge characterisation, we sought to identify potential mRNA targets that miR-34a was regulating. A small list of validated miR-34a targets were screened upon transient overexpression of miR-34a in CHO-K1-SEAP cells. Targets were identified and chosen from the review by Andreas G. Bader (Bader 2012) (**Table 4.1 in Discussion**). Primers were designed based on the CHO sequence genome database (<http://www.chogenome.org/>). Primer sequences are shown in **table 2.1 of materials and methods section 2.4.3**. RNA was harvested 24 h after transfection (see **section 2.4.6 of Materials and Methods**) and reverse transcribed (see **section 2.4.2 of Materials and Methods**). Semi-quantitative PCR was carried out on a small subset of targets including *E2F3*, *BCL2*, *CCND1*, *DCR-1*, *CDK4*, *CDK6* and *FUT8* using β -actin as an endogenous control (**materials and methods section 2.4.3**).

Cells were assayed 48 h after transfection as a means to confirm both transfection efficiency and retention of the miR-34a induced phenotype (**Fig. 3.10 A**). Gel-based visualisation indicated that several cell cycle-related targets were under the influence of miR-34a with *CCND1* potentially the most dramatic (**Fig. 3.10 B**).

Real-time quantitative (qRT)-PCR using SYBR[®] Green (see **section 2.4.4 of Materials and Methods**) showed a 50% ($p \leq 0.001$) reduction in the mRNA abundance of *CCND1* (**Fig. 3.10 C**).

Figure 3.10: semi-quantitative and qRT-PCR identification of miR-34a targets

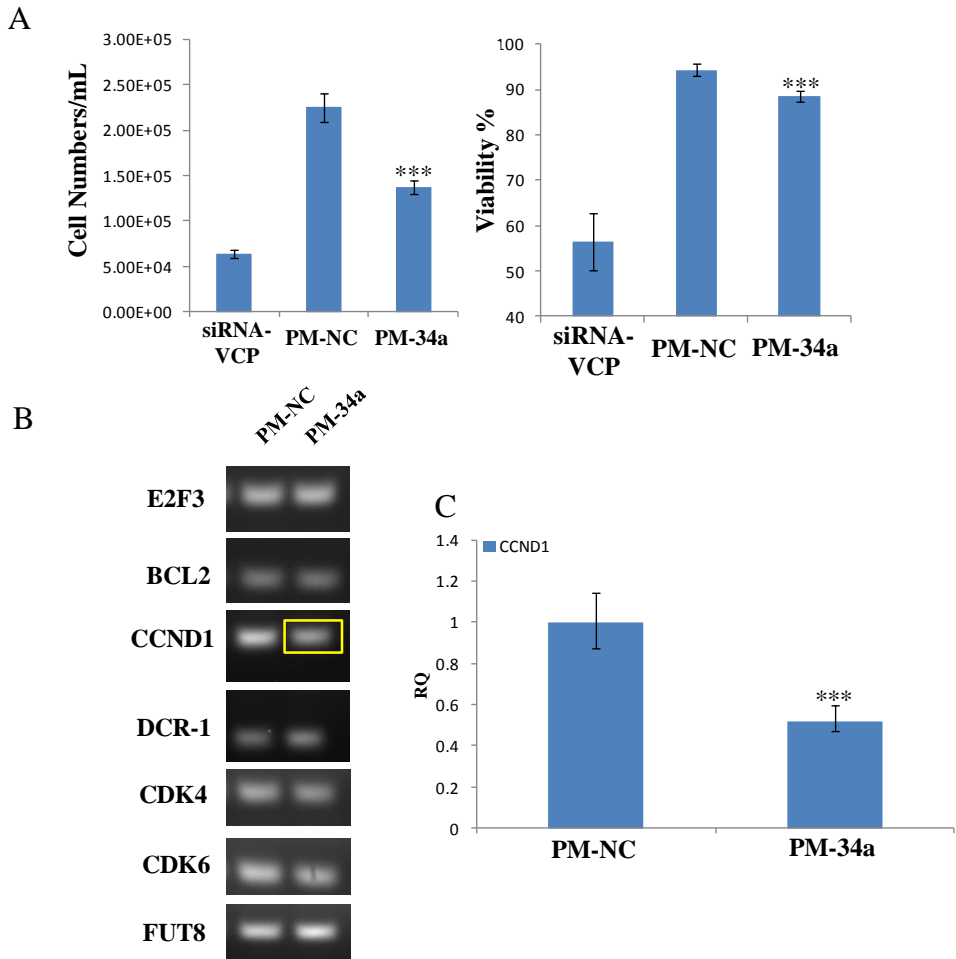


Figure 3.10: Assessment of validated miR-34a targets upon miR-34a over-expression (PM-34a) compared to a negative control (PM-NC) in addition to a positive control (siRNA-VCP) A) Influence of miR-34a overexpression on proliferation and viability in CHO-SEAP cells 24 h post transfection. B) Gel-based semi-quantitative PCR using a panel of primers for validated targets. C) Real-time quantitative PCR on *CCND1* upon miR-34a overexpression when compared to pre-miR-NC transfection. Statistical analysis was calculated based on cyclic threshold (C_t) values using a standard student t-test ($p \leq 0.001^{*}$).**

3.2.3.4 miR-34 sponge influence on endogenous miR-34a and CCND1

To further explore the influence of the miR-34 sponge on the endogenous levels of miR-34a, we evaluated the levels of miR-34a in a stable CHO-1.14 clone expressing our miR-sponge. We further assessed the levels of *CCND1*, which were shown to be reduced by 50% upon transient miR-34a overexpression, in the same clone to identify if its levels were increased.

miR-34a abundance was assessed using Singleplex Taqman qRT-PCR (**section 2.4.8 of Materials and Methods**) on three miR-NC-spg clones and three miR-34 spg clones. A ~5-fold reduction in the mature levels of miR-34a ($p \leq 0.001$) was observed in clones engineered with the miR-34 sponge when compared to non-specific controls (**Fig. 3.11 A**).

Next siRNA-mediated knockdown of the miR-34 sponge construct was carried out in miR-34 sponge clone 21.

Knockdown of the miR-34 sponge was achieved using a siRNA designed against the GFP (siGFP) gene sequence. RNA was harvested 72 h after transfection and qRT-PCR was carried out for mature miR-34a expression. As observed before, the miR-34 sponge clone exhibited a 5-7-fold reduction in mature miR-34a levels when compared to the miR-NC sponge control (**Fig. 3.11 B**). However, a 2-fold increase in the mature levels of miR-34a was observed in the case of miR-34 sponge treated with siGFP compared to miR-NC-treated miR-34 sponge (**Fig. 3.11 B**). Knockdown of the miR-34 sponge was demonstrated by a 90% ($p \leq 0.001$) reduction in GFP expression (**Fig. 3.11 B inset**). The levels of miR-34a however did not return to levels comparable with that of the miR-NC sponge control (**Fig. 3.11 B**) which could potentially be due to the presence of residual sponge construct. This does however, indicate that the miR-34 sponge construct is specific for miR-34.

Finally, we attempted to assess the impact that the miR-34 sponge construct exerted on a previously validated target of miR-34a, *CCND1*. The greatest difference was observed in the case of miR-34 sponge clone 21 which demonstrated a 1.2-3.5-fold increase in endogenous *CCND1* levels when compared to all three control sponge clones (**Fig. 3.11 C**). However, the abundance of *CCND1* in 2 of the 3 miR-34 sponge clones (3 and 4) exhibited lower levels when compared to 2 of the 3 control clones (15 and 20).

Figure 3.11: The influence of stable miR-34 sponge expression on miR-34a and CCND1 abundance

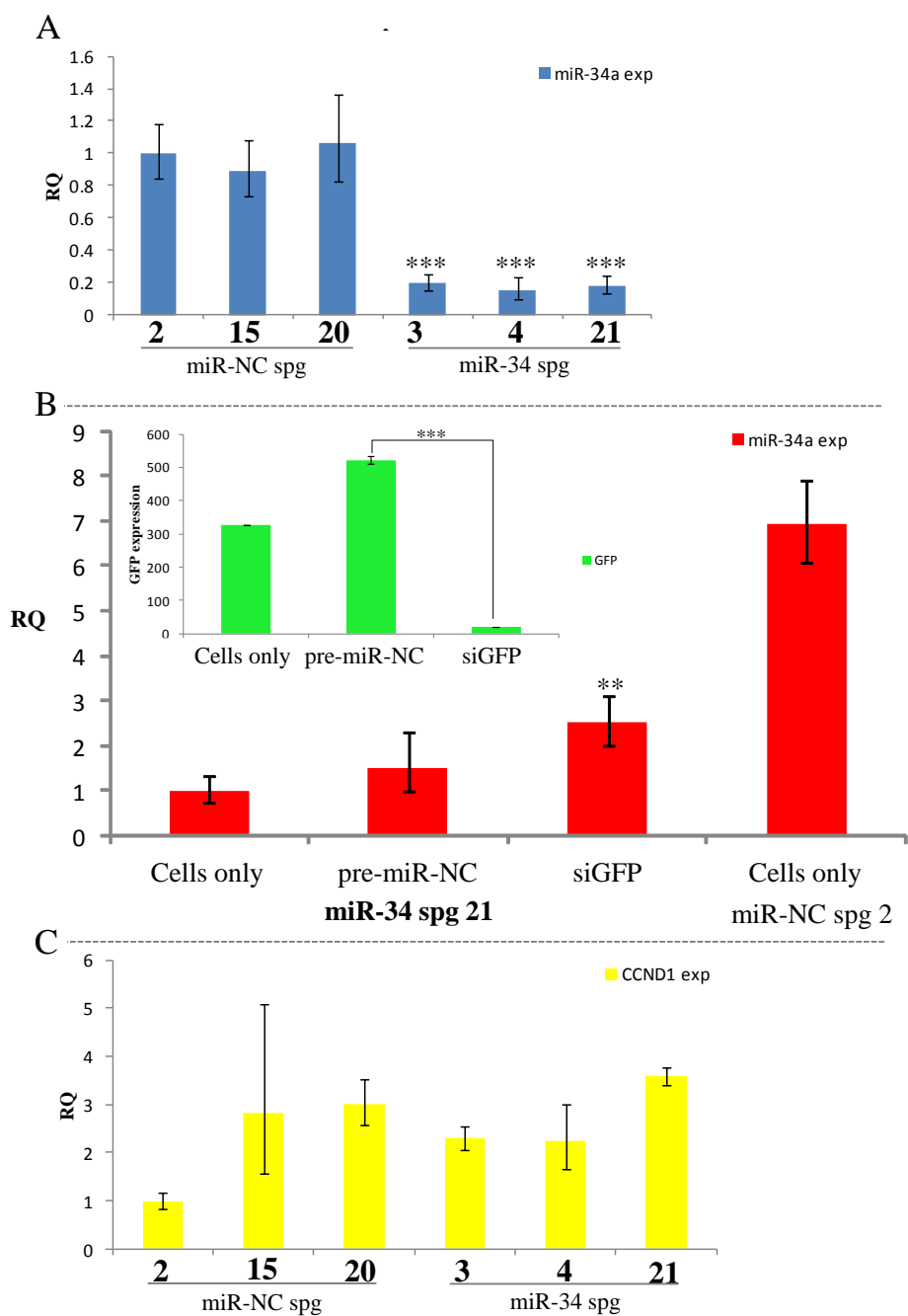


Figure 3.11: Impact of the miR-34 specific sponge on the endogenous levels of mature miR-34a and the target CCND1. A) Taqman qRT-PCR for miR-34a in a panel of miR-34 and control sponge clones. B) [Inset] The knockdown of the miR-34 sponge construct using siGFP compared to pre-miR-NC control. Endogenous levels of miR-34a in a miR-34 sponge clone untreated (Cells only) and transfected with a control (pre-miR-NC) and siRNA for GFP (siGFP). Endogenous levels of miR-34a are also shown for an untreated control sponge clone (miR-NC spg 2) compared to cells only miR-34 spg 21 C) qRT-PCR for the validated miR-34a target, CCND1.

3.2.4 Evaluation of miR-34 depletion in CHO mixed pool populations

Two CHO cell lines (CHO-SEAP and CHO-1.14) secreting recombinant human-secreted alkaline phosphatase (SEAP) and the more industrially relevant antibody (IgG) were generated using the miR-34 sponge construct discussed earlier in **section 3.2.3.1**. Both stable mixed pools were evaluated under several culture conditions in an attempt to identify the potential benefit of the stable inhibition of miR-34.

3.2.4.1 miR-34 depletion in CHO-K1-SEAP cells

miR-34 sponge CHO-SEAP mixed pools - Batch

Stable miR-34 sponge mixed populations were cultured in batch mode over a 6 day period and sampled every 48 h along with a non-specific control sponge population. Cells were seeded initially at 2×10^5 cells/mL in a 5 mL culture volume of CHO-S-SFM II in the absence of Hygromycin selection reagent.

There was a 55% ($p \leq 0.05$) improvement in cell density on day 2 of culture (**Fig. 3.12 A**). Repeated experiments demonstrated increased growth over various stages of the culture process. Furthermore, cellular viability appeared to be mildly enhanced by 6-15% ($p \leq 0.05$) late in culture across all three replicates (**Fig. 3.12 B**).

No impact was observed on volumetric SEAP yield when both test and controls were compared (**Fig. 3.12 C**). However, the increase in cell numbers on day 2 of culture correlated with a reduction in normalised productivity (**Fig. 3.12 D**).

Figure 3.12: Stable miR-34 sponge mixed pool CHO-SEAP under batch conditions

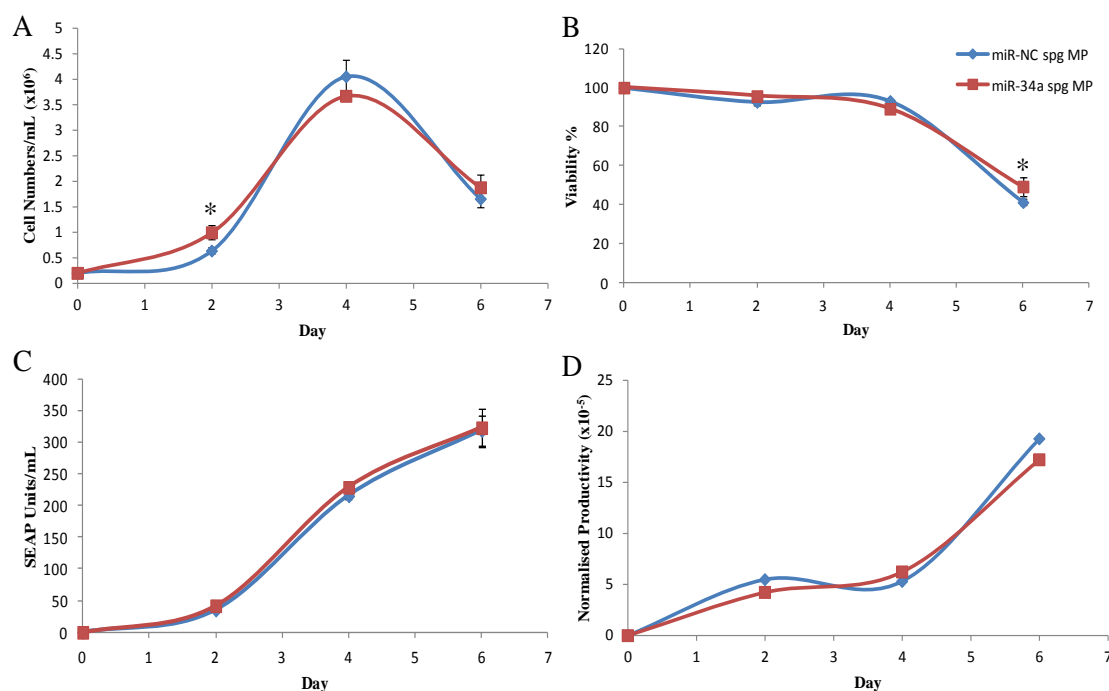


Figure 3.12: The influence of stable miR-34 depletion in batch mode is demonstrated compared to a negative control sponge. A) Cells numbers sampled on day 2,4 and 6 B) Cellular viability C) Volumetric SEAP yield/mL designated as SEAP Units D) Normalised SEAP activity.

miR-34 sponge CHO-SEAP mixed pool – Fed-batch

Feeding strategies are commonly implemented in biopharma as a means to further boost maximal cell densities and mediate a prolonged viable production phase. An initial feed of 15% (v/v) of CD CHO-Efficient Feed A was supplemented on day 0 of culture with subsequent feeding of 10% (v/v) every 3 days of culture. Cell growth was dramatically enhanced in the case of the non-specific control by almost 2-fold at its apex upon feed addition, however, this was not observed in the case of miR-34 pools (**Fig. 3.13 A**). Cellular viability on day 8 of culture was reduced in the miR-34 sponge population by ~20% (**Fig. 3.13 B**). However, both volumetric SEAP and specific productivities were observed to be enhanced by a range of about 1.6 to 3-fold in miR-34 depleted pools (**Fig. 3.13 C and D**).

Figure 3.13: Stable miR-34 sponge mixed pool CHO-SEAP under fed-batch conditions

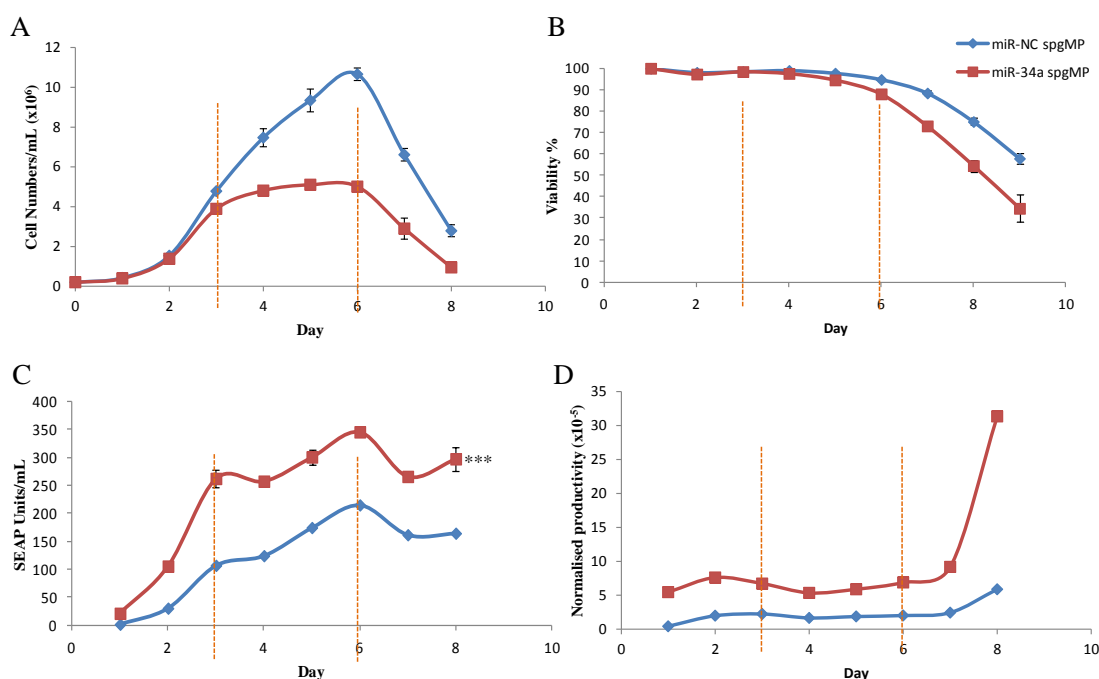


Figure 3.13: Fed-batch (feed represented as a broken orange line) results for the miR-34 sponge mixed pools alongside a non-specific control sponge assessed over the course of a 6 day culture. A) Cell Numbers/mL B) Cellular viability C) Volumetric SEAP yield D) Specific SEAP productivity (n = 3), statistics were carried out using a paired student t-test ($p \leq 0.001^{*}$).**

3.2.4.2 miR-34 depletion in IgG-secreting CHO-1.14 cells

miR-34 sponge CHO-1.14 mixed population - Batch

A 40% ($p \leq 0.01$) improvement in cell density was recorded on day 2 of culture with a 20% ($p \leq 0.001$) increase observed on day 4 and 6 when compared to controls (**Fig. 3.14 A**). Cell density was improved consistently across separate replicates but varied in magnitude with viability appearing unaffected (**Fig. 3.14 B**). Volumetric IgG (see section **2.6.8 of Materials and Methods**) was determined to be unchanged with a small increase of about 10% late in culture (**Fig. 3.14 C**). This could potentially be due to the elevated cell numbers, as cell specific productivity was reduced (**Fig. 3.14 D**).

Figure 3.14: Stable miR-34 sponge mixed pool CHO-1.14 under batch conditions

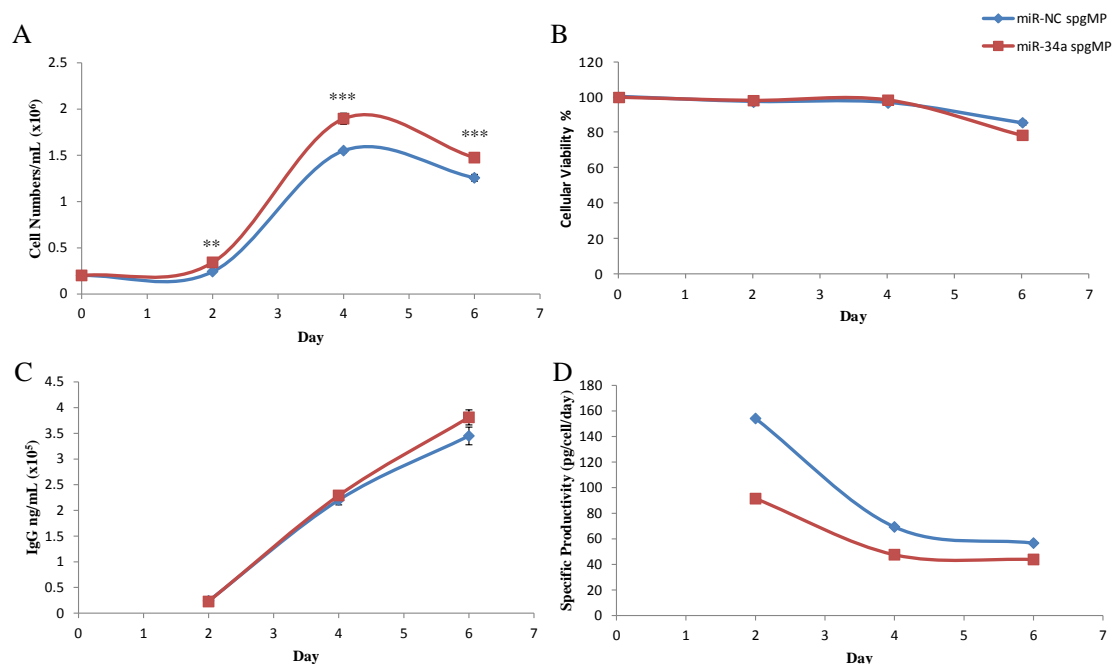


Figure 3.14: CHO-1.14 cells stably engineered to inhibit miR-34 were cultured under batch conditions and sampled over the course of a 6 day batch process reporting on the phenotypes, A) Cell numbers/mL B) Cellular viability C) Volumetric titres, IgG ng/mL and D) Cell specific productivity.

3.2.5 Generation of miR-34 sponge clones

As a means of further investigating the phenotype observed within the mixed populations, we isolated a panel of clones from the mixed pools using fluorescent activated cell sorting (FACS, see section 2.3.4 of Materials and Methods).

3.2.5.1 GFP fluorescence across clonal panels

Clones were selected that exhibited a medium-to-high GFP intensity as a means to isolate clones that expressed the miR-34 sponge at levels sufficient to sequester all endogenous miR-34a/b/c. A range of GFP intensities were observed across all clonal panels in both cell lines (**Fig. 3.9**). Both miR-34 sponge clone panels were assessed for performance in 1 mL batch suspension culture.

3.2.5.2 Impact of miR-34 depletion across a CHO-SEAP cell panel

Previous characterisation in mixed pools indicated that in fed-batch culture, stable miR-34 inhibition potentially enhanced specific productivity while batch conditions mildly enhanced CHO cell growth with no benefit to volumetric SEAP yield. Upon clonal isolation, clones were seeded at 1×10^5 cells/mL and cultured over a 6 day suspension batch process in parafilm sealed 24-well culture plates. As in the case of previous batch processes, samples were taken every 48 h and assessed for the primary phenotypes, growth, viability and productivity. Phenotypic characterisation was carried out across the entire panel of clones, both test and control, in an effort to assess the average impact of miR-34 depletion in addition to isolating exceptional clones.

When cultured in a 24-well format, miR-34 depleted clones did not display a similar phenotype to what was indicated in mixed pool batch culture. Growth was reduced by ~30% ($p \leq 0.01$), ~75% ($p \leq 0.001$) and ~80% ($p \leq 0.01$) on day 2, 4 and 6, respectively (**Fig. 3.15**). Furthermore, although the average performance was reduced, not a single miR-34 depleted clone demonstrated higher growth than the top control performers. This reduced growth was observed in 1 mL culture despite mixed pools and subsequently selected clones demonstrating “normal” growth patterns in 5 mL.

Figure 3.15: CHO-SEAP miR-34 sponge clonal panel – Cell Numbers/mL

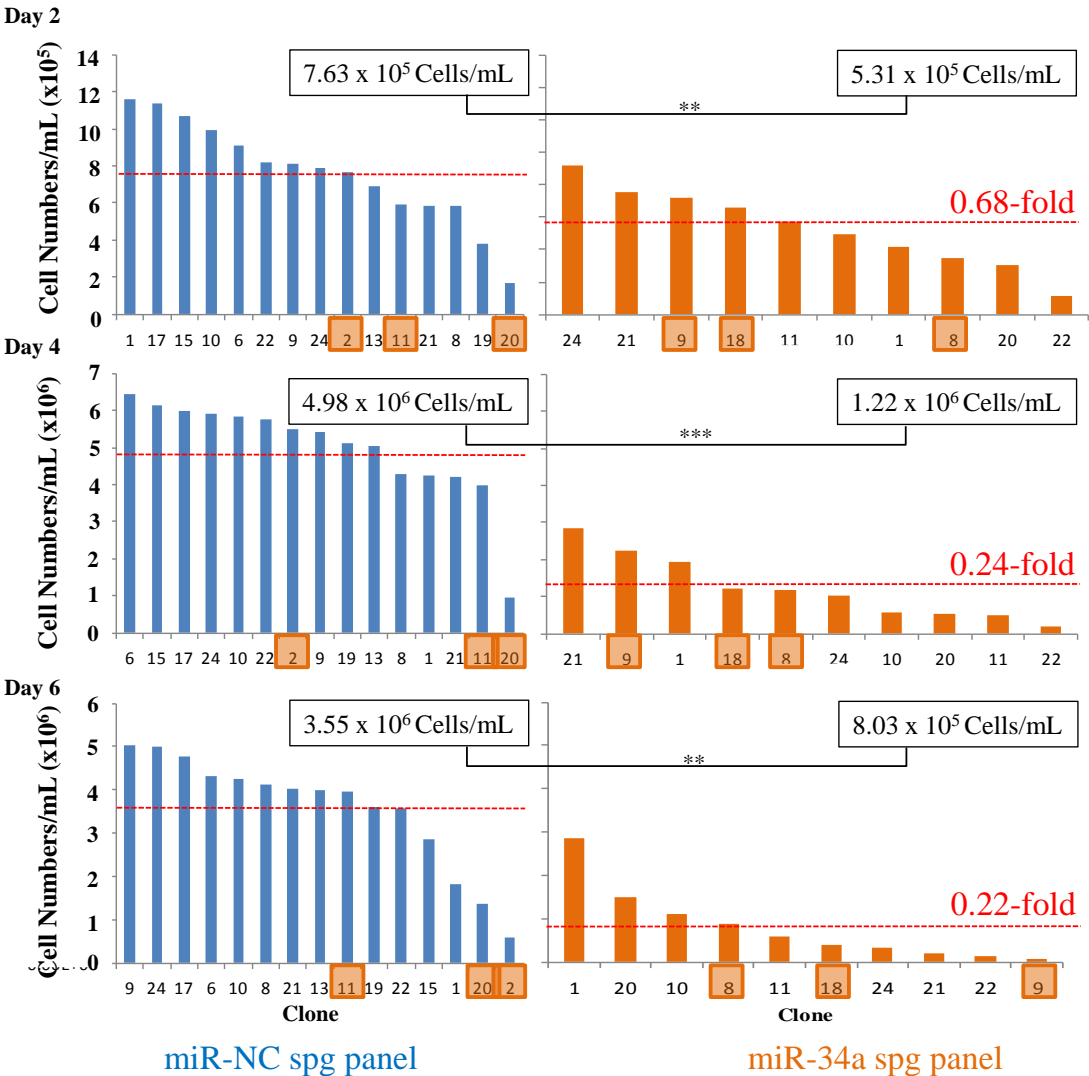


Figure 3.15: Growth of individual miR-34 and miR-NC stable sponge clones in 1 mL batch conditions. Average panel performance at each time point is represented as a **broken red line**. Clones highlighted in an **orange box** are clones that were subsequently selected for further characterisation. Statistical analysis was carried out using a standard student t-test ($p \leq 0.01^{**}$ and $p \leq 0.001^{***}$).

Figure 3.16: CHO-SEAP miR-34 sponge clonal panel – Cellular Viability

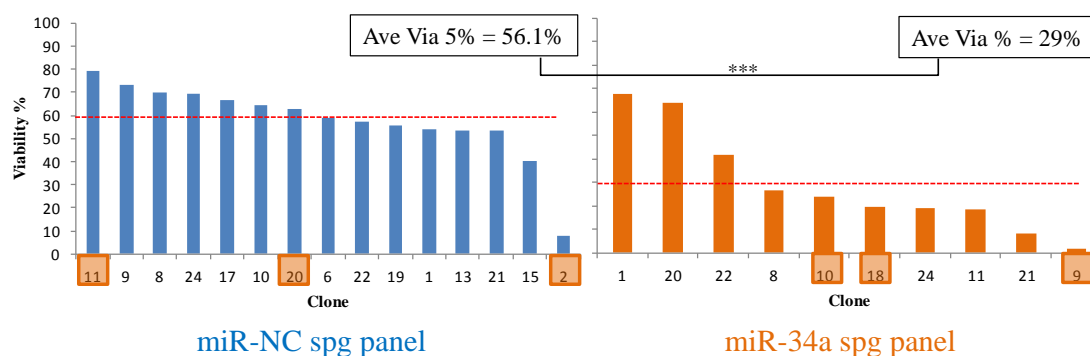


Figure 3.16: Clonal viability in both miR-34 and miR-NC sponge stable CHO-SEAP panels on day 6 of culture. There was no gross difference in clonal cell viability on the preceding time points of day 2 and 4. Average viability across each clonal panel is represented as a **broken red line. Clones selected for scale up are highlighted in an **orange box**. Statistical analysis was carried out using a standard student t-test ($p \leq 0.001^{***}$).**

The majority of miR-34 depleted clones preformed significantly worse than the panel of miR-NC spg clones with a considerable reduction in average viability from 56% in the case of the control panel to 29% ($p \leq 0.001$) in the case of the miR-34 test panel (**Fig. 3.16**).

Figure 3.17: CHO-SEAP miR-34 sponge clonal panel – Volumetric SEAP yield/mL

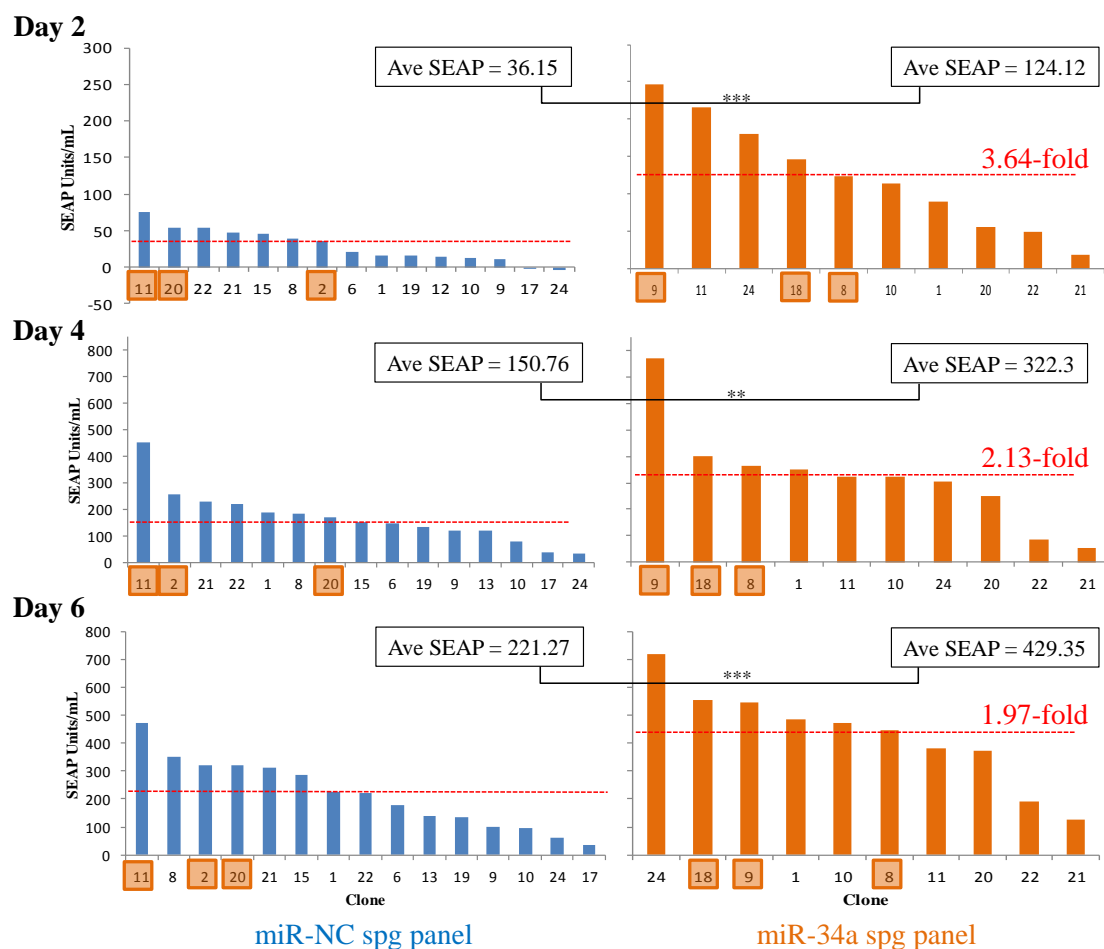


Figure 3.17: Volumetric output of SEAP/mL of each clone in both the miR-34 and miR-NC sponge panels. The average SEAP yield across each panel is represented as a broken red line while each clone subsequently selected for scale up is highlighted in an orange box. Statistical analysis was carried out using a standard student t-test ($p \leq 0.01^{}$ and $p \leq 0.001^{***}$).**

A significant 3.64-fold ($p \leq 0.001$), 2.13-fold ($p \leq 0.01$) and 1.97-fold ($p \leq 0.001$) increase was observed when the average volumetric SEAP yields of the miR-34 sponge panel was compared to the miR-NC spg panel on days 2, 4 and 6, respectively (**Fig. 3.17**).

Figure 3.18: CHO-SEAP miR-34 sponge clonal panel – Specific SEAP productivity

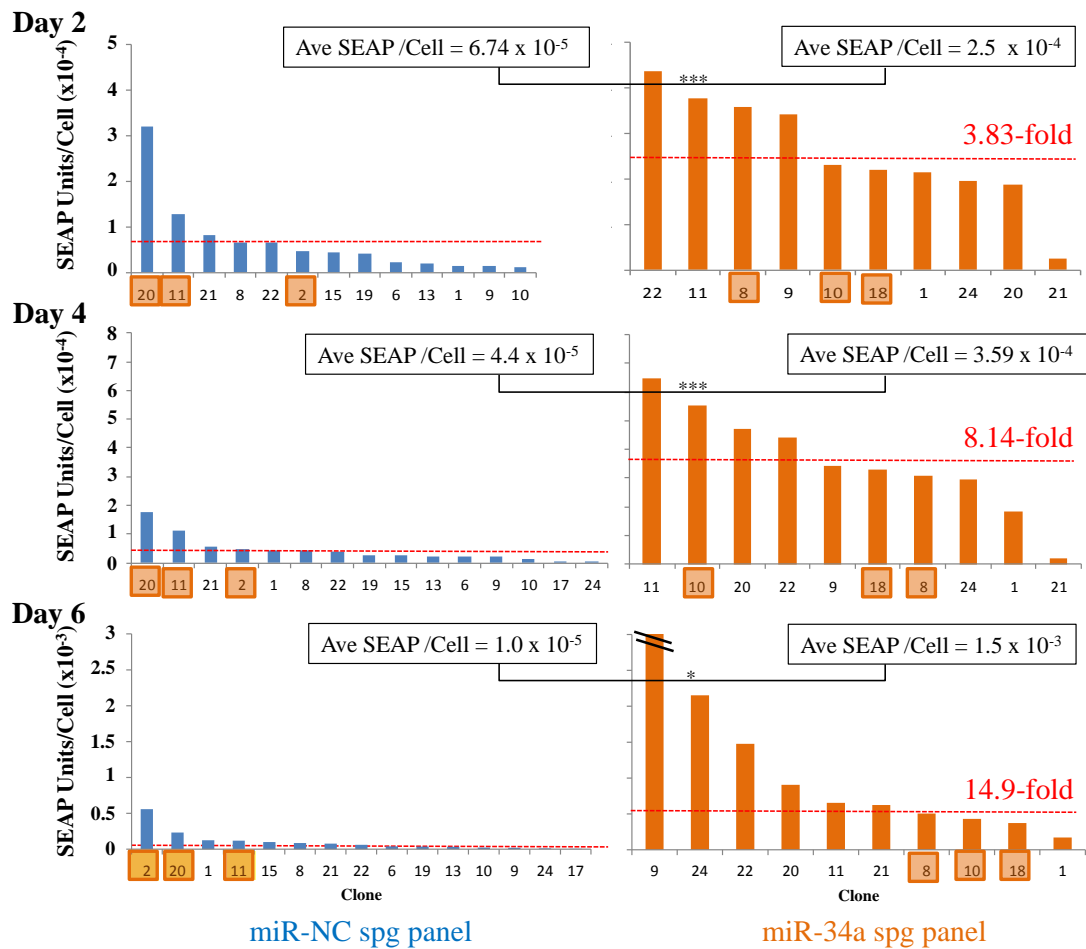


Figure 3.18: Normalised SEAP productivity per cell for each clone within both miR-34 and miR-NC sponge panels. Average normalised productivity is represented as a broken red line while clones selected for scale up are highlighted in orange boxes. Normalised productivity was calculated based on the value of SEAP produced divided by the number of cells present. The outlier (miR-34a sponge clone 9-day 6) has a value of 7.96×10^{-3} . Statistical analysis was calculated using a standard student t-test ($p \leq 0.05^*$ and $p \leq 0.001^{*}$).**

An increase of 3.83-fold ($p \leq 0.001$), 8.14-fold ($p \leq 0.001$) and 14.9-fold ($p \leq 0.05$) was observed in normalised productivity for the miR-34 sponge panel (**Fig. 3.18**).

There was no indication that viability was enhanced by the stable depletion of miR-34. Furthermore, at this scale, growth appeared to be diminished in comparison to control clones. For these reasons, to eliminate bias, clones were selected based on their

volumetric productivity attributes, a process that was indicated to be enhanced during the fed-batch cultivation in mixed pools. Clones 8, 10 and 18 were selected from the miR-34 sponge panel while clones 2, 11 and 20 were selected from the miR-NC sponge panel (highlighted in orange boxes, **Fig. 3.17**). The clones selected demonstrated a spread within the other phenotypic categories such as viability and growth; however, attempting to encompass all performance categories into the one clone would have compromised the selection of high SEAP producers and would ultimately give an inappropriate indication of performance. The clones selected were progressed for further study in 5 mL culture scale up. By selecting clones based on their enhanced productivity attributes, this could potentially introduce a bias when clones are scaled up to higher culture volumes. Clones have been seen across the literature to perform differently within various culture formats. By selecting clones based on phenotypic attributes other than those suggested to be enhanced during mixed population assays, a bias can be introduced thereby selecting clones whose observed phenotypes are potentially not a result of miRNA intervention. This should be considered throughout this thesis for all clones.

3.2.5.3 Impact of miR-34 depletion across a CHO-1.14 cell panel

We previously showed that the CHO-1.14 mixed pools grew to better cell densities in batch culture without any impact on cell viability or product yield. This improvement was not maintained when pool-derived clones were cultured in 24-well plates.

Cell growth across all time points was reduced by 22% ($p \leq 0.05$), 8% and 39% ($p \leq 0.01$) on days 2, 4 and 6, respectively when compared to non-specific controls (**Fig. 3.19**). Additionally, no clone within the miR-34 sponge panel demonstrated a superior growth capacity to any of the top performing controls.

Figure 3.19: CHO-1.14 (IgG) miR-34 sponge clonal panel – Cell Numbers/mL

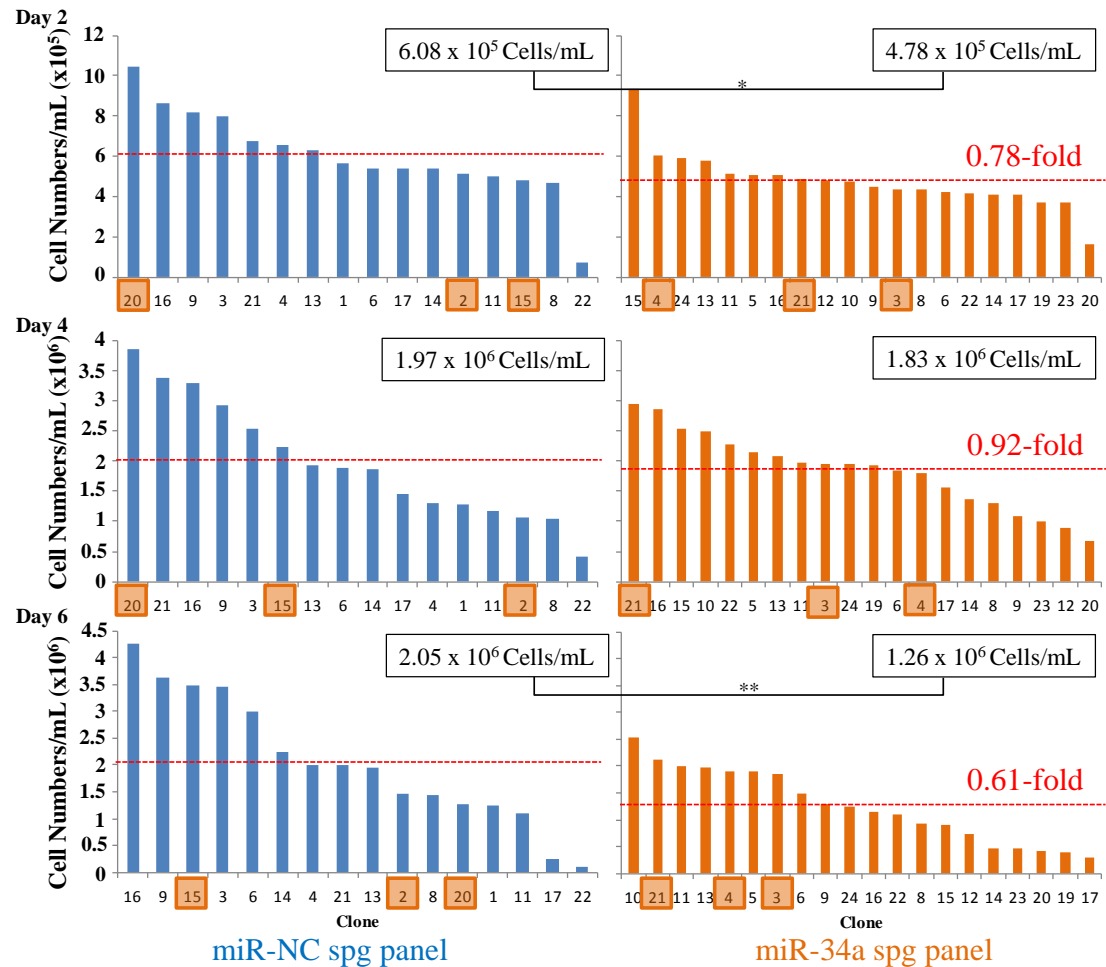


Figure 3.19: The individual growth performance of the clones that make up the miR-34 and miR-NC sponge panels with the average growth being represented as a broken red line. Clones that were subsequently selected for scale up are highlighted in orange boxes. Statistical analysis was carried out using a standard student t-test to include all clones ($p \leq 0.05^*$ and $p \leq 0.01^{}$).**

Cellular viability remained constant in the early stages of culture (Days 2 and 4, Data not included). Within each population there were some poor performers but the average viability across miR-NC and miR-34 sponge was 63.4% and 66%, respectively (**Fig. 3.20**).

Figure 3.20: CHO-1.14 (IgG) miR-34 sponge clonal panel – Cell Viability %

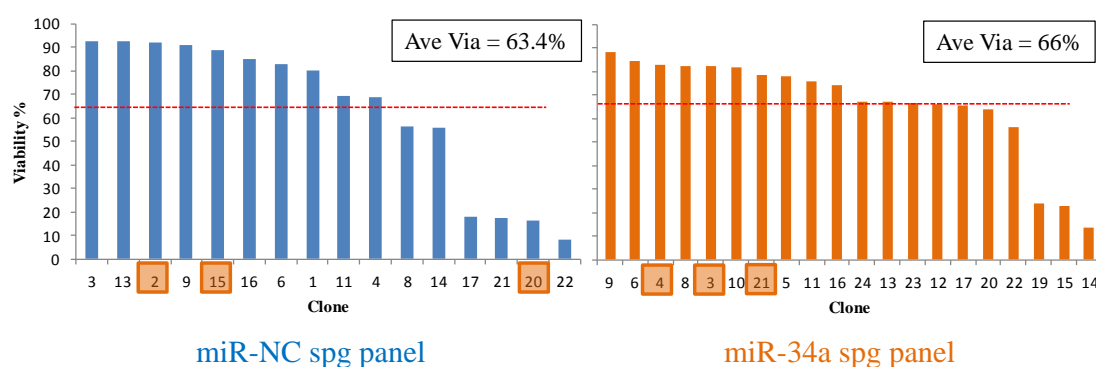


Figure 3.20: The cellular viability of each individual clone of both miR-34 and miR-NC stable sponge clonal panels with the average viability across each panel being represented as a broken red line. Clones that were selected for scale up are highlighted in orange boxes.

When volumetric IgG levels were assessed, there were a large number of clones that did not produce IgG above the detectable limits of the ELISA assay. Although these poor performing clones did pull down the average performance across the population, there were still some reasonably high performing clones within both groups. There was an average reduction of 23%, 36% and 28% observed in volumetric IgG on days 2, 4 and 6 of culture, respectively (**Fig. 3.21**). No single clone from the miR-34 sponge panel demonstrated a volumetric IgG output above the top performing clone from the control group. However, clones that did produce IgG did so above the average level of the control panel.

Figure 3.21: CHO-1.14 (IgG) miR-34 sponge clonal panel – Volumetric productivity

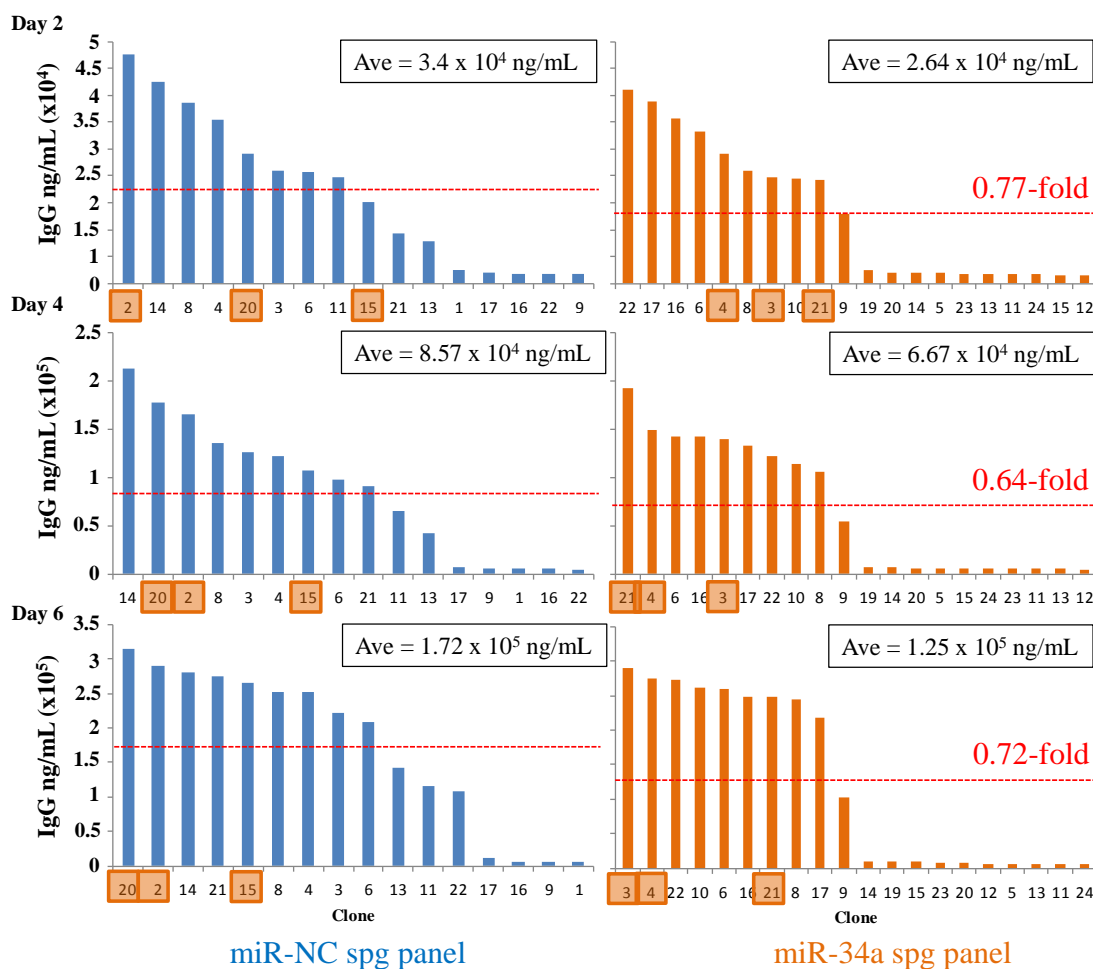


Figure 3.21: Volumetric IgG secreted product of all individual clones within both the miR-34 and miR-NC sponge clonal panels. The average IgG product across each panel is represented as a broken red line. Clones subsequently selected for scale up are highlighted in an orange box.

It is not surprising that when the specific productivities of each panel was calculated the values observed reflected that of the proliferative capacity of each clone versus their volumetric output (**Fig. 3.22**).

Figure 3.22: CHO-1.14 (IgG) miR-34a sponge clonal panel – specific productivity

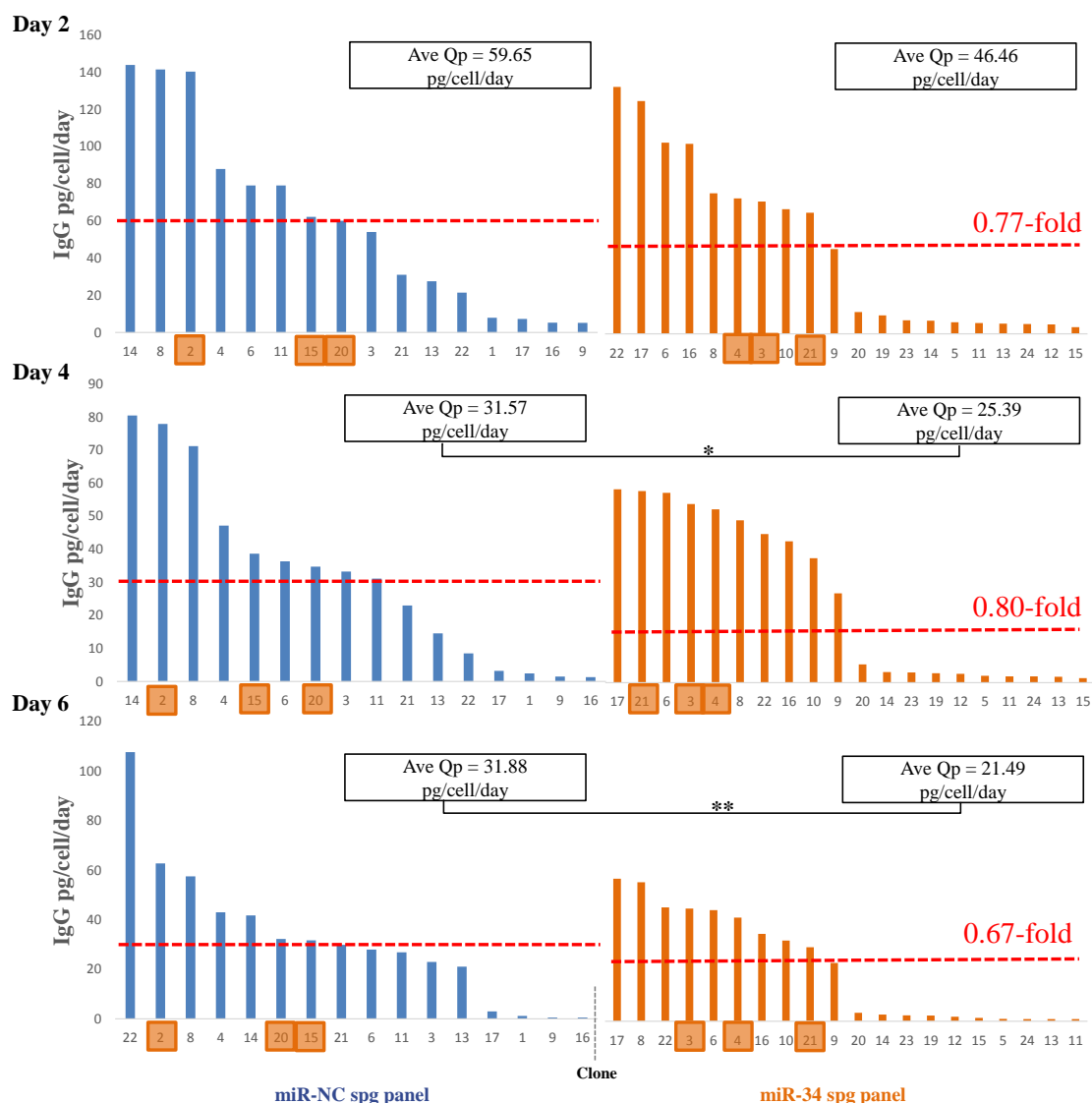


Figure 3.22: Specific IgG productivity of each individual clone from both the miR-34 and miR-NC sponge panel. The average specific productivity is represented as a broken red line. Clones selected for scale up are highlighted in an orange box.

The performance of the clonal panel did not reflect the phenotype determined within the predecessor mixed pool population. From this perspective we decided to select those clones that displayed good volumetric IgG characteristics. Clones selected are highlighted in orange boxes in all the graphs. The clones selected from the miR-34 sponge panel

were clones 3, 4 and 21. These clones displayed reasonable phenotypes across all categories with an emphasis on volumetric productivity. Additionally, miR-NC sponge clones 2, 15 and 20 were selected based on similar criteria.

3.2.6 Phenotypic evaluation of miR-34 depleted clones in a 5 mL volume

miR-34 depletion has been observed to elicit two distinct phenotypes in two recombinant CHO cell lines, SEAP and IgG. In CHO-SEAP mixed populations, volumetric SEAP yield was enhanced in fed-batch while clones in 1 mL batch displayed enhanced SEAP yield. CHO-1.14 mixed pools demonstrated increased growth with reduced specific productivity while clone panels showed reduced performance across all traits (Growth, yield and specific productivity). This section explores the potential of miR-34 depletion in individual clones selected from both the CHO-SEAP and CHO-1.14 panels isolated for their production characteristics.

3.2.6.1 Selected miR-34 depleted CHO-SEAP clones

miR-34 sponge CHO-SEAP clones - Batch

All miR-34 depleted clones were observed to achieve a reduced maximal cell density of between 20-50% when compared to the two control clones (miR-NC spg 2 and 11) that reached the highest cell density (**Fig. 3.23 A**). However, when compared to the worst performing control clone, all miR-34 sponge clones demonstrated 1.9-2.3-fold higher cell numbers (**Fig. 3.23 A**). This control clone would be considered an outlier as the “normal” growth profile of the CHO-SEAP cell line would be greater than this ($\sim 3.5 \times 10^6$ cell/mL in the case of miR-NC mixed pools). All miR-34 sponge clones demonstrated reduced viability on day 6 of culture (**Fig. 3.23 B**) with two clone in particular (miR-34 spg clone 9 and 18) exhibiting the lowest viability at ~1%. Furthermore, these miR-34 sponge clones appeared to clump early in culture (days 3-4) contributing to a sudden drop in apparent cell density.

Figure 3.23: miR-34 sponge clones culture under batch conditions

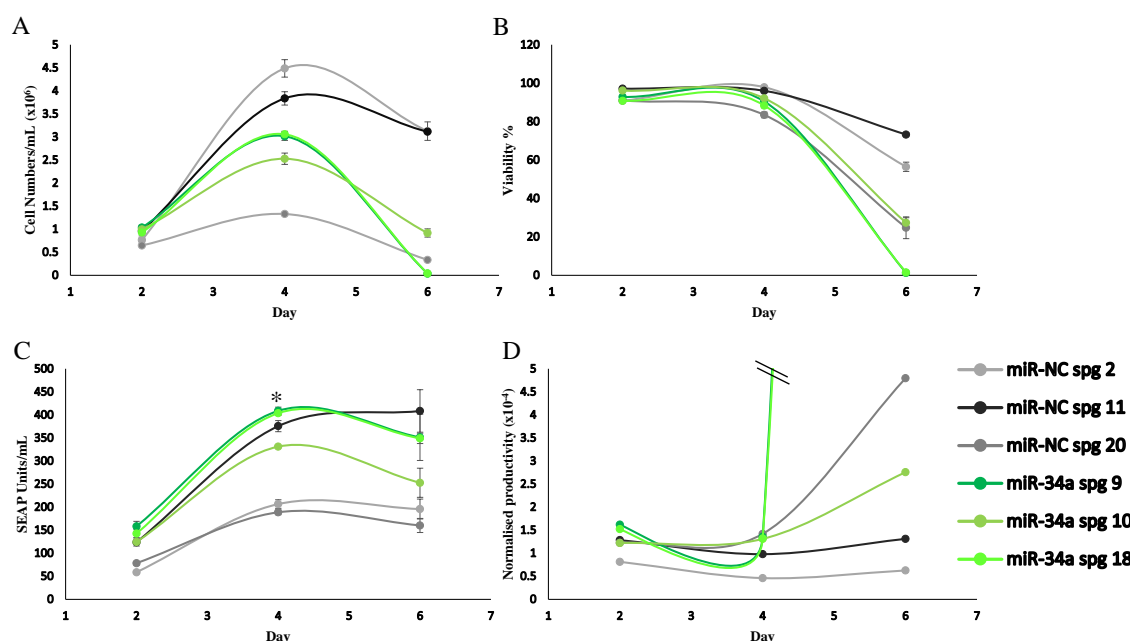


Figure 3.23: Batch culture results in a 5 mL volume for miR-34 depleted CHO-SEAP clones selected from the clonal panel when compared to non-specific control clones. Phenotypes assessed were A) Cell growth, B) Culture viability, C) SEAP yield/mL and D) Normalised productivity. Statistical analysis was calculated using a standard student t-test ($p \leq 0.05^*$ and an $n = 3$).

All miR-34 sponge clones displayed an enhanced SEAP secretion when compared to the two lowest producing control clones (Fig. 3.23 C). One control sponge clone (Clone 11) did reach comparable maximal SEAP levels when compared to miR-34 sponge clones (Fig. 3.23 C). Two miR-34 sponge clones (9 and 10) demonstrated a high normalised productivity potentially due to their propensity to clump and display low cell viability resulting in a low cell density on day 6 of culture (Fig. 3.23 D). miR-34 sponge clones exhibited a tendency to clump early in culture regardless of the addition of PVA or the process of cloning out non-clumping cells from these cultures. At this point, Fed-batch was not pursued and assessment of miR-34 depletion in CHO-SEAP cells was terminated.

3.2.6.2 Selected miR-34 depleted CHO-1.14 clones

miR-34 sponge CHO-1.14 clones - Batch

3 clones were selected from both control and test panels based on their volumetric productivity. However, a growth benefit was observed in the case of mixed pools that was

not retained in 1 mL batch culture. When scaled up to a 5 mL volume, all clones demonstrated enhanced growth of 1.3-5-fold ($p \leq 0.001$) on day 2 and 1.5-3-fold ($p \leq 0.01$ and 0.001) on day 4 (**Fig. 3.24 A**). While all three clones reached higher cell numbers on day 6 when compared to two control clones (miR-NC spg 2 and 15), one control clone had increased cell numbers as well as comparable cell viability (**Fig. 3.24 A and B**). Despite the varied performance of the control clones, siRNA-mediated knockdown of the miR-34 sponge construct in miR-34 sponge 21 caused a 30% ($p \leq 0.001$) reduction in density on day 3, suggesting that the presence of the sponge had a growth benefit (**Fig. 3.25**). Efficient knockdown of the miR-34 sponge was previously demonstrated (**Fig. 3.11 B**).

All three miR-34 sponge clones demonstrated enhanced viability on day 6 of culture of between 65-80% while the miR-NC sponge control clones exhibited viability between 21-53% (**Fig. 3.24 B**). However, one control clone (miR-NC spg clone 20) demonstrated a viability comparable to miR-34 sponge clones. This would suggest that miR-34 depletion is conferring a potential benefit by delaying the onset of apoptosis and that miR-NC clone 20 is displaying high viability due to the nature of clonality, selecting clones with inherent beneficial attributes, by chance.

When volumetric IgG productivity and specific productivity were assessed, there was a dramatic reduction in the production capacity of all three miR-34 sponge clones of around 10-60% across all time points when compared to the range of titres produced by all three control clones (**Fig. 3.24 C**). As cell numbers were observed to be enhanced in the case of the miR-34 depleted clones, specific productivity was further reduced to a range of 10-80% (**Fig. 3.24 D**).

Figure 3.24: CHO-1.14 stable miR-34 sponge clones under batch growth conditions

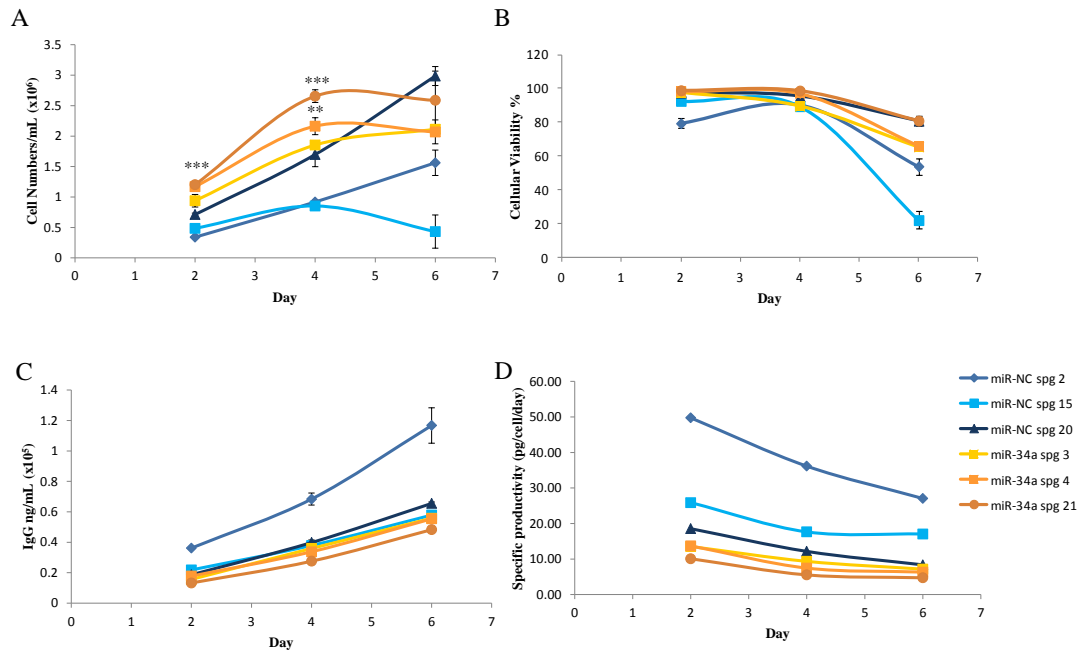


Figure 3.24: Clones selected from each panel (miR-34 and miR-NC sponge in batch conditions in a scaled up 5 mL culture volume. A) Cell numbers/mL B) Cellular viability C) Volumetric IgG secretion and D) Specific productivity. Statistical analysis was determined using a standard student t-test with each miR-34a sponge clone being compared to all three controls. ($p \leq 0.01^{}$ and $p \leq 0.001^{***}$).**

Figure 3.25: sponge knockdown mediates a reversal in the growth phenotype

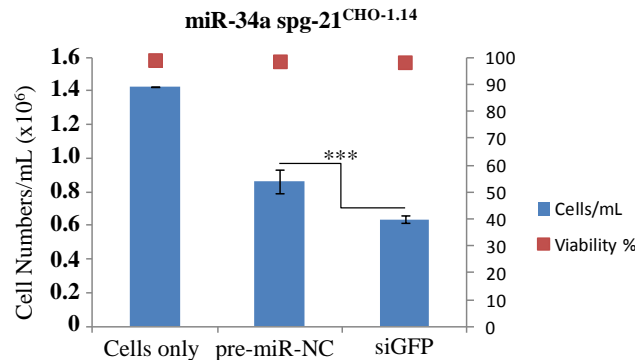


Figure 3.25: The impact that miR-34 sponge knockdown exerted on the growth profile of a stable miR-34a sponge clone (clone 21) upon transient transfection of a siRNA designed against the deGFP (siGFP) reporter construct. Cells were sampled on day 3 of culture after transfection with GFP fluorescence inhibition reported in Figure 3.11.

miR-34 sponge CHO-1.14 clones – Fed-batch

Clone 3 from the miR-34 sponge panel was omitted from this Fed-batch study as it exhibited the poorest growth phenotype. Once again, miR-34 sponge clones achieved an increased maximal cell density of 1.5 to 2-fold when compared to two of the three control clones (**Fig. 3.26 A**). Furthermore, both miR-34 depleted clones demonstrated an extended productivity phase by maintaining viability above 80% until day 8 (**Fig. 3.26 B**). However, as observed in the case of batch culture, one control sponge exhibited a comparable phenotype, miR-NC spg clone 20, when both growth and viability were assessed.

A reduction of about 20-40% was observed for both miR-34 depleted clones when compared to control clones 15 and 20 while a large reduction of around 80% was observed in the case of the high producing clone miR-NC spg 2 in IgG productivity (**Fig. 3.26 C**). When specific productivity was determined, there was a 40-90% reduction in both miR-34 sponge clones when compared to all three control clones (**Fig. 3.26 D**).

Figure 3.26: CHO-1.14 stable miR-34 sponge clones under fed-batch growth conditions

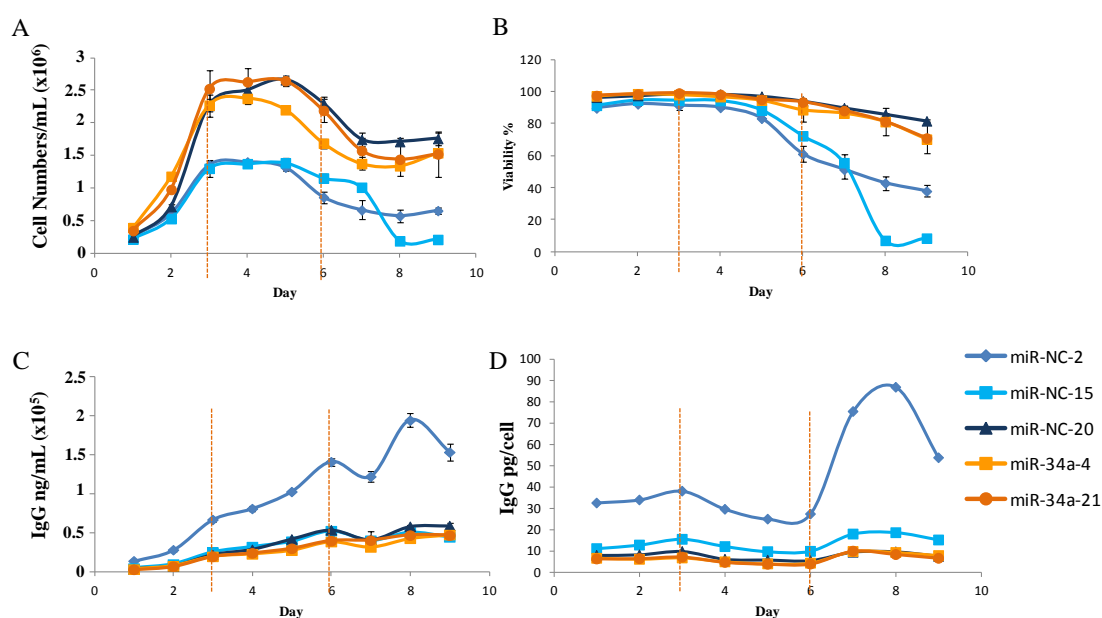


Figure 3.26: Fed-batch culture for the selected clones engineered to stably deplete miR-34 and the non-specific control. Addition of feed media is represented as a broken orange line. Phenotypes reported are A) Cell numbers/mL B) Cell viability C) Volumetric IgG secretion and D) specific productivity.

From this section it can be seen that the depletion of miR-34 mediated improved growth in CHO-1.14 cells. However, this growth benefit did not push the cells to reach higher cell densities than previously observed for the parental population with the addition of potentially compromising the production capacity of each clone. Although miR-34 sponge clones did perform better in regards to growth and viability when compared to 2 of the 3 control clones selected, one control clone exhibited comparable phenotypic attributes.

With miR-34 proving an interesting miRNA but potentially not a viable miRNA for CHO engineering, we decided to explore its potential role in influencing the glycoprofile of secreted IgG.

3.2.7 miRNA-mediated interference of CHO cell antibody glycoforms

Section 1.4 introduced the importance of antibody glycoforms to the functionality and potency of antibody-mediated effector functions such as ADCC. Increased ADCC has shown to be enhanced for main-stream anti-cancer therapeutics such as Herceptin through the manipulation of the core fucose added to the N-acetylglucosamine at the conserved Asparagine-297 (Suzuki et al. 2007a)(Li et al. 2013b) and Rituxan (Li et al. 2013b). The report that miR-34a could interact with the 3'UTR of FUT8 (Bernardi et al. 2013a) and interfere with its mature protein levels led us to explore the stable depletion of miR-34 contributing to an altered antibody glycoform, fucosylation, in the case of recombinant CHO-1.14 cells. The protocol followed is as described by Mittermayr and Bones *et al.*, (Mittermayr et al. 2011) and **section 2.6.11 in Materials and Methods**.

Two clones were selected from the CHO-1.14 parental population engineered to stably deplete miR-34 including a separate non-specific sponge clone. When the antibody glycoform profile was determined for both the selected miR-34 sponge and miR-NC sponge clone, it was observed that there was no change in the peak ratios between each sample indicating no alteration in the fucosylation profile (G0F, G1F and G2F (see section 1.4.2 of Introduction for nomenclature, Fig. 3.27)).

Figure 3.27: Glyco-profile of a miR-34 sponge clone versus miR-NC sponge clone

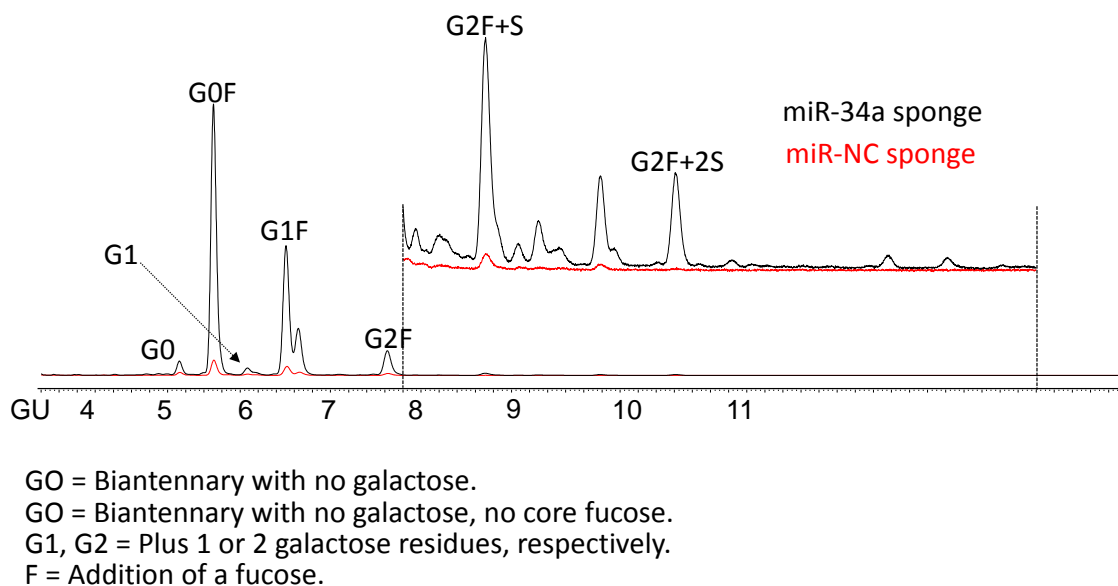


Figure 3.27: The peak intensities and elution times (min) for the N-glycans isolated and fluorescently labelled with 2-AB (2-aminobenzoic acid) with the core fucosylated N-acetylglucosamine of interest being G0F, G1F and G2F, i.e. biantennary N-glycan no, one or two galactose groups on either terminal N-acetylglucosamine. GU indicates glucose units

However, one interesting observation was that the intensity of the peak profile was considerably higher in the case of the secreted antibody derived from the miR-34 sponge clone when compared to the miR-NC sponge clone (**Fig. 3.27**).

As a means to ensure that antibody quantification was accurate, potentially contributing to the difference in peak intensities, 10 µg of each antibody was run on a 4-12% Bis-Tris SDS gel and stained with Coomassie Blue. One antibody pair was reduced using iodoacetamide to break apart disulphide bonds, liberating the individual heavy and light chains.

Coomassie blue stained gel showed that there was similar quantities of IgG antibody in both miR-NC and miR-34 sponge clone samples (**Fig. 3.28**).

Figure 3.28: Coomassie blue semi-quantification of secreted IgG from miR-34 and miR-NC sponge clones

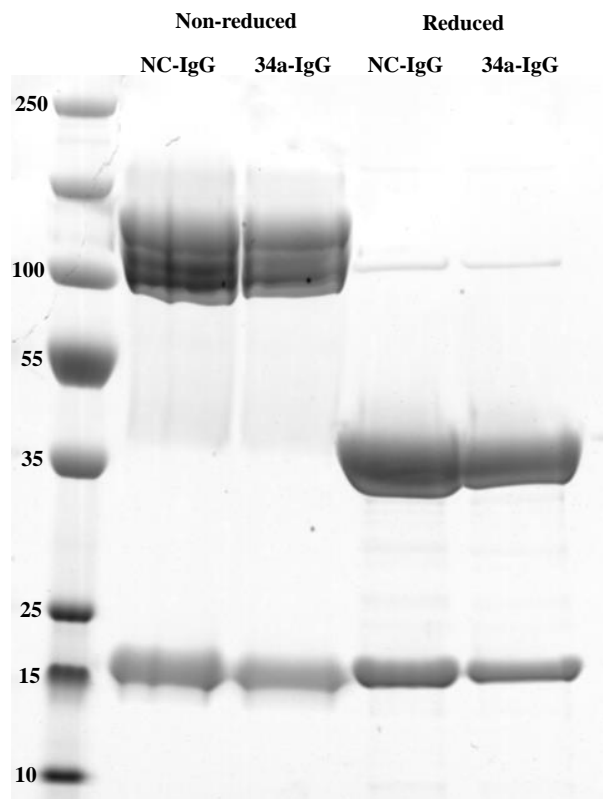


Figure 3.28: 10 µg of purified non-reduced and reduced IgG antibody secreted from a miR-NC and miR-34 sponge CHO-1.14 clone stained with Coomassie Blue.

Following these observations, we designed several treatments of the miR-34 sponge clone 21 as a means to assess the stable depletion of miR-34 on influencing the IgG glycoprofile.

Firstly, as the intensity of the glycoprofile peaks were higher in the case of the miR-34 sponge compared to the control, we assessed the glycoprofile of the parental CHO-1.14 from which both sponge clones were derived. It was anticipated that the parental CHO-1.14 would demonstrate a similar low intensity profile to that of the negative control. When this was assessed, both parental and miR-34 sponge clones exhibited a similar glycoprofile of equal intensity (**Fig. 3.29 Sample A compared to Sample C or E**).

Secondly, if miR-34 depletion was mediating this increased peak intensity, we attempted to knockdown the sponge using a siRNA against GFP with the hope of observing a reduced intensity when compared to the control miR-34 sponge treated with pre-miR-NC. Successful inhibition of the sponge was demonstrated previously for this clone (**Fig.**

3.11 B inset). However, no change in peak intensity was observed (**Fig. 3.29 Sample D compared to Sample C or E**).

From the perspective of fucosylation, CHO cells secrete antibody of which >90% are fucosylated (Jefferis 2009a). It is possible that by depleting miR-34 and increasing the expression of FUT8, an increase in fucosylation would not be apparent. We next transiently over-expressed miR-34a in a stable miR-34 sponge clone with the anticipation of observing a shift in the fucosylation profile towards reduced fucosylation. No shift in the three peaks associated with fucosylation (G0, G1 and G2) was observed (**Fig. 3.29 Sample B compared to Sample C or E**).

Figure 3.29: Glyco-profile of IgG produced from a miR-34 sponge clone 21 treated with pre-miR-34a and siRNA for GFP

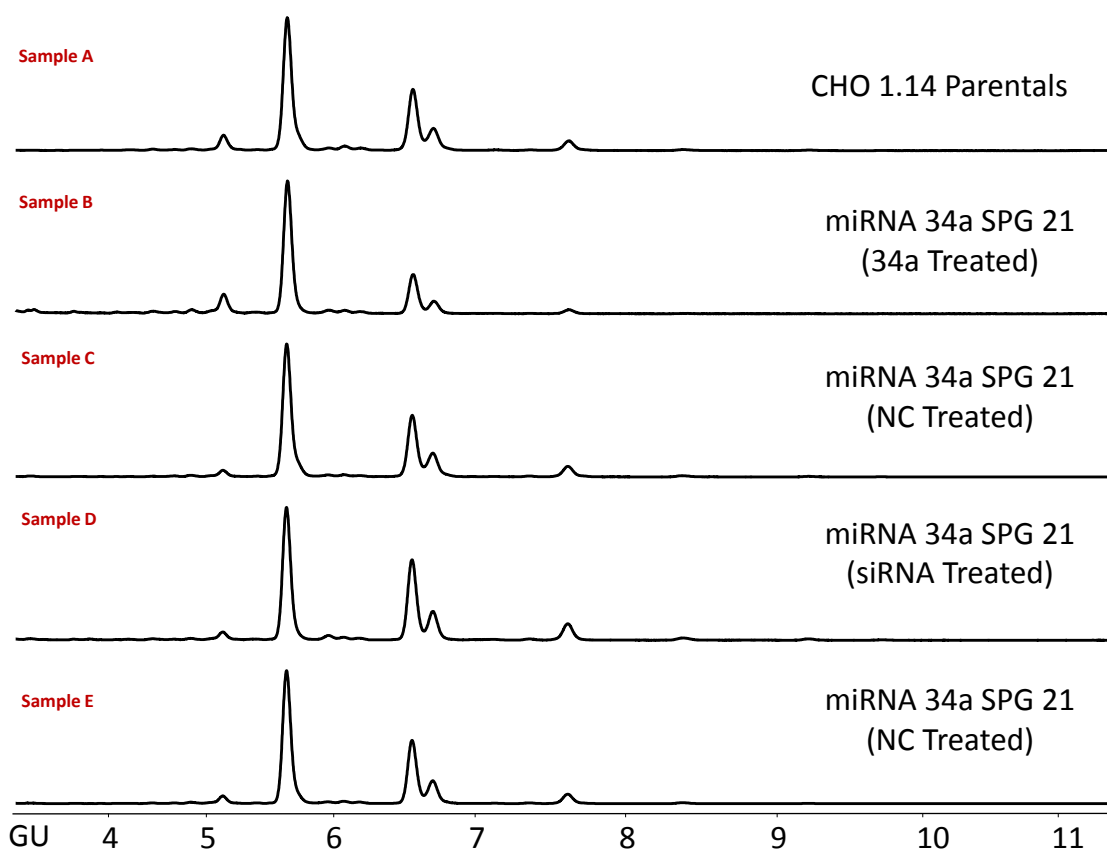


Figure 3.29: The IgG glyco-profiles of various sample conditions including A) CHO-1.14 parentals untransfected, B) miR-34a sponge clone 21 transfected with pre-miR-34a, C) miR-34a sponge clone 21 transfected with a pre-miR-NC control, D) miR-34a sponge clone 21 transfected with a siRNA specific for the GFP in the miR-34a sponge construct and E) miR-34a sponge clone 21 transfected with a pre-miR-NC control. The primary fucosylated glycan peaks are labelled including G0F, G1F and G2F. GU indicates glucose units.

The focus of CHO cell line engineering towards glyco-manipulation has proven to be a promising endeavour from literature reports. Further evaluation of the impact of miR-34a on the fucosylation capacity in CHO cells would be required starting by assessing the mature protein levels of the FUT8 gene upon overexpression of miR-34a. Additionally, several IgG producing cell lines would have to be assessed for their resulting glycoforms following miR-34a transfection. Increased miR-34a expression elicits an undesirable phenotype such as cell death and growth inhibition. From this perspective, the identification of alternative miRNA targets of FUT8 that do not contribute this unwanted phenotype would be invaluable.

Section 3.3

Stable depletion of independent microRNA duplex components: miR-23b and miR-23b*

3.3. CHO cell engineering using miR-23b and miR-23b*

Several miRNAs that were screened, such as miR-23b*, impacted negatively on the CHO cell phenotype despite their positive correlation with improved growth in the profiling experiment. This section describes and characterises two miRNA partners, miR-23b and its passenger miR-23b*, selected for stable CHO cell line engineering within both a SEAP and IgG-secreting cell line derived from the same CHO-K1 parental background.

3.3.1. Selection of miR-23b and miR-23b* for stable knockdown

Transient miR-23b* overexpression inhibited growth by 90% and cell viability was reduced by 30%. However, it was anticipated that stable inhibition of this miRNA might induce a reversed phenotype, enhancing growth and potentially inhibiting cell death. Past experience in CHO using miR-7, demonstrated that overexpression of miR-7 caused growth inhibition (Barron et al. 2011a) while stable inhibition improved CHO cell growth and product yield (Sanchez et al. 2013b).

The mature guide strand miR-23b was selected based on previous identification and evaluation within our research group. A previous study by Gammell *et al.*, (Gammell et al. 2007) identified components of the miR-23a~27a~24-2 cluster to be down-regulated when subjected to hypothermic growth conditions. Stable depletion of all three miRNA members improved both CHO cell growth and volumetric productivity (Data not shown) in a CHO-SEAP mixed population. We sought to dissect the role that miR-23 plays in mediating the enhanced rCHO-SEAP phenotype by diverting its actions away from its endogenous targets. Although specified as miR-23b in this instance, the mature sequence of miR-23b and miR-23a only differ by a single nucleotide (**Appendix Figure A5**), which lies outside the miRNA seed region. miRNA sponges have been shown to sequester entire seed families (Kluiver et al. 2012a) as miRNA recognition elements (MREs) are fully complementary to the mature seed sequence thus effectively targeting both miR-23a and miR-23b in our stable cell line (here in referred to as miR-23).

3.3.2 miR-sponge vector design and stable CHO cell line generation

Two individual miRNA sponge vectors were generated for miR-23 and miR-23b* using the same miR-sponge construct described for the stable depletion of miR-7 (Sanchez et al. 2013b). Both mature miRNA sequences are conserved across human (*hsa*) and CHO (*cgr*) (**Fig. 3.30 A**). The miRNA sponge design for miR-23 and miR-23b* follows the same vector construct shown in **Figure 3.30 B**. Molecular cloning and stable cell line generation was carried out as described for the miR-34 sponge (**section 3.2**).

The miRNA sponge sequences for miR-23 and miR-23b* are shown in **Table 3.3** and included the same base-pair mis-matches across nucleotides 9-12 (miR-23) and 10-13 (miR-23b*). Molecular cloning gels for construct preparation and sequence information can be found in the appendix (**Appendix fig. A6 and A7**, respectively).

Figure 3.30: miR-23b and -23b* sequence conservation and sponge design

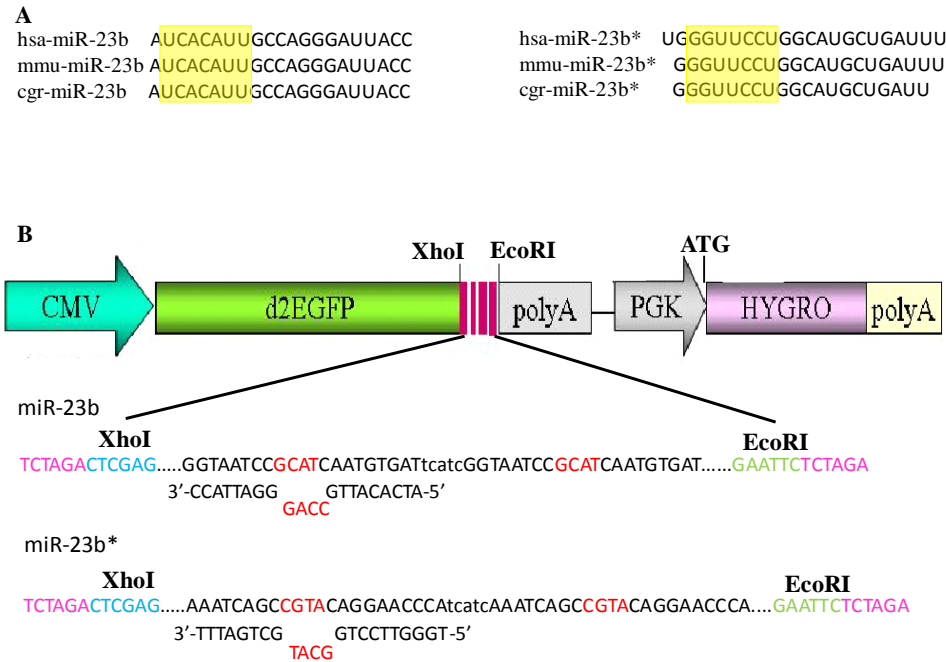


Figure 3.30: A) Demonstrates the conservation of miR-23 and miR-23b* across the species of *Homo sapiens* (*hsa*), *Mus musculus* (*mmu*) and *Cricetulus griseus* (*cgr*) including the dogmatic “seed” region (yellow box). **B)** Schematic diagram of the miR-sponge vector backbone expressing dEGFP and under Hygromycin selection with XhoI and EcoRI restriction sites for insertion of miR-23b* sequence carrying fully complementary concatemeric repeats (5'-3') to each respective microRNAs (5'-3') including base-pair mismatch “Wobble” at nucleotides 9-12 (miR-23) and 10-13 (miR-23b*) (red).

Table 3.3: miRNA sponge sequence design for miR-23b/-23b*

5'-3' microRNA Sponge sequence					
miR Sponge	XbaI Res.	XhoI Res.	Sponge seq.	EcoRI Res.	XbaI Res.
miR- 23b*	TCTA GA	CTCGA G	acgcgAAATCAGC CGTA CAGGAACCCA tcataAAATCAGC CGTA CAGGAACCCAa ccgtaAAATCAGC CGTA CAGGAACCCAa cgagAAATCAGC CGTA CAGGAACCCA catc	GAA TTC	TCTA GA
miR- 23b	TCTA GA	CTCCG A	acgcgGGTAATCC GCAT CAATGTGATtca tcGGTAATCC GCAT CAATGTGATaccgta GGTAATCC GCAT CAATGTGATacgagG GTAATCC GCAT CAATGTGATtcac	GAA TTC	TCTA GA

3.3.3 Investigation of GFP fluorescence

Binding specificity of each miRNA sponge was assessed for its target miRNA. All three miRNA sponges were transfected (NC-spg, 23b-spg and 23b*-spg) with their appropriate pre-miR and separately with a negative control mimic (pre-miR-NC). A ~90% ($p \leq 0.001$) reduction in the levels of GFP expression was achieved when pre-miR-23b* and pre-miR-23b*-mod (pre-miR-23b) were transfected into the appropriate CHO-sponge population with the NC-sponge demonstrating little specificity (**Fig. 3.31 A and B**).

One point to note was the nomenclature for pre-miR-23b referred to as pre-miR-23b*-mod. This “mod” implies a modification that we sought when ordering the commercial hairpins. Normal pre-miR-23b and pre-miR-23b* take the form of siRNA-like constructs, that being a fully complementary duplex with terminal modifications to allow selection of the desired strand. In the case of pre-miR-23b*-mod, the hairpin structure mimics that of the endogenous miR-23b/23b* duplex (**Appendix Fig. A8**) thus thermodynamically favouring the selection of the mature miR-23b strand while generating the by-product passenger strand miR-23b*. The modified version (pre-miR-23b*-mod) repressed GFP expression with over 5-fold greater potency than the commercial siRNA-like pre-miR-23b. This suggested that processing of the commercial pre-miR-23b duplex resulted in a lower mature miR-23b copy number.

The non-specific sponge mixed pool population demonstrated an average higher fluorescence when compared to both miR-23 and miR-23b* sponge mixed pools (**Fig. 3.31 B**). This reduced GFP fluorescence is likely a reflection of the repression caused by

endogenous miR-23/23b*, similar to the observation for the miR-34 sponge, in the previous section.

The heterogeneity within all populations generated is evident from the various GFP expression arising from individual clones within the mixed populations (Fig. 3.31 A).

Figure 3.31: miR-23b/23b* spg binding specificity through GFP suppression

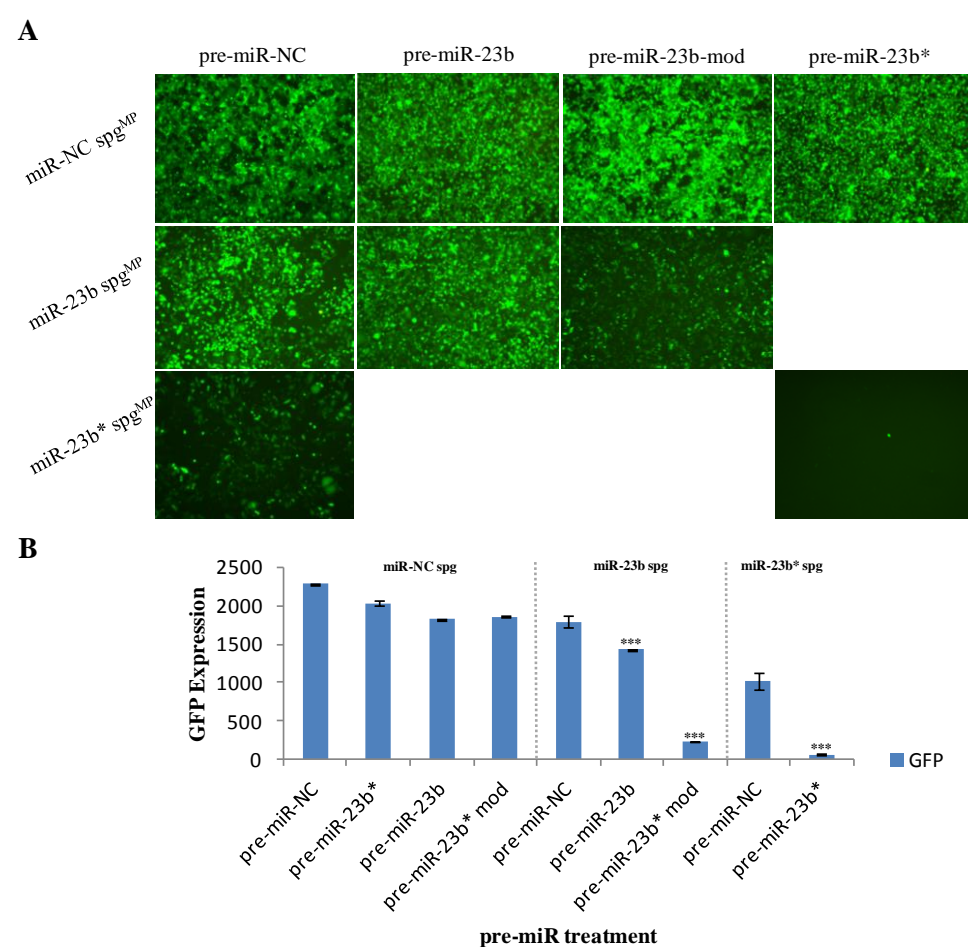


Figure 3.31: miR-sponge specificity was carried out for the miR-23 and miR-23b* sponge through the transient over-expression pre-miR-23b* and pre-miR-23b. miR-23b*-mod is a specifically designed pre-miRNA that is composed of the mature miR-23b and miR-23b* and is processed according to their natural thermodynamic properties with the miR-23b* strand being tagged with a biotin group. Sponge specificity was determined based on inhibition of GFP expression through monitoring with A) Fluorescent microscopy and B) Guava ExpressPlus programme. Non-specific stable sponge was transfected in order to identify its lack of specificity. Statistical significance was calculated using a standard student t-test ($p \leq 0.001^{*}$).**

3.3.4 Analysis in mixed populations

The following section assesses the impact both stable miRNA depletion of miR-23 and miR-23b* had in both rCHO populations (SEAP and IgG) under various bioprocess conditions (Batch and Fed-batch).

3.3.4.1 Impact on bioprocess phenotypes in CHO-K1-SEAP: Batch and Fed-batch

miR-23 sponge mixed population - Batch

Mixed pool rCHO-SEAP cells with stable inhibition of miR-23 exhibited no growth or viability benefit when compared to NC-spg cells (**Fig. 3.32 A and B**). However, an increase ranging from ~30-50% ($p \leq 0.001$) in volumetric SEAP activity was observed (**Fig. 3.32 C**).

Figure 3.32: Batch process of mixed pool CHO-SEAP cells stably depleting miR-23

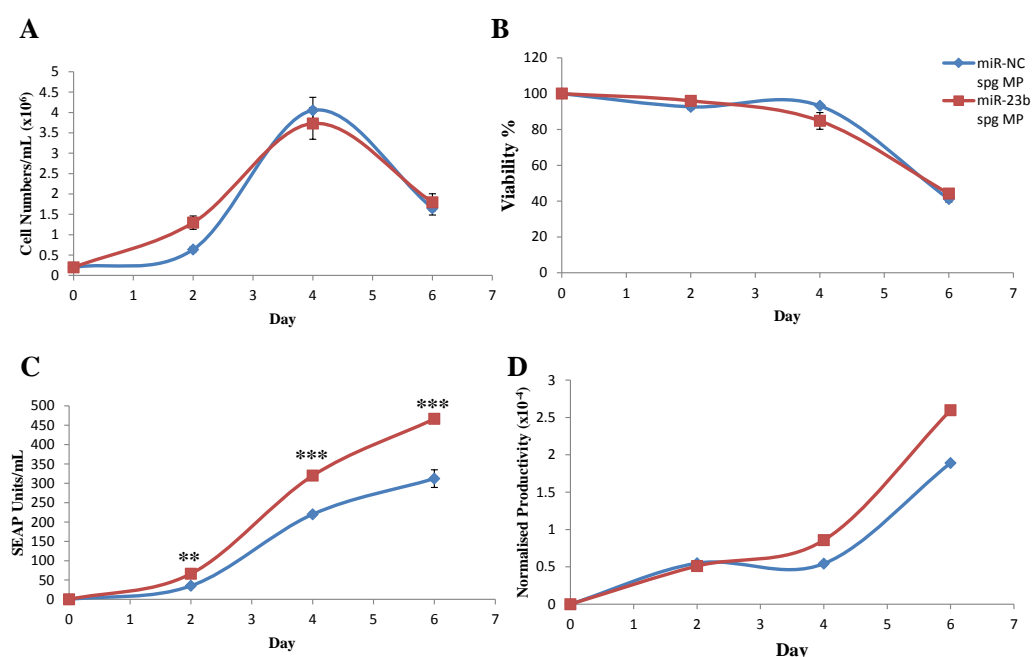


Figure 3.32: CHO-SEAP cells engineered to stably deplete miR-23 in a mixed pool population were evaluated for bioprocess relevant phenotypes A) Cellular proliferation, B) Cellular viability, C) Volumetric SEAP yield/mL and D) specific SEAP productivity/cell over the course of a 6 day batch process and compared to a stable mixed pool population expressing a non-specific control sponge (miR-NC spg). Statistical analysis was calculated using a standard student t-test ($p \leq 0.01^{}$ and $\leq 0.001^{***}$) with an $n = 3$ of experimental replicates.**

miR-23 sponge mixed population – Fed-batch

miR-23 depletion conferred no growth benefit, however, addition of the feed improved maximal cell density by 2-fold when compared to batch culture (**Fig. 3.33 A**). Viability was extended a further 3 days above 80% for both miR-23/-NC sponge pools with no additional benefit observed in the case of miR-23 depletion (**Fig. 3.33 B**).

Figure 3.33: Fed-batch process of mixed pool CHO-SEAP cells stably depleting miR-23

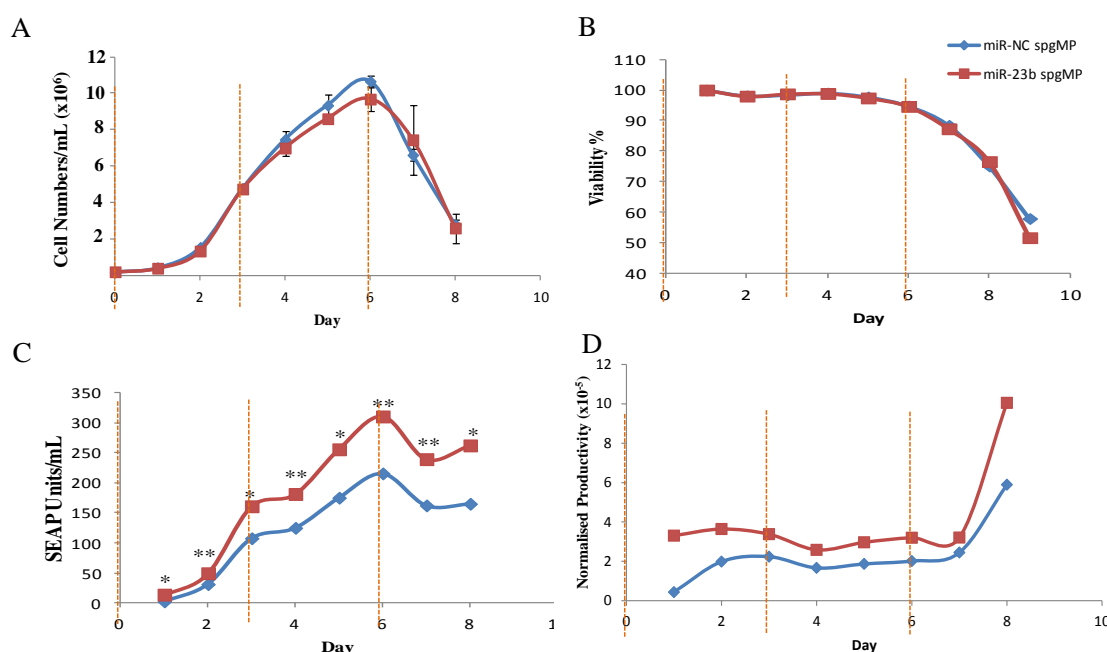


Figure 3.33: Stable miR-23 sponge mixed pool populations were cultured in a fed-batch format over the course of an 8 day assay. Nutrient Feed (CD CHO Efficient Feed A) was initially inoculated at 15% (v/v) on day 0 and subsequent feeds of 10% (v/v) every 72 hs (Feed signified in orange). Stable inhibition of miR-23b was assessed for its influence on A) Cellular proliferation, B) Cell viability, C) Volumetric SEAP activity and D) Specific SEAP activity. Statistical significance was calculated using a standard student t-test ($p \leq 0.05^*$ and $\leq 0.01^{}$) with an experimental replication of $n = 3$.**

A ~50% ($p \leq 0.05$ and $p \leq 0.01$ at various time points) increase in volumetric SEAP activity was achieved across various time points for miR-23 depleted mixed pools (**Fig. 3.33 C**). The maximum SEAP units calculated for the mixed pool miR-23 sponge in the

fed-batch process was lower when compared to batch. This reduced SEAP activity between miR-23 depleted mixed pools under different culture conditions could potentially be due to the 2-fold increase in cell growth resulting in an increased demand on cellular energy metabolism to be pledged toward cellular division rather than productivity. Finally, there was a range of 30-80% enhanced normalised SEAP productivity observed for miR-23 depleted mixed pools compared to controls (**Fig. 3.33 D**).

miR-23b sponge mixed population - Batch*

Stable depletion of miR-23b* in an rCHO-SEAP mixed pool demonstrated an average increase of 30-40% in the maximal cell density on day 4 of culture with no benefit to culture viability when compared to NC-spg pools (**Fig. 3.34 A and B**). A trend towards an enhanced growth phenotype was observed over the course of several replicates although not significant. A 40-50% ($p \leq 0.01$, $p \leq 0.001$) reduced volumetric SEAP activity was observed when compared to non-specific control sponge cells (**Fig. 3.34 C**). Normalised productivity was observed to be reduced by ~60% (**Fig. 3.34 D**). This reduction in volumetric/normalised productivity could potentially be due to the enhanced proliferation phenotype diverting cellular resources from productivity.

Figure 3.34: Batch process of mixed pool CHO-SEAP cells stably depleting miR-23b*

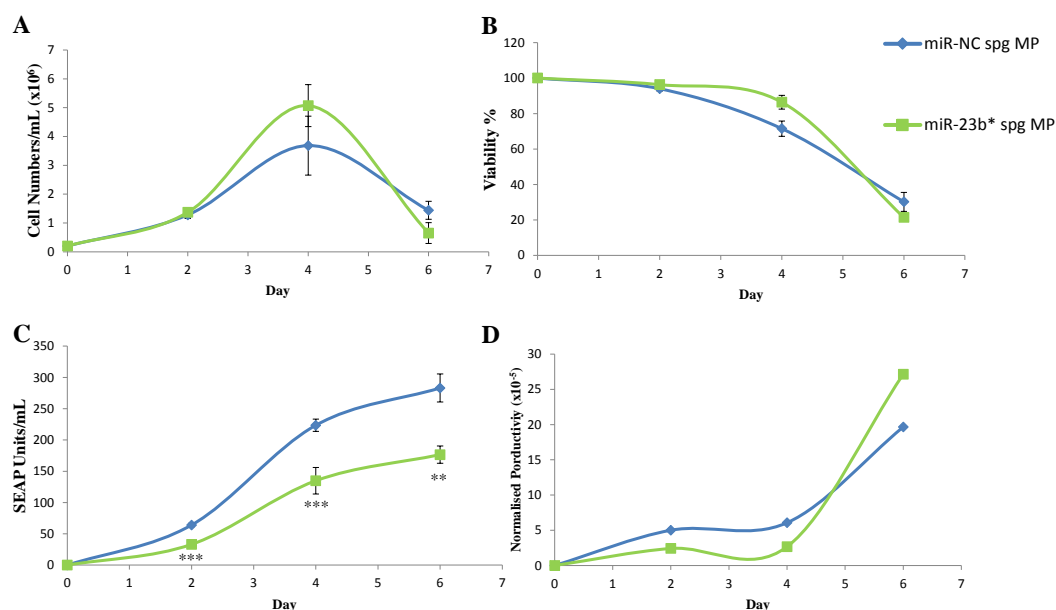


Figure 3.34: Mixed populations engineered to stably deplete miR-23b* (miR-23b* spg MP) were cultured in a batch process over a 6 day time course with a control population expressing a non-specific miRNA sponge. Phenotypes recorded were A) Cellular proliferation, B) Cellular viability, C) Volumetric SEAP activity and D) Specific SEAP activity. Statistical significance was calculated based on a standard student t-test ($p \leq 0.01^{}$ and $\leq 0.001^{***}$) and an experimental repeat of $n = 3$.**

miR-23b sponge mixed population – Fed-batch*

When the same mixed pool populations were evaluated in a fed-batch format, a 60-70% ($p \leq 0.01$, $p \leq 0.001$) increase in maximal cell density was achieved (**Fig. 3.35 A**) with no impact on cellular viability.

Volumetric SEAP output was observed to be reduced by 40-75%, as was described for batch culture (**Fig. 3.35 B**). However, at the later time points in culture, volumetric productivity achieved comparative levels to that of sponge controls (**Fig. 3.35 B**). This gradual increase in SEAP activity per mL is potentially attributed to the increase in the viable cell population. A consistent reduction in normalised productivity of 50-80% throughout various time points was observed (**Fig. 3.35 C**).

Figure 3.35: Fed-Batch process of mixed pool CHO-SEAP cells stably depleting miR-23b*

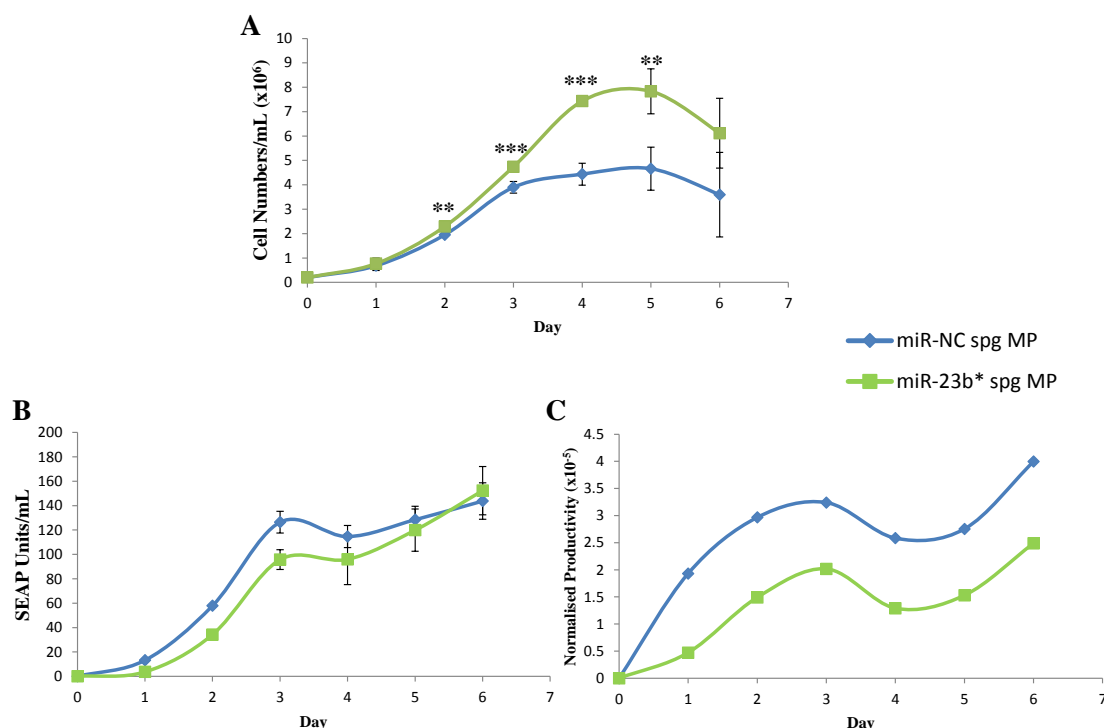


Figure 3.35: CHO-SEAP mixed populations engineered with a miRNA sponge specific for miR-23b* (miR-23b* spg MP) were cultured over a 6 day fed-batch period alongside a non-specific control sponge population (miR-NC spg MP). Cultured were fed initially with a nutrient rich feed on day 0 (15% v/v) and subsequently every 3 days (10% v/v). Bioprocess phenotypes assessed were A) Cellular proliferation, B) Cell viability, C) Volumetric SEAP activity and D) Specific SEAP activity. Statistical significance was calculated using a standard student t-test ($p \leq 0.01^{}$ and $\leq 0.001^{***}$) with an experimental repeat of $n = 3$.**

3.3.4.2 Impact of miR-23 and -23b* depletion on Mab producing clones

Both miRNA sponge mixed populations were next evaluated in a cell line secreting an IgG antibody.

miR-23 sponge mixed population - Batch

The maximal cell density achieved was increased~2-fold ($p \leq 0.001$) in miR-23 depleted CHO-1.14 cells with an improved viability of 15-20% ($p \leq 0.001$) when compared to

control sponge cells (**Fig. 3.36 A and B**). When volumetric IgG concentration was determined, a ~60% ($p \leq 0.001$) reduction early in culture but only ~30% ($p \leq 0.001$) in late culture was observed when compared to non-specific sponge controls (**Fig. 3.36 C**). The gradual increase could be a result of the higher viable density of producing cells, especially when productivity on a per cell basis was determined to be reduced by ~60% across all time points (**Fig. 3.36 D**).

Figure 3.36: Batch process of a CHO-1.14 mixed pool population with stable depletion of miR-23

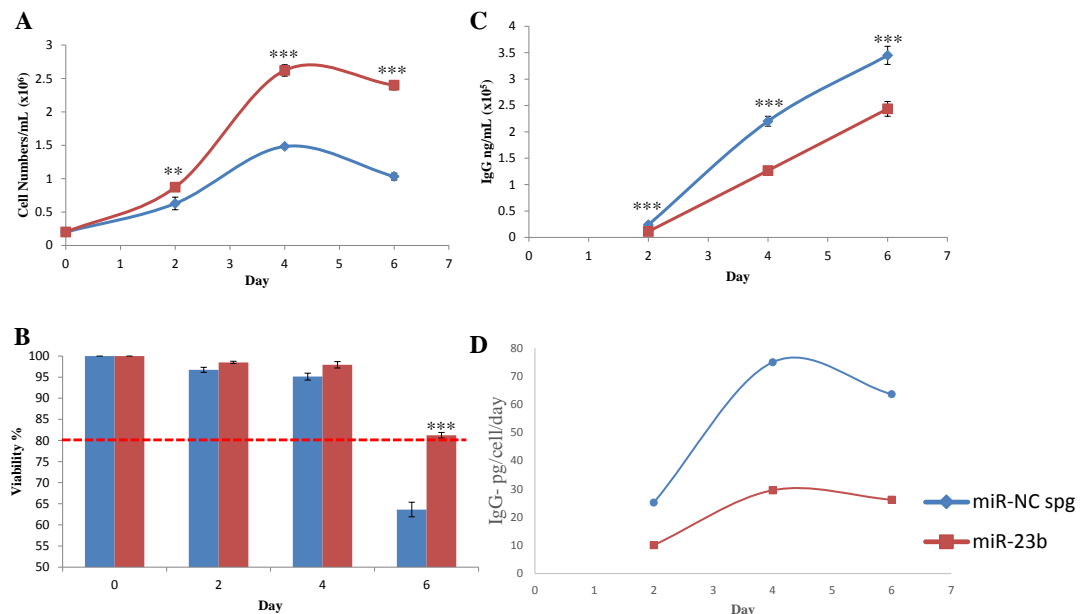


Figure 3.36: CHO-1.14 cells engineered with a sponge specific for miR-23 and a non-specific control sponge were cultured in a batch process over 6 days. Phenotypes assessed were A) Cellular proliferation, B) Cellular viability with an 80% viability threshold flagged with a red broken line, C) Volumetric IgG concentration and D) Specific IgG concentration. Statistical analysis was determined using a standard student t-test ($p \leq 0.01^{}$ and $\leq 0.001^{***}$) with an experimental repeat of $n = 3$.**

miR-23b sponge mixed population - Batch*

CHO-1.14 mixed pool populations demonstrated a similar phenotype to what was observed in CHO-SEAP mixed pools. An increase in CHO cell growth of 20-50% ($p \leq 0.01$, $p \leq 0.001$) was observed for miR-23b* sponge cells when compared to non-specific

pools (**Fig. 3.37 A**). Additionally, an increase in cellular viability of 10-15% ($p \leq 0.001$) was observed on day 6 of culture (**Fig. 3.37 B**). When volumetric IgG was assessed, a 30-40% ($p \leq 0.001$) decrease was determined across all time points with a higher decrease in cell-specific productivity of 50-60% (**Fig. 3.37 C and D**).

Figure 3.37: Batch culture for IgG-secreting miR-23b* sponge stable CHO-1.14

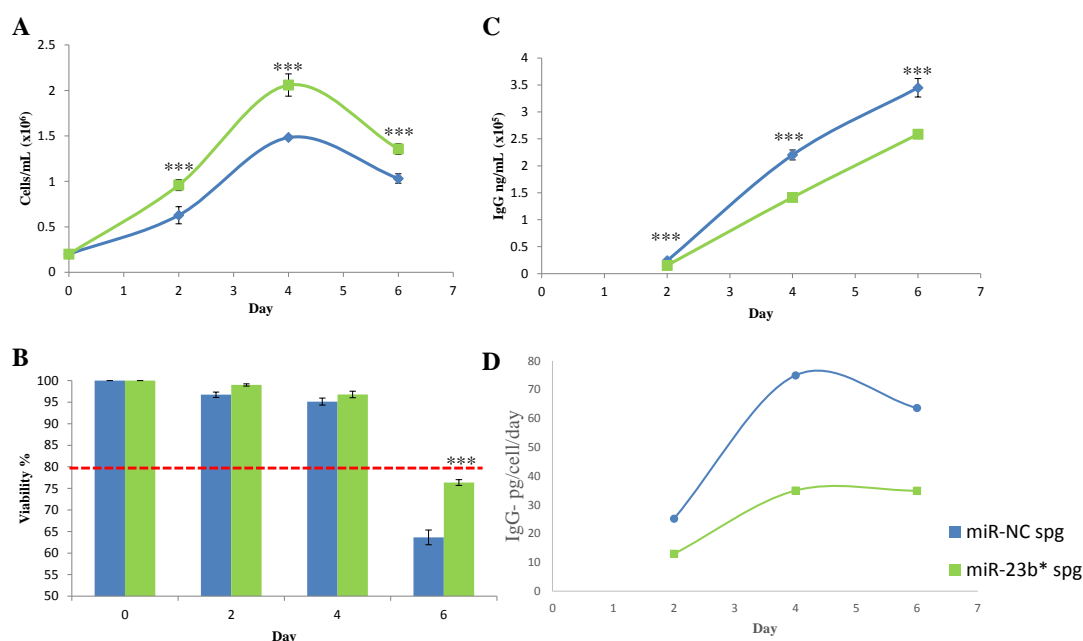


Figure 3.37: Stable mixed pool CHO-1.14 population engineered with a sponge specific for miR-23b* and a non-specific sponge sequence were cultured over a 6 day batch process. Bioprocess phenotypes under investigation were A) Cellular proliferation, B) Cellular viability with an 80% threshold marked with a red broken line, C) Volumetric IgG concentration and D) Specific IgG concentration. Statistical significance was calculated using a standard student t-test ($p \leq 0.01^{}$ and $\leq 0.001^{***}$) and an experimental repeat of $n = 3$.**

3.3.5 Analysis of single cell clones in 24-well plate

Clones from all mixed populations (miR-23, miR-23b* and miR-NC) were selected based on a medium-high level of GFP fluorescence to ensure that clones selected were expressing the miR-sponge constructs to a degree sufficient enough to meet the minimum threshold levels to achieve saturated target miRNA diversion (**Fig. 3.38**).

Figure 3.38: GFP distribution of miR-sponge clones isolated using FACS

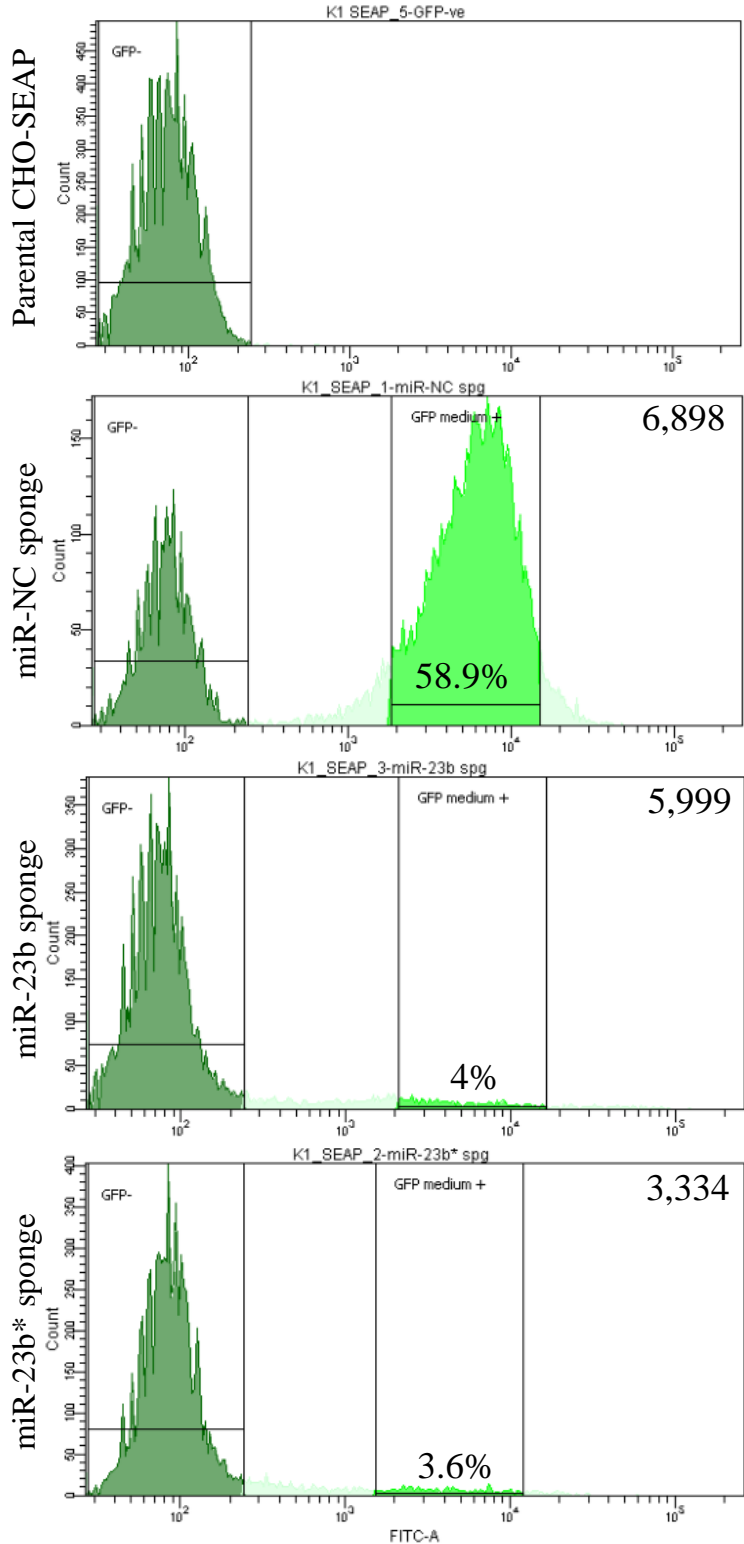


Figure 3.38: miR-sponge clones were sorted based on a medium-high range of GFP intensity. Mixed populations were gated based on a non-fluorescent parental CHO-K1-SEAP cell line. The average GFP intensity is shown in the top right hand corner of the graphs. The percentage of medium-high GFP cells is represented as a percentage compared to all cells.

Before phenotypic evaluation was performed, all clones were passaged at least 3 times in the presence of PVA and pulsed with G418 (Neomycin Phosphotransferase) and HYG (Hygromycin phosphotransferase).

3.3.5.1 GFP fluorescence across clonal panels

From the panel of 24 clones in each group (miR-NC-spg, miR-23-spg and miR-23b*-spg) in both cell lines (CHO-SEAP and CHO-1.14), GFP fluorescence was determined using the Guava ExpressPlus programme on the GuavaTM benchtop cytometer. It revealed that there was a spread in GFP expression intensity throughout all clonal panels ranging from very high to low expression levels (**Fig. 3.39**). Similar to what was observed for the miR-34 sponge, the average GFP intensity of both miR-23 and miR-23b* panels was reduced compared to controls and similarly observed in FACS readouts of miR-23/23b* sponge mixed pools (**Fig. 3.38**). It was also observed that the reduced GFP expression in the case of the miR-23b* panel was of a lower magnitude when compared to the control panel as opposed to miR-23 (**Fig. 3.39**). This could potentially be attributed to the nature of miR* strands being predominantly less abundant in addition to suggesting a potential lesser phenotype. The range in GFP intensity across the panel of clones is potentially attributed to plasmid integration site within the genome in addition to copy number and not as a result of transfection efficiency. Efficiency of transfection would have been assessed 24 h post-transfection (Data not shown) with a ~70% efficiency in the case of both miR-NC and miR-34 sponge mixed pools.

Figure 3.39: GFP expression across miR-spg clonal panel (miR-NC, miR-23b and miR-23b*) in both CHO-K1-SEAP and CHO-1.14 cells

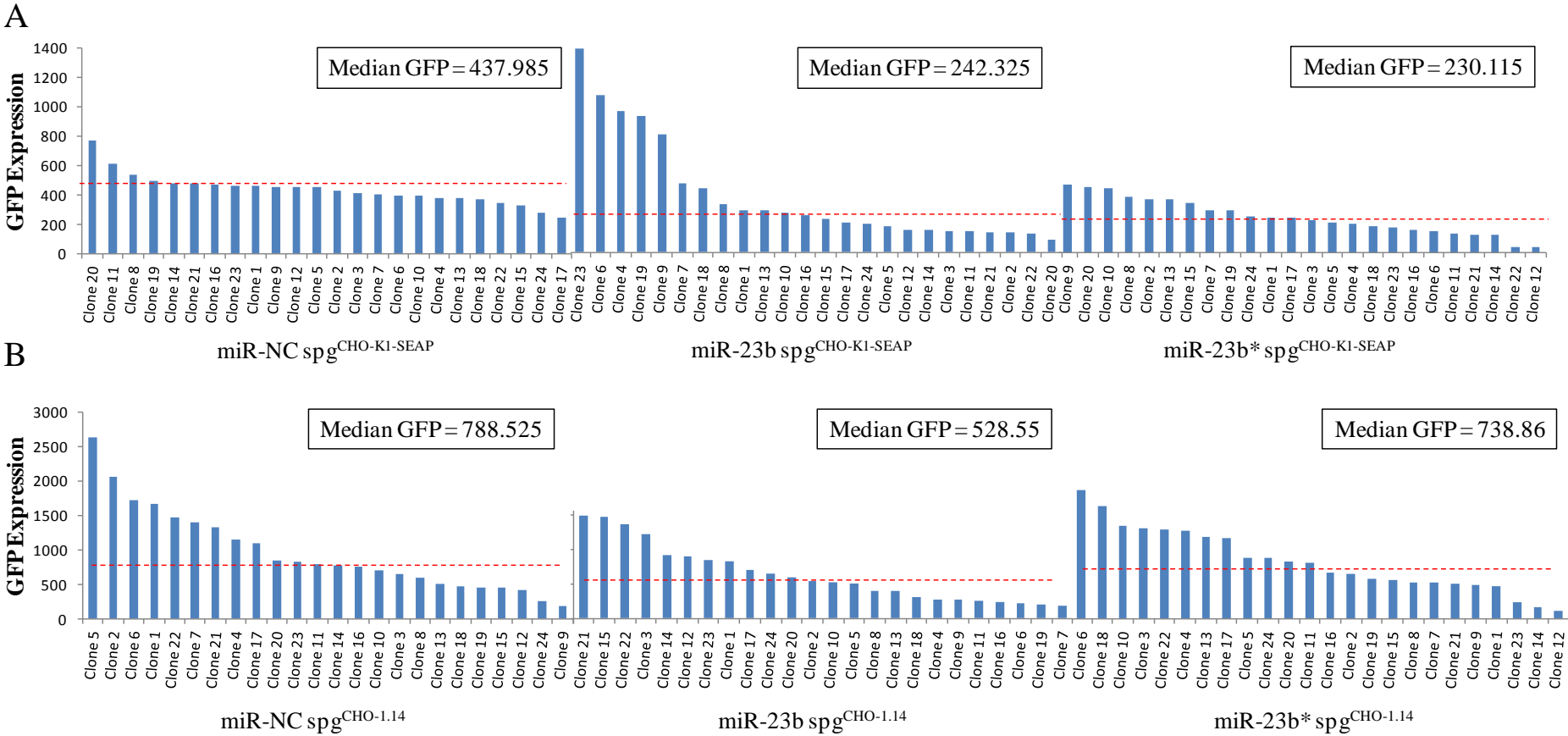


Figure 3.39: GFP expression for each individual clone from all stable miR-sponge populations (miR-NC spg, miR-23b spg and miR-23b* spg) in two different CHO cell lines (CHO-K1-SEAP and CHO-1.14). The Median GFP fluorescence for each panel is represented as a **broken red line. GFP intensity was analysed using the Guava ExpressPlus programme on a Guava EasyCyte benchtop cytometer.**

3.3.5.2 Impact on bioprocess phenotypes across CHO-K1-SEAP clonal panels

In the mixed pool populations under various culture conditions, stable depletion of miR-23 in our rCHO-SEAP cell line demonstrated no impact on CHO cell growth or viability yet significantly improved volumetric SEAP production due to enhanced specific productivity. On the other hand, miR-23b* depletion appeared to have a subtle beneficial effect on CHO cell growth at the expense of specific productivity. Clones isolated from both panels were evaluated on a clonal level as a means of assessing the gross phenotype as a function of the average panel performance.

miR-23 sponge clonal panel - Batch

After adaption to suspension culture, clones were grown in a 1 mL volume of serum-free medium and cultured in a 24-well suspension plate. The original panel of 24 clones, previously assessed for GFP fluorescence, was reduced to a panel of 14 clones due to loss during the adaption process as well as a contamination event over the course of several passages. The same occurred for miR-NC sponge clones of which 15 clones were recovered.

Both clonal panels were cultured over the course of a 6 day batch period and sampled on days 2, 4 and 6.

The average growth was not observed to differ when clones were assessed on day 2 (**Fig. 3.40^{Day 2}**), as observed in the mixed pools. However, clones stably expressing the miR-23 sponge decoy achieved half the maximal cell density on day 4 when compared to the miR-NC sponge panel (**Fig. 3.40^{Day 4}**), despite a subset of clones reaching “normal” cell densities. Cell density was further reduced by ~70% on day 6, potentially attributed to the 25% drop in cell viability at this late culture time point (**Fig. 3.40^{Day 6}**, **Fig. 3.41**).

Figure 3.40: CHO-SEAP miR-23 sponge clonal panel – Cell numbers/mL

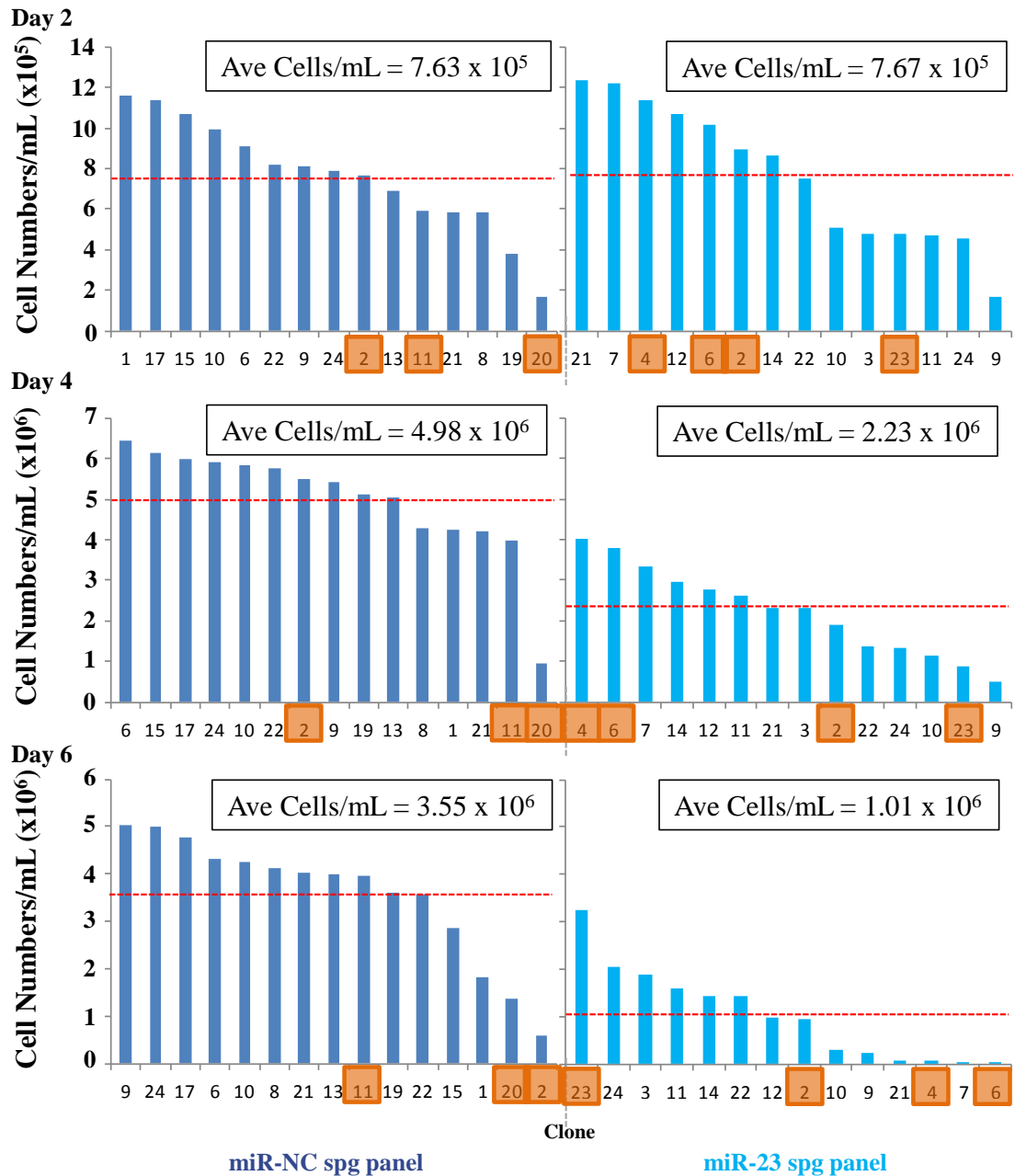


Figure 3.40: CHO-SEAP clonal panel demonstrating stable depletion of miR-23 and assessed for their growth phenotype in 1 mL suspension culture in a 24-well plate format and sampled at days 2, 4 and 6 in a batch process. Average cell numbers calculated across the entire clonal panels is represented by the **broken red line with the miR-NC-spg panel represented in dark blue and miR-23b spg panel in light blue. **Yellow boxes** highlight the individual sponge clones that were subsequently selected from each group for scale up and an n = 2.**

Figure 3.41: Day 6 cell viability of miR-23b CHO-SEAP sponge panel

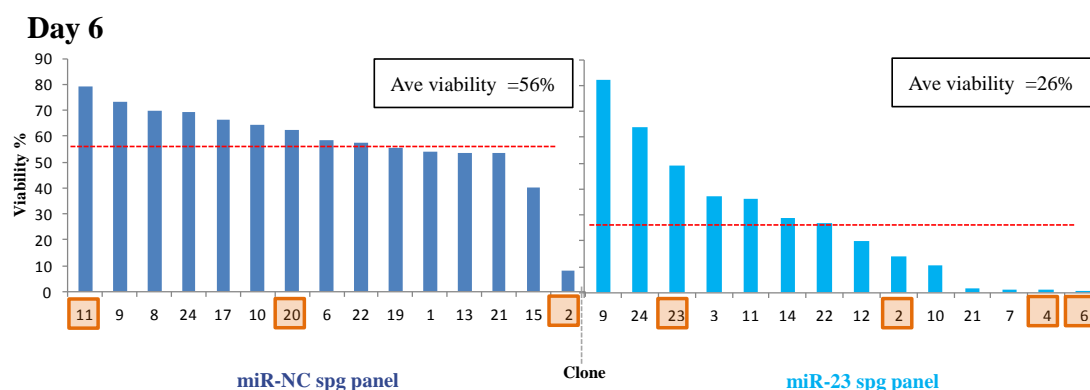


Figure 3.41: As cellular viability was comparable between both clonal panels on day 2 and 4, for both the miR-23 spg and miR-NC spg panel only the viability of each individual clone from both panel for day 6 of culture is presented above. The average viability across each panel is represented as a **broken red line** with the corresponding value enclosed. Clones ultimately selected for scale up are highlighted in **orange boxes** and an $n = 2$.

An increase of 3.1, 2.9 and 2.5-fold ($p \leq 0.001$) in SEAP production per mL was observed on days 2, 4 and 6, respectively in the miR-23 depleted panel despite the negative impact on cell density (**Fig. 3.42**). Although some clones from the NC-sponge group possessed a high level of SEAP production, 11 of the 15 miR-23 sponge clones outperformed the highest performing control clone. In the miR-23 sponge panel, average volumetric SEAP activity was observed to be 2.5-fold increased on day 4. This translated to a 5.8-fold ($p \leq 0.001$) increase in normalised productivity due to the reduced cell numbers (**Fig. 3.40^{Day 4}**, **3.42^{Day 4}** and **3.43^{Day 4}**). This suggests that although miR-23 may be contributing to enhanced specific productivity, the extent to which an individual cell will respond relies on various cellular processes such as proliferation, an energetically demanding process.

Figure 3.42: miR-23 sponge clonal panel – Volumetric SEAP activity

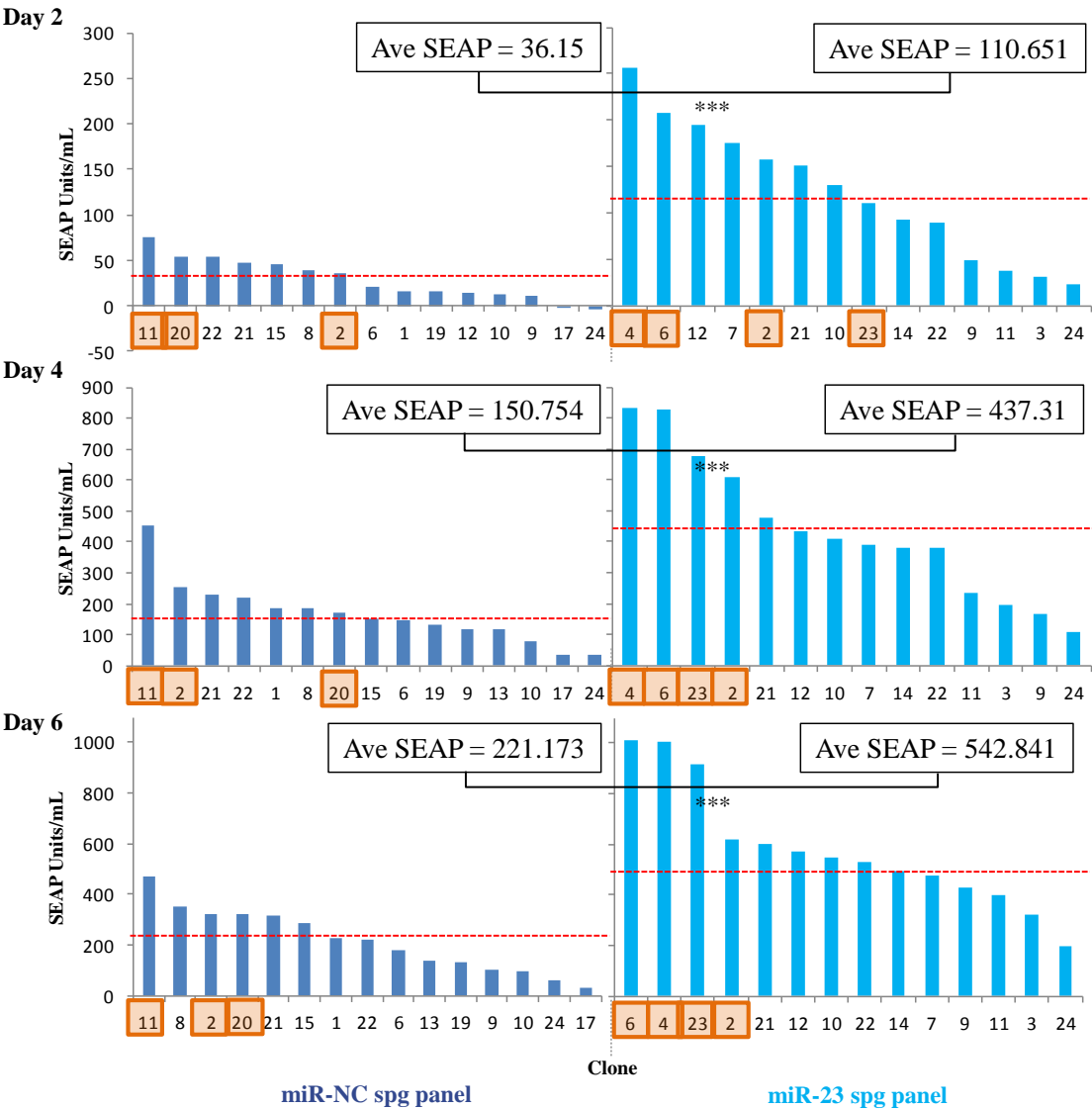


Figure 3.42: Individual volumetric SEAP activity is presented above for both miR-23 sponge and NC-sponge clones with the average performance across both panels represented as a **red broken line**. **Orange boxes** highlight the individual sponge clones that were subsequently selected from each group for scale up. Statistical significance was determined using a standard student t-test ($p \leq 0.001^{***}$), $n = 2$.

Figure 3.43: miR-23 sponge clonal panel – specific SEAP productivity

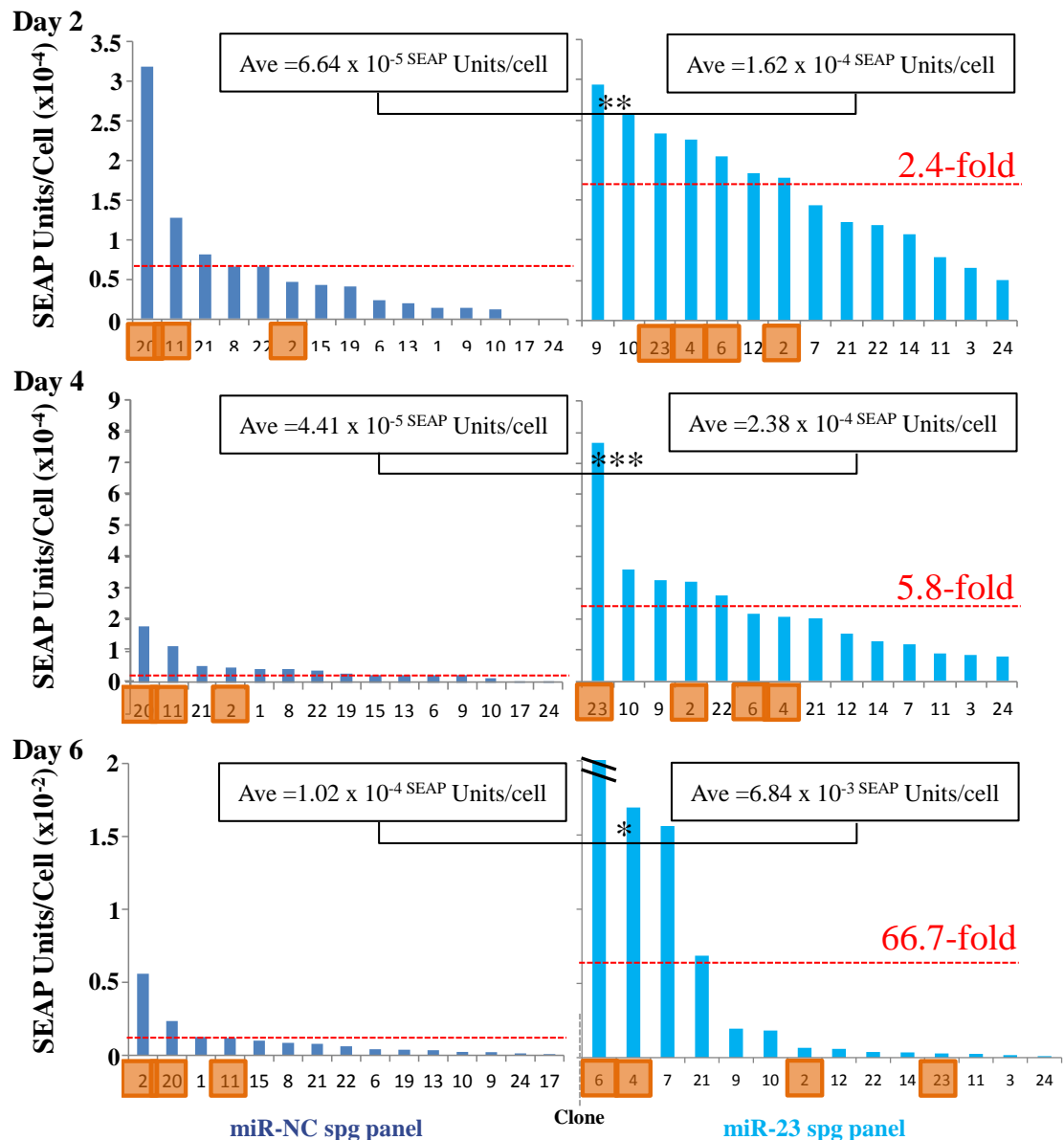


Figure 3.43: Specific SEAP productivity for all clones in both miR-23 and miR-NC sponge panels. Average specific productivity is represented as a **red broken line**. **Orange boxes** highlight the individual sponge clones that were subsequently selected for scale up. Statistical analysis was calculated using a standard student t-test ($p \leq 0.05^*$, $\leq 0.01^{**}$ and $\leq 0.001^{***}$), $n = 2$. The outlier, miR-23 clone 6 on day 6, is at a value of 4.98×10^{-2} .

Finally, clones selected from both miR-23 sponge and the miR-NC sponge panels were chosen based on volumetric SEAP production, highlighted in orange boxes (**Fig. 3.42**). From the miR-23 sponge panel, the four best producing clones were chosen for scale up (miR-23 sponge 2, 4, 6 and 23). A similar approach was taken for the selection of the miR-NC sponge clones (miR-NC sponge 2 and 11) except that miR-NC sponge clone 20

was also selected based on its high normalised productivity as well as its high volumetric productivity.

miR-23b sponge clonal panel - Batch*

In 1 mL suspension culture, the miR-23b* sponge clonal panel did not exhibit a beneficial growth phenotype as was suggested from previous characterisation in mixed pools. Although some individual clones did demonstrate an enhanced growth phenotype early into batch culture (miR-23b* spg clone 18 and 22, **Fig. 3.44^{Day 2}**), on average across the entire clonal panel, there was no growth benefit evident with clones behaving similarly to that of the miR-NC sponge panel. Furthermore, similar to what was observed for the miR-23 sponge panel, there was a 50% reduction in the maximal cell density achieved by miR-23b* sponge clones (**Fig. 3.44^{Day 4+6}**). However, unlike the observation from the miR-23 sponge panel, cell viability was similar when compared to the control panel (**Fig. 3.45**).

Figure 3.44: CHO-SEAP miR-23b* sponge clonal panel – Cell numbers/mL

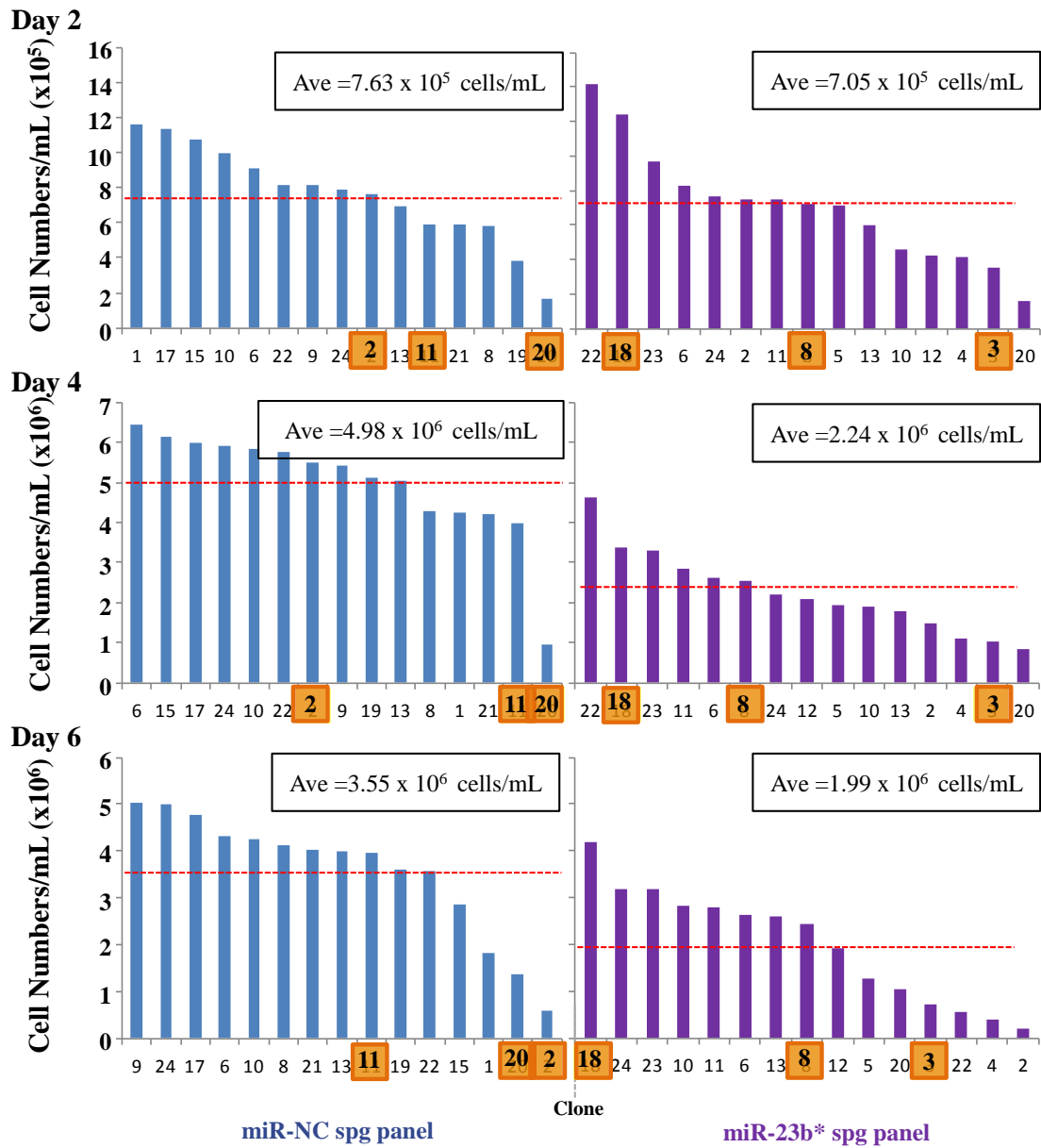


Figure 3.44: The individual performance of each clone derived from both miR-23b* sponge and miR-NC sponge mixed pools when cell growth was evaluated over a batch culture process. Average performance across all clones is represented by the broken red line with each clone that was ultimately selected for further validation highlighted with an orange box.

Figure 3.45: Day 6 cell viability of miR-23b* sponge panel

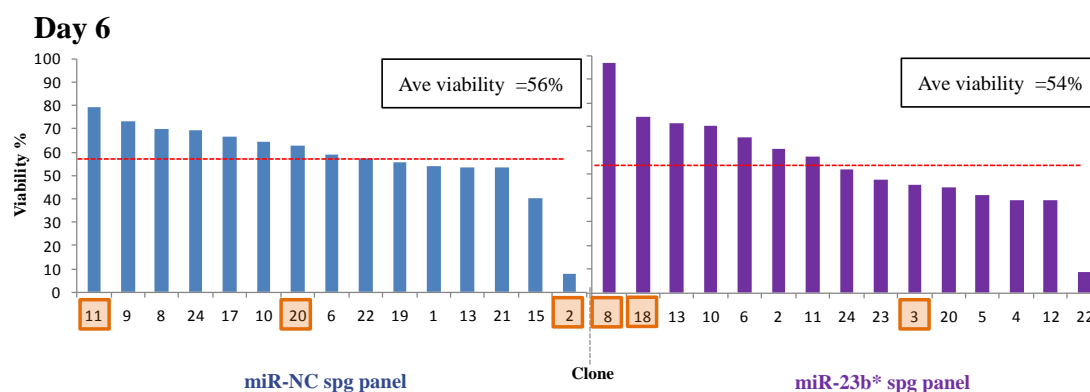


Figure 3.45: Day 6 viability for the miR-23b* and miR-NC sponge panels with average viability represented as a broken red line. No impact was observed at the earlier time points of day 2 and 4 with clones selected highlighted with an orange box.

The drastic impact previously observed on both volumetric and specific SEAP activity for the miR-23b* sponge mixed pools was not reflected in the clonal panel. SEAP activity remained unchanged on day 2 of culture while a ~20% reduction was observed on day 4 of culture (**Fig. 3.46^{Day 2+4}**). Normalised productivity also remained unchanged on day 2 of culture while being enhanced by ~2-fold ($p \leq 0.05$) on day 4 (**Fig. 3.47^{Day 2+4}**). Furthermore, although a 2-fold increase in normalised productivity was observed, this coincided with a reduction in volumetric yield by ~20% on day 4. However, on day 6 of culture, SEAP yield was measured to be ~35% increased with a further improved normalised productivity of ~3.5-fold (**Fig. 46^{Day 6}, 47^{Day 6}**).

Figure 3.46: CHO-SEAP miR-23b* sponge clonal panel – Volumetric SEAP

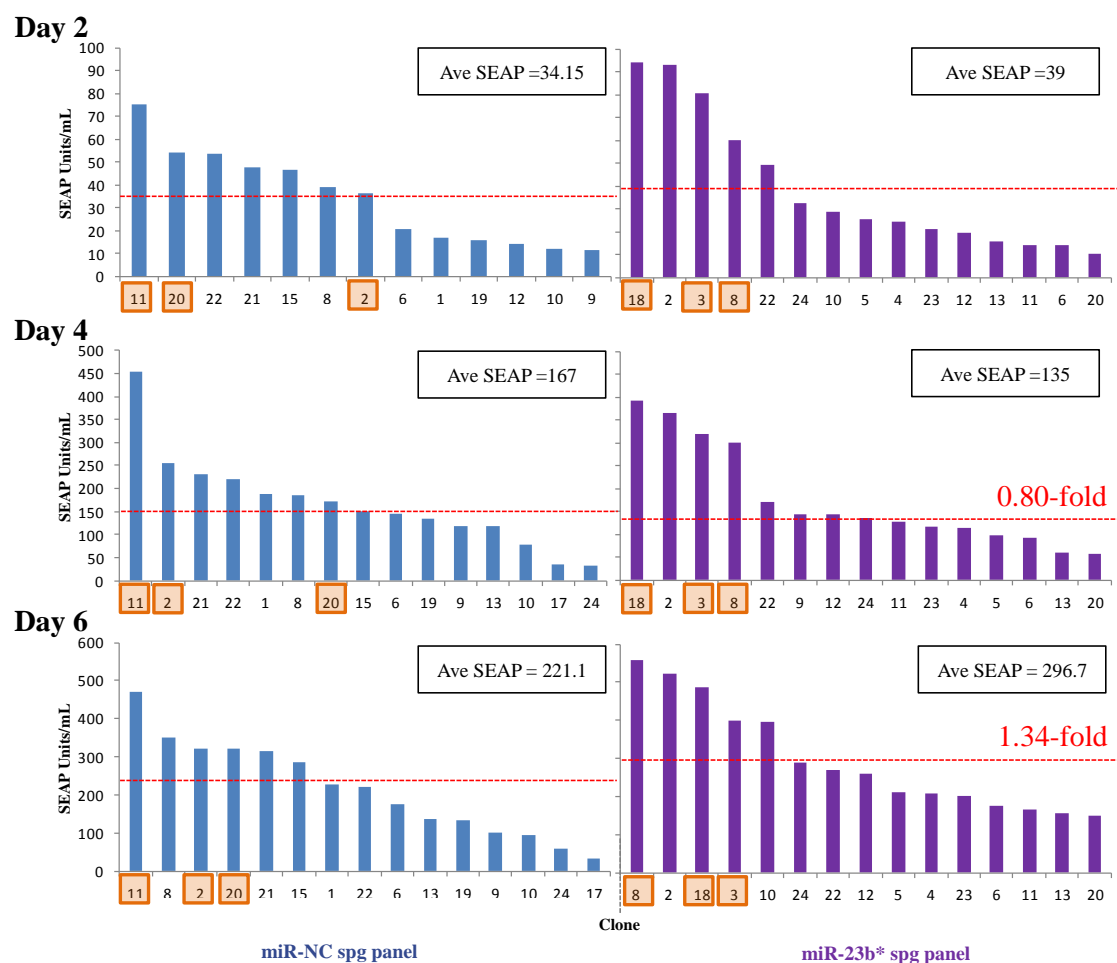


Figure 3.46: Volumetric SEAP activity for each individual clone from both miR-23b* and miR-NC sponge panels is represented above with the average performance across the clonal panels shown as a broken red line. Clones selected for scale-up are highlighted in orange boxes with no statistical significance observed for phenotypic differences calculated using a standard student t-test.

Figure 3.47: CHO-SEAP miR-23b* sponge clonal panel – Specific productivity

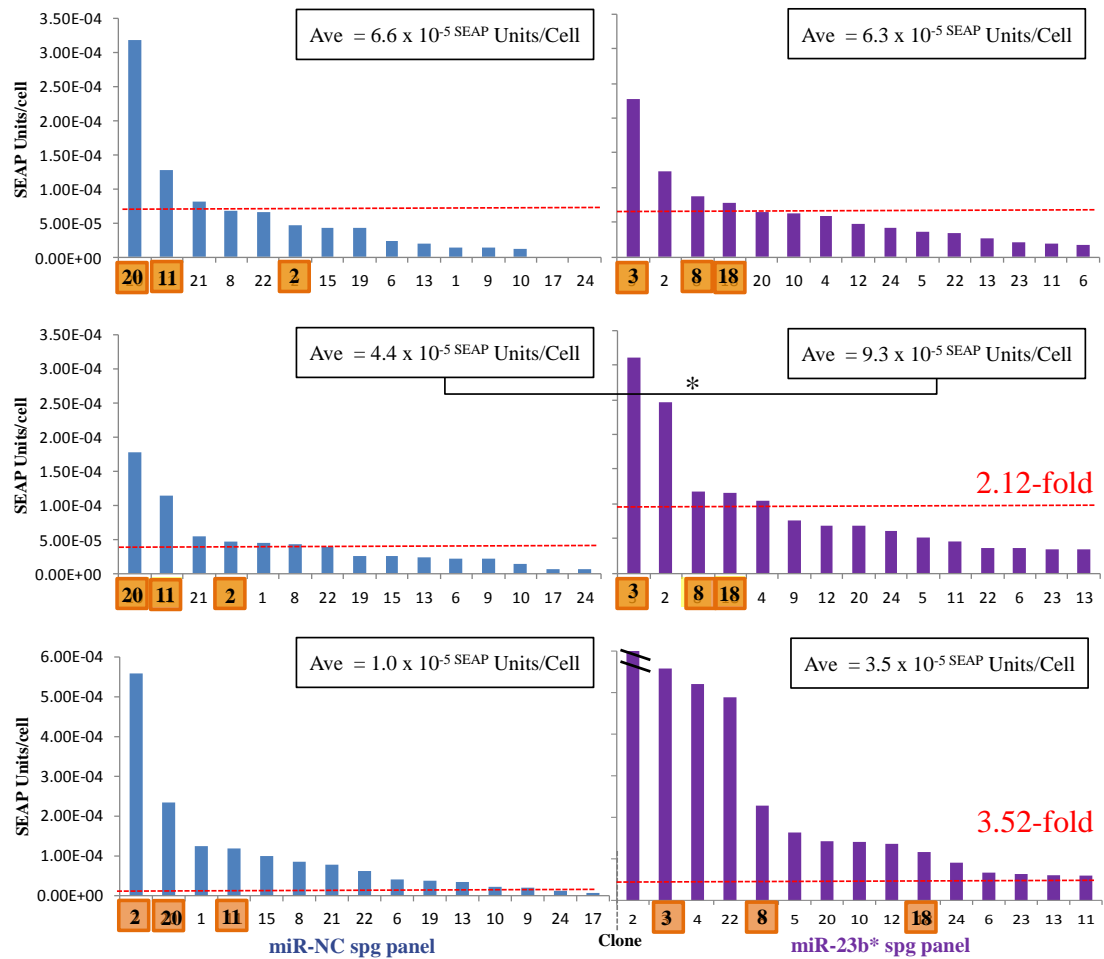


Figure 3.47: Specific SEAP productivity was calculated and graphed for each individual clone form both miR-23b* and miR-NC sponge clones. Average panel performance is represented as a **broken red line again with selected clones highlighted in an **orange box**. Statistical significance was calculated using a standard student t-test ($p \leq 0.05^*$). miR-23b* sponge clone 2 on day 6 has a value of 2.55×10^{-3} SEAP units/cell.**

Summary of miR-23 and miR-23b clonal panels*

As in indicated in mixed pools, miR-23 depleted clones demonstrated an enhanced volumetric and normalised productivity of ~ 3 -fold. Maximum cell densities achieved were observed to be reduced by $\sim 50\%$ when compared to controls resulting in a further boost in normalised productivity. miR-23b* depleted clones demonstrated no growth benefit with the exception of a couple of clones early in culture (Day 2). Similar to the miR-23 sponge clones, these clones also reached lower maximum cell densities which

could be contributing to the enhanced normalised productivity observed. SEAP yield was observed to be reduced except late in culture where it was increased by 34%. Viability was not observed to differ from control clones as opposed to miR-23 sponge clones whose viability was reduced despite exhibiting reduced cell numbers. Clones were selected based on volumetric productivity.

3.3.5.3 Impact on bioprocess phenotypes across CHO-1.14 clonal panels

Subsequent to the characterisation of the influence of both miR-23 sponge and miR-23b* sponge constructs in an stable mixed pool IgG-secreting rCHO-1.14 cell line, individual clones were sorted using FACS under the same selection criteria as was previously applied to the selection of both miR-spg SEAP clonal panels.

miR-23 sponge clonal panel - Batch

CHO-1.14 cell clones stably expressing a sponge specific for miR-23 were cultured in a 1 mL volume of CHO-S-SFM II media in suspension batch culture over the course of 6 days. As previously described, a certain number of clones were lost over the course of suspension adaptation and suitability to suspension culture. The improved cellular growth, as first observed in the predecessor mixed pools, was not as potent in the case of clones although, on average, growth was enhanced ~10% on days 2 and 4 with a more significant ~40% ($p \leq 0.001$) observed on day 6 (**Fig. 3.48**).

13 out of 22 miR-23 sponge clones demonstrated higher cell numbers when compared to the average cell density of the controls. This less potent growth benefit could potentially be attributed to the nature of the 1 mL suspension culture process of which both miR-23/23b* sponge CHO-SEAP clones demonstrated reduced growth.

Figure 3.48: CHO-1.14 (IgG) miR-23 sponge clonal panel – Cell numbers/mL

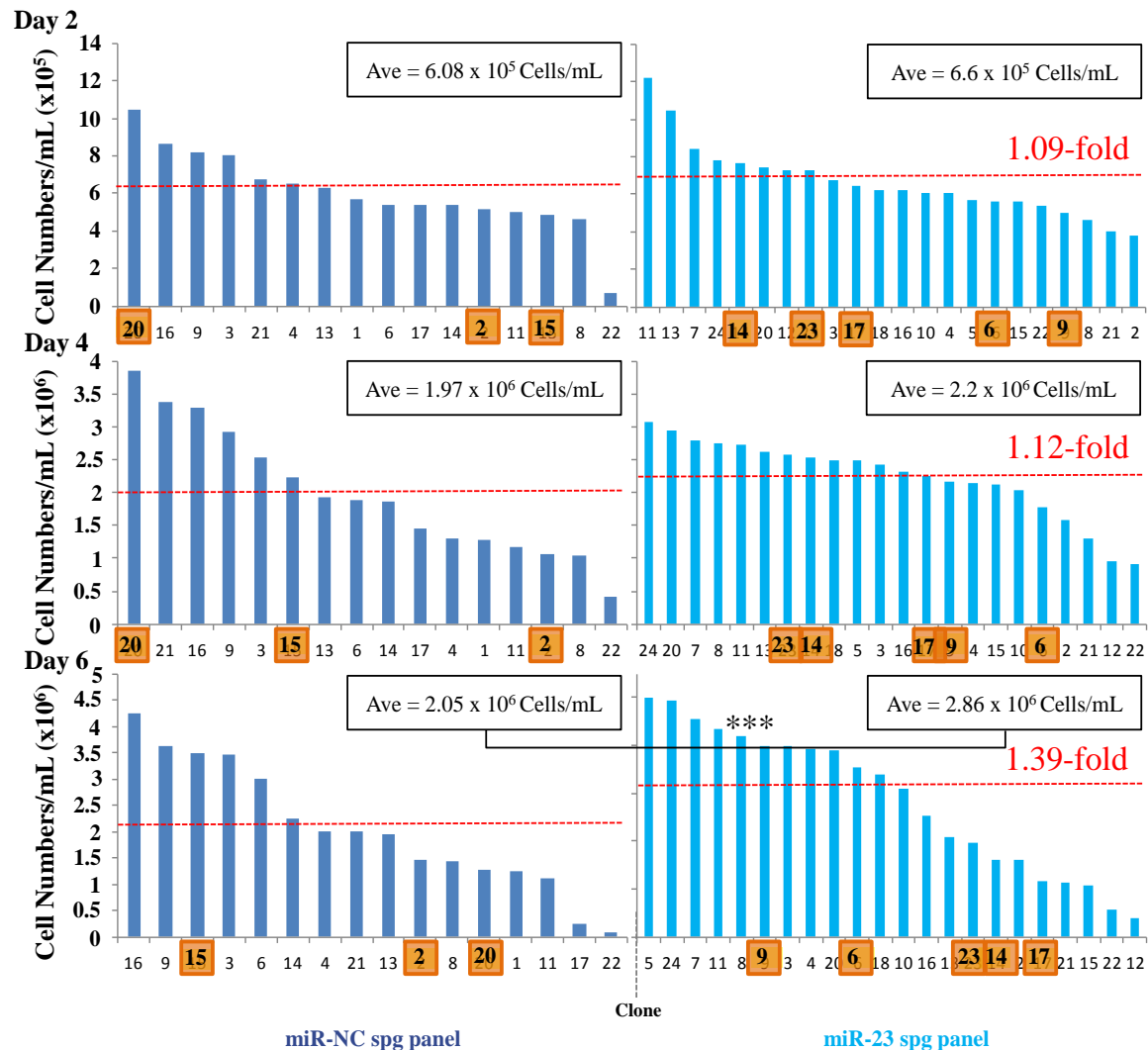


Figure 3.48: Cellular proliferation for each individual clone within the miR-23 sponge panel is represented above with the comparative miR-NC sponge panel in a CHO-1.14 cell line. The average cell numbers/mL was calculated across each panel and is represented as a **broken red line. Statistical significance was calculated using a standard student t-test ($p \leq 0.001^{***}$). Each clones ultimately selected for scale up is highlighted in an **orange box**.**

The enhanced cell density at day 6 was potentially attributed to the increased cell viability of 87.7% ($p \leq 0.001$) for miR-23 sponge clones when compared to 63.4% for controls (Fig. 3.49). The direct impact of miR-23 depletion on viability is potentially reflected in the large percentage (18/22 or 81.1%) of clones that maintained a viability of over 80% when compared to controls (8/16 or 50%).

Figure 3.49: CHO-1.14 (IgG) miR-23 sponge clonal panel – Cell viability %

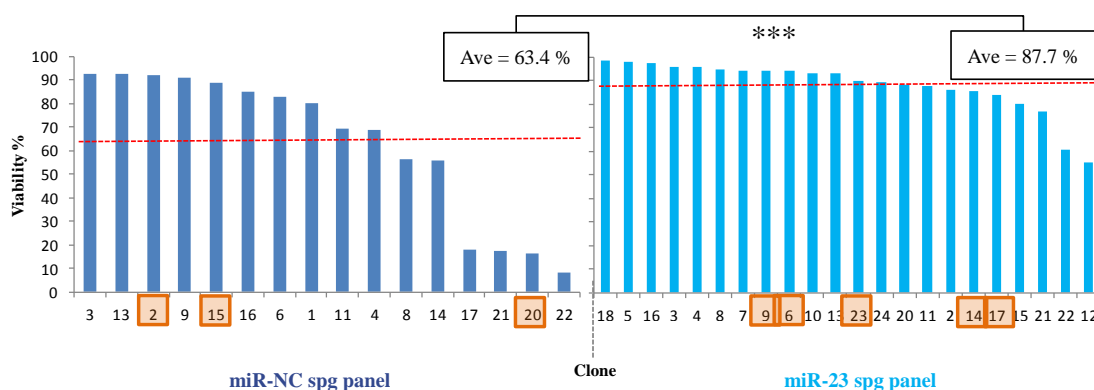


Figure 3.49: As viability remained relatively unchanged when comparing miR-23 sponge and miR-NC sponge clones on day 2 and 4, only day 6 cell viability was reported. The average cellular viability across both sponge panels is represented as a **broken red line**. Statistical significance was calculated using a standard student t-test ($p \leq 0.001^{***}$) with each clone ultimately selected for scale up being highlighted in an **orange box**.

Figure 3.50: CHO-1.14 (IgG) miR-23 sponge clonal panel – Volumetric productivity

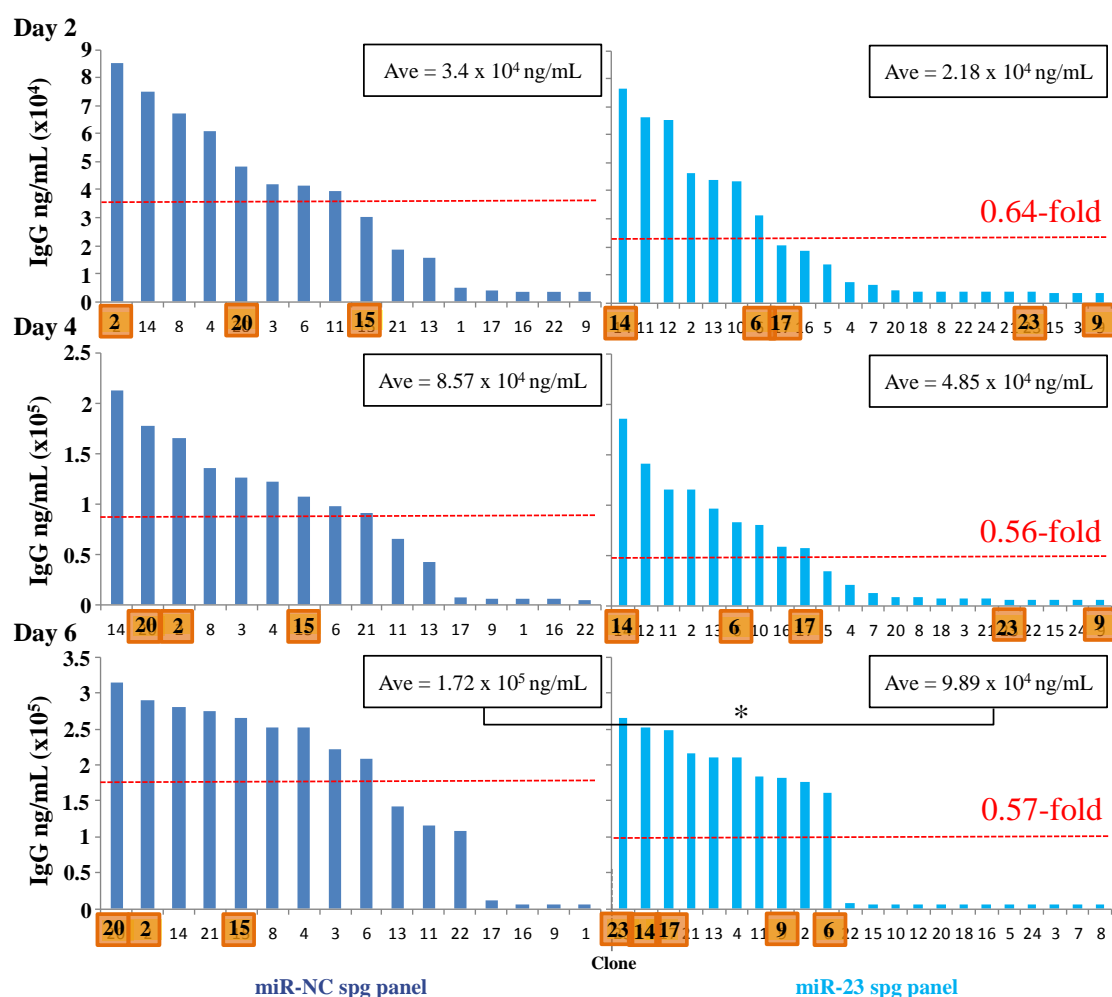


Figure 3.50: Volumetric IgG production is represented above for all clones across both sponge panels with average performance shown as a **red broken line over a 6 day batch culture process. Clones selected for scale up are highlighted in **orange boxes**. Statistical significance was calculated using a standard student t-test ($p \leq 0.05^*$).**

It was observed that a significant number of individual clones completely lost IgG production, with a higher proportion in miR-23 sponge clones. Statistical analysis was performed on all clones. A reduction in volumetric IgG was observed on days 2 (~35%) and 4 (~45%), and 6 (~40%, $p \leq 0.05$) in miR-23 depleted clone panels (**Fig. 3.50**). Day 6 demonstrated the largest reduction in specific productivity (~60%, **Fig. 3.51**).

Figure 3.51: CHO-1.14 (IgG) miR-23b sponge clonal panel – Specific productivity

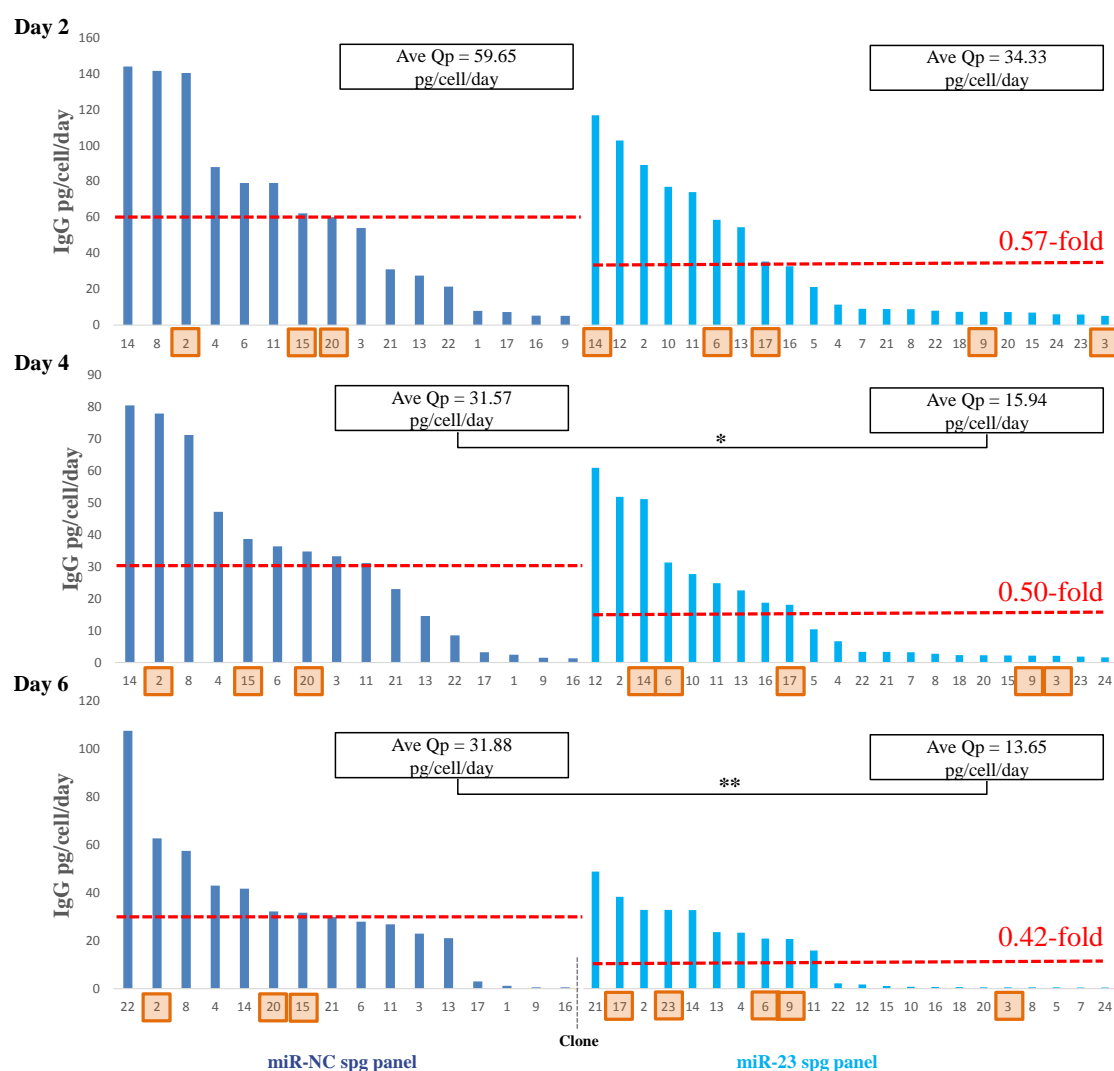


Figure 3.51: Specific productivity for CHO clones engineered with a sponge specific for miR-23 versus a control non-specific sponge. Average specific productivity is represented a broken red line. Clones selected for scale up are highlighted in an orange box. Statistical analysis was calculated using a standard student t-test ($p \leq 0.05^*$ and $p \leq 0.01^{}$).**

As improved viability was observed to be potentially mediated through miR-23 depletion, all clones selected from the miR-23 panel demonstrated a viability above 80%. Additionally, although enhanced cellular proliferation was observed within the mixed pools to the detriment of productivity, a combination of both proliferation and productivity was considered when selecting clones. For example, of the 5 best performing miR-23 sponge clones (clone 5, 7, 8, 11 and 24), when viable cell numbers were assessed

(**Fig. 3.48**^{Day 6}), only 1 clone (clone 11) remained in the topmost performing group of clones when volumetric IgG secretion was assessed, with the remaining 4 clones producing below detectable limits. For these reasons clones were chosen based on day 6 volumetric IgG values (miR-23 sponge clones 6, 9, 14, 17 and 23) as particular clones (clone 9 and 23) demonstrated high secreted IgG levels at this time point while producing below the ELISA sensitivity on days 2 and 4. Clonal selection from the miR-NC sponge panel (clones 2, 15 and 20) was based on similar criteria.

miR-23b sponge clonal panel - Batch*

Next, the influence of miR-23b* depletion was assessed in clones derived from the stable IgG-secreting CHO-1.14 mixed pool. These were observed previously to have an enhanced proliferation capacity of 20-50% at the expense of productivity. Furthermore, cell viability late into the culture process was increased by 10-15% when compared to controls.

An increase in growth of ~50% ($p \leq 0.001$) was observed on day 2 of culture when compared to control sponge panels (**Fig. 3.52**^{Day 2}) with a ~30% ($p \leq 0.01$) improved maximal cell density. However, it was noted that particular NC-sponge clones (clone 20, 21 and 16) reached similar cell numbers at this time point (**Fig. 3.52**^{Day 4}). 20 of 22 (90%) of miR-23b* sponge clones exceeded the average growth performance of the control panel. Furthermore, an average 50% ($p \leq 0.01$) increase in cell density was maintained at day 6 of culture potentially resulting from an extended viability (**Fig. 3.52**^{Day 6}).

An average additional 25% ($p \leq 0.001$) viability was observed when compared to the average of the control panel (87.9% versus 63.4%, **Fig. 3.53**), a phenotype previously seen to a lesser extent in mixed pools.

Figure 3.52: CHO-1.14 (IgG) miR-23b* sponge clonal panel – Cell numbers/mL

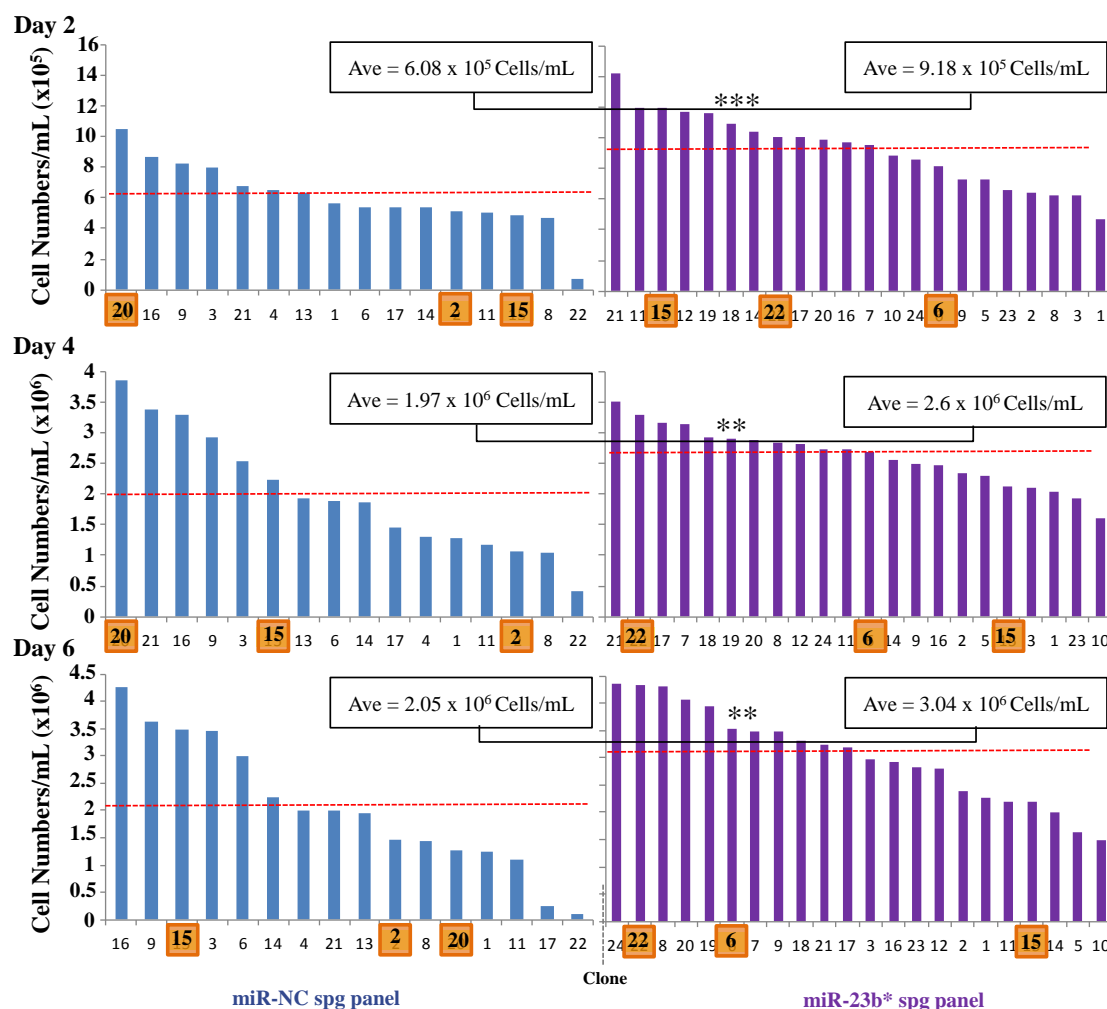


Figure 3.52: The viable cell numbers/mL for clonal miR-23b* and miR-NC sponge populations derived from their predecessor mixed pools. Individual clonal performance is represented with the average performance across the panel being shown as a **broken red line. Clones selected for scale up are highlighted in an **orange box**. Statistical significance was calculated using a standard student t-test ($p \leq 0.01^{**}$ and $\leq 0.001^{***}$).**

Figure 3.53: CHO-1.14 (IgG) miR-23b* sponge clonal panel – Cell viability %

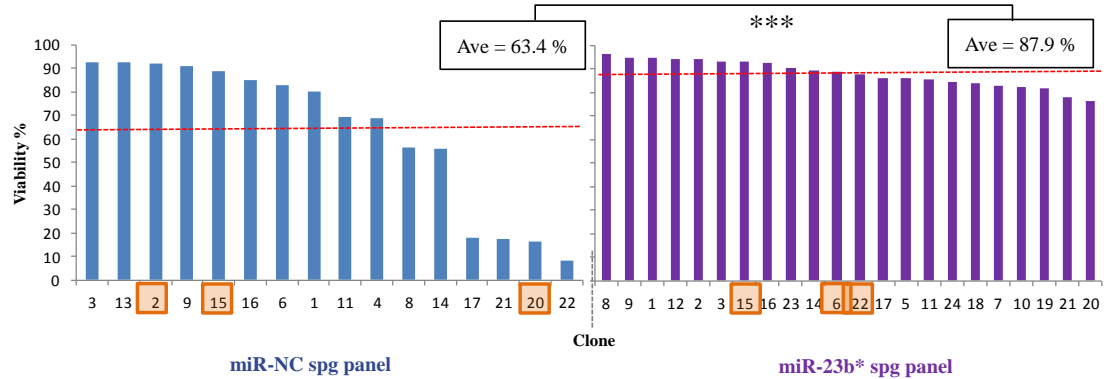


Figure 3.53: Cellular viability status of both miR-23b* and miR-NC rCHO-1.14 clones late in culture. Average viability across each clonal panel is represented by a **broken red line. Clones that were ultimately selected for scale up are highlighted in **orange boxes**. Statistical significance is was calculated using a standard student t-test ($p \leq 0.001^{***}$).**

Day 2

miR-NC spg panel: Ave = 3.4×10^4 ng/mL

miR-23b* spg panel: Ave = 2.35×10^4 ng/mL

Day 4

miR-NC spg panel: Ave = 8.57×10^4 ng/mL

miR-23b* spg panel: Ave = 4.69×10^4 ng/mL

Day 6

miR-NC spg panel: Ave = 1.72×10^5 ng/mL

miR-23b* spg panel: Ave = 9.51×10^5 ng/mL

0.69-fold (Day 2), 0.54-fold (Day 4), 0.55-fold (Day 6)

Similarly to the miR-23 sponge panel, a significant number of miR-23b* clones completely lost IgG production but were included in statistical analysis. An average reduction of 30-45% was observed in volumetric IgG across all time points (**Fig. 3.54**). Cell specific productivity was significantly reduced by ~50% ($p \leq 0.05$) on day 2 and ~60-65% on day 4 and 6 ($p \leq 0.01$), respectively (**Fig. 3.55**).

Figure 3.55: CHO-1.14 (IgG) miR-23b* sponge clonal panel – Specific productivity

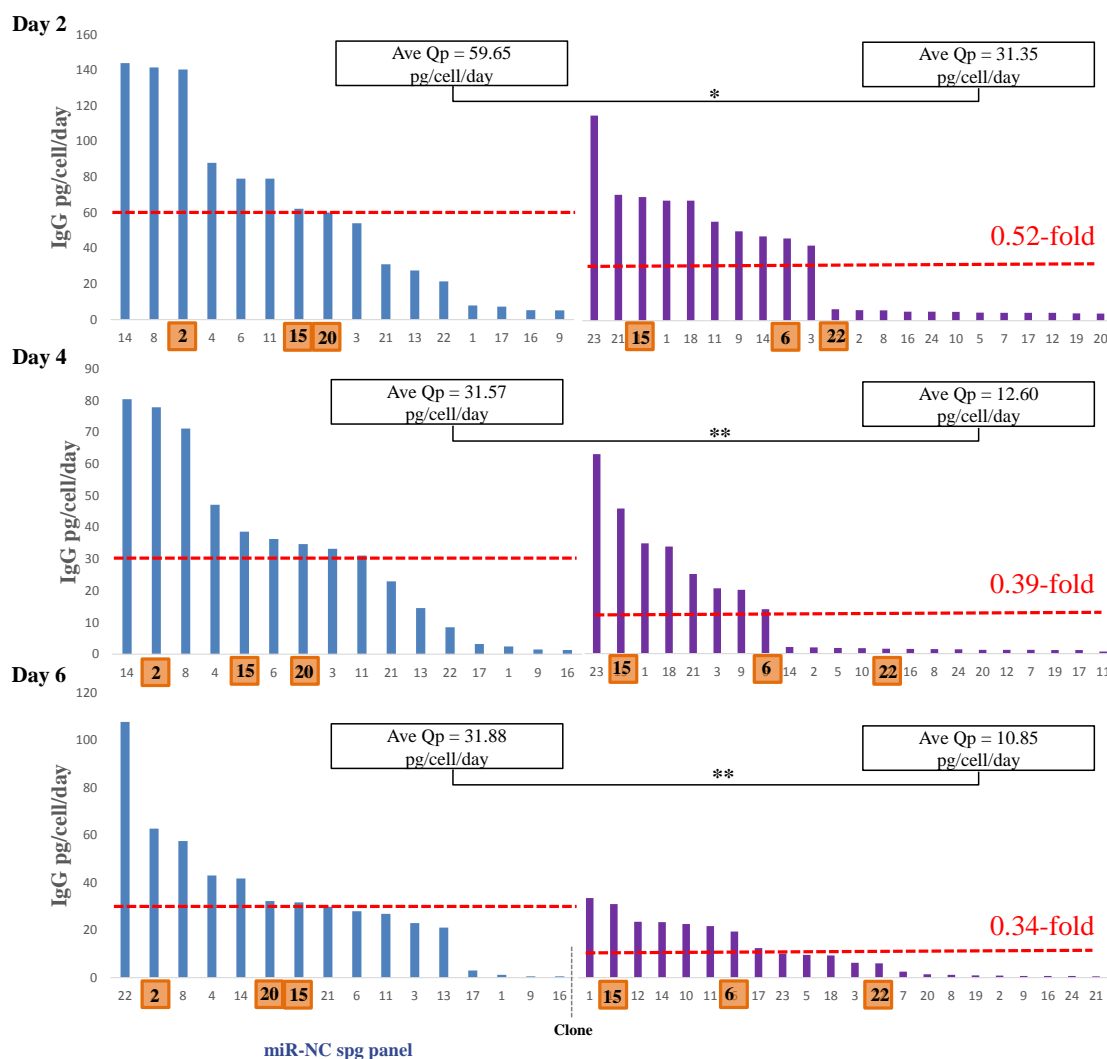


Figure 3.55: Specific productivity for each clone from both miR-23b* and miR-NC sponge panels are shown above with the average performance represented as a **broken red line. Statistics were calculated using a standard student t-test ($p \leq 0.05^*$ and $\leq 0.01^{**}$) with each clone chosen for scale up highlighted in an **orange box**.**

The significant number of miR-23b* depleted clones that exhibited a reduced IgG titre below the detectable limits of the ELISA is potentially due to the inherent reduction in productivity due to the enhanced growth phenotype as previously observed for mixed populations in CHO-1.14 and additionally conserved in CHO-SEAP stables (not as dramatic a growth impact). Clones ultimately selected for 5 mL scale up were based on their viability and cell growth attributes while also maintaining a production capacity. Although clonal selection proved difficult, it was anticipated that if miR-23b* depletion

mediated apoptosis resistance in selected clones, their inherent reduced specific productivity would be overcome by a potential prolonged production phase, potentially achieving higher volumetric titres. Clones 6, 15 and 22 were selected from the miR-23b* sponge panel and clones 2, 15 and 20 were selected from the miR-NC sponge panel, as before for miR-23 sponge comparison.

3.3.6 Investigation of miR-23 and -23b* depletion on selected clones in 5mL Batch, Fed-Batch and Fed-batch temperature shift

This next section characterises the performance of clonal behaviour for both stable miR-23 and miR-23b* sponge CHO-SEAPs over a series of commonly implemented bioprocess regimes including batch, fed-batch and temperature shift fed-batch.

3.3.6.1 miR-23 and miR-23b* sponge CHO-SEAP clones

miR-23 sponge clones - Batch

Clones selected from the clonal panel screen (Clones 2, 4, 6 and 23) were seeded at 2×10^5 cells/mL in a 5 mL working volume in a 50 mL vented spin tube (37 °C at 170 rpm). A slight variation in maximal cell density was evident between all clones to within a range of 1×10^6 /mL, potentially attributed to clonal variation (**Fig. 3.56 A**). A range of viabilities was observed with a single control clone remaining above 80%, potentially an innate clonal benefit (**Fig. 3.56 B**).

Productivity was represented as a range with each test clone being compared to the best and worst performing control clone. Statistical analysis was calculated for each test clone against the pooled values for each control clone. The best performing clones were miR-23 spg 4 and 6, both demonstrating similar SEAP activity increases of 2-6-fold ($p \leq 0.001$) while exhibiting a 2-5-fold enhanced normalised productivity as a result of a slightly higher cell density (**Fig. 3.56 C and D**). The lowest performing miR-23 sponge clone (miR-23 spg 2) still maintained a higher SEAP activity when compared to the best performing control clone ranging from 1.25-3-fold ($p \leq 0.001$).

A note to make at this point would be the apparent dramatic increase in normalised productivity of the control clone, miR-NC spg 20. When cultured in 5 mL volumes, this clone had a propensity to clump therefore exhibiting an apparent reduced cell density thus resulting in an enhanced normalised productivity calculation. Subsequent bioprocess characterisation was carried out with this clone omitted. Additionally, miR-23 sponge clone 4 and 6 were retained as they both exhibited similar characteristics.

Figure 3.56: miR-23 sponge clones 2, 4, 6 and 23 under 5 mL batch conditions

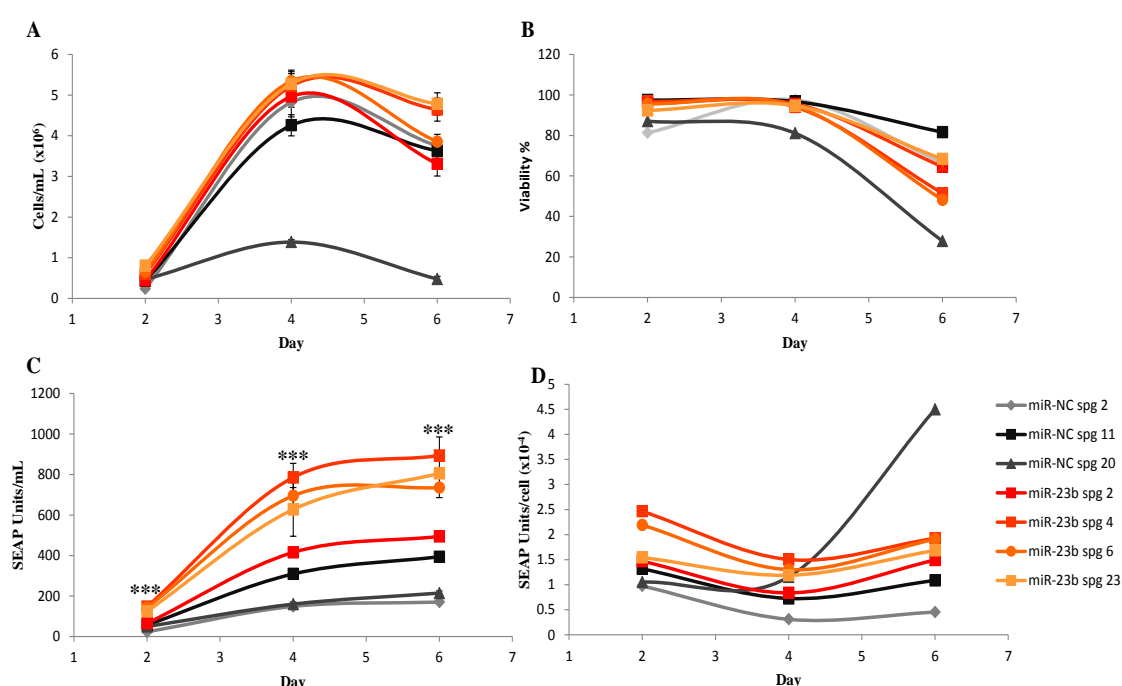


Figure 3.56: CHO-SEAP stable clones 2, 4, 6 and 23 stably depleted of miR-23 grown under batch condition in a 5 mL volume seeded at 2×10^5 cell/mL are represented above in different shades of red while miR-NC clones 2, 11 and 20 are shown in various shades of black (n = 3). Clone performance is reported in text as a range compared to the best and worst control clone while statistical significance was calculated based on the combined values for all control clones ($p \leq 0.001^{*}$, standard student t-test).**

It is evident that miR-23 depleted clones selected from the mixed pool exhibited a maximum 2-fold increase in volumetric SEAP activity when compared to their mixed population predecessors under batch conditions (**Fig. 3.57**), highlighting the benefits of clonal isolation.

Another interesting observation was that a similar SEAP activity was observed in miR-23 sponge clones cultured in 1 mL and 5 mL batch culture despite reduced maximal cell densities achieved in 1 mL culture. This SEAP activity was attributed to an increased normalised productivity (~2-fold) for those clones that reached a lower cell density.

Figure 3.57: Volumetric SEAP performance of miR-23 sponge clones versus miR-23 sponge mixed pools

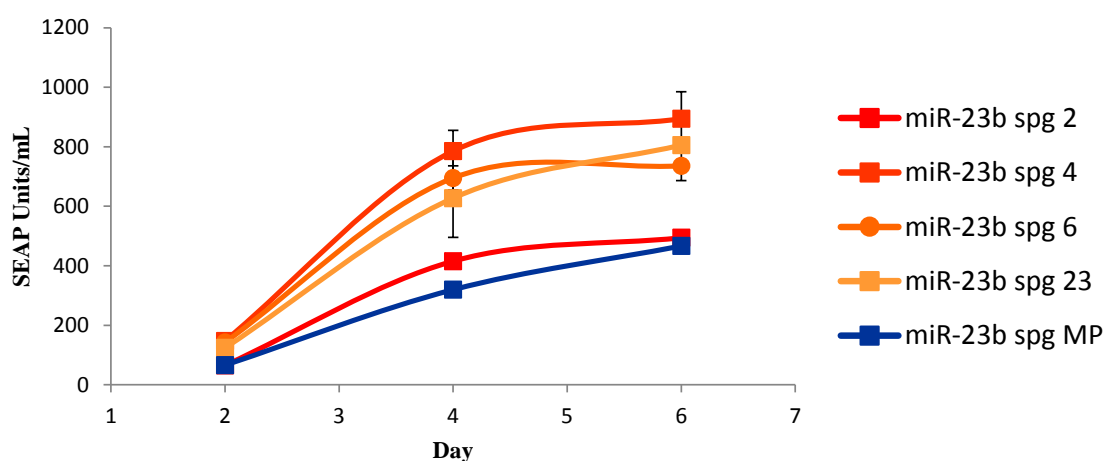


Figure 3.57: Various performing clones that make up a mixed population as a result of the nature of plasmid integration and expression upon transgenic CHO cell line generation. The SEAP activity is compared between the predecessor miR-23 sponge mixed CHO cell population and the subsequently isolated clones.

miR-23 sponge clones – Fed-batch

Next we assessed whether a fed-batch process would further enhance cell density of these high SEAP producing clones potentially improving productivity. miR-23 sponge clones 4 and 6 were evaluated as they both demonstrated similar attributes as well as miR-NC spg 2 and 11. Clonal variation was once again evident upon the addition of a feed with a range of maximal cell densities being observed (**Fig. 3.58 A**).

Figure 3.58: miR-23 sponge clone 4 and 6 under 5 mL Fed-Batch conditions

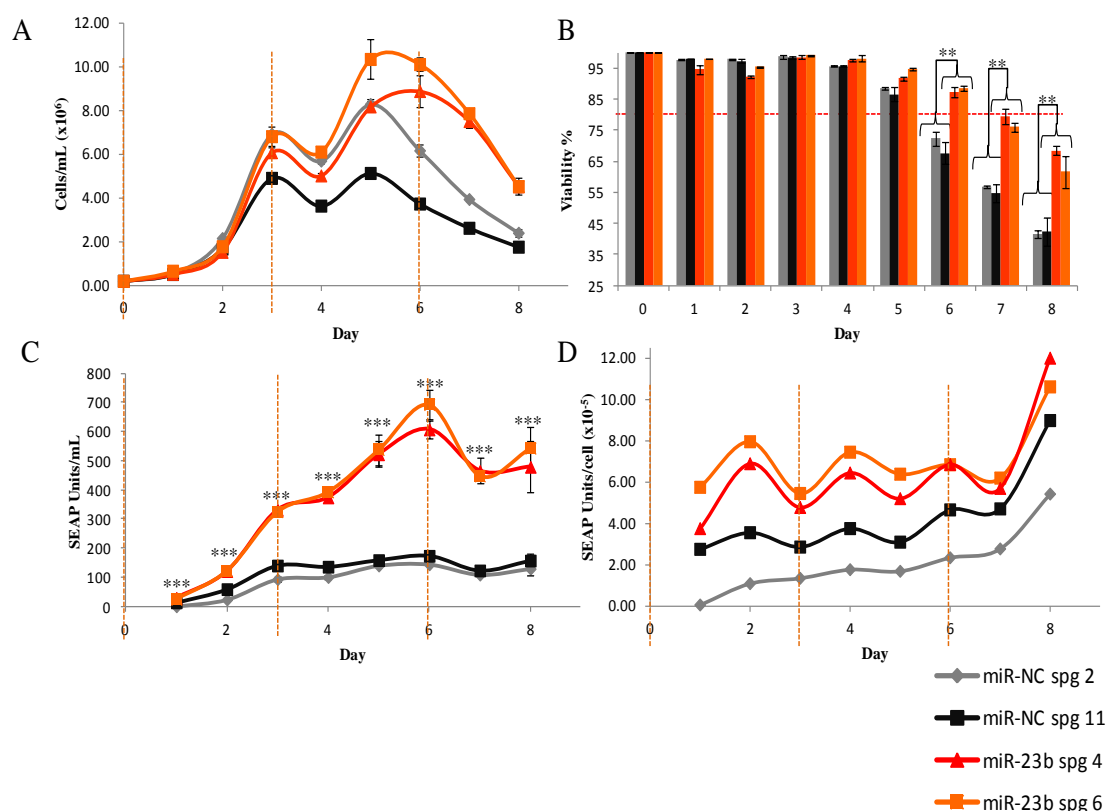


Figure 3.58: An 8 day fed-batch culture with a working volume of 5 mL (+ initial feed of 15% v/v, represented with a broken orange line) seeded at 2×10^5 cell/mL with subsequent feeding of 10% (v/v) every 3 days. A) Cell numbers/mL, B) Cell viability with 80% viability threshold represented as a broken red line, C) Volumetric SEAP activity/mL with statistical significance calculated based on each test clone versus all three combined control clones ($p \leq 0.001$, student t-test) and D) specific SEAP activity per cell, $n = 2$.

Both miR-23 sponge clones 4 and 6 exhibited an enhanced viability of $\sim 20\%$ ($p \leq 0.01$) on days 6, 7 and 8 of culture when compared to control clones while also maintaining a prolonged viability above the 80% threshold for an additional 48 h (**Fig. 3.58 B**). Both miR-23 depleted clones exhibited a 2-6-fold ($p \leq 0.001$) increase in SEAP activity when compared to controls (**Fig. 3.58 C**). Given the various growth phenotypes observed, normalised productivity was improved but not proportional to volumetric productivity (**Fig. 3.58 D**). It was observed that that maximum SEAP produced was reduced in Fed-batch for miR-23 depleted clones when compared to batch despite the improved cell densities, possibly due to a compromise in normalised SEAP production.

miR-23 sponge clones – Fed-batch with Temperature shift

Another commonly implemented process utilised in industry is hypothermic growth conditions (Kumar, Gammell & Clynes 2007). By reducing the culture temperature from 37 °C to ~31 °C, specific CHO cell productivity can be enhanced through arrest in the G₁-phase of the cell cycle, the most transcriptionally active phase.

With the observation that fed-batch boosted both growth and maximum cell density of our miR-23 sponge CHO-SEAP clones with the addition of imparting an extended viable production phase above 80% for a further 48 h, we sought to overcome the reduced SEAP activity when compared to batch culture by inducing a temperature shift thus potentially enhancing specific productivity and prolonging culture longevity.

Fed-batch was carried out as previously described with a temperature shift to 31 °C after 72 h of culture. Both miR-23 and miR-NC sponge clones performed similar over the first three days of fed-batch culture reaching cell densities of ~ 6 x 10⁶ cells/mL prior to temperature shift, as observed previously. Cellular proliferation was observed to be halted upon shift to 31 °C three days into culture for all clones except miR-NC spg 2 which climbed a further 2 x 10⁶ cell/mL at its maximum (**Fig. 3.59 A**). A gradual decrease in cell density, forming the induced production phase, can be observed upon TS which was due to a combination of both cell death and cellular clumping. Another interesting observation was that miR-23 sponge clones appeared to be sensitive to TS demonstrating a negative response to hypothermic culture conditions dropping below the 80% viability threshold on day 5 (**Fig. 3.59 B**) when compared to day 7 in the absence of TS (**Fig. 3.58 B**). However, a viable production phase of ~60% was maintained as far as day 13 of culture. Furthermore, miR-NC clones declined faster in viability at very late culture time points with a significant separation observed of ~10-20% ($p \leq 0.05$) (**Fig. 3.59 B**).

Enhanced SEAP productivity of 2-4-fold (Volumetric, $p \leq 0.001$) and 2-5-fold (Normalised) respectively, was observed for miR-23 depleted clones (**Fig. 3.59 C and D**).

Figure 3.59: miR-23 sponge clones under Fed-batch temperature shift

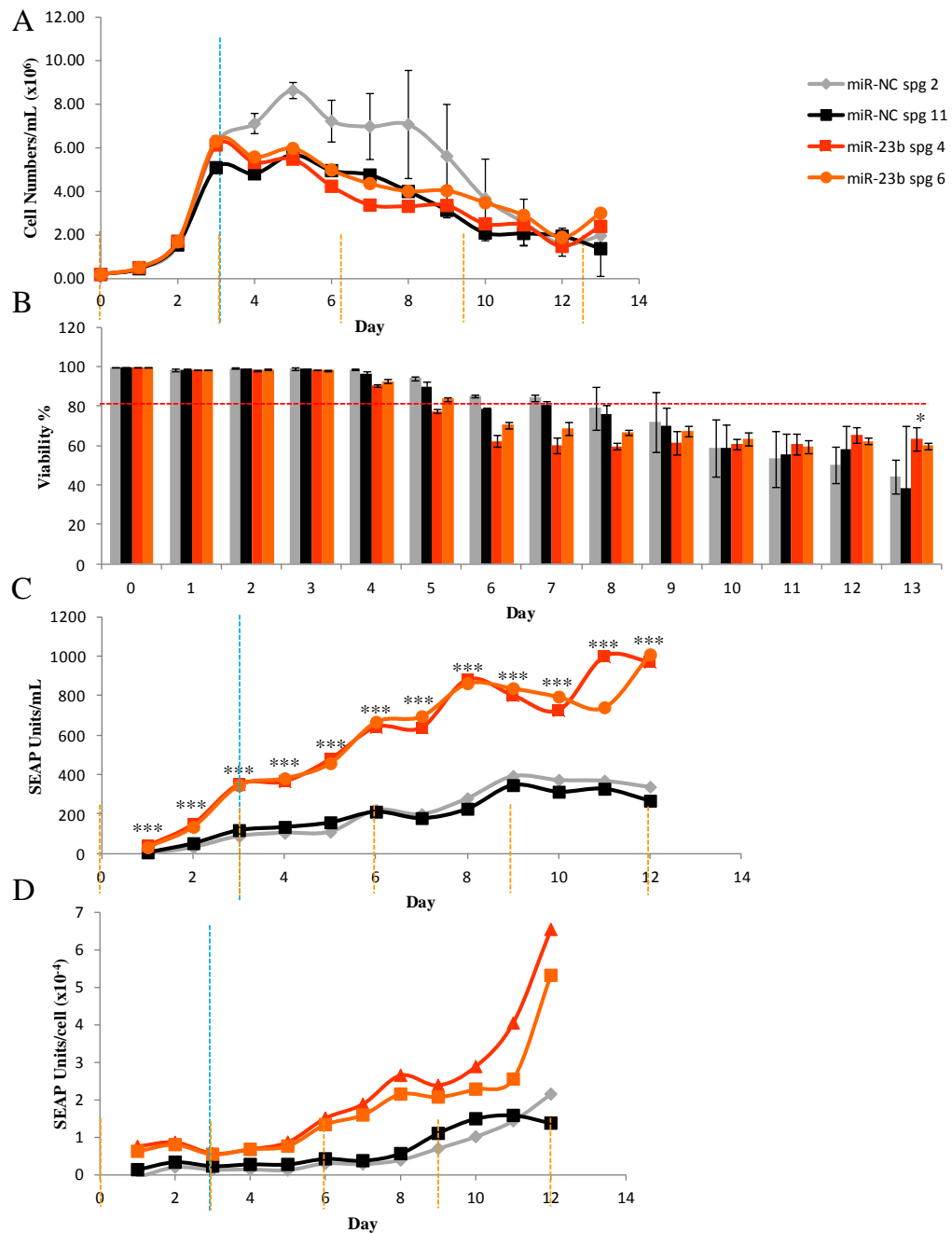


Figure 3.59: miR-23 sponge clones 4 and 6 were subjected to fed-batch (Orange broken line) temperature shift (broken blue line) as a means to exploit the increased cell densities accumulated in early culture while subsequently potentially improving specific productivity and reducing the onset of apoptosis. Nutrient feeds were as described in the case of a fed-batch. Phenotypes assessed were A) Viable cell numbers/mL, B) Cellular viability with an 80% viability threshold represented as a broken red line, C) Volumetric SEAP activity and D) specific productivity. Statistics were calculated using a standard student t-test ($p \leq 0.05$, $p \leq 0.001$ *) and an $n = 2$.**

Normalised productivity was observed to be increased in fed-batch with temperature shift when compared to fed-batch only for miR-23 sponge clones, with normalised productivity spikes in late culture potentially attributed to clumping (**Fig. 3.60**).

Figure 3.60: miR-23 sponge 4 and 6 clones specific productivity under Fed-batch and fed-batch temperature shift

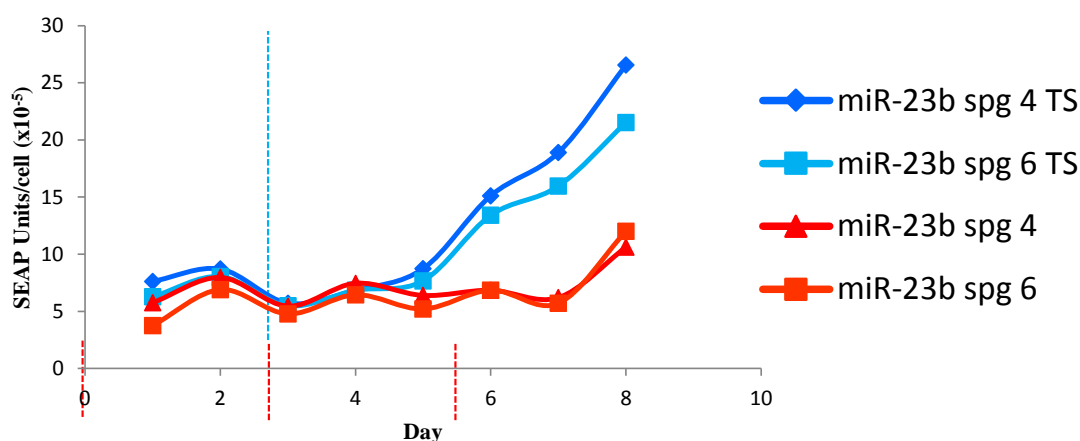


Figure 3.60: The influence of a fed-batch versus a fed-batch with temperature shift on specific SEAP productivity is compared above for clone 4 and 6 that have been engineered to stably deplete miR-23. Nutrient feeds are as previously described (15% v/v on Day 0 and 10% v/v every 72 hs) and represented as a broken orange line. Temperature shift (TS) to 31°C is denoted on day 3 as a broken blue line.

miR-23b sponge clones - Batch*

miR-23b* sponge SEAP clones (clone 3,8 and 18) were selected based on their growth and productivity phenotype when evaluated under 1 mL suspension.. A range of growth phenotypes were observed when clones were cultured under 5 mL batch conditions. One clone in particular, miR-23b* spg 18, demonstrated an enhanced growth phenotype on day 4 of culture achieving an improved maximum cell concentration of 42% ($p \leq 0.01$) when compared to the highest performing control clone (**Fig. 3.61 A**). Furthermore, this clone maintained a high viable cell density of 91.1% ($p \leq 0.05$) late in culture when compared to controls (66.4, 81.6 and 27.8) (**Fig. 3.61 B**). When normalised productivity was compared to miR-NC spg 11, the highest producing control clone, all miR-23b* spg

clones demonstrated a reduced output across all time points ranging from 75-35% (**Fig. 3.61 D**). However, miR-23b* spg 18 produced an equivalent volumetric SEAP yield on day 6 despite this observed reduced normalised SEAP activity (**Fig. 3.61 C**). This observation was potentially due to the enhanced maximal cell density achieved coupled with the prolonged viability thus mediating a prolonged viable production phase.

With the observation of this highly attractive phenotype, miR-23b* spg clone 18 was carried on for further validation using various culture conditions.

Figure 3.61: miR-23b* sponge CHO-SEAP clones under batch conditions

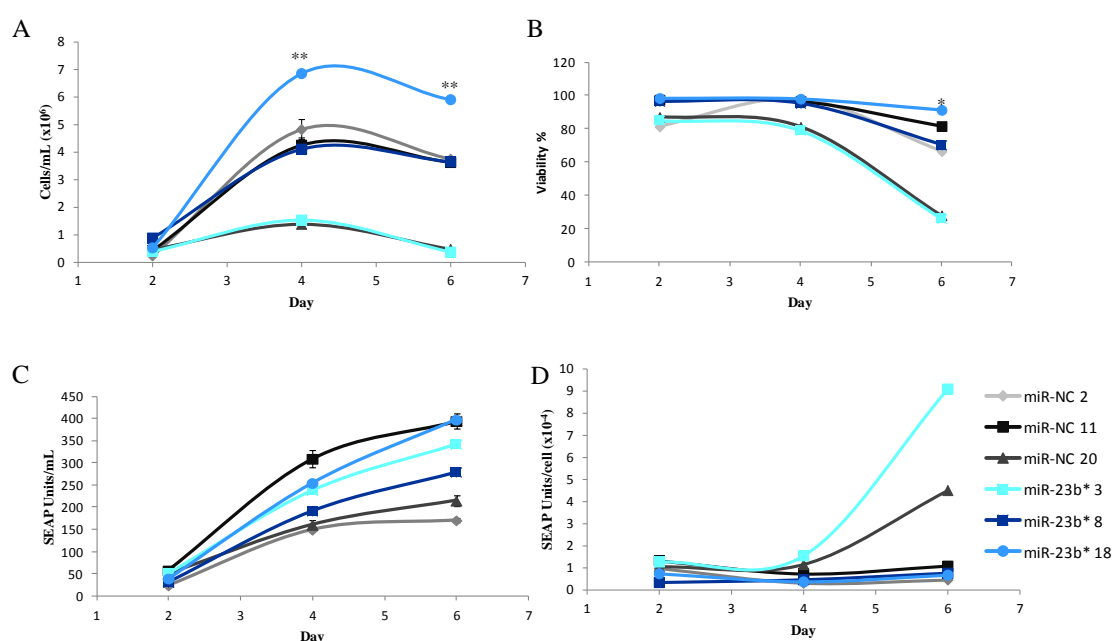


Figure 3.61: miR-23b* sponge CHO-SEAP clones cultured under batch conditions are represented above for all bioprocess phenotypes including A) Cell numbers/mL, B) Cellular viability, C) Volumetric SEAP activity/mL and D) Specific SEAP activity/cell. Statistical significance was calculated using the standard student t-test ($p \leq 0.01^{}$) and an $n = 3$.**

miR-23b sponge clone 18 – Fed-batch*

A similar phenotype was observed when miR-23b* sponge clone 18 was cultured in the presence of a feed as had been observed when under batch conditions. The addition of a feed did not boost maximal cell densities achieved by the miR-23b* spg 18 clone as its

growth profile was previously observed to be high under batch conditions. This clone demonstrated an intermediate growth profile when compared to both miR-NC 2 and miR-NC 11 (**Fig. 3.62 A**). An extended viability was observed for clone 18 with a further 48 hs of culture above 80% viability ($p \leq 0.001$) when compared to control clones (**Fig. 3.62 B**). The benefit of this extended viable production phase was again reflected in the gradual increase in volumetric SEAP activity of miR-23b* spg 18 producing ~10% more than the highest producing control clone (**Fig. 3.62 C**) despite a reduced normalised productivity, 75-30% (**Fig. 3.62 D**).

Figure 3.62: miR-23b* sponge clone 18 CHO-SEAP under fed-batch conditions

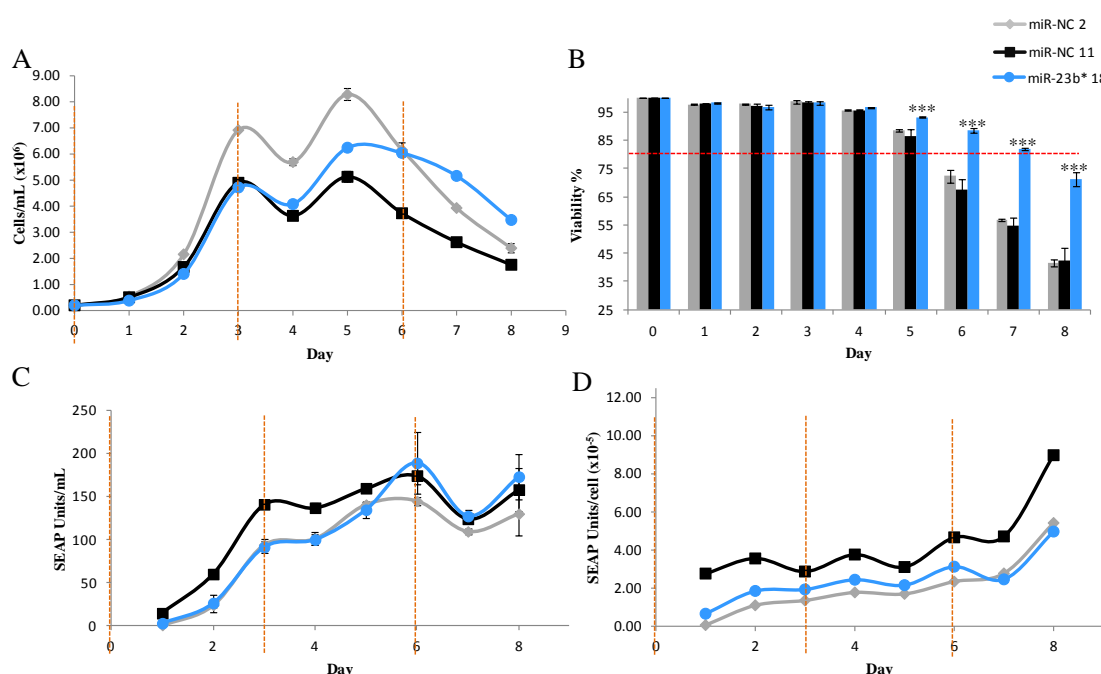


Figure 3.62: Fed-batch culture results for miR-23b* spg 18 versus two top performing control sponge clones (miR-NC spg 2 and 11). Cells were seeded at 2×10^5 cells/mL with an initial feed of 15% (v/v) and an additional subsequent feed of 10% (v/v) every 72 h represented as a **broken orange line**. Graphs demonstrate A) Cell numbers/mL, B) Cell viability with an 80% viability threshold shown as a **broken red line**, C) Volumetric SEAP activity/mL and D) Normalised productivity. Statistical significance was calculated using the standard student t-test ($p \leq 0.001^{***}$), $n = 2$.

miR-23b sponge clone 18 – Fed-batch with Temperature shift*

With the observation that this miR-23b* sponge clone exhibited a beneficial viability phenotype when compared to controls that ultimately improved the production phenotype, we sought to further enhance the production phase through the utilisation of hypothermic growth conditions.

miR-23b* spg clone 18 exhibited similar cell densities to controls over the three days prior to TS with an immediate growth arrest being observed upon transfer to 31 °C (**Fig. 3.63 A**). A prolonged viable production phase was observed in the case of miR-23b* depletion in clone 18 ($p \leq 0.001$ -0.05 at various time points) while remaining above 80% viability for a further 5 days when compared to controls (**Fig. 3.63 B**). Volumetric yield was boosted by 20-80% ($p \leq 0.001$) over various time points (**Fig. 3.63 C**). Normalised productivity was observed to be lower than controls at the early stages of the culture process but appeared to be gradually improved later into culture due to the gradual reduction in cell numbers and the increase in SEAP activity (**Fig. 3.63 D**).

From progressing particular CHO clones generated from both the miR-23 sponge and miR-23b* panels through various culture processes, it was evident that both miRNA engineering approaches endowed a beneficial CHO cell phenotype although miR-23 depletion was more consistent than miR-23b*, which allowed for the isolation of a single clone (clone 18) with an enhanced viability performance. The observed prolonged viability suited this miR-23b* sponge clone to the bioprocess of fed-batch with temperature shift. miR-23 sponge clones exhibited an attractive phenotype suitable to several production platforms (batch, fed-batch and fed-batch with TS) and for this reason was pursued for further validation.

Figure 3.63: miR-23b* sponge clone 18 CHO-SEAP under batch conditions

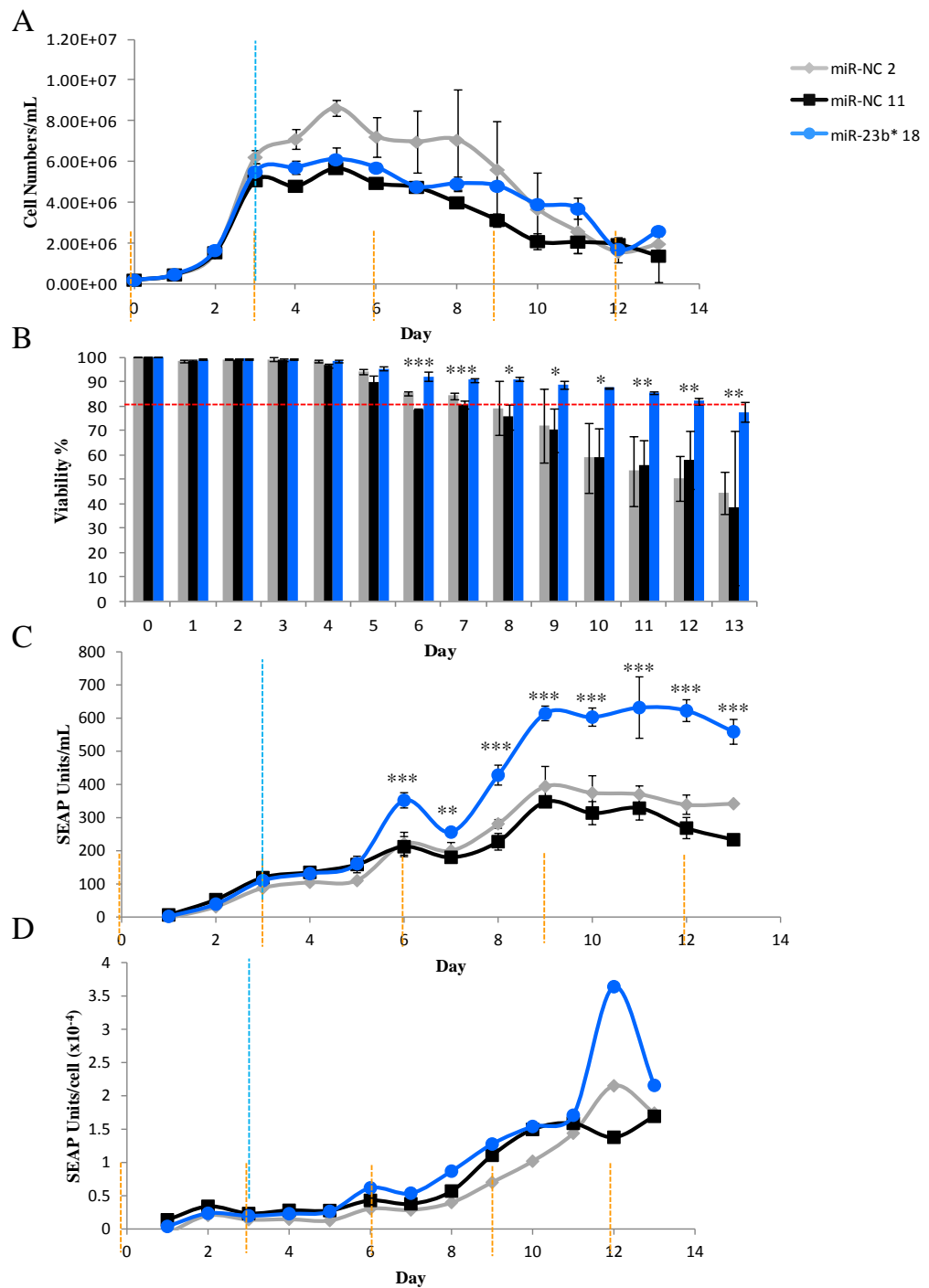


Figure 3.63: Fed-batch (Orange broken line) culture with an additional temperature shift to 31 °C (Broken blue line) for the CHO-SEAP clone 18 stably depleted of miR-23b* and control sponge clones. A) Cell numbers/mL, B) cell viability with an 80% viability threshold represented as a **broken red line, C) Volumetric SEAP activity/mL and D) Specific SEAP activity. Statistical analysis was calculated using the standard student t-test ($p \leq 0.05^*$, $\leq 0.01^{**}$ and $\leq 0.001^{***}$), $n = 2$.**

3.3.6.2 miR-23 sponge CHO-1.14 (IgG) clones

miR-23 sponge clones - Batch

As reported previously, miR-23 depletion in the IgG-secreting CHO-1.14 cells was different from what was observed in SEAP cells. Growth and viability were enhanced in the case of CHO-1.14 to the detriment of productivity. Furthermore, it was observed within the clonal panel study that viability was improved by ~20%. Although, volumetric and specific productivity was observed to be reduced, miR-23 sponge CHO-1.14 clones were selected based on IgG levels, i.e. attempting to isolate the best producers while considering both growth and viability traits. From the clones chosen (miR-23 spg 6, 9, 14, 17 and 23), various bioprocess conditions were tested.

Enhanced growth of ~1.5-2-fold ($p \leq 0.001$) on days 2 and 4 of batch culture was observed for all miR-23 sponge clones when compared to all three control clones (**Fig. 3.64 A**). One control clone (miR-NC spg 20) demonstrated a comparable viability (above 80%) to that of miR-23 depleted clones unlike its counterparts whose viability on day 6 of culture were 54% and 22% (**Fig. 3.64 B**). Although all 5 miR-23 depleted clones demonstrated higher viability than the two lowest performing control clones, only two retained enhanced viability over the best performing control clone. It is still evident from the number of clones selected that miR-23 depletion does have a positive and beneficial impact on CHO cell growth.

Figure 3.64: miR-23 depleted CHO-1.14 clones under batch conditions

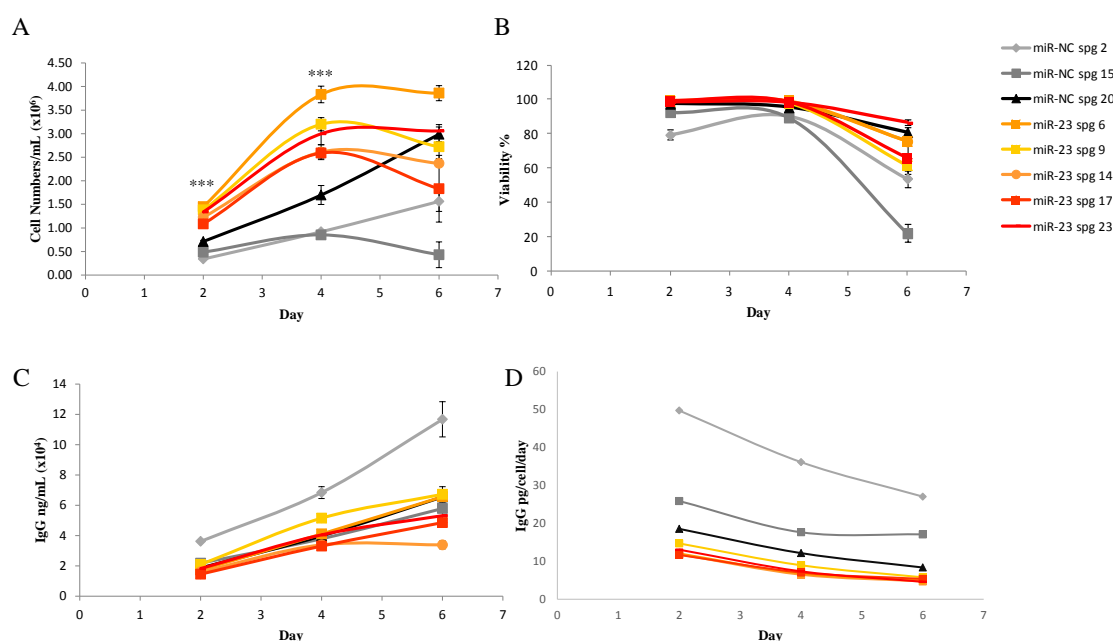


Figure 3.64: CHO-1.14 clones stably engineered to be depleted of miR-23 under batch culture conditions. A) Cell numbers/mL, B) Cellular viability, C) Volumetric productivity (ng/mL) and D) Specific productivity. Statistical analysis was determined using a standard student t-test and was based on a comparison between each individual test clone and all control clones ($p \leq 0.001^{*}$), $n = 3$.**

All miR-23 sponge clones demonstrated a ~40-60% reduction in volumetric IgG when compared to the best performing control clone, miR-NC sponge clone 2 (**Fig. 3.64 C**). When compared to the lower producing controls, there was a less dramatic reduction in volumetric IgG titre observed of ~20% as far as +20% in some instances, for all miR-23 sponge clones. However, all miR-23 depleted clones demonstrated a reduction in specific productivity ranging from 25-90% (**Fig. 3.64 D**) when compared to control clones. It is evident that from batch cultivation of a selected panel of miR-23 sponge clones in a recombinant IgG-secreting CHO cell line exhibit an enhanced growth phenotype at the expense of specific productivity.

miR-23 sponge clones – Fed-batch

We sought to attempt to further boost cell numbers with the addition of a feed and potentially mediate a prolonged production phase to ultimately improve volumetric titres considering the reduced specific productivity. One immediate observation was that the addition of a feed did not appear to enhance cellular proliferation past normal levels, a phenotype which had been previously noted in the case of CHO-SEAP during fed-batch. miR-23 depleted clones demonstrated an enhanced growth phenotype early into culture of ~50% on day 1 and 2 while achieving an increased maximal cell density of ~50-70% on day 3 when compared to control clone 2 and 15 (**Fig. 3.65 A**). One control clone however (miR-NC spg 20), as observed in batch culture, demonstrated similar maximal cell densities and a superior viability profile (**Fig. 3.65 B**). Although culture under batch conditions suggested a potential viability benefit, there was no discernible improvement observed when a feed was added.

Figure 3.65: miR-23 depleted CHO-1.14 clones under fed-batch conditions

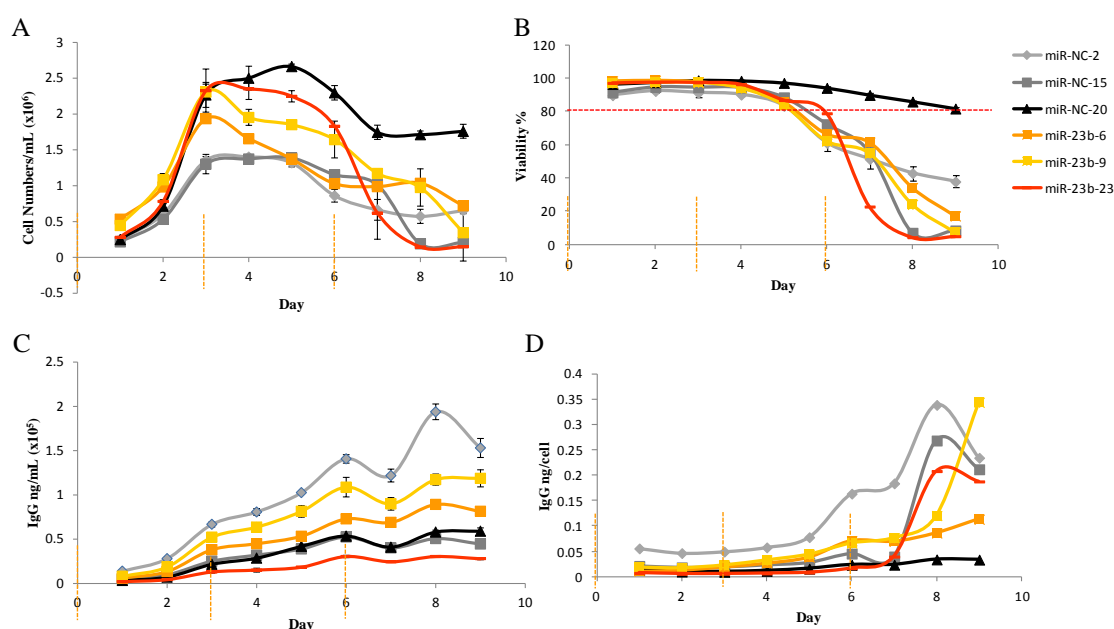


Figure 3.65: miR-23 depleted clones secreting IgG under fed-batch conditions with the broken orange line indicating the addition of a nutrient feed. Phenotypes monitored were A) cell numbers/mL, B) Cellular viability with an 80% threshold represented as a broken red line, C) Volumetric IgG titres and D) Specific productivity (n =2).

The three miR-23 sponge clones selected for fed-batch culture demonstrated the highest cell densities when grown under batch conditions and demonstrated a potential improved volumetric IgG titre at various time points when compared to the two lowest producing control clones. In the case of fed-batch, this improved volumetric productivity was more potent in the case of miR-23 spg clone 6 and 9 with a maximum increased IgG titre on day 9 of ~40-80% and 2-2.6-fold, respectively. miR-23 spg clone 23 exhibited the lowest productivity profile of all clones under investigation while miR-NC spg clone 2 surpassed all clones when both volumetric and specific productivity were assessed (**Fig. 3.65 C and D**). Specific IgG productivity was observed to be enhanced for 2 out of three clones when fed-batch was carried out possibly due to the observation of no dramatic improvement in cell growth, potentially resulting in an excess of nutrients available for protein synthesis. This demonstrates that miR-23 depletion in our IgG-secreting CHO-1.14 cell line improves cellular growth and maximal cell density with a benefit to viability. These enhanced phenotypes appear to be at the cost of productivity. However, it is evident that the process of clonal selection and the inherent heterogeneity present within CHO cell clones can in itself mediate a beneficial phenotype that can be selected for. The selection of a larger panel of clones would give a better understanding of the impact that miR-23 depletion has on this CHO-1.14 cell line.

At this point however, the depletion of miR-23 in CHO-SEAP cells was more beneficial and consistent upon scale up and will be the primary focus for the rest of this thesis. As both IgG and SEAP secreting CHO cell lines were derived from the same parental cell line, it is possible that the impact of stable miR-23 depletion is product specific with the culture format also having an influence. The fact that clones selected throughout the various phases of scale-up were selected based on their volumetric productivity could have introduced a bias. However, the initial phenotype observed within mixed pools was observed to be retained throughout.

Section 3.4

Investigation of the molecular impact of miR-23 depletion in CHO-SEAP cells

3.4.1 miR-23 depletion improves CHO-SEAP specific productivity

miR-23 depleted clones exhibited an improved SEAP productivity of ~3-fold with a slight variation in cellular growth over various culture conditions. This section focuses on the elucidation of how the depletion of miR-23 is conferring this advantage on cellular productivity.

3.4.2 SEAP transcript levels appear elevated in miR-23 sponge clones

As all secreted mammalian proteins are translocated to the lumen of the endoplasmic reticulum either post- or co-translationally for modification, folded and assembled before release to the cis-Golgi compartment (Tigges, Fussenegger 2006), they are susceptible to secretory bottlenecks in the event of high protein turnover. We evaluated the transcript levels of SEAP within a small panel of selected clones. Clones were cultured under the same batch conditions as reported previously in **section 3.3.6.1** and harvested for RNA (see **section 2.4.6 of Materials and Methods**) on day 3 of culture. Semi-quantitative PCR indicated that SEAP mRNA levels were elevated in all test clones when compared to control (**Fig. 3.66 A**).

A more definitive comparison in the levels of SEAP mRNA abundance in our miR-23 engineered clones was carried out using qRT-PCR (see **section 2.4.4 of Materials and Methods**). The intermediate SEAP producing control clone (miR-NC spg 11) was chosen as the calibrator when data was normalised during data analysis. A 2-3-fold increase in SEAP transcript ($p \leq 0.05$ and 0.01) was observed for all miR-23 sponge clones (**Fig. 3.66 B**). Significance was calculated based on Ct (Cyclic threshold) values for each individual miR-23 sponge clone versus a combination of all three controls. Although error bars to appear to cover a significant portion of the overall dataset, the Ct values were quite tight and resulted in significant statistics when a t-test was carried out. Inclusion of a larger number of technical replicates would have aided in reducing the level of variation within samples ultimately contributing to a reduction in error.

These results would suggest that the enhanced SEAP yields observed are potentially as a result of an elevation in the rate of transcription of the SEAP gene in miR-23 depleted cells.

Figure 3.66: Semi-quantitative/qPCR for SEAP transcript in miR-23 sponge clones

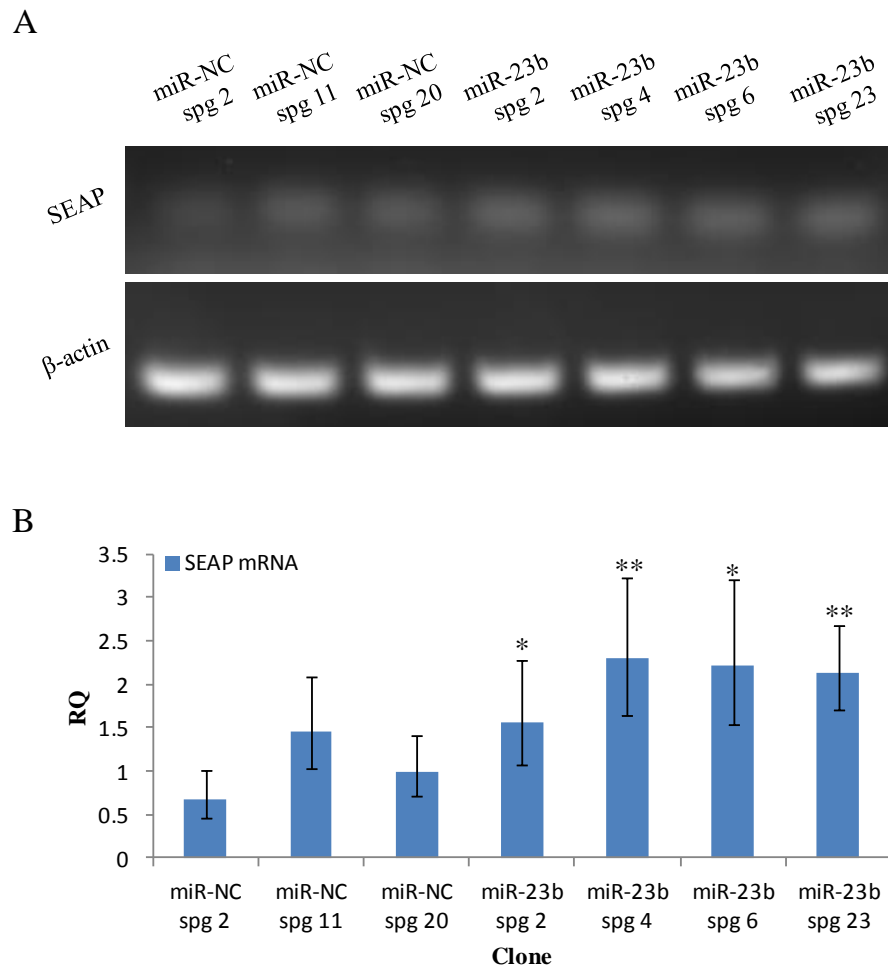


Figure 3.66: A) Semi-quantitative gel-based PCR and quantitative real-time PCR (qPCR) was carried out on miR-23 depleted CHO-SEAP clones in an attempt to assess the potential difference in transcript levels. **A)** Represents the ethidium bromide (EtBr)-stained agarose gel primed for the SEAP mRNA transcript in all miR-23b clones and control clones. **B)** Quantitative real-time PCR was carried out to accurately determine the relative fold change in transcript levels of SEAP. miR-NC spg 20 was chosen as the clone to calibrate the relative quantity (RQ) of SEAP across all clones while statistical analysis was determined for each individual test clone by using a standard student t-test for all Ct values across all three controls, ($p \leq 0.05^*$ and $p \leq 0.01^{**}$).

When the mature levels of miR-23b were assessed by qRT-PCR (see **section 2.4.8 of Materials and Methods**), there was a 5-fold ($p \leq 0.001^{***}$) reduction observed in clones expressing a miR-23 specific sponge compared to controls (**Fig. 3.67**). This reduction in mature miR-23 levels was similar to what was observed in the case of miR-34a.

Figure 3.67: Endogenous miR-23b levels in miR-23 sponge clones

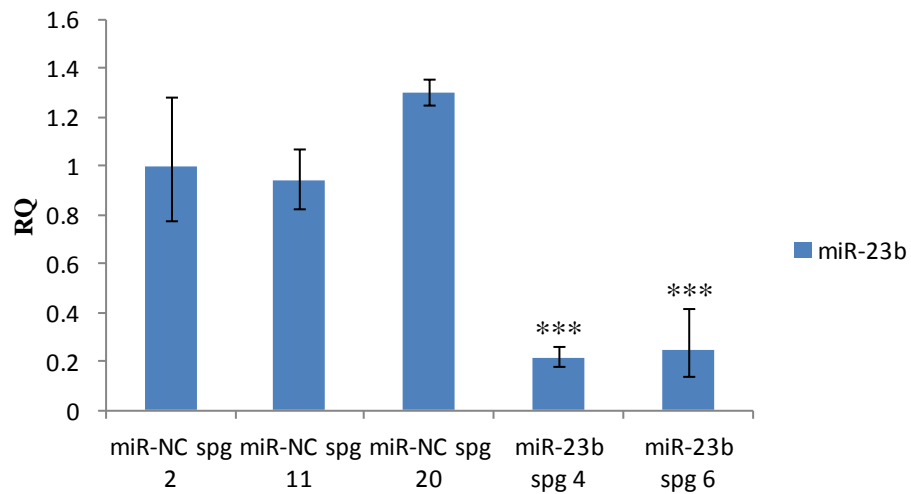


Figure 3.67: qRT-PCR was utilised to assess mature levels of endogenous miR-23b in miR-23 sponge clones when compared to control clones. Significance was calculated for each miR-23 clone across all 3 miR-NC sponge clones using a standard student t-test ($p \leq 0.001$ *).**

3.4.3 SEAP mRNA stability is not a contributing factor to enhanced productivity

To further confirm that the elevated SEAP productivity was due to enhanced transcription and not increased mRNA stability, we measured the stability of the SEAP mRNA transcript in both control and miR-23 sponge clones after Actinomycin-D (Act-D) treatment. Actinomycin-D treatment is used as a transcriptional block due to its high affinity binding for DNA GC-rich duplexes at transcription initiation complexes and preventing elongation by RNA polymerase (Kang, Park 2009). By inhibiting transcription, the rate of mRNA decay, i.e. stability, can be determined. The two best performing miR-23 sponge clones (4 and 6) and the best control clones (2 and 11) were selected for stability assessment. RNA was harvested 6, 18 and 24 hs after the addition of Act-D and assessed for SEAP mRNA levels using SYBR Green qPCR with β -actin as the endogenous control. The cyclic threshold (Ct) values for each time point of each sample is graphed below as a means to best depict the trend in mRNA stability across all conditions (**Fig. 3.68**).

Figure 3.68: miR-23 sponge SEAP mRNA stability assay

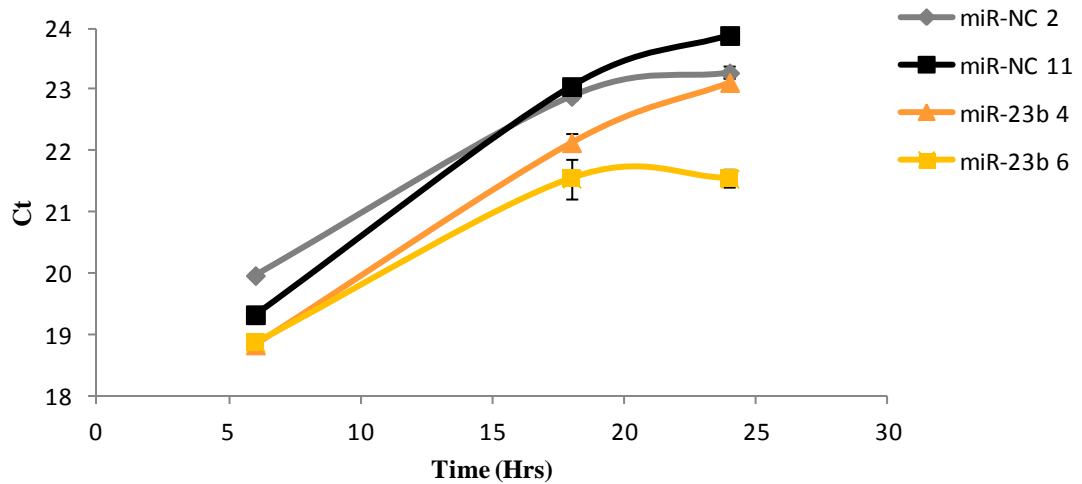


Figure 3.68: qRT-PCR was used to evaluate the stability of the SEAP mRNA transcript in miR-23 sponge clones versus miR-NC sponge clones upon the addition of Actinomycin-D. Upon transcriptional inhibition RNA was sampled 6, 18 and 24 hs later with the respective Ct values of each clone graphed and slopes calculated as a means to assess the rate of decay.

We chose to represent mRNA stability as a function of the Ct from each time point and calculate the slope of the line as a means to measure the change over time because expressing changes in mRNA levels quantitatively was hindered by the fact that the endogenous control (β -actin) displayed an accelerated decay rate to that of the SEAP transcript. It can be observed that both miR-NC sponge clones and miR-23 sponge clones behaved similarly reflecting both the similar SEAP production capacity previously observed and the elevated SEAP transcript exhibited by both miR-23 sponge clones indicated by the lower Ct values recorded for each time point. Furthermore, the slope calculated for each clone miR-NC sponge 2 and 11 and miR-23 sponge 4 and 6 was 0.9493, 0.9743, 0.9873 and 0.9828, respectively. This observation indicated that the rate of decay of the SEAP transcript was comparable between both the control and the test sponge clones and that mRNA stability was not playing a role in the enhanced SEAP activity seen in our CHO-SEAP clones engineered to stably deplete miR-23.

3.4.4 Cell size is not a contributing factor to clonal differences in productivity

Cell size has been a variable considered to play a part in the specific production capacity of rCHO cells. Larger cells have been shown to possess inherently longer duplication times (Kang et al. 2013a). This increased duplication time could correlate with a longer period of G₁ during the cell cycle or in the case of larger cells without increased genomic size, an increased availability of biogenesis machinery.

Using the Cedex XS analyzer (see section 2.2.3.3 of **Materials and Methods**), the size of the CHO-SEAP sponge clones were evaluated. miR-23 sponge clone 4 and 6 and miR-NC sponge clone 2 and 11 were selected as these clones exhibited a similar SEAP production profile. A size range of 11.3 μm to 12 μm was observed with miR-NC sponge clone 11 falling at the higher end of this scale (**Fig. 3.69**). This indicated that clone cell size was not contributing to the increase in productivity in miR-23 depleted clones.

Figure 3.69: Comparison of miR-23 sponge and miR-NC sponge clonal cell size

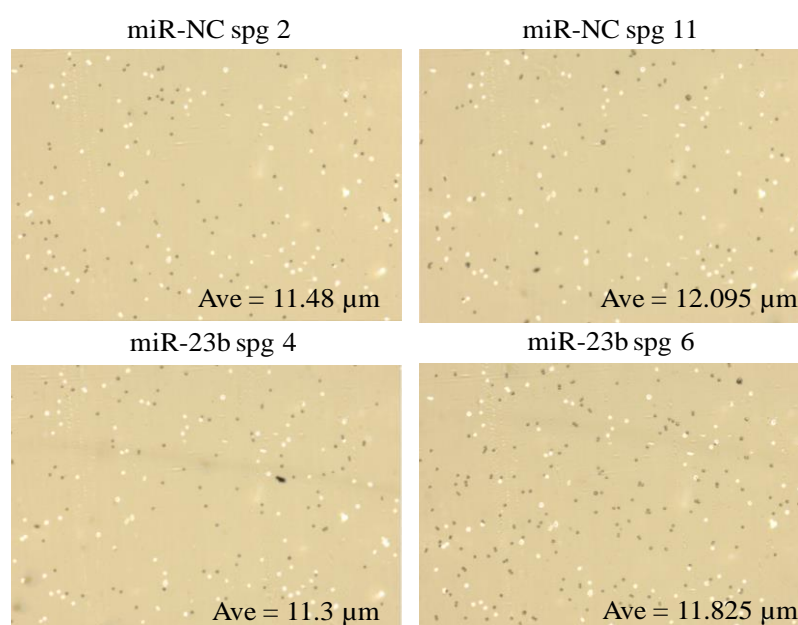


Figure 3.69: Using the Cedex XS analyzer, a Trypan blue-based cell imager, miR-23 sponge and miR-NC sponge clones were assessed for their cell size. Cell size for each clonal population is represented as an average value across the entire population.

3.4.5 miR-23 depleted CHO clones exhibited elevated Glutamate levels

Both miR-23a and miR-23b have previously been shown to target the mRNA of glutaminase (GLS), an enzyme that mediates the conversion of glutamine to glutamate (Gao et al. 2009), which has been proposed to play a role in the Warburg effect through anaplerosis, the replenishment of TCA cycle intermediates through glutaminolysis (Dang 2010) potentially boosting oxidative metabolism, a process previously associated with productivity (Templeton et al. 2013). For this reason, we measured the levels of secreted glutamate within the supernatants of day 4 cultures (**section 2.6.9 of Materials and Methods**).

Figure 3.70: Glutamate levels across sponge clones

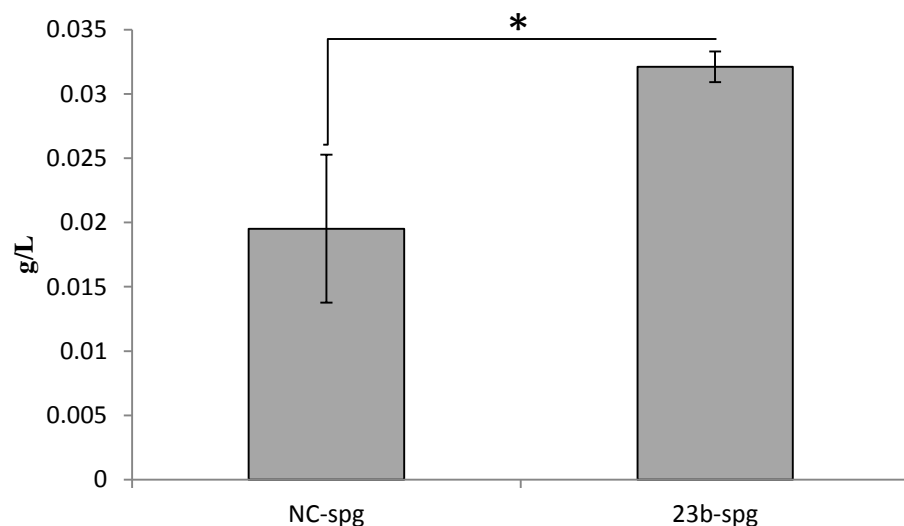


Figure 3.70: Glutamate levels were measured from the supernatants of rCHO-SEAP clones engineered with a miR-23 specific sponge (clone 4 and 6) and a non-specific control sponge (clone 2 and 11). Glutamate levels were calculated based on the average across both test and control groups with statistical significance being calculated using a standard student t-test ($p \leq 0.05^*$).

The average glutamate levels across both clonal groups was observed to be increased by 65% ($p \leq 0.05$, **Fig. 3.70**). This potentially suggested that glutamate levels were elevated through de-repression of translation of the glutaminase enzyme. However, semi-quantitative and quantitative PCR analysis did not indicate any change in the mRNA

levels of glutaminase (GLS), (**Fig. 3.77** and **Fig. 3.78**). This however does not discount miR-23 interfering with the translation of GLS. The conversion of glutamine to glutamate by GLS generating ammonia (NH_4) is not the only source of glutamate. Glutamate dehydrogenase (GDH) can catalyse the reversible conversion of glutamate to α -ketoglutarate (Spanaki, Plaitakis 2012). Glutamate oxaloacetate transaminase also mediates the reversible conversion of oxaloacetate and glutamate to aspartate and α -ketoglutarate (Perez-Mato et al. 2014). This would suggest that the levels of glutamate can either contribute to cellular bioenergetics or balance the availability of TCA cycle intermediates. It would be expected that the primary source of glutamate generation would be intracellular, however, secreted glutamate levels would be expected to reflect the internal glutamate levels.

3.4.6 miR-23 depletion impacts positively on CHO cell mitochondrial activity

Although the observation of increased availability of glutamate could not be definitively attributed to enhanced GLS activity without the assessment of its mature protein levels, we decided to assess the impact on mitochondrial function in a miR-23 depleted clone by using high resolution respirometry (HRR) (see **section 2.5.2 of Materials and Methods**). As glutamate provides essential electron donors (NADH and FADH_2) critical to mitochondrial function, we speculated that a miR-23 sponge clone would demonstrate an increased mitochondrial activity, be it either directly or indirectly through miR-23's influence on GLS. Oxidative phosphorylation (OXPHOS) is a measure of oxygen consumption culminating in the synthesis of ATP and the respiratory by-product, water. By measuring oxygen consumption using HRR, we were able to compare the mitochondrial function of intact cells under normal environmental conditions. Additionally, permeabilization assays allowed for the interrogation of individual complex components of the electron transport system (ETS, **Fig. 3.71**). A series of mitochondrial substrates, uncouplers and inhibitors are listed in **table 3.4**.

Table 3.4: SUIT protocol substrates, uncouplers and inhibitors

Substrate	Abbreviation	Site of action	Volume (μL)	Final Conc in 2mL
Pyruvate	P	Complex I (CI)	5	5 mM
Malate	M	CI	2.5	0.5 mM
Glutamate	G	CI	10	10 mM
Succinate	S	CI	20	10 mM
Ascorbate	As	CIV	5	2 mM
TMPD	Tm	CIV	5	0.5 mM
Cytochrome c	C	CIV	5	10 μM
ADP	D	CV	4	1 mM
Uncoupler				
FCCP	F	Inner Mitochondrial membrane	1 μL steps	0.05 μM steps
Inhibitors				
Rotenone	Rot	CI	1	0.5 μM
Malonic Acid	Mna	CII	5	5 mM
Antimycin A	Ama	CIII	1	2.5 μM
Sodium Azide	Az	CIV	50	100 mM
Oligomycin	Omy	CV	1	2 μg/mL

Figure 3.71: Schematic diagram of the electron transport system (ETS) and its component complexes

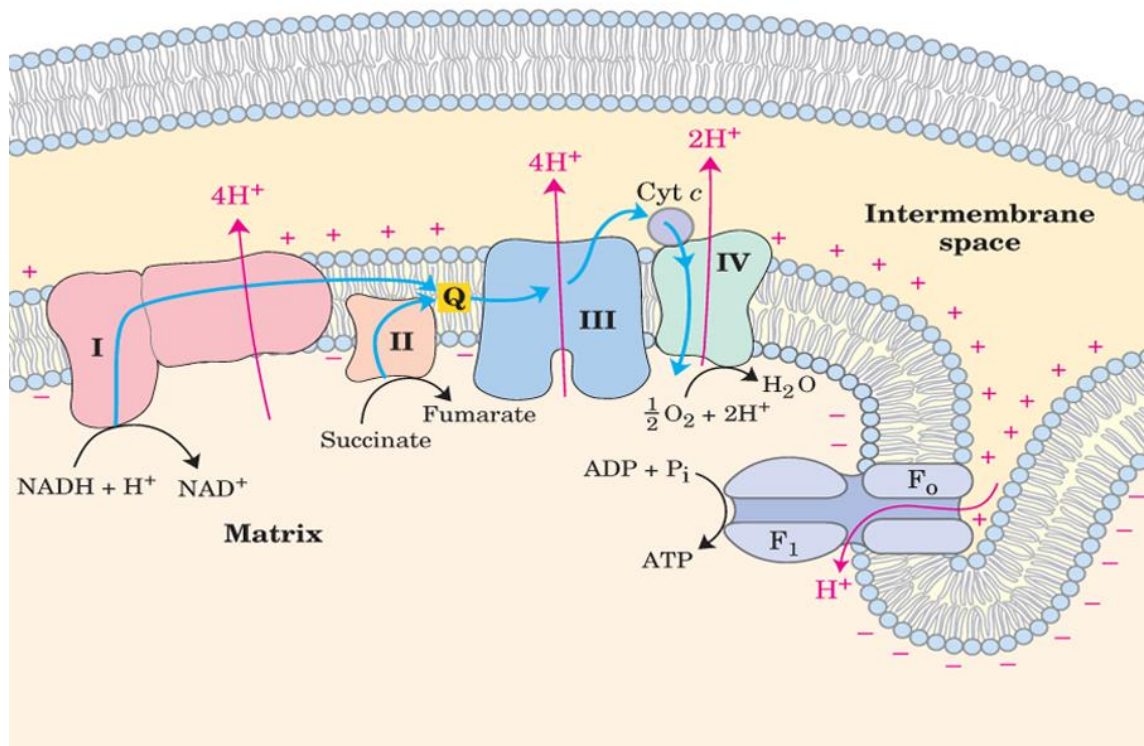


Figure 3.71: A schematic diagram showing the components of the electron transport system (complex I, II, III and IV) culminating at the generation of ATP through Complex V. These complexes are localised to the inner mitochondrial membrane and are responsible for transporting electrons from donors (NADH and FADH_2) along the chain ending in the generation of water from molecular oxygen at complex IV. Additionally, generation of the proton gradient is also contributed to by these complexes mediating the transfer of protons from the matrix to the inner membrane space. (Image sourced from <http://www.robertlfurler.com/category/systems-biology/>).

3.4.6.1 Mitochondrial function of intact rCHO cells

Routine respiration (R) is a measure of mitochondrial oxygen consumption and normal cellular homeostasis that is supported by exogenous substrates from the culture media. Dissection of mitochondrial activity via the various components that make up the mitochondrial electron transport system (ETS) cannot be measured in intact cells as the plasma membrane is impermeable to various mitochondrial substrates and ADP.

Once, R has stabilised, ATP synthesis is inhibited through the addition of oligomycin (ATP synthase-Complex V inhibitor). LEAK respiration (L) is a measure of cellular

substrate utilisation accommodated by the proton leak (intrinsic uncoupling) at maximum mitochondrial potential. As ATP synthase has been inhibited, the electrochemical proton gradient is not regulated as proton import into the mitochondrial matrix cannot occur. The mitochondrial respiratory control (proton gradient exerting a regulatory electrochemical backpressure) system is fully released or uncoupled by the addition of FCCP (Carbonilcyanide p-trifluoromethoxyphenylhydrazone) which cycles across the inner mitochondrial membrane with the transport of protons and dissipates the proton gradient. This allows the non-coupled state of ETS capacity to be determined irrespective of the contribution from the proton pumps (CI, CIII and CIV).

Two clonal pairs were compared for their mitochondrial activity as intact cells (miR-NC spg 2 and miR-23 spg 4: miR-NC spg 11 and miR-23 spg 6). Cells were cultured at an initial density of 2×10^5 cells/mL in a 5 mL volume and grown under batch process conditions for 72 h. Cells were counted and resuspended in a 4 mL volume of fresh culture media at a final density of 1×10^6 cells/mL. Prior to inoculation of the OROBOROS chambers, the oxygen sensors were calibrated using culture media. Given the limited nature of the OROBOROS system, only two samples could be assessed at any one time, therefore a test and corresponding control clone were assessed with results and statistics calculated based on the values obtained from three replicates.

Routine (R) and LEAK (L) respiration of miR-23 depleted CHO cells was found to be increased ($p \leq 0.05$) as a function of the maximum ETS (E) determined by the addition of FCCP (**Fig. 3.72 B**). Although the maximum ETS was observed to be lower in the case of CHO cells exhibiting an increased volumetric yield (**Fig. 3.72 A**), respiratory control ratios (RCRs) revealed that miR-23 depleted CHO cells produced a higher percentage of their maximum energy capability as opposed to NC-sponge cells. This indicated that miR-23 depleted clones under normal growth conditions have a more efficient mitochondrial function. miR-23 sponge clone 4 was observed to perform at 54% of its maximum capacity routinely (R) compared to 44% in miR-NC sponge clone 2 while leak was observed to be 32% of its maximum compared to 27 (**Fig. 3.72 B**).

Figure 3.72: Mitochondrial function of intact miR-23 depleted rCHO cells clone 4 and miR-NC sponge 2

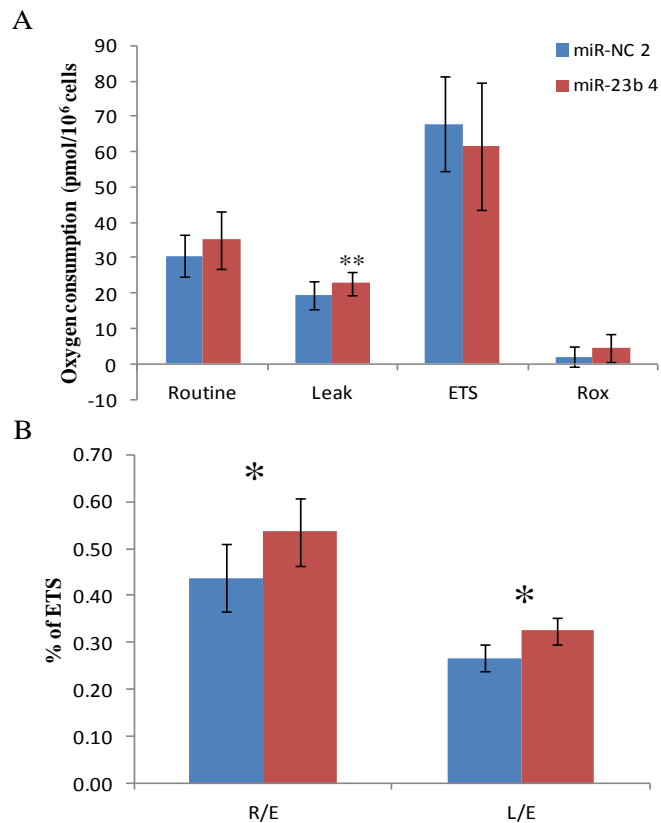


Figure 3.72: Comparison of mitochondrial activity based on the rate of oxygen consumption between the miR-23 sponge clone 4 and the control sponge clone, miR-NC sponge 2. A) Represents the raw values for the rate of oxygen consumption between both miR-sponge clones. B) Flux control ratios (FCRs) are normalised to a common reference state after normalisation to residual oxygen (ROX). R/E ratio is an expression of how close ROUTINE respiration operates to ETS capacity while L/E follows the same trend. All calculations were made based on the individual values obtained over the course of three experimental replicates (n = 3) with statistical significance calculated using a type 1 paired standard student t-test ($p \leq 0.05^*$ and $\leq 0.01^{}$).**

Interestingly, when a second set of clones were evaluated for their mitochondrial activity, miR-23 sponge clone 6 and miR-NC sponge clone 11, it was observed that there was a significantly enhanced routine respiration by 22% ($p \leq 0.01$) and maximum ETS by 13% ($p \leq 0.05$). Although there was an elevated ETS observed in this case, it did not translate into a significant increase in the ratio of energy utilisation when normalised to the maximum ETS (Fig. 3.73).

Figure 3.73: Mitochondrial function of intact miR-23 depleted rCHO cells clone 6 and miR-NC sponge 11

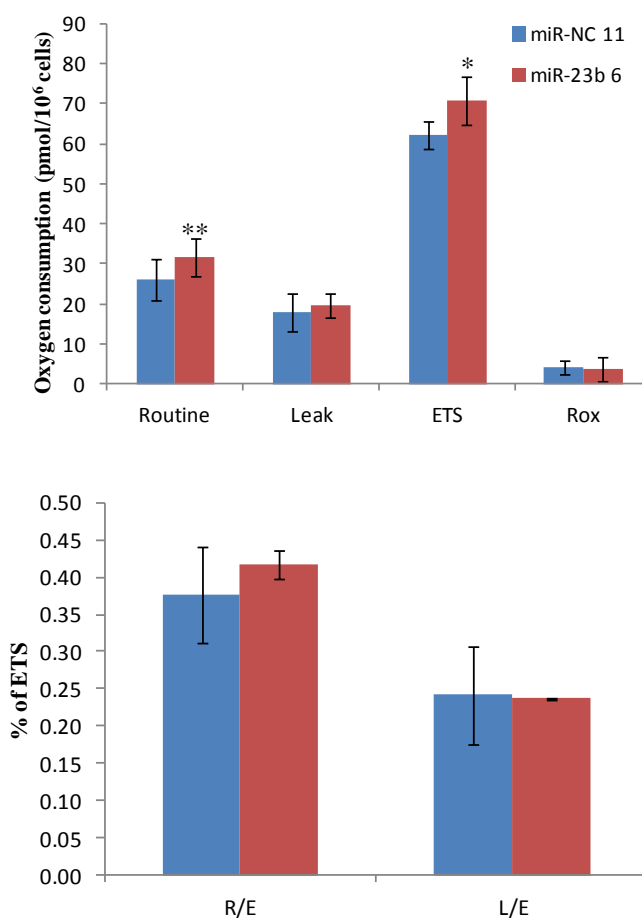


Figure 3.73: Comparison of mitochondrial activity based on the rate of oxygen consumption between the miR-23 sponge clone 6 and the control sponge clone, miR-NC sponge 11. A) Represents the raw values for the rate of oxygen consumption between both miR-sponge clones. B) Flux control ratios (FCRs) are normalised to a common reference state. R/E ratio is an expression of how close ROUTINE respiration operates to ETS capacity while L/E follows the same trend. All calculations were made based on the individual values obtained over the course of three experimental replicates (n = 3) with statistical significance calculated using a type 1 paired standard student t-test ($p \leq 0.05^*$ and $\leq 0.01^{}$).**

Both miR-23 depleted clones appeared to demonstrate an enhanced mitochondrial activity be it when directly compared to the rate of oxygen consumption in the case of miR-23 spg clone 6, or be it through the more opportunistic utilisation of energy when compared to their maximum ETS capacity, in the case of miR-23 sponge clone 4.

Ideally, assessing and comparing the various combinations of test versus control sponge clones would have been both desirable and beneficial, however, the limited number of chambers in the OROBOROS system would make this a time consuming endeavour which unfortunately could not be explored.

3.4.6.2 Mitochondrial function of permeabilised rCHO cells

Next we sought to evaluate if this enhanced mitochondrial function was as a result of the hyperactivity of individual complex components that make up the electron transport system (ETS). Permeabilised experimental evaluation of mitochondrial function was carried out in mitochondrial respiration media (MiR05) which contains no exogenous substrates. As a result, routine mitochondrial respiration cannot be assessed within permeabilised mitochondrial assays as this is a natural state of respiration dependent on exogenous sources.

The first exercise was to determine the concentration of Digitonin (Dgt) to achieve full membrane permeabilization. Each chamber was inoculated with 2 mL of MiR05 buffer containing 1×10^6 cells/mL. Cells were initially treated with 1 μ L Rotenone (Complex I (C1) inhibitor), 20 μ L Succinate (CII substrate) and 4 μ L ADP (precursor for ATP production – see **table 3.4 for final concentrations**). In intact cells, CI inhibition via rotenone addition suspends respiration through CII because succinate cannot cross the cell membrane and succinate production through the TCA cycle is stopped when NADH cannot be oxidised. Therefore, inhibition of CI in this instance allows us to assess cell membrane permeability with mitochondrial respiration via CII being dependent purely on exogenous sources of succinate. After inoculation of both chambers, Digitonin was titrated 1 μ L at a time with one chamber remaining as a control. As the cell membrane becomes permeabilised, succinate moves into the mitochondria thus stimulating oxygen consumption through CII activity. After each addition of Dgt, the rate of oxygen consumption is allowed to stabilise before the addition of the next μ L. We determined that our rCHO cells reached a plateau of permeability upon the addition of 3-4 μ L of Dgt (**Fig. 3.74**). Subsequent permeabilization experiments were carried out by initially adding 4 μ L of digitonin.

Figure 3.74: Cell membrane permeabilization optimisation using Digitonin

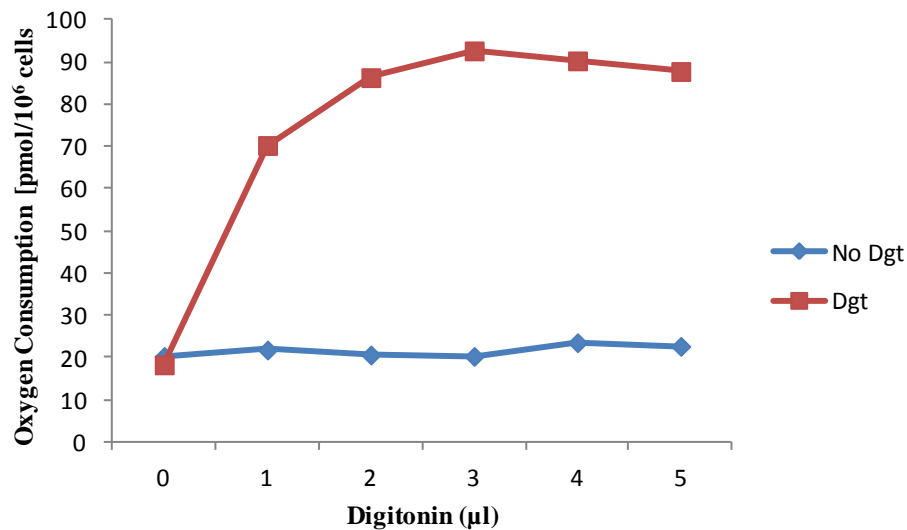


Figure 3.74: The addition of Digitonin (Dgt) was titrated in order to assess the optimal concentration that would fully permeabilise the CHO cell membrane. As succinate cannot cross the cell membrane, intact cells are initially dosed with the complex II substrate, succinate (S). Dgt is subsequently titrated until maximum oxygen consumption has been achieved through full permeabilization of the cell membrane allowing succinate and ADP to fully cross into the mitochondria.

The systematic evaluation of the activity of individual mitochondrial membrane components that contribute to cellular respiration was assessed when miR-23 sponge clone 4 and miR-NC sponge clone 2 were compared (**Fig. 3.75 A and B**). Part A of **Figure 3.75** shows the real-time change in oxygen consumption of both control and test clones with each substrate/inhibitor/uncoupler being indicated whereas part B demonstrates the average values and statistics across a triplicate run.

A 29% increase in mitochondrial respiration was observed upon addition of glutamate/malate as substrates for Complex I. However a significant 26% increase ($p \leq 0.05$) in OXPHOS in miR-23 depleted CHO cells was observed when ADP was no longer the limiting factor (**Fig. 3.75 B^{ADP}**).

The addition of cytochrome c confirmed that in both cases mitochondrial membrane integrity was not compromised either through the permeabilization process itself or as a result of mitochondrial hyperactivity, in the case of miR-23 sponge cells.

OXPPOS maintained the increased of ~ 29% ($p \leq 0.05$) upon the addition of succinate, a substrate for Complex II, suggesting that complex I was responsible for the observed increase in mitochondrial respiration. However, upon acquisition of the ETS, complex I was inhibited by the addition of Rotenone (Rot) resulting in a marginal drop in oxygen consumption when compared to the addition of succinate (CI and CII). This suggested that both complex I and complex II are mediating a ~30% ($p \leq 0.05$) increase in cellular respiration in miR-23 depleted CHO cells but do not appear to display an additive advantage. However, complex II on its own in an uncoupled state maintained a 44% higher ($p \leq 0.05$) activity upon complex I inhibition (**Fig. 3.75 B^{Rot}**).

Subsequent inhibition of complex II and III followed by the activation of CIV through the addition of the electron donor TMPD resulted in a marginal drop in oxygen consumption in miR-23 depleted cells (**Fig. 3.75 B^{TMPPD}**).

Dissection of the mitochondrial membrane complexes suggested that complex I and II contribute to a higher degree of respiration at levels comparable to each other but do not display synergy when co-stimulated possibly due to a saturation point centred on the downstream electron chaperone complexes III and IV.

Figure 3.75: Mitochondrial permeabilization assay on miR-23 sponge clone 4 versus miR-NC sponge clone 2

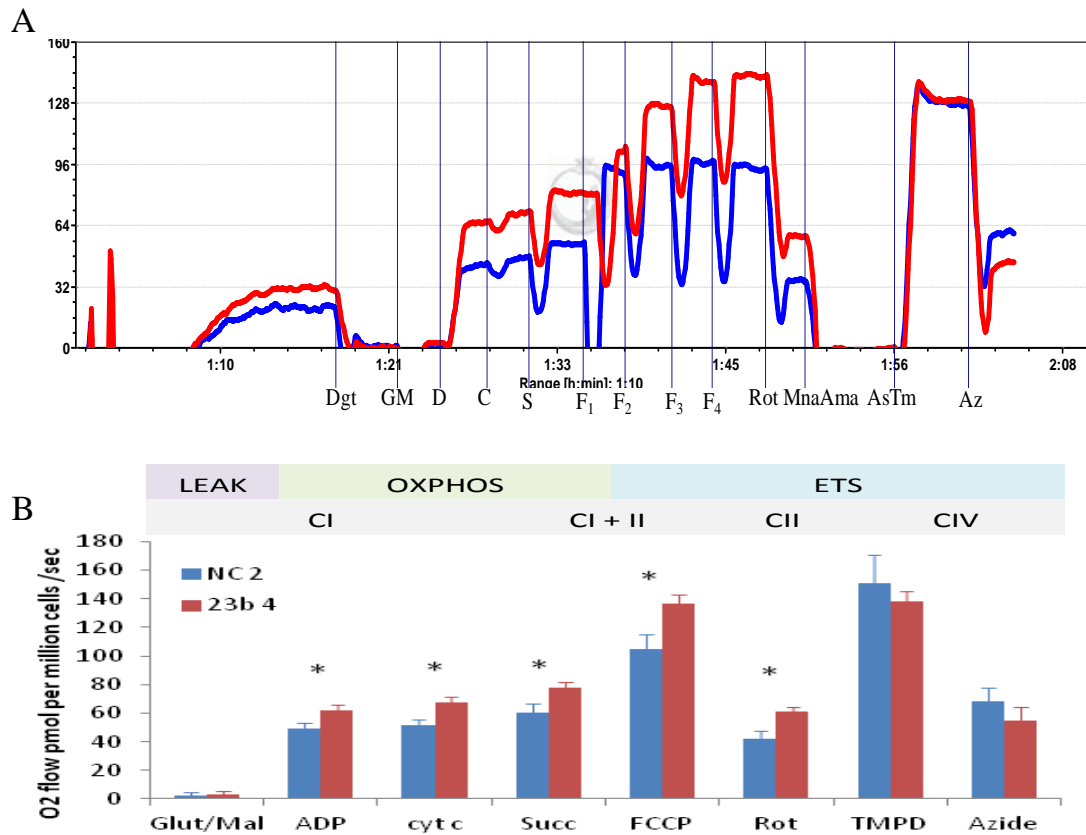


Figure 3.75: Mitochondrial activity of permeabilised rCHO cells (miR-23 sponge clone 4 and miR-NC sponge clone 2) using a SUIT protocol. A) Is a representation of a real-time read out of oxygen consumption from one of the replicates (n = 3) indicating the addition of each substrate/inhibitor/uncoupler over the time course (h: min). Oxygen consumption is allowed to stabilise before the addition of Dgt. At each step, oxygen consumption is allowed to stabilise before the addition of the next substrate/inhibitor/uncoupler. Glutamate/Malate (GM) is added to stimulate CI activity while ADP (D) further stimulates OXPHOS through CI by relieving ADP availability as a limiting factor. Cytochrome c (C) assessed the integrity of the mitochondrial membrane. Succinate (S) additionally stimulates the activity of CII while the uncoupler FCCP (F) assessed the ETS though titration at 2 μ l intervals. Rotenone (Rot) addition inhibits CI allowing OXPHOS through CII and CIII. Malonic acid/Antimycin A (Mna/Ama) inhibits CII and CIII, respectively. CIV is then stimulated by the artificial electron donor TMPD in the presence of Ascorbate (AsTm) which serves to maintain TMPD in a reduced state. Finally complex CIV is inhibited through the addition of Sodium Azide (Az). B) Represents the same data normalised to ROX, with averages across all replicates being shown. The states of mitochondrial activity is broken up in LEAK, OXPHOS and ETS with statistical analysis calculated using a type 1 paired student t-test ($p \leq 0.05^*$).

3.4.7 Mitochondrial content

Although mitochondrial function based on oxygen consumption was performed on a fixed and equal number of cells (1×10^6 cells/mL) it does not account for the potential intrinsic change in mitochondria per cell that could ultimately contribute to the elevated mitochondrial activity. Several biomarkers have been assessed for their utility as candidates whose activity correlate well with mitochondrial content including cardiolipin, citrate synthase (CS) and complex I, in that order (Larsen et al. 2012). However, we decided to use a fluorescent-based assay, MitoTracker Deep Red (MTDR, **section 2.5.1 of Material and Methods**), which is routinely used to evaluate mitochondrial content (Kitami et al. 2012). Cells were cultured in a similar fashion to those that were evaluated for mitochondrial activity using the OROBOROS in the previous section.

Sample fluorescence signals are affected by signal levels, auto-fluorescence, non-specific staining, electronic noise, and optical background from other fluorochromes. These factors can contribute to the noise and/or signals observed and increase the width of a negative population (i.e. variance or standard deviation). Stain index (SI) normalization was used to adjust for the influence of such factors. SI is defined as D/W , where D is the difference between positive and negative populations and W is equal to 2 S.D. of the negative population.

This data indicates that the enhanced mitochondrial function observed in the case of miR-23 sponge clones is not as a result of increased mitochondrial mass/content (**Fig. 3.76**). FACS-based assessment of mitochondrial content using MitotrackerTM Deep red does not discriminate between mitochondrial mass and content. Immuno-histochemical staining would provide further information as to the nature of mass being attributed to content variation. Furthermore, the emission of MitotrackerTM DR at 665 nm did not interfere with the inherent emission signal at 506 nm for the GFP positive sponge clones.

Figure 3.76: Mitochondrial mass/content assessment using FACS analysis

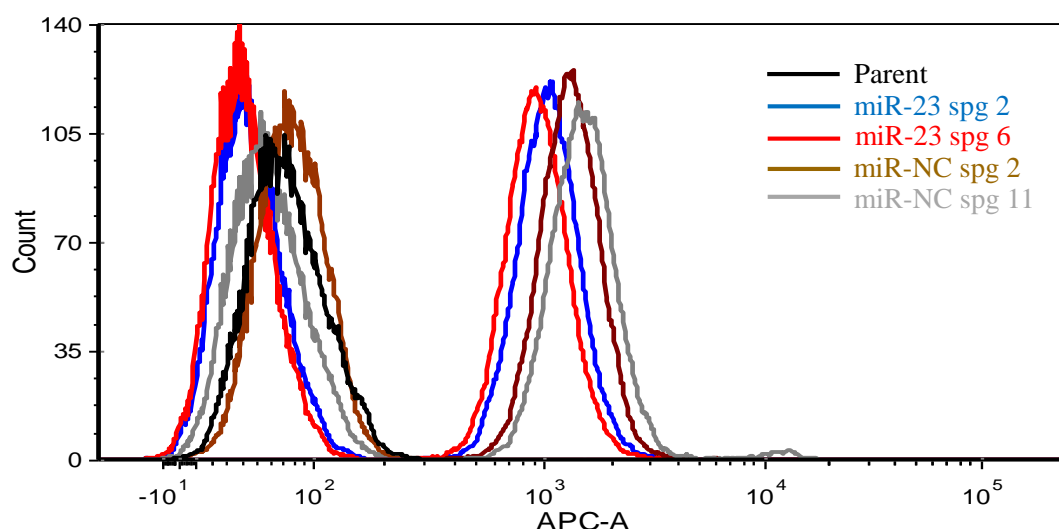


Figure 3.76: Assessment of mitochondrial content in stable miRNA sponge expressing CHO cells. Mitochondrial content of control miR-NC2, -NC11 sponge and miR-23-6 and miR-24-4 expressing CHO cells were examined by MTDR staining and flow cytometry. Data were obtained from ~10,000 events and stain index used to normalize fluorescent signals for each sample. A representative histogram shows Mitotracker™ deep red signals for stained and unstained test and control samples.

3.4.8 Assessment of miR-23 target transcript levels

Several candidate genes were chosen for evaluation of their endogenous transcript levels for two reasons. Firstly, the enzyme glutaminase (GLS) has been validated to be a target of miR-23a/b which in the case of our stable miR-23 sponge CHO cells could potentially contribute to the elevated glutamate levels (Gao et al. 2009). Furthermore, another interesting target of miR-23 is the mitochondrial transcription factor A (TFAM) which has been shown to play a critical role in the transcriptional initiation of mitochondrial encoded genes (Jiang et al. 2013b). Secondly, increased mitochondrial activity has been correlated with enhanced global transcriptional activity (das Neves et al. 2010). From this perspective we selected this panel of genes including another validated target of miR-23, *XIAP* (X-linked inhibitor of apoptosis), for the assessment of their mRNA levels (Siegel et al. 2011). As miRNA function predominantly lies at the post-transcriptional level, the observation of unchanged transcript levels of the aforementioned targets does not discount the possibly of miR-23 depletion impact on the mature protein levels. However,

if enhanced mitochondrial activity was having an effect on global gene transcription, it was suspected that all three genes could be elevated at an mRNA level.

Semi-quantitative PCR was carried out on all three selected targets of miR-23 using the designed primers listed in the appendix (**Table 2.2 of Materials and Methods**) using DreamTaq (Thermo Scientific) following the protocol in **section 2.4.3 of Materials and Methods**.

Figure 3.77: Semi-quantitative PCR for miR-23 targets

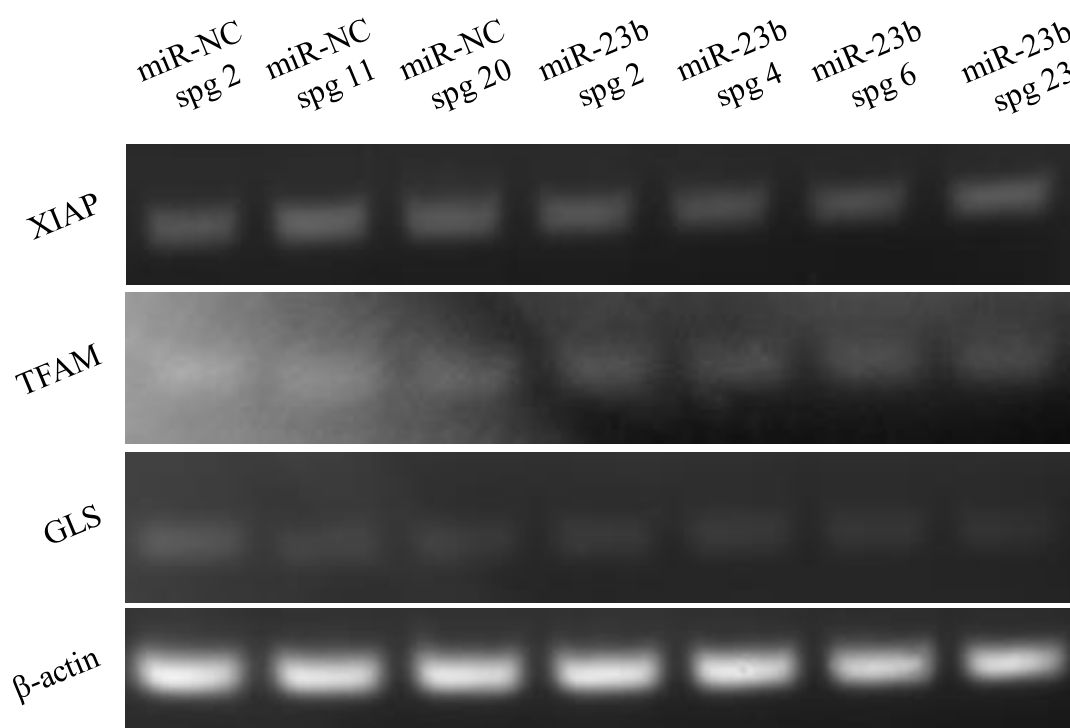


Figure 3.77: Semi-quantitative assessment of the mRNA transcript levels for a select panel of previously validated targets of miR-23 (GLS, TFAM and XIAP). A moderate number of cycles, 25, was used so as not to saturate the amplification signal thus allowing visual identification of potential fluorescent changes. B-actin was used as an endogenous control to ensure efficient sample loading. All PCR amplicons were pre-designed to be small, in the range of 150-200 bp, so were ultimately ran on a high percentage (2%) agarose gel stained with ethidium bromide and ran slowly for the acquisition of clean bands.

There appeared to be no apparent changes in the abundance levels of the mRNA transcripts for XIAP and TFAM in all rCHO-SEAP clones from both non-specific and miR-23 sponge panels that were selected for clonal screening (**Fig. 3.77**). There did appear to be a reduced level of expression for the transcript of glutaminase (GLS). However, minute changes in expression can be difficult to observe at best even if an optimal number of cycles has been utilised.

We next sought to evaluate the abundance of transcript levels for the same targets using quantitative real-time RT-PCR (see **section 2.4.4 of Materials and Methods**). Clones chosen to take part in this screen were the two best producing miR-23 sponge clone 4 and 6 and the two best non-specific control clones, miR-NC sponge clone 2 and 11.

Little to no change was observed for the expression of GLS and TFAM when qPCR was carried out (**Figure 3.78**). A moderate increase in the expression of XIAP was observed in the case of miR-23 sponge clone 6 and for a single control miR-NC sponge clone 11 (**Figure 3.78^{XIAP}**), potentially a result of clonal variation. This observation does not discount the possibility that miR-23 depletion is having an effect on one or all of these validated targets due to the nature of miRNA mode of action, translational inhibition.

To fully understand the potential influence of miR-23 depletion on these target genes, analysis on the protein level would have to be carried out through western blot. Label-free mass-spectrometry will be explored in these stable rCHO-SEAP clones in the next section as a means to identify potential targets of miR-23 and to isolate pathways potentially contributing to the observed phenotype of enhanced target protein productivity with elevated mitochondrial respiration. For this reason, identification of protein abundance of the three targets was not explored at this time through western blot analysis.

Figure 3.78: qPCR of miR-23 validated targets GLS, TFAM and XIAP

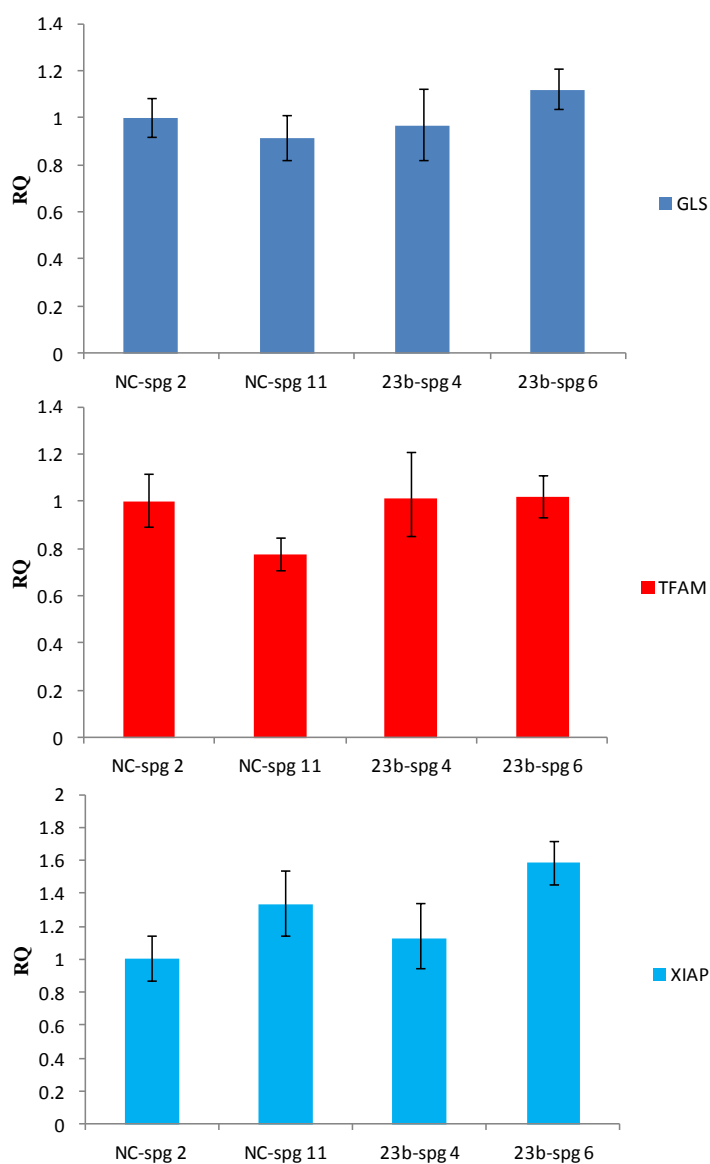


Figure 3.78: Quantitative evaluation of changes in the expression of the mature transcript of a panel of validated targets of miR-23, GLS, TFAM and XIAP. Fast SYBR® Green was used to evaluate the expression of three targets previously assessed at a semi-quantitative level. Data was normalised to one of the two control clones (miR-NC spg 2). Relative quantification was calculated using the $2^{-\Delta\Delta C_t}$ method.

It has been demonstrated so far that stable depletion of miR-23 improves the productivity of SEAP by an average of 3-fold when compared to non-specific controls. Further evaluation found that SEAP productivity may be attributed in part to an increase in the level of SEAP mRNA. Furthermore, mRNA stability and cell size were ruled out as contributing to this.

miR-23 has been strongly implicated in mitochondrial function both through the reprogramming of the “Warburg effect” through anapleurotic replenishment of TCA cycle intermediates such as α -ketoglutarate (α KG) via enhanced translation of the enzyme glutaminase (*GLS*) (Liu et al. 2012) and additionally through the post-transcriptional attenuation of the mitochondrial transcription factor A (*TFAM*) (Campbell, Kolesar & Kaufman 2012). Although the mRNA levels of these genes remained unchanged in our clones, it does not rule out the possibility of their mature protein products being influenced especially when considering the elevated glutamate levels observed in the miR-23 depleted clones. Using high resolution respirometry (HRR), oxygen consumption was assessed as a measure of mitochondrial activity. A ~30% increase in oxygen consumption was observed in the miR-23 sponge cells attributed to Complex I and Complex II stimulation. Both complexes contributed to this enhanced mitochondrial function independently of each other but did not appear to act synergistically, potentially suggesting a bottleneck downstream. Using a mitochondria-specific fluorescent dye, we managed to rule out an increase in cellular mitochondrial mass/content as a contributing factor to this enhanced activity.

The next section explores the discovery of potential targets of miR-23 that could have a role in mediating this observed influence on CHO cell bioenergetics in addition to identifying molecular pathways directly or indirectly influenced by miR-23 depletion.

Section 3.5

miR-23 target identification and pathway analysis

3.5 microRNA target identification

Previous characterisation has so far identified that stable miR-23 depletion results in increased specific SEAP productivity without any impact on cellular growth thus ultimately enhancing volumetric SEAP yield. Across a panel of clones the enhanced SEAP activity appears to be somewhat attributable to the increase in transcription of the SEAP mRNA. Previous characterisation from the literature has implicated miR-23 to be involved in cellular bioenergetics through the regulation of targets associated with mitochondrial function such as GLS and TFAM. However, analysis of the expression of these transcripts using qPCR revealed no difference in the case of miR-23 depletion in CHO cells. Given the nature of miRNA, this observation does not rule out the possibility that the mechanism of action of miR-23 is being mediated through blocking translation. In order to attempt to identify how miR-23 depletion selectively appears to enhance SEAP transcription and influence mitochondrial functional, we set out to identify potential targets of miR-23 through a novel process of biotin-labelled microRNA mimics and Label-free Mass Spectrometry on rCHO-SEAP clones stably engineered to deplete miR-23. It was hoped that the global mRNA targeting capacity would be identified in the case of biotin-tagged mRNA pull down thus indicating potential pathways under miR-23 regulatory control as well as high priority candidate targets, while proteomic profiling was intended to unveil a snap shot of mature molecular pathways under functional interference from miR-23, be it either directly or indirectly.

3.5.1 Identification of global mRNA targets through Biotinylated miRNA tags

A recently described method of identifying miRNA targets is the use of biotinylated-labelled miRNA mimics (Orom, Lund 2007) and successfully reported for miR-34a (Lal et al. 2011). This technique exploits the use of miRNA mimics (pre-miRs) whose 3'-end has been covalently modified to carry a biotinylated tag (**Fig. 3.79 A**). Streptavidin, isolated from *Streptomyces avidinii* and immobilised to sepharose beads has a high binding affinity for biotin or biotinylated components (**Fig. 3.79 A**).

Figure 3.79: Schematic diagram of biotin-labelled miRNA-mediated mRNA pull down

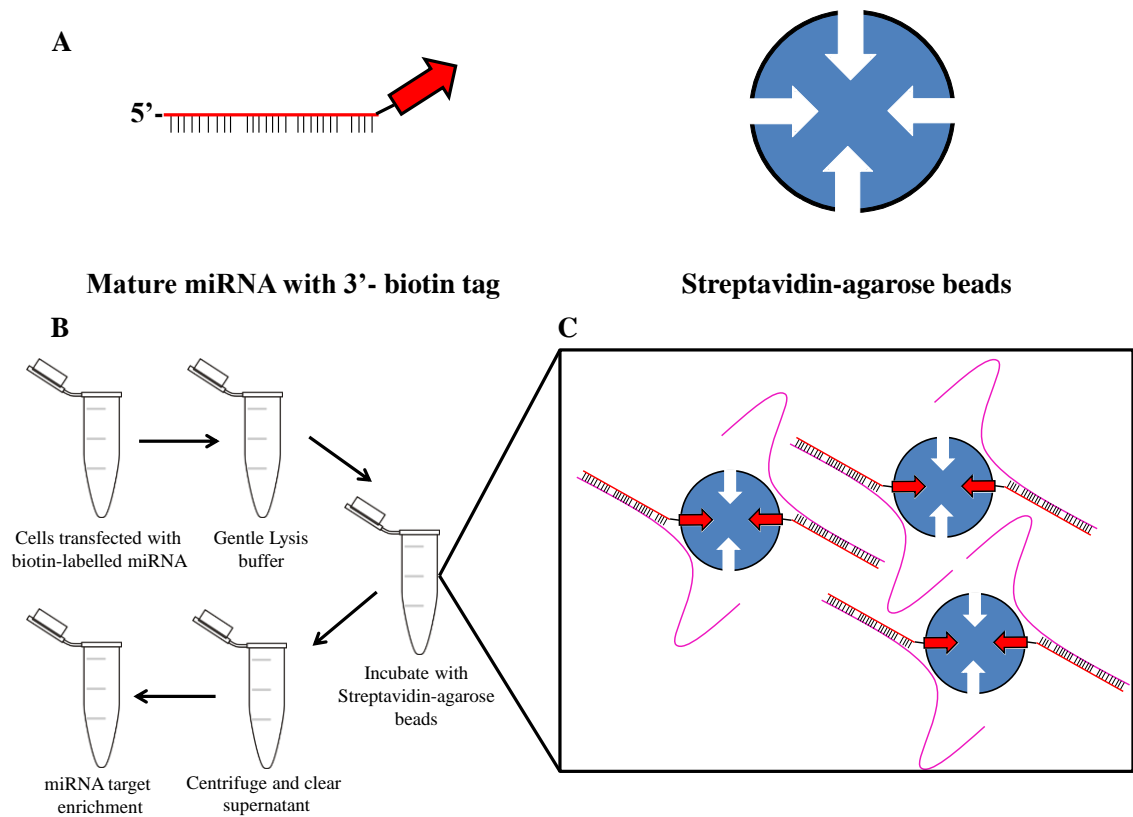


Figure 3.79: A) Shows a mature miRNA with a chemically modified 3' - end (red arrow) to include a linked Biotinylated group as well as the streptavidin-agarose beads with high affinity binding sites for biotin **B)** Represents the general flow diagram for miRNA target enrichment. RNA is isolated from streptavidin-agarose beads through the Tri Reagent protocol **C)** During the incubation period of cell lysate with streptavidin-agarose beads mRNAs bound to the biotin labelled miRNA will remain bound to the SA beads and enriched for after clearing of the cell lysate.

By incubating CHO cell lysates that have been lysed through the utilisation of a gentle lysis buffer so as not to disturb miRNA-RISC bound target mRNAs in the presence of streptavidin beads, it is possible to wash away the majority of non-bound mRNAs and enrich for those that have a high binding affinity for the mature biotin-tagged miRNA. Using microarray technology (**section 2.4.10 of Material and Methods**), it is possible to identify enrichment of a panel of mRNA targets whose identification is potentially a function of their association with the pre-tagged miRNA of interest.

Both miR-23b and its counterpart passenger strand miR-23b* were selected for mRNA target identification through this novel method in an attempt to determine firstly what targets and molecular networks are under their influence and secondly if there is complementary, antagonistic or unique cellular process under their individual regulation.

3.5.1.1 Evaluation of biotin-miRNA workflow

Prior to committing to a full scale microarray analysis, validation of the protocol was assessed using a validated target as previously reported for the miRNA bantam (*Hid* gene) (Orom, Lund 2007) and miR-34a (*CDK4/6*) (Lal et al. 2011).

We undertook some validation steps using qPCR to assess the utility of this method using validated miR-23b* targets such as proline dehydrogenase (PRODH) (Liu et al. 2010a). However, a challenge presented was the lack of validated targets of miR-23b* other than PRODH. A panel of potential targets of miR-23b* was selected by generating a list of mRNAs that were anti-correlated to the expression of miR-23b* from the datasets acquired during the DE of miRNA in fast and slow growing CHO cells (section 3.1 of results and (Clarke et al. 2012)), unveiling 319 mRNAs.

Next, the miRWalk prediction algorithm was utilised to generate two lists of potential miR-23b* targets, one predicted and one validated (Dweep et al. 2011a). From here, both lists were analysed for any overlap with the list of mRNAs found to be anti-correlated with miR-23b* expression. 11 mRNAs were found to overlap with the list of 856 predicted targets while none were found to overlap with the list of 98 validated targets (**Table 3.5**). The search criteria for “Validated targets” uses an algorithm that searches abstract and paper content for commands such as “miR-23b*” and associated gene names. Therefore, this list of 98 validated targets would not necessarily be accurate and reading the paper content would be essential to establish if they could truly be considered “validated”.

Table 3.5: miRWalk Predicted targets of miR-23b* overlapping with targets anti-correlated to miR-23b* expression

Top 10 predicted targets	Overlapping targets	Selected Targets
DNAJC3	Rapgef1	Rapgef1
GRIP1	BSG	CSTA
CRYBB2	Plod1	DNAJC3
CTSA	C6orf89	GRIP-1
HCG9	GGA2	PRODH
PGK1	BEST1	PGK-1
SMPD1	ACYL	BEST-1
STX4	YARS	CALU
ACLY	RARRES2	GGA2
SPRN	CALU	YARS
	Pomt2	

Although PRODH did appear in the list of validated targets, it was not predicted to be a target of miR-23b* nor did it appear to be anti-correlated with miR-23b* from the miRNA:mRNA profile.

Biotin-labelled miR-23b* and miR-NC were transfected into CHO-SEAP cells at the usual concentration of 50 nM in 1×10^5 cells/mL (see section 2.3.2.2 of Materials and Methods). After 72 h, cells were harvested and processed according to the protocol described by Ørum and Lund (Orom, Lund 2007) and described in detail in section 2.7 of Material and Methods. Two miR-23b* biotin –tagged mimics were designed, miR-23b*-1 and miR-23b*-2 (natural). miR-23b*-1 comprises a duplex miRNA with a complementary strand designed to promote strand selection of miR-23b* (Appendix Figure A8). miR-23b*-2 (natural) was specifically designed to mimic the wild-type hairpin and would result in the selection of the mature miR-23b. When both biotin-tagged miRNA were transfected separately, qRT-PCR was carried out for both miR-23b*-1 and miR-23b*-2 (natural) (see section 2.4.8 of Materials and Methods) probing for miR-23b and the miR-23b*.

When miR-23b* levels were assessed, an increase was observed of ~600-fold for miR-23b*-1 and ~12,000-fold for miR-23b*-2 (natural) in bead enriched samples (Fig. 3.80 A). Furthermore, a ~2000-fold increase of miR-23b* was detected for miR-23b*-1 and ~9,000-fold for miR-23b*-2 (modified) in the input samples prior to bead exposure (Fig. 3.80 B). Input samples, are samples taken after gentle lysis but prior to incubation with streptavidin beads.

Figure 3.80: Quantification of miR-23 and miR-23b* by qPCR from streptavidin pull-down

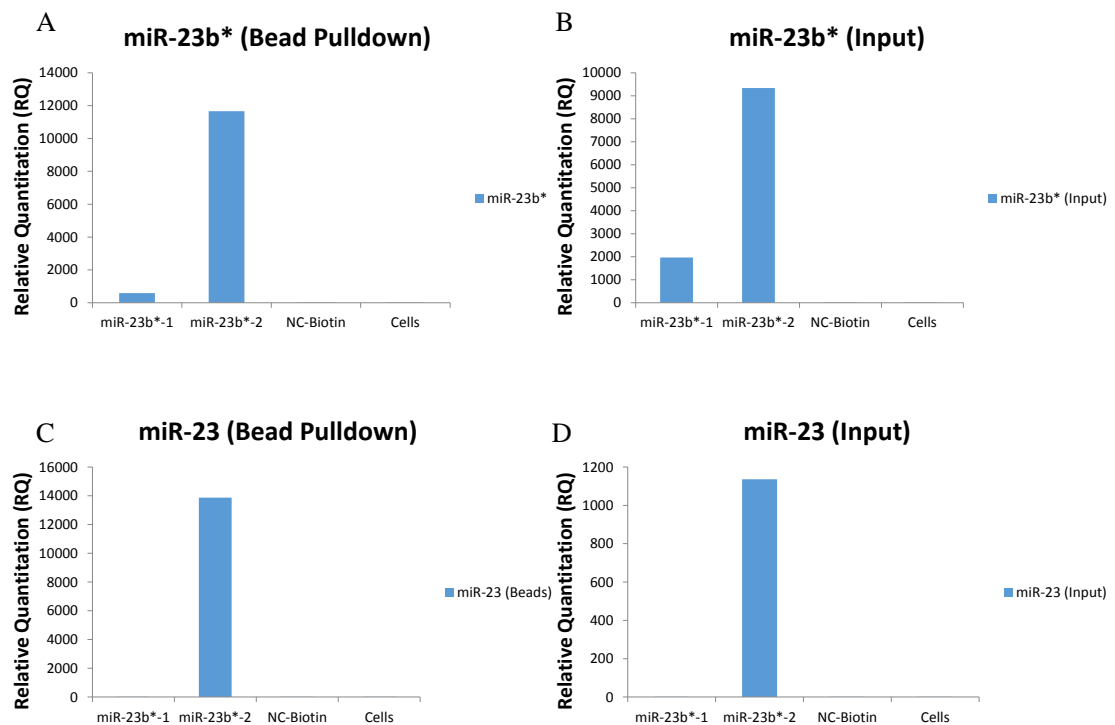


Figure 3.80: qRT-PCR data assessing the mature levels of miR-23b and miR-23b* when biotin-labelled miR-23b*-1 and miR-23b*-2 (modified) were transfected into CHO-SEAP cells. miR-23b* is probed for in A) streptavidin captured samples and B) Input samples taken after gentle lysis but before incubation in streptavidin beads. miR-23b is probed for in C) streptavidin captured samples and D) Input samples.

As an additional level of quality control, miR-23b levels were assessed in the same samples. No fold change of miR-23b was observed in either streptavidin captured or input samples in the case of miR-23b*-1 as expected as this biotin-labelled pre-miRNA is designed to exclusively express miR-23b* as its complementary strand does not contain mis-matches therefore has a different sequence to miR-23b (**Fig. 3.80 A and B**). Furthermore, when miR-23b levels were measured in the case of the miR-23b*-2 (modified) transfectant, a ~14,000-fold and 1,000-fold increase was observed for streptavidin captured and input samples, respectively (**Fig. 3.80 C and D**). This enrichment for miR-23b in the case of the tailored miR-23b*-2 (natural) biotin-tagged duplex was expected as it should mimic a naturally occurring miR-duplex. The miR-

23b*-1 biotin-tagged pre-miR was ultimately selected for experimental evaluation as it best represents the processing steps that culminate at RISC loading.

Next, we assessed if successful pull-down of the list of potential miR-23b* targets could be observed in samples transfected with miR-23b*-1 and -2 and exposed to streptavidin beads. The amount of RNA pull-down was approaching the sub-nanomolar concentration when assessed using a NanoDrop, however, enough template was retrieved that enabled reverse transcription and subsequent PCR analysis. Of the list of 10 candidates selected for evaluation, Pgk-1 resulted in the most consistent enrichment. miR-23b*-1 proved to enrich for Pgk-1 compared to miR-23b*-2 in cell lysates exposed to streptavidin (**Fig. 3.81 Beads**). An inconsistency can be observed across input samples possibly due to the quality of the RNA harvested.

Figure 3.81: Enrichment for Pgk-1 in miR-23b*-biotin pull-down

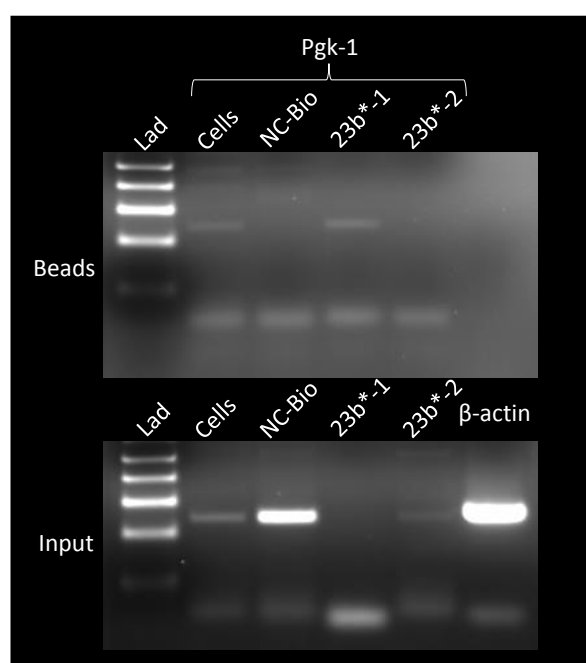


Figure 3.81: Analysis of Pgk-1 expression in CHO-SEAP cells transfected with biotin-tagged pre-miRs, miR-23b*-1 and miR-23b*-2, and incubated with streptavidin beads (Beads). RNA samples were taken prior to exposure to streptavidin (Input).

Assessment of Pgk-1 pull-down by miR-23b*-1 biotin-tagged pre-miR upon several repeats demonstrated inconsistent yet strong indications that Pgk-1 specific binding and enrichment was occurring (**Fig. 3.82**).

Figure 3.82: Enrichment for Pgk-1 in miR-23b*-1 biotin-labelled transfected CHO-SEAP cells

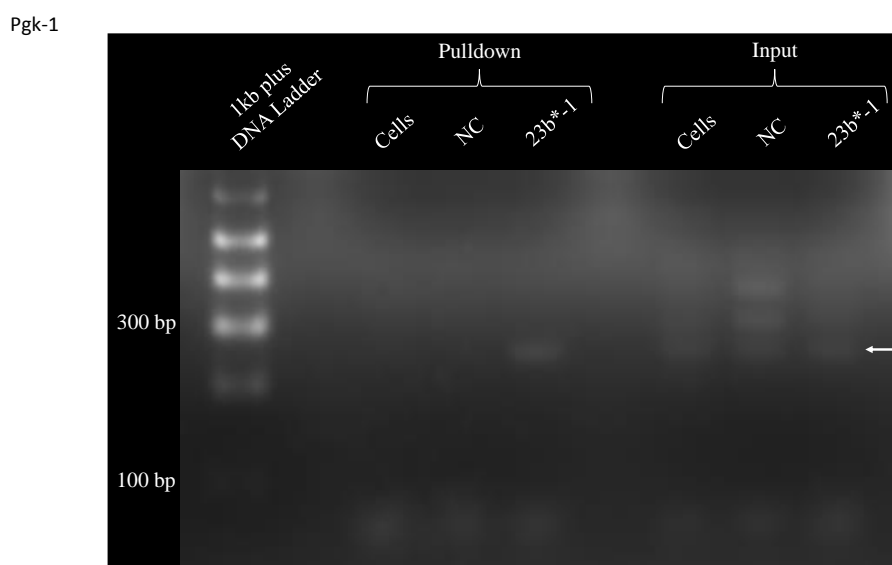


Figure 3.82: pPCR analysis to measure enrichment of the potential target of miR-23b*, pgk-1 (white arrow), in CHO-SEAP cells transfected with miR-23b*-1. “Pull-down” indicates samples incubated in streptavidin beads while “input” indicates RNA sampled prior to bead incubation.

3.5.1.2 Microarray identification of mRNA targets specific for miR-23b and miR-23b* using biotin-labelled mimics

Following initial optimisation, biotin-labelled miR-23b and miR-23b*-1 pre-miRs were transfected into parental CHO-SEAP cells and processed according to section **2.7.5 of Materials and Methods**. As 12.5 µg of aRNA (antisense RNA) was required for loading of CHO-specific microarray chips, an amplification process (MessageAmp™ II aRNA amplification, section **2.4.9 of materials and methods**) was undertaken prior to processing of the aRNA (section **2.4.10 of Materials and Methods**).

Subsequent to generating aRNA, samples were hybridized to CHO-specific microarrays. Across all samples (cells only, miR-NC-biotin, miR-23b-biotin and miR-23b*-1-biotin),

1933 annotated genes were identified as being present, however, none demonstrated a significant fold change or enrichment between conditions. One of the first quality control tests undertaken in microarray analysis is the use of hierarchal clustering. This is an unbiased means by which a dataset is grouped into sample families based on a similar gene expression pattern. This revealed that there were no similarities between samples of the same group (**Fig. 3.83**).

Figure 3.83: Cluster Dendrogram of microarray results

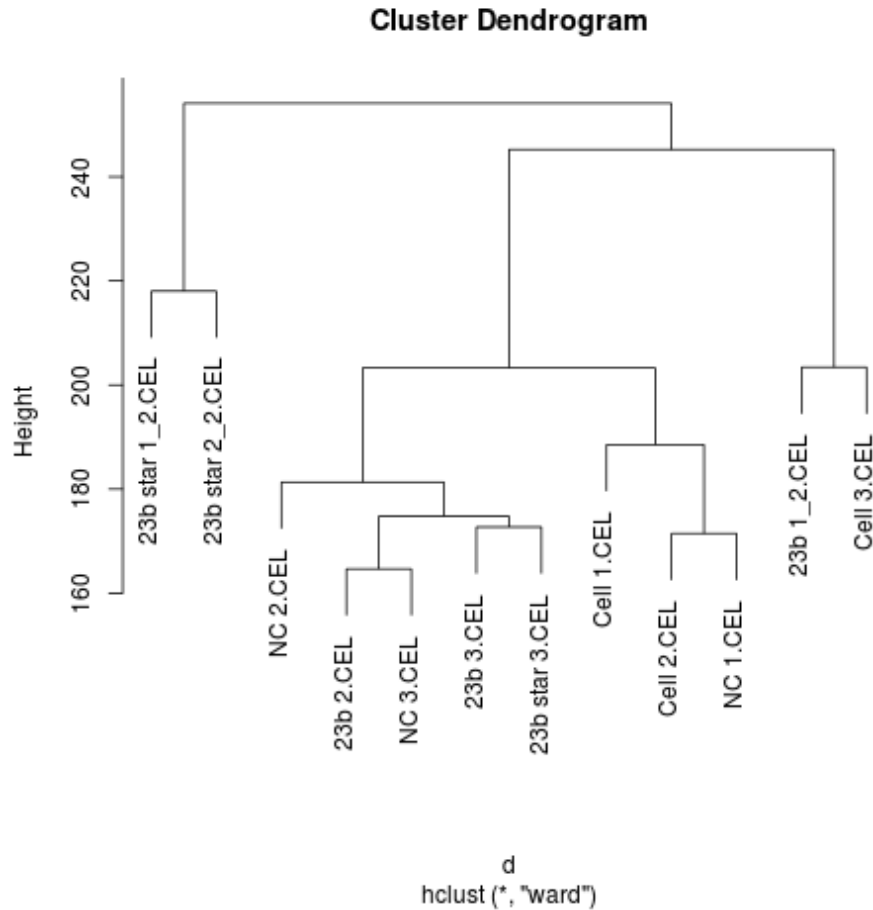


Figure 3.83: Dendrogram demonstrating the unsupervised hierarchal clustering of samples based on gene expression.

Any changes observed between biotin-tagged miRNAs compared to biotin-tagged non-specific controls equated to inherent background noise that would ordinarily be observed

between replicate samples. Although this method of miRNA:mRNA identification has proved valuable and successful in the past, in this case, no candidates were generated from our experiment.

The reasons for this was not immediately apparent so we decided to check bead-elutes for enrichment of both miR-23b and miR-23b* in case the capture step failed.

Figure 3.84: miR-23b/23b* enrichment in main experimental run

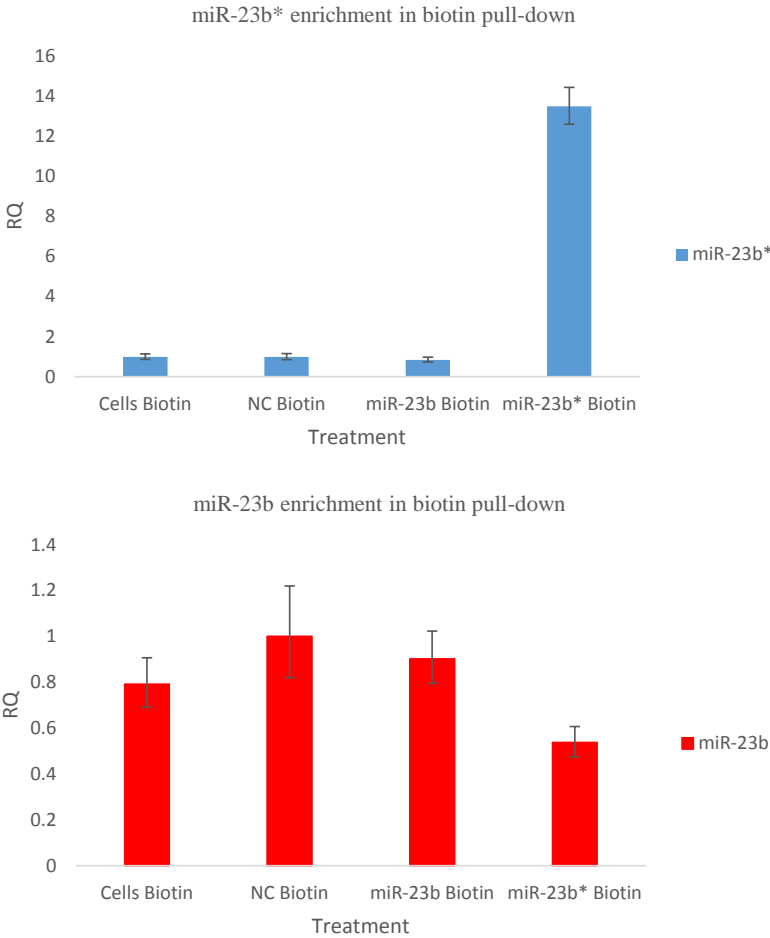


Figure 3.84: qRT-PCR analysis using singleplex PCR specific for miR-23b* (blue) and miR-23b (red) was carried out on the streptavidin incubated biotin-labelled pre-miRNA for the mature miR-23b and miR-23b*.

Singleplex qRT-PCR carried out on samples captured for microarray analysis revealed that there was a ~14-fold enrichment of miR-23b* with no apparent enrichment of miR-

23b (**Fig. 3.84**). This latter result would explain the lack of clustering observed in **figure 3.83** for miR-23b samples but, miR-23b* at least, seemed to have been successfully pulled down although not to as high a magnitude as previously achieved.

3.5.2 Identification of global protein targets using Label-free Mass Spectrometry

As miRNAs ultimately influence translation, we sought to carry out label-free mass spectrometry as a means to identify the potential finite changes in the proteome elicited by the stable depletion of miR-23 through sponge intervention. In addition, we attempted to identify potential molecular networks and/or biological processes associated with mitochondrial function.












3.5.2.1 Differentially expressed proteins in miR-23 depleted clones

Differential protein expression analysis was performed on two miR-23 sponge clones (clone 4 and 6) and two miR-NC sponge clones (clone 2 and 11), the same clones that were evaluated for mitochondrial function in section 3.4.6. CHO cells were cultured under normal batch conditions in an identical manner as had been previously described for mitochondrial function assays and harvested for whole cell proteome analysis after 72 hs. A maximum of 500 µg of protein was prepped using a Ready-prep 2D clean-up kit (Bio-Rad, #163-2130, **and see materials and methods section 2.8.3**) as a means to further concentrate, if necessary, and remove any contaminating salts, reagents and buffers from the lysis process. 10 µg of protein was then subsequently digested with Lys-c and trypsin overnight to cleave all protein into polypeptides for mass spec identification.

41 proteins were found to be differentially expressed (25 up-regulated and 16 down-regulated) in miR-23 depleted CHO-SEAP clones when compared to their non-specific control counterparts (**Table 3.6**). Proteins are listed in order of MASCOT score output which overlaps the mass spectral data of the target peptides with that of the reference database, including the number of identifications (numbers of peptides associated with a single protein). MASCOT also incorporates a false discovery rate (FDR) which compares the same mass spectral data of the target peptides to that of a randomised reference database of similar length as a means to identify the probability of identifications by

chance. Statistical significance is then assigned to each identified protein after normalisation (Anova value) to determine that the observed fold-changes demonstrate low variation within replicates and/or pooled clones in the case of our experiment.

Table 3.6: DE proteins identified through label-free mass spectrometry in miR-23 (test) depleted CHO-SEAP clones

Accession	Peptides	Score	Anova (p)*	Fold	Tags	Description	Gene I.D.	Average Normalised		Up in Test
								Control	Test	
gi 860908	6	271.74	7.74E-03	1.5		vimentin [Cricetulus griseus] [MASS=44524]	VIM	2.91E+06	1.94E+06	Down in Test
gi 344235837	3 (2)	188	3.36E-05	1.74		Glutathione S-transferase Mu 6 [Cricetulus griseus] [MASS=86559]	GSTM6	2.15E+05	3.75E+05	0.67
gi 344236438	3	148.52	6.85E-05	2.07		Bifunctional aminoacyl-tRNA synthetase [Cricetulus griseus] [MASS=154896]	EPRS	4.09E+05	1.98E+05	1.74
gi 344257633	2	145.81	2.72E-08	1.98		Lactadherin [Cricetulus griseus] [MASS=16152]	MFGE8	1.41E+05	2.79E+05	0.48
gi 344255736	3	144.97	3.12E-04	2.16		Non-muscle caldesmon [Cricetulus griseus] [MASS=61921]	CALD1	2.09E+05	4.52E+05	1.98
gi 354487570	2	133.91	6.64E-05	1.85		PREDICTED: ATP-binding cassette sub-family F member 1-like [Cricetulus griseus] [MASS=95446]	ABCF1	1.39E+05	7.53E+04	2.16
gi 344237556	2 (1)	132.94	0.02	1.52		Glyceraldehyde-3-phosphate dehydrogenase [Cricetulus griseus] [MASS=36889]	GAPDH	4.80E+05	3.15E+05	0.54
gi 354479271	2	118.37	8.74E-07	2.49		PREDICTED: perilipin-4-like [Cricetulus griseus] [MASS=184216]	PLIN4	1.06E+05	2.63E+05	0.66
gi 354507545	2 (1)	98.26	4.80E-03	1.56		PREDICTED: glutathione S-transferase Mu 1-like [Cricetulus griseus]	GSTM1	1.32E+04	2.07E+04	2.48
gi 344238611	1	91.09	2.48E-03	1.68		Isocitrate dehydrogenase [NADP] cytoplasmic [Cricetulus griseus] [MASS=12467]	IDH1	2.58E+04	4.33E+04	1.57
gi 344244293	1	89.46	4.33E-07	2.73		LETM1 and EF-hand domain-containing protein 1, mitochondrial [Cricetulus griseus] [MASS=79070]	LETM1	2.71E+04	7.39E+04	1.68
										2.73

gi 354474417	1	86.11	5.14E-05	1.54		PREDICTED: ras GTPase-activating protein-binding protein 1 [Cricetulus griseus] [MASS=51797]	G3BP1	1.07E+05	6.96E+04	0.65
gi 354473301	2	85.25	6.20E-04	1.54		PREDICTED: septin-9 [Cricetulus griseus]	SEPT9	1.76E+05	2.71E+05	1.54
gi 344251753	1	85.03	0.02	317.52		Heat shock cognate 71 kDa protein [Cricetulus griseus] [MASS=22696]	HSPA8	5.32E+05	1676.73	0.00
gi 4504445	1	78	0.04	2877.1		heterogeneous nuclear ribonucleoprotein A1 isoform a [Homo sapiens]	HNRNPA1	2.24E+05	77.98	0.00
gi 344254200	1	77.24	1.48E-04	1.84		Prolyl 4-hydroxylase subunit alpha-1 [Cricetulus griseus] [MASS=58084]	P4HA1	7.12E+04	1.31E+05	1.84
gi 354489184	1	72.31	1.05E-03	1.65		PREDICTED: lysosomal alpha-glucosidase-like [Cricetulus griseus]	GAA	3.96E+04	6.55E+04	1.65
gi 344255594	1	71.25	4.95E-04	1.76		Calcium/calmodulin-dependent protein kinase type II delta chain [Cricetulus griseus] [MASS=25006]	CaMK2D	8.60E+04	1.51E+05	1.76
gi 344248788	1	65.91	0.04	2.50E+04		Eukaryotic translation initiation factor 5A-1 [Cricetulus griseus] [MASS=7244]	EIF5A1	3.45E+05	13.79	0.00
gi 344236520	1	61.57	0.02	1.55		40S ribosomal protein S13 [Cricetulus griseus] [MASS=15245]	RSP13	1.16E+05	1.79E+05	1.54
gi 354503637	1	61.06	3.85E-03	1.77		PREDICTED: STE20-like serine/threonine-protein kinase isoform 1 [Cricetulus griseus] [MASS=142185]	SLK	4.87E+04	2.75E+04	0.56
gi 344247607	1	60.45	9.02E-06	20.57		Suprabasin [Cricetulus griseus] [MASS=63932]	SBSN	2685.43	5.52E+04	20.56
gi 346421390	1	58.73	0.02	5.36		C-X-C motif chemokine 3 precursor [Cricetulus griseus]	CXC3	1.56E+05	2.91E+04	0.19
gi 344250293	1	57.66	0.01	1.86		rRNA 2'-O-methyltransferase fibrillarin [Cricetulus griseus] [MASS=25970]	FBL	4.21E+04	7.84E+04	1.86
gi 71043900	1	56.08	0.03	Infinity		60S ribosomal protein L11 [Rattus norvegicus]	RPL11	2.89E+05	0	0.00
gi 354468793	1	53.47	1.96E-06	2.49		PREDICTED: leukocyte elastase inhibitor A [Cricetulus griseus]	SERPINB	8.27E+04	2.06E+05	2.49

gi 344249602	1	51.72	1.48E-03	1.64		Ras GTPase-activating-like protein IQGAP1 [Cricetulus griseus] [MASS=191377]	IQGAP1	7.88E+04	4.80E+04	0.61
gi 354471687	1	51.7	0.02	1.59		PREDICTED: sorbitol dehydrogenase [Cricetulus griseus]	SDH	8.25E+04	1.31E+05	1.59
gi 354504447	1	51.44	1.18E-04	5.77		PREDICTED: hypothetical protein LOC100755523 [Cricetulus griseus] [MASS=7910]	SPRR2E	1.95E+04	1.13E+05	5.79
gi 344253587	1	50.88	2.66E-03	1.67		Thioredoxin reductase 1, cytoplasmic [Cricetulus griseus] [MASS=61858]	TXNDR1	6.61E+04	1.10E+05	1.66
354479983	1	50.38	2.50E-03	1.67		PREDICTED: malate dehydrogenase, cytoplasmic-like [Cricetulus griseus]	MDH	4.07E+05	6.79E+05	1.67
354493216	1	48.45	0.03	1.53		PREDICTED: 26S proteasome non-ATPase regulatory subunit 7-like [Cricetulus griseus]	PSMD7	7.40E+04	4.85E+04	0.66
gi 344254748	1	48.09	2.30E-04	1.62		Cytosolic acyl coenzyme A thioester hydrolase [Cricetulus griseus] [MASS=35644]	ACOT7	1.44E+05	8.90E+04	0.62
gi 344248399	1	48.08	5.56E-03	1.82		hypothetical protein I79_019528 [Cricetulus griseus] [MASS=271141]	PRUNE2	4.81E+04	8.74E+04	1.82
gi 344245117	1	47.43	2.41E-03	1.69		Fermitin family-like 2 [Cricetulus griseus] [MASS=65673]	FERMT2	1.95E+05	3.30E+05	1.69
gi 344241413	1	47.22	2.07E-03	1.66		Epidermal growth factor receptor substrate 15-like 1 [Cricetulus griseus] [MASS=82827]	EPS15L1	3.26E+04	1.96E+04	0.60
gi 344242484	1	46.57	0.01	1.79		Cytoplasmic dynein 1 light intermediate chain 2 [Cricetulus griseus] [MASS=68816]	DYNC1L12	1.54E+04	2.75E+04	1.79
gi 354499825	1	45.47	0.01	2.33		PREDICTED: heme oxygenase 1-like [Cricetulus griseus]	HMOX1	3.45E+04	8.05E+04	2.33
gi 354468396	1	43.47	0.02	1.97		PREDICTED: serine/threonine-protein phosphatase PP1-beta catalytic subunit-like [Cricetulus griseus] [MASS=37328]	PPP1CB	4.02E+04	7.92E+04	1.97
gi 354495432	1	41.82	5.41E-04	2.24		PREDICTED: asparagine synthetase [glutamine-hydrolyzing]-like isoform 1 [Cricetulus griseus]	ASNS	8.78E+04	3.92E+04	0.45
gi 344244307	1	40.44	5.84E-06	2.77		14-3-3 protein eta [Cricetulus griseus] [MASS=27084]	YWHAH	6.50E+04	1.80E+05	2.77

Table 3.6: The fold change highlighted in Green or Red denotes the direction in expression of each identified gene in relation to miR-23 sponge clones with Green being up and Red being down. Tags indicate the implementation of analytical criteria including fold change above 1.5 and an Anova value below 0.01.

We conducted our own quality control tests as a means to identify proteins whose identification were potentially by chance. The average protein expression of a test group is compared to the average protein expression of the control group resulting in identifying DE. By un-supervising the samples, large variation within samples contributing to DE can be identified. The “6 replicates” of each group (control and test) were stripped of their identifiers and randomised, ultimately resulting in two groups for comparison whose occupants potentially spanned samples from both control and test groups. When DE analysis was carried out in this instance, only two proteins were found to be DE, neither of which overlapped with those identified in the list of 41 above (**Appendix fig. A9**).

For example, after carrying out the various comparisons, LETM1 was found to be a potential target of miR-23 (**Fig. 3.85**). This figure demonstrates that LETM1 expression range is tight and consistent throughout control clones (pink box) and significantly increased in expression in miR-23-depleted clones (blue box). Furthermore, the data suggests that titrational effects are potentially occurring due to differential sponge expression, as two triplicate clusters appear to demonstrate distinct patterns of expression within the miR-23 test samples (**Fig. 3.85-Black box**).

Figure 3.85: Differential expression of LETM1 in control and miR-23 sponge clones

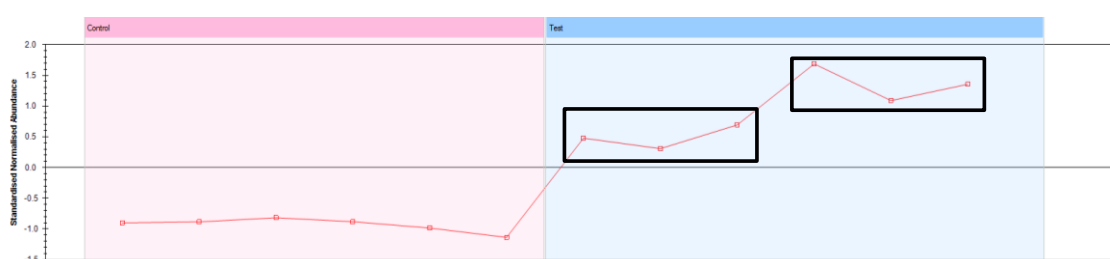


Figure 3.85: Progenesis software output of the protein expression pattern of LETM1 for each of the samples replicates within both control (Pink) and test (Blue) groups that ultimately contribute to the calculation of both fold change and statistical significance.

Furthermore, when both negative control clones were compared, LETM1 was not found to be DE as indicated in **Figure 3.85**. Additionally, when both miR-23 clones were compared, LETM1 was not found to be DE further strengthening that LETM1 is

potentially increased as a product of sharing a post-translational controller (miR-23) and not as a result of clonal variation.

When the control clones (miR-NC sponge clone 2 and 11) were compared, 69 proteins were found to be DE, compared, to 19 proteins DE between the test clones (miR-23 sponge clone 4 and 6). Interestingly, 4 proteins determined to be DE in miR-23 depleted clones when compared to controls were also found to be DE between control clones themselves: Malate dehydrogenase (MDH), heme-oxygenase-1 (HMOX1), non-muscle caldesmon (CALD1) and 26S proteasome non-ATPase regulatory subunit 7-like (PSMD7). By comparing both control and test clones against each other it examines the potential for clonal variation irrespective of the introduction of a miRNA sponge. By grouping all clones into their respective groups these inter-clonal differences will ultimately be accounted for resulting in a lower statistical significance. Profiling a larger panel of clones would be a means to further refine the data output accounting for expressional variations that are not a product of or indeed specific to the introduction of a sponge specific for miR-23.

Figure 3.86: Progenesis output of 4 proteins DE in control clones

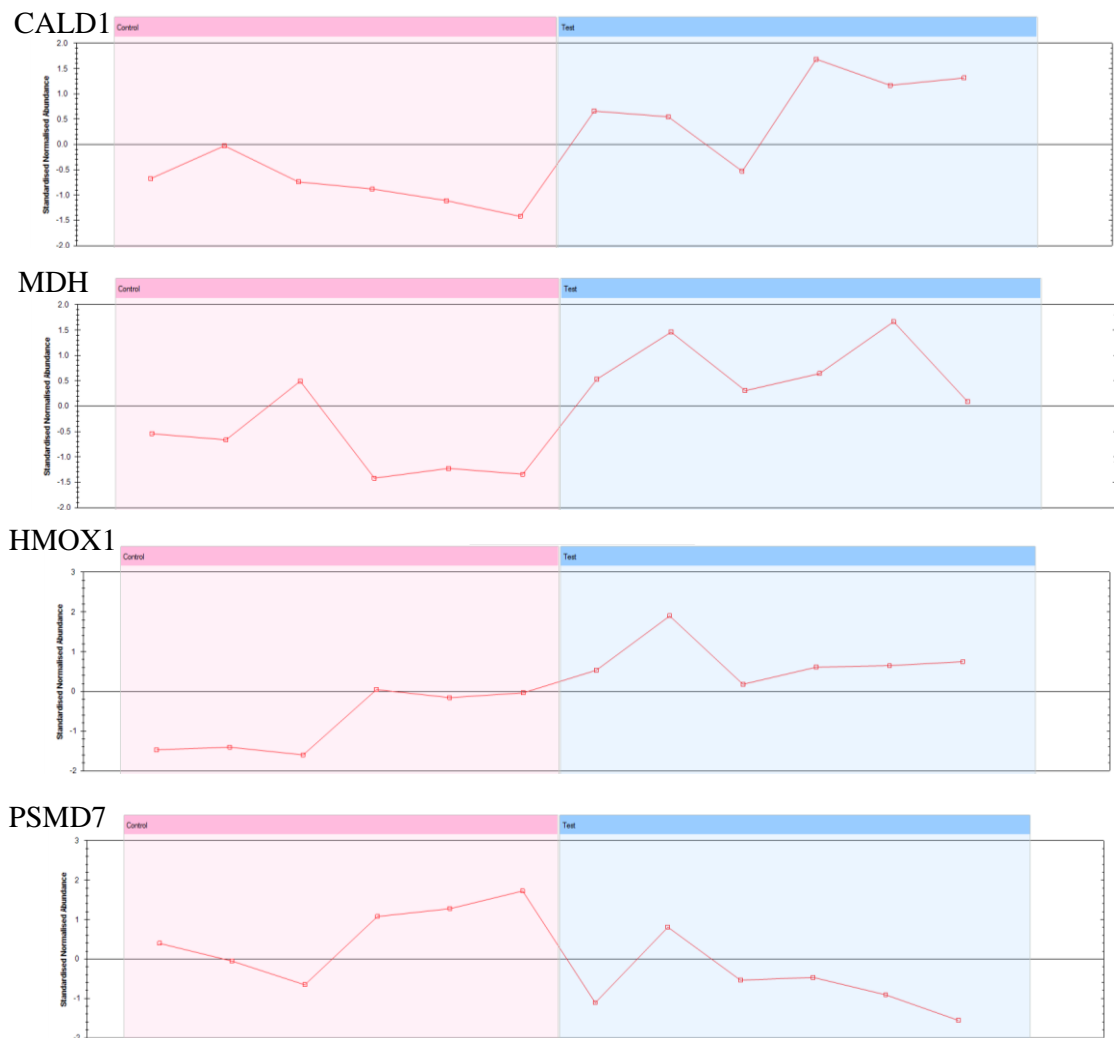


Figure 3.86: Progenesis output diagram of the DE of four proteins in miR-23 clones versus miR-NC controls. The four proteins listed above, however, were determined to be DE between both control clones.

3.5.2.2 High Priority targets of miR-23

Of the list of 41 proteins found to be DE across the miR-23 depleted CHO-SEAP clones when compared to control clones, it was necessary to identify which of these proteins were DE as a result of miR-23 diversion and not as a byproduct of the CHO cell phenotype. The online resource, miRWalk (Dweep et al. 2011b), was utilised to generate a list of potential mRNA targets of miR-23. miRWalk assesses binding potential of a selected miRNA for all possible mRNAs by identifying a hetpamer complementary

sequence to the miRNA seed region and extending or “walking” in the 3’ direction for further complementarity and scored accordingly. Additionally, miRWalk considers binding sites within the coding sequences (CDS) and 10kb upstream of the CDS including the 5’UTR, a criteria not encompassed in the vast majority of prediction algorithms. Furthermore, miRWalk compares the readouts of up to 8 separate prediction algorithms (3’UTR only) scoring predicted mRNAs based on the number of algorithms that overlap in their prediction.

Of the 41 proteins found to be DE, 13 were found to overlap with the miRWalk algorithms (**Table 3.7**). These proteins are listed according to their statistical significance (Anova value) with the addition of the number of algorithms predicting each protein. Given the nature of the miRNA sponge construct and its influence on the cells translatoe, it was possible to further reduce this list of 13 to a more refined and manageable list of proteins. As the presence of the miRNA sponge provides a surplus of binding sites for endogenous miR-23, the activity of this miRNA is being sequestered away from its normal cellular targets thus ultimately resulting in their translational de-repression. Taking this into account, DE proteins from this list of 13 that exhibit an increased-fold change would correlate with the diversion of miR-23 away from its natural suppressive role.

Table 3.7: Predicted targets of miR-23 using the miRWalk algorithm

Gene I.D	Accession No.	FC	Anova Value	Algorithm overlap	Biological Process
Predicted targets demonstrating up-regulation					
LETM1	gi 344244293	2.73	4.33×10^{-7}	3	ETS Biogenesis/ Mitochondria
CALD1	gi 344255736	2.16	3.12×10^{-4}	1	Calcium Signalling
CAMK2D	gi 344255594	1.76	4.95×10^{-4}	2	Calcium binding
FERMT2	gi 344245117	1.69	2.41×10^{-3}	2	Actin assembly
IDH1	gi 344238611	1.68	2.48×10^{-3}	1	TCA cycle / α -KG
TXNRD1	gi 344253587	1.67	2.66×10^{-3}	4	Oxidative stress
PPP1CB	gi 354468396	1.97	2.01×10^{-2}	3	Glycogen metabolism, protein synthesis and chromatin structure
P4HA1	gi 344254200	1.84	1.48×10^{-4}	2	Collagen synthesis
Predicted targets demonstrating down-regulation					
ABCF1	gi 354487570	1.85	6.64×10^{-5}	2	ATP binding
ASNS	gi 354495432	2.24	5.41×10^{-4}	3	Asparagine synthesis
IQGAP1	gi 344249602	1.64	1.48×10^{-3}	1	Cell morphology and motility
CXCL3	gi 346421390	5.36	1.95×10^{-2}	1	Cell migration and adhesion
HNRNPA1	gi 4504445	2877.1	4.07×10^{-2}	1	pre-mRNA processing

Of the shortlist of 7 proteins found to be increased in their levels of expression as a result of miR-23 depletion, several appear to be involved in cellular processes that potentially reflect the observed phenotype of enhanced mitochondrial function such as LETM1 (mitochondrial biogenesis), IDH1 (TCA cycle, α -ketoglutarate synthesis) and TXNRD1 (oxidative stress response).

Further experiments would be required to validate these proteins as true targets of miR-23. Western blot could be utilised to determine the sensitivity and accuracy of mass spectrometry by selecting a small panel of high priority candidates such as LETM1. Ultimately, functional characterisation of priority targets could be explored by siRNA

knockdown of the protein to examine whether their DE could be linked to observed phenotype.

3.5.2.3 Gene Ontology analysis of differentially expressed proteins

To give an indication if the list of DE expressed proteins within the miR-23 clones displayed any enrichment for their involvement in similar biological processes, the entire list of 42 were analysed using the DAVID (Database for Annotation, Visualisation and integrated Discovery: <http://david.abcc.ncifcrf.gov/home.jsp>) algorithm. From the biological processes identified, cellular metabolism was apparent (**Table 3.8**).

Table 3.8: Gene Ontology of miR-23 sponge DE proteins

GO ID	GO Term	P-value	BH adj.
0015980	Energy derived by oxidation of organic compounds	8.4×10^{-4}	2.5×10^{-1}
0006091	Generation of precursor metabolites	1.4×10^{-3}	2.2×10^{-1}
0051186	Cofactor catabolic process	1.7×10^{-3}	1.8×10^{-1}
0006006	Glucose metabolic process	2.3×10^{-3}	1.8×10^{-1}
0055114	Oxidation reduction	3.7×10^{-3}	7.3×10^{-1}
0006099	Tricarboxylic acid cycle	4.3×10^{-2}	7.5×10^{-1}
0046356	Acetyl-CoA catabolic process	4.5×10^{-2}	7.3×10^{-1}
0009060	Aerobic respiration	5.0×10^{-2}	7.2×10^{-1}
0006084	Acetyl-CoA metabolic process	5.8×10^{-2}	7.2×10^{-1}

3.5.3 Identification of differential protein expression in isolated mitochondria

miR-23 depletion was previously observed to impact on mitochondrial function in addition to mitochondrial-associated proteins being identified as increased such as LETM1. Mitochondrial extraction was carried out 72 h into culture as before (**see section 2.5.3 of Materials and Methods**) and processed for label-free mass spectrometry following the same procedure as previously described for proteomic profiling of whole cell cultures.

3.5.3.1 Differentially expressed proteins

When label-free mass spectrometry was carried out on the isolated mitochondria of the same miR-23 sponge clones (4 and 6) and miR-NC sponge clones (2 and 11), 499 proteins were determined to be DE exhibiting a fold change of ≥ 1.2 and a peptide identification of ≥ 1 (**Appendix fig. A10**). When this list was subjected to more stringent analytical filters (≥ 1.5 FC in addition to ≥ 2 peptide identifications), a shorter list of 99 proteins were found to be DE. Overlap of the entire list of 499 with the 42 found to be DE in the whole cell identified 15 proteins common to both lists (**Table 3.9**) demonstrating the same direction of expression in addition to a similar FC in most cases (10 up-regulated and 5 down-regulated). One interesting observation was the identification of the cytoplasmic MDH1 to be upregulated by 1.79-fold in miR-23 sponge clones in the whole cell lysate. Whereas the mitochondrial-specific MDH2 and the cytoplasmic MDH1 were identified to be up-regulated by 1.3 and 2.7, respectively, in mitochondrial enriched miR-23 sponge samples.

Table 3.9: DE proteins common to both Whole cell and Mitochondrial

Whole Cell Lysate		Mitochondria	
Protein	FC	Protein	FC
GSTM6	2.73	GSTM6	2.4
MFGE8	2.49	MFGE8	2.2
CALD1	2.77	CALD1	1.9
P4HA1	2.24	P4HA1	1.7
GAA	1.54	GAA	2.5
RPS13	1.66	RPS13	1.3
SBSN	1.68	SBSN	3.6
TXNRD1	1.86	TXNRD1	1.8
HMOX1	Infinity	HMOX1	2
MDH1	1.79	MDH1	2.7
YWHAH	2877.10	YWHAH	1.7
EPRS	2.49	EPRS	2.6
ABCF1	20.57	ABCF1	2.4
GAPDH	1.74	GAPDH	1.4
HNRNPA1	1.76	HNRNPA1	1.5
IQGAP1	1.82	IQGAP1	1.6

Table 3.9: DE proteins common to both label-free MS list (Whole cell lysates and Mitochondrial enriched). Fold-change (FC) comparisons are listed to demonstrate similarities across both lists and MS sensitivity in addition to an identical direction of expression (Green – upregulated and Red – down regulated). FC and colour-coding refers to the expression in miR-23 depleted clones compared to controls.

When cell component association of both DE protein lists from the whole cell (42 proteins) and the mitochondrial enriched (499 proteins) was assessed, there was a 10% enrichment for proteins associated with the mitochondria (47 proteins) in the mitochondrial enriched samples compared to no apparent mitochondrial association in the case of the DE proteins from the whole cell lysate. This indicated a significant enrichment over what would be expected by chance.

3.5.3.2: Gene Ontology analysis

Similar to the case of miR-23 sponge whole cell lysate DE proteins, GO analysis was performed for the 499 proteins DE in the mitochondrial enriched samples. Biological processes associated with translation, RNA processing, ribosome biogenesis and protein folding were found to be enriched. This is potentially in agreement with the miR-23 depleted associated phenotype of high SEAP production. When all ribosomal proteins found to be DE were further analysed, it was found that 26 out of 35 (74.2%) were up-regulated in miR-23 sponge clones, in keeping with what would be expected in cells with an increased protein output. Only one of these ribosomal proteins was determined to be specific to the mitochondria (Mitochondrial Ribosomal protein S7 – MRPS7) and was decreased in its expression.

With a far greater degree of statistical significance, GO on the 499 DE proteins also indicated biological processes related to cellular respiration including aerobic respiration and the Tricarboxylic acid cycle (**Table 3.10**).

Table 3.10: GO for 499 DE proteins

GO ID	GO Term	P-value	BH adj.
0006414	Translation elongation	1.8×10^{-34}	3.7×10^{-31}
0006412	Translation	2.9×10^{-26}	3.0×10^{-23}
0006396	RNA processing	2.4×10^{-12}	1.6×10^{-9}
0006397	mRNA processing	1.4×10^{-10}	5.7×10^{-8}
0016071	mRNA metabolic process	1.4×10^{-9}	4.9×10^{-7}
0006457	Protein folding	5.6×10^{-9}	1.7×10^{-6}
0009060	Aerobic respiration	3.9×10^{-7}	7.3×10^{-5}
0046356	Acetyl-CoA catabolic process	2.3×10^{-6}	3.7×10^{-4}
0006099	Tricarboxylic acid cycle	2.3×10^{-6}	3.6×10^{-4}
0042254	Ribosome biogenesis	8.9×10^{-6}	1.1×10^{-3}
0006084	Acetyl-CoA metabolic process	2.0×10^{-5}	2.1×10^{-3}

Table 3.10: GO categories for DE expressed proteins in mitochondrial enriched miR-23 samples versus miR-NC clones using DAVID.

Finally, of the 47 DE proteins that were found to be associated with the mitochondrion when assessed for cell compartment affiliation, gene ontology enrichment was carried out as a means to determine which elements of mitochondrial function were predominately under regulation (**Table 3.11**). The highest scoring biological processes found to be enriched were aerobic respiration, cellular respiration, Tricarboxylic acid cycle and acetyl-CoA catabolic processes indicating that, of the mitochondrial related proteins that were DE, a significant proportion of them were influencing pathways responsible for cellular energy, as indicated by the observation of enhanced oxygen consumption (OXPHOS) by miR-23 depleted clones (**Section 3.4.6**).

Table 3.11: GO analysis of DE proteins associated with the mitochondria

GO ID	GO Term	P-value	BH adj.
0009060	Aerobic respiration	1.2×10^{-13}	7.8×10^{-11}
0045333	Cellular respiration	1.6×10^{-11}	5.3×10^{-9}
0006099	Tricarboxylic acid cycle	7.0×10^{-11}	1.6×10^{-8}
0046356	Acetyl-CoA catabolic process	7.0×10^{-11}	1.6×10^{-8}
0009109	Coenzyme catabolic process	1.6×10^{-10}	2.7×10^{-8}
0006084	Acetyl-CoA catabolic process	5.0×10^{-10}	6.7×10^{-8}
0051186	Cofactor catabolic process	5.0×10^{-10}	6.7×10^{-8}
0015980	Energy derivation by oxidation of organic compounds	5.7×10^{-10}	6.4×10^{-8}
0006732	Coenzyme metabolic process	9.7×10^{-10}	9.4×10^{-8}
0055114	Oxidation reduction	5.2×10^{-9}	4.4×10^{-7}
0006091	Generation of precursor metabolites	3.7×10^{-8}	2.5×10^{-6}
0043648	Dicarboxylic acid metabolic process	3.8×10^{-8}	2.4×10^{-4}
0006105	Succinate metabolic process	3.5×10^{-4}	2.0×10^{-2}
0022904	Respiratory electron transport chain	1.1×10^{-3}	5.5×10^{-2}
0022900	Electron transport chain	5.6×10^{-3}	2.4×10^{-1}
0007005	Mitochondrion organisation	9.5×10^{-3}	9.5×10^{-1}

Table 3.11: Gene Ontology categories for differentially expressed proteins in mitochondrial enriched miR-23 samples versus miR-NC clones using DAVID.

However, upon further interrogation of the proteins involved in these biological processes associated with mitochondrial energy production, several participating candidates were found to be decreased in their levels of expression such as IDH3A (Isocitrate dehydrogenase [NAD] subunit alpha) and COX5A (Cytochrome c oxidase subunit 5A). Further analysis of the proteins related to these processes will be considered later within the discussion (**Section 4.8**).

3.5.3.3: Potential targets of miR-23

Similar to the exercise carried out in the case of the list of DE proteins from the whole cell lysate experiment, the predicted output of targets of miR-23 was overlapped with the 499 DE proteins in the mitochondrial proteomics profiling experiment. This generated a total list of 143 potential targets of miR-23 (64 up-regulated and 79 down-regulated, **Table 3.11**). To further refine this extensive list of potential targets, those that appeared in the short list of 99 DE proteins reduced this list to 32 (10 up-regulated and 22 down-regulated), highlighted in yellow in **Table 3.12**. Finally, as it would be expected that the diversion of miR-23 away from its endogenous targets should result in the translational

de-repression of potential targets, only the 10 upregulated proteins from this short list were considered high priority.

Table 3.12: Potential targets of miR-23 from isolated mitochondria

Gene ID	FC	Anova (p)	Algorithm Overlap
Genes Upregulated in miR-23 sponge clones			
LIMA1	1.7	1.41E-06	3
CALD1	1.9	2.30E-06	2
HMGB2	1.5	5.57E-06	3
AKAP12	6.9	9.29E-06	4
SCP2	1.6	1.06E-05	1
P4HA1	1.7	1.97E-05	2
CALU	2	2.13E-05	2
CAPRIN1	1.8	2.25E-05	1
ITGB1	1.6	2.66E-05	2
CTSB	1.7	2.70E-05	1
TXNRD1	1.8	2.92E-05	1
CLINT1	2	4.73E-05	1
HSP90B1	1.5	4.78E-05	3
ALCAM	3.1	7.11E-05	3
TWSG1	2.5	8.00E-05	3
CNN2	1.7	8.38E-05	3
NUFIP2	1.4	0.00034	4
PSAP	3.5	0.00041	1
MAP4	1.4	0.00044	3
ANXA2	1.4	0.00051	2
BCL9L	2.3	0.00074	2
CETN3	1.9	0.00076	2
HDDC2	1.7	0.00112	3
TPI	1.2	0.00127	2
WBP2	1.3	0.00172	4
PRKCSH	1.4	0.00181	3
AIM2	2	0.00191	2
SNX1	1.5	0.00217	2
MAGOH	1.4	0.00231	2
LAMC1	1.5	0.00381	1
LAMP1	2.9	0.0042	4
SET	1.6	0.00451	2
IDI1	2	0.00466	1
PDIA6	1.8	0.00534	3
CACYBP	1.3	0.00543	3
TMED9	1.4	0.00601	1
HEXIM1	1.3	0.00685	4
CRK	1.9	0.00926	2
PLEKHO2	1.4	0.00936	3
RAB14	1.4	0.00956	3

PPIB	1.4	0.0098	1
RPL10	1.7	0.01005	4
BCLAF1	2.2	0.01103	4
CTSL	1.3	0.0118	1
SNAP29	1.4	0.01615	2
FXR1	1.4	0.01785	1
LMAN2	1.1	0.01836	3
RRAS2	1.5	0.01912	4
PEX19	1.3	0.01968	2
RPL27A	1.7	0.02155	3
TPI	1.2	0.02234	2
FKBP10	1.4	0.02374	1
SEPT7	1.2	0.02385	3
RCN2	1.6	0.02611	1
HYPK	2.2	0.0274	2
DSC1	1.2	0.02788	2
PRPF40A	1.5	0.03643	3
FUBP1	1.5	0.03698	2
RPL31	1.5	0.03785	1
TMOD3	1.2	0.0386	4
RPS23	1.5	0.04037	2
ENO2	1.2	0.04215	4
GIGYF2	1.1	0.04946	2
PRDX2	1.3	0.04984	1
Genes Down-regulated in miR-23 sponge clones			
IQGAP1	1.6	3.40E-05	1
SKIV2L2	2.1	5.12E-05	3
TOP2A	1.7	5.99E-05	2
VCP	1.9	6.71E-05	3
VCL	1.5	7.35E-05	1
MYH10	1.5	8.17E-05	2
PLAA	1.8	0.00011	2
GRSF1	1.4	0.00012	3
H2AFV	3	0.00013	2
FASN	2.8	0.00014	2
SLC7A1	2	0.00026	3
RRP15	1.6	0.00027	4
HDAC2	1.7	0.00028	3
MCM2	1.8	0.00032	2
OXCT1	1.5	0.00041	3
SND1	1.9	0.00041	2
WDR43	1.8	0.00042	2
NPM1	1.3	0.00048	1
HSPH1	2.3	0.00053	2
RRM1	1.3	0.00056	1
ABCF1	2.4	0.00057	2
CLTC	1.7	0.00062	2
LRPPRC	1.6	0.00069	3

FLNB	1.5	0.00073	2
SLC25A3	1.8	0.00083	1
LYAR	1.3	0.00088	1
CAND1	1.9	0.0009	1
TES	1.4	0.00104	2
EIF4G1	1.4	0.00108	1
TMPO	1.3	0.0011	3
HMGCS1	1.4	0.00121	2
MAP1B	1.5	0.00165	1
PPP2R1A	1.3	0.00195	2
MATR3	1.6	0.00196	1
SMARCC1	1.3	0.00199	3
MRPS7	1.4	0.00229	1
SUCLA2	1.4	0.0023	1
HAT1	1.5	0.00233	1
TOP1	1.5	0.00269	4
RPN1	2.3	0.00309	1
GATAD2B	1.4	0.00327	1
SF3B3	2	0.00328	1
SFPQ	1.3	0.00379	2
RBM14	1.4	0.00379	1
DDB1	1.5	0.00511	2
MKI67	1.5	0.00516	2
WNK1	1.3	0.00519	4
SPTBN1	2	0.00575	2
HNRNPU	1.8	0.0058	3
DDX21	1.8	0.00583	2
HNRNPC	3.1	0.00664	1
MTAP	1.5	0.00757	3
CPSF6	1.4	0.00803	3
ILF3	1.4	0.00914	1
HNRNPA1	1.5	0.01038	1
KIF5B	1.3	0.01132	1
SMC1A	1.5	0.01164	4
DDX5	1.4	0.0128	2
ZC3HAV1	1.5	0.01293	2
CTNND1	1.4	0.01374	2
HIST1H2AG	2.1	0.0142	1
LBR	1.6	0.01466	2
SPTBN1	1.8	0.01533	3
ACTR2	1.2	0.01651	3
TBL2	1.5	0.01816	4
HNRNPA2B1	1.2	0.0182	3
HIST1H2AG	1.4	0.01858	1
OPA1	1.3	0.01882	2
KHSRP	1.6	0.02496	3
SAFB	1.3	0.02618	3
CSE1L	1.5	0.02706	4

RRP12	1.5	0.0278	1
EZR	1.5	0.02814	2
VAPA	1.2	0.02995	4
IRF2BP2	1.2	0.03608	2
NCAM1	9.4	0.03793	3
CKAP4	1.2	0.0392	3
IQCE	1.3	0.04587	3
MAPRE1	16.6	0.0487	4

Table 3.12: Potential targets of miR-23 are shown by overlapping the hits generated by the miRWalk algorithm with the list of DE proteins from isolated mitochondria. The list is broken up into two, low priority targets found to be down-regulated in miR-23 clones and high priority targets found to be up-regulated in miR-23 clones. Cells highlighted in yellow passed more stringent criteria of over 1.5-fold change in expression with the addition of 2 or more peptide identifications.

Of the two short-lists generated from both label-free MS experiments (DE proteins that overlapped with prediction algorithms demonstrating an increased expression) and taking into account the two common targets CALD1 and P4HA1, a list of 18 targets were identified to be high priority targets of miR-23 that would be subject to further validation. These targets are LIMA1, HMGB2, SCP2, CALU, ITGB1, CTSB, SNX1 and PDIA6 in the mitochondrial extracted list and LETM1, CaMKII δ , FERMT2, IDH1, TXNDR1 and PPP1CB in the whole cell lysate.

Chapter 4

Discussion

4.1 CHO cell engineering using miR-23

miR-23 depletion presented itself as the most viable candidate for stable miRNA intervention when assessed in CHO-K1-SEAP cells. Although not directly derived from the initial miRNA profile carried out on CHO cells with varying growth rates, previous manipulation of the miR-23~27~24 cluster using miRNA sponge technology proved to be an attractive engineering route enhancing both CHO-SEAP cell growth and product yield.

Stable depletion of a single component of this cluster, miR-23, in the same CHO-SEAP cell line was observed not to play a role in growth but did elicit an improved product yield of ~ 3-fold. These high producing CHO clones were identified to possess an enhanced mitochondrial function with an increase in oxidative metabolism of ~ 30% centred on complex I and II of the mitochondrial electron transport chain. Protein processing and biogenesis has been identified as an energetically demanding process highlighting the potential contribution of enhanced mitochondrial activity to accommodate this cellular burden. Calcium signalling not only is suggested to be an ATP sensor within the endoplasmic reticulum (Kaufman, Malhotra 2014) thus monitoring energy requirements but is also implicated in TCA cycle function through the activation of vital enzymes of the TCA cycle thus driving energy provisions (Osellame, Blacker & Duchen 2012). It was discovered that the increase in SEAP yield was potentially attributed partially to an increase in SEAP transcription. This poses the question of whether there lies a reciprocal relationship between transcriptional activity/protein processing with enhanced OXPHOS or vice versa.

Label-free mass spectrometry identified various protein targets whose expression was increased suggesting potential targets of miR-23 itself that are associated with mitochondrial function and cellular metabolism, *IDH1/MDH1* and *LETM1*, in addition to proteins implicated in transcriptional control, *CaMKII δ* and *14-3-3- η* (**Fig. 4.1**). This schematic forms the basis of our hypothesis of the impact miR-23 is having in these CHO-SEAP clones ultimately boosting productivity of the bioprocess.

Figure 4.1: Schematic of miR-23s hypothetical role in rCHO-SEAP cells

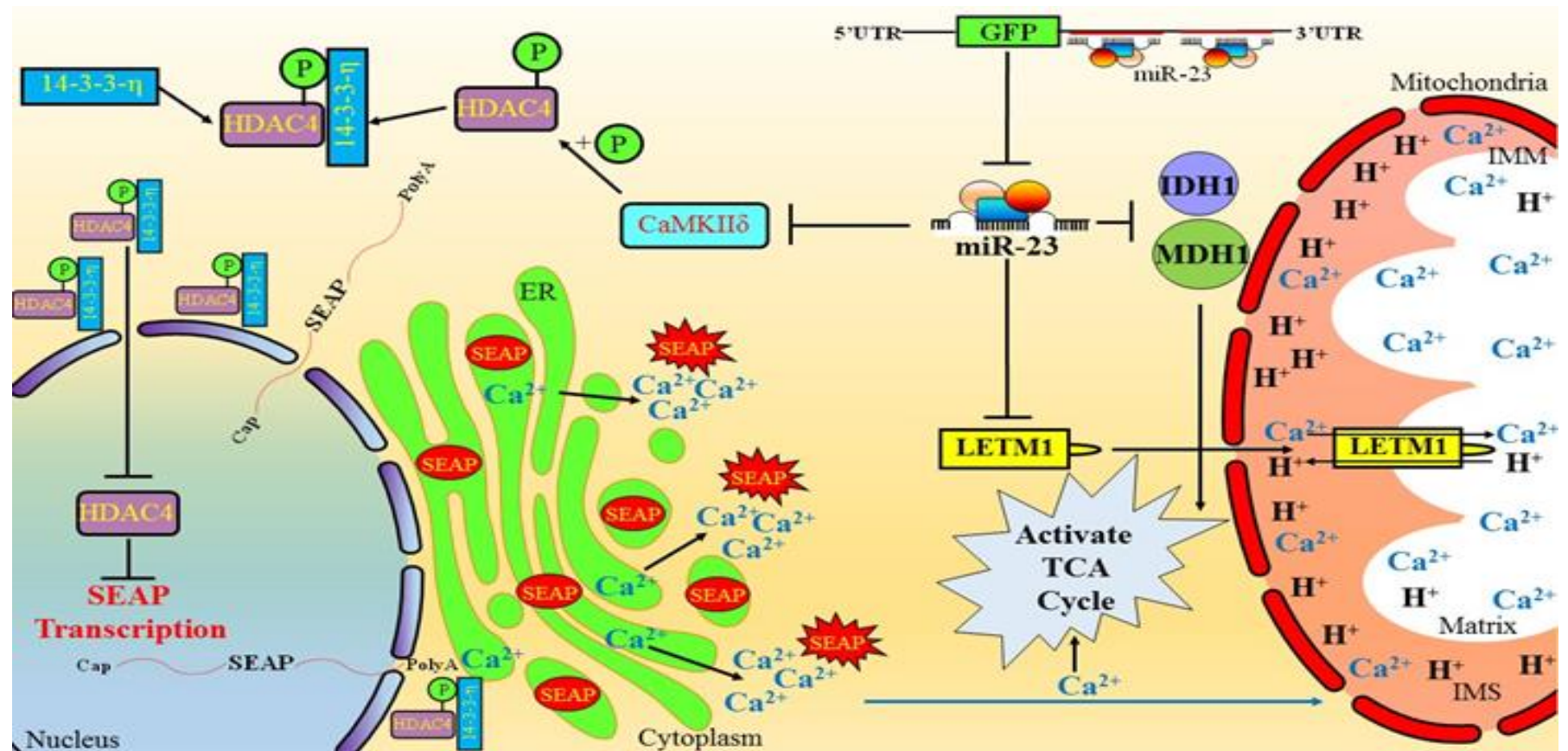


Figure 4.1: The depletion of miR-23 could impact directly or indirectly on mitochondrial function given the suggested panel of potential targets from the proteomics profiling. Isocitrate dehydrogenase (*IDH1*) and Malate dehydrogenase (*MDH1*) provide TCA cycle metabolites. *LETM1* is an inner mitochondrial membrane (IMM) protein acting as a Ca²⁺/H⁺ antiporter with calcium activating TCA cycle enzymes in the matrix while H⁺ provides energy to the proton gradient. Indirectly, increased expression of *CaMKIIδ* targets *HDAC4* for phosphorylation, tagging it for *14-3-3-η* thus preventing nuclear localisation. *HDAC4* inhibits transcription through deacetylation. Enhanced SEAP processing in the endoplasmic reticulum (ER) is an energy-demanding process, releasing Ca²⁺ as ATP is used which stimulates mitochondrial oxidative metabolism.

4.1.1 Selection of miR-23 for stable depletion

The pioneering study by Gammell *et al.*, identified a panel of miRNAs to be DE upon hypothermic growth conditions such as let-7f and miR-21 (Gammell et al. 2007). Two cluster components, miR-27a and miR-24, were found to be up-regulated upon temperature shift-induced growth arrest and late culture growth arrest. Despite being transcribed from a single transcriptional unit, the levels of miR-23a remained unchanged, an outcome influenced by RNA-binding proteins and processing pathway (Chhabra et al. 2009). Interestingly, these miRNAs demonstrated no change in expression when evaluated in CHO cells with varying growth rates (Clarke et al. 2012). Previous characterisation within our research group by Dr. Noelia Sanchez demonstrated that transient overexpression of miR-23a in CHO-K1-SEAP cells elicited a growth arrest of 61% whereas its inhibition did not reverse the phenotype. Transient overexpression of miR-24 induced a 27% arrest in cell numbers while transient inhibition reversed this phenotype to improve cellular growth by the same magnitude. miR-27a overexpression in two individual cell lines (CHO-1.14 and CHO2B6) resulted in a growth reduction and improvement, respectively, demonstrating a cell specific influence. It was for this reason that targeting of the entire miR-23a~27a~24-2 cluster using miRNA-sponge technology was explored resulting in a 1.7-fold increase in cell numbers and a 2-fold increase in specific productivity.

This was a beneficial observation in that specific productivity is often observed to be compromised during enhanced growth (Sunley, Tharmalingam & Butler 2008a). The co-existence of a fast growing CHO cell and the retention of increased specific productivity in the case of miR-23a~27a~24-2 depletion offers encouragement in terms of a viable and robust engineering strategy. CHO cell engineering using decoy technology against miR-7 (Sanchez et al. 2013b) or stable miR-17 overexpression (Jadhav et al. 2014) have both enhanced CHO cell growth without the compromise of specific productivity achieving 2-3 fold improvements in product yield.

miR-23 has also been associated with the reprogramming of cellular bioenergetics (Gao et al. 2012). The “Warburg effect” describes the propensity of cancer cells to avidly take up glucose and almost exclusively convert it to lactate in a process known as aerobic glycolysis (Vander Heiden, Cantley & Thompson 2009). Although energetically inefficient, it provides critical fuel for biomass production (Catapleurosis) and it highlights the role that energy metabolism plays in tumorigenesis (**Fig. 4.2**).

It has however been demonstrated that weakening of the TCA cycle by Acetyl-CoA starvation mediated through the Warburg effect (Dell'Antone 2012) can be overcome by anapleurotic reactions that resupply mitochondrial intermediates of the TCA cycle such as α -ketoglutarate through miR-23s role in glutaminolysis (Gao et al. 2012).

Figure 4.2: Schematic of Aerobic and Anaerobic glycolysis in various cellular conditions

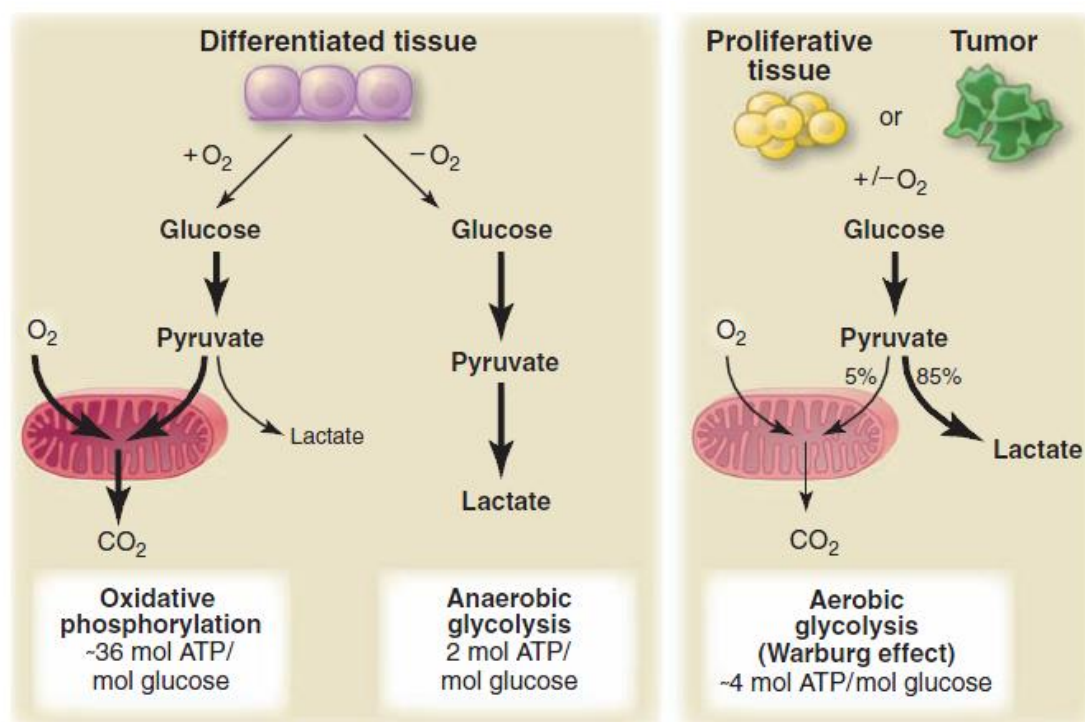


Figure 4.2: A schematic representation of “normal” channelling between Oxidative phosphorylation and anaerobic glycolysis under high and low oxygen concentrations, respectively. In addition, the utilisation of excess glucose sources via the Warburg effect in both normal and diseased tissues. This figure was sourced from (Vander Heiden, Cantley & Thompson 2009).

The primary carbon sources, Glucose and Glutamine, have been extensively considered in the area CHO cell research. Monoclonal antibody production has been positively correlated with the metabolism of glucose and lactate (Chen et al. 2012). Metabolic by-product accumulation such as lactate and ammonia from glucose and glutamine metabolism, respectively, has been extensively considered for their impact on cell growth and productivity, not to mention product quality (Yang, Butler 2000). Studies centred on glutamate supplementation have contributed to enhanced productivity and galactosylation of recombinant IgG (Hong, Cho & Yoon 2010) and optimisation of fed-

batch cultures through galactose/glutamate replacement (Altamirano et al. 2000). Various CHO cell phenotypes have also been affiliated with particular metabolic states such as growth, glycolytic metabolism, productivity and oxidative metabolism (Templeton et al. 2013). Metabolic re-programming using miR-23 depletion could enhance productivity through enhanced mitochondrial function while maintaining growth through an unperturbed glycolytic process.

4.1.2 GFP as an effective reporter for clone selection and sponge efficiency

The utilisation of a reporter construct has enabled the selection of rCHO clones demonstrating high specific productivities (Lai, Yang & Ng 2013a). Additionally, they have proved useful in the implementation of miRNA-based technology, such as miR-sponges. We utilised a destabilised GFP (deGFP) reporter construct to monitor miRNA sponge efficacy (Kitsera, Khobta & Epe 2007). When expressed at supraphysiological levels, miRNA sponges act as decoy transcripts (Mullokandov et al. 2012) but when expressed at physiological levels they can be used as miRNA “sensors” allowing for the evaluation of endogenous miRNA activity (Mansfield et al. 2004). Despite a wide range of GFP intensities, we observed an average reduction in GFP expression across the miR-23 sponge clonal panel when compared to the miR-NC controls. This reduced GFP expression was presumably a result of endogenously expressed miR-23a/b, which should not influence the non-specific sponge, as observed by Sanchez and colleagues for miR-7 (Sanchez et al. 2013b).

To further confirm the specificity of the miR-23 sponge construct, mixed pools were transfected with a miR-23b mimic as a means to repress translation of the GFP reporter. One interesting observation however was that transient transfection of the miR-23b mimic resulted in a mild repression of GFP (**Fig. 3.31 B**). One explanation is the reported low proficiency of miR-23 derived from its “weak seed”-pairing stability (SPS) due to its A+U-rich seed region (Garcia et al. 2011). Furthermore, miRNAs with A+U-rich seeds have a greater target abundance due to the A+U-rich composition of 3'UTRs (Grimson et al. 2007) ultimately titrating miRNA function (Franco-Zorrilla et al. 2007). With this in mind, we attempted to transfect a miRNA that was specifically designed to mimic the natural structure of the miR-23b duplex (pre-miR-23b*-mod) meaning that upon exogenous introduction into cells, would be processed based on thermodynamic stability of the duplex ends giving rise to both miR-23b and miR-23b*. When transfected, both

miR-23 sponge mixed populations and two clones (4 and 6), demonstrated a 90% reduction in GFP (**Fig. 3.31 B^{pre-miR-23b*-mod}** and **Appendix Fig. A14**). These observations suggested that the first miR-23b mimic was not being processed efficiently whereas the modified, pre-miR-23b* mod was, achieving GFP inhibition. miR-23 sponge specificity was also explored by assessing the endogenous levels of mature miR-23b in clones stably expressing the sponge construct compared to controls. A 5-fold reduction in mature miR-23b levels were observed in our clones when compared to clones expressing a non-specific sponge (**Fig. 3.67**).

The rapid degradation of mature miRNAs have been reported in cases of target availability such as miR-27a/b by murine cytomegalovirus (Marcinowski et al. 2012), miR-15a/16-1 by hepatitis B virus (HBV) (Liu et al. 2013), miR-122 by HBV (Li et al. 2013c) and the miR-let-7 family have been observed using a miRNA sponge (Yang et al. 2012). Although contradictory observations have been reported for miR-7 (Sanchez et al. 2013b), the mechanism behind the decrease of endogenous miR-23 in stable sponge clones remains uncertain.

4.1.3 Stable depletion of miR-23 improves CHO-SEAP productivity

Specific productivity was enhanced by 30-50% in the case of CHO mixed pools with an average 3-fold improved SEAP activity in a clonal panel. Of the four top SEAP producing clones selected, 3 demonstrated the highest level of GFP intensity compared to the majority of the miR-23 clones suggesting the highest levels of miR-23 depletion. One clone in particular however, miR-23 clone 2, possessed the third lowest GFP expression yet was the fourth highest producing clone. This would suggest that the intensity of the fluorescent signal is not necessarily proportional to the level of productivity. miR-23 sponge clone 9 for example displayed a high GFP signal compared to miR-23 sponge clone 7 (**Fig. 3.39**) yet its productivity value is one of the lowest. It is possible that by selecting clones with mid-high GFP intensities, a titrational influence of miR-23 depletion is lost and the productivity differences are due to clonal variation. The selection of clones exhibiting a low-medium GFP intensity might allow the assessment of a correlation of sponge expression with productivity improvements.

Protein folding and secretory bottlenecks have been shown to restrict mammalian cells from exploiting their physiologic production capacity (Tigges, Fussenegger 2006). As a means to investigate whether miR-23 depleted clones possessed an enhanced ability to

process and secrete the SEAP protein, we determined there to be a ~2-fold increase in the levels of the SEAP mRNA transcript when compared to control clones. This indicated that there were no processing bottlenecks in either control or test clones as the levels of SEAP transcript reflected SEAP enzymatic activity.

mRNA stability has been demonstrated to contribute to specific productivity as in the case of CHO cells expressing TNFR-Fc subject to hypothermic growth conditions (Kou et al. 2011). After translational inhibition through Actinomycin-D treatment, the rate of mRNA decay was determined by calculating the slope across the various time points when qPCR was carried out. Ideally, a similar decrease at each time when compared to time zero would provide information as to the rate of decay independent of varying Ct values due to differing transcript concentrations. It was observed that the endogenous control (β -actin) displayed an accelerated rate of decay when compared to the SEAP transcript, therefore $2^{-\Delta\Delta C_t}$ calculation would not have been suitable. miR-23 sponge clones demonstrated no change in decay suggesting there to be no increase in SEAP mRNA stability when compared to controls.

It has been strongly suggested that lessons from nature could aid in the identification of attractive engineering targets for the use in CHO cell manipulation, in particular the antibody producing B-cell (Dinnis, James 2005). Resting B-cells, once stimulated, differentiate into nature's own antibody factories, plasma cells, and have presented engineering targets such as *XBP-1* (Tigges, Fussenegger 2006), *BiP* and *PDI* (Pybus et al. 2013) and *ATF4* (Ohya et al. 2008b). In the case of miR-23, its down-regulation has been associated with the progression of chronic lymphocytic leukemia (Chhabra, Dubey & Saini 2010b). A recent study by Li and colleagues demonstrated that malignant transformation of B-cells closely resemble the activation of resting B-cells (Li et al. 2011a). Among the panel of miRNAs found to be similarly deregulated across both phenotypes, miR-23a/b, miR-24 and miR-27b were shown to be down-regulated in activated B-cells. Additionally, hematopoietic progenitors expressing the miR-23a cluster and cultured in the presence of B-cell promoting conditions were observed to undergo a dramatic reduction in B-lymphopoiesis (Kong et al. 2010). The expression of miR-23a has also been observed to be negatively associated with the up-regulation of *Blimp-1* (B lymphocyte-induced maturation protein 1) (Parlato et al. 2013). These studies demonstrate that the miR-23a cluster plays a central role not only in regulating the molecular frame work of B-cells but also further in their activation. B-cells are of an equal

size to that of CHO cells (10-15 μm) with a specific production capability of 100 pg/cell/day (Dinnis, James 2005), the suggested maximum production capacity of CHO (De Jesus, Wurm 2011). As B-cells are considered antibody factories, the implication of miR-23 and its cluster components in the activation of B-cells could suggest a similar influence in CHO-SEAP cells, specifically stimulating productivity in the case of miR-23.

4.1.4 miR-23 depletion improves CHO cell growth in a cell type and product-dependent manner

Although miR-23 depletion was not observed to impact on the growth of rCHO-SEAP cells, it did appear to elicit a positive impact on a second cell line, rCHO-1.14 upon its stable depletion, both derived from the same CHO-K1 parent. In both stable mixed populations and clonal populations cultured in a 1 mL format, there was an increase in cell growth to the detriment of IgG productivity. Various expression patterns of the members of miR-23 have been recorded across many cancer states with over-expression dominating (**Table 4.1**). Inhibition in this instance enhanced growth within the CHO-1.14 cell line. It is possible that this cell line exhibits a completely different set of gene targets as its inherent growth is markedly reduced when compared to CHO-SEAP cells. The oncogenic transcription factor, *c-myc*, despite being demonstrated to inhibit the expression of miR-23a/b to ultimately alleviate their inhibitory role on glutaminase (Gao et al. 2009), has also been shown to up-regulate the miR-23a cluster in mammary carcinoma (Li et al. 2013).

Furthermore, a significant improvement in apoptosis resistance was mediated by the depletion of miR-23 in CHO-1.14s in batch culture. miR-23a has been demonstrated to directly inhibit the caspase-inhibitor, X-linked inhibitor of apoptosis (*XIAP*) (Siegel et al. 2011). *XIAP* over-expression has been previously explored in CHO cells exposed to sodium butyrate treatment as a means to prolong cell survival while exploiting the induced high specific productivity phase (Kim, Kim & Lee 2009) offering no viability benefit. A prior study demonstrated that stable *XIAP* over-expression could inhibit CHO cell apoptosis upon Sindbis virus infection (Sauerwald, Betenbaugh & Oyler 2002b). This suggests that the benefit of *XIAP* can be both cell line specific and potentially influenced by the route of apoptosis activation. As a result, this could be why miR-23 depletion offers a protective phenotype in rCHO-1.14 cells but not in rCHO-SEAP cells under batch

conditions. Ongoing work by a colleague within our research group has demonstrated that miR-23 retains its functionality in targeting *XIAP* in CHO cells thus validating its capacity to regulate the gene but again in a cell type and context-dependent manner.

It was observed that the improved growth phenotype came hand-in-hand with a reduction in specific IgG productivity. However, upon clonal characterisation, there was a mixture in the observed phenotype. Although all clones stably depleted of miR-23 retained a fast growing phenotype with increased maximal cell density, volumetric productivity was enhanced in the case of 2 out of the three clones. This could have been due to the bias introduced during clonal selection, when clones were selected based on their high volumetric productivity in addition to growth. Furthermore, a single control clone demonstrated an enhanced viable phenotype exposing the natural variation in clones. It is possible that the influence on rCHO-SEAP cells in regards to growth is a factor of the expressed mRNA targets when compared to the rCHO-1.14. Inducing a faster growth phenotype may not be possible due to the limited availability of miR-23s targets in an already fast growing cell type.

Table 4.1: Table of expression of miR-23 cluster components in various disease states

Diseased condition	23a	27a	24	23b	27b
Acute lymphoblastic leukemia (ALL)	u	u	u	u	u
Acute myeloid leukemia (AML)	u	u	u	u	u
Acute promyelocytic leukemia (APL)	d	d	d		
Autism spectrum disorder (ASD)	d	d			
Bladder cancer	u			u	
Breast cancer		u			
Cardiac hypertrophy	u	u	u	u	u
Colorectal cancer	d	d	u		d
Gastric cancer (stomach)	u	u	u		
Glioblastoma	u		u	u	
Heart failure	u		u	u	
Hepatocellular carcinoma (HCC)	u	u	u		
Kidney cancer		u			
Lung cancer			u		d
Lupus nephritis					
Malignant melanoma		d		d	
Oral squamous cell carcinoma (OSCC)	d	d			d
Pancreatic cancer	u		u	u	
Papillary thyroid carcinoma (PTC)			u		
Prostate cancer	u/d	u/d	u	u/d	u/d
Schizophrenia			d		
Serous ovarian cancer	u	u		u	
Ulcerative colitis (UC)	u		u	u	
Uterine leiomyoma (ULM)		u		u	
Vesicular stomatitis				NA	

Table 4.1: Deregulated expression of the miR-23 cluster paralogs in various disease states as demonstrated above. “u” denotes up regulation whereas “d” denotes down-regulation. The table was sourced from the review (Chhabra, Dubey & Saini 2010b).

4.1.5 Clonal variation and culture conditions impact on the CHO cell phenotype

The process of recombinant cell line generation has its inherent pitfalls depending on the context. For example, non-site specific integration of the experimental transgene, in our case the miR-23/NC sponge constructs, can result in various genetic phenotypes such as copy number variation, intensity of expression due to insert location and potential

insertional mutagenesis. Random integration and amplification may also interfere with or de-regulate endogenous genes (Winnard, Glackin & Raman 2006) ultimately creating the potential for variation in other cellular traits (Kim, Lee 2007). This in particular was observed when cellular proliferation was characterised upon the isolation of a panel of clones derived by FACS from the original CHO-SEAP mixed pool. Across both miR-23 and miR-NC sponge clones, a range of growth profiles were identified despite the observation of no gross differences in growth of the recombinant mixed pool populations. This heterogeneity within clones, as a function of the transgenesis process, is routinely exploited in the selection of clones showing an advantage for a particular phenotype (Pichler et al. 2011).

The parental rCHO-SEAP cell used as the basis for stable miR-sponge generation was a clonal line and presumed to demonstrate a similar level of SEAP production and genetic homogeneity. An additional layer of complexity has been demonstrated in that not only are there variations in the performance from clone to clone but that protein expression can be heterogeneous within clones themselves. One study demonstrated a 50-70% deviation in antibody expression within clones upon 2-11 generations (Pilbrough, Munro & Gray 2009). This could have potentially contributed to a production variance, originating within the parental CHO-K1-SEAP, across all clones generated irrespective of the process of recombinant cell line generation.

One very interesting observation was that when miR-23 sponge clones were selected and cultured in a 1 mL suspension format, the maximum achievable cell density on day 4 was less than half of that of miR-NC sponge clones, again in contrast to the similar growth profiles observed in the case of mixed pools. The similarity in cell numbers between both clonal panels on day 2 of growth suggested that miR-23 depletion itself was not exerting a direct impact on the CHO cell growth. Interestingly, of the 4 clones selected from this panel demonstrating a range of maximal cell densities ($\sim 1 \times 10^6$ to $\sim 4 \times 10^6$ cells/mL in 1 mL), each clone exhibited a similar maximal cell density of $\sim 5 \times 10^6$ cells/mL upon culture in a 5mL volume in a vented spin tube. Cell line behaviour has been previously shown to be sensitive to vessel type and process conditions such as pH, temperature and dissolved oxygen tension (Trummer et al. 2006, Liu et al. 2011). A comprehensive study by Porter and colleagues (Porter et al. 2010) followed the progression of 175 antibody-secreting clones isolated from the same transfected population throughout various phases of cell line characterisation using a “typical strategy” of cell line development (**Fig. 4.3**).

It was evident that clonal performance was dependent on the culture environment which ultimately presents a difficult task when empirically selecting clones for phase development.

Early stage platforms tend not to have strict regulation on particular environmental conditions such as pH and dissolved oxygen tension (DOT). In the case of our miR-23/NC sponge screen, the microenvironment of the parafilm-sealed 24-well suspension plate potentially possessed a less consistent oxygen environment as opposed to the vented spin flasks, potentially contributing to the miR-23 sponge specific growth inhibition. Kulshreshtha and colleagues demonstrated a panel of miRNAs responsive to hypoxic growth conditions with miR-23/-27 and -24 being upregulated (Kulshreshtha et al. 2007). An independent study demonstrated a reduced expression of miR-23a/b and miR-27a/b in hypoxia induced apoptosis with an anti-correlation with *Apaf-1* (Chen et al. 2014). Overexpression of these two miRNAs was further demonstrated to protect against apoptosis. Both of these studies suggest a protective role of miR-23 in response to hypoxia. It is possible that depletion of miR-23 in CHO-SEAP clones is preventing these CHO clones from responding to the potential hypoxic conditions of this culture format compared to control clones resulting in the reduced cell viability observed.

Interestingly, despite the reduced maximal cell densities, a similar average 3-fold increase in volumetric SEAP productivity was exhibited when compared to individual clones selected for 5 mL culture. This retention in volumetric SEAP activity appeared to be as a result of enhanced specific productivity in the case of clones cultured at 1 mL volume potentially attributed to a prolonged residence in the highly transcriptionally active phase of the cell cycle, G₁ (Kumar, Gammell & Clynes 2007).

Figure 4.3: CHO clone behaviour across multiple phase development platforms

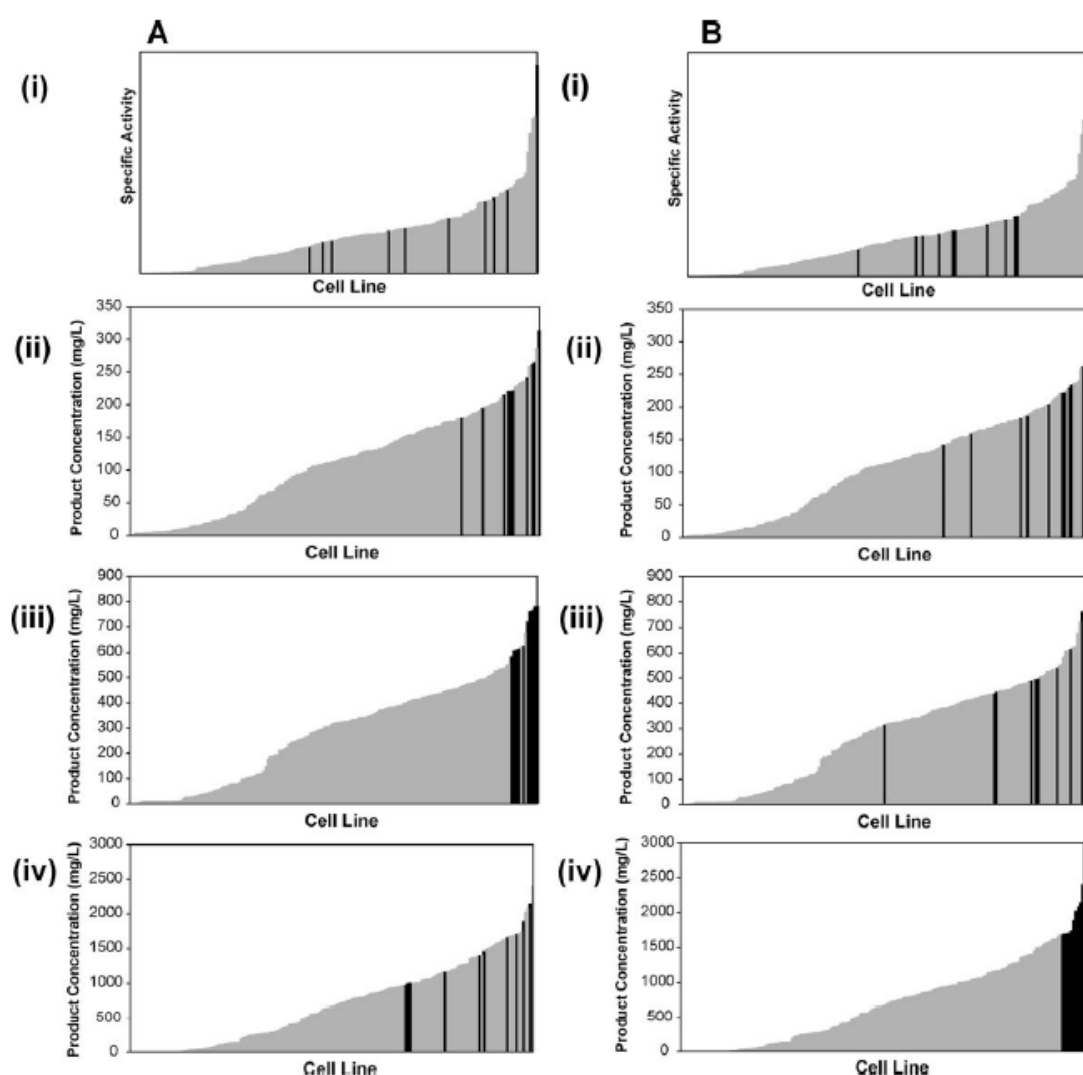


Figure 4.3: Heterogeneity within clonal populations along with the variations in performance across multiple culture conditions ultimately contributing to the complexity in clonal selection during phase development. A) Represents the “selected top 10” based on their volumetric productivity in batch suspension culture and B) represents the “real top 10” based on their volumetric productivity in fed-batch suspension culture. From these two categories, clonal ranking was highlighted within all phase platforms including (i) spot test, (ii) 24-well plate, (iii) batch culture and (iv) Fed-batch culture. This figure was sourced from (Porter et al. 2010).

In the same study by Porter and colleagues (Porter et al. 2010), the addition of a feed resulted in the largest variation (25%) in ranking position across all clones. This was observed in the case of all miR-23 sponge and miR-NC sponge clones cultured with a feed supplement causing larger variations in growth and maximum cell density (**Fig. 3.58 A**). Volumetric SEAP production was still retained at 3-fold increase when compared to non-specific controls (**Fig. 3.58 A**). However, when volumetric SEAP activity was

compared to that of miR-23 sponge clones cultured under a 6 day batch, it was not improved, in fact mildly reduced, (**Fig. 3.56 C** and **3.58 C**) despite the significant increase in maximal cell density. One report observed that in the case of CHO cells producing tissue plasminogen activator (t-PA), the reduced volumetric yield associated with a 2.5-fold increase in IVCC was mediated by a possible secretory bottleneck when intracellular t-PA mRNA levels were identified to be increased (Dowd, Kwok & Piret 2000). Another possibility is that the enhanced cellular growth has resulted in a trade off in CHO cell specific productivity conferring no significant production advantage despite the extension of 2 days in the culture life time. Both miR-23 sponge clones subject to a nutrient feed also retained a viability above 80% for an additional 48 h compared to control clones. The introduction of nutrient feeds have greatly improved pharmaceutical recombinant protein manufacturing by boosting maximal cell densities, improving cell productivities and enhancing viability (Butler, Meneses-Acosta 2012, Huang et al. 2010). This enhanced cell viability was evident in both miR-23 and miR-NC sponge clones upon fed-batch cultivation when compared to batch, however, stable miR-23 depletion did appear to confer a further extended viability (**Fig. 3.58 B**).

Low culture temperature results in growth arrest, meaning that cell density is significantly reduced at 31°C, nutrients are consumed at a slower rate and the culture can be run for a longer period of time prior to the onset of cell death, in a cell-type specific manner. We thought it prudent to exploit the potential enhanced viability phenotype of a fed-batch with that of a temperature shift as a means to boost volumetric SEAP production. When specific productivity was compared between miR-23 sponge clones 4 and 6 cultured under fed-batch conditions with or without temperature shift to 33°C (**Fig. 3.60**), there was an average ~2-fold increase in cell specific SEAP productivity in the case of hypothermic culture conditions. Furthermore, volumetric productivity was enhanced by ~30% in the case of clones subject to temperature shift with feed addition (**Fig. 3.58 C** and **3.59 C**). A similar observation was made by Fox and colleagues in the case of Interferon- γ production (Fox et al. 2004). The highest volumetric SEAP production observed in the case of fed-batch with temperature shift may be due to the extended production phase. Another possibility that has been reported is that reduced culture temperatures can have the added advantage of stabilizing the product and reducing intramolecular aggregation (Tharmalingam, Sunley & Butler 2008, Oguchi et al. 2006). The highest level of SEAP activity was recorded under hypothermic growth conditions. Although, the presence of the miR-23 sponge in fed-batch appeared to delay the onset of

apoptosis, the extended production phase under hypothermic growth conditions appeared to be maintained below the industry standard of 80%, with the anti-apoptosis benefits appearing from day 11 onwards (**Fig. 3.59 B**).

It is possible that clones under batch conditions will exhibit a unique transcriptome to a clone grown in fed-batch culture. This could ultimately provide a completely new set of targets for miR-23 impeding its role in regulating particular phenotypes. It was found that cell death in fed-batch was primarily induced via death receptor- and mitochondria-mediated signalling pathways rather than endoplasmic reticulum-mediated signalling compared to batch (Wong et al. 2006) with *Fas* being demonstrated to be a target of miR-23a/b (Li et al. 2013a). Despite miR-7 over-expression yielding no negative impact on CHO cell viability (Barron et al. 2011b) and being associated with the de-regulation of pro/anti-apoptotic genes (Sanchez et al. 2013a), its stable inhibition mediated a prolonged viable phenotype under fed-batch conditions (Sanchez et al. 2013b) again suggesting the availability of a new cohort of targets. It is possible that fed-batch with temperature shift would best suit the stable depletion of miR-23 in our CHO-SEAP population with further optimisation such as adapting miR-23 sponge clones to hypothermic growth conditions (Sunley, Tharmalingam & Butler 2008b).

4.1.6 miR-23 depletion enhances CHO cell mitochondrial function at Complex I and II

Mitochondria are vital to normal cellular function as they are responsible for energy production in eukaryotes, including the synthesis of phospholipids and heme, calcium homeostasis and apoptosis activation. Deregulation in mitochondrial activity is often associated with numerous disease states such as diabetes mellitus. Furthermore, alterations in the metabolic pathways that ultimately feed oxidative phosphorylation (OXPHOS) at the electron transport system such as glycolysis and the tricarboxylic acid cycle (TCA) can lead to changes in cell fate. The Warburg effect, a process also observed in CHO cells (Martinez et al. 2013), has been observed to be reprogrammed through miR-23's interaction with glutaminase and sparked the exploration of mitochondrial activity (Gao et al. 2009). Each of the enzymes that constitute the glycolytic pathways have been found to be over-expressed and/or deregulated in several cancer cell lines and tumours *in vivo* (Pelicano et al. 2006a) ultimately contributing to enhanced cell growth. However, in this instance, miR-23 depletion resulted in enhanced SEAP

transcription without contributing to growth. A recent study demonstrated the metabolic flux in an antibody producing CHO cell line exposing variations in metabolism during growth (Glycolytic) and production (TCA) (Templeton et al. 2013). This has further been supported with observations that increased oxidative metabolism can be favoured in situations of nutrient depletion and/or reduced growth rate (Young 2013). These studies implicate certain metabolic states with particular CHO cell phenotypes, mainly productivity with oxidative metabolism encouraging the exploration of miR-23 depletion. Eliminating proliferation as a variable, it has been observed that the protein folding process consumes much energy, which is provided for by the mitochondria (Bravo et al. 2011, Simmen et al. 2010). With this in mind, enhanced mitochondrial function could further aid miR-23 depleted clones in efficiently processing and turning over the additional SEAP mRNA transcripts (**Fig. 4.1**).

When intact, non-permeabilised miR-23 clones were assessed for their mitochondrial function, one set of clonal pairs exhibited an increased Routine and Leak respiration due to the reduced calculated maximum ETS when applying the respiratory control ratios (RCRs) (**Fig. 3.71 B**). RCRs are defined as the O₂ flux in different respiratory control states normalised for the maximum flux of the ETS capacity. Despite an overall reduced maximum ETS in the case of miR-23 sponge clone 4 compared to miR-NC sponge clone 2, energy turnover is potentially more efficient. Muscle cell mitochondria have demonstrated increased RCRs indicating efficient energy production (Larsen et al. 2011). The proton gradient is the source of electrochemical energy and regulates electron movement across the transport system, electrochemical backpressure (**Fig. 4.4**).

Figure 4.4: Schematic diagram of the mitochondrial proton gradient

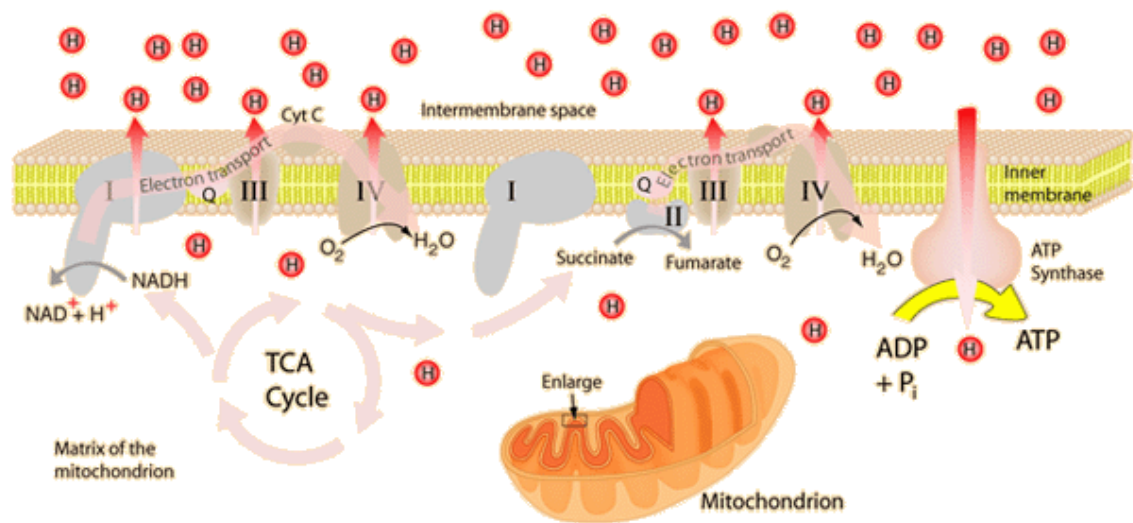


Figure 4.4: The propagation of electrons through the ETS is regulated by the electrochemical backpressure exerted by the proton gradient. Protons are translocated from the mitochondrial matrix to the inner mitochondrial membrane through the various complexes (I, III and IV) as electrons are donated from NADH/FADH₂. Inner membrane protons are then translocated back into the matrix through ATP Synthase generating ATP or lost to proton leak.

<http://hyperphysics.phy-astr.gsu.edu/hbase/biology/etrans.html>.

However, both protons and electrons can leak across the membrane without contributing to ATP production yet ultimately allowing electron transport from the reducing equivalents (NADH and FADH₂). Leak respiration is dependent on internal energy sources as ATP Synthase has been inhibited by the addition of oligomycin thus preventing the translocation of exogenous metabolites into the mitochondrial matrix. Leak respiration also accounts for a large proportion of resting metabolic rates (20-25%) (Rolfe et al. 1999). The observed increase in leak respiration indicated that internal substrates for mitochondrial turnover are more readily available. This is in contrast to the other clonal pair, miR-23 sponge clone 6 and miR-NC sponge clone 11, whose RCRs remained similar while miR-23 sponge clone 6 demonstrated an enhanced routine respiration and ETS capacity (**Fig. 3.72**). This would suggest that mitochondrial function may not be contributing directly to an increase in the transcriptional activity of the SEAP mRNA transcript. However, an increase in cellular ATP levels can activate transcription from promoters by RNA polymerase II (Conaway, Conaway 1988) indicating a role in transcriptional control. To put the change of 5% difference in Leak respiration into perspective, a study reported a difference of 5% in leak respiration in skeletal muscle

mitochondria in diet resistant and diet responsive patients (Harper et al. 2002), i.e. 5% would be considered significant as it does not vary hugely.

Systematic stimulation and inhibition of the various complex components of the electron transport system, when cells were permeabilised with Digitonin, revealed that there was a 30% increase in oxygen consumption attributed to Complex I and II (**Fig. 3.74 B**). This indicated that there was an increase in the availability of the reducing equivalents NADH and FADH₂ which provides electrons that drive the pumping of protons from the matrix to the inner membrane space contributing to energy production or a more effective and efficient assembly of these components on the inner mitochondrial membrane (**Fig. 4.5**).

Cell-to-cell variation in the rate of transcription has been correlated to higher mitochondrial mass or higher membrane potential, with the presence of anti-/pro-oxidants and increased ATP substantially improving transcription rates (das Neves et al. 2010), indicating the possibility of a contribution to enhanced SEAP transcription. However, this enhanced transcription was reported to be on a global level which we investigated by probing a set of genes (GLS, XIAP and TFAM). These showed no increase in miR-23 sponge clones. However, in hindsight, if global gene transcription was enhanced then so would the transcription of the endogenous control used for comparison in qPCR indicating that no difference would be detected.

A kinetic model of cellular energetics in CHO cells subjected to sodium butyrate exposure demonstrated a shift in energy metabolism towards increased efficiency of glucose utilisation through the TCA cycle (Ghorbaniaghdam, Henry & Jolicoeur 2013). As sodium butyrate treatment is routinely used to artificially induce higher specific productivity, the 30% increase in mitochondrial function observed in the miR-23 sponge clones supports this notion of oxidative metabolism being linked to specific productivity. NaBu treatment has also been observed to stimulate the release of Ca²⁺ from the ER (Sun et al. 2012a) with Ca²⁺ itself being previously demonstrated to activate enzymes of the TCA cycle thus enhancing OXPHOS (Osellame, Blacker & Duchon 2012). It still remains difficult to speculate as to how there appears to be a selective increase in SEAP transcription. This increase of 30% is significant as reports in the literature of variations in mitochondrial function are mild, usually in the range of 5-70% (Hirsch et al. 2012).

Figure 4.5: Schematic Diagram linking the TCA cycle to ATP production

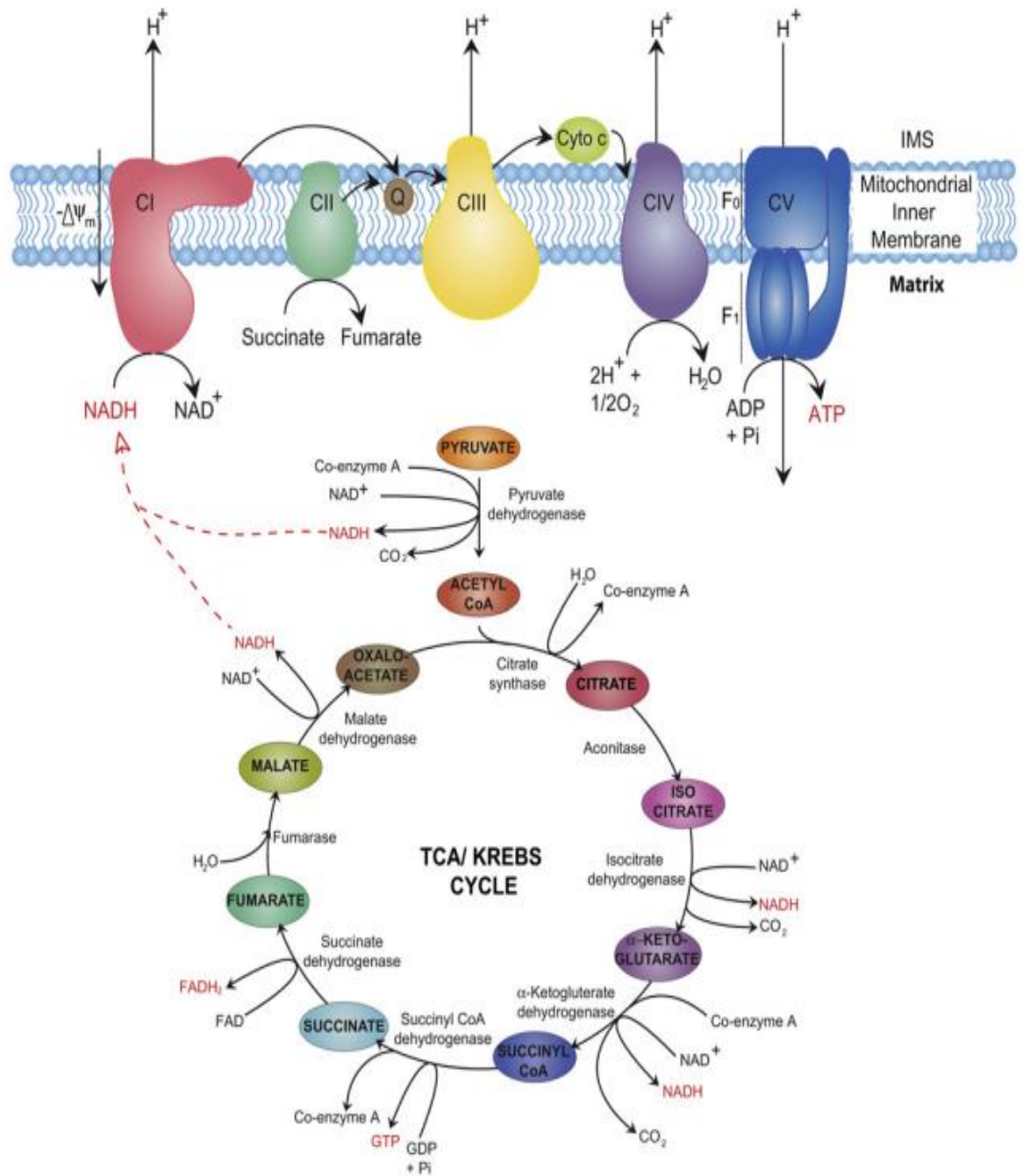


Figure 4.5: The schematic representation of the complex components of the electron transport system (ETS) in addition to its coupled behaviour with the TCA cycle and the reducing equivalents produced (Osellame, Blacker & Duchon 2012).

Despite the potential increase in mitochondrial function, there did not seem to be an apparent compromise in mitochondrial membrane integrity. Complex I and III of the electron transport system have been described as the primary location of electron loss or

leak (Jastroch et al. 2010). This could potentially contribute to the lack of synergy observed upon co-stimulation of both complexes I and II when ADP was not the limiting factor. Both CI and CII demonstrated a ~30% increase in oxygen consumption independently, yet maintained this increase upon co-stimulation. This could potentially be attributed to electron leak downstream of both complexes. Mitochondrial membrane integrity was demonstrated to be unaffected in miR-23 depleted clones both through the addition of cytochrome c during HRR-SUIT permeabilization and the evaluation of mitochondrial content/mass using the Mitotracker™ deep red assay. Mitotracker™ deep red probes are sensitive to membrane integrity and will diffuse out which we assessed not to be a contributing factor.

Upon inhibition of the activity of complex II and III by Malonic acid and Antimycin A, respectively, there was an observed drop in oxygen consumption on complex IV for miR-23 depleted clone upon its stimulation by the artificial electron donor TMPD. This again could potentially be another contributing factor to the lack of synergy between the stimulation of complex I and II with electrons potentially reaching a bottle neck at complex IV.

When we assessed the levels of glutamate, there was an observed increase of 65% across all clones (**Fig. 3.70**). Assessment of this metabolite was suggested by the identification of the role that miR-23a/b plays in targeting the enzyme glutaminase (Gao et al. 2009). The process of glutaminolysis is an anapleurotic reaction that provides that TCA cycle with vital intermediates such as α -ketoglutarate (**Fig. 4.5**). This is a potential mechanism in which cancer cells can overcome what's been termed "the Crabtree effect" in which excessive turnover of glucose via the "Warburg effect" can quench and ultimately starve the TCA cycle of Acetyl-CoA through exclusive conversion of pyruvate to lactate (Dell'Antone 2012). This increase in glutamate availability could explain the increase in respiration observed at complex I and II during permeabilised assays as well as the increase in routine and leak respiration with the potential of an alternative endogenous source of TCA cycle substrates.

Peak antibody production in CHO cells has been associated with a highly metabolic oxidative state while peak cell growth was characterised by a highly glycolytic state (Templeton et al. 2013). This would suggest that the observed SEAP productivity could be attributed to enhanced mitochondrial function also indicating why cellular proliferation was not influenced. However, it would be necessary to assess the glycolytic

status of miR-23 sponge clones to rule this a plausible explanation. Glutamate dehydrogenase (GDH) can also convert α -ketoglutarate into glutamate providing an alternative source of glutamate that is not derived from glutaminolysis (Friday et al. 2012). Interestingly, when proteomic analysis was carried out between miR-NC and miR-23 sponge clones, glutaminase was not identified to be DE suggesting that the formation of glutamate could be as a result of catapleurosis derived from downstream sources to TCA intermediates.

These results suggest that miR-23 depletion is potentially playing a role in enhancing CHO cell mitochondrial function. The link between oxidative metabolism and productivity is a strong indication that the improved mitochondrial function is influencing SEAP transcription. Without assessing ATP levels it would be premature to equate this increased oxygen consumption to energy synthesis. Furthermore, identifying and comparing the presence of lactate would indicate if CHO cells are favouring the glycolytic pathway which could be an explanation as to why miR-23 sponge cells demonstrate no growth advantage.

4.1.7 Summary of miR-23 depletion in CHO cells

miR-23 depletion appeared to influence the CHO cell phenotype in a product-dependent manner as both SEAP and IgG secreting cell lines were generated from the same CHO-K1 parent. miR-23 depletion in CHO-1.14 cells improved CHO cell growth and extended cell viability at the expense of IgG productivity. This phenotype was maintained as far as clonal isolation at which point particular control clones exhibited a comparable phenotype. Depletion of miR-23 in CHO-SEAP cells improved SEAP productivity to a maximum average of 3-fold without influencing growth. Under fed-batch culture conditions, miR-23 depletion was observed to prolong the onset of cell death. Improved specific SEAP productivity was shown to be, in part at least, at the transcriptional level with cell size and mRNA stability being ruled out as contributing factors. miR-23 sponge clones exhibited an enhanced mitochondrial function with permeabilised assays revealing a hyperactivity of 30% at Complex I and Complex II. The difference in mitochondrial mass/content between miR-23 and miR-NC clones was demonstrated to be negligible. However, the specificity of miR-23 depletion influencing SEAP transcription remained undetermined at this point despite the indication of oxidative metabolism being associated with specific productivity.

4.2 Biotinylated miRNA mimics as a novel method for mRNA target identification

A novel method of isolating and identifying potential miRNA targets was carried out by exploiting the use of biotin-labelled miRNAs. Previous studies have demonstrated the utility of selective enrichment of target mRNAs associated with a specific miRNA such as the immunoprecipitation of epitope-tagged *Ago2* in HEK293 cells transfected with miR-124a (Karginov et al. 2007). The inherent benefits of using biotin-tagged miRNA would be the identification of direct targets, excluding genes whose expression is indirectly influenced by changes in miRNA expression, a refinement not possible in microarray or proteomics of whole cell lysates. Furthermore, affinity pull-down would isolate mRNAs that exhibit a binding affinity for a selected miRNA. Upon assessing the utility of this technique using miR-23b*, we carried out pull-down followed by microarray target identification, using CHO-specific arrays, for both biotin-tagged miR-23b and miR-23b*. When both datasets were compared to that of the biotin-tagged non-specific control, no enrichment was detected (no hierarchical clustering of samples) when data were assessed for trends.

miR:miR* partners have been demonstrated to have complementary functionality be it through the same mRNA targets or similar signalling networks (Yang et al. 2013); or unique functionality through an independent set of mRNA targets (Shan et al. 2013). By comparing the targets pulled down with miR-23 and miR-23b*, we sought to shed light on the relationship and potential functional redundancy between both miRNAs. Furthermore, we designed a biotin-labelled miR-23b* (miR-23b*-2 modified) whose duplex gave rise to both miR-23b and miR-23b* during processing. The biotin-linker was located on the miR-23b* passenger strand and was intended to examine the fate of a “discarded” passenger strand when compared to a biotin-linked miR-23b* favoured for selection and RISC-loading. However, only 12 CHO-specific array cards were available and the inclusion of both cells only and biotin-labelled non-specific control was essential resulting in the utilisation of both miR-23b and miR-23b* biotin-labelled mimics.

As previously mentioned, miR-23 possesses an inherently weak seed-pairing due to its AT-rich seed region (Garcia et al. 2011). Despite the gentle lysis process, carried out to avoid disturbing any ribonucleoprotein complexes that would otherwise fall apart in harsher protocols, this weak pairing could have contributed to the poor pull-down of miR-23-specific mRNAs resulting in the isolation predominantly of non-specific mRNA transcripts. When qRT-PCR was carried out, it was observed that there was no enrichment

detected for miR-23b in either streptavidin-bead-incubated lysates as well as input samples prior to streptavidin incubation. It was possible that the biotin-tagged miR-23b mimic was not being processed efficiently. Keeping in mind the potential for poor transfection efficiency on the day, with a 14-fold enrichment of miR-23b*, it was possible that this could have further contributed to the absence of enrichment of miR-23b ultimately resulting in no capture of target mRNAs.

The over-expression of biotin-tagged miR-23b*-1 did not mediate the phenotype previously observed for the transient expression of miR-23b* during the primary miRNA screen reported in **section 3.1** of results (reduced cell growth and viability). This observation would suggest that the biotin-labelled miR-23b*-1 was not being sufficiently processed in the cell to yield the mature biotin-labelled, RISC-loaded, miR-23b* that would otherwise interact with endogenous miR-23b*-specific transcripts mediating their degradation or translational suppression. Despite this potential lack of cellular processing of the miR-23b*-1 miRNA, enrichment and quantification was observed both in the optimisation process and the main experimental run. It is possible that regardless of efficient processing, the RNA extraction process would separate the exogenously introduced miRNA duplex leaving the miR-23b* strand available for qRT-PCR amplification and detection. This would explain how a high fold-change of ~600 was identified for miR-23b* during optimisation. However, a ~14-fold change was detected for samples that were subsequently loaded on to microarrays. It is possible that the reduced enrichment of miR-23b* compared to the enrichment achieved during optimisation was due to a poor transfection efficiency on the day ultimately contributing to no mRNA target enrichment when microarrays were hybridised and analysed. Lal and colleagues reported a >40-fold enrichment of miR-34a in a similar experiment where 982 genes were found to be captured (ranging from 4-10-fold) and common to two cell lines including the identification of 14 new targets of miR-34a (Lal et al. 2011). One of the genes predicted to be a target of miR-23b* was phosphoglycerokinase (Pgk-1). It was the detection of this gene that gave us the most confident indication that we were achieving selective enrichment with miR-23b* (Dheda et al. 2004). On the other hand, its role as a housekeeping gene and therefore relatively high and consistent expression could have contributed to its identification during optimization, when it was potentially a contaminant or non-specifically bound.

At the time, the lack of characterisation of miR-23b* and the limited knowledge of bona fide targets impeded the validation and optimisation of this method of identifying targets of miR-23b and miR-23b*. Previous studies implementing this technology had the fundamental resource of validated targets in the cell lines under investigation such as the miRNA *bantam* and its gene target *Hid* in *Drosophila* (Orom, Lund 2007) and *CDK4/6* for miR-34a in HEK293 cells (Lal et al. 2011). In future, optimisation of this process would be essential with a target previously validated in CHO cells or validated prior to using this biotin capture approach. Furthermore, if numerous biotin-tagged miRNA were being explored, it would be essential to validate each miRNA independently for criteria such as efficient cellular processing, execution of an expected phenotype following its over-expression, qPCR enrichment for mature miRNA levels and finally mRNA target association and enrichment. Although this method was unsuccessful in our case, we propose several viable reasons as to the potential reasons behind its failure. Nonetheless, it still remains an attractive approach for the identification of miRNA specific mRNA interactions.

4.3 Analysis of the whole cell proteome reveals potential miR-23 regulated processes

As miRNA regulation ultimately culminates at the interference of mature protein levels due to post-transcriptional suppression/de-repression, label-free mass spectrometry was carried out as a means to identify finite changes in the translome of miR-23 depleted CHO-SEAP clones demonstrating enhanced specific productivity and mitochondrial function. 41 proteins were identified to be DE in miR-23 depleted clones when compared to control CHO clones. The influence of miR-23 diversion is of importance when attempting to identify potential candidates under miR-23s influence in addition to which of these candidates are contributing to the observed phenotype. For this reason, a small sub-list of DE proteins are discussed below that could potentially be involved in the observed elevated SEAP transcription in addition to enhanced mitochondrial activity.

4.3.1 LETM1

LETM1 (Leucine zipper-EF-hand-containing transmembrane protein) is a nuclear encoded mitochondrial inner membrane protein that is involved in respiratory chain biogenesis and calcium (Ca^{2+}) homeostasis in mitochondria. It has been implicated in the

onset of Wolf-Hirschhorn syndrome in which its deletion mediates an impaired mitochondrial ATP generation, reduced glucose oxidation, altered metabolism and increased seizures (Jiang et al. 2013a). We identified *LETM1* to be up-regulated by 2.73-fold in CHO-SEAP cells engineered with a sponge specific against miR-23.

Oxidative phosphorylation is regulated by cross-talk with cellular calcium signalling, so that the transfer of Ca^{2+} into the mitochondrial matrix signals an increased energy demand (Jacobson, Duchen 2004). The rise in matrix Ca^{2+} concentration $[\text{Ca}^{2+}]_m$ activates the rate limiting enzymes of the TCA cycle – pyruvate dehydrogenase, α -ketoglutarate dehydrogenase and NAD-isocitrate dehydrogenase as well as ATP synthase although the mechanism remains unclear (Osellame, Blacker & Duchen 2012). These processes ultimately drive the increase in the availability of NADH to the respiratory chain (a substrate for complex I), an increase in respiration and ATP synthesis. *LETM1* has been characterised as a $\text{Ca}^{2+}/\text{H}^+$ antiporter contributing to Ca^{2+} influx into the mitochondria along with other Ca^{2+} regulatory genes such as the mitochondrial calcium uniporter (*MCU*) (**Fig. 4.6**).

Figure 4.6: LETM1s function as a $\text{Ca}^{2+}/\text{H}^+$ antiporter in the mitochondria

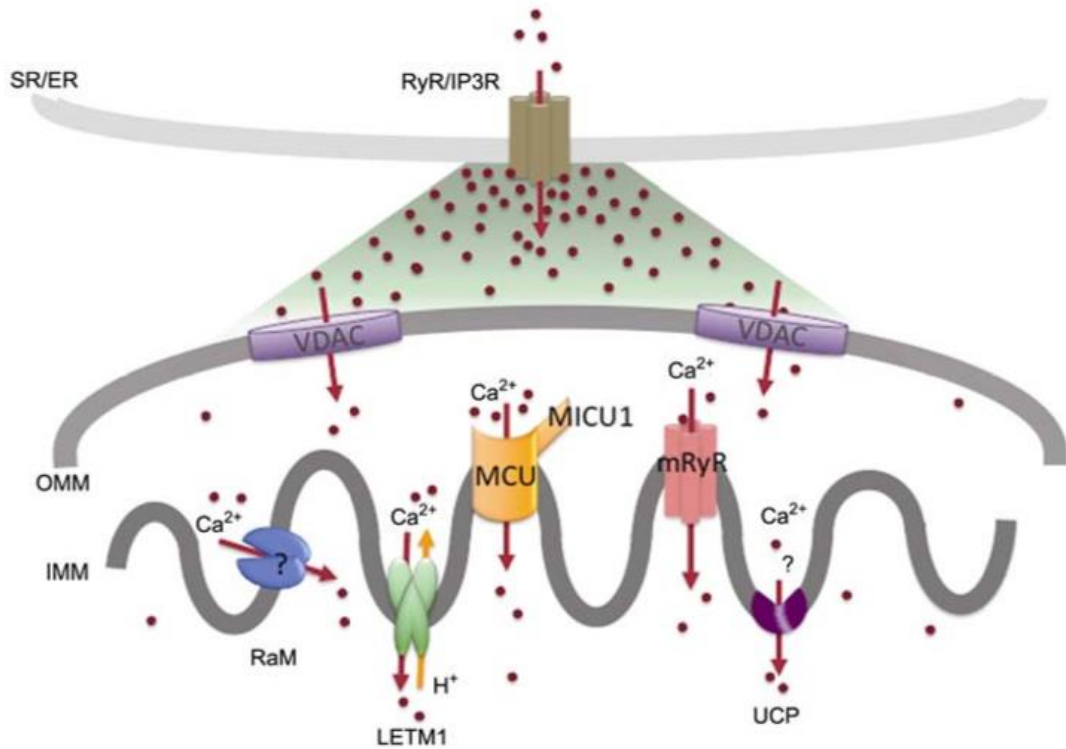


Figure 4.6: Illustration of the various methods exploited by the mitochondria to import cytosolic Ca^{2+} into the mitochondrial matrix with LETM1 acting as a $\text{Ca}^{2+}/\text{H}^+$ antiporter. This figure was sourced from (Pan, Ryu & Sheu 2011).

With the previous observation that Ca^{2+} drives mitochondrial energy demand, it is possible that *LETM1* overexpression contributes to the enhanced OXPHOS observed. Furthermore, RNAi-mediated inhibition of *LETM1* was demonstrated to nearly abolish both mitochondrial Ca^{2+} and pH increases which indicated that *LETM1* catalysed the slow uptake of Ca^{2+} into the mitochondria (Jiang, Zhao & Clapham 2009). The study also demonstrated a sustained Ca^{2+} increase upon *LETM1* inhibition suggesting that Ca^{2+} efflux is highly regulated by this protein. Additionally, as the formation of the proton gradient by Complex I, III and IV is vital for harnessing electrochemical energy for the synthesis of ATP, it has further been suggested that the uptake of Ca^{2+} into the matrix by *LETM1* not only drives energy demand by the activation of TCA cycle enzymes but also contributes to the electrochemical gradient ending at ATP production via the export of H^+ out of the matrix (Poburko, Demarex 2012) (**Fig. 4.1**).

Another interesting role of *LETM1/mdm38* (its *Saccharomyces cerevisiae* homolog) is its capability to bind mitochondrial ribosomes through a conserved 14-3-3-like ribosomal binding domain (RBD) (Lupo et al. 2011). Enhanced respiratory chain biogenesis has been observed to be specific to the effective translation and synthesis of the complex III component cytochrome b reductase (*Cyt-b*) and the complex IV component cytochrome c oxidase (*COXI*) (Bauerschmitt et al. 2010) mediated by *LETM1/mdm38* while its loss leads to respiratory chain defects. Interestingly, when we assessed mitochondrial function in permeabilised CHO cells, a ~30% increase in oxygen consumption was observed for complex I and II while a drop in oxygen consumption was observed at complex IV in the case of the miR-23 sponge clone 4. It has been demonstrated that overexpression of *LETM1* can abrogate mitochondrial chain biogenesis (Piao et al. 2009) suggesting a potential reasoning behind this reduced activity at complex IV and the lack of synergy between complex I and II. *LETM1* overexpression has additionally been documented in various cancerous phenotypes and its inhibition of mitochondrial function has correlated with an increase in glycolysis, compensating for ATP production and resulting in a shift from NADH to NADPH production (Chen et al. 2007, Pelicano et al. 2006b). Although components specific to the mitochondrial transport chain were not found to be DE in miR-23 depleted clones, it is possible that their assembly is being perturbed. Furthermore, mitochondrial enrichment and label-free mass spectrometry was carried out in an attempt to identify subtle alterations taking place within the mitochondria that may have been missed through whole cell proteomic analysis. The enhanced mitochondrial function may be as a result of the activation of particular TCA cycle enzymes as suggested by *LETM1*'s role in Ca^{2+} homeostasis and the observed up-regulation of metabolic enzymes such as isocitrate dehydrogenase (*IDH1*) and malate dehydrogenase (*MDH*) (**Fig. 4.1**). With reference to the literature, *LETM1* appears to have a regulatory influence in mitochondrial function both directly and indirectly spanning the majority of the respiratory chain complex components.

4.3.2 14-3-3-eta (YWHAH)

The 14-3-3 protein family is a well conserved family of heterogeneous dimeric proteins whose activation is dependent upon calcium and the cAMP-dependent kinase or Calmodulin-dependent protein kinase. They are involved in cell signalling, regulation of cell cycle progression, intracellular trafficking/targeting, cytoskeletal structure and

transcription and commonly require the phosphorylation of a serine or threonine residue in their target sequences (Ferl, Manak & Reyes 2002). There are 7 known isoforms in mammals (α/β , ϵ , η , γ , τ/θ , δ/ζ , and σ) suggesting that each exert a distinct function. However, knockout studies have demonstrated no definite phenotype which may reflect the fact that in many cases isoforms can compensate for each other (Aitken 2006).

14-3-3-eta (*14-3-3- η*) was found to be elevated in its abundance in miR-23 depleted CHO-SEAP cells by 2.7 fold. The regular functions of *14-3-3* proteins encompasses activation, inhibition, stabilization or orientation of their binding partners (Gardino, Smerdon & Yaffe 2006). This is through the sequestration of target proteins in the cytoplasm ultimately inhibiting nuclear or mitochondrial localisation of specific binding partners and includes cellular functions such as metabolism (Kleppe et al. 2011) and insulin secretion (Chen et al. 2011b).

Although we are not observing a tumour-like phenotype as previously demonstrated for this family of proteins, one interesting role is their involvement in the regulation of gene expression, reviewed in (Healy, Khan & Davie 2011). 14-3-3-epsilon's expression in CHO has been previously demonstrated to be induced upon the induction of hypothermic growth conditions (Thaisuchat et al. 2011) potentially implicating a role in increased specific productivity (Kumar, Gammell & Clynes 2007). Additionally, 14-3-3-epsilon, among other 14-3-3 family members, was identified to be increased in their expression/translation upon transient transfection with pre-miR-7 (Meleady et al. 2012a) whose transient overexpression was also found to mimic a temperature-shift-like phenotype including enhanced specific productivity (Barron et al. 2011b). This would suggest that the expression of this family of *14-3-3* proteins is involved in enhancing transcription in a temperature-dependent and independent manner.

It has been further demonstrated that the *14-3-3* family of proteins can interfere with gene expression at an epigenetic level by binding to and sequestering (*Shahbazian, Grunstein 2007*) *HDAC4* activity (Wang et al. 2000) and *HDAC5* (Grozinger, Schreiber 2000). Histone deacetyltransferases (*HDACs*) regulate gene expression by the phosphorylation of H3 of the histone complex rendering surrounding DNA inaccessible. Although the association with *HDAC4* and *14-3-3* does not interfere with *HDAC4s* activity, retention within the cytoplasm prevents its nuclear localisation and ultimately inhibition of transcriptional repression mediated through deacetylation (**Fig. 4.1**). Additionally, prevention of nuclear entry of *HDAC4* via *14-3-3* was demonstrated to be activated upon

Ca²⁺/Calmodulin signalling, a biological process found to be activated within miR-23 depleted CHO clones (Guan et al. 2012) including *CaMKIIδ* found also to be increased in expression in miR-23 depleted CHO clones (Zhang et al. 2007). HDACs lack intrinsic DNA-binding activity and are therefore recruited to target sites by their direct association with transcriptional activators and repressors (Shahbazian, Grunstein 2007). Target site specificity to the SEAP CMV-promoter and enhanced SEAP transcription in the case of miR-23 sponge clones is partially suggested when considering the binding specificity can be dictated by endogenous transcriptional activators that would be cell type specific yet potentially similar within our rCHO-SEAP cell line. To explore the possibility of *14-3-3* mediating specific transcriptional enhancement of the SEAP gene further validation would be required such as siRNA-mediated knockdown of the *14-3-3-eta* gene expecting to observe reduction in SEAP secretion and transcription or immunoprecipitation of *14-3-3-eta* as means to identify its binding partners, *HDAC4* potentially being one. Interestingly, a recent paper by Yang and colleagues demonstrated that the addition of the small molecule inhibitor of HDACs, Valporic acid (VPA), enhanced antibody titres by >20% in numerous cell lines without impacting on glyco-profiles (Yang et al. 2014). Several miRNA have been previously demonstrated to regulate the translation of *14-3-3* proteins in various types of cancer such as miR-193b in MCF7 cells (Leivonen et al. 2011) and miR-375 in gastric cancer (Tsukamoto et al. 2010). Interestingly, miR-375 has been widely implicated in the regulation of glucose-stimulated insulin secretion through targeting multiple factors such as *PDK1* and myotrophin in pancreatic β-cells (Li 2014). Its previously characterised impact on *14-3-3* proteins expression offers a potential and alternative explanation to how it mediates elevated levels of insulin transcript. Despite the large regulatory capabilities of this family of proteins, it is possible that *14-3-3* is mediating the enhanced SEAP transcription phenotype be it through direct de-repression due to miR-23 diversion or as a result of other targets more dramatically de-repressed such as *CaMKIIδ*.

4.3.3 Calcium signalling

This ubiquitous second messenger, Calcium (Ca²⁺), is intricately involved in numerous cellular processes including signal transduction, muscle contraction, secretion of proteins/hormones and gene expression. Within the cell, Ca²⁺ is stored in specialised compartments (endosomes, lysosomes and golgi) as well as within the endoplasmic

reticulum (ER)/sarcoplasmic reticulum (SR) (Rizzuto, Pozzan 2006). Protein folding in the ER is a very energy-demanding process as many of the molecular chaperones (*BiP* and *GP94*) hydrolyse ATP during their binding/release cycles. It has been suggested that the depletion of intraluminal ER ATP may be an energy deprivation signal to stimulate Ca^{2+} release for uptake by the mitochondria ultimately stimulating OXPHOS as described earlier through the activation of TCA cycle enzymes (Kaufman, Malhotra 2014). This would suggest that enhanced transcription of the SEAP gene within our miR-23 depleted clones is exerting a high energy demand on the ER for efficient folding and processing ultimately driving energy demand through Ca^{2+} release and mitochondrial stimulation (**Fig. 4.1**). Excessive cytosolic/mitochondrial Ca^{2+} can result in mitochondrial swelling, pore opening and collapse of the mitochondrial membrane potential resulting in apoptosis by cyt-c release (Osellame, Blacker & Duchen 2012). This would suggest that if mitochondrial function is being stimulated by Ca^{2+} influx, it is as a result of energy demand and not the direct influence of miR-23 intervention providing unphysiological amounts of Ca^{2+} through the over-activity of *LETM1*, for example. An additional layer of Ca^{2+} -mediated OXPHOS regulation comes from the observation that extra-mitochondrial Ca^{2+} can influence the transport of glutamate into the mitochondria (Gellerich et al. 2010), suggesting the observed increased availability of glutamate is being channelled into the mitochondria for utilisation.

CaMKs (Ca^{2+} /Calmodulin-dependant protein kinases) are a family of serine/threonine kinases regulated by calcium and Calmodulin. One member, *CaMKII δ* , was observed to be increased in expression by 1.75-fold in miR-23 depleted clones. Another protein found to be up-regulated and activated by *CaMKs* was Caldesmon (*CALD*), an actin binding protein (2.16-fold). Both *CaMKII δ* and *CALD* presented themselves as potential targets of miR-23 and both are responsive to calcium signalling.

CaMKII δ has previously been found to be expressed at relatively high levels in β -cells (Easom 1999) in addition to its activation upon glucose stimulation following the entry of Ca^{2+} (Norling et al. 1994, Wenham, Landt & Easom 1994). Furthermore, *CaMKII δ* was found to be directly related to the metabolic control of insulin secretion at a transcriptional level (Osterhoff et al. 2003). As mentioned previously, *CaMKII δ* has been demonstrated to phosphorylate the two conserved phosphorylation sites, ser-246/467 in *HDAC4*, ultimately flagging it for the mobilisation of *14-3-3-eta* which recognises phosphorylated serine/threonine residues (Little et al. 2007). Retention of HDAC4 in the

cytosol prevents histone deacetylation maintaining DNA in a relaxed and transcriptionally accessible state (**Fig. 4.1**) Furthermore, *CaMKII δ* possesses two splice variants (δ_B and δ_C) the former of which contains a nuclear localisation signal (NLS) (Zhang, Brown 2004) further suggesting its potential role in enhancing SEAP transcription. Perhaps elevated SEAP productivity could be as a result of this process with mitochondrial function being a by-product of calcium signalling stimulated by ATP-depleted ER-release. It would be interesting to evaluate the levels of intracellular calcium in our miR-23 stable clones in addition to inhibiting *CaMKII δ* .

4.3.4 TCA cycle and metabolism

Several proteins were found to be DE in CHO-SEAP-sponge-23 that could potentially be playing a role in cellular metabolism including isocitrate dehydrogenase 1 (*IDH1*-1.68-fold up regulated), malate dehydrogenase (*MDH* – 1.67-fold up regulated), Lysosomal alpha glucosidase (1.65-fold up regulated) and prolyl-4-hydroxylase (*P4HAI* – 1.84-fold up-regulated). It's been suggested that some of these candidates can be activated by an influx of Ca^{2+} into the mitochondrial matrix suggesting their function to be responsive to internal cellular cues and potentially not causative. Nevertheless, their increased abundance could be responsible for the increase in mitochondrial OXPHOS previously observed in miR-23 depleted CHO-SEAP cells (**Fig. 4.1**).

Lysosomal alpha glycosidase is an enzyme encoded by the *GAA* gene that mediates the degradation of glycogen to glucose from lysosomes. Lysosomal alpha-glucosidase is known to be responsible for a lysosomal storage disease, Pompe(Manganelli, Ruggiero 2013) disease, whereby a build-up of lysosomal glycogen results in the inhibition of lysosome activity, aberration of autophagy and ultimately muscle wasting characterised by the build-up of cellular debris (Manganelli, Ruggiero 2013). Mitochondrial dysfunction has also been implicated in the onset of Pompe disease, however, this lull in mitochondria function is potentially coupled to the inhibited autophagic turnover of cellular organelles in addition to broken cristae due to the accumulation of membrane bound glycogen particles within the mitochondria (Raben et al. 2012). Increased expression of this enzyme in miR-23 depleted CHO cell could potentially supply excess glucose through glycolysis into the TCA cycle resulting in the observed increase in OXPHOS in addition to ensuring effective and optimal lysosome function.

IDH is a family of enzymes that include three distinct enzymes: *IDH1*, *IDH2* and *IDH3*. All three enzymes catalyse the conversion of isocitrate to α -KG, a central metabolite for the TCA cycle. *IDH1* and 2 use NADP^+ while *IDH3* uses NAD^+ with *IDH1* being located in the cytosol and the latter two being localised to the mitochondria (Yang et al. 2012). As NADH is a reducing equivalent providing electrons to the ETS and *IDH3*s reaction being irreversible, this isoform is considered central to oxidative phosphorylation (**Fig. 4.7**).

Figure 4.7: The role of *IDH* in cellular metabolism

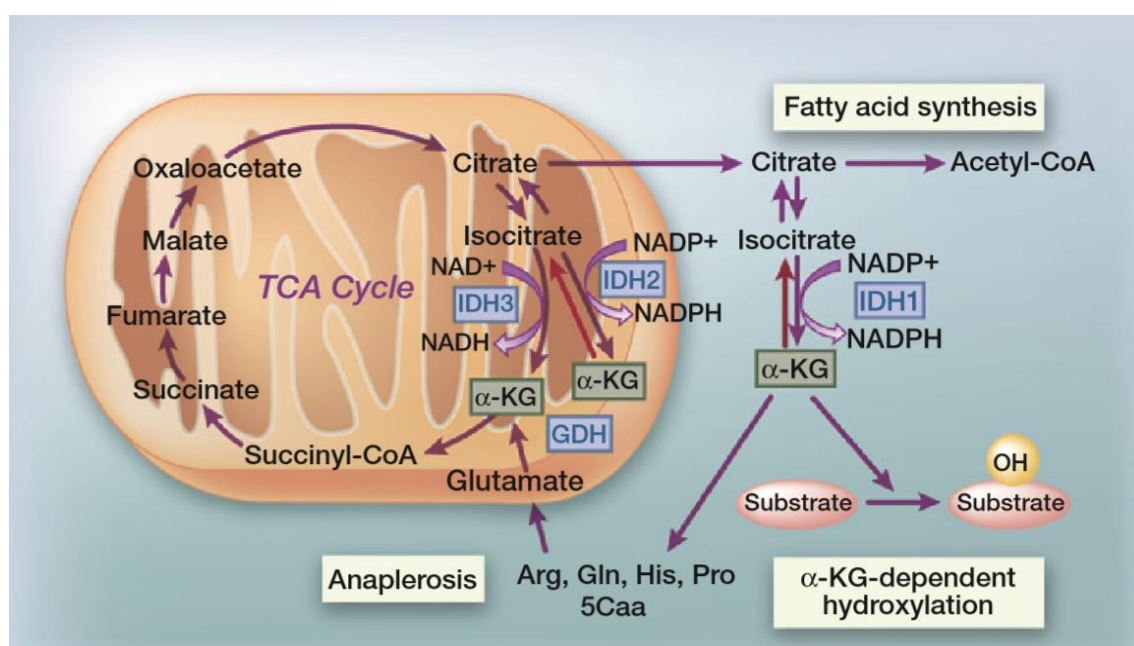


Figure 4.7: The role of the IDH family of enzymes in cellular metabolism including the central role *IDH3* plays in the TCA cycle and both the compensatory roles *IDH1/2* play in the TCA cycle in addition to downstream molecular pathways. This figure was sourced from (Yang et al. 2012).

NADPH on the other hand is involved in many cellular processes including defence against oxidative stress, fatty acid synthesis and cholesterol biosynthesis (Kim et al. 2007). It is possible that the cytosolic *IDH1* enzyme reaction might compensate for the loss of the mitochondrial *IDH2/3* by producing metabolites in the cytosol that can be transported into the mitochondria as it has previously been observed that rapid transport of metabolites can take place between the cytosol and the mitochondria such as citrate, isocitrate and α -ketoglutarate (**Fig. 4.8**).

Figure 4.8: The role of *IDH1* in supplementing the TCA cycle

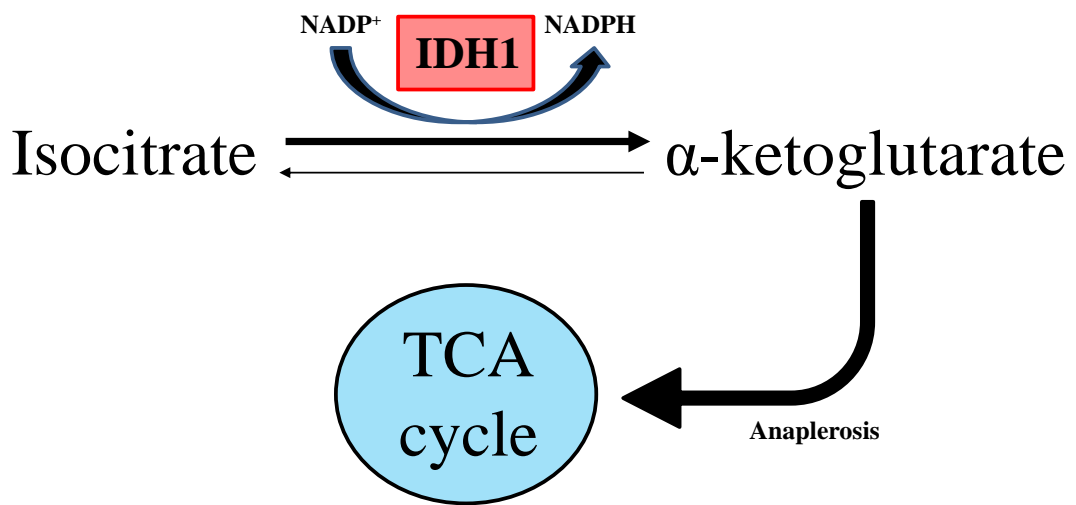


Figure 4.8: The potential role of *IDH1* in rCHO-SEAP cells inducing an increased OXPHOS. *IDH1* catalysis the reversible conversion of isocitrate to α -KG with the forward reaction being predominant. This reaction takes place in the cytoplasm whereby α -KG is then transported into the mitochondria for entrance into the TCA cycle in what's known as anaplerosis.

Mitochondrial export of citrate/isocitrate was demonstrated to be an important step in glucose-stimulated insulin secretion with the overexpression of citrate/isocitrate carriers (CICs) enhancing GSIS (Joseph et al. 2006). Furthermore, siRNA knockdown of cytosolic *IDH1* inhibited GSIS by 59% (Ronnebaum et al. 2006). This observation reinforces the suggested function of α -KG as a co-factor for other cellular pathways such as the activation of α -KG-dependent dioxygenases and that the predominant mutations in *IDH1/2* isotypes influence these alternative molecular pathways. Although *IDH1* is redundant for the *IDH2/3* interconversion of isocitrate to α -KG, its knockdown impacting on insulin secretion suggests a non-redundant role in this pathway. Elevated expression of *IDH1*, for example as a result of miR-23 diversion, could potentially provide the cell with excess α -KG ultimately providing elevated NADH through TCA cycle processing. However, the exclusive production of NADPH in the cytosol, through export of TCA cycle intermediates via excess downstream sources, could possibly be playing a part in signalling networks such as its interaction with dioxygenases and its role in oxidative stress as *IDH1* mutations have been associated with increased oxidative stress in gliomas (Gilbert et al. 2014). Furthermore, *IDH1* is one of the key genes found to be up-regulated in breast cancer stem cells, which were identified to have lower levels of reactive oxygen species (ROS) (Diehn et al. 2009). The overabundance of α -KG in addition to Fe^{2+} serve

as cofactors for the activity of histone demethylases such as Jumonji C ultimately switching gene expression on (Horbinski 2013).

Prolyl-4-hydroxylase is an intracellular enzyme required for the synthesis of all types of collagens and is stimulated by the levels of α -KG, potentially provided for by *IDH1* in miR-23 depleted CHO cells. The functional roles of prolyl-hydroxylases or 2-OG oxygenases (2-OG is 2-oxoglutarate also known as α -ketoglutarate or α -KG) have a wide range of functional roles including hypoxic response (oxygen sensing), nucleic acid repair and modification, fatty acid metabolism and chromatin modification (Loenarz, Schofield 2008). Prolyl-hydroxylase catalyses the conversion of proline and α -KG into hydroxyproline, succinate and CO₂ in the presence of iron and dioxygen. Prolyl-4-hydroxylase has been demonstrated to have a higher affinity of α -KG than other PDHs. This high affinity would suggest that the cell would possess an inherent increased sensitivity in responding to TCA cycle defects. It is possible that the α -KG being produced exclusively in the cytosol by *IDH1* is being sensed and processed by *P4HA1* into its products hydroxyproline and succinate. Succinate could be shuttled into the mitochondria where it serves as a substrate for succinate dehydrogenase (complex II) resulting in the increased oxygen consumption observed at this complex. A study by Zhao *et al* (Zhao et al. 2009) demonstrated that ectopic expression of an *IDH1* mutant was found to result in the inhibition of the activity of prolyl hydroxylase (*PDH*) which could be restored by feeding cells with α -KG. Various pathways are under the influence of these hydroxylases including collagen synthesis, histone modification and transcription. It is estimated that there are over 60 α -KG-dependent dioxygenases (Rose et al. 2011) suggesting that changes in *IDH1* levels could potentially affect multiple pathways.

With the observation of glutaminase not being elevated in its translation due to miR-23 depletion, the increase in the glutamate concentration of 65% across all miR-23 depleted clones could be as a result of the catapleurotic export of α -ketoglutarate due to elevated IDH1 (increased synthesis of α -KG from isocitrate) and its conversion into glutamate (Owen, Kalhan & Hanson 2002).

Malate dehydrogenase (*MDH*) catalyses the conversion of malate to oxaloacetate in a NAD⁺-dependent manner generating the reducing equivalent NADH, contributing to the electron transport chain. It is considered the second rate limiting step in the TCA cycle as oxaloacetate is the terminal substrate required to produce citrate in the presence of acetyl-CoA to start the cycle over again. *MDH* was found to be increased in its expression in

miR-23 depleted CHO-SEAP clones. This increase in *MDH* expression could be providing surplus NADH reducing equivalent for electron donation at complex I thus contributing to the elevated OXPHOS previously observed. As an aside, interference at these rate limiting steps can be responsible for mitochondrial dysfunction due to metabolite starvation such as the “Crabtree effect” whereby exclusive conversion of glucose to lactate inhibits TCA cycle recycling by reducing Acetyl-CoA production from pyruvate (Dell'Antone 2012) (**Fig. 4.9**).

Figure 4.9: The “Warburg” and “Crabtree” effect

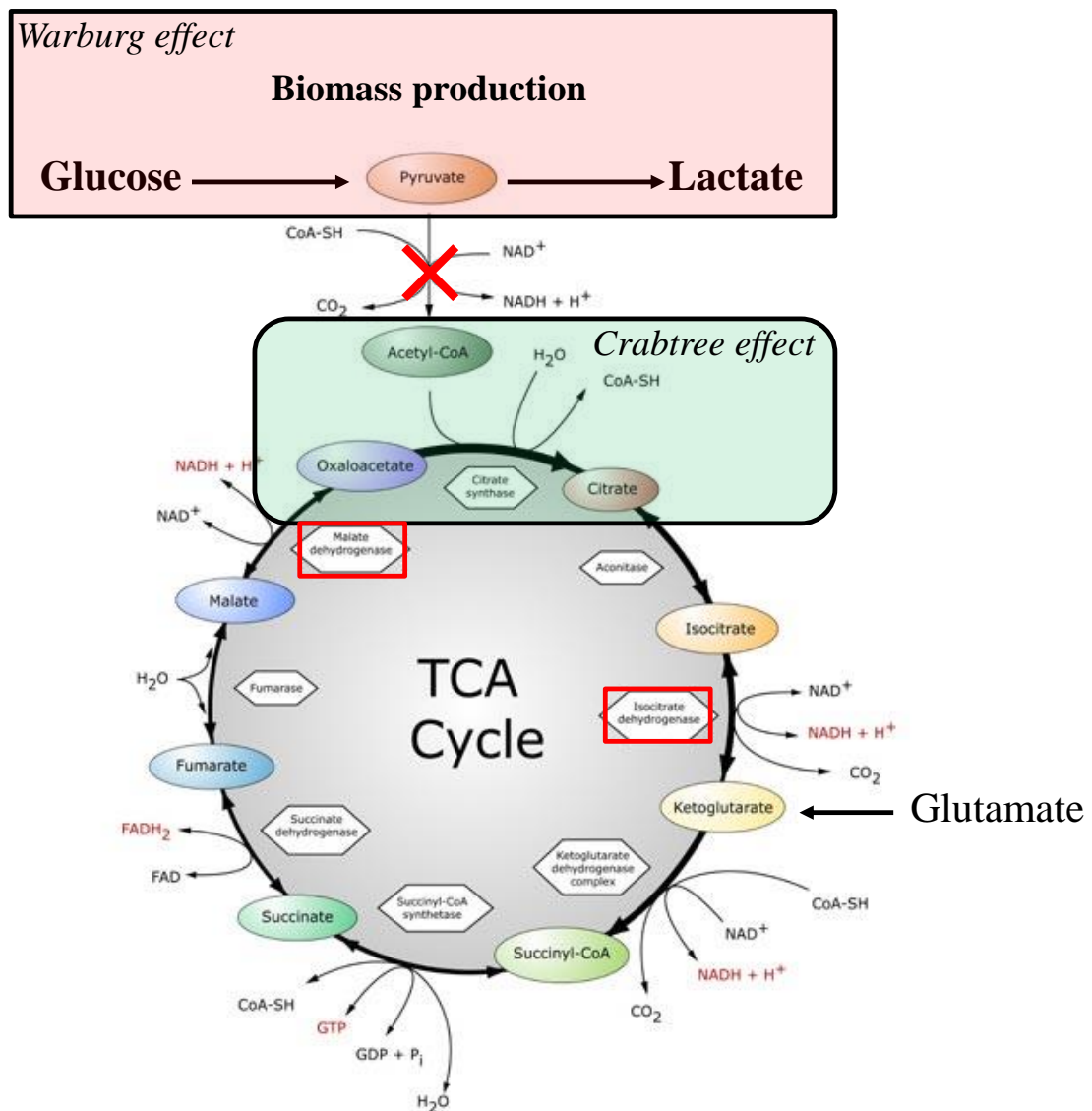


Figure 4.9: The “Warburg effect” (Red Box) demonstrates the high consumption of glucose by cancer/CHO cells with exclusive conversion to lactate. Although energetically inefficient, intermediates provide key substrates for biomass production to actively proliferating cells. As pyruvate is converted to lactate and not Acetyl-CoA, the TCA cycle is starved of essential starting metabolites (Acetyl-CoA and oxaloacetate) causing TCA cycle weakening termed the “Crabtree effects” (Green box). However, the overexpression of certain enzyme such as *IDH1* and *MDH*, in addition to the increased abundance of glutamate, can supplement and strengthen the TCA cycle by providing key intermediates such as α -KG and encouraging forward reactions.

Overexpression of *MDH II* in CHO resulted in increases in intracellular ATP and NADH with a corresponding 1.9-fold improvement in integral viable cell density (Chong et al. 2010). Growth improvement was not an observed benefit in our miR-23 depleted stable

SEAP cell line despite NADH concentration being correlated with cellular proliferation. It would be interesting to assess miR-23 depleted clones for their metabolic profiles including ATP, NADH, NADPH, as well as TCA intermediate metabolites such as malate, α -KG, citrate and isocitrate.

4.3.5 Combating oxidative stress

Evidence suggests that protein folding and the generation of reactive oxygen species (ROS) is a byproduct of protein oxidation in the ER. Additionally, one of the main cellular organelles involved in the production of ROS is the mitochondria which, in a state of chronic nutrient/energy overload, the flux of nutrients through the mitochondrial ETS can result in enhanced ROS production and ultimately oxidative stress (Malhotra, Kaufman 2007). The observation of elevated transcription of the SEAP gene as well as increased oxidative phosphorylation within miR-23 depleted clones, in addition to metabolic enzymes of the TCA cycle fuelling OXPHOS, suggests that miR-23 sponge clones by comparison to their control counterparts have a higher degree of oxidative stress. Numerous proteins were found to be up-regulated that have been shown to respond to oxidative stress including Thioredoxin reductase 1 (*TXNRD1*: 1.66-fold), Heme oxygenase-1 (*HMOX-1* or HO-1: 2.33-fold), glutathione-s-transferase Mu-1 and glutathione-s-transferase Mu-6 (*GSTM1/GSTM6* – 1.56/1.74-fold up-regulated respectively).

Thioredoxin reductase-1 is a cytosolic antioxidant which is known to reduce various cellular compounds including Thioredoxin using NADPH. Reduction of thioredoxin (TXN) activates it allowing for the reduction of oxidised cysteins in cellular proteins and scavenge peroxides by peroxidoredoxins (*PRDX*), thus protecting the cell against oxidative stress (Cadenas et al. 2010). Thioredoxin reductase does appear to be able to directly remove ROS by reducing oxidants and hydrogen peroxide due to its highly reactive selenocystein (Cenas et al. 2004). Activated thioredoxin has a redox-active cystein pair through which it interacts with other proteins to regenerate proteins damaged by ROS for example H₂O₂-inactivated GAPDH (Fernando et al. 1992). Thioredoxin is also a co-factor for methionine sulfoxide reductase, whereby it can reduce methionine sulfoxide residues in oxidised proteins caused by ROS (Watson et al. 2004). Thioredoxin reductase deficient cells demonstrated a decreased basal mitochondrial oxygen consumption rates (Lopert,

Day & Patel 2012) suggesting its role in maintaining efficient mitochondrial function under harsh oxidative stressful conditions.

Heme oxygenase 1 is a ubiquitous inducible cellular antioxidant stress protein that catalyses the conversion of the pro-oxidant molecule heme into the products biliverdin, iron and CO. *HMOX1* is up-regulated in response to cellular stress such as hydrogen peroxide. Mitochondrial localisation of *HMOX1* has been demonstrated to confer resistance to oxidative stress, correct mitochondrial dysfunction and inhibit apoptosis and gastric injury (Bindu et al. 2011). Interestingly, Thioredoxin reductase has been demonstrated to regulate the induction of heme-oxygenase-1 expression (Trigona et al. 2006) suggesting a synergistic link between both pathways and that the increased expression of *HMOX1* in miR-23 depleted CHO-SEAP cells could be a result of oxidative stress and not as a function of miR-23 diversion.

The ubiquitin-proteasome pathway (UPP) is the primary cytosolic proteolytic machinery for the selective degradation and removal of damaged proteins. Studies have demonstrated that the 26S proteasome is highly susceptible to inactivation during oxidative stress whereas the 20S proteasome is relatively stable under a variety of oxidative stresses (Reinheckel et al. 1998). The 26S proteasome has been found to be responsible for the unfolding and degradation of most normal ubiquitinated proteins (missense mutations) but shows poor selectivity for oxidised proteins (Ding, Dimayuga & Keller 2006). Unlike the 26S proteasome, the 20S exhibits a high degree of selectivity for degrading oxidised or otherwise damaged proteins resulting from oxidative stress (Pickering, Davies 2012). The 26S proteasome is composed of a 20S and two 19S subunits. Cellular adaptation to oxidative stress has revealed that dissociation of the 26S proteasome liberates the oxidative-damaged specific 20S subunit as a means of combatting potential cellular damage in a transcriptional-independent manner (Grune et al. 2011). It is possible that the down-regulation of *PSMD7* (26S proteasome non-ATPase regulatory subunit 7-like) which is a component of the 19S subunit is reducing the association and formation of the 26S proteasome thus providing increased availability of the 20S subunit potentially providing assistance for mitochondrial/ER derived oxidative stress.

In addition to their role in cellular metabolism and other molecular pathways such as biosynthesis, *IDH1/2* have been observed to play a vital role in cell protection against a variety of insults that produce oxidative stress (Chang, Xu & Shu 2011). Reduced expression of both *IDH1* and *IDH2* was observed to result in higher levels of ROS and a

greater oxidative damage in response to an oxidative insult (Jo et al. 2001, Lee et al. 2002). Additionally, several reports have demonstrated that the overexpression of *IDH1/2* can offer cellular protection against oxidative stress (Kim et al. 2007, Shin et al. 2004). For examples, NADPH produced by IDH1/2 can be utilised by glutathione reductase to convert the oxidised form of glutathione (GSSG) to the reduced form (GSH) which can neutralise free radicals and ROS species (Lee et al. 2002).

Following from this, two glutathione-s-transferase of the Mu (μ) isoform (1 and 6) were found to be up-regulated in miR-23 depleted CHO cells. Maintenance of the cellular antioxidant glutathione (GSH) in different cellular compartments is under the critical regulation of GSTs. GSTs function in cellular detoxification of endogenous toxic metabolites, superoxide radicals and exogenous toxic chemicals (Raza 2011). Reports have documented the presence of the mu class of GSTs in rat and mouse mitochondria in addition to rat brain mitochondria (Addya et al. 1994, Raza et al. 2002, Bhagwat et al. 1998). The reduced expression of *GSTM2* was observed to increase oxidative stress in spontaneously hypertensive rats (Zhou et al. 2008). The observation of the elevated abundance of these antioxidant proteins further suggests that cellular and molecular pathways, mediating an enhanced SEAP productivity are inducing oxidative stress which is being compensated for by numerous cellular responses. Glutathione (GSH) and Thioredoxin are considered the most important out of the four antioxidant systems in the cell. The observation of both of these systems potentially being overactive again suggest that miR-23 depleted CHO cells are under oxidative stress which is being adequately dealt with. Without measuring the internal levels of ROS, it is premature to assume that the elevated expression of these oxidative stress responding proteins are activated as a result of elevated mitochondrial function and SEAP production, in addition to their expression (*TXNDR1*) being a result of miR-23 depletion or responsive to cellular cues.

4.4 Proteomic analysis of enriched mitochondria

Cell fractionation to isolate mitochondria and profile them directly not only serves to identify low abundant proteins that would be otherwise over-shadowed by high abundant proteins, but also serves to refine the localisation of previously identified proteins as functioning specifically in the mitochondria (Drissi, Dubois & Boisvert 2013).

The previous link between miR-23 and cellular bioenergetics through glutaminolysis (Gao et al. 2009) highlights its potential role in our enhanced mitochondrial function

through other pathways such as the various proteins mentioned previously. Another mitochondrial-related gene found to be under the translational control of miR-23 is the mitochondrial transcription factor A (*TFAM*) (Jiang et al. 2013b). This gene is involved in the transcriptional initiation of the mitochondrial genome (Campbell, Kolesar & Kaufman 2012) in addition to mtDNA packaging and copy number (Uchiumi, Kang 2012). Although several of these validated gene targets of miR-23 (*GLS*, *TFAM* and *XIAP*) did not appear to be DE when label-free mass spectrometry was carried out, it is possible that miR-23 can influence cellular metabolism through various molecular means. However, given the previous association of high CHO cell specific productivity with oxidative metabolism (Young 2013) and the ability of the endoplasmic reticulum to increase energy provisions through calcium signalling (Kaufman, Malhotra 2014), it is possible that this enhanced mitochondrial function is not causative but symptomatic of the enhanced production phenotype of miR-23 sponge CHO-SEAP cells.

4.4.1 A deeper insight into mitochondrial function

Lactate dehydrogenase (*LDH*) directly catalyses the interconversion of pyruvate to lactate with the concurrent interconversion of NADH and NAD⁺. *LDH-A* was observed to be down-regulated in miR-23 sponge clones by 1.3-fold. Although lactate is considered the lesser of two evils when compared to ammonia (Kim do et al. 2013), the propensity of CHO cells to act like some cancers with respect to the Warburg effect, excessive accumulation of lactate is an issue. Inhibition of *LDH-A* has been demonstrated to decrease glucose flux in the glycolytic pathway (Chen et al. 2001) and has further been demonstrated in CHO, upon siRNA-mediated inhibition, to increase hTPO production by 2.2-fold without influencing growth or viability (Kim, Lee 2007). These authors suggested that the viability benefit of reduced *LDH-A* activity may be more apparent under fed-batch conditions whereby a high glucose feed would result in faster accumulation of lactate. Although measurement of lactate levels would be required within our miR-23 sponge clones, this could be a potential explanation for the extended viability phase observed under fed-batch conditions that was not apparent when in batch culture.

It has been suggested that the increase in recombinant protein production may drive pyruvate into the TCA cycle or divert glucose towards the pentose phosphate pathway (Sengupta, Rose & Morgan 2011). With the observation of enhanced mitochondrial

function in miR-23 depleted clones, it is likely that oxidative metabolism is favoured. The reduced expression of *LDH-A* could also make pyruvate transiently more abundant for channelling into the TCA cycle (**Fig. 4.9**). With the observation that glycolytic metabolism and oxidative metabolism being associated with growth and productivity, respectively (Young 2013), the potential reduced glycolysis not impacting on miR-23 sponge clone growth is interesting. It has been reported that a 20% reduction in glucose consumption in a CHO cell engineered with reduced *LDH-A* and enhanced *Bcl2* expression, had no impact on growth (Jeon, Yu & Lee 2011). Another interesting report demonstrated that the co-inhibition of *LDH-A* and pyruvate dehydrogenase kinase (*PDHK*, the enzyme responsible for PDH inhibition) resulted in the 90% increase in IgG specific productivity without any appreciable impact on CHO cell growth (Zhou et al. 2011a).

The enzyme pyruvate kinase (*PKM*) was found to be down-regulated in miR-23 sponge clones by 1.9-fold. This enzyme is responsible for the generation of pyruvate from phosphoenolpyruvic acid and is a key regulator of the metabolic fate of the glycolytic intermediates (Iqbal et al. 2014). Its expression has been demonstrated to promote the Warburg effect and tumour growth (Sun et al. 2011). Down-regulation of this gene could be mediating a reduced dependency on glycolytic metabolism in miR-23 depleted clones starving the TCA cycle of its perquisite metabolite Acetyl-CoA. Acetyl-CoA catabolic processes were also found to be enriched for in GO assessment. Oxidative metabolism is possibly supplemented, as indicated by the enhanced mitochondrial function, through the various isotypes of TCA cycle enzyme such as *IDH1* and *MDH1*. This is irrespective of the potential enhanced activity of various TCA cycle enzymes through calcium signalling suggested by the increased expression of *LETM1* and the energy requirements of the ER (**Fig. 4.1**). However, without assessing the specific consumption rate of glucose, it would be premature to conclude that glycolytic metabolism is being perturbed in our miR-23 sponge clones or if they are simply eliciting an enhanced mitochondrial function.

Both *MDH* isotypes were identified as being overexpressed in miR-23 depleted CHO cells indicating that the isolation of mitochondria was successful in unveiling mitochondrial specific proteins such as the mitochondrial specific *MDH2*. These enzymes mediate the conversion of malate to oxaloacetate in addition to generating the reducing equivalent NADH (Marín-García 2012)

. Overexpression of *MDH2* in CHO cells has been demonstrated to increase intracellular ATP and NADH levels by 1.9-fold contributing to an increase in IVCC (Chong et al.

2009b). Weakening of the TCA cycle has been observed due to the export of vital intermediates such as α -ketoglutarate and malate out of the mitochondrial matrix (Dell'Antone 2012). The constant supply of oxaloacetate via *MDH1* and 2 may allow for the efficient energy turn over as indicated when respiratory control ratios were calculated for miR-23 sponge clones, as no bottleneck is provided in addition to the reduced *LDH-A* activity potentially providing excess pyruvate. The restoration of oxaloacetate has been observed to drive continued TCA cycle function (DeBerardinis et al. 2007). Another rate limiting metabolite α -ketoglutarate could be in constant supply through the elevated abundance of *IDH1*, identified in both whole cell and mitochondria enriched experiments. This could potentially compensate for the observation of the reduced expression of the mitochondrial-specific isotype, *IDH3A*, the predominant isotype involved in the TCA cycle (Yang et al. 2012). It was also observed that other enzymes involved in the TCA cycle were found to be down-regulated such as 2-oxoglutarate dehydrogenase (*KGDI*) and aconitate hydratase (*ACO2*). However, it is possible that the small changes in abundance may not be impacting significantly on mitochondrial function as indicated in intact and permeabilise assays.

Enzymes involved in combatting oxidative stress were found to be increased in miR-23 sponge clones including those previously identified in the whole lysate experiment such as *TXNDR1*, *HMOX1* and *GSTM1/6*. Mitochondrial Glutathione reductase (GSR) was found to be upregulated 1.3-fold and serves as a key enzyme that converts oxidised glutathione (GSSG) to its reduced form (GSH) which ultimately scavenges ROS (Gill et al. 2013). Peroxiredoxin-2 (*PRDX2*) was also found to be increased in expression and has been linked with protecting proteins against oxidative damage (Rhee et al. 2012). The observation of the increase in expression of additional proteins involved in conferring resistance to oxidative stress further suggest the increase in mitochondrial function despite certain TCA cycle members being reduced.(Li et al. 2005)

Several proteins found to be associated with the electron transport system were found to be DE in mitochondrial enriched miR-23 sponge clone extracts. Cytochrome c oxidase (*COX*), also known as Complex IV, is the terminal enzyme complex of the mitochondrial electron transport system that couples the transfer of electrons from reduced cytochrome c to molecular oxygen and is composed of 13 subunits of both nuclear and mitochondrial origin. The subunit *COX5A*, nuclear in origin, was found to be down-regulated in miR-23 sponge clones by 1.8-fold. This complex has been associated with efficient assembly

of the *COX* supercomplex. The first step in *COX* assembly is the membrane integration of *COX1* followed by *COX4-COX5A* (Stiburek et al. 2005). Furthermore, direct depletion of *COX5A* resulted in the decreased levels of assembly of the *COX* enzyme with a parallel accumulation of *COX* sub-(Fornuskova et al. 2010)complexes and unassembled subunits (Fornuskova et al. 2010). Another mitochondrial complex associated protein *UQCRC1* (ubiquinol-cytochrome b-c1 reductase) was found to be down-regulated by 1.5-fold in miR-23 sponge clones. This enzyme is responsible for transferring electrons from QH_2 to ferricytochrome c. Specific loss of *UQCRC1* has been demonstrated to be induced upon exposure to oxidative stress (Shibanuma et al. 2011). The reduction in abundance of both these Complex III and IV related proteins could potentially explain the bottleneck in electron transfer suggested earlier for the lack of synergy upon stimulation of Complex I and II in permeabilised assays. Furthermore, stimulation of Complex IV by TMPD demonstrated a reduction in oxygen consumption in miR-23 sponge clones potentially due to the reduced expression of *COX5A* and associated assembly of *COX*. The continued healthy phenotype of miR-23 deplete clones would suggest that the reduced expression of these mitochondrial related proteins is not detrimental to the cell.

The protein *NDUFA1* was once thought to be associated with complex I is now emerging as having a role with complex IV (Carroll et al. 2006). *NDUFA4* has been shown to be associated with *COX* function but not in its assembly (Pitceathly et al. 2013) suggesting that, despite its increased expression, will not enhance *COX* function. One observation however indicates that enhanced mitochondrial function maybe due to the increased abundance of metabolites providing excess quantities of the reducing equivalent NADH and FADH_2 . This observation was the reduction in abundance of two components of Complex II, Succinate dehydrogenase (*SDH*), A and B. *SDH* catalyses the oxidation of succinate to fumarate in addition to the reduction of ubiquinone to ubiquinol (Kim et al. 2013). The dual role this enzyme plays links the oxidation of glucose in the TCA cycle with the production of ATP. The reduced expression of two components does not correlate the increased oxygen consumption previously observed at complex II during permeabilised assays. However, this could be due to the mild reduction in abundance of 1.3 and 1.4 for *SDHA* and *SDHB*, respectively, potentially not abrogating enzymatic function. Furthermore, the enhanced activity of other TCA cycle enzymes such as *IDH* and *MDH* could provide excess metabolites mediating the observed enhanced activity.

The indication towards enhanced mitochondrial function with elevated SEAP productivity as a result of stable miR-23 depletion begs the question: Is SEAP productivity enhanced as a function of oxidative metabolism or is oxidative metabolism elevated as a result of enhanced SEAP transcription and processing? Previous studies have documented the ability of MYC to induce mitochondrial biogenesis, function and enhanced oxygen consumption (Li et al. 2005). Metabolic reprogramming in activated B-cells has also been recently reported with both an increase in glycolytic and oxidative metabolism being observed (Le et al. 2012). The ability of MYC to regulate the expression of several (O'Donnell et al. 2005b) miRNAs (O'Donnell et al. 2005b), miR-23a/b included (Gao et al. 2009), including its role in metabolic reprogramming (Eilers, Eisenman 2008) and the association of miR-23 with B-cell differentiation (Li et al. 2011a), further strengthens the potential of miR-23 playing a direct role in cellular metabolism.

4.5 Potential bona-fide targets of miR-23

Identification of true miRNA targets is a cumbersome and trialling task, which without appropriate validation, leaves the researcher with an extensive list of potential targets all of which have question marks over them. Earlier, we demonstrated that by integrating multiple “omics” datasets, low scoring *in-silico* predicted targets that would otherwise be discounted can ultimately be discovered. However, when posed with a list of DE proteins from a single dataset, prediction algorithms are still the number one source for narrowing down the potential target list. Of the 41 protein targets found to be DE in the whole cell lysates of stable miR-23 depleted clones, 13 were found to overlap with the list generated from the miRWalk algorithm. Given that the miR-23 sponge clones divert miR-23 away from its endogenous mRNA targets, mRNA transcripts under direct influence of miR-23 should demonstrate an increase in their level of translation. When this was considered, 8 protein targets (*LETM1*, *CALM1*, *CaMKII δ* , *FERMT2*, *IDH1*, *TXNRD1*, *PPP1CB* and *P4HA1*) of the 13 overlapping targets were found to be up-regulated. These eight targets present themselves as priority targets of miR-23a/b. miRNAs impact on an endogenous target is generally accepted to be modest, mediating an impact of ~ 2-fold increase/decrease in the level of translation of the target protein (Meleady et al. 2012b). All of these candidates demonstrate this modest change in translation ranging from 1.67-2.73 with *LETM1* exhibiting the highest level of translational de-repression. Of course

using the term de-repression is premature at this point as further validation would be required as a means to assess the totality of miR-23s influence on these targets.

Detecting translational de-repression has been observed in the past to be easier than translational inhibition despite both eliciting modest impacts on the translatoome (Martinez-Sanchez, Murphy 2013). From this perspective, it would be worth carrying out label-free mass spectrometry on the parental CHO-SEAP cell line upon the transient overexpression of miR-23 such as in the case of miR-7 overexpression with subsequent proteomic analysis (Meleady et al. 2012a). Transient over-expression of miR-23a/b with subsequent analysis of each of the above targets on both the mRNA and protein levels would be the next step in elucidating their potential as true targets. Furthermore, siRNA inhibition of each target in stable CHO clones engineered to deplete miR-23 would be a means to determine which of the panel of targets is mediating the observed phenotype of enhanced SEAP mRNA transcription contributing to elevated specific productivity and those candidates whose expression is potentially symptomatic and not causative of the induced phenotype. Lastly, cloning the 3'UTR of the highest priority targets downstream of a reporter gene would be required to validate the potential suppressive role of miR-23a/b.

LETMI presents itself as the most attractive and high priority candidate in relation to being a target of miR-23. As a means to account for variation between clones, all clones were grouped together i.e. triplicate samples of miR-23 sponge clone 4 and 6 being analysed as 6 miR-23 replicates. This would allow for the variation within clones themselves to be accounted for with only protein candidates under the influence of miR-23 demonstrating significant differences between the control groups. When replicates from both miR-23 and miR-NC groups were randomised and compared, two proteins were found to be DE that did not overlap with the final DE list. This was performed to assess whether identifications were a result of random chance. *LETMI* demonstrated no DE between control groups while not exhibiting DE when both miR-23 sponge clones were compared. To further refine the list and potentially eliminate clonal variation and background noise, more miR-23 sponge clones and control clones could be selected and assessed for differential protein expression.

4.6 Integrated “omics” profile of CHO cells with varying growth rates

The use of miRNAs in CHO cell engineering has flourished in the past few years and have been secured in the toolbox of viable engineering strategies (reviewed recently in (Jadhav et al. 2013)) and highlighted in the stable manipulation of miR-23 in CHO-SEAP cells. Numerous DE profiles have been carried out to date in an attempt to identify miRNAs involved in the regulation of bioprocess relevant phenotypes including temperature shift (TS) (Gammell et al. 2007, Barron et al. 2011a), growth phases (Hernandez Bort et al. 2012), apoptosis induction (Druz et al. 2011) and CHO cells grown in serum-containing medium (Jadhav et al. 2013). These profiles have resulted in stable CHO cell manipulation of candidates such as miR-7 (Sanchez et al. 2013b) and miR-466h (Druz et al. 2013) enhancing bioprocess phenotypes.

With the advent of biphasic culture, accumulation of cell density is crucial before entering the “production phase” whereby growth is compromised to the benefit of specific productivity. We sought to potentially enhance growth early in culture using miRNAs derived from this profile with an application in temperature shift culture, published in BMC Genomics in 2012 (Clarke et al. 2012).

Additionally, by acquiring transcriptomic data, mRNA and protein, a systems level perspective of the molecular networks surrounding CHO cell growth was revealed, demonstrating gene ontology enrichment for cellular processes such as translation and RNA splicing. Furthermore, the integration of all three datasets facilitated the identification of potential mRNA targets under the direct regulatory control of the DE miRNAs. This approach also highlighted targets that can be scored poorly by prediction algorithms, Rab14-miR451 (Wang et al. 2011a), in addition to identifying “non-seed” mRNA targets whose miRNA: mRNA interaction does not follow the binding criteria by which most prediction algorithms are based upon (Pasquinelli 2012).

Given the large inherent genetic heterogeneity between CHO cell lines, demonstrated when comparing the genomes of 6 CHO cell lines including CHO-K1, DG-44 and CHO-S against the ancestral sequenced CHO-K1 genome (Lewis et al. 2013), it was essential to minimise variation through the careful selection of CHO cells that would form the basis of the DE profile. Chromosomal heterogeneity has also been observed even among cells within a clonal population (Wurm, Hacker 2011), not to mention the genetic

heterogeneity associated with recombinant CHO cell line development (Matasci et al. 2011).

All things considered, the study sought to minimise variation through the careful selection of mAb-secreting CHO cell lines that were derived from the same transfection pool, exhibiting a range of growth rates spanning from 0.011-0.044 hr⁻¹. To further eliminate biological noise and expose variations related to the proliferation phenotype, sister clones selected demonstrated a similar level of cell specific productivity of 24 pg/cell/day (± 3), an attribute that commonly varies with growth rate (Barron et al. 2011a)

4.6.1 Identification of miRNAs associated with cellular growth rate

Of the 51 DE miRNAs identified within this study, a number of them have previously been associated with cell growth. Several miRNAs that were found to be upregulated form part of a well-studied oncogenic cluster, miR-17~92 (e.g. miR-17, miR-18a, miR-18b, miR-20a, miR-20b and miR-106a) (Olive, Li & He 2013). This cluster has been shown to be directly activated by the oncogenic transcription factor *Myc* (Dews et al. 2006b) and *E2F1* (O'Donnell et al. 2005a). Its repression has also been demonstrated to be influenced by p53 (Yan et al. 2009b). Individual cluster components contribute to the clusters pleiotropic function through the regulation of various phenotypes such as proliferation (*p21*), apoptosis (*Bim*) and angiogenesis (*Tsp1*) (Olive, Jiang & He 2010a) (**Fig. 1.3 of the Introduction**). This miRNA cluster has previously been identified in CHO (Hernandez Bort et al. 2012). Functional redundancy has been suggested by Hackl *et al.*, by identifying the conservation of MREs within 26 validated targets of this cluster through next-generation sequencing (such as *E2F1*, *CCND1*, *BCL211* and *PTEN*) in CHO (Hackl et al. 2011).

Among the 51 miRNAs DE within fast growing CHO cells, 15 make up the lesser characterised miR-passenger (miR*) strands. Thought initially to be a by-product or carrier (Guo, Lu 2010) of miRNA processing, it is now emerging that miRNA* strands accumulate to substantial levels *in-vivo*, indicating a functional role (Chiang et al. 2010). Bioinformatics' analysis has demonstrated that a substantial fraction of miR* species are conserved throughout vertebrate evolution with the greatest degree of conservation lying within their seed regions and MREs (Yang et al. 2011). Growing evidence has supported the functional role miR* strands play in genetic regulation such as target reporter gene suppression as a function of endogenous miR: miR* reads (Yang et al. 2011), the

generation of mature miRNAs from both arms of a miRNA precursor (Okamura et al. 2008), the sporadic switch from the dominantly selected miRNA (Griffiths-Jones et al. 2011), the capacity of particular miRNA precursors to generate comparable levels of mature miRNAs from both arms (miR-3p/5p) and ultimately their role in various disease states such as arthritis (Niederer et al. 2012) and cancer (Chang et al. 2013).

13 of the 15 miR* strands DE in fast growing CHO cells were observed to be upregulated. In some cases (miR-34a* and miR-23b*), this apparent increase in miR* strand accumulation was not accompanied by an increase in transcription based-on the constant levels of the mature guide miRNA strand. This could be as a result of a phenomenon known as target-mediated miRNA protection (TMMP), a proposed mechanism by which increased target availability can lead to the accumulation of miRNAs protected by exoribonuclease turnover through target association (Chatterjee et al. 2011, Chatterjee, Grosshans 2009).

miR-34a* has been observed to be down-regulated in Rheumatoid arthritis increasing apoptosis resistance in synovial fibroblasts through the regulation of *XIAP* with its overexpression inducing apoptosis (Niederer et al. 2012). This is in contrast to the observation of its increased expression in fast growing CHO cells. However, the transient overexpression of miR-34a* in CHO did correlate with this observation. Other miR* strands over-represented are part of the well characterised miRNA clusters such as the miR-17~92 and miR-23b~27b/miR-23a~27a clusters. There have been observations of functional redundancy between partner strands through target sharing or pathway overlap. One study demonstrated the induction of prostate tumour growth through co-ordinated suppression of *TIMP3* by both the guide miRNA, miR-17-5p, and the passenger miR-17-3p (Yang et al. 2013). The miR: miR* relationship is further exemplified with the observation that both miR-17-5p and miR-17-3p act synergistically to induce hepatocellular carcinoma through the interference of independent signalling pathways via knockdown of *PTEN* (-5p), *GalNT7* and *vimentin* (-3p) (Shan et al. 2013). This would suggest that miR* strands identified as DE could mimic their guide counterparts.

Several miRNAs found to be down-regulated as growth rate increased included miR-338-3p, miR-204, miR-206 and miR-30e. One interesting observation was the down-regulation of miR-30e in fast growing CHO cells and its up-regulation in CHO cells subject to temperature shift growth arrest (Barron et al. 2011b). miR-451 has been shown

to inhibit growth (Li et al. 2013) and induce apoptosis (Bian et al. 2011) upon its overexpression whereby it was observed to be down-regulated in fast growing CHO cells. It is extensively reported within the literature that miRNAs are both species and cell type/tissue specific. The nature of this variance is dependent on the availability of miRNA targets and the sensitivity of the molecular pathways subjected to translational influence. Several miRNAs play a recurring role within the literature, such as miR-34a and the oncogenic cluster miR-17~92, earning themselves an almost p53-like status. From the list of miRNAs found to be DE in our fast growing CHO cell phenotype, many correlated well with reported function in the literature in addition to a subset of miRNAs previously studied in CHO such as members of the miR-17~92 cluster (Jadhav et al. 2014) and miR-30e (Barron et al. 2011a).

4.6.2 Transient screening of miRNA

Numerous miRNA profiling experiments have been carried out in CHO cells to include subsequent screening strategies (Barron et al. 2011b, Jadhav et al. 2014, Strotbek et al. 2013, Jadhav et al. 2012). One such strategy began with an initial screen of 879 miRNA mimics at a high concentration of 1 μ M isolating candidates based on improved volumetric productivity (Strotbek et al. 2013). Although this study identified that the stable overexpression of miR-557/-1287 improved viable CHO cell density and specific productivity, it highlights the potential loss of information because of the assessment of a single phenotype (volumetric productivity) or the screening of only miRNA mimics. Selection of the host cell line that will form the basis of a screening project will also contribute to the outcome of the screen. This primarily is due to the variation in the miRNA/mRNA expression across species, tissues and cell types. This is a critical factor to consider when the cell system forming the basis of the DE profile is different to that of the cell type exposed to transient evaluation. This potential variation was evident within our primary screen with candidates such as miR-23b*, miR-34a*, miR-206 and miR-639 inducing a contrary phenotype.

The absence of phenotypic conservation within the CHO-SEAP screen could be due to various reasons. One study demonstrated that predicted mRNA targets of highly conserved tissue-specific miRNAs were expressed at low abundance in comparison to tissues that did not express these tissue specific miRNAs. It also highlighted that highly expressed genes were enriched that do not contain MREs within their 3'UTR for certain

tissue specific miRNAs (Sood et al. 2006). A study using a miRNA decoy library found that over 60% of miRNAs had no discernible activity which indicated that the functional “miRNome” may be quite limited and that only the most abundant miRNAs mediate target suppression (Mullokandov et al. 2012). It has been identified that a “threshold” relationship is apparent between miRNAs and their cognate mRNA targets (Pasquinelli 2012) and that a non-linear trend exists between a targets transcription and translation (Mukherji et al. 2011). Published screens as mentioned previously have reported a small numbers of impactful miRNAs which is in keeping with the results observed during transient evaluation.

The fundamental point to take from these observations is that a miRNAs influence is complex, to say the least. The observation that many miRNA candidates did not elicit the anticipated phenotype as suggested from the profile does not rule out the potential for these miRNA candidates to control CHO cell growth in a different CHO cell type. It is possible that the molecular make-up of the CHO-K1-SEAP cell line used for transient screening is different to that of the fast and slow CHO clones, thereby presenting a wealth of differing molecular targets.

4.6.2.1 miR-23b*

Of the 15 miR passenger strands found to be DE in fast growing CHO cells, miR-23b* exhibited the highest increased fold change of 121. Very little is known about the specific role that miR-23b* plays. However, a recent report has identified it to be elevated in renal cancers (Liu et al. 2010a) mediating its function through inhibition of the mitochondrial tumour suppressor Proline Oxidase (POX) or alternatively Proline Dehydrogenase (PRODH), correlating with its increased abundance in fast-growing CHO cells. Transient overexpression, however, of miR-23b* demonstrated contrary results to both the literature and the profile, with miR-23b* inhibition being demonstrated to elicit a similar outcome (Liu et al. 2010a). A maximal inhibition of ~70% peak cell density was observed upon miR-23b* overexpression with a mild induction of cell death. A more in-depth analysis using the Guava Nexin assay was carried out to determine the degree of influence this miRNA played in apoptosis. It was noted that there was an almost 2-fold increase of cells entering early apoptosis ($p \leq 0.05$) at both 48 and 96 h. The results are in contrast to the reports above and suggests that the apparent increase in miR-23b* expression is a by-

product of the changing molecular environment and not a causative influence on the fast growing phenotype.

One potential mechanism for the increased levels of this passenger strand in fast growing CHO cells is the recently hypothesised target-mediated miRNA protection (TMMP). Although the reciprocal relationship between miRNAs and their targets is not a new concept (Pasquinelli 2012), TMMP is an experimentally validated mechanism by which mRNAs, once thought to be passive targets of miRNAs, prevent the active turnover and degradation of miRNA duplex components by cytoplasmic exoribonucleolytic enzymes such as XRN-2 in *Caenorhabditis elegans* (Chatterjee, Grosshans 2009) and XRN-1 in humans (Bail et al. 2010) (**Fig. 4.10**). Target availability has been shown to be a stabilizing factor for Ago-bound mature miRNAs (Chi et al. 2009). Chatterjee *et al.*, has demonstrated that target availability can also exhibit a protective effect on certain miR: miR* strands (Chatterjee et al. 2011) (**Fig 4.10 C**). It potentially plays a role in RISC and non-RISC bound miRNAs adding further complexity to the regulatory role that mRNAs can elicit on endogenous miRNAs.

Figure 4.10: Enzyme-mediated microRNA turnover with miR* strand TMMP

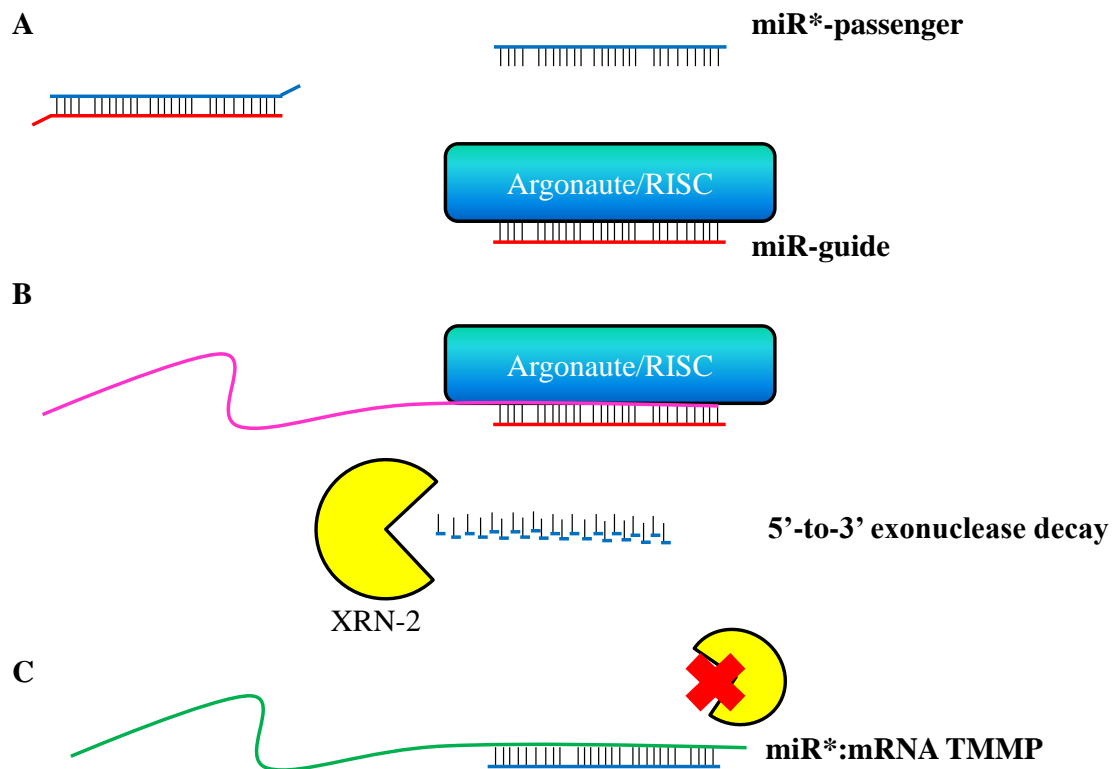


Figure 4.10: A) Shows a pre-miRNA duplex with 3' 2 nt overhangs being loaded into the Ago/RISC protein complex with selection of the miRNA **guide/passenger** strand based on thermodynamic stability of the 5' end B) **mRNA** target binding by RISC directed by the miRNA guide strand with exonuclease decay of the free passenger (miR*) strand by XRN-2 C) **mRNA** target availability prevents decay of miR* strands through this TMMP process.

From the raw TLDA profiling data of the expression patterns of miR-23b and miR-23b* (**Appendix Fig. A10**), it was observed that in slow growing CHO cells, a classical expressional relationship between star and guide strand existed, one strand present at high levels (miR-23b) and one strand at low levels (miR-23b*). However, in Fast-growing cells, expression levels of both strands were comparable. It has been shown that some miRNA precursors can be processed to produce significant amounts of mature miRNAs from both arms (Okamura et al. 2008), in addition to arm-switching being tissue specific (Griffiths-Jones et al. 2011). The increase in miR-23b* levels in fast growing CHO cells versus slow with no associated change in the levels of mature miR-23b suggests that arm-switching is not taking place in this instance. However, without assessing the transcriptional levels of the precursor pre-miRNA, it cannot be concluded whether an increase in transcription is compensating for the steady mature miR-23b levels or if arm-

switching was taking place. A recent report has suggested that the abundance of target transcript is primarily more selective at “protecting or mediating arm-switching” of miR* strands over their more abundant guides (Kang et al. 2013b), perhaps due to the inherently low miR* copy number. This dramatic impact on miR* strands was demonstrated by Kang and colleagues whereby a 10-fold increase of miR-7b was observed compared to ~250-fold for miR-7b* in stable sponge models (Kang et al. 2013b). One major factor for consideration from the perspective of “does the level of miR-23b* contribute to this fast growing phenotype?” is whether the apparent elevated levels of miR-23b* are associated with a functionally active RISC or are they merely a by-product of miRNA processing? Stable depletion of miR-23b* in a fast growing clone from the profile was observed to elicit a reduction in growth (Data not shown) suggesting that in this cell, miR-23b* may contribute functionally.

From a productivity perspective, miR-23b* overexpression resulted in a maximum reduction in SEAP production of 55%. This was attributed to the reduced cell density, similar to transient miR-7 overexpression in the same CHO-K1-SEAP cell line (Barron et al. 2011b). Although an increase in cell specific productivity is often observed upon growth arrest, miR-23b*-mediated growth arrest did not generate such a phenotype. As miR-23b* has been linked with the G₂-phase of the cell cycle through POX interaction (Liu et al. 2009), it is possible that no significant increase in specific productivity is a result of the potential arrest in G₂ whereas high specific productivity is often associated with G₁ phase arrest (Bi, Shuttleworth & Al-Rubeai 2004, Carvalhal, Marcelino & Carrondo 2003).

Although miR-23b* overexpression did not present itself as an attractive option for CHO cell engineering, a reversal of this observed phenotype would be desirable. Evidence supporting reversing CHO cell phenotype was observed by Sanchez and colleagues (Sanchez et al. 2013b) upon the stable depletion of miR-7 despite its overexpression resulting in cell cycle arrest with reduced product yields (Sanchez et al. 2013a, Meleady et al. 2012b, Barron et al. 2011c). Although little is known about the functionality of miR-23b*, it is part of a well characterised miRNA cluster implicated in human disease, miR-23a~27a~24-2 and its paralog miR-23b~27b~24-1 (Discussed briefly in the Introduction). The pleiotropic functionality of this miRNA cluster is evident from the multiple processes regulated by its members such as metabolism, oncogenesis, proliferation or differentiation, with the additional observation from profiling studies in various disease

conditions that all three miRNA members are simultaneously deregulated (Chhabra, Dubey & Saini 2010b). Individual members have been documented as potent modulators of cellular processes such as miR-23b; found to regulate a plethora of phenotypes including apoptosis, angiogenesis and invasion (Zhang et al. 2011). Interestingly, both miR-23b and miR-23b* have been implicated in mitochondrial function, ultimately contributing to metabolite introduction to the TCA cycle under the regulation of the oncogenic *c-MYC* (**Fig. 4.11**).

In the case of miR-23a/b, *c-MYC* suppresses their expression thus derepressing inhibition of glutaminase (*GLS*) and mediating the conversion of glutamine to glutamate (Dang 2010). In the case of miR-23b*, *c-MYC* enhances its expression levels thereby decreasing *POX* expression (Liu et al. 2009). Genetic alternations linking the regulation of glucose metabolism in cancers are evident by the aberrant expression of the oncogenic transcription factor, *c-myc*, which directly regulates the expression of glucose metabolic enzymes and additionally genes involved in mitochondrial biogenesis (Li et al. 2005, Eilers, Eisenman 2008). Mitochondrial dysfunction has been observed in various metabolic diseases including obesity, aging, diabetes and cancer, with miRNAs emerging as key regulators of mitochondrial proteins encoded by nuclear genes (Tomasetti, Neuzil & Dong 2013). Re-programming of mitochondrial metabolism to depend on glutamine catabolism circumvents the requirement of glucose as a primary carbon source, starving the TCA cycle of essential metabolites as observed via the “Warburg effect” (Dell'Antone 2012). Glutaminolysis, conversion of glutamine to glutamate, is mediated by the enzyme glutaminase (*GLS*) of which miR-23a/b have been shown to target of whose transcription is repressed by *c-myc* (Gao et al. 2009). The implication of miR-23a/b in cellular bioenergetics encouraged the exploration of its stable inhibition in CHO cells.

Figure 4.11: Mitochondrial metabolic contribution of miR-23b and miR-23b*

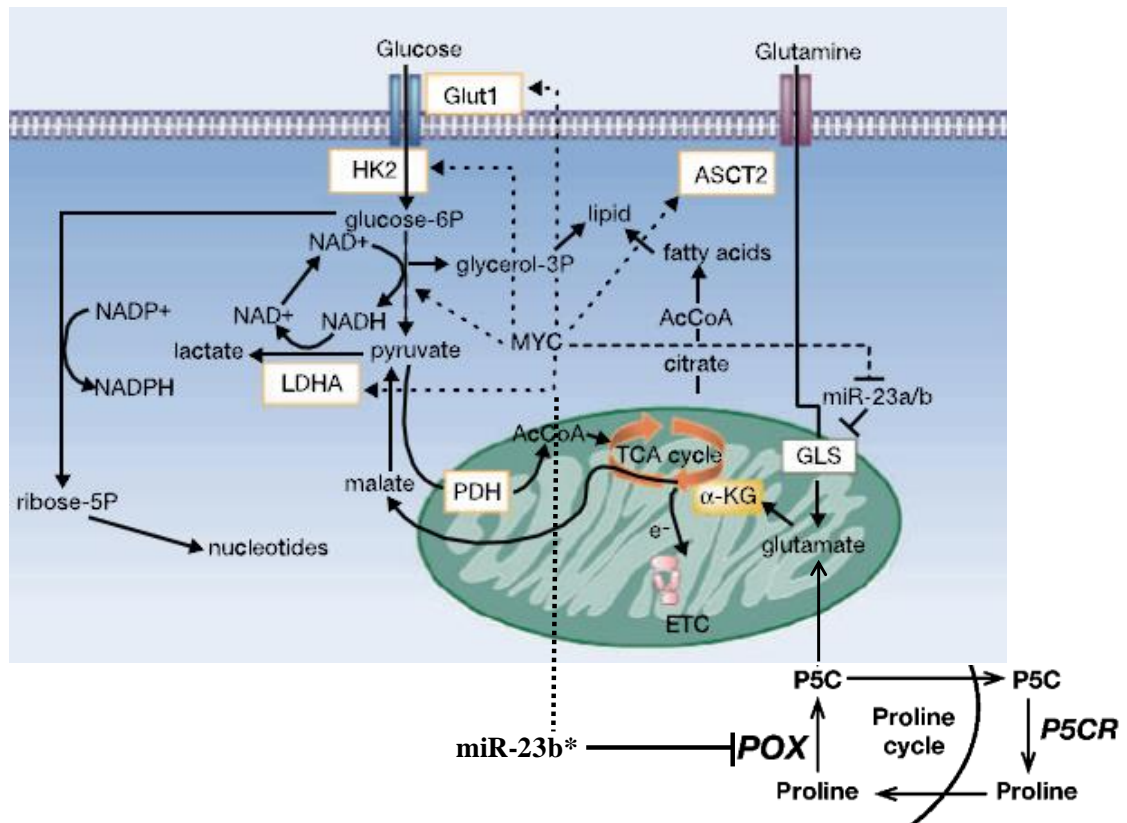


Figure 4.11: The influence that miR-23a/b suppression plays in the release of Glutaminase under c-MYC suppression thus alternatively feeding mitochondrial respiration through glutamate metabolism independent of glucose. Additionally, as an alternative fuel source to glucose, miR-23b* also contributes to mitochondrial function through proline metabolism. Figure was sourced and modified from (Dang 2010) and (Liu et al. 2009).

4.6.2.2 miR-34a/34a*

miR-34a* was found to be elevated in fast growing CHO cells and displayed a similar but less dramatic expression pattern with its partner strand miR-34a as miR-23b* demonstrated with its counterpart. Given the extensive characterisation of miR-34a in the literature, we thought it prudent to evaluate the phenotypic impact of both miRNAs on the CHO cell despite only the star strand being DE. Transient transfection of either miRNA resulted in a similar phenotype: i.e. detriment to cellular proliferation and viability. This also supported a previous notion of miR:miR* components demonstrating functional redundancy. miR-34a has been shown to be transcriptionally activated by the “master tumour suppressor” *p53* (Hermeking 2009), a transcription factor capable of halting cell cycle progression or ultimately activating programmed cell death (PCD) (Hermeking 2007). Ectopic expression of miR-34a has been observed to induce G₁/S-

phase arrest through direct inhibition of pro-cell cycle targets such as *CCND1* and its binding partner *CDK6* (Sun et al. 2008b). Its counterpart on the other hand, miR-34a*, is less well characterised and has been validated to target a member of the family of apoptosis inhibitors, X-linked inhibitor of apoptosis (*XIAP*) (Niederer et al. 2012). Reduced expression of *XIAP* has been correlated with a reduction in the level of expression of *CCND1* (Cao et al. 2013) inducing G₁-phase arrest while another study demonstrated that selective inhibition of *XIAP* arrested cells in S and G₂/M-phase with an associated deregulation of targets such as *cyclin-B1* and *CDK1/2* (Wang et al. 2013).

The small molecule inhibitor of *XIAP*, Embelin, induced the shift in expression of apoptosis related proteins *Bcl-1*, *Bax* and *Bcl-xL* destabilising the mitochondrial membrane potential allowing for the release of cytochrome c (Wang et al. 2013), supporting the 30% reduction in cell viability reported for miR-34a* overexpression in CHO in addition to a similar observation of its overexpression in synovial fibroblasts (Niederer et al. 2012). Numerous anti-apoptotic genes have been validated within the literature as direct targets of miR-34a including *Bcl2* (Cole et al. 2008) and the inhibitor of apoptosis (IAP) member, *survivin* (Shen et al. 2012) supporting its impact on CHO cell viability, similar to miR-34a*. A recent study has identified *XIAP* to be a target of miR-34a to add to the extensive list of validated targets (**see table 4.2**) (Truettner, Motti & Dietrich 2013). On top of this, despite limited studies of miR-34a*, the realisation that transient overexpression of both pre-miRs mediate similar phenotypes, it is possible that both miRNAs share more common targets, beyond *XIAP*, associated with proliferation and apoptosis than is currently known.

Table 4.2: Validated targets of miR-34a

Cellular process	Gene	Gene name	Reference
Cell cycle	CDK4 CCNE2 CCND1 CDK6	Cyclin-dependent kinase 4 Cyclin E2 Cyclin D1 Cyclin-dependent kinase 6	(He et al. 2007a) (He et al. 2007a) (Sun et al. 2008b) (Sun et al. 2008b)
Apoptosis/ p53 pathway	BCL2 SIRT1 YY1 BIRC5	B-cell leukemia/lymphoma 2 Sirtuin, silent information regulator 1 Ying yang 1 transcription factor (TF) Survivin	(Cole et al. 2008) (Yamakuchi, Ferlito & Lowenstein 2008) (Chen et al. 2011a) (Shen et al. 2012)
Wnt signalling/ metastasis	JAG1 WNT1 NOTCH1 LEF1 WNT3* CTNNB1* LRP6* MTA2+ TPD52+ AXL+	Jagged 1 Wingless-related MMTV integration site member 1 Notch homolog 1, translocation-associated Lymphoid enhancer binding factor 1 Wingless-type MMTV integration site member 3 Beta-catenin Low density lipoprotein receptor-related protein 6 Metastasis associated 1 family member 2 Tumor protein D52 AXL receptor tyrosine kinase	(Hashimi et al. 2009) (Hashimi et al. 2009) (Du et al. 2012) (Kim et al. 2011) * (Kaller et al. 2011b) +
Cancer	MYCN CD44 NANOG SOX2	v-myc myelocytomatosis viral related oncogen N Heparan sulphate proteoglycan NANOG homeobox transcription factor SRY (sex determining region Y)-box 2 TF	(Cole et al. 2008) (Liu et al. 2011) (Choi et al. 2011) (Choi et al. 2011)
Mitotic signalling	MET MAP2K1 (Silber et al. 2012) RRAS PDGFRA	Met proto-oncogen (hepatocyte growth factor receptor) Mitogen-activated protein kinase 1 (MEK1) Related RAS viral (r-ras) oncogen homolog Platelet-derived growth factor receptor, alpha	(He et al. 2007c) (Ichimura et al. 2010) (Kaller et al. 2011b) (Silber et al. 2012)
Oncogenic Transcription	E2F3 MYB MYC	E2F transcription factor 3 v-myb myeloblastosis viral oncogen homolog v-myc myelocytomatosis viral oncogen homolog	(Welch, Chen & Stallings 2007) (Navarro et al. 2009) (Christoffersen et al. 2010)
Metabolism	ACSL1 LDHA IMPDH	Acyl-CoA synthetase long-chain family member Lactate dehydrogenase A IMP (inosine 5'-monophosphate) dehydrogenase	(Li et al. 2011b) (Kaller et al. 2011b) (Kim et al. 2012)
Post-translational modifications	FUT8	α -1,6-Fucosyltransferase	(Bernardi et al. 2013a)

Table sourced and modified from (Bader 2012)

A maximum reduction of ~75-80% in SEAP activity was observed which was in parallel with an almost 90% drop in maximal cell density upon overexpression of both miR-34a/-34a*. As seen before, this decrease in yield is due to the limited number of actively

producing cells within the bioprocess. One interesting observation however was the increase in normalised productivity for cultures treated with pre-miR-34a (section 3.1.2.3.1) compared to those treated with pre-miR-34a* (section 3.1.2.2.2). The maximum increase of ~80% in normalised productivity in CHO-SEAP cells may be perhaps due to the role that miR-34a plays in G₁-phase arrest (Sun et al. 2008b) compared to the association of miR-34a* with G₂ (Wang et al. 2013).

4.6.2.3 miR-181d/200a

We pursued miR-200a to assess its possible functional conservation, low in relapsed patients subsequent to prostatectomy (Barron et al. 2012), in CHO cells and observed a reduction in cell density of 20-65% upon its overexpression (n = 7). This reduced cellular proliferation coincided with improved normalised productivity, however, in some instances volumetric SEAP yields were enhanced, suggesting that normalised productivity was improved irrespective of growth. A study by Hennessy and colleagues (Hennessy et al. 2010) found miR-200a to be down-regulated in glucose non-responsive MIN6 cells. Transient inhibition of miR-200a decreased glucose-stimulated insulin secretion (GSIS) which seems in keeping with the observation that its overexpression in CHO cells potentially enhances SEAP production. The tumour suppressive nature of miR-200a is exemplified in the study by Saydam and colleagues (Saydam et al. 2009) whereby the expression of miR-200a was found to be ~25-fold down-regulated in meningiomas with targets such as *Cyclin-D1* and *β-catenin* (Su et al. 2012). Previous characterisation of this miRNA to regulate *CCND1* coincides with our observation of reduced cell growth with enhanced normalised productivity (Kumar, Gammell & Clynes 2007). This would further suggest that miR-200a knockdown might improve CHO cell growth thus allowing for the rapid accumulation of cellular biomass. Interestingly, miR-200a was observed to be involved in a positive-feedback loop through the translational inhibition of histone deacetylase 4 (HDAC4) in human hepatocellular carcinoma implicating a role in transcription (Yuan et al. 2011). The specificity of HDACs is an area of continuous research as to whether a set panel of genes or global gene expression is influenced by their mechanism of action (Haberland, Montgomery & Olson 2009). The potential of miR-200a to interfere with the translation of HDAC4 could potentially contribute to the increased specific productivity independent of growth, if its panel of targets excluded growth related genes for example.

The transient over-expression of miR-181d demonstrated a less potent and consistent phenotype than miR-200a when screened in CHO-SEAP cells. Although selected for its potential tumour suppressor influence, overexpression resulted in a varied suppressive influence on CHO cell growth. One study reported that miR-181d, miR-34a and miR-193b were down-regulated subsequent to *MAPK* activity (Ikeda et al. 2012). Although miR-181d and the miR-181 family have been validated to target various cancer associated genes such as *k-ras*, *bcl2* (Wang et al. 2012), *Mcl-1* (Ouyang et al. 2012) and *Tcl1* in chronic lymphocytic leukemia (Pekarsky et al. 2006), the expression profile of these targets and fundamentally the retention of target conservation will dictate the potency of this miRNA to elicit an effect in CHO. Of the two miRNAs screened, miR-181d and miR-200a, it would be interesting to explore the potential synergy between the two however; miR-200a would be a prime candidate for stable inhibition, in the future.

4.6.2.4 miR-532-5p

It has been suggested that lessons can be learned from nature such as mimicking the differentiation of B-lymphocytes into plasma cells (Dinnis, James 2005) with a view to potentially improving the secretory capacity of host rCHO cells. Numerous miRNAs have been identified to be directly involved in glucose-stimulated insulin secretion (GSIS) such as miR-375 (Poy et al. 2004) and miR-124a (Lovis, Gattesco & Regazzi 2008) in pancreatic islet β -cells. miR-532-5p was found to be down-regulated in glucose non-responsive MIN6 β -cells and was explored for its potential role in CHO cell productivity (Hennessy et al. 2010).

Transient overexpression of miR-532-5p (Guide strand) had no impact on cellular proliferation or viability but did impact negatively on specific productivity, ranging from a ~20-30% reduction. Without assessing intracellular SEAP levels, it would be premature to attribute this observed phenotype to a reduction in the secretory capacity of treated cells or an impact on rSEAP transcription. In an attempt to reverse this phenotype, anti-miRs designed against miR-532-5p were transiently transfected into CHO-K1-SEAP cells with no impact on volumetric productivity. It was noted that the expression of miR-532-5p in fast growing CHO cell clones was low (**Appendix fig. A11**) upon analysis of the raw C_T values from the original profiling study. It is possible that if miR-532-5p is related to a fast growing phenotype then its low level of expression could be similar in CHO-K1-SEAP. If that was the case, further inhibition may not yield a measurable

phenotype. However, upon exploring transient knockdown of this miRNA to mediate enhanced SEAP secretion, there was a mild increase of around 20-30%, at its highest, in cell numbers on day 2-4 of culture, suggesting that stable inhibition might be an interesting route to pursue.

4.6.2.5 miR-639

miR-639 expression was increased in fast growing CHO cells, yet when over expressed in our model CHO-K1-SEAP cell line, it caused a contrary but consistent reduction in cellular growth with an associated increased normalised productivity. One study showed miR-639 to be upregulated in the serum samples of patients with bladder cancer in an attempt to evaluate the potential of miRNAs as candidates to assess prognosis and as diagnostic biomarkers (Scheffer et al. 2012). This suggests it could act as an oncogene in addition to a report of it targeting the tumour suppressor *p21* (Wu et al. 2010). Despite the suggestion from the literature, the transient overexpression of miR-639 induced a reduction in CHO cell proliferation. It is possible that the increased expression of miR-639 is a result of the phenotype and not a cause of it. The increase in normalised productivity indicates that the observed reduced growth could be due to an arrest in G₁ phase of the cell cycle potentially inducing an associated highly transcriptionally active production phase (Kumar, Gammell & Clynes 2007). Despite its lack of characterisation, miR-639 presents itself as an attractive candidate for stable depletion.

4.6.2.6 miR-206

Reduced expression of miR-206 in fast growing CHO cells agreed with numerous studies reporting its decreased expression in gastric cancer samples and cell lines (Zhang et al. 2013), estrogen-dependent ER α -positive breast cancer (Kondo et al. 2008), melanoma cell lines (Georgantas et al. 2014) and laryngeal cancer (Zhang et al. 2011). Several characterised targets of this miRNA support its tumour suppressive capacity such as *CCND2* (Kondo et al. 2008), *CCND1*, *CDK4* (Georgantas et al. 2014), *VEGF* (Zhang et al. 2011) and *Notch3* (Song, Zhang & Wang 2009). It was interesting to observe that transient inhibition of miR-206 in CHO-K1-SEAP cells mediated a reduction in CHO cell proliferation by 30% with an associated elevated normalised productivity of 15% on day 4 of culture.

The reason for its negative impact on CHO cell growth upon its transient inhibition remains elusive. Reports of this miRNA in apoptosis suggests the potential for it to prolong a viable production phase upon its inhibition (Wang et al. 2012). The observation of enhanced normalised productivity suggests that cell cycle interference may be at the G₁ phase. It would be interesting to pursue its transient overexpression as a means of assessing any conserved impact on CHO cell growth through targets such as *CCND1/2* or *CDK4*.

4.6.3 Final miRNA screen comments

Several candidate miRNAs were highlighted from the transient screening process, including miR-34a/34a*, miR-23b*, miR-200a, miR-206 and miR-639, some of which were more potent than others and all of which demonstrated growth inhibition. The observation that numerous miRNAs selected for screening either had no phenotypic impact or the opposite of what was expected could be due to a point made earlier in that over 60% of miRNAs expressed in any given cell type have no apparent functional influence (Mullokandov et al. 2012). Additionally, the varied expression pattern of miRNAs and mRNAs across various cell lines would suggest that miRNAs screened in the CHO-K1-SEAP cell line could elicit a varied phenotype given the potential differences in the expression profile of its mRNA targets. In essence, a miRNAs function is dependent on the abundance and sensitivity of its gene targets.

The non-linear relationship between miRNA abundance and mRNA expression (Mukherji et al. 2011) potentially contributes to a layer of complexity when assessing miRNA function. When screening miRNAs in combination, a compromise has to be made when selecting the concentration of each miRNA under investigation. Exogenously introducing a high concentration, as in our transient screening process (50 nM), could potentially saturate the miRNA biogenesis machinery when assessing multiple miRNAs in combination leading to a potential transfection concentration of 150 nM and upward. Aberrant expression of miRNA biogenesis components have been associated with negative cellular phenotypes, for example Dicer knockdown inducing G₁ arrest in MCF-7 breast carcinoma cells (Bu et al. 2009) and the induction of mouse embryonic lethality (Bernstein et al. 2003). We demonstrated that siRNA-mediated dicer knockdown was detrimental to the CHO cell phenotype both inducing apoptosis and inhibiting cellular proliferation, an observation also made by others in CHO (Hackl et al. 2014a). A CHO

specific observation was made that both Dicer expression and global miRNA abundance were enhanced in CHO cells cultured in serum containing media (Hackl et al. 2011, Hackl et al. 2014a). These observations not only exemplify the beneficial role that miRNAs play in sustaining and maintaining cellular homeostasis but also that interference in global miRNA processing can be detrimental to the cell. Compromising miRNA concentration when screening multiples can potentially dilute miRNA activity to a point where a phenotype is not perturbed which ties into this titrational effect that was previously mentioned. Several miRNA candidates from the fast versus slow profile were assessed in combination such as miR-338-3p, miR-455-3p/5p and miR-409-3p, members from the panel screened that did not generate a significant/consistent phenotype. Additionally, in combination with each other, a more consistent or potent phenotype was observed.

Not observing a phenotype upon transient manipulation of these miRNAs does not prove that they do not play a role in the phenotype in which they were implicated. However, it is possible that a large number of DE miRNAs in any profile are a result of the phenotype and not the cause of it. The CHO-SEAP cell line is innately a fast growing cell line by comparison to the fast growing clones used in the original profiling experiment. This would suggest that a similar miRNA profile could be shared between both cell lines in relation to growth. As a result, further manipulation of particular candidates may not elicit a phenotype. Furthermore, the CHO-SEAP cell line could potentially demonstrate a completely unique miRNA and mRNA profile thus not expressing targets of these miRNAs. This suggests the benefit of profiling a panel of CHO cell lines from an industrial point of view to determine the diversity of a particular targets across a range of cell and product types. It would also suggest that profiling of candidates from a profile should be carried out in the same cell line as used in the original profiling such as in the case of miR-7 (Barron et al. 2011b) and miR-466 (Druz et al. 2011) in CHO.

By assessing and understanding the miRNA/mRNA expression patterns of CHO cell lines two things can potentially be achieved. The first is the prediction of CHO cell performance if miRNA/mRNA expression patterns are correlated with production phenotypes such as growth or productivity. A study like this was carried out by Clarke and colleagues which predicted CHO cell specific productivity to within 4.44 pg/cell/day by using microarray technology generating a panel of 287 genes associated with productivity (Clarke et al. 2011b). miRNA profiles across various CHO cell types, could help to predict which CHO cells will respond to miRNA intervention.

Secondly, rudimentary inducible systems could be developed if miRNA expression profiling data has been catalogued. For example, the cell cycle inhibitor *p27* could be engineered to include a miRNA sponge that contains MREs for a miRNA whose temporal expression profile is confidently understood within a given CHO cell. If this miRNA has a high expression early into culture then *p27* will not be translated thus allowing for the propagation of exponential growth (**Fig. 1.7 of Introduction**). If this miRNA is naturally switched off or down-regulated in mid-late exponential growth then *p27* translation would be de-repressed inducing a growth arrest in G₁ mediating an artificial, high producing, temperature-shift like phenotype. This system could potentially provide industry with an alternative to the use of exogenously inducible systems or the exploration of temperature sensitive promoters. Profiling of tens or hundreds of CHO cell lines may be costly but could present itself with numerous benefits such as those mentioned above. The screening process also highlights the importance of selecting an appropriate cell line for transient screening or suggests the necessity of carrying out screens in multiple cell lines as a means of pin-pointing master miRNAs that possess conserved function across various CHO cell types.

4.7 CHO cell engineering using miR-34

Our transient screening assay revealed potent suppression of CHO cell growth when miR-34a was overexpressed. This observation prompted us to attempt a stable depletion approach in anticipation of having the opposite outcome i.e. improved cell densities and/or increased culture longevity.

4.7.1 miR-34's depletion on various CHO cell types

The impact of a miRNA on a late stage culture phenotype such as apoptosis is difficult to evaluate due to their short life-time. This can be caused by the stability of the exogenously introduced miRNA in addition to cellular proliferation diluting cytoplasmic miRNAs across daughter cells ultimately titrating their effect (Song et al. 2003, Bartlett, Davis 2006). To navigate around this, we cultured CHO-SEAP cells in nutrient-depleted media and transiently inhibited miR-34a function resulting in a ~10% reduction in cell death. This mild improvement in cell viability was similar to an observation by Druz and colleagues upon transient inhibition of miR-466h in nutrient depleted cells (Druz et al. 2011). The inconsistent improvement in cell viability observed in the case of CHO-SEAP

cells could be attributed to the low endogenous levels of miR-34a in CHO cells reported by next-generation sequencing (Hackl et al. 2011). Additionally, the successful profiling of miR-466h by Druz and colleagues could be due to the same cell type being used in both profiling and miRNA transient/stable inhibition (Druz et al. 2013). Transient inhibition of miR-34a also demonstrated an inconsistent improvement of 30% in maximal cell density. This increase in cell numbers could have contributed to the apparent increase of 10% in culture viability.

The mild and inconsistent impact of miR-34a upon its inhibition may also be due to a multitude of reasons: 1) the transient inhibition of miRNAs being less potent on endogenous targets compared to their overexpression (Martinez-Sanchez, Murphy 2013), 2) the potential absence of molecular targets for miR-34a in combination with its low abundance in CHO cells (Hackl et al. 2011) and 3) the dilution effect of miR-34a inhibitor through multiple rounds of cellular proliferation. Stable inhibition of miR-34 was based on previous observations in our group (Barron et al. 2011b), whereby stable depletion of miR-7 enhanced cell density and boosted volumetric SEAP yield (Sanchez et al. 2013b) despite increased apparent normalised productivity. Similar to miR-466h, miR-7 was identified, characterised and stably engineered in the same cell line again highlighting the selection of cell line having a contribution to outcome. Of course, from the perspective of identifying a high priority miRNA candidate for industrial application, the effect should be verified in several CHO cell lines.

When miR-34 depletion was assessed in a CHO-SEAP stable mixed population, there was an increase in growth observed with an elevated viable cell density of 6-15% (**Fig. 3.12 A and B**). No benefit was observed in SEAP yield. However, when these cells were cultured under fed-batch conditions, a considerable increase in SEAP yield was observed (**Fig. 3.13 C and D**). This increase in productivity could have been attributed to the reduced proliferation of miR-34 depleted cells when compared to controls, suggesting a longer residence in the highly transcriptionally active G₁-phase of the cell cycle (Kumar, Gammell & Clynes 2007). When clones were assessed as a panel, volumetric SEAP productivity was enhanced across all time points (**Fig. 3.17**). Cellular proliferation in 1 mL batch culture was reduced, possibly explaining the considerable increase in specific productivity. Studies have demonstrated that CHO clones not only behave differently to each other in respect to a certain phenotype but vary under differing bioprocess conditions

(Porter et al. 2010). Clones were selected based on their productivity and when cultured in batch conditions continued to demonstrate an enhanced volumetric yield as observed within the clonal screen. Interestingly, miR-34 clones exhibited a propensity to clump when compared to controls and other miR-sponge clones generated (miR-23 and -23b*). miR-34a has previously been associated with biological processes contributing to cell adhesion (Jo et al. 2011), potentially explain this increased cellular interaction resulting in clumping when clones were derived.

On the other hand, when miR-34 was stably depleted in IgG-secreting CHO-1.14 cells, mixed populations grew better (**Fig. 3.14 A**). This agrees with numerous reports of loss of miR-34a expression influencing cancer cell proliferation through mediating the increased expression of numerous oncogenes such as *CCND1*, *CCNE2* and *CDK4/6* (He et al. 2007b, Sun et al. 2008b). Loss of miR-34a function has been observed in a range of cancers such as prostate (Fujita et al. 2008), breast (Vogt et al. 2011), pancreas (Chang et al. 2007) and ovary (Corney et al. 2010) due to epigenetic mechanisms and genomic instability (Calin et al. 2008, Vogt et al. 2011, Lodygin et al. 2008). The observation that miR-34a overexpression reduced the mRNA levels of *CCND1* in CHO suggested its potential role in mediating a beneficial growth phenotype. However, the expression of *CCND1* in miR-34 depleted CHO clones varied considerably when compared to controls (**Fig. 3.11 C**). It has been reported that mild changes of as little as 1.23-fold in the expression levels of miR-34a targets have been sufficient to drive tumorigenesis (Kaller et al. 2011a). It is possible that other targets both known and unknown are mediating this enhanced proliferation such as *CDK4/6*. Additionally, siRNA knockdown of the miR-34 sponge did reduce growth suggesting that miR-34 depletion was eliciting an enhanced growth phenotype.

Specific productivity was reduced across all time points in these mixed pool CHO-1.14 populations potentially as a result of enhanced proliferation. It has been suggested that energy provisions can be redirected in fast growing cells from productivity to proliferation and accumulation of biomass (Clarke et al. 2012). Furthermore, miR-34a has been implicated in the arrest of cells in the G₁-phase of the cell cycle upon its expression (Navarro et al. 2009) ultimately prolonging their residence in this highly transcriptionally active phase (Kumar, Gammell & Clynes 2007). Swift propagation through the cell cycle could be contributing to the observed reduced specific productivity.

When miR-34 sponge clones were selected through FACS, the GFP expression pattern across both CHO-SEAP and CHO-1.14 panels was suggestive that endogenous miR-34 was targeting the sponge as there was an average drop in GFP fluorescence across the miR-34 sponge panels compared to controls, an observation made previously by Sanchez and colleagues for miR-7 sponge clones (Sanchez et al. 2013b). Furthermore, it was demonstrated that mature miR-34a levels when assessed in a set of miR-34a clones exhibited a 5-fold reduction (**Fig. 3.11 A**). siRNA inhibition of the miR-34a sponge was also shown to increase levels of endogenous miR-34a though not to resting levels when compared to control sponges. This is possibly as a result of incomplete knockdown of the sponge.

The enhanced growth phenotype observed in the case of CHO-1.14 mixed populations was not retained when miR-34 clones were cultured in a 1 mL volume. However, once introduced back into 5 mL volumes, miR-34 sponge clones showed an improved growth phenotype over all control clones except one, which maintained high cell density and viability. Volumetric IgG and specific productivity was observed to be reduced considerably in the case of miR-34 sponge clones. This could be due to the more potent increase in growth exerted by the miR-34 sponge thus contributing more significantly to reduced specific productivity. When fed-batch was carried out, a similar trend was observed in the case of miR-34 sponge clones, i.e. enhanced growth to the detriment of productivity. However, individual miR-NC clones also performed well, showing high cell densities and viability, miR-NC sponge clone 20, and high productivity, miR-NC sponge 2. This could be as a result of clonal selection, isolating individual clones that exhibit desirable phenotypes potentially mediated by insertional mutagenesis resulting from plasmid integrating or inherent heterogeneity.

From assessing miR-34a depletion across various culture formats within two cell lines, it can be seen that it enhanced the specific production capacity of CHO-SEAP cells but possibly caused these cells to clump mid-culture. This observation of miR-34 depletion to improve productivity in selected clones suggests its potential use under an inducible promoter, whereby a high specific production phase could be induced through depletion of miR-34 mid-culture after biomass has accumulated. In the IgG-secreting CHO-1.14 cell line, miR-34 depletion potentially enhanced CHO cell growth at the expense of productivity. However, the selection of a large clonal panel would be required before concluding the miR-34 does confer a growth benefit to these cells. It is also possible that

in the case of the CHO-SEAP cell line, whose growth characteristics are far superior to that of the CHO-1.14s, miR-34 depletion did not mediate an enhanced growth phenotype as the potential molecular targets of miR-34 in this cell line would not mediate a further improvement upon their deregulation. However, by investigating the potential role that miR-34 could play in the bioprocess, the process of glyco-engineering would not have been highlighted nor would the significant impact this engineering process would have on industry be appreciated.

4.7.2 miRNA-based glycoform engineering of recombinant antibodies

It has been suggested that the maximum specific production capacity of CHO has been achieved at 100 pg/cell/day (De Jesus, Wurm 2011), although not routinely accomplished. An alternative means of indirectly increasing yield to meet the global demand for these products could be offered through enhancing antibody effector function, ADCC, thus reducing patient doses. The addition of a biantennary glycan (heptasaccharide) to the conserved asparagine-297 considerably influences antibody effector functions (Jefferis 2009b). In fact, when the glycosylation is eliminated, binding of the target antigen has been observed to decrease or not take place at all (Walsh, Jefferis 2006). The proportion of non-fucosylated IgG-Fc produced in CHO is low with >90% of N-linked glycans containing a core fucose group. It is possible that this high frequency of fucosylation stems from their inability to add a bisecting N-acetylglucosamine as they do not express despite containing a genomic homolog of the gene, β -1-4-N-acetylglucosaminyltransferase III (GnTIII) (Xu et al. 2011). This was suggested by a study whereby CHO cells engineered to express the GnTIII gene produced a non-fucosylated Rituximab-like antibody product with enhanced ADCC due to prior addition of a bisecting-GlcNAc (Ferrara et al. 2006).

shRNA technology designed against the FUT8 gene resulted in an 88% reduction in fucosylation of an IGF-1R antibody with enhanced ADCC and little impact on productivity in a CHO-DG44 clone (Beuger et al. 2009). Several studies have reported improved ADCC function of CHO-produced antibodies for clinically relevant products such as Herceptin and Rituxan exploring routes such as genetic knockout of FUT8 (Yamane-Ohnuki et al. 2004), GMD knockout (GDP-fucose 4, 6-dehydratase (Kanda et al. 2007), siRNA-double knockdown of both FUT8/GMD (Imai-Nishiya et al. 2007) and siRNA inhibition of FUT8 alone (Mori et al. 2004).

Having found that the stable depletion of miR-34 did not generally mediate a beneficial phenotype, despite enhancing cell growth in the IgG-secreting CHO-1.14 cell line, we explored its potential impact on the fucosylation of secreted antibodies following the observation by Bernardi and colleagues that miR-34a could regulate the translation of FUT8 (Bernardi et al. 2013a).

CHO cells produce predominantly fucosylated glycans (Kanda et al. 2006) with the main glycoforms being G0F, G1F and G2F (Ucakturk 2012). It is possible that the increased expression of FUT8, potentially as a result of miR-34 depletion, does not increase antibody fucosylation. This is potentially due to the high abundance of fucosylated antibodies (>90%) already produced by CHO. However, despite no change in fucosylation being observed, there was a considerable reduction in peak intensity for the miR-NC sponge clone when compared to miR-34 sponge clone possibly indicating a reduced frequency in the post-translational addition of the N-Glycan at asparagine-297 (**Fig. 3.27 in Results**). Discrepancies have been observed in the glycosylation patterns of clones derived from the same cell line indicating that clonal variation can contribute to differences in post-translational modifications (Singh 2011). However, we were hopeful that the depletion of miR-34 was enhancing the post-translational process occurring in the CHO-1.14 cells. Little literature support could be found regarding the frequency at which monoclonal antibodies are successfully glycosylated, however, we evaluated the peak intensities of the parental CHO-1.14 cells and anticipated that a similarity would be observed when compared to miR-NC sponge clones, i.e. reduced intensity by comparison to miR-34 depleted clones. Both miR-34 sponge and parental CHO-1.14 demonstrated a similar glyco-profile of comparable intensity (**Fig. 3.29 in Results**). Furthermore, siRNA knockdown of the miR-34 sponge did not lower the peak intensity of the glycoprofile suggesting that the presence of the miR-34-specific sponge was not influencing the frequency of N-glycan addition.

Interestingly, we observed no change in the glycoprofile (**Fig. 3.28 in Results**) of the miR-34 sponge clone 21 transfected with miR-34a mimic. This was carried out in an effort to reduce FUT8 levels in the hope of reducing core fucosylation. In hindsight, this was not the most ideal experimental setup as it is possible that the presence of a highly expressed sponge specific for miR-34 could dilute miR-34a away from its endogenous targets, including FUT8, in this instance (Mullokandov et al. 2012). When the miR-34 sponge clone 21 was transfected with miR-34a, there was a significant reduction in

maximum cell density observed (Data not shown). However, no decline in cellular viability was observed, as had been previously induced in parental cell lines. This would suggest that the presence of the miR-34 sponge competed for exogenously introduced miR-34a preventing its suppression of genes involved in apoptosis resistance for example *Bcl2* (Yang et al. 2014) or *XIAP* (Truettner, Motti & Dietrich 2013). Although its potent inhibition on cell growth was maintained, this could be due to the multitude of validated targets of miR-34a involved in cellular proliferation such as *CCND1*, *CCNE2*, *CDK4*, *CDK6* and *E2F1* thus hitting this phenotype from multiple angles. Transfection of miR-34a into an IgG-secreting cell line not containing a sponge specific for miR-34a would be a more desirable approach.

miR-34a function upon its overexpression in CHO appears to be conserved, as indicated from the literature, in regards to reducing proliferation and inducing cell death (**section 3.1.2.3.1**). If its influence on FUT8 was also demonstrated to be conserved in CHO resulting in reduced antibody fucosylation, as an engineering target it would still not prove viable. As miR-34a overexpression would be required to reduce FUT8 translational, this could also result in it eliciting other phenotypes such as reduced cell growth and cell death. As miRNAs are renowned for their ability to bind multiple mRNA targets, it is possible that multiple miRNAs target the FUT8 gene. A method to identify bound miRNAs to specific mRNAs has been reported and offers an attractive option to achieve this goal (Hassan et al. 2013). By identifying novel miRNA targets of FUT8, subsequent screening could identify those that mediate a potent inhibition of FUT8 translation without negatively impacting on other cellular processes such as growth or apoptosis.

The benefit of exploring miRNA/siRNA inhibition of FUT8 in antibody producing CHO cells would potentially navigate around the generation of multiple cell lines, i.e. the primary or parental FUT8 knockout CHO cell lines and the subsequent introduction of the specific antibody for large-scale production. A bi-cistronic expression vector has been reported for the co-expression of the miR-183 family and a protein coding gene (GFP/Atoh1) by exploiting the naturally occurring intronic pathway of miRNA processing (Stoller, Chang & Fekete 2013). This technology would allow for the simultaneous engineering of target therapeutic and miRNA. Although the generation of a FUT8 genetic knockout cell line, as demonstrated by complete de-fucosylation of a Rituxan antibody with enhanced ADCC (Yamane-Ohnuki et al. 2004), would be an

attractive option for industrial implementation, the availability of a co-expression system could accommodate engineering of the multiple cell types suited for particular bioprocesses and certain “hard-to-process” recombinant proteins. Glycoform engineering offers industry a new option to produce highly active, less immunogenic and controlled (Mode-of-action executed to suit treatment) antibodies that can indirectly address the strain of global demand. As mentioned previously, current blockbuster antibodies such as Herceptin and Rituxan will more than likely not be manufactured in these FUT8 engineered cell lines due to the costs involved in characterising their new structure in clinical testing. The technology will, however, provide a viable platform for the production and large-scale manufacture of the 350 antibodies currently in development (Reichert 2013). Additionally, as patents expire, new parental cell lines will have to be generated allowing for the introduction and implementation of this highly beneficial engineering strategy. In addition, increasing the effector function of current antibodies could also mediate the development of “Bio-betters”.

4.8 CHO cell engineering using miR-23b*

Previous characterisation of this miRNA in CHO-K1-SEAP cells demonstrated it to be detrimental to the CHO cell phenotype upon its overexpression, resulting in reduced maximum cell densities and the induction of apoptosis. This observation was in contrast to that indicated from the profile. As previously suggested, the phenomenon of target-mediated miRNA protection (TMMP) (Chatterjee et al. 2011) is potentially causing the apparent increase in mature miR-23b* although the nature of it exerting a phenotypic influence remains in question.

When miR-23b* levels were measured in miR-23b* sponge clones, there was no apparent change when compared to non-specific controls (**Appendix Fig. A13**). This was in contrast to the reduced levels of endogenous miR-34a and miR-23b in their respective sponge clones as well as reports of miR-7 being up in its sponge cell line (Sanchez et al. 2013b). Despite an observed phenotype upon miR-23b* depletion and the demonstration of the sponges specificity for miR-23b* via GFP inhibition, it was interesting to observe no influence on endogenous miR-23b* levels. It has been demonstrated in HeLa cells that miRNAs are expressed in a 13-fold excess relative to that of Ago1-4 indicating that there are more freely available miRNAs than RISC-bound. Additionally, there is a 7-fold excess of free miRNAs associated with mRNA targets compared to Ago-bound miRNAs

demonstrating that free miRNAs can associate with mRNAs and do so in excess to RISC-bound miRNAs (Janas et al. 2012). This would also suggest that free miRNAs can compete for and interfere with the regulatory capacity of their RISC-bound counterparts also suggesting that TMMP can influence any miRNA within the transcriptome. On the other hand, if there are more RISC-bound miRNAs than free, the interaction with mRNAs could accelerate the turnover of these RISC-bound miRNAs upon dissociation from the mRNA target. The fate of the miRNA-RISC complex is not something reported on in the literature so the reduction in miR-23b/-34a levels through this increased instability upon mRNA dissociation is purely speculative. By sequentially assessing numerous miR-sponge constructs specific to miR-34a/23/23b* with various mismatches within the MREs, it could be possible to evaluate if finite changes in complementarity will dictate the observation of TMMP or reduced mature miR levels. The above questions the influence of TMMP in both influencing apparent miRNA abundance and additionally in the regulation of a miRNAs phenotypic influence.

miR-23b* depletion in CHO-SEAP mixed pools enhanced growth in both batch and fed-batch conditions at the cost of specific productivity, resulting ultimately in reduced volumetric SEAP output. This phenotype was conserved when assessed in the IgG-secreting CHO-1.14 cell line with the addition of improved cell viability. Only one validated target of miR-23b* has been reported, Proline Oxidase (POX) or Proline Dehydrogenase (PRODH) (Liu et al. 2010a). This is a mitochondrial inner-membrane tumour suppressor gene involved in proline catabolism. The absence or reduction of PRODH has been observed in a variety of human tumours (Liu et al. 2010a, Liu et al. 2009) with its induction being observed to be regulated by p53 (Polyak et al. 1997) resulting in cell cycle arrest in G₂-M (Donald et al. 2001) and the initiation of apoptosis through its ability to generate ROS (Liu et al. 2006). In miR-23b* depleted clones, the enhanced growth was potentially associated with an increase in the target PRODH, contradicting the reports mentioned. It is possible that the enhanced growth phenotype is being mediated by a variety of potential miR-23b* targets that have not yet been identified due to the little attention previously paid to miR* strands. Enhanced growth was not observed when clones were assessed in a 1 mL volume, an observation made in the case of miR-23 depleted CHO-SEAP clones also. As specific productivity and cell density appeared to be equivalent on day 2 of culture, it is possible that the reduced cell numbers observed on day 4 contributed to the increased specific productivity. However, in the case of the IgG-secreting CHO-1.14 cells (mixed pool, clonal panel and clones), cell density

was enhanced at the cost of productivity. The phenotype mediated by miR-23b* was observed to be retained in the CHO-1.14 cell line.

Upon selection of miR-23b* depleted CHO-SEAP clones, a range of growth phenotypes were observed with clone 18 demonstrating the highest cell density and culture longevity. miR-23b* sponge clones demonstrated a higher productivity than previously documented for mixed pools but still lower when compared to controls. This potentially could have resulted from the selection of clones based on productivity values thus introducing a bias. Clone 18 produced a comparative amount of SEAP on D6 of batch culture despite its reduced specific productivity. This may have been as a consequence of extended viability towards the latter part of the culture compared to controls. This comparative productivity was retained under fed-batch conditions with viability being maintained above 80% for a further 72 h. Temperature shift was explored with the aim of improving specific productivity and further delaying the induction of apoptosis which ultimately resulted in improved SEAP yield of 50%.

One observation was that, upon subsequent experimental repeat of miR-23b* sponge clone 18 in CHO-SEAP cells in fed-batch conditions including a temperature shift, a reduction in GFP expression was observed which coincided with a decrease in viability at an earlier time point in culture (Data not shown). This potentially implicates the presence of the sponge in mediating the observed phenotype. Given the variation observed within clones themselves over several generations (Pilbrough, Munro & Gray 2009), this reduction in GFP expression could also be attributed to an increase in endogenous miR-23b* expression. Of the three miR-23b* sponge CHO-SEAP clones selected from the panel screen, clone 18 demonstrated the lowest level of GFP expression with clone 8 being the highest and clone 3 falling in between. Only clone 18 demonstrated enhanced viability in 5 mL scale up suggesting that the presence of the sponge is not influencing extended viability and may be a result of mutagenesis in addition to the influence of the culture format (Porter et al. 2010). This type of forward genetic characterisation has been explored to identify genes involved in cancer onset by using a transposon, *Sleeping Beauty* (Dupuy, Jenkins & Copeland 2006) supporting the possibility of beneficial CHO phenotypes induced by plasmid integration. No viability benefit was observed across the panel of miR-23b* sponge clones indicating that this is a phenotype not effected by miR-23b* depletion. Selection of a larger number of clones

carried over into the various culture formats would have given a better indication as to whether this prolonged culture longevity observed for clone 18 was more than a by-product of the cloning process. Regardless, the phenotype observed in miR-23b* sponge clone 18 would be desirable under perfusion culture conditions. This bioprocess configuration has been shown to compensate for low specific activity, as in the case of miR-23b* depletion, due to the maintenance of high viable cell densities (Clincke et al. 2013) and demonstrates the utility of process selection for exploiting innate CHO cell characteristics.

Although it would be pre-mature to conclude that miR-23b* depletion is mediating the observed phenotype, it is evident that by selecting and adapting particular bioprocess regimes to suit a clonal attributes, a desirable outcome can be achieved.

4.9 miRNAs place in the bioprocess

Although the specific production capacity of CHO cells has been proposed to have reached its natural limit at 100 pg/cell/day (De Jesus, Wurm 2011), acquisition of this is not routinely achieved and further drives the requirement for alternative engineering approaches. One such alternative is boosting CHO cell densities and/or prolonging culture viability without compromising specific productivity. It is for this reason that miRNA profiling of CHO cells with varying growth rates but similar specific productivities was explored (Clarke et al. 2012) identifying miRNAs associated with growth such as the miR-17~92 cluster (Olive, Li & He 2013). This miRNA has already demonstrated promising results in the manipulation of the CHO cell phenotype including the overexpression of miR-17 enhancing growth performance, increasing specific productivity 2-fold and boosting yield 3-fold of an EPO-Fc protein (Jadhav et al. 2014). More recently, miR-17, -19b and -92a overexpression was observed to enhance antibody titres by 130-140% in clonal cells without interfering with product quality (Loh et al. 2014). Other reports have demonstrated beneficial outcomes as a function of miRNA intervention including miR-7 depletion (Sanchez et al. 2013b), miR-466h inhibition (Druz et al. 2013) and miR-557/-1287 overexpression (Strotbek et al. 2013) all resulting in enhanced product titres in SEAP and IgG producing cell lines. Characterisation of the benefits of miRNAs over a range of recombinant products further enhances their utility as engineering targets. Furthermore, several of the above reports demonstrate the

improvement in cell growth without compromising specific productivity, a common trade-off often reported (Lai, Yang & Ng 2013a).

To add to this list, miR-23 depletion in CHO-SEAP cells was observed to enhance specific productivity ~3-fold without impacting cell growth. However, pursuit of inhibition of the entire miR-23~27~24 cluster could offer a more adventitious phenotype, given its association with B-cell differentiation, and preliminary data in mixed pools demonstrating both enhanced growth and specific SEAP productivity.

In the 7 years since the first miRNA differential expression profile of CHO cells subjected to temperature shift (Gammell et al. 2007), numerous reviews have been published that have documented the progress in the field and further speculating on miRNAs future in the bioprocess (Wu 2009b, Jadhav et al. 2013, Muller, Katinger & Grillari 2008, Barron et al. 2011d). Significant efforts have been invested to the understanding and control of CHO cells and the molecular tools available for their engineering including the release of the CHO genome (Xu et al. 2011), the utility of endogenous CHO miRNA clusters (Klanert et al. 2013) and the large-scale transfection of CHO cultures with miRNAs (Fischer et al. 2013) (**Fig. 1.4 of the introduction**).

Furthermore, the ongoing profiling strategies (Barron et al. 2011b, Hernandez Bort et al. 2012, Druz et al. 2011) in CHO have been suggested to benefit the bioprocess in the form of inducible systems dependent on the innate expression profile of miRNAs over the culture process (**Fig. 1.7**).

The possibility for miRNAs potential in bioprocess engineering does not end here. An exciting area of research has been in the manipulation and control of particular antibody glycoforms produced by CHO cells with the goal of enhancing antibody effector functions such as ADCC (Jefferis 2009b). We explored the potential of miR-34a to retain its function of suppressing the translation of the FUT8 gene (Bernardi et al. 2013b) as a means of reducing the level of fucosylated IgG antibody. Although we were unsuccessful in demonstrating miR-34a to impact on antibody fucosylation, this particular area of research will have vast implications for the industry. By enhancing antibody effector functions, therapeutic dosages can be reduced which could ultimately aid in achieving global demands. This indirect route of meeting demand, or bringing the demand down, will reduce costs involved in bioprocess design, allow for the derivation away from the construction of large-scale pharmaceutical production plants and ultimately reduce consumer costs.

With patents of major blockbuster therapeutics coming to an end, the drive for the development of “bio-similars” and “bio-betters” is in full swing with over 350 antibody products alone currently in pre-clinical development (Reichert 2013), a new era of cell line development will be opened allowing for the re-optimisation of the parental production cell lines for industrial scale manufacture. The various success stories reported for miRNAs, miR-23 included, effectively enhancing CHO cell performance across a range of recombinant products, implicates these small molecules as additional tools to compliment other approaches.

Conclusions

1 Integrated microRNA profile of CHO cells with varying degrees of growth rates and subsequent phenotypic characterisation through transient screening

- 51 miRNAs were found to be differentially expressed (DE) demonstrating a positive or negative correlation with increasing CHO cell growth rate such as the oncogenic miR-17~92 cluster.
- Transient screening revealed miR-34a/34a* and miR-23b* to negatively impact cell growth and viability: miR-206, miR-639 and miR-200a to negatively impact growth with potential improved productivity in the case of miR-200a: and miR-532-5p and miR-15a~16-1 to positively influence CHO cell growth.
- Target-mediated miRNA protection (TMMP) could influence and reshape the apparent miRNA transcriptome ultimately contributing to a symptomatic change in mature miRNA levels, as indicated in the case of miR-23b*.

2 miR-34a as a potential candidate for CHO cell engineering

- miR-34a overexpression was demonstrated to arrest cellular proliferation and to induce cell death with concomitant improved specific SEAP productivity.
- miR-34a was observed to enhance CHO cell specific productivity when stably depleted in CHO-K1-SEAP cells but appeared to cause clones to clump mid-late exponential phase of culture with clones demonstrating reduced culture viability.
- In IgG-secreting CHO-1.14 clones, miR-34 depletion was observed to enhance CHO cell growth at the expense of specific productivity potentially through the regulation of targets such as CCND1.
- Stable depletion of miR-34 did not appear to further increase antibody fucosylation potentially attributed to the inherently high (>90%) level of fucosylated IgG secreted by CHO.
- Overexpression of miR-34a did not reduce the level of antibody fucosylation potentially resulting from the presence of the miR-34 sponge titrating miR-34a function away from FUT8.

3 miR-23b* as a potential candidate for CHO cell engineering

- The over-expression of miR-23b* inhibited cell growth and induced cell death in CHO-SEAP cells.
- Stable depletion of miR-23b* appeared to enhance CHO cell growth at the expense of productivity in both CHO-SEAP and CHO-1.14 cells.
- In a stable CHO-SEAP clone, miR-23b* sponge clone 18, was observed to produce ~50% more SEAP in a fed-batch temperature shift, despite its reduced

specific productivity compared to controls. This enhanced phenotype was attributed to a prolonged production phase due to its enhanced culture longevity.

4 miR-23 depletion as an attractive tool for industrial application

- miR-23 depletion using a miRNA sponge enhanced CHO-SEAP cell productivity by an average of ~3-fold without affecting cell growth.
- Productivity was demonstrated to be enhanced at the transcriptional level with no influence on post-translational/secretory bottlenecks and mRNA stability.
- Stable depletion of miR-23 in IgG-secreting CHO-1.14 cells enhanced cell growth and appeared to prolong viability at the expense of productivity.
- The variation of miR-23's impact on two separate CHO cell lines, both derived from the same parent, suggests that this variation is product-specific.
- Mitochondrial function appeared to be enhanced in miR-23 depleted CHO-SEAP clones.
- Proteomic profiling of whole cell lysates identified a high priority target LETM1 (associated with mitochondrial function) to be elevated in miR-23 sponge clones by 2.7-fold.
- Elevated SEAP transcription is enhanced in miR-23 sponge clones possibly due to the increased expression of CaMKII δ and 14-3-3 η which have been demonstrated to interact with HDAC4/5 sequestering them in the cytoplasm resulting in elevated transcriptional activation through reduced deacetylation in a co-factor dependent manner.
- Whole cell proteomic analysis further identified 8 potential targets of miR-23 which were found to overlap with predicted targets using the miRWalk algorithm including LETM1, CALD1, CaMKII δ , FERMT2, IDH1, TXNDR1, PPP1CB and P4HA1.
- Several proteins found to be enriched in both whole cell lysate and mitochondrial extracts have been previously associated with cellular bioenergetics and mitochondrial metabolism including MDH, SDH, GAA and IDH1 in addition to proteins involved in oxidative stress such as TXNRD1, GSTM1/6, IDH1, PSMD7 and HMOX1 further indicating that CHO cell mitochondrial function is potentially elevated as indicated through miR-23 depletion.

Future work

1 Identify additional miRNA targets for stable CHO cell engineering

- It would be interesting to screen the full panel of DE miRNAs from the profile in both a slow growing clone and the model CHO-SEAP cell line.
- Explore the potential of TMMP playing a role in the apparent increase of miR-23b* levels in fast growing CHO clones and if miR-23b* is itself influencing this fast growing phenotype.

2 Validate the selectivity for enhanced SEAP transcription in CHO-SEAP cells upon stable depletion of miR-23

- siRNA-mediated inhibition of a selection of potential targets of miR-23 derived from label-free MS such as LETM1, CaMKII δ and IDH1 including other interesting targets such as 14-3-3- η would assess whether these targets are playing a role in the enhanced SEAP productivity phenotype.
- Immunoprecipitation of candidates such as 14-3-3- η and LETM1 followed by label-free mass spectrometry would give an indication of the cohort of proteins associated with these upregulated targets such as the hypothesised family of HDACs.
- Over-expression of miR-23a/b in CHO-SEAP cells and western blot analysis of the 8 high priority predicted targets (LETM1, CADL1, CaMKII δ , FERMT2, IDH1, TXNDR1, PPP1CB and P4HA1) would further prioritize their candidacy as targets of miR-23 with the expectation of reduced translation. Following this, 3'UTR cloning of miR-23 responsive targets placed downstream of a GFP reporter would confirm them as bona fide targets upon miR-23 overexpression.
- Assess transcript levels of IgG (heavy/light chain) in miR-23-depleted CHO-1.14 clones to determine enhanced transcription with a potential down-stream processing bottleneck.

3 Investigate the impact miR-23 depletion is exerting on mitochondrial function

- Select a larger number of miR-23 and miR-NC sponge clones and assess mitochondrial function using the OROBOROS under both intact and permeabilised conditions. Furthermore, it would be interesting to assess variation within clonal groups for differences in mitochondrial function.
- siRNA-mediated sponge knockdown of both miR-23 and miR-NC sponges within selected clones and subsequent mitochondrial function characterisation using the OROBOROS.
- siRNA-mediated knockdown of the SEAP transcript with subsequent OROBOROS assessment could potentially determine if protein processing is driving energy demand.

- Carry out the quantification of the various metabolites such as isocitrate, α -ketoglutarate, malate, oxaloacetate, lactate and ammonia in miR-23 sponge CHO-SEAP clones versus controls. Additionally, determining the availability of NADH and FADH₂ could indicate the direction of metabolic reactions. Ultimately, evaluating the levels of ATP will provide insight as to whether the enhanced mitochondrial function is contributing to an increased energy provision.

4 Investigation of the role of miR-23~27~24 depletion in a panel of CHO cells producing a range of recombinant products

- With the previous observation that depletion of the entire miR-23~27~24 cluster enhanced both cell growth and productivity without compromising specific SEAP productivity, stable depletion and generation of CHO-SEAP (various recombinant products) clones exhibiting stable cluster diversion could further enhance volumetric titres due to increased cell densities.

5 Further explore the manipulation of antibody glycoforms using miRNAs

- Assess the capability of miR-34a to interfere with the fucosylation of antibodies produced in rCHO cells. Transiently transfect antibody-secreting cells with miR-34a followed by western blot analysis of the α -1,6-fucosyltransferase (FUT8) to determine effective targeting of FUT8 itself. Following this, glyco-profiling will be explored to confirm reduced core fucosylation.
- As miR-34a overexpression does not present itself as a viable option for CHO cell engineering given its widely conserved phenotypic influence of reduced cell growth and induction of apoptosis, additional miRNAs that target FUT8 will be explored. The use of biotin-labelled anti-sense DNA oligonucleotides will be used to pull down FUT8 with any associated miRNAs followed by miRNA target identification using miRNA arrays.
- From a practical application perspective, identified miRNAs will be validated as bona fide targets of FUT8 in addition to interfering with core fucosylation. Furthermore, overexpression of these miRNAs will be screened for any potential adverse effects such as a negative impact on cell growth, viability and/or productivity.
- Finally, ADCC studies with the antibody products of these stable engineered miRNA cells will be essential to confirm the enhanced benefits of antibody effector functions.

6 miRNA profiling of the natural antibody producing B-cell

- It has already been suggested that lessons from nature can be explored in the identification of attractive engineering targets for CHO cell manipulation, B-cells being one. Differential miRNA expression profiling could be explored on resting B-cells and activated B-cells with subsequent screening of these identified miRNA candidates in CHO.

Bibliography

- Addya, S., Mullick, J., Fang, J.K. & Avadhani, N.G. 1994, "Purification and characterization of a hepatic mitochondrial glutathione S-transferase exhibiting immunochemical relationship to the alpha-class of cytosolic isoenzymes", *Archives of Biochemistry and Biophysics*, vol. 310, no. 1, pp. 82-88.
- Aitken, A. 2006, "14-3-3 Proteins: a Historic Overview", *Seminars in cancer biology*, vol. 16, no. 3, pp. 162-172.
- Alexiou, P., Maragkakis, M., Papadopoulos, G.L., Reczko, M. & Hatzigeorgiou, A.G. 2009, "Lost in translation: an assessment and perspective for computational microRNA target identification", *Bioinformatics (Oxford, England)*, vol. 25, no. 23, pp. 3049-3055.
- Al-Fageeh, M.B., Marchant, R.J., Carden, M.J. & Smales, C.M. 2006, "The cold-shock response in cultured mammalian cells: harnessing the response for the improvement of recombinant protein production", *Biotechnology and bioengineering*, vol. 93, no. 5, pp. 829-835.
- Altamirano, C., Paredes, C., Cairo, J.J. & Godia, F. 2000, "Improvement of CHO cell culture medium formulation: simultaneous substitution of glucose and glutamine", *Biotechnology progress*, vol. 16, no. 1, pp. 69-75.
- Altamirano, C., Paredes, C., Illanes, A., Cairo, J.J. & Godia, F. 2004, "Strategies for fed-batch cultivation of t-PA producing CHO cells: substitution of glucose and glutamine and rational design of culture medium", *Journal of Biotechnology*, vol. 110, no. 2, pp. 171-179.
- Ambros, V. 2008, "The evolution of our thinking about microRNAs", *Nature medicine*, vol. 14, no. 10, pp. 1036-1040.
- Ambros, V., Bartel, B., Bartel, D.P., Burge, C.B., Carrington, J.C., Chen, X., Dreyfuss, G., Eddy, S.R., Griffiths-Jones, S., Marshall, M., Matzke, M., Ruvkun, G. & Tuschl, T. 2003, "A uniform system for microRNA annotation", *RNA (New York, N.Y.)*, vol. 9, no. 3, pp. 277-279.
- An, J., Pan, Y., Yan, Z., Li, W., Cui, J., Jiao, Y., Tian, L., Xing, R. & Lu, Y. 2013, "MiR-23a in Amplified 19p13.13 Loci Targets Metallothionein 2A and Promotes Growth in Gastric Cancer Cells", *Journal of cellular biochemistry*, .
- Arden, N. & Betenbaugh, M.J. 2004, "Life and death in mammalian cell culture: strategies for apoptosis inhibition", *Trends in biotechnology*, vol. 22, no. 4, pp. 174-180.
- Arvey, A., Larsson, E., Sander, C., Leslie, C.S. & Marks, D.S. 2010, "Target mRNA abundance dilutes microRNA and siRNA activity", *Molecular systems biology*, vol. 6, pp. 363.

- Bader, A.G. 2012, "miR-34 - a microRNA replacement therapy is headed to the clinic", *Frontiers in genetics*, vol. 3, pp. 120.
- Bagga, S., Bracht, J., Hunter, S., Massirer, K., Holtz, J., Eachus, R. & Pasquinelli, A.E. 2005, "Regulation by let-7 and lin-4 miRNAs results in target mRNA degradation", *Cell*, vol. 122, no. 4, pp. 553-563.
- Baik, J.Y., Lee, M.S., An, S.R., Yoon, S.K., Joo, E.J., Kim, Y.H., Park, H.W. & Lee, G.M. 2006, "Initial transcriptome and proteome analyses of low culture temperature-induced expression in CHO cells producing erythropoietin", *Biotechnology and bioengineering*, vol. 93, no. 2, pp. 361-371.
- Bail, S., Swerdel, M., Liu, H., Jiao, X., Goff, L.A., Hart, R.P. & Kiledjian, M. 2010, "Differential regulation of microRNA stability", *RNA (New York, N.Y.)*, vol. 16, no. 5, pp. 1032-1039.
- Barron, N., Keenan, J., Gammell, P., Martinez, V.G., Freeman, A., Masters, J.R. & Clynes, M. 2012, "Biochemical relapse following radical prostatectomy and miR-200a levels in prostate cancer", *The Prostate*, vol. 72, no. 11, pp. 1193-1199.
- Barron, N., Kumar, N., Sanchez, N., Doolan, P., Clarke, C., Meleady, P., O'Sullivan, F. & Clynes, M. 2011a, "Engineering CHO cell growth and recombinant protein productivity by overexpression of miR-7", *Journal of Biotechnology*, vol. 151, no. 2, pp. 204-211.
- Barron, N., Kumar, N., Sanchez, N., Doolan, P., Clarke, C., Meleady, P., O'Sullivan, F. & Clynes, M. 2011b, "Engineering CHO cell growth and recombinant protein productivity by overexpression of miR-7", *Journal of Biotechnology*, vol. 151, no. 2, pp. 204-211.
- Barron, N., Kumar, N., Sanchez, N., Doolan, P., Clarke, C., Meleady, P., O'Sullivan, F. & Clynes, M. 2011c, "Engineering CHO cell growth and recombinant protein productivity by overexpression of miR-7", *Journal of Biotechnology*, vol. 151, no. 2, pp. 204-211.
- Barron, N., Sanchez, N., Kelly, P. & Clynes, M. 2011d, "MicroRNAs: tiny targets for engineering CHO cell phenotypes?", *Biotechnology Letters*, vol. 33, no. 1, pp. 11-21.
- Barron, N., Sanchez, N., Kelly, P. & Clynes, M. 2011e, "MicroRNAs: tiny targets for engineering CHO cell phenotypes?", *Biotechnology Letters*, vol. 33, no. 1, pp. 11-21.
- Bartel, D.P. 2009, "MicroRNAs: target recognition and regulatory functions", *Cell*, vol. 136, no. 2, pp. 215-233.
- Bartel, D.P. 2004, "MicroRNAs: Genomics, Biogenesis, Mechanism, and Function", *Cell*, vol. 116, no. 2, pp. 281-297.

- Bartlett, D.W. & Davis, M.E. 2006, "Insights into the kinetics of siRNA-mediated gene silencing from live-cell and live-animal bioluminescent imaging", *Nucleic acids research*, vol. 34, no. 1, pp. 322-333.
- Bauerschmitt, H., Mick, D.U., Deckers, M., Vollmer, C., Funes, S., Kehrein, K., Ott, M., Rehling, P. & Herrmann, J.M. 2010, "Ribosome-binding proteins Mdm38 and Mba1 display overlapping functions for regulation of mitochondrial translation", *Molecular biology of the cell*, vol. 21, no. 12, pp. 1937-1944.
- Baumgart, E., Fahimi, H.D., Stich, A. & Volkl, A. 1996, "L-lactate dehydrogenase A4- and A3B isoforms are bona fide peroxisomal enzymes in rat liver. Evidence for involvement in intraperoxisomal NADH reoxidation", *The Journal of biological chemistry*, vol. 271, no. 7, pp. 3846-3855.
- Becker, E., Florin, L., Pfizenmaier, K. & Kaufmann, H. 2008, "An XBP-1 dependent bottle-neck in production of IgG subtype antibodies in chemically defined serum-free Chinese hamster ovary (CHO) fed-batch processes", *Journal of Biotechnology*, vol. 135, no. 2, pp. 217-223.
- Becker, J., Hackl, M., Rupp, O., Jakobi, T., Schneider, J., Szczepanowski, R., Bekel, T., Borth, N., Goesmann, A., Grillari, J., Kaltschmidt, C., Noll, T., Puhler, A., Tauch, A. & Brinkrolf, K. 2011, "Unraveling the Chinese hamster ovary cell line transcriptome by next-generation sequencing", *Journal of Biotechnology*, vol. 156, no. 3, pp. 227-235.
- Bensing, S.J. & Christofk, H.R. 2012, "New aspects of the Warburg effect in cancer cell biology", *Seminars in cell & developmental biology*, vol. 23, no. 4, pp. 352-361.
- Bernardi, C., Soffientini, U., Piacente, F. & Tonetti, M.G. 2013a, "Effects of MicroRNAs on Fucosyltransferase 8 (FUT8) Expression in Hepatocarcinoma Cells", *PloS one*, vol. 8, no. 10, pp. e76540.
- Bernardi, C., Soffientini, U., Piacente, F. & Tonetti, M.G. 2013b, "Effects of microRNAs on fucosyltransferase 8 (FUT8) expression in hepatocarcinoma cells", *PloS one*, vol. 8, no. 10, pp. e76540.
- Bernstein, E., Kim, S.Y., Carmell, M.A., Murchison, E.P., Alcorn, H., Li, M.Z., Mills, A.A., Elledge, S.J., Anderson, K.V. & Hannon, G.J. 2003, "Dicer is essential for mouse development", *Nature genetics*, vol. 35, no. 3, pp. 215-217.
- Beuger, V., Kunkele, K.P., Koll, H., Gartner, A., Bahner, M., Burtscher, H. & Klein, C. 2009, "Short-hairpin-RNA-mediated silencing of fucosyltransferase 8 in Chinese-hamster ovary cells for the production of antibodies with enhanced antibody immune effector function", *Biotechnology and applied biochemistry*, vol. 53, no. Pt 1, pp. 31-37.
- Bhagwat, S.V., Vijayasathy, C., Raza, H., Mullick, J. & Avadhani, N.G. 1998, "Preferential effects of nicotine and 4-(N-methyl-N-nitrosamine)-1-(3-pyridyl)-1-butanone on mitochondrial glutathione S-transferase A4-4 induction and increased

- oxidative stress in the rat brain", *Biochemical pharmacology*, vol. 56, no. 7, pp. 831-839.
- Bi, J.X., Shuttleworth, J. & Al-Rubeai, M. 2004, "Uncoupling of cell growth and proliferation results in enhancement of productivity in p21CIP1-arrested CHO cells", *Biotechnology and bioengineering*, vol. 85, no. 7, pp. 741-749.
- Bian, H.B., Pan, X., Yang, J.S., Wang, Z.X. & De, W. 2011, "Upregulation of microRNA-451 increases cisplatin sensitivity of non-small cell lung cancer cell line (A549)", *Journal of experimental & clinical cancer research : CR*, vol. 30, pp. 20-9966-30-20.
- Bindu, S., Pal, C., Dey, S., Goyal, M., Alam, A., Iqbal, M.S., Dutta, S., Sarkar, S., Kumar, R., Maity, P. & Bandyopadhyay, U. 2011, "Translocation of heme oxygenase-1 to mitochondria is a novel cytoprotective mechanism against non-steroidal anti-inflammatory drug-induced mitochondrial oxidative stress, apoptosis, and gastric mucosal injury", *The Journal of biological chemistry*, vol. 286, no. 45, pp. 39387-39402.
- Birch, J.R. & Arathoon, R. 1990, "Suspension culture of mammalian cells", *Bioprocess technology*, vol. 10, pp. 251-270.
- Bleckwenn, N.A. & Shiloach, J. 2004, "Large-scale cell culture", *Current protocols in immunology / edited by John E.Coligan et al.*, vol. Appendix 1, pp. Appendix 1U.
- Bohnsack, M.T., Czaplinski, K. & Gorlich, D. 2004, "Exportin 5 is a RanGTP-dependent dsRNA-binding protein that mediates nuclear export of pre-miRNAs", *RNA (New York, N.Y.)*, vol. 10, no. 2, pp. 185-191.
- Boland, A., Huntzinger, E., Schmidt, S., Izaurralde, E. & Weichenrieder, O. 2011, "Crystal structure of the MID-PIWI lobe of a eukaryotic Argonaute protein", *Proceedings of the National Academy of Sciences of the United States of America*, vol. 108, no. 26, pp. 10466-10471.
- Bommer, G.T., Gerin, I., Feng, Y., Kaczorowski, A.J., Kuick, R., Love, R.E., Zhai, Y., Giordano, T.J., Qin, Z.S., Moore, B.B., MacDougald, O.A., Cho, K.R. & Fearon, E.R. 2007, "p53-mediated activation of miRNA34 candidate tumor-suppressor genes", *Current biology : CB*, vol. 17, no. 15, pp. 1298-1307.
- Borth, N., Mattanovich, D., Kunert, R. & Katinger, H. 2005, "Effect of increased expression of protein disulfide isomerase and heavy chain binding protein on antibody secretion in a recombinant CHO cell line", *Biotechnology progress*, vol. 21, no. 1, pp. 106-111.
- Bortolin-Cavaille, M.L., Dance, M., Weber, M. & Cavaille, J. 2009, "C19MC microRNAs are processed from introns of large Pol-II, non-protein-coding transcripts", *Nucleic acids research*, vol. 37, no. 10, pp. 3464-3473.

- Bradley, S.A., Ouyang, A., Purdie, J., Smitka, T.A., Wang, T. & Kaerner, A. 2010, "Fermentanomics: monitoring mammalian cell cultures with NMR spectroscopy", *Journal of the American Chemical Society*, vol. 132, no. 28, pp. 9531-9533.
- Bravo, R., Vicencio, J.M., Parra, V., Troncoso, R., Munoz, J.P., Bui, M., Quiroga, C., Rodriguez, A.E., Verdejo, H.E., Ferreira, J., Iglewski, M., Chiong, M., Simmen, T., Zorzano, A., Hill, J.A., Rothermel, B.A., Szabadkai, G. & Lavandero, S. 2011, "Increased ER-mitochondrial coupling promotes mitochondrial respiration and bioenergetics during early phases of ER stress", *Journal of cell science*, vol. 124, no. Pt 13, pp. 2143-2152.
- Brennecke, J., Stark, A., Russell, R.B. & Cohen, S.M. 2005, "Principles of microRNA-target recognition", *PLoS biology*, vol. 3, no. 3, pp. e85.
- Brooks, A.R., Harkins, R.N., Wang, P., Qian, H.S., Liu, P. & Rubanyi, G.M. 2004, "Transcriptional silencing is associated with extensive methylation of the CMV promoter following adenoviral gene delivery to muscle", *The journal of gene medicine*, vol. 6, no. 4, pp. 395-404.
- Bruggemann, M., Williams, G.T., Bindon, C.I., Clark, M.R., Walker, M.R., Jefferis, R., Waldmann, H. & Neuberger, M.S. 1987, "Comparison of the effector functions of human immunoglobulins using a matched set of chimeric antibodies", *The Journal of experimental medicine*, vol. 166, no. 5, pp. 1351-1361.
- Bruhns, P., Iannascoli, B., England, P., Mancardi, D.A., Fernandez, N., Jorieux, S. & Daeron, M. 2009, "Specificity and affinity of human Fcγ receptors and their polymorphic variants for human IgG subclasses", *Blood*, vol. 113, no. 16, pp. 3716-3725.
- Bu, Y., Lu, C., Bian, C., Wang, J., Li, J., Zhang, B., Li, Z., Brewer, G. & Zhao, R.C. 2009, "Knockdown of Dicer in MCF-7 human breast carcinoma cells results in G1 arrest and increased sensitivity to cisplatin", *Oncology reports*, vol. 21, no. 1, pp. 13-17.
- Burd, C.E., Jeck, W.R., Liu, Y., Sanoff, H.K., Wang, Z. & Sharpless, N.E. 2010, "Expression of linear and novel circular forms of an INK4/ARF-associated non-coding RNA correlates with atherosclerosis risk", *PLoS genetics*, vol. 6, no. 12, pp. e1001233.
- Butler, M. 2005, "Animal cell cultures: recent achievements and perspectives in the production of biopharmaceuticals", *Applied Microbiology and Biotechnology*, vol. 68, no. 3, pp. 283-291.
- Butler, M. & Meneses-Acosta, A. 2012, "Recent advances in technology supporting biopharmaceutical production from mammalian cells", *Applied Microbiology and Biotechnology*, vol. 96, no. 4, pp. 885-894.
- Byrd, A.E., Aragon, I.V. & Brewer, J.W. 2012, "MicroRNA-30c-2* limits expression of proadaptive factor XBP1 in the unfolded protein response", *The Journal of cell biology*, vol. 196, no. 6, pp. 689-698.

- Cacciatore, J.J., Chasin, L.A. & Leonard, E.F. 2010, "Gene amplification and vector engineering to achieve rapid and high-level therapeutic protein production using the Dhfr-based CHO cell selection system", *Biotechnology Advances*, vol. 28, no. 6, pp. 673-681.
- Cadenas, C., Franckenstein, D., Schmidt, M., Gehrman, M., Hermes, M., Geppert, B., Schormann, W., Maccoux, L.J., Schug, M., Schumann, A., Wilhelm, C., Freis, E., Ickstadt, K., Rahnenfuhrer, J., Baumbach, J.I., Sickmann, A. & Hengstler, J.G. 2010, "Role of thioredoxin reductase 1 and thioredoxin interacting protein in prognosis of breast cancer", *Breast cancer research : BCR*, vol. 12, no. 3, pp. R44.
- Cai, H., Wang, C.C. & Tsou, C.L. 1994, "Chaperone-like activity of protein disulfide isomerase in the refolding of a protein with no disulfide bonds", *The Journal of biological chemistry*, vol. 269, no. 40, pp. 24550-24552.
- Cai, X., Hagedorn, C.H. & Cullen, B.R. 2004, "Human microRNAs are processed from capped, polyadenylated transcripts that can also function as mRNAs", *RNA (New York, N.Y.)*, vol. 10, no. 12, pp. 1957-1966.
- Calin, G.A., Cimmino, A., Fabbri, M., Ferracin, M., Wojcik, S.E., Shimizu, M., Taccioli, C., Zanesi, N., Garzon, R., Aqeilan, R.I., Alder, H., Volinia, S., Rassenti, L., Liu, X., Liu, C.G., Kipps, T.J., Negrini, M. & Croce, C.M. 2008, "MiR-15a and miR-16-1 cluster functions in human leukemia", *Proceedings of the National Academy of Sciences of the United States of America*, vol. 105, no. 13, pp. 5166-5171.
- Campbell, C.T., Kolesar, J.E. & Kaufman, B.A. 2012, "Mitochondrial transcription factor A regulates mitochondrial transcription initiation, DNA packaging, and genome copy number", *Biochimica et biophysica acta*, vol. 1819, no. 9-10, pp. 921-929.
- Cao, Z., Zhang, R., Li, J., Huang, H., Zhang, D., Zhang, J., Gao, J., Chen, J. & Huang, C. 2013, "X-linked inhibitor of apoptosis protein (XIAP) regulation of cyclin D1 protein expression and cancer cell anchorage-independent growth via its E3 ligase-mediated protein phosphatase 2A/c-Jun axis", *The Journal of biological chemistry*, vol. 288, no. 28, pp. 20238-20247.
- Carlage, T., Hincapie, M., Zang, L., Lyubarskaya, Y., Madden, H., Mhatre, R. & Hancock, W.S. 2009a, "Proteomic profiling of a high-producing Chinese hamster ovary cell culture", *Analytical Chemistry*, vol. 81, no. 17, pp. 7357-7362.
- Carlage, T., Hincapie, M., Zang, L., Lyubarskaya, Y., Madden, H., Mhatre, R. & Hancock, W.S. 2009b, "Proteomic profiling of a high-producing Chinese hamster ovary cell culture", *Analytical Chemistry*, vol. 81, no. 17, pp. 7357-7362.
- Carrington, J.C. & Ambros, V. 2003, "Role of MicroRNAs in Plant and Animal Development", *Science*, vol. 301, no. 5631, pp. 336-338.
- Carroll, J., Fearnley, I.M., Skehel, J.M., Shannon, R.J., Hirst, J. & Walker, J.E. 2006, "Bovine complex I is a complex of 45 different subunits", *The Journal of biological chemistry*, vol. 281, no. 43, pp. 32724-32727.

- Carvalho, A.V., Marcelino, I. & Carrondo, M.J. 2003, "Metabolic changes during cell growth inhibition by p27 overexpression", *Applied Microbiology and Biotechnology*, vol. 63, no. 2, pp. 164-173.
- Casagrande, R., Stern, P., Diehn, M., Shamu, C., Osario, M., Zuniga, M., Brown, P.O. & Ploegh, H. 2000, "Degradation of proteins from the ER of *S. cerevisiae* requires an intact unfolded protein response pathway", *Molecular cell*, vol. 5, no. 4, pp. 729-735.
- Cenas, N., Nivinskas, H., Anusevicius, Z., Sarlauskas, J., Lederer, F. & Arner, E.S. 2004, "Interactions of quinones with thioredoxin reductase: a challenge to the antioxidant role of the mammalian selenoprotein", *The Journal of biological chemistry*, vol. 279, no. 4, pp. 2583-2592.
- Chan, A.C. & Carter, P.J. 2010, "Therapeutic antibodies for autoimmunity and inflammation", *Nature reviews.Immunology*, vol. 10, no. 5, pp. 301-316.
- Chan, J.A., Krichevsky, A.M. & Kosik, K.S. 2005, "MicroRNA-21 is an antiapoptotic factor in human glioblastoma cells", *Cancer research*, vol. 65, no. 14, pp. 6029-6033.
- Chang, C., Xu, K. & Shu, H. 2011, "The role of isocitrate dehydrogenase mutations in glioma brain tumors", *Molecular targets of CNS tumors*, pp. 413-436.
- Chang, K.W., Kao, S.Y., Wu, Y.H., Tsai, M.M., Tu, H.F., Liu, C.J., Lui, M.T. & Lin, S.C. 2013, "Passenger strand miRNA miR-31* regulates the phenotypes of oral cancer cells by targeting RhoA", *Oral oncology*, vol. 49, no. 1, pp. 27-33.
- Chang, T.C., Wentzel, E.A., Kent, O.A., Ramachandran, K., Mullendore, M., Lee, K.H., Feldmann, G., Yamakuchi, M., Ferlito, M., Lowenstein, C.J., Arking, D.E., Beer, M.A., Maitra, A. & Mendell, J.T. 2007, "Transactivation of miR-34a by p53 broadly influences gene expression and promotes apoptosis", *Molecular cell*, vol. 26, no. 5, pp. 745-752.
- Chatterjee, S., Fasler, M., Bussing, I. & Grosshans, H. 2011, "Target-mediated protection of endogenous microRNAs in *C. elegans*", *Developmental cell*, vol. 20, no. 3, pp. 388-396.
- Chatterjee, S. & Grosshans, H. 2009, "Active turnover modulates mature microRNA activity in *Caenorhabditis elegans*", *Nature*, vol. 461, no. 7263, pp. 546-549.
- Chen, C.Z., Li, L., Lodish, H.F. & Bartel, D.P. 2004, "MicroRNAs modulate hematopoietic lineage differentiation", *Science (New York, N.Y.)*, vol. 303, no. 5654, pp. 83-86.
- Chen, F., Ye, Z., Zhao, L., Liu, X., Fan, L. & Tan, W.S. 2012, "Correlation of antibody production rate with glucose and lactate metabolism in Chinese hamster ovary cells", *Biotechnology Letters*, vol. 34, no. 3, pp. 425-432.
- Chen, K., Liu, Q., Xie, L., Sharp, P.A. & Wang, D.I. 2001, "Engineering of a mammalian cell line for reduction of lactate formation and high monoclonal antibody production", *Biotechnology and bioengineering*, vol. 72, no. 1, pp. 55-61.

- Chen, Q., Xu, J., Li, L., Li, H., Mao, S., Zhang, F., Zen, K., Zhang, C.Y. & Zhang, Q. 2014, "MicroRNA-23a/b and microRNA-27a/b suppress Apaf-1 protein and alleviate hypoxia-induced neuronal apoptosis", *Cell death & disease*, vol. 5, pp. e1132.
- Chen, Q.R., Yu, L.R., Tsang, P., Wei, J.S., Song, Y.K., Cheuk, A., Chung, J.Y., Hewitt, S.M., Veenstra, T.D. & Khan, J. 2011a, "Systematic proteome analysis identifies transcription factor YY1 as a direct target of miR-34a", *Journal of proteome research*, vol. 10, no. 2, pp. 479-487.
- Chen, S., Synowsky, S., Tinti, M. & MacKintosh, C. 2011b, "The capture of phosphoproteins by 14-3-3 proteins mediates actions of insulin", *Trends in endocrinology and metabolism: TEM*, vol. 22, no. 11, pp. 429-436.
- Chen, Z., Lu, W., Garcia-Prieto, C. & Huang, P. 2007, "The Warburg effect and its cancer therapeutic implications", *Journal of Bioenergetics and Biomembranes*, vol. 39, no. 3, pp. 267-274.
- Chendrimada, T.P., Gregory, R.I., Kumaraswamy, E., Norman, J., Cooch, N., Nishikura, K. & Shiekhattar, R. 2005, "TRBP recruits the Dicer complex to Ago2 for microRNA processing and gene silencing", *Nature*, vol. 436, no. 7051, pp. 740-744.
- Chhabra, R., Adlakha, Y.K., Hariharan, M., Scaria, V. & Saini, N. 2009, "Upregulation of miR-23a-27a-24-2 cluster induces caspase-dependent and -independent apoptosis in human embryonic kidney cells", *PloS one*, vol. 4, no. 6, pp. e5848.
- Chhabra, R., Dubey, R. & Saini, N. 2010a, "Cooperative and individualistic functions of the microRNAs in the miR-23a~27a~24-2 cluster and its implication in human diseases", *Molecular cancer*, vol. 9, pp. 232-4598-9-232.
- Chhabra, R., Dubey, R. & Saini, N. 2010b, "Cooperative and individualistic functions of the microRNAs in the miR-23a~27a~24-2 cluster and its implication in human diseases", *Molecular cancer*, vol. 9, pp. 232-4598-9-232.
- Chi, S.W., Hannon, G.J. & Darnell, R.B. 2012, "An alternative mode of microRNA target recognition", *Nature structural & molecular biology*, vol. 19, no. 3, pp. 321-327.
- Chi, S.W., Zang, J.B., Mele, A. & Darnell, R.B. 2009, "Argonaute HITS-CLIP decodes microRNA-mRNA interaction maps", *Nature*, vol. 460, no. 7254, pp. 479-486.
- Chiang, G.G. & Sisk, W.P. 2005, "Bcl-x(L) mediates increased production of humanized monoclonal antibodies in Chinese hamster ovary cells", *Biotechnology and bioengineering*, vol. 91, no. 7, pp. 779-792.
- Chiang, H.R., Schoenfeld, L.W., Ruby, J.G., Auyeung, V.C., Spies, N., Baek, D., Johnston, W.K., Russ, C., Luo, S., Babiarz, J.E., Blelloch, R., Schroth, G.P., Nusbaum, C. & Bartel, D.P. 2010, "Mammalian microRNAs: experimental evaluation of novel and previously annotated genes", *Genes & development*, vol. 24, no. 10, pp. 992-1009.

- Choi, Y.J., Lin, C.P., Ho, J.J., He, X., Okada, N., Bu, P., Zhong, Y., Kim, S.Y., Bennett, M.J., Chen, C., Ozturk, A., Hicks, G.G., Hannon, G.J. & He, L. 2011, "miR-34 miRNAs provide a barrier for somatic cell reprogramming", *Nature cell biology*, vol. 13, no. 11, pp. 1353-1360.
- Chong, W.P., Goh, L.T., Reddy, S.G., Yusufi, F.N., Lee, D.Y., Wong, N.S., Heng, C.K., Yap, M.G. & Ho, Y.S. 2009a, "Metabolomics profiling of extracellular metabolites in recombinant Chinese Hamster Ovary fed-batch culture", *Rapid communications in mass spectrometry : RCM*, vol. 23, no. 23, pp. 3763-3771.
- Chong, W.P., Goh, L.T., Reddy, S.G., Yusufi, F.N., Lee, D.Y., Wong, N.S., Heng, C.K., Yap, M.G. & Ho, Y.S. 2009b, "Metabolomics profiling of extracellular metabolites in recombinant Chinese Hamster Ovary fed-batch culture", *Rapid communications in mass spectrometry : RCM*, vol. 23, no. 23, pp. 3763-3771.
- Chong, W.P., Reddy, S.G., Yusufi, F.N., Lee, D.Y., Wong, N.S., Heng, C.K., Yap, M.G. & Ho, Y.S. 2010, "Metabolomics-driven approach for the improvement of Chinese hamster ovary cell growth: overexpression of malate dehydrogenase II", *Journal of Biotechnology*, vol. 147, no. 2, pp. 116-121.
- Chong, W.P., Thng, S.H., Hiu, A.P., Lee, D.Y., Chan, E.C. & Ho, Y.S. 2012, "LC-MS-based metabolic characterization of high monoclonal antibody-producing Chinese hamster ovary cells", *Biotechnology and bioengineering*, vol. 109, no. 12, pp. 3103-3111.
- Chong, W.P., Yusufi, F.N., Lee, D.Y., Reddy, S.G., Wong, N.S., Heng, C.K., Yap, M.G. & Ho, Y.S. 2011, "Metabolomics-based identification of apoptosis-inducing metabolites in recombinant fed-batch CHO culture media", *Journal of Biotechnology*, vol. 151, no. 2, pp. 218-224.
- Chotteau, V. & Lindqvist, A. 2012, "Study of the Effect of High pH and Alkali Addition in a Cultivation of Chinese Hamster Ovary Cell", *Proceedings of the 21st Annual Meeting of the European Society for Animal Cell Technology (ESACT), Dublin, Ireland, June 7-10, 2009* Springer, pp. 323.
- Christoffersen, N.R., Shalgi, R., Frankel, L.B., Leucci, E., Lees, M., Klausen, M., Pilpel, Y., Nielsen, F.C., Oren, M. & Lund, A.H. 2010, "p53-independent upregulation of miR-34a during oncogene-induced senescence represses MYC", *Cell death and differentiation*, vol. 17, no. 2, pp. 236-245.
- Chung, J.Y., Lim, S.W., Hong, Y.J., Hwang, S.O. & Lee, G.M. 2004, "Effect of doxycycline-regulated calnexin and calreticulin expression on specific thrombopoietin productivity of recombinant Chinese hamster ovary cells", *Biotechnology and bioengineering*, vol. 85, no. 5, pp. 539-546.
- Clarke, C., Doolan, P., Barron, N., Meleady, P., O'Sullivan, F., Gammell, P., Melville, M., Leonard, M. & Clynes, M. 2011a, "Large scale microarray profiling and coexpression network analysis of CHO cells identifies transcriptional modules associated with growth and productivity", *Journal of Biotechnology*, 20:155(3), pp. 530-9.

- Clarke, C., Doolan, P., Barron, N., Meleady, P., O'Sullivan, F., Gammell, P., Melville, M., Leonard, M. & Clynes, M. 2011b, "Predicting cell-specific productivity from CHO gene expression", *Journal of Biotechnology*, vol. 151, no. 2, pp. 159-165.
- Clarke, C., Henry, M., Doolan, P., Kelly, S., Aherne, S., Sanchez, N., Kelly, P., Kinsella, P., Breen, L., Madden, S.F., Zhang, L., Leonard, M., Clynes, M., Meleady, P. & Barron, N. 2012, "Integrated miRNA, mRNA and protein expression analysis reveals the role of post-transcriptional regulation in controlling CHO cell growth rate", *BMC genomics*, vol. 13, pp. 656-2164-13-656.
- Clincke, M.F., Molleryd, C., Zhang, Y., Lindskog, E., Walsh, K. & Chotteau, V. 2013, "Very high density of CHO cells in perfusion by ATF or TFF in WAVE bioreactor. Part I. Effect of the cell density on the process", *Biotechnology progress*, vol. 29, no. 3, pp. 754-767.
- Cole, K.A., Attiyeh, E.F., Mosse, Y.P., Laquaglia, M.J., Diskin, S.J., Brodeur, G.M. & Maris, J.M. 2008, "A functional screen identifies miR-34a as a candidate neuroblastoma tumor suppressor gene", *Molecular cancer research : MCR*, vol. 6, no. 5, pp. 735-742.
- Conaway, R.C. & Conaway, J.W. 1988, "ATP activates transcription initiation from promoters by RNA polymerase II in a reversible step prior to RNA synthesis", *The Journal of biological chemistry*, vol. 263, no. 6, pp. 2962-2968.
- Congy-Jolivet, N., Probst, A., Watier, H. & Thibault, G. 2007, "Recombinant therapeutic monoclonal antibodies: mechanisms of action in relation to structural and functional duality", *Critical reviews in oncology/hematology*, vol. 64, no. 3, pp. 226-233.
- Corney, D.C., Hwang, C.I., Matoso, A., Vogt, M., Flesken-Nikitin, A., Godwin, A.K., Kamat, A.A., Sood, A.K., Ellenson, L.H., Hermeking, H. & Nikitin, A.Y. 2010, "Frequent downregulation of miR-34 family in human ovarian cancers", *Clinical cancer research : an official journal of the American Association for Cancer Research*, vol. 16, no. 4, pp. 1119-1128.
- Cost, G.J., Freyvert, Y., Vafiadis, A., Santiago, Y., Miller, J.C., Rebar, E., Collingwood, T.N., Snowden, A. & Gregory, P.D. 2010, "BAK and BAX deletion using zinc-finger nucleases yields apoptosis-resistant CHO cells", *Biotechnology and bioengineering*, vol. 105, no. 2, pp. 330-340.
- Danan, M., Schwartz, S., Edelheit, S. & Sorek, R. 2012, "Transcriptome-wide discovery of circular RNAs in Archaea", *Nucleic acids research*, vol. 40, no. 7, pp. 3131-3142.
- Dang, C.V. 2010, "Rethinking the Warburg effect with Myc micromanaging glutamine metabolism", *Cancer research*, vol. 70, no. 3, pp. 859-862.
- das Neves, R.P., Jones, N.S., Andreu, L., Gupta, R., Enver, T. & Iborra, F.J. 2010, "Connecting variability in global transcription rate to mitochondrial variability", *PLoS biology*, vol. 8, no. 12, pp. e1000560.

- Datta, P., Linhardt, R.J. & Sharfstein, S.T. 2013, "An 'omics approach towards CHO cell engineering", *Biotechnology and bioengineering*, vol. 110, no. 5, pp. 1255-1271.
- Davalos, A., Goedeke, L., Smibert, P., Ramirez, C.M., Warriar, N.P., Andreo, U., Cirera-Salinas, D., Rayner, K., Suresh, U., Pastor-Pareja, J.C., Esplugues, E., Fisher, E.A., Penalva, L.O., Moore, K.J., Suarez, Y., Lai, E.C. & Fernandez-Hernando, C. 2011, "miR-33a/b contribute to the regulation of fatty acid metabolism and insulin signaling", *Proceedings of the National Academy of Sciences of the United States of America*, vol. 108, no. 22, pp. 9232-9237.
- Davie, J.R. 2003, "Inhibition of histone deacetylase activity by butyrate", *The Journal of nutrition*, vol. 133, no. 7 Suppl, pp. 2485S-2493S.
- Davies, J., Jiang, L., Pan, L.Z., LaBarre, M.J., Anderson, D. & Reff, M. 2001, "Expression of GnTIII in a recombinant anti-CD20 CHO production cell line: Expression of antibodies with altered glycoforms leads to an increase in ADCC through higher affinity for FC gamma RIII", *Biotechnology and bioengineering*, vol. 74, no. 4, pp. 288-294.
- Davis, R., Schooley, K., Rasmussen, B., Thomas, J. & Reddy, P. 2000, "Effect of PDI overexpression on recombinant protein secretion in CHO cells", *Biotechnology progress*, vol. 16, no. 5, pp. 736-743.
- De Jesus, M. & Wurm, F.M. 2011, "Manufacturing recombinant proteins in kg-ton quantities using animal cells in bioreactors", *European journal of pharmaceuticals and biopharmaceutics : official journal of Arbeitsgemeinschaft fur Pharmazeutische Verfahrenstechnik e.V.*, vol. 78, no. 2, pp. 184-188.
- De Leon Gatti, M., Wlaschin, K.F., Nissom, P.M., Yap, M. & Hu, W.S. 2007, "Comparative transcriptional analysis of mouse hybridoma and recombinant Chinese hamster ovary cells undergoing butyrate treatment", *Journal of bioscience and bioengineering*, vol. 103, no. 1, pp. 82-91.
- Dean, N.M. 2001, "Functional genomics and target validation approaches using antisense oligonucleotide technology", *Current opinion in biotechnology*, vol. 12, no. 6, pp. 622-625.
- DeBerardinis, R.J., Mancuso, A., Daikhin, E., Nissim, I., Yudkoff, M., Wehrli, S. & Thompson, C.B. 2007, "Beyond aerobic glycolysis: transformed cells can engage in glutamine metabolism that exceeds the requirement for protein and nucleotide synthesis", *Proceedings of the National Academy of Sciences of the United States of America*, vol. 104, no. 49, pp. 19345-19350.
- Dechant, M., Beyer, T., Schneider-Merck, T., Weisner, W., Peipp, M., van de Winkel, J.G. & Valerius, T. 2007, "Effector mechanisms of recombinant IgA antibodies against epidermal growth factor receptor", *Journal of immunology (Baltimore, Md.: 1950)*, vol. 179, no. 5, pp. 2936-2943.
- Dell'Antone, P. 2012, "Energy metabolism in cancer cells: how to explain the Warburg and Crabtree effects?", *Medical hypotheses*, vol. 79, no. 3, pp. 388-392.

- DeMaria, C.T., Cairns, V., Schwarz, C., Zhang, J., Guerin, M., Zuena, E., Estes, S. & Karey, K.P. 2008, "Accelerated Clone Selection for Recombinant CHO Cells Using a FACS-Based High-Throughput Screen", *Biotechnology progress*, vol. 23, no. 2, pp. 465-472.
- Dews, M., Homayouni, A., Yu, D., Murphy, D., Seignani, C., Wentzel, E., Furth, E.E., Lee, W.M., Enders, G.H., Mendell, J.T. & Thomas-Tikhonenko, A. 2006a, "Augmentation of tumor angiogenesis by a Myc-activated microRNA cluster", *Nature genetics*, vol. 38, no. 9, pp. 1060-1065.
- Dews, M., Homayouni, A., Yu, D., Murphy, D., Seignani, C., Wentzel, E., Furth, E.E., Lee, W.M., Enders, G.H., Mendell, J.T. & Thomas-Tikhonenko, A. 2006b, "Augmentation of tumor angiogenesis by a Myc-activated microRNA cluster", *Nature genetics*, vol. 38, no. 9, pp. 1060-1065.
- Dheda, K., Huggett, J.F., Bustin, S.A., Johnson, M.A., Rook, G. & Zumla, A. 2004, "Validation of housekeeping genes for normalizing RNA expression in real-time PCR", *BioTechniques*, vol. 37, no. 1, pp. 112-4, 116, 118-9.
- Diehn, M., Cho, R.W., Lobo, N.A., Kalisky, T., Dorie, M.J., Kulp, A.N., Qian, D., Lam, J.S., Ailles, L.E., Wong, M., Joshua, B., Kaplan, M.J., Wapnir, I., Dirbas, F.M., Somlo, G., Garberoglio, C., Paz, B., Shen, J., Lau, S.K., Quake, S.R., Brown, J.M., Weissman, I.L. & Clarke, M.F. 2009, "Association of reactive oxygen species levels and radioresistance in cancer stem cells", *Nature*, vol. 458, no. 7239, pp. 780-783.
- Dill, H., Linder, B., Fehr, A. & Fischer, U. 2012, "Intronic miR-26b controls neuronal differentiation by repressing its host transcript, ctdsp2", *Genes & development*, vol. 26, no. 1, pp. 25-30.
- Ding, Q., Dimayuga, E. & Keller, J.N. 2006, "Proteasome regulation of oxidative stress in aging and age-related diseases of the CNS", *Antioxidants & redox signaling*, vol. 8, no. 1-2, pp. 163-172.
- Dinnis, D.M. & James, D.C. 2005, "Engineering mammalian cell factories for improved recombinant monoclonal antibody production: lessons from nature?", *Biotechnology and bioengineering*, vol. 91, no. 2, pp. 180-189.
- Djuranovic, S., Nahvi, A. & Green, R. 2012, "miRNA-mediated gene silencing by translational repression followed by mRNA deadenylation and decay", *Science (New York, N.Y.)*, vol. 336, no. 6078, pp. 237-240.
- Donald, S.P., Sun, X.Y., Hu, C.A., Yu, J., Mei, J.M., Valle, D. & Phang, J.M. 2001, "Proline oxidase, encoded by p53-induced gene-6, catalyzes the generation of proline-dependent reactive oxygen species", *Cancer research*, vol. 61, no. 5, pp. 1810-1815.
- Donaldson, M., Wood, H.A., Kulakosky, P.C. & Shuler, M.L. 1999, "Glycosylation of a recombinant protein in the Tn5B1-4 insect cell line: influence of ammonia, time of harvest, temperature, and dissolved oxygen", *Biotechnology and bioengineering*, vol. 63, no. 3, pp. 255-262.

- Dong, C.G., Wu, W.K., Feng, S.Y., Wang, X.J., Shao, J.F. & Qiao, J. 2012, "Co-inhibition of microRNA-10b and microRNA-21 exerts synergistic inhibition on the proliferation and invasion of human glioma cells", *International journal of oncology*, 41(31), pp. 1005-12.
- Doolan, P., Clarke, C., Kinsella, P., Breen, L., Meleady, P., Leonard, M., Zhang, L., Clynes, M., Aherne, S. & Barron, N. 2013, "Transcriptomic analysis of clonal growth rate variation during CHO cell line development", *Journal of Biotechnology*, 10; 166(3), pp. 105-13.
- Doolan, P., Meleady, P., Barron, N., Henry, M., Gallagher, R., Gammell, P., Melville, M., Sinacore, M., McCarthy, K., Leonard, M., Charlebois, T. & Clynes, M. 2010, "Microarray and proteomics expression profiling identifies several candidates, including the valosin-containing protein (VCP), involved in regulating high cellular growth rate in production CHO cell lines", *Biotechnology and bioengineering*, vol. 106, no. 1, pp. 42-56.
- Dowd, J.E., Kwok, K.E. & Piret, J.M. 2000, "Increased t-PA yields using ultrafiltration of an inhibitory product from CHO fed-batch culture", *Biotechnology progress*, vol. 16, no. 5, pp. 786-794.
- Drissi, R., Dubois, M.L. & Boisvert, F.M. 2013, "Proteomics methods for subcellular proteome analysis", *The FEBS journal*, vol. 280, no. 22, pp. 5626-5634.
- Druz, A., Chu, C., Majors, B., Sanctuary, R., Betenbaugh, M. & Shiloach, J. 2011, "A novel microRNA mmu-miR-466h affects apoptosis regulation in mammalian cells", *Biotechnology and bioengineering*, vol. 108, no. 7, pp. 1651-1661.
- Druz, A., Son, Y.J., Betenbaugh, M. & Shiloach, J. 2013, "Stable inhibition of mmu-miR-466h-5p improves apoptosis resistance and protein production in CHO cells", *Metabolic engineering*, vol. 16C, pp. 87-94.
- Du, G., Yonekubo, J., Zeng, Y., Osisami, M. & Frohman, M.A. 2006, "Design of expression vectors for RNA interference based on miRNAs and RNA splicing", *The FEBS journal*, vol. 273, no. 23, pp. 5421-5427.
- Du, R., Sun, W., Xia, L., Zhao, A., Yu, Y., Zhao, L., Wang, H., Huang, C. & Sun, S. 2012, "Hypoxia-induced down-regulation of microRNA-34a promotes EMT by targeting the Notch signaling pathway in tubular epithelial cells", *PloS one*, vol. 7, no. 2, pp. e30771.
- Du, W.W., Fang, L., Li, M., Yang, X., Liang, Y., Peng, C., Qian, W., O'Malley, Y.Q., Askeland, R.W., Sugg, S.L., Qian, J., Lin, J., Jiang, Z., Yee, A.J., Sefton, M., Deng, Z., Shan, S.W., Wang, C.H. & Yang, B.B. 2013, "MicroRNA miR-24 enhances tumor invasion and metastasis by targeting PTPN9 and PTPRF to promote EGF signaling", *Journal of cell science*, vol. 126, no. Pt 6, pp. 1440-1453.
- Dupuy, A.J., Jenkins, N.A. & Copeland, N.G. 2006, "Sleeping beauty: a novel cancer gene discovery tool", *Human molecular genetics*, vol. 15 Spec No 1, pp. R75-9.

- Dweep, H., Sticht, C., Pandey, P. & Gretz, N. 2011a, "miRWalk--database: prediction of possible miRNA binding sites by "walking" the genes of three genomes", *Journal of Biomedical Informatics*, vol. 44, no. 5, pp. 839-847.
- Dweep, H., Sticht, C., Pandey, P. & Gretz, N. 2011b, "miRWalk--database: prediction of possible miRNA binding sites by "walking" the genes of three genomes", *Journal of Biomedical Informatics*, vol. 44, no. 5, pp. 839-847.
- Easom, R.A. 1999, "CaM kinase II: a protein kinase with extraordinary talents germane to insulin exocytosis", *Diabetes*, vol. 48, no. 4, pp. 675-684.
- Ebert, M.S., Neilson, J.R. & Sharp, P.A. 2007, "MicroRNA sponges: competitive inhibitors of small RNAs in mammalian cells", *Nature methods*, vol. 4, no. 9, pp. 721-726.
- EDELMAN, G.M. & BENACERRAF, B. 1962, "On structural and functional relations between antibodies and proteins of the gamma-system", *Proceedings of the National Academy of Sciences of the United States of America*, vol. 48, pp. 1035-1042.
- Ehrenreich, I.M. & Purugganan, M. 2008, "MicroRNAs in plants: Possible contributions to phenotypic diversity", *Plant signaling & behavior*, vol. 3, no. 10, pp. 829-830.
- Eilers, M. & Eisenman, R.N. 2008, "Myc's broad reach", *Genes & development*, vol. 22, no. 20, pp. 2755-2766.
- Eizirik, D.L., Miani, M. & Cardozo, A.K. 2013, "Signalling danger: endoplasmic reticulum stress and the unfolded protein response in pancreatic islet inflammation", *Diabetologia*, vol. 56, no. 2, pp. 234-241.
- Elkan-Miller, T., Ulitsky, I., Hertzano, R., Rudnicki, A., Dror, A.A., Lenz, D.R., Elkon, R., Irmeler, M., Beckers, J., Shamir, R. & Avraham, K.B. 2011, "Integration of transcriptomics, proteomics, and microRNA analyses reveals novel microRNA regulation of targets in the mammalian inner ear", *PloS one*, vol. 6, no. 4, pp. e18195.
- Eng, K.E., Panas, M.D., Karlsson Hedestam, G.B. & McInerney, G.M. 2010, "A novel quantitative flow cytometry-based assay for autophagy", *Autophagy*, vol. 6, no. 5, pp. 634-641.
- Esau, C., Davis, S., Murray, S.F., Yu, X.X., Pandey, S.K., Pear, M., Watts, L., Booten, S.L., Graham, M., McKay, R., Subramaniam, A., Propp, S., Lollo, B.A., Freier, S., Bennett, C.F., Bhanot, S. & Monia, B.P. 2006a, "miR-122 regulation of lipid metabolism revealed by in vivo antisense targeting", *Cell metabolism*, vol. 3, no. 2, pp. 87-98.
- Esau, C., Davis, S., Murray, S.F., Yu, X.X., Pandey, S.K., Pear, M., Watts, L., Booten, S.L., Graham, M., McKay, R., Subramaniam, A., Propp, S., Lollo, B.A., Freier, S., Bennett, C.F., Bhanot, S. & Monia, B.P. 2006b, "miR-122 regulation of lipid metabolism revealed by in vivo antisense targeting", *Cell metabolism*, vol. 3, no. 2, pp. 87-98.

- Ferl, R.J., Manak, M.S. & Reyes, M.F. 2002, "The 14-3-3s", *Genome biology*, vol. 3, no. 7, pp. REVIEWS3010.
- Fernando, M.R., Nanri, H., Yoshitake, S., Nagata-Kuno, K. & Minakami, S. 1992, "Thioredoxin regenerates proteins inactivated by oxidative stress in endothelial cells", *European journal of biochemistry / FEBS*, vol. 209, no. 3, pp. 917-922.
- Ferrara, C., Brunker, P., Suter, T., Moser, S., Puntener, U. & Umana, P. 2006, "Modulation of therapeutic antibody effector functions by glycosylation engineering: influence of Golgi enzyme localization domain and co-expression of heterologous beta1, 4-N-acetylglucosaminyltransferase III and Golgi alpha-mannosidase II", *Biotechnology and bioengineering*, vol. 93, no. 5, pp. 851-861.
- Figuerola, B., Jr, Chen, S., Oyler, G.A., Hardwick, J.M. & Betenbaugh, M.J. 2004, "Aven and Bcl-xL enhance protection against apoptosis for mammalian cells exposed to various culture conditions", *Biotechnology and bioengineering*, vol. 85, no. 6, pp. 589-600.
- Filipowicz, W., Bhattacharyya, S.N. & Sonenberg, N. 2008, "Mechanisms of post-transcriptional regulation by microRNAs: are the answers in sight?", *Nature reviews. Genetics*, vol. 9, no. 2, pp. 102-114.
- Fiore, M., Zanier, R. & Degrossi, F. 2002, "Reversible G(1) arrest by dimethyl sulfoxide as a new method to synchronize Chinese hamster cells", *Mutagenesis*, vol. 17, no. 5, pp. 419-424.
- Fischer, S., Wagner, A., Kos, A., Aschrafi, A., Handrick, R., Hannemann, J. & Otte, K. 2013, "Breaking limitations of complex culture media: functional non-viral miRNA delivery into pharmaceutical production cell lines", *Journal of Biotechnology*, vol. 168, no. 4, pp. 589-600.
- Flowers, E., Froelicher, E.S. & Aouizerat, B.E. 2012, "MicroRNA regulation of lipid metabolism", *Metabolism: clinical and experimental*, 62(1), pp. 12-20.
- Ford, L.P. 2006, "Using synthetic miRNA mimics for diverting cell fate: a possibility of miRNA-based therapeutics?", *Leukemia research*, vol. 30, no. 5, pp. 511-513.
- Fornuskova, D., Stiburek, L., Wenchich, L., Vinsova, K., Hansikova, H. & Zeman, J. 2010, "Novel insights into the assembly and function of human nuclear-encoded cytochrome c oxidase subunits 4, 5a, 6a, 7a and 7b", *The Biochemical journal*, vol. 428, no. 3, pp. 363-374.
- Forstemann, K., Tomari, Y., Du, T., Vagin, V.V., Denli, A.M., Bratu, D.P., Klattenhoff, C., Theurkauf, W.E. & Zamore, P.D. 2005, "Normal microRNA maturation and germ-line stem cell maintenance requires Loquacious, a double-stranded RNA-binding domain protein", *PLoS biology*, vol. 3, no. 7, pp. e236.
- Fox, S.R., Patel, U.A., Yap, M.G. & Wang, D.I. 2004, "Maximizing interferon-gamma production by Chinese hamster ovary cells through temperature shift optimization:

- experimental and modeling", *Biotechnology and bioengineering*, vol. 85, no. 2, pp. 177-184.
- Franco-Zorrilla, J.M., Valli, A., Todesco, M., Mateos, I., Puga, M.I., Rubio-Somoza, I., Leyva, A., Weigel, D., Garcia, J.A. & Paz-Ares, J. 2007, "Target mimicry provides a new mechanism for regulation of microRNA activity", *Nature genetics*, vol. 39, no. 8, pp. 1033-1037.
- Freedman, R.B., Hirst, T.R. & Tuite, M.F. 1994, "Protein disulphide isomerase: building bridges in protein folding", *Trends in biochemical sciences*, vol. 19, no. 8, pp. 331-336.
- Friday, E., Oliver, R., Turturro, F. & Welbourne, T. 2012, "Role of glutamate dehydrogenase in cancer growth and homeostasis", *Dehydrogenases.Rijeka, Croatia: InTech*, pp. 181-190.
- Friedman, R.C., Farh, K.K., Burge, C.B. & Bartel, D.P. 2009, "Most mammalian mRNAs are conserved targets of microRNAs", *Genome research*, vol. 19, no. 1, pp. 92-105.
- Frost, R.J. & Olson, E.N. 2011, "Control of glucose homeostasis and insulin sensitivity by the Let-7 family of microRNAs", *Proceedings of the National Academy of Sciences of the United States of America*, vol. 108, no. 52, pp. 21075-21080.
- Fujita, Y., Kojima, K., Hamada, N., Ohhashi, R., Akao, Y., Nozawa, Y., Deguchi, T. & Ito, M. 2008, "Effects of miR-34a on cell growth and chemoresistance in prostate cancer PC3 cells", *Biochemical and biophysical research communications*, vol. 377, no. 1, pp. 114-119.
- Furukawa, N., Sakurai, F., Katayama, K., Seki, N., Kawabata, K. & Mizuguchi, H. 2011, "Optimization of a microRNA expression vector for function analysis of microRNA", *Journal of controlled release : official journal of the Controlled Release Society*, vol. 150, no. 1, pp. 94-101.
- Fussenegger, M., Mazur, X. & Bailey, J.E. 1997, "A novel cytostatic process enhances the productivity of Chinese hamster ovary cells", *Biotechnology and bioengineering*, vol. 55, no. 6, pp. 927-939.
- Gammell, P., Barron, N., Kumar, N. & Clynes, M. 2007, "Initial identification of low temperature and culture stage induction of miRNA expression in suspension CHO-K1 cells", *Journal of Biotechnology*, vol. 130, no. 3, pp. 213-218.
- Gao, P., Sun, L., He, X., Cao, Y. & Zhang, H. 2012, "MicroRNAs and the Warburg Effect: new players in an old arena", *Current gene therapy*, vol. 12, no. 4, pp. 285-291.
- Gao, P., Tchernyshyov, I., Chang, T.C., Lee, Y.S., Kita, K., Ochi, T., Zeller, K.I., De Marzo, A.M., Van Eyk, J.E., Mendell, J.T. & Dang, C.V. 2009, "c-Myc suppression of miR-23a/b enhances mitochondrial glutaminase expression and glutamine metabolism", *Nature*, vol. 458, no. 7239, pp. 762-765.

- Garcia, D. 2008, "A miRacle in plant development: role of microRNAs in cell differentiation and patterning", *Seminars in cell & developmental biology*, vol. 19, no. 6, pp. 586-595.
- Garcia, D.M., Baek, D., Shin, C., Bell, G.W., Grimson, A. & Bartel, D.P. 2011, "Weak seed-pairing stability and high target-site abundance decrease the proficiency of lsy-6 and other microRNAs", *Nature structural & molecular biology*, vol. 18, no. 10, pp. 1139-1146.
- Gardino, A.K., Smerdon, S.J. & Yaffe, M.B. 2006, "Structural determinants of 14-3-3 binding specificities and regulation of subcellular localization of 14-3-3-ligand complexes: a comparison of the X-ray crystal structures of all human 14-3-3 isoforms", *Seminars in cancer biology*, vol. 16, no. 3, pp. 173-182.
- Gaziel-Sovran, A. & Hernando, E. 2012, "miRNA-mediated GALNT modulation of invasion and immune suppression: A sweet deal for metastatic cells", *Oncoimmunology*, vol. 1, no. 5, pp. 746-748.
- Gellerich, F.N., Gizatullina, Z., Trumbeckaite, S., Nguyen, H.P., Pallas, T., Arandarcikaite, O., Vielhaber, S., Seppet, E. & Striggow, F. 2010, "The regulation of OXPHOS by extramitochondrial calcium", *Biochimica et biophysica acta*, vol. 1797, no. 6-7, pp. 1018-1027.
- Georgantas, R.W., 3rd, Streicher, K., Luo, X., Greenlees, L., Zhu, W., Liu, Z., Brohawn, P., Morehouse, C., Higgs, B.W., Richman, L., Jallal, B., Yao, Y. & Ranade, K. 2014, "MicroRNA-206 induces G1 arrest in melanoma by inhibition of CDK4 and Cyclin D", *Pigment cell & melanoma research*, vol. 27, no. 2, pp. 275-286.
- Gething, M.J. & Sambrook, J. 1992, "Protein folding in the cell", *Nature*, vol. 355, no. 6355, pp. 33-45.
- Ghorbaniaghdam, A., Henry, O. & Jolicoeur, M. 2013, "A kinetic-metabolic model based on cell energetic state: study of CHO cell behavior under Na-butyrate stimulation", *Bioprocess and biosystems engineering*, vol. 36, no. 4, pp. 469-487.
- Giglio, S., Cirombella, R., Amodeo, R., Portaro, L., Lavra, L. & Vecchione, A. 2013, "MicroRNA miR-24 promotes cell proliferation by targeting the CDKs inhibitors p27 and p16", *Journal of cellular physiology*, 228(10), pp. 2015-23.
- Gilbert, M.R., Liu, Y., Neltner, J., Pu, H., Morris, A., Sunkara, M., Pittman, T., Kyprianou, N. & Horbinski, C. 2014, "Autophagy and oxidative stress in gliomas with IDH1 mutations", *Acta Neuropathologica*, vol. 127, no. 2, pp. 221-233.
- Gill, S.S., Anjum, N.A., Hasanuzzaman, M., Gill, R., Trivedi, D.K., Ahmad, I., Pereira, E. & Tuteja, N. 2013, "Glutathione and glutathione reductase: a boon in disguise for plant abiotic stress defense operations", *Plant Physiology and Biochemistry : PPB / Societe francaise de physiologie vegetale*, vol. 70, pp. 204-212.
- Godlewski, J., Nowicki, M.O., Bronisz, A., Nuovo, G., Palatini, J., De Lay, M., Van Brocklyn, J., Ostrowski, M.C., Chiocca, E.A. & Lawler, S.E. 2010, "MicroRNA-451

- regulates LKB1/AMPK signaling and allows adaptation to metabolic stress in glioma cells", *Molecular cell*, vol. 37, no. 5, pp. 620-632.
- Griffiths-Jones, S. 2004, "The microRNA Registry", *Nucleic acids research*, vol. 32, no. Database issue, pp. D109-11.
- Griffiths-Jones, S., Hui, J.H., Marco, A. & Ronshaugen, M. 2011, "MicroRNA evolution by arm switching", *EMBO reports*, vol. 12, no. 2, pp. 172-177.
- Griffiths-Jones, S., Saini, H.K., van Dongen, S. & Enright, A.J. 2008, "miRBase: tools for microRNA genomics", *Nucleic acids research*, vol. 36, no. Database issue, pp. D154-8.
- Grimm, D., Streetz, K.L., Jopling, C.L., Storm, T.A., Pandey, K., Davis, C.R., Marion, P., Salazar, F. & Kay, M.A. 2006, "Fatality in mice due to oversaturation of cellular microRNA/short hairpin RNA pathways", *Nature*, vol. 441, no. 7092, pp. 537-541.
- Grimson, A., Farh, K.K., Johnston, W.K., Garrett-Engele, P., Lim, L.P. & Bartel, D.P. 2007, "MicroRNA targeting specificity in mammals: determinants beyond seed pairing", *Molecular cell*, vol. 27, no. 1, pp. 91-105.
- Grozinger, C.M. & Schreiber, S.L. 2000, "Regulation of histone deacetylase 4 and 5 and transcriptional activity by 14-3-3-dependent cellular localization", *Proceedings of the National Academy of Sciences of the United States of America*, vol. 97, no. 14, pp. 7835-7840.
- Grune, T., Catalgol, B., Licht, A., Ermak, G., Pickering, A.M., Ngo, J.K. & Davies, K.J. 2011, "HSP70 mediates dissociation and reassociation of the 26S proteasome during adaptation to oxidative stress", *Free radical biology & medicine*, vol. 51, no. 7, pp. 1355-1364.
- Gu, S., Jin, L., Zhang, F., Huang, Y., Grimm, D., Rossi, J.J. & Kay, M.A. 2011, "Thermodynamic stability of small hairpin RNAs highly influences the loading process of different mammalian Argonautes", *Proceedings of the National Academy of Sciences of the United States of America*, vol. 108, no. 22, pp. 9208-9213.
- Guan, Y., Chen, Q., Yang, X., Haines, P., Pei, M., Terek, R., Wei, X., Zhao, T. & Wei, L. 2012, "Subcellular relocation of histone deacetylase 4 regulates growth plate chondrocyte differentiation through Ca²⁺/calmodulin-dependent kinase IV", *American journal of physiology. Cell physiology*, vol. 303, no. 1, pp. C33-40.
- Guo, L. & Lu, Z. 2010, "The fate of miRNA* strand through evolutionary analysis: implication for degradation as merely carrier strand or potential regulatory molecule?", *PloS one*, vol. 5, no. 6, pp. e11387.
- Haberland, M., Montgomery, R.L. & Olson, E.N. 2009, "The many roles of histone deacetylases in development and physiology: implications for disease and therapy", *Nature reviews. Genetics*, vol. 10, no. 1, pp. 32-42.

- Hackl, M., Borth, N. & Grillari, J. 2012, "miRNAs--pathway engineering of CHO cell factories that avoids translational burdening", *Trends in biotechnology*, vol. 30, no. 8, pp. 405-406.
- Hackl, M., Jadhav, V., Jakobi, T., Rupp, O., Brinkrolf, K., Goesmann, A., Puhler, A., Noll, T., Borth, N. & Grillari, J. 2012, "Computational identification of microRNA gene loci and precursor microRNA sequences in CHO cell lines", *Journal of Biotechnology*, vol. 158, no. 3, pp. 151-155.
- Hackl, M., Jadhav, V., Klanert, G., Karbiener, M., Scheideler, M., Grillari, J. & Borth, N. 2014a, "Analysis of microRNA transcription and post-transcriptional processing by Dicer in the context of CHO cell proliferation", *Journal of Biotechnology*, 2014 Jan 28. pii: S0168-1656(14)00037-6. doi: 10.1016/j.jbiotec.2013.12.018.
- Hackl, M., Jakobi, T., Blom, J., Doppmeier, D., Brinkrolf, K., Szczepanowski, R., Bernhart, S.H., Honer Zu Siederdissen, C., Bort, J.A., Wieser, M., Kunert, R., Jeffs, S., Hofacker, I.L., Goesmann, A., Puhler, A., Borth, N. & Grillari, J. 2011, "Next-generation sequencing of the Chinese hamster ovary microRNA transcriptome: Identification, annotation and profiling of microRNAs as targets for cellular engineering", *Journal of Biotechnology*, vol. 153, no. 1-2, pp. 62-75.
- Hammell, M., Long, D., Zhang, L., Lee, A., Carmack, C.S., Han, M., Ding, Y. & Ambros, V. 2008, "mirWIP: microRNA target prediction based on microRNA-containing ribonucleoprotein-enriched transcripts", *Nature methods*, vol. 5, no. 9, pp. 813-819.
- Hammond, S., Kaplarevic, M., Borth, N., Betenbaugh, M.J. & Lee, K.H. 2012, "Chinese hamster genome database: an online resource for the CHO community at www.CHOgenome.org", *Biotechnology and bioengineering*, vol. 109, no. 6, pp. 1353-1356.
- Han, B.W., Hung, J.H., Weng, Z., Zamore, P.D. & Ameres, S.L. 2011, "The 3'-to-5' exoribonuclease Nibbler shapes the 3' ends of microRNAs bound to Drosophila Argonaute1", *Current biology : CB*, vol. 21, no. 22, pp. 1878-1887.
- Han, J., Lee, Y., Yeom, K.H., Kim, Y.K., Jin, H. & Kim, V.N. 2004, "The Drosha-DGCR8 complex in primary microRNA processing", *Genes & development*, vol. 18, no. 24, pp. 3016-3027.
- Han, J., Lee, Y., Yeom, K.H., Nam, J.W., Heo, I., Rhee, J.K., Sohn, S.Y., Cho, Y., Zhang, B.T. & Kim, V.N. 2006, "Molecular basis for the recognition of primary microRNAs by the Drosha-DGCR8 complex", *Cell*, vol. 125, no. 5, pp. 887-901.
- Han, Y.K., Ha, T.K., Lee, S.J., Lee, J.S. & Lee, G.M. 2011, "Autophagy and apoptosis of recombinant Chinese hamster ovary cells during fed-batch culture: effect of nutrient supplementation", *Biotechnology and bioengineering*, vol. 108, no. 9, pp. 2182-2192.
- Hansen, T.B., Wiklund, E.D., Bramsen, J.B., Villadsen, S.B., Statham, A.L., Clark, S.J. & Kjems, J. 2011, "miRNA-dependent gene silencing involving Ago2-mediated

- cleavage of a circular antisense RNA", *The EMBO journal*, vol. 30, no. 21, pp. 4414-4422.
- Haraguchi, T., Ozaki, Y. & Iba, H. 2009, "Vectors expressing efficient RNA decoys achieve the long-term suppression of specific microRNA activity in mammalian cells", *Nucleic acids research*, vol. 37, no. 6, pp. e43.
- Harper, M.E., Dent, R., Monemdjou, S., Bezaire, V., Van Wyck, L., Wells, G., Kavaslar, G.N., Gauthier, A., Tesson, F. & McPherson, R. 2002, "Decreased mitochondrial proton leak and reduced expression of uncoupling protein 3 in skeletal muscle of obese diet-resistant women", *Diabetes*, vol. 51, no. 8, pp. 2459-2466.
- Hashimi, S.T., Fulcher, J.A., Chang, M.H., Gov, L., Wang, S. & Lee, B. 2009, "MicroRNA profiling identifies miR-34a and miR-21 and their target genes JAG1 and WNT1 in the coordinate regulation of dendritic cell differentiation", *Blood*, vol. 114, no. 2, pp. 404-414.
- Hassan, T., Smith, S.G., Gaughan, K., Oglesby, I.K., O'Neill, S., McElvaney, N.G. & Greene, C.M. 2013, "Isolation and identification of cell-specific microRNAs targeting a messenger RNA using a biotinylated anti-sense oligonucleotide capture affinity technique", *Nucleic acids research*, vol. 41, no. 6, pp. e71.
- He, L., He, X., Lim, L.P., de Stanchina, E., Xuan, Z., Liang, Y., Xue, W., Zender, L., Magnus, J., Ridzon, D., Jackson, A.L., Linsley, P.S., Chen, C., Lowe, S.W., Cleary, M.A. & Hannon, G.J. 2007a, "A microRNA component of the p53 tumour suppressor network", *Nature*, vol. 447, no. 7148, pp. 1130-1134.
- He, L., He, X., Lim, L.P., de Stanchina, E., Xuan, Z., Liang, Y., Xue, W., Zender, L., Magnus, J., Ridzon, D., Jackson, A.L., Linsley, P.S., Chen, C., Lowe, S.W., Cleary, M.A. & Hannon, G.J. 2007b, "A microRNA component of the p53 tumour suppressor network", *Nature*, vol. 447, no. 7148, pp. 1130-1134.
- He, L., He, X., Lim, L.P., de Stanchina, E., Xuan, Z., Liang, Y., Xue, W., Zender, L., Magnus, J., Ridzon, D., Jackson, A.L., Linsley, P.S., Chen, C., Lowe, S.W., Cleary, M.A. & Hannon, G.J. 2007c, "A microRNA component of the p53 tumour suppressor network", *Nature*, vol. 447, no. 7148, pp. 1130-1134.
- Healy, S., Khan, D.H. & Davie, J.R. 2011, "Gene expression regulation through 14-3-3 interactions with histones and HDACs", *Discovery medicine*, vol. 11, no. 59, pp. 349-358.
- Hendrick, V., Winnepenninckx, P., Abdelkafi, C., Vandeputte, O., Cherlet, M., Marique, T., Renemann, G., Loa, A., Kretzmer, G. & Werenne, J. 2001a, "Increased productivity of recombinant tissular plasminogen activator (t-PA) by butyrate and shift of temperature: a cell cycle phases analysis", *Cytotechnology*, vol. 36, no. 1-3, pp. 71-83.
- Hendrick, V., Winnepenninckx, P., Abdelkafi, C., Vandeputte, O., Cherlet, M., Marique, T., Renemann, G., Loa, A., Kretzmer, G. & Werenne, J. 2001b, "Increased productivity of recombinant tissular plasminogen activator (t-PA) by butyrate and

- shift of temperature: a cell cycle phases analysis", *Cytotechnology*, vol. 36, no. 1-3, pp. 71-83.
- Hennessy, E., Clynes, M., Jeppesen, P.B. & O'Driscoll, L. 2010, "Identification of microRNAs with a role in glucose stimulated insulin secretion by expression profiling of MIN6 cells", *Biochemical and biophysical research communications*, vol. 396, no. 2, pp. 457-462.
- Hermeking, H. 2009, "MiR-34a and p53", *Cell cycle (Georgetown, Tex.)*, vol. 8, no. 9, pp. 1308.
- Hermeking, H. 2007, "p53 enters the microRNA world", *Cancer cell*, vol. 12, no. 5, pp. 414-418.
- Hernandez Bort, J.A., Hackl, M., Hoflmayer, H., Jadhav, V., Harreither, E., Kumar, N., Ernst, W., Grillari, J. & Borth, N. 2012, "Dynamic mRNA and miRNA profiling of CHO-K1 suspension cell cultures", *Biotechnology journal*, vol. 7, no. 4, pp. 500-515.
- Hirano, N., Muroi, T., Takahashi, H. & Haruki, M. 2011, "Site-specific recombinases as tools for heterologous gene integration", *Applied Microbiology and Biotechnology*, vol. 92, no. 2, pp. 227-239.
- Hirsch, A., Hahn, D., Kempna, P., Hofer, G., Mullis, P.E., Nuoffer, J.M. & Fluck, C.E. 2012, "Role of AMP-activated protein kinase on steroid hormone biosynthesis in adrenal NCI-H295R cells", *PloS one*, vol. 7, no. 1, pp. e30956.
- Ho, S.C., Tong, Y.W. & Yang, Y. 2013, "Generation of monoclonal antibody-producing mammalian cell lines", *Pharmaceutical Bioprocessing*, vol. 1, no. 1, pp. 71-87.
- Hong, J.K., Cho, S.M. & Yoon, S.K. 2010, "Substitution of glutamine by glutamate enhances production and galactosylation of recombinant IgG in Chinese hamster ovary cells", *Applied Microbiology and Biotechnology*, vol. 88, no. 4, pp. 869-876.
- Horbinski, C. 2013, "What do we know about IDH1/2 mutations so far, and how do we use it?", *Acta Neuropathologica*, vol. 125, no. 5, pp. 621-636.
- Hsieh, J.K., Fredersdorf, S., Kouzarides, T., Martin, K. & Lu, X. 1997, "E2F1-induced apoptosis requires DNA binding but not transactivation and is inhibited by the retinoblastoma protein through direct interaction", *Genes & development*, vol. 11, no. 14, pp. 1840-1852.
- Hu, H.Y., Yan, Z., Xu, Y., Hu, H., Menzel, C., Zhou, Y.H., Chen, W. & Khaitovich, P. 2009, "Sequence features associated with microRNA strand selection in humans and flies", *BMC genomics*, vol. 10, pp. 413.
- Huang, Y.M., Hu, W., Rustandi, E., Chang, K., Yusuf-Makagiansar, H. & Ryll, T. 2010, "Maximizing productivity of CHO cell-based fed-batch culture using chemically defined media conditions and typical manufacturing equipment", *Biotechnology progress*, vol. 26, no. 5, pp. 1400-1410.

- Hwang, S.O., Chung, J.Y. & Lee, G.M. 2003, "Effect of doxycycline-regulated ERp57 expression on specific thrombopoietin productivity of recombinant CHO cells", *Biotechnology progress*, vol. 19, no. 1, pp. 179-184.
- Hwang, S.O. & Lee, G.M. 2009, "Effect of Akt overexpression on programmed cell death in antibody-producing Chinese hamster ovary cells", *Journal of Biotechnology*, vol. 139, no. 1, pp. 89-94.
- Hwang, S.O. & Lee, G.M. 2008, "Nutrient deprivation induces autophagy as well as apoptosis in Chinese hamster ovary cell culture", *Biotechnology and bioengineering*, vol. 99, no. 3, pp. 678-685.
- Ichimura, A., Ruike, Y., Terasawa, K., Shimizu, K. & Tsujimoto, G. 2010, "MicroRNA-34a inhibits cell proliferation by repressing mitogen-activated protein kinase kinase 1 during megakaryocytic differentiation of K562 cells", *Molecular pharmacology*, vol. 77, no. 6, pp. 1016-1024.
- Ikeda, Y., Tanji, E., Makino, N., Kawata, S. & Furukawa, T. 2012, "MicroRNAs associated with mitogen-activated protein kinase in human pancreatic cancer", *Molecular cancer research : MCR*, vol. 10, no. 2, pp. 259-269.
- Imai-Nishiya, H., Mori, K., Inoue, M., Wakitani, M., Iida, S., Shitara, K. & Satoh, M. 2007, "Double knockdown of alpha1,6-fucosyltransferase (FUT8) and GDP-mannose 4,6-dehydratase (GMD) in antibody-producing cells: a new strategy for generating fully non-fucosylated therapeutic antibodies with enhanced ADCC", *BMC biotechnology*, vol. 7, pp. 84.
- Iqbal, M.A., Gupta, V., Gopinath, P., Mazurek, S. & Bamezai, R.N. 2014, "Pyruvate kinase M2 and cancer: an updated assessment", *FEBS letters*, 19;588(16), pp. 2685-92.
- Ishteiw, R.A., Ward, T.M., Dykxhoorn, D.M. & Burnstein, K.L. 2012, "The microRNA -23b/-27b cluster suppresses the metastatic phenotype of castration-resistant prostate cancer cells", *PloS one*, vol. 7, no. 12, pp. e52106.
- Itani, S., Kunisada, T., Morimoto, Y., Yoshida, A., Sasaki, T., Ito, S., Ouchida, M., Sugihara, S., Shimizu, K. & Ozaki, T. 2012, "MicroRNA-21 correlates with tumorigenesis in malignant peripheral nerve sheath tumor (MPNST) via programmed cell death protein 4 (PDCD4)", *Journal of cancer research and clinical oncology*, vol. 138, no. 9, pp. 1501-1509.
- Ivanovska, I., Ball, A.S., Diaz, R.L., Magnus, J.F., Kibukawa, M., Schelter, J.M., Kobayashi, S.V., Lim, L., Burchard, J., Jackson, A.L., Linsley, P.S. & Cleary, M.A. 2008, "MicroRNAs in the miR-106b family regulate p21/CDKN1A and promote cell cycle progression", *Molecular and cellular biology*, vol. 28, no. 7, pp. 2167-2174.
- Jacobson, J. & Duchon, M.R. 2004, "Interplay between mitochondria and cellular calcium signalling", *Molecular and cellular biochemistry*, vol. 256-257, no. 1-2, pp. 209-218.

- Jadhav, V., Hackl, M., Bort, J.A., Wieser, M., Harreither, E., Kunert, R., Borth, N. & Grillari, J. 2012, "A screening method to assess biological effects of microRNA overexpression in Chinese hamster ovary cells", *Biotechnology and bioengineering*, vol. 109, no. 6, pp. 1376-1385.
- Jadhav, V., Hackl, M., Druz, A., Shridhar, S., Chung, C.Y., Heffner, K.M., Kreil, D.P., Betenbaugh, M., Shiloach, J., Barron, N., Grillari, J. & Borth, N. 2013, "CHO microRNA engineering is growing up: Recent successes and future challenges", *Biotechnology Advances*, 2013 Dec;31(8):1501-13. doi: 10.1016/j.biotechadv.2013.07.00.
- Jadhav, V., Hackl, M., Klanert, G., Hernandez Bort, J.A., Kunert, R., Grillari, J. & Borth, N. 2014, "Stable overexpression of miR-17 enhances recombinant protein production of CHO cells", *Journal of Biotechnology*, vol. 175C, pp. 38-44.
- Jahn, R. & Scheller, R.H. 2006, "SNAREs--engines for membrane fusion", *Nature reviews.Molecular cell biology*, vol. 7, no. 9, pp. 631-643.
- Jaluria, P., Betenbaugh, M., Konstantopoulos, K. & Shiloach, J. 2007, "Enhancement of cell proliferation in various mammalian cell lines by gene insertion of a cyclin-dependent kinase homolog", *BMC biotechnology*, vol. 7, pp. 71.
- Janas, M.M., Wang, B., Harris, A.S., Aguiar, M., Shaffer, J.M., Subrahmanyam, Y.V., Behlke, M.A., Wucherpfennig, K.W., Gygi, S.P., Gagnon, E. & Novina, C.D. 2012, "Alternative RISC assembly: binding and repression of microRNA-mRNA duplexes by human Ago proteins", *RNA (New York, N.Y.)*, vol. 18, no. 11, pp. 2041-2055.
- Jastroch, M., Divakaruni, A.S., Mookerjee, S., Treberg, J.R. & Brand, M.D. 2010, "Mitochondrial proton and electron leaks", *Essays in biochemistry*, vol. 47, pp. 53-67.
- Jayapal, K.P., Wlaschin, K.F., Hu, W. & Yap, M.G.S. 2007, "Recombinant protein therapeutics from CHO cells-20 years and counting", *Chemical Engineering Progress*, vol. 103, no. 10, pp. 40.
- Jeck, W.R., Sorrentino, J.A., Wang, K., Slevin, M.K., Burd, C.E., Liu, J., Marzluff, W.F. & Sharpless, N.E. 2013, "Circular RNAs are abundant, conserved, and associated with ALU repeats", *RNA (New York, N.Y.)*, vol. 19, no. 2, pp. 141-157.
- Jefferis, R. 2009a, "Glycosylation as a strategy to improve antibody-based therapeutics", *Nature reviews.Drug discovery*, vol. 8, no. 3, pp. 226-234.
- Jefferis, R. 2009b, "Recombinant antibody therapeutics: the impact of glycosylation on mechanisms of action", *Trends in pharmacological sciences*, vol. 30, no. 7, pp. 356-362.
- Jefferis, R. 2007, "Antibody therapeutics: isotype and glycoform selection", *Expert opinion on biological therapy*, vol. 7, no. 9, pp. 1401-1413.

- Jeon, M.K., Yu, D.Y. & Lee, G.M. 2011, "Combinatorial engineering of ldh-a and bcl-2 for reducing lactate production and improving cell growth in dihydrofolate reductase-deficient Chinese hamster ovary cells", *Applied Microbiology and Biotechnology*, vol. 92, no. 4, pp. 779-790.
- Jeong, D., Kim, T.S., Lee, J.W., Kim, K.T., Kim, H.J., Kim, I.H. & Kim, I.Y. 2001, "Blocking of acidosis-mediated apoptosis by a reduction of lactate dehydrogenase activity through antisense mRNA expression", *Biochemical and biophysical research communications*, vol. 289, no. 5, pp. 1141-1149.
- Jiang, D., Zhao, L. & Clapham, D.E. 2009, "Genome-wide RNAi screen identifies Letm1 as a mitochondrial Ca²⁺/H⁺ antiporter", *Science (New York, N.Y.)*, vol. 326, no. 5949, pp. 144-147.
- Jiang, D., Zhao, L., Clish, C.B. & Clapham, D.E. 2013a, "Letm1, the mitochondrial Ca²⁺/H⁺ antiporter, is essential for normal glucose metabolism and alters brain function in Wolf-Hirschhorn syndrome", *Proceedings of the National Academy of Sciences of the United States of America*, vol. 110, no. 24, pp. E2249-54.
- Jiang, J., Yang, J., Wang, Z., Wu, G. & Liu, F. 2013b, "TFAM is directly regulated by miR-23b in glioma", *Oncology reports*, vol. 30, no. 5, pp. 2105-2110.
- Jiang, Q., Wang, Y., Hao, Y., Juan, L., Teng, M., Zhang, X., Li, M., Wang, G. & Liu, Y. 2009, "miR2Disease: a manually curated database for microRNA deregulation in human disease", *Nucleic acids research*, vol. 37, no. Database issue, pp. D98-104.
- Jiang, X.R., Song, A., Bergelson, S., Arroll, T., Parekh, B., May, K., Chung, S., Strouse, R., Mire-Sluis, A. & Schenerman, M. 2011, "Advances in the assessment and control of the effector functions of therapeutic antibodies", *Nature reviews. Drug discovery*, vol. 10, no. 2, pp. 101-111.
- Jiang, Z. & Sharfstein, S.T. 2008, "Sodium butyrate stimulates monoclonal antibody over-expression in CHO cells by improving gene accessibility", *Biotechnology and bioengineering*, vol. 100, no. 1, pp. 189-194.
- Jo, D.H., Kim, J.H., Park, W.Y., Kim, K.W., Yu, Y.S. & Kim, J.H. 2011, "Differential profiles of microRNAs in retinoblastoma cell lines of different proliferation and adherence patterns", *Journal of pediatric hematology/oncology*, vol. 33, no. 7, pp. 529-533.
- Jo, S.H., Son, M.K., Koh, H.J., Lee, S.M., Song, I.H., Kim, Y.O., Lee, Y.S., Jeong, K.S., Kim, W.B., Park, J.W., Song, B.J. & Huh, T.L. 2001, "Control of mitochondrial redox balance and cellular defense against oxidative damage by mitochondrial NADP⁺-dependent isocitrate dehydrogenase", *The Journal of biological chemistry*, vol. 276, no. 19, pp. 16168-16176.
- John, B., Enright, A.J., Aravin, A., Tuschl, T., Sander, C. & Marks, D.S. 2004, "Human MicroRNA targets", *PLoS biology*, vol. 2, no. 11, pp. e363.

- Johnson, K.C., Jacob, N.M., Nissom, P.M., Hackl, M., Lee, L.H., Yap, M. & Hu, W.S. 2011, "Conserved microRNAs in Chinese hamster ovary cell lines", *Biotechnology and bioengineering*, vol. 108, no. 2, pp. 475-480.
- Joseph, J.W., Jensen, M.V., Ilkayeva, O., Palmieri, F., Alarcon, C., Rhodes, C.J. & Newgard, C.B. 2006, "The mitochondrial citrate/isocitrate carrier plays a regulatory role in glucose-stimulated insulin secretion", *The Journal of biological chemistry*, vol. 281, no. 47, pp. 35624-35632.
- Joung, J.K. & Sander, J.D. 2013, "TALENs: a widely applicable technology for targeted genome editing", *Nature reviews.Molecular cell biology*, vol. 14, no. 1, pp. 49-55.
- Junttila, T.T., Parsons, K., Olsson, C., Lu, Y., Xin, Y., Theriault, J., Crocker, L., Pabonan, O., Baginski, T., Meng, G., Totpal, K., Kelley, R.F. & Sliwkowski, M.X. 2010, "Superior in vivo efficacy of afucosylated trastuzumab in the treatment of HER2-amplified breast cancer", *Cancer research*, vol. 70, no. 11, pp. 4481-4489.
- Juvvuna, P.K., Khandelvia, P., Lee, L.M. & Makeyev, E.V. 2012, "Argonaute identity defines the length of mature mammalian microRNAs", *Nucleic acids research*, 40(14), pp. 6808-20.
- Kabeya, Y., Mizushima, N., Ueno, T., Yamamoto, A., Kirisako, T., Noda, T., Kominami, E., Ohsumi, Y. & Yoshimori, T. 2000, "LC3, a mammalian homologue of yeast Apg8p, is localized in autophagosome membranes after processing", *The EMBO journal*, vol. 19, no. 21, pp. 5720-5728.
- Kaller, M., Liffers, S.T., Oeljeklaus, S., Kuhlmann, K., Roh, S., Hoffmann, R., Warscheid, B. & Hermeking, H. 2011a, "Genome-wide characterization of miR-34a induced changes in protein and mRNA expression by a combined pulsed SILAC and microarray analysis", *Molecular & cellular proteomics : MCP*, vol. 10, no. 8, pp. M111.010462.
- Kaller, M., Liffers, S.T., Oeljeklaus, S., Kuhlmann, K., Roh, S., Hoffmann, R., Warscheid, B. & Hermeking, H. 2011b, "Genome-wide characterization of miR-34a induced changes in protein and mRNA expression by a combined pulsed SILAC and microarray analysis", *Molecular & cellular proteomics : MCP*, vol. 10, no. 8, pp. M111.010462.
- Kameyama, Y., Kawabe, Y., Ito, A. & Kamihira, M. 2010, "An accumulative site-specific gene integration system using Cre recombinase-mediated cassette exchange", *Biotechnology and bioengineering*, vol. 105, no. 6, pp. 1106-1114.
- Kanda, Y., Imai-Nishiya, H., Kuni-Kamochi, R., Mori, K., Inoue, M., Kitajima-Miyama, K., Okazaki, A., Iida, S., Shitara, K. & Satoh, M. 2007, "Establishment of a GDP-mannose 4,6-dehydratase (GMD) knockout host cell line: a new strategy for generating completely non-fucosylated recombinant therapeutics", *Journal of Biotechnology*, vol. 130, no. 3, pp. 300-310.
- Kanda, Y., Yamane-Ohnuki, N., Sakai, N., Yamano, K., Nakano, R., Inoue, M., Misaka, H., Iida, S., Wakitani, M., Konno, Y., Yano, K., Shitara, K., Hosoi, S. & Satoh, M.

- 2006, "Comparison of cell lines for stable production of fucose-negative antibodies with enhanced ADCC", *Biotechnology and bioengineering*, vol. 94, no. 4, pp. 680-688.
- Kang, H.J. & Park, H.J. 2009, "Novel molecular mechanism for actinomycin D activity as an oncogenic promoter G-quadruplex binder", *Biochemistry*, vol. 48, no. 31, pp. 7392-7398.
- Kang, S., Ren, D., Xiao, G., Daris, K., Buck, L., Enyenihi, A.A., Zubarev, R., Bondarenko, P.V. & Deshpande, R. 2013a, "Cell line profiling to improve monoclonal antibody production", *Biotechnology and bioengineering*, 111(4), pp. 748-60.
- Kang, S.M., Choi, J.W., Hong, S.H. & Lee, H.J. 2013b, "Up-Regulation of microRNA* Strands by Their Target Transcripts", *International journal of molecular sciences*, vol. 14, no. 7, pp. 13231-13240.
- Kanitz, A. & Gerber, A.P. 2010, "Circuitry of mRNA regulation", *Wiley interdisciplinary reviews. Systems biology and medicine*, vol. 2, no. 2, pp. 245-251.
- Kantardjieff, A., Jacob, N.M., Yee, J.C., Epstein, E., Kok, Y.J., Philp, R., Betenbaugh, M. & Hu, W.S. 2010, "Transcriptome and proteome analysis of Chinese hamster ovary cells under low temperature and butyrate treatment", *Journal of Biotechnology*, vol. 145, no. 2, pp. 143-159.
- Karginov, F.V., Conaco, C., Xuan, Z., Schmidt, B.H., Parker, J.S., Mandel, G. & Hannon, G.J. 2007, "A biochemical approach to identifying microRNA targets", *Proceedings of the National Academy of Sciences of the United States of America*, vol. 104, no. 49, pp. 19291-19296.
- Karreth, F.A., Tay, Y., Perna, D., Ala, U., Tan, S.M., Rust, A.G., DeNicola, G., Webster, K.A., Weiss, D., Perez-Mancera, P.A., Krauthammer, M., Halaban, R., Provero, P., Adams, D.J., Tuveson, D.A. & Pandolfi, P.P. 2011, "In vivo identification of tumor-suppressive PTEN ceRNAs in an oncogenic BRAF-induced mouse model of melanoma", *Cell*, vol. 147, no. 2, pp. 382-395.
- Kaufman, R.J. & Malhotra, J.D. 2014, "Calcium trafficking integrates endoplasmic reticulum function with mitochondrial bioenergetics", *Biochimica et biophysica acta*, 1843(10), pp. 2233-9.
- Kawabe, Y., Makitsubo, H., Kameyama, Y., Huang, S., Ito, A. & Kamihira, M. 2012, "Repeated integration of antibody genes into a pre-selected chromosomal locus of CHO cells using an accumulative site-specific gene integration system", *Cytotechnology*, vol. 64, no. 3, pp. 267-279.
- Kertesz, M., Iovino, N., Unnerstall, U., Gaul, U. & Segal, E. 2007, "The role of site accessibility in microRNA target recognition", *Nature genetics*, vol. 39, no. 10, pp. 1278-1284.

- Ketting, R.F., Fischer, S.E., Bernstein, E., Sijen, T., Hannon, G.J. & Plasterk, R.H. 2001, "Dicer functions in RNA interference and in synthesis of small RNA involved in developmental timing in *C. elegans*", *Genes & development*, vol. 15, no. 20, pp. 2654-2659.
- Khvorova, A., Reynolds, A. & Jayasena, S.D. 2003, "Functional siRNAs and miRNAs exhibit strand bias", *Cell*, vol. 115, no. 2, pp. 209-216.
- Kim do, Y., Chaudhry, M.A., Kennard, M.L., Jardon, M.A., Braasch, K., Dionne, B., Butler, M. & Piret, J.M. 2013, "Fed-batch CHO cell t-PA production and feed glutamine replacement to reduce ammonia production", *Biotechnology progress*, vol. 29, no. 1, pp. 165-175.
- Kim, Y.G., Kim, J.Y. & Lee, G.M. 2009, "Effect of XIAP overexpression on sodium butyrate-induced apoptosis in recombinant Chinese hamster ovary cells producing erythropoietin", *Journal of Biotechnology*, vol. 144, no. 4, pp. 299-303.
- Kim, H.R., Roe, J.S., Lee, J.E., Hwang, I.Y., Cho, E.J. & Youn, H.D. 2012, "A p53-inducible microRNA-34a downregulates Ras signaling by targeting IMPDH", *Biochemical and biophysical research communications*, vol. 418, no. 4, pp. 682-688.
- Kim, H.S. & Lee, G.M. 2007, "Differences in optimal pH and temperature for cell growth and antibody production between two Chinese hamster ovary clones derived from the same parental clone", *Journal of microbiology and biotechnology*, vol. 17, no. 5, pp. 712-720.
- Kim, J.Y., Kim, Y.G., Han, Y.K., Choi, H.S., Kim, Y.H. & Lee, G.M. 2011, "Proteomic understanding of intracellular responses of recombinant Chinese hamster ovary cells cultivated in serum-free medium supplemented with hydrolysates", *Applied Microbiology and Biotechnology*, vol. 89, no. 6, pp. 1917-1928.
- Kim, J.Y., Kim, Y.G. & Lee, G.M. 2012, "CHO cells in biotechnology for production of recombinant proteins: current state and further potential", *Applied Microbiology and Biotechnology*, vol. 93, no. 3, pp. 917-930.
- Kim, N.H., Kim, H.S., Kim, N.G., Lee, I., Choi, H.S., Li, X.Y., Kang, S.E., Cha, S.Y., Ryu, J.K., Na, J.M., Park, C., Kim, K., Lee, S., Gumbiner, B.M., Yook, J.I. & Weiss, S.J. 2011, "p53 and microRNA-34 are suppressors of canonical Wnt signaling", *Science signaling*, vol. 4, no. 197, pp. ra71.
- Kim, N.S. & Lee, G.M. 2002, "Inhibition of sodium butyrate-induced apoptosis in recombinant Chinese hamster ovary cells by constitutively expressing antisense RNA of caspase-3", *Biotechnology and bioengineering*, vol. 78, no. 2, pp. 217-228.
- Kim, S., Kim, D.H., Jung, W.H. & Koo, J.S. 2013, "Succinate dehydrogenase expression in breast cancer", *SpringerPlus*, vol. 2, no. 1, pp. 299.
- Kim, S.H. & Lee, G.M. 2007, "Down-regulation of lactate dehydrogenase-A by siRNAs for reduced lactic acid formation of Chinese hamster ovary cells producing

- thrombopoietin", *Applied Microbiology and Biotechnology*, vol. 74, no. 1, pp. 152-159.
- Kim, S.Y., Lee, S.M., Tak, J.K., Choi, K.S., Kwon, T.K. & Park, J.W. 2007, "Regulation of singlet oxygen-induced apoptosis by cytosolic NADP⁺-dependent isocitrate dehydrogenase", *Molecular and cellular biochemistry*, vol. 302, no. 1-2, pp. 27-34.
- Kim, Y.G., Kim, J.Y., Mohan, C. & Lee, G.M. 2009a, "Effect of Bcl-xL overexpression on apoptosis and autophagy in recombinant Chinese hamster ovary cells under nutrient-deprived condition", *Biotechnology and bioengineering*, vol. 103, no. 4, pp. 757-766.
- Kim, Y.K., Yu, J., Han, T.S., Park, S.Y., Namkoong, B., Kim, D.H., Hur, K., Yoo, M.W., Lee, H.J., Yang, H.K. & Kim, V.N. 2009b, "Functional links between clustered microRNAs: suppression of cell-cycle inhibitors by microRNA clusters in gastric cancer", *Nucleic acids research*, vol. 37, no. 5, pp. 1672-1681.
- Kinoshita, T., Nohata, N., Yoshino, H., Hanazawa, T., Kikkawa, N., Fujimura, L., Chiyomaru, T., Kawakami, K., Enokida, H., Nakagawa, M., Okamoto, Y. & Seki, N. 2012, "Tumor suppressive microRNA-375 regulates lactate dehydrogenase B in maxillary sinus squamous cell carcinoma", *International journal of oncology*, vol. 40, no. 1, pp. 185-193.
- Kitami, T., Logan, D.J., Negri, J., Hasaka, T., Tolliday, N.J., Carpenter, A.E., Spiegelman, B.M. & Mootha, V.K. 2012, "A chemical screen probing the relationship between mitochondrial content and cell size", *PloS one*, vol. 7, no. 3, pp. e33755.
- Kitsera, N., Khobta, A. & Epe, B. 2007, "Destabilized green fluorescent protein detects rapid removal of transcription blocks after genotoxic exposure", *BioTechniques*, vol. 43, no. 2, pp. 222-227.
- Klanert, G., Jadhav, V., Chanoumidou, K., Grillari, J., Borth, N. & Hackl, M. 2013, "Endogenous MicroRNA Clusters Outperform Chimeric Sequence Clusters in Chinese Hamster Ovary Cells", *Biotechnology journal*, 9(4), pp. 538-44.
- Kleppe, R., Martinez, A., Doskeland, S.O. & Haavik, J. 2011, "The 14-3-3 proteins in regulation of cellular metabolism", *Seminars in cell & developmental biology*, vol. 22, no. 7, pp. 713-719.
- Klionsky, D.J., Cuervo, A.M. & Seglen, P.O. 2007, "Methods for monitoring autophagy from yeast to human", *Autophagy*, vol. 3, no. 3, pp. 181-206.
- Kloosterman, W.P., Wienholds, E., Ketting, R.F. & Plasterk, R.H. 2004, "Substrate requirements for let-7 function in the developing zebrafish embryo", *Nucleic acids research*, vol. 32, no. 21, pp. 6284-6291.
- Kluiser, J., Gibcus, J.H., Hettinga, C., Adema, A., Richter, M.K., Halsema, N., Slezak-Prochazka, I., Ding, Y., Kroesen, B.J. & van den Berg, A. 2012a, "Rapid generation of microRNA sponges for microRNA inhibition", *PloS one*, vol. 7, no. 1, pp. e29275.

- Kluiver, J., Slezak-Prochazka, I., Smigielska-Czepiel, K., Halsema, N., Kroesen, B.J. & van den Berg, A. 2012b, "Generation of miRNA sponge constructs", *Methods (San Diego, Calif.)*, 58(2), pp. 113-7.
- Kobayashi, H., Tan, E.M. & Fleming, S.E. 2004, "Acetylation of histones associated with the p21WAF1/CIP1 gene by butyrate is not sufficient for p21WAF1/CIP1 gene transcription in human colorectal adenocarcinoma cells", *International journal of cancer. Journal international du cancer*, vol. 109, no. 2, pp. 207-213.
- Kondo, N., Toyama, T., Sugiura, H., Fujii, Y. & Yamashita, H. 2008, "miR-206 Expression is down-regulated in estrogen receptor alpha-positive human breast cancer", *Cancer research*, vol. 68, no. 13, pp. 5004-5008.
- Kong, K.Y., Owens, K.S., Rogers, J.H., Mullenix, J., Velu, C.S., Grimes, H.L. & Dahl, R. 2010, "MIR-23A microRNA cluster inhibits B-cell development", *Experimental hematology*, vol. 38, no. 8, pp. 629-640.e1.
- Koscianska, E., Starega-Roslan, J. & Krzyzosiak, W.J. 2011, "The role of Dicer protein partners in the processing of microRNA precursors", *PloS one*, vol. 6, no. 12, pp. e28548.
- Kou, T.C., Fan, L., Zhou, Y., Ye, Z.Y., Liu, X.P., Zhao, L. & Tan, W.S. 2011, "Detailed understanding of enhanced specific productivity in Chinese hamster ovary cells at low culture temperature", *Journal of bioscience and bioengineering*, vol. 111, no. 3, pp. 365-369.
- Kozomara, A. & Griffiths-Jones, S. 2011, "miRBase: integrating microRNA annotation and deep-sequencing data", *Nucleic acids research*, vol. 39, no. Database issue, pp. D152-7.
- Krapp, S., Mimura, Y., Jefferis, R., Huber, R. & Sondermann, P. 2003, "Structural analysis of human IgG-Fc glycoforms reveals a correlation between glycosylation and structural integrity", *Journal of Molecular Biology*, vol. 325, no. 5, pp. 979-989.
- Krek, A., Grun, D., Poy, M.N., Wolf, R., Rosenberg, L., Epstein, E.J., MacMenamin, P., da Piedade, I., Gunsalus, K.C., Stoffel, M. & Rajewsky, N. 2005, "Combinatorial microRNA target predictions", *Nature genetics*, vol. 37, no. 5, pp. 495-500.
- Krol, J., Loedige, I. & Filipowicz, W. 2010, "The widespread regulation of microRNA biogenesis, function and decay", *Nature reviews. Genetics*, vol. 11, no. 9, pp. 597-610.
- Ku, S.C., Ng, D.T., Yap, M.G. & Chao, S.H. 2008, "Effects of overexpression of X-box binding protein 1 on recombinant protein production in Chinese hamster ovary and NS0 myeloma cells", *Biotechnology and bioengineering*, vol. 99, no. 1, pp. 155-164.
- Kulshreshtha, R., Ferracin, M., Wojcik, S.E., Garzon, R., Alder, H., Agosto-Perez, F.J., Davuluri, R., Liu, C.G., Croce, C.M., Negrini, M., Calin, G.A. & Ivan, M. 2007, "A microRNA signature of hypoxia", *Molecular and cellular biology*, vol. 27, no. 5, pp. 1859-1867.

- Kumar, N., Gammell, P. & Clynes, M. 2007, "Proliferation control strategies to improve productivity and survival during CHO based production culture: A summary of recent methods employed and the effects of proliferation control in product secreting CHO cell lines", *Cytotechnology*, vol. 53, no. 1-3, pp. 33-46.
- Kumar, N., Gammell, P., Meleady, P., Henry, M. & Clynes, M. 2008, "Differential protein expression following low temperature culture of suspension CHO-K1 cells", *BMC biotechnology*, vol. 8, pp. 42-6750-8-42.
- Kuystermans, D. & Al-Rubeai, M. 2009, "cMyc increases cell number through uncoupling of cell division from cell size in CHO cells", *BMC biotechnology*, vol. 9, pp. 76-6750-9-76.
- Lagana, A., Russo, F., Sismeiro, C., Giugno, R., Pulvirenti, A. & Ferro, A. 2010, "Variability in the incidence of miRNAs and genes in fragile sites and the role of repeats and CpG islands in the distribution of genetic material", *PloS one*, vol. 5, no. 6, pp. e11166.
- Lagos-Quintana, M., Rauhut, R., Lendeckel, W. & Tuschl, T. 2001, "Identification of novel genes coding for small expressed RNAs", *Science (New York, N.Y.)*, vol. 294, no. 5543, pp. 853-858.
- Lai, T., Yang, Y. & Ng, S.K. 2013a, "Advances in Mammalian cell line development technologies for recombinant protein production", *Pharmaceuticals (Basel, Switzerland)*, vol. 6, no. 5, pp. 579-603.
- Lai, T., Yang, Y. & Ng, S.K. 2013b, "Advances in Mammalian cell line development technologies for recombinant protein production", *Pharmaceuticals (Basel, Switzerland)*, vol. 6, no. 5, pp. 579-603.
- Lal, A., Navarro, F., Maher, C.A., Maliszewski, L.E., Yan, N., O'Day, E., Chowdhury, D., Dykxhoorn, D.M., Tsai, P., Hofmann, O., Becker, K.G., Gorospe, M., Hide, W. & Lieberman, J. 2009a, "miR-24 Inhibits cell proliferation by targeting E2F2, MYC, and other cell-cycle genes via binding to "seedless" 3'UTR microRNA recognition elements", *Molecular cell*, vol. 35, no. 5, pp. 610-625.
- Lal, A., Navarro, F., Maher, C.A., Maliszewski, L.E., Yan, N., O'Day, E., Chowdhury, D., Dykxhoorn, D.M., Tsai, P., Hofmann, O., Becker, K.G., Gorospe, M., Hide, W. & Lieberman, J. 2009b, "miR-24 Inhibits cell proliferation by targeting E2F2, MYC, and other cell-cycle genes via binding to "seedless" 3'UTR microRNA recognition elements", *Molecular cell*, vol. 35, no. 5, pp. 610-625.
- Lal, A., Thomas, M.P., Altschuler, G., Navarro, F., O'Day, E., Li, X.L., Concepcion, C., Han, Y.C., Thiery, J., Rajani, D.K., Deutsch, A., Hofmann, O., Ventura, A., Hide, W. & Lieberman, J. 2011, "Capture of microRNA-bound mRNAs identifies the tumor suppressor miR-34a as a regulator of growth factor signaling", *PLoS genetics*, vol. 7, no. 11, pp. e1002363.

- Larsen, F.J., Schiffer, T.A., Borniquel, S., Sahlin, K., Ekblom, B., Lundberg, J.O. & Weitzberg, E. 2011, "Dietary inorganic nitrate improves mitochondrial efficiency in humans", *Cell metabolism*, vol. 13, no. 2, pp. 149-159.
- Larsen, S., Nielsen, J., Hansen, C.N., Nielsen, L.B., Wibrand, F., Stride, N., Schroder, H.D., Boushel, R., Helge, J.W., Dela, F. & Hey-Mogensen, M. 2012, "Biomarkers of mitochondrial content in skeletal muscle of healthy young human subjects", *The Journal of physiology*, vol. 590, no. Pt 14, pp. 3349-3360.
- Lau, N.C., Lim, L.P., Weinstein, E.G. & Bartel, D.P. 2001, "An abundant class of tiny RNAs with probable regulatory roles in *Caenorhabditis elegans*", *Science (New York, N.Y.)*, vol. 294, no. 5543, pp. 858-862.
- Laurila, E.M., Sandstrom, S., Rantanen, L.M., Autio, R. & Kallioniemi, A. 2012, "Both inhibition and enhanced expression of miR-31 lead to reduced migration and invasion of pancreatic cancer cells", *Genes, chromosomes & cancer*, vol. 51, no. 6, pp. 557-568.
- Le, A., Lane, A.N., Hamaker, M., Bose, S., Gouw, A., Barbi, J., Tsukamoto, T., Rojas, C.J., Slusher, B.S., Zhang, H., Zimmerman, L.J., Liebler, D.C., Slebos, R.J., Lorkiewicz, P.K., Higashi, R.M., Fan, T.W. & Dang, C.V. 2012, "Glucose-independent glutamine metabolism via TCA cycling for proliferation and survival in B cells", *Cell metabolism*, vol. 15, no. 1, pp. 110-121.
- Lebbink, R.J., Lowe, M., Chan, T., Khine, H., Wang, X. & McManus, M.T. 2011, "Polymerase II promoter strength determines efficacy of microRNA adapted shRNAs", *PloS one*, vol. 6, no. 10, pp. e26213.
- Lee, H.C., Yang, C.W., Chen, C.Y. & Au, L.C. 2011, "Single point mutation of microRNA may cause butterfly effect on alteration of global gene expression", *Biochemical and biophysical research communications*, vol. 404, no. 4, pp. 1065-1069.
- Lee, J.S., Ha, T.K., Park, J.H. & Lee, G.M. 2013, "Anti-cell death engineering of CHO cells: co-overexpression of Bcl-2 for apoptosis inhibition, Beclin-1 for autophagy induction", *Biotechnology and bioengineering*, vol. 110, no. 8, pp. 2195-2207.
- Lee, J.S. & Lee, G.M. 2012, "Effect of sodium butyrate on autophagy and apoptosis in Chinese hamster ovary cells", *Biotechnology progress*, vol. 28, no. 2, pp. 349-357.
- Lee, M.S., Kim, K.W., Kim, Y.H. & Lee, G.M. 2003, "Proteome analysis of antibody-expressing CHO cells in response to hyperosmotic pressure", *Biotechnology progress*, vol. 19, no. 6, pp. 1734-1741.
- Lee, R., Feinbaum, R. & Ambros, V. 2004, "A short history of a short RNA", *Cell*, vol. 116, no. 2 Suppl, pp. S89-92, 1 p following S96.
- Lee, R.C. & Ambros, V. 2001, "An extensive class of small RNAs in *Caenorhabditis elegans*", *Science (New York, N.Y.)*, vol. 294, no. 5543, pp. 862-864.

- Lee, R.C., Feinbaum, R.L. & Ambros, V. 1993, "The *C. elegans* heterochronic gene *lin-4* encodes small RNAs with antisense complementarity to *lin-14*", *Cell*, vol. 75, no. 5, pp. 843-854.
- Lee, S.J., Jiko, C., Yamashita, E. & Tsukihara, T. 2011, "Selective nuclear export mechanism of small RNAs", *Current opinion in structural biology*, vol. 21, no. 1, pp. 101-108.
- Lee, S.M., Koh, H.J., Park, D.C., Song, B.J., Huh, T.L. & Park, J.W. 2002, "Cytosolic NADP(+)-dependent isocitrate dehydrogenase status modulates oxidative damage to cells", *Free radical biology & medicine*, vol. 32, no. 11, pp. 1185-1196.
- Leivonen, S.K., Rokka, A., Ostling, P., Kohonen, P., Corthals, G.L., Kallioniemi, O. & Perala, M. 2011, "Identification of miR-193b targets in breast cancer cells and systems biological analysis of their functional impact", *Molecular & cellular proteomics: MCP*, vol. 10, no. 7, pp. M110.005322.
- Lempiainen, H. & Shore, D. 2009, "Growth control and ribosome biogenesis", *Current opinion in cell biology*, vol. 21, no. 6, pp. 855-863.
- Lennox, K.A. & Behlke, M.A. 2010, "A direct comparison of anti-microRNA oligonucleotide potency", *Pharmaceutical research*, vol. 27, no. 9, pp. 1788-1799.
- Levine, B. & Yuan, J. 2005, "Autophagy in cell death: an innocent convict?", *The Journal of clinical investigation*, vol. 115, no. 10, pp. 2679-2688.
- Lewis, B.P., Shih, I.H., Jones-Rhoades, M.W., Bartel, D.P. & Burge, C.B. 2003, "Prediction of mammalian microRNA targets", *Cell*, vol. 115, no. 7, pp. 787-798.
- Lewis, N.E., Liu, X., Li, Y., Nagarajan, H., Yerganian, G., O'Brien, E., Bordbar, A., Roth, A.M., Rosenbloom, J., Bian, C., Xie, M., Chen, W., Li, N., Baycin-Hizal, D., Latif, H., Forster, J., Betenbaugh, M.J., Famili, I., Xu, X., Wang, J. & Palsson, B.O. 2013, "Genomic landscapes of Chinese hamster ovary cell lines as revealed by the *Cricetulus griseus* draft genome", *Nature biotechnology*, vol. 31, no. 8, pp. 759-765.
- Ley, D., Harraghy, N., Le Fourn, V., Bire, S., Girod, P.A., Regamey, A., Rouleux-Bonnin, F., Bigot, Y. & Mermoud, N. 2013, "MAR elements and transposons for improved transgene integration and expression", *PloS one*, vol. 8, no. 4, pp. e62784.
- Li, B., Sun, M., Gao, F., Liu, W., Yang, Y., Liu, H., Cheng, Y., Liu, C. & Cai, J. 2013a, "Up-regulated expression of miR-23a/b targeted the pro-apoptotic Fas in radiation-induced thymic lymphoma", *Cellular physiology and biochemistry : international journal of experimental cellular physiology, biochemistry, and pharmacology*, vol. 32, no. 6, pp. 1729-1740.
- Li, C., Rossomando, A., Wu, S.L. & Karger, B.L. 2013b, "Comparability analysis of anti-CD20 commercial (rituximab) and RNAi-mediated fucosylated antibodies by two LC-MS approaches", *mAbs*, vol. 5, no. 4, pp. 565-575.

- Li, C., Wang, Y., Wang, S., Wu, B., Hao, J., Fan, H., Ju, Y., Ding, Y., Chen, L., Chu, X., Liu, W., Ye, X. & Meng, S. 2013c, "Hepatitis B virus mRNA-mediated miR-122 inhibition upregulates PTTG1-binding protein, which promotes hepatocellular carcinoma tumor growth and cell invasion", *Journal of virology*, vol. 87, no. 4, pp. 2193-2205.
- Li, F., Vijayasankaran, N., Shen, A.Y., Kiss, R. & Amanullah, A. 2010, "Cell culture processes for monoclonal antibody production", *mAbs*, vol. 2, no. 5, pp. 466-479.
- Li, F., Wang, Y., Zeller, K.I., Potter, J.J., Wonsey, D.R., O'Donnell, K.A., Kim, J.W., Yustein, J.T., Lee, L.A. & Dang, C.V. 2005, "Myc stimulates nuclearly encoded mitochondrial genes and mitochondrial biogenesis", *Molecular and cellular biology*, vol. 25, no. 14, pp. 6225-6234.
- Li, H.Y., Zhang, Y., Cai, J.H. & Bian, H.L. 2013, "MicroRNA-451 inhibits growth of human colorectal carcinoma cells via downregulation of Pi3k/Akt pathway", *Asian Pacific journal of cancer prevention: APJCP*, vol. 14, no. 6, pp. 3631-3634.
- Li, J., Menzel, C., Meier, D., Zhang, C., Dubel, S. & Jostock, T. 2007, "A comparative study of different vector designs for the mammalian expression of recombinant IgG antibodies", *Journal of immunological methods*, vol. 318, no. 1-2, pp. 113-124.
- Li, S., Moffett, H.F., Lu, J., Werner, L., Zhang, H., Ritz, J., Neuberg, D., Wucherpfennig, K.W., Brown, J.R. & Novina, C.D. 2011a, "MicroRNA expression profiling identifies activated B cell status in chronic lymphocytic leukemia cells", *PloS one*, vol. 6, no. 3, pp. e16956.
- Li, W.Q., Chen, C., Xu, M.D., Guo, J., Li, Y.M., Xia, Q.M., Liu, H.M., He, J., Yu, H.Y. & Zhu, L. 2011b, "The rno-miR-34 family is upregulated and targets ACSL1 in dimethylnitrosamine-induced hepatic fibrosis in rats", *The FEBS journal*, vol. 278, no. 9, pp. 1522-1532.
- Li, X. 2014, "MiR-375, a microRNA related to diabetes", *Gene*, vol. 533, no. 1, pp. 1-4.
- Li, X., Liu, X., Xu, W., Zhou, P., Gao, P., Jiang, S., Lobie, P.E. & Zhu, T. 2013, "c-MYC-regulated miR-23a/24-2/27a cluster promotes mammary carcinoma cell invasion and hepatic metastasis by targeting Sprouty2", *The Journal of biological chemistry*, vol. 288, no. 25, pp. 18121-18133.
- Liew, J.C., Tan, W.S., Alitheen, N.B., Chan, E.S. & Tey, B.T. 2010, "Over-expression of the X-linked inhibitor of apoptosis protein (XIAP) delays serum deprivation-induced apoptosis in CHO-K1 cells", *Journal of bioscience and bioengineering*, vol. 110, no. 3, pp. 338-344.
- Lim, Y., Seah, V.X., Mantalaris, A., Yap, M.G. & Wong, D.C. 2010, "Elucidating the role of requiem in the growth and death of Chinese hamster ovary cells", *Apoptosis: An International Journal on Programmed Cell Death*, vol. 15, no. 4, pp. 450-462.

- Lin, N., Davis, A., Bahr, S., Borgschulte, T., Achtien, K. & Kayser, K. 2010, "Profiling highly conserved microRNA expression in recombinant IgG-producing and parental chinese hamster ovary cells", *Biotechnology progress*, 27(4), pp. 1163-71.
- Lin, Q., Gao, Z., Alarcon, R.M., Ye, J. & Yun, Z. 2009, "A role of miR-27 in the regulation of adipogenesis", *The FEBS journal*, vol. 276, no. 8, pp. 2348-2358.
- Little, G.H., Bai, Y., Williams, T. & Poizat, C. 2007, "Nuclear calcium/calmodulin-dependent protein kinase IIdelta preferentially transmits signals to histone deacetylase 4 in cardiac cells", *The Journal of biological chemistry*, vol. 282, no. 10, pp. 7219-7231.
- Little, P. 1993, "Genetics. Small and perfectly formed", *Nature*, vol. 366, no. 6452, pp. 204-205.
- Liu, C., Chu, I. & Hwang, S. 2001, "Pentanoic acid, a novel protein synthesis stimulant for Chinese Hamster Ovary (CHO) cells", *Journal of bioscience and bioengineering*, vol. 91, no. 1, pp. 71-75.
- Liu, C., Kelnar, K., Liu, B., Chen, X., Calhoun-Davis, T., Li, H., Patrawala, L., Yan, H., Jeter, C., Honorio, S., Wiggins, J.F., Bader, A.G., Fagin, R., Brown, D. & Tang, D.G. 2011, "The microRNA miR-34a inhibits prostate cancer stem cells and metastasis by directly repressing CD44", *Nature medicine*, vol. 17, no. 2, pp. 211-215.
- Liu, C.J., Tsai, M.M., Hung, P.S., Kao, S.Y., Liu, T.Y., Wu, K.J., Chiou, S.H., Lin, S.C. & Chang, K.W. 2010, "miR-31 ablates expression of the HIF regulatory factor FIH to activate the HIF pathway in head and neck carcinoma", *Cancer research*, vol. 70, no. 4, pp. 1635-1644.
- Liu, J., Carmell, M.A., Rivas, F.V., Marsden, C.G., Thomson, J.M., Song, J.J., Hammond, S.M., Joshua-Tor, L. & Hannon, G.J. 2004, "Argonaute2 is the catalytic engine of mammalian RNAi", *Science (New York, N.Y.)*, vol. 305, no. 5689, pp. 1437-1441.
- Liu, N., Zhang, J., Jiao, T., Li, Z., Peng, J., Cui, Z. & Ye, X. 2013, "Hepatitis B virus inhibits apoptosis of hepatoma cells by sponging the MicroRNA 15a/16 cluster", *Journal of virology*, vol. 87, no. 24, pp. 13370-13378.
- Liu, W., Le, A., Hancock, C., Lane, A.N., Dang, C.V., Fan, T.W. & Phang, J.M. 2012, "Reprogramming of proline and glutamine metabolism contributes to the proliferative and metabolic responses regulated by oncogenic transcription factor c-MYC", *Proceedings of the National Academy of Sciences of the United States of America*, vol. 109, no. 23, pp. 8983-8988.
- Liu, W., Zabirnyk, O., Wang, H., Shiao, Y.H., Nickerson, M.L., Khalil, S., Anderson, L.M., Perantoni, A.O. & Phang, J.M. 2010a, "miR-23b targets proline oxidase, a novel tumor suppressor protein in renal cancer", *Oncogene*, vol. 29, no. 35, pp. 4914-4924.
- Liu, X., Sempere, L.F., Ouyang, H., Memoli, V.A., Andrew, A.S., Luo, Y., Demidenko, E., Korc, M., Shi, W., Preis, M., Dragnev, K.H., Li, H., Drenzo, J., Bak, M.,

- Freemantle, S.J., Kauppinen, S. & Dmitrovsky, E. 2010b, "MicroRNA-31 functions as an oncogenic microRNA in mouse and human lung cancer cells by repressing specific tumor suppressors", *The Journal of clinical investigation*, vol. 120, no. 4, pp. 1298-1309.
- Liu, Y., Borchert, G.L., Donald, S.P., Diwan, B.A., Anver, M. & Phang, J.M. 2009, "Proline oxidase functions as a mitochondrial tumor suppressor in human cancers", *Cancer research*, vol. 69, no. 16, pp. 6414-6422.
- Liu, Y., Borchert, G.L., Surazynski, A., Hu, C.A. & Phang, J.M. 2006, "Proline oxidase activates both intrinsic and extrinsic pathways for apoptosis: the role of ROS/superoxides, NFAT and MEK/ERK signaling", *Oncogene*, vol. 25, no. 41, pp. 5640-5647.
- Lodygin, D., Tarasov, V., Epanchintsev, A., Berking, C., Knyazeva, T., Korner, H., Knyazev, P., Diebold, J. & Hermeking, H. 2008, "Inactivation of miR-34a by aberrant CpG methylation in multiple types of cancer", *Cell cycle (Georgetown, Tex.)*, vol. 7, no. 16, pp. 2591-2600.
- Loenarz, C. & Schofield, C.J. 2008, "Expanding chemical biology of 2-oxoglutarate oxygenases", *Nature chemical biology*, vol. 4, no. 3, pp. 152-156.
- Loh, W.P., Loo, B., Zhou, L., Zhang, P., Lee, D.Y., Yang, Y. & Lam, K.P. 2014, "Overexpression of microRNAs enhances recombinant protein production in Chinese hamster ovary cells", *Biotechnology journal*, 9(9), pp. 1140-51.
- Lopert, P., Day, B.J. & Patel, M. 2012, "Thioredoxin reductase deficiency potentiates oxidative stress, mitochondrial dysfunction and cell death in dopaminergic cells", *PloS one*, vol. 7, no. 11, pp. e50683.
- Lovis, P., Gattesco, S. & Regazzi, R. 2008, "Regulation of the expression of components of the exocytotic machinery of insulin-secreting cells by microRNAs", *Biological chemistry*, vol. 389, no. 3, pp. 305-312.
- Lovis, P., Roggli, E., Laybutt, D.R., Gattesco, S., Yang, J.Y., Widmann, C., Abderrahmani, A. & Regazzi, R. 2008, "Alterations in microRNA expression contribute to fatty acid-induced pancreatic beta-cell dysfunction", *Diabetes*, vol. 57, no. 10, pp. 2728-2736.
- Lupo, D., Vollmer, C., Deckers, M., Mick, D.U., Tews, I., Sinning, I. & Rehling, P. 2011, "Mdm38 is a 14-3-3-like receptor and associates with the protein synthesis machinery at the inner mitochondrial membrane", *Traffic (Copenhagen, Denmark)*, vol. 12, no. 10, pp. 1457-1466.
- Lytle, J.R., Yario, T.A. & Steitz, J.A. 2007, "Target mRNAs are repressed as efficiently by microRNA-binding sites in the 5' UTR as in the 3' UTR", *Proceedings of the National Academy of Sciences of the United States of America*, vol. 104, no. 23, pp. 9667-9672.

- Ma, J.B., Ye, K. & Patel, D.J. 2004, "Structural basis for overhang-specific small interfering RNA recognition by the PAZ domain", *Nature*, vol. 429, no. 6989, pp. 318-322.
- Ma, N., Ellet, J., Okediadi, C., Hermes, P., McCormick, E. & Casnocha, S. 2009, "A single nutrient feed supports both chemically defined NS0 and CHO fed-batch processes: Improved productivity and lactate metabolism", *Biotechnology progress*, vol. 25, no. 5, pp. 1353-1363.
- Majors, B.S., Arden, N., Oyler, G.A., Chiang, G.G., Pederson, N.E. & Betenbaugh, M.J. 2008, "E2F-1 overexpression increases viable cell density in batch cultures of Chinese hamster ovary cells", *Journal of Biotechnology*, vol. 138, no. 3-4, pp. 103-106.
- Majors, B.S., Betenbaugh, M.J., Pederson, N.E. & Chiang, G.G. 2009, "Mcl-1 overexpression leads to higher viabilities and increased production of humanized monoclonal antibody in Chinese hamster ovary cells", *Biotechnology progress*, vol. 25, no. 4, pp. 1161-1168.
- Malhotra, J.D. & Kaufman, R.J. 2007, "Endoplasmic reticulum stress and oxidative stress: a vicious cycle or a double-edged sword?", *Antioxidants & redox signaling*, vol. 9, no. 12, pp. 2277-2293.
- Mali, P., Esvelt, K.M. & Church, G.M. 2013, "Cas9 as a versatile tool for engineering biology", *Nature methods*, vol. 10, no. 10, pp. 957-963.
- Malphettes, L., Freyvert, Y., Chang, J., Liu, P.Q., Chan, E., Miller, J.C., Zhou, Z., Nguyen, T., Tsai, C., Snowden, A.W., Collingwood, T.N., Gregory, P.D. & Cost, G.J. 2010, "Highly efficient deletion of FUT8 in CHO cell lines using zinc-finger nucleases yields cells that produce completely nonfucosylated antibodies", *Biotechnology and bioengineering*, vol. 106, no. 5, pp. 774-783.
- Manganelli, F. & Ruggiero, L. 2013, "Clinical features of Pompe disease", *Acta myologica : myopathies and cardiomyopathies : official journal of the Mediterranean Society of Myology / edited by the Gaetano Conte Academy for the study of striated muscle diseases*, vol. 32, no. 2, pp. 82-84.
- Mansfield, J.H., Harfe, B.D., Nissen, R., Obenauer, J., Srineel, J., Chaudhuri, A., Farzan-Kashani, R., Zuker, M., Pasquinelli, A.E., Ruvkun, G., Sharp, P.A., Tabin, C.J. & McManus, M.T. 2004, "MicroRNA-responsive 'sensor' transgenes uncover Hox-like and other developmentally regulated patterns of vertebrate microRNA expression", *Nature genetics*, vol. 36, no. 10, pp. 1079-1083.
- Marcinowski, L., Tanguy, M., Krmpotic, A., Radle, B., Lisnic, V.J., Tuddenham, L., Chane-Woon-Ming, B., Ruzsics, Z., Erhard, F., Benkartek, C., Babic, M., Zimmer, R., Trgovcich, J., Koszinowski, U.H., Jonjic, S., Pfeffer, S. & Dolken, L. 2012, "Degradation of cellular mir-27 by a novel, highly abundant viral transcript is important for efficient virus replication in vivo", *PLoS pathogens*, vol. 8, no. 2, pp. e1002510.

- Mariani, M.R., Carpaneto, E.M., Ulivi, M., Allfrey, V.G. & Boffa, L.C. 2003, "Correlation between butyrate-induced histone hyperacetylation turn-over and c-myc expression", *The Journal of steroid biochemistry and molecular biology*, vol. 86, no. 2, pp. 167-171.
- Marín-García, J. 2012, *Mitochondria and Their Role in Cardiovascular Disease*, Springer.
- Martinez, V.S., Dietmair, S., Quek, L.E., Hodson, M.P., Gray, P. & Nielsen, L.K. 2013, "Flux balance analysis of CHO cells before and after a metabolic switch from lactate production to consumption", *Biotechnology and bioengineering*, vol. 110, no. 2, pp. 660-666.
- Martinez-Sanchez, A. & Murphy, C.L. 2013, "MicroRNA Target Identification—Experimental Approaches", *Biology*, vol. 2, no. 1, pp. 189-205.
- Matasci, M., Baldi, L., Hacker, D.L. & Wurm, F.M. 2011, "The PiggyBac transposon enhances the frequency of CHO stable cell line generation and yields recombinant lines with superior productivity and stability", *Biotechnology and bioengineering*, vol. 108, no. 9, pp. 2141-2150.
- Mazur, X., Fussenegger, M., Renner, W.A. & Bailey, J.E. 1998, "Higher productivity of growth-arrested Chinese hamster ovary cells expressing the cyclin-dependent kinase inhibitor p27", *Biotechnology progress*, vol. 14, no. 5, pp. 705-713.
- Meents, H., Enenkel, B., Werner, R.G. & Fussenegger, M. 2002, "p27Kip1-mediated controlled proliferation technology increases constitutive sICAM production in CHO-DUKX adapted for growth in suspension and serum-free media", *Biotechnology and bioengineering*, vol. 79, no. 6, pp. 619-627.
- Meerbrey, K.L., Hu, G., Kessler, J.D., Roarty, K., Li, M.Z., Fang, J.E., Herschkowitz, J.I., Burrows, A.E., Ciccia, A., Sun, T., Schmitt, E.M., Bernardi, R.J., Fu, X., Bland, C.S., Cooper, T.A., Schiff, R., Rosen, J.M., Westbrook, T.F. & Elledge, S.J. 2011, "The pINDUCER lentiviral toolkit for inducible RNA interference in vitro and in vivo", *Proceedings of the National Academy of Sciences of the United States of America*, vol. 108, no. 9, pp. 3665-3670.
- Meister, G., Landthaler, M., Patkaniowska, A., Dorsett, Y., Teng, G. & Tuschl, T. 2004, "Human Argonaute2 mediates RNA cleavage targeted by miRNAs and siRNAs", *Molecular cell*, vol. 15, no. 2, pp. 185-197.
- Meleady, P., Gallagher, M., Clarke, C., Henry, M., Sanchez, N., Barron, N. & Clynes, M. 2012a, "Impact of miR-7 over-expression on the proteome of Chinese hamster ovary cells", *Journal of Biotechnology*, vol. 160, no. 3-4, pp. 251-262.
- Meleady, P., Gallagher, M., Clarke, C., Henry, M., Sanchez, N., Barron, N. & Clynes, M. 2012b, "Impact of miR-7 over-expression on the proteome of Chinese hamster ovary cells", *Journal of Biotechnology*, vol. 160, no. 3-4, pp. 251-262.

- Meleady, P., Hoffrogge, R., Henry, M., Rupp, O., Bort, J.H., Clarke, C., Brinkrolf, K., Kelly, S., Muller, B., Doolan, P., Hackl, M., Beckmann, T.F., Noll, T., Grillari, J., Barron, N., Puhler, A., Clynes, M. & Borth, N. 2012c, "Utilization and evaluation of CHO-specific sequence databases for mass spectrometry based proteomics", *Biotechnology and bioengineering*, vol. 109, no. 6, pp. 1386-1394.
- Memczak, S., Jens, M., Elefsinioti, A., Torti, F., Krueger, J., Rybak, A., Maier, L., Mackowiak, S.D., Gregersen, L.H., Munschauer, M., Loewer, A., Ziebold, U., Landthaler, M., Kocks, C., le Noble, F. & Rajewsky, N. 2013, "Circular RNAs are a large class of animal RNAs with regulatory potency", *Nature*, vol. 495, no. 7441, pp. 333-338.
- Mertens-Talcott, S.U., Chintharlapalli, S., Li, X. & Safe, S. 2007, "The oncogenic microRNA-27a targets genes that regulate specificity protein transcription factors and the G2-M checkpoint in MDA-MB-231 breast cancer cells", *Cancer research*, vol. 67, no. 22, pp. 11001-11011.
- Mimura, Y., Church, S., Ghirlando, R., Ashton, P.R., Dong, S., Goodall, M., Lund, J. & Jefferis, R. 2000, "The influence of glycosylation on the thermal stability and effector function expression of human IgG1-Fc: properties of a series of truncated glycoforms", *Molecular immunology*, vol. 37, no. 12-13, pp. 697-706.
- Mishima, Y., Fukao, A., Kishimoto, T., Sakamoto, H., Fujiwara, T. & Inoue, K. 2012, "Translational inhibition by deadenylation-independent mechanisms is central to microRNA-mediated silencing in zebrafish", *Proceedings of the National Academy of Sciences of the United States of America*, vol. 109, no. 4, pp. 1104-1109.
- Mittermayr, S., Bones, J., Doherty, M., Guttman, A. & Rudd, P.M. 2011, "Multiplexed analytical glycomics: rapid and confident IgG N-glycan structural elucidation", *Journal of proteome research*, vol. 10, no. 8, pp. 3820-3829.
- Mizuochi, T., Taniguchi, T., Shimizu, A. & Kobata, A. 1982, "Structural and numerical variations of the carbohydrate moiety of immunoglobulin G", *Journal of immunology (Baltimore, Md.: 1950)*, vol. 129, no. 5, pp. 2016-2020.
- Mizushima, N., Yoshimori, T. & Levine, B. 2010, "Methods in mammalian autophagy research", *Cell*, vol. 140, no. 3, pp. 313-326.
- Mohan, C., Kim, Y.G., Koo, J. & Lee, G.M. 2008a, "Assessment of cell engineering strategies for improved therapeutic protein production in CHO cells", *Biotechnology journal*, vol. 3, no. 5, pp. 624-630.
- Mohan, C., Kim, Y.G., Koo, J. & Lee, G.M. 2008b, "Assessment of cell engineering strategies for improved therapeutic protein production in CHO cells", *Biotechnology journal*, vol. 3, no. 5, pp. 624-630.
- Mohan, C., Park, S.H., Chung, J.Y. & Lee, G.M. 2007, "Effect of doxycycline-regulated protein disulfide isomerase expression on the specific productivity of recombinant CHO cells: thrombopoietin and antibody", *Biotechnology and bioengineering*, vol. 98, no. 3, pp. 611-615.

- Mori, K., Kuni-Kamochi, R., Yamane-Ohnuki, N., Wakitani, M., Yamano, K., Imai, H., Kanda, Y., Niwa, R., Iida, S., Uchida, K., Shitara, K. & Satoh, M. 2004, "Engineering Chinese hamster ovary cells to maximize effector function of produced antibodies using FUT8 siRNA", *Biotechnology and bioengineering*, vol. 88, no. 7, pp. 901-908.
- Morin, R.D., O'Connor, M.D., Griffith, M., Kuchenbauer, F., Delaney, A., Prabhu, A.L., Zhao, Y., McDonald, H., Zeng, T., Hirst, M., Eaves, C.J. & Marra, M.A. 2008, "Application of massively parallel sequencing to microRNA profiling and discovery in human embryonic stem cells", *Genome research*, vol. 18, no. 4, pp. 610-621.
- Moss, E.G., Lee, R.C. & Ambros, V. 1997, "The cold shock domain protein LIN-28 controls developmental timing in *C. elegans* and is regulated by the *lin-4* RNA", *Cell*, vol. 88, no. 5, pp. 637-646.
- Mukherji, S., Ebert, M.S., Zheng, G.X., Tsang, J.S., Sharp, P.A. & van Oudenaarden, A. 2011, "MicroRNAs can generate thresholds in target gene expression", *Nature genetics*, vol. 43, no. 9, pp. 854-859.
- Muller, D., Katinger, H. & Grillari, J. 2008, "MicroRNAs as targets for engineering of CHO cell factories", *Trends in biotechnology*, vol. 26, no. 7, pp. 359-365.
- Mullokandov, G., Baccarini, A., Ruzo, A., Jayaprakash, A.D., Tung, N., Israelow, B., Evans, M.J., Sachidanandam, R. & Brown, B.D. 2012, "High-throughput assessment of microRNA activity and function using microRNA sensor and decoy libraries", *Nature methods*, vol. 9, no. 8, pp. 840-846.
- Nam, S., Kim, B., Shin, S. & Lee, S. 2008, "miRGator: an integrated system for functional annotation of microRNAs", *Nucleic acids research*, vol. 36, no. Database issue, pp. D159-64.
- Navarro, F., Gutman, D., Meire, E., Caceres, M., Rigoutsos, I., Bentwich, Z. & Lieberman, J. 2009, "miR-34a contributes to megakaryocytic differentiation of K562 cells independently of p53", *Blood*, vol. 114, no. 10, pp. 2181-2192.
- Neermann, J. & Wagner, R. 1996, "Comparative analysis of glucose and glutamine metabolism in transformed mammalian cell lines, insect and primary liver cells", *Journal of cellular physiology*, vol. 166, no. 1, pp. 152-169.
- Niederer, F., Trenkmann, M., Ospelt, C., Karouzakis, E., Neidhart, M., Stanczyk, J., Kolling, C., Gay, R.E., Detmar, M., Gay, S., Jungel, A. & Kyburz, D. 2012, "Down-regulation of microRNA-34a* in rheumatoid arthritis synovial fibroblasts promotes apoptosis resistance", *Arthritis and Rheumatism*, vol. 64, no. 6, pp. 1771-1779.
- Nimmerjahn, F. & Ravetch, J.V. 2008, "Fcgamma receptors as regulators of immune responses", *Nature reviews.Immunology*, vol. 8, no. 1, pp. 34-47.
- Nissom, P.M., Sanny, A., Kok, Y.J., Hiang, Y.T., Chuah, S.H., Shing, T.K., Lee, Y.Y., Wong, K.T., Hu, W.S., Sim, M.Y. & Philp, R. 2006, "Transcriptome and proteome profiling to understanding the biology of high productivity CHO cells", *Molecular biotechnology*, vol. 34, no. 2, pp. 125-140.

- Norling, L.L., Colca, J.R., Kelly, P.T., McDaniel, M.L. & Landt, M. 1994, "Activation of calcium and calmodulin dependent protein kinase II during stimulation of insulin secretion", *Cell calcium*, vol. 16, no. 2, pp. 137-150.
- Obad, S., dos Santos, C.O., Petri, A., Heidenblad, M., Broom, O., Ruse, C., Fu, C., Lindow, M., Stenvang, J., Straarup, E.M., Hansen, H.F., Koch, T., Pappin, D., Hannon, G.J. & Kauppinen, S. 2011, "Silencing of microRNA families by seed-targeting tiny LNAs", *Nature genetics*, vol. 43, no. 4, pp. 371-378.
- O'Donnell, K.A., Wentzel, E.A., Zeller, K.I., Dang, C.V. & Mendell, J.T. 2005a, "c-Myc-regulated microRNAs modulate E2F1 expression", *Nature*, vol. 435, no. 7043, pp. 839-843.
- O'Donnell, K.A., Wentzel, E.A., Zeller, K.I., Dang, C.V. & Mendell, J.T. 2005b, "c-Myc-regulated microRNAs modulate E2F1 expression", *Nature*, vol. 435, no. 7043, pp. 839-843.
- Oguchi, S., Saito, H., Tsukahara, M. & Tsumura, H. 2006, "pH Condition in temperature shift cultivation enhances cell longevity and specific hMab productivity in CHO culture", *Cytotechnology*, vol. 52, no. 3, pp. 199-207.
- Ohya, T., Hayashi, T., Kiyama, E., Nishii, H., Miki, H., Kobayashi, K., Honda, K., Omasa, T. & Ohtake, H. 2008a, "Improved production of recombinant human antithrombin III in Chinese hamster ovary cells by ATF4 overexpression", *Biotechnology and bioengineering*, vol. 100, no. 2, pp. 317-324.
- Ohya, T., Hayashi, T., Kiyama, E., Nishii, H., Miki, H., Kobayashi, K., Honda, K., Omasa, T. & Ohtake, H. 2008b, "Improved production of recombinant human antithrombin III in Chinese hamster ovary cells by ATF4 overexpression", *Biotechnology and bioengineering*, vol. 100, no. 2, pp. 317-324.
- Okamura, K., Hagen, J.W., Duan, H., Tyler, D.M. & Lai, E.C. 2007, "The mirtron pathway generates microRNA-class regulatory RNAs in *Drosophila*", *Cell*, vol. 130, no. 1, pp. 89-100.
- Okamura, K., Phillips, M.D., Tyler, D.M., Duan, H., Chou, Y.T. & Lai, E.C. 2008, "The regulatory activity of microRNA* species has substantial influence on microRNA and 3' UTR evolution", *Nature structural & molecular biology*, vol. 15, no. 4, pp. 354-363.
- Olena, A.F. & Patton, J.G. 2010, "Genomic organization of microRNAs", *Journal of cellular physiology*, vol. 222, no. 3, pp. 540-545.
- Olive, V., Jiang, I. & He, L. 2010a, "mir-17-92, a cluster of miRNAs in the midst of the cancer network", *The international journal of biochemistry & cell biology*, vol. 42, no. 8, pp. 1348-1354.
- Olive, V., Jiang, I. & He, L. 2010b, "mir-17-92, a cluster of miRNAs in the midst of the cancer network", *The international journal of biochemistry & cell biology*, vol. 42, no. 8, pp. 1348-1354.

- Olive, V., Li, Q. & He, L. 2013, "Mir-17-92: a Polycistronic Oncomir with Pleiotropic Functions", *Immunological reviews*, vol. 253, no. 1, pp. 158-166.
- Omasa, T., Takami, T., Ohya, T., Kiyama, E., Hayashi, T., Nishii, H., Miki, H., Kobayashi, K., Honda, K. & Ohtake, H. 2008, "Overexpression of GADD34 enhances production of recombinant human antithrombin III in Chinese hamster ovary cells", *Journal of bioscience and bioengineering*, vol. 106, no. 6, pp. 568-573.
- Orom, U.A. & Lund, A.H. 2007, "Isolation of microRNA targets using biotinylated synthetic microRNAs", *Methods (San Diego, Calif.)*, vol. 43, no. 2, pp. 162-165.
- Orom, U.A., Nielsen, F.C. & Lund, A.H. 2008, "MicroRNA-10a binds the 5'UTR of ribosomal protein mRNAs and enhances their translation", *Molecular cell*, vol. 30, no. 4, pp. 460-471.
- Osellame, L.D., Blacker, T.S. & Duchon, M.R. 2012, "Cellular and molecular mechanisms of mitochondrial function", *Best practice & research. Clinical endocrinology & metabolism*, vol. 26, no. 6, pp. 711-723.
- Osterhoff, M., Mohlig, M., Schwanstecher, M., Seufert, J., Ortmann, J., Schatz, H. & Pfeiffer, A.F. 2003, "Ca²⁺/calmodulin-dependent protein kinase II delta2 regulates gene expression of insulin in INS-1 rat insulinoma cells", *Cell calcium*, vol. 33, no. 3, pp. 175-184.
- Ota, A., Tagawa, H., Karnan, S., Tsuzuki, S., Karpas, A., Kira, S., Yoshida, Y. & Seto, M. 2004a, "Identification and characterization of a novel gene, C13orf25, as a target for 13q31-q32 amplification in malignant lymphoma", *Cancer research*, vol. 64, no. 9, pp. 3087-3095.
- Ota, A., Tagawa, H., Karnan, S., Tsuzuki, S., Karpas, A., Kira, S., Yoshida, Y. & Seto, M. 2004b, "Identification and characterization of a novel gene, C13orf25, as a target for 13q31-q32 amplification in malignant lymphoma", *Cancer research*, vol. 64, no. 9, pp. 3087-3095.
- Ouyang, Y.B., Lu, Y., Yue, S. & Giffard, R.G. 2012, "miR-181 targets multiple Bcl-2 family members and influences apoptosis and mitochondrial function in astrocytes", *Mitochondrion*, vol. 12, no. 2, pp. 213-219.
- Owen, O.E., Kalhan, S.C. & Hanson, R.W. 2002, "The key role of anaplerosis and cataplerosis for citric acid cycle function", *The Journal of biological chemistry*, vol. 277, no. 34, pp. 30409-30412.
- Pan, S., Ryu, S.Y. & Sheu, S.S. 2011, "Distinctive characteristics and functions of multiple mitochondrial Ca²⁺ influx mechanisms", *Science China. Life sciences*, vol. 54, no. 8, pp. 763-769.
- Panzitt, K., Tschernatsch, M.M., Guelly, C., Moustafa, T., Stradner, M., Strohmaier, H.M., Buck, C.R., Denk, H., Schroeder, R., Trauner, M. & Zatloukal, K. 2007, "Characterization of HULC, a novel gene with striking up-regulation in

- hepatocellular carcinoma, as noncoding RNA", *Gastroenterology*, vol. 132, no. 1, pp. 330-342.
- Park, C.Y., Choi, Y.S. & McManus, M.T. 2010, "Analysis of microRNA knockouts in mice", *Human molecular genetics*, vol. 19, no. R2, pp. R169-75.
- Parlato, S., Bruni, R., Fragapane, P., Salerno, D., Marcantonio, C., Borghi, P., Tataseo, P., Ciccaglione, A.R., Presutti, C., Romagnoli, G., Bozzoni, I., Belardelli, F. & Gabriele, L. 2013, "IFN- α regulates Blimp-1 expression via miR-23a and miR-125b in both monocytes-derived DC and pDC", *PloS one*, vol. 8, no. 8, pp. e72833.
- Pasquinelli, A.E. 2012, "MicroRNAs and their targets: recognition, regulation and an emerging reciprocal relationship", *Nature reviews.Genetics*, vol. 13, no. 4, pp. 271-282.
- Pasquinelli, A.E., Reinhart, B.J., Slack, F., Martindale, M.Q., Kuroda, M.I., Maller, B., Hayward, D.C., Ball, E.E., Degan, B., Muller, P., Spring, J., Srinivasan, A., Fishman, M., Finnerty, J., Corbo, J., Levine, M., Leahy, P., Davidson, E. & Ruvkun, G. 2000, "Conservation of the sequence and temporal expression of let-7 heterochronic regulatory RNA", *Nature*, vol. 408, no. 6808, pp. 86-89.
- Pattingre, S., Tassa, A., Qu, X., Garuti, R., Liang, X.H., Mizushima, N., Packer, M., Schneider, M.D. & Levine, B. 2005, "Bcl-2 antiapoptotic proteins inhibit Beclin 1-dependent autophagy", *Cell*, vol. 122, no. 6, pp. 927-939.
- Pekarsky, Y., Santanam, U., Cimmino, A., Palamarchuk, A., Efanov, A., Maximov, V., Volinia, S., Alder, H., Liu, C.G., Rassenti, L., Calin, G.A., Hagan, J.P., Kipps, T. & Croce, C.M. 2006, "Tcl1 expression in chronic lymphocytic leukemia is regulated by miR-29 and miR-181", *Cancer research*, vol. 66, no. 24, pp. 11590-11593.
- Pelicano, H., Martin, D.S., Xu, R.H. & Huang, P. 2006a, "Glycolysis inhibition for anticancer treatment", *Oncogene*, vol. 25, no. 34, pp. 4633-4646.
- Pelicano, H., Xu, R.H., Du, M., Feng, L., Sasaki, R., Carew, J.S., Hu, Y., Ramdas, L., Hu, L., Keating, M.J., Zhang, W., Plunkett, W. & Huang, P. 2006b, "Mitochondrial respiration defects in cancer cells cause activation of Akt survival pathway through a redox-mediated mechanism", *The Journal of cell biology*, vol. 175, no. 6, pp. 913-923.
- Peng, R.W., Abellan, E. & Fussenegger, M. 2011, "Differential effect of exocytic SNAREs on the production of recombinant proteins in mammalian cells", *Biotechnology and bioengineering*, vol. 108, no. 3, pp. 611-620.
- Peng, R.W. & Fussenegger, M. 2009, "Molecular engineering of exocytic vesicle traffic enhances the productivity of Chinese hamster ovary cells", *Biotechnology and bioengineering*, vol. 102, no. 4, pp. 1170-1181.
- Perez-Mato, M., Ramos-Cabrera, P., Sobrino, T., Blanco, M., Ruban, A., Mirelman, D., Menendez, P., Castillo, J. & Campos, F. 2014, "Human recombinant glutamate

- oxaloacetate transaminase 1 (GOT1) supplemented with oxaloacetate induces a protective effect after cerebral ischemia", *Cell death & disease*, vol. 5, pp. e992.
- Piao, L., Li, Y., Kim, S.J., Byun, H.S., Huang, S.M., Hwang, S.K., Yang, K.J., Park, K.A., Won, M., Hong, J., Hur, G.M., Seok, J.H., Shong, M., Cho, M.H., Brazil, D.P., Hemmings, B.A. & Park, J. 2009, "Association of LETM1 and MRPL36 contributes to the regulation of mitochondrial ATP production and necrotic cell death", *Cancer research*, vol. 69, no. 8, pp. 3397-3404.
- Pichinuk, E., Broday, L. & Wreschner, D.H. 2011, "Endogenous RNA cleavages at the ribosomal SRL site likely reflect miRNA (miR) mediated translational suppression", *Biochemical and biophysical research communications*, vol. 414, no. 4, pp. 706-711.
- Pichler, J., Galosy, S., Mott, J. & Borth, N. 2011, "Selection of CHO host cell subclones with increased specific antibody production rates by repeated cycles of transient transfection and cell sorting", *Biotechnology and bioengineering*, vol. 108, no. 2, pp. 386-394.
- Pickering, A.M. & Davies, K.J. 2012, "Degradation of damaged proteins: the main function of the 20S proteasome", *Progress in molecular biology and translational science*, vol. 109, pp. 227-248.
- Pilbrough, W., Munro, T.P. & Gray, P. 2009, "Intracloal protein expression heterogeneity in recombinant CHO cells", *PloS one*, vol. 4, no. 12, pp. e8432.
- Pitceathly, R.D., Rahman, S., Wedatilake, Y., Polke, J.M., Cirak, S., Foley, A.R., Sailer, A., Hurles, M.E., Stalker, J., Hargreaves, I., Woodward, C.E., Sweeney, M.G., Muntoni, F., Houlden, H., Taanman, J.W., Hanna, M.G. & UK10K Consortium 2013, "NDUFA4 mutations underlie dysfunction of a cytochrome c oxidase subunit linked to human neurological disease", *Cell reports*, vol. 3, no. 6, pp. 1795-1805.
- Poburko, D. & Demarex, N. 2012, "Regulation of the mitochondrial proton gradient by cytosolic Ca(2)(+) signals", *Pflugers Archiv : European journal of physiology*, vol. 464, no. 1, pp. 19-26.
- Poliseno, L., Salmena, L., Zhang, J., Carver, B., Haveman, W.J. & Pandolfi, P.P. 2010, "A coding-independent function of gene and pseudogene mRNAs regulates tumour biology", *Nature*, vol. 465, no. 7301, pp. 1033-1038.
- Polyak, K., Xia, Y., Zweier, J.L., Kinzler, K.W. & Vogelstein, B. 1997, "A model for p53-induced apoptosis", *Nature*, vol. 389, no. 6648, pp. 300-305.
- Pontiller, J., Gross, S., Thaisuchat, H., Hesse, F. & Ernst, W. 2008, "Identification of CHO endogenous promoter elements based on a genomic library approach", *Molecular biotechnology*, vol. 39, no. 2, pp. 135-139.
- Ponting, C.P., Oliver, P.L. & Reik, W. 2009, "Evolution and functions of long noncoding RNAs", *Cell*, vol. 136, no. 4, pp. 629-641.

- Porter, A.J., Racher, A.J., Preziosi, R. & Dickson, A.J. 2010, "Strategies for selecting recombinant CHO cell lines for cGMP manufacturing: improving the efficiency of cell line generation", *Biotechnology progress*, vol. 26, no. 5, pp. 1455-1464.
- Poy, M.N., Eliasson, L., Krutzfeldt, J., Kuwajima, S., Ma, X., Macdonald, P.E., Pfeffer, S., Tuschl, T., Rajewsky, N., Rorsman, P. & Stoffel, M. 2004, "A pancreatic islet-specific microRNA regulates insulin secretion", *Nature*, vol. 432, no. 7014, pp. 226-230.
- Pybus, L.P., Dean, G., West, N.R., Smith, A., Daramola, O., Field, R., Wilkinson, S.J. & James, D.C. 2013, "Model-directed engineering of "difficult-to-express" monoclonal antibody production by Chinese hamster ovary cells", *Biotechnology and bioengineering*, 111(2), pp. 372-85.
- Qiu, X., Friedman, J.M. & Liang, G. 2011, "Creating a flexible multiple microRNA expression vector by linking precursor microRNAs", *Biochemical and biophysical research communications*, vol. 411, no. 2, pp. 276-280.
- Qu, B., Han, X., Tang, Y. & Shen, N. 2012, "A novel vector-based method for exclusive overexpression of star-form microRNAs", *PloS one*, vol. 7, no. 7, pp. e41504.
- Quan, H., Fan, G. & Wang, C.C. 1995, "Independence of the chaperone activity of protein disulfide isomerase from its thioredoxin-like active site", *The Journal of biological chemistry*, vol. 270, no. 29, pp. 17078-17080.
- Raben, N., Wong, A., Ralston, E. & Myerowitz, R. 2012, "Autophagy and mitochondria in Pompe disease: nothing is so new as what has long been forgotten", *American journal of medical genetics. Part C, Seminars in medical genetics*, vol. 160C, no. 1, pp. 13-21.
- Rahimpour, A., Vaziri, B., Moazzami, R., Nematollahi, L., Barkhordari, F., Kokabee, L., Adeli, A. & Mahboudi, F. 2013, "Engineering the Cellular Protein Secretory Pathway for Enhancement of Recombinant Tissue Plasminogen Activator Expression in Chinese Hamster Ovary cells: Effects of CERT and XBP1s Genes", *Journal of microbiology and biotechnology*, 23(8), pp. 1116-22.
- Raju, T.S. 2008, "Terminal sugars of Fc glycans influence antibody effector functions of IgGs", *Current opinion in immunology*, vol. 20, no. 4, pp. 471-478.
- Raza, H. 2011, "Dual localization of glutathione S-transferase in the cytosol and mitochondria: implications in oxidative stress, toxicity and disease", *The FEBS journal*, vol. 278, no. 22, pp. 4243-4251.
- Raza, H., Robin, M.A., Fang, J.K. & Avadhani, N.G. 2002, "Multiple isoforms of mitochondrial glutathione S-transferases and their differential induction under oxidative stress", *The Biochemical journal*, vol. 366, no. Pt 1, pp. 45-55.
- Reichert, J.M. 2013, "Which are the antibodies to watch in 2013?", *mAbs*, vol. 5, no. 1, pp. 1-4.

- Reichert, J.M. 2010, "Antibodies to watch in 2010", *mAbs*, vol. 2, no. 1, pp. 84-100.
- Reinhart, B.J., Slack, F.J., Basson, M., Pasquinelli, A.E., Bettinger, J.C., Rougvie, A.E., Horvitz, H.R. & Ruvkun, G. 2000, "The 21-nucleotide let-7 RNA regulates developmental timing in *Caenorhabditis elegans*", *Nature*, vol. 403, no. 6772, pp. 901-906.
- Reinheckel, T., Sitte, N., Ullrich, O., Kuckelkorn, U., Davies, K.J. & Grune, T. 1998, "Comparative resistance of the 20S and 26S proteasome to oxidative stress", *The Biochemical journal*, vol. 335 (Pt 3), no. Pt 3, pp. 637-642.
- Rhee, S.G., Woo, H.A., Kil, I.S. & Bae, S.H. 2012, "Peroxiredoxin functions as a peroxidase and a regulator and sensor of local peroxides", *The Journal of biological chemistry*, vol. 287, no. 7, pp. 4403-4410.
- Rizzuto, R. & Pozzan, T. 2006, "Microdomains of intracellular Ca²⁺: molecular determinants and functional consequences", *Physiological Reviews*, vol. 86, no. 1, pp. 369-408.
- Robertson, K.D. & Jones, P.A. 2000, "DNA methylation: past, present and future directions", *Carcinogenesis*, vol. 21, no. 3, pp. 461-467.
- Rolfe, D.F., Newman, J.M., Buckingham, J.A., Clark, M.G. & Brand, M.D. 1999, "Contribution of mitochondrial proton leak to respiration rate in working skeletal muscle and liver and to SMR", *The American Journal of Physiology*, vol. 276, no. 3 Pt 1, pp. C692-9.
- Ronchetti, D., Lionetti, M., Mosca, L., Agnelli, L., Andronache, A., Fabris, S., Delilieri, G.L. & Neri, A. 2008, "An integrative genomic approach reveals coordinated expression of intronic miR-335, miR-342, and miR-561 with deregulated host genes in multiple myeloma", *BMC medical genomics*, vol. 1, pp. 37.
- Ronnebaum, S.M., Ilkayeva, O., Burgess, S.C., Joseph, J.W., Lu, D., Stevens, R.D., Becker, T.C., Sherry, A.D., Newgard, C.B. & Jensen, M.V. 2006, "A pyruvate cycling pathway involving cytosolic NADP-dependent isocitrate dehydrogenase regulates glucose-stimulated insulin secretion", *The Journal of biological chemistry*, vol. 281, no. 41, pp. 30593-30602.
- Roopenian, D.C. & Akilesh, S. 2007, "FcRn: the neonatal Fc receptor comes of age", *Nature reviews.Immunology*, vol. 7, no. 9, pp. 715-725.
- Rose, N.R., McDonough, M.A., King, O.N., Kawamura, A. & Schofield, C.J. 2011, "Inhibition of 2-oxoglutarate dependent oxygenases", *Chemical Society Reviews*, vol. 40, no. 8, pp. 4364-4397.
- Rossi, J.J. 2008, "Expression strategies for short hairpin RNA interference triggers", *Human Gene Therapy*, vol. 19, no. 4, pp. 313-317.
- Ruepp, A., Kowarsch, A., Schmidl, D., Buggenthin, F., Brauner, B., Dunger, I., Fobo, G., Frishman, G., Montrone, C. & Theis, F.J. 2010, "PhenomiR: a knowledgebase for

- microRNA expression in diseases and biological processes", *Genome biology*, vol. 11, no. 1, pp. R6.
- Running Deer, J. & Allison, D.S. 2004, "High-level expression of proteins in mammalian cells using transcription regulatory sequences from the Chinese hamster EF-1alpha gene", *Biotechnology progress*, vol. 20, no. 3, pp. 880-889.
- Ruvkun, G. & Giusto, J. 1989, "The *Caenorhabditis elegans* heterochronic gene *lin-14* encodes a nuclear protein that forms a temporal developmental switch", *Nature*, vol. 338, no. 6213, pp. 313-319.
- Ryll, T., Dutina, G., Reyes, A., Gunson, J., Krummen, L. & Etcheverry, T. 2000, "Performance of small-scale CHO perfusion cultures using an acoustic cell filtration device for cell retention: characterization of separation efficiency and impact of perfusion on product quality", *Biotechnology and bioengineering*, vol. 69, no. 4, pp. 440-449.
- Saini, H.K., Griffiths-Jones, S. & Enright, A.J. 2007, "Genomic analysis of human microRNA transcripts", *Proceedings of the National Academy of Sciences of the United States of America*, vol. 104, no. 45, pp. 17719-17724.
- Salmena, L., Poliseno, L., Tay, Y., Kats, L. & Pandolfi, P.P. 2011, "A ceRNA hypothesis: the Rosetta Stone of a hidden RNA language?", *Cell*, vol. 146, no. 3, pp. 353-358.
- Sanchez, N., Gallagher, M., Lao, N., Gallagher, C., Clarke, C., Doolan, P., Aherne, S., Blanco, A., Meleady, P., Clynes, M. & Barron, N. 2013a, "MiR-7 Triggers Cell Cycle Arrest at the G1/S Transition by Targeting Multiple Genes Including Skp2 and Psme3", *PloS one*, vol. 8, no. 6, pp. e65671.
- Sanchez, N., Kelly, P., Gallagher, C., Lao, N.T., Clarke, C., Clynes, M. & Barron, N. 2013b, "CHO cell culture longevity and recombinant protein yield are enhanced by depletion of miR-7 activity via sponge decoy vectors", *Biotechnology journal*, 9(3), pp. 396-404.
- Sangokoya, C., Telen, M.J. & Chi, J.T. 2010, "microRNA miR-144 modulates oxidative stress tolerance and associates with anemia severity in sickle cell disease", *Blood*, vol. 116, no. 20, pp. 4338-4348.
- Sauerwald, T.M., Betenbaugh, M.J. & Oyler, G.A. 2002a, "Inhibiting apoptosis in mammalian cell culture using the caspase inhibitor XIAP and deletion mutants", *Biotechnology and bioengineering*, vol. 77, no. 6, pp. 704-716.
- Sauerwald, T.M., Betenbaugh, M.J. & Oyler, G.A. 2002b, "Inhibiting apoptosis in mammalian cell culture using the caspase inhibitor XIAP and deletion mutants", *Biotechnology and bioengineering*, vol. 77, no. 6, pp. 704-716.
- Sauerwald, T.M., Figueroa, B., Jr, Hardwick, J.M., Oyler, G.A. & Betenbaugh, M.J. 2006, "Combining caspase and mitochondrial dysfunction inhibitors of apoptosis to limit cell death in mammalian cell cultures", *Biotechnology and bioengineering*, vol. 94, no. 2, pp. 362-372.

- Sauerwald, T.M., Oyler, G.A. & Betenbaugh, M.J. 2003, "Study of caspase inhibitors for limiting death in mammalian cell culture", *Biotechnology and bioengineering*, vol. 81, no. 3, pp. 329-340.
- Saydam, O., Shen, Y., Wurdinger, T., Senol, O., Boke, E., James, M.F., Tannous, B.A., Stemmer-Rachamimov, A.O., Yi, M., Stephens, R.M., Fraefel, C., Gusella, J.F., Krichevsky, A.M. & Breakefield, X.O. 2009, "Downregulated microRNA-200a in meningiomas promotes tumor growth by reducing E-cadherin and activating the Wnt/beta-catenin signaling pathway", *Molecular and cellular biology*, vol. 29, no. 21, pp. 5923-5940.
- Scheffer, A.R., Holdenrieder, S., Kristiansen, G., von Ruecker, A., Muller, S.C. & Ellinger, J. 2012, "Circulating microRNAs in serum: novel biomarkers for patients with bladder cancer?", *World journal of urology*, 32(2), pp. 353-8.
- Schwarz, D.S., Hutvagner, G., Du, T., Xu, Z., Aronin, N. & Zamore, P.D. 2003, "Asymmetry in the assembly of the RNAi enzyme complex", *Cell*, vol. 115, no. 2, pp. 199-208.
- Seitz, H. 2009, "Redefining microRNA targets", *Current biology: CB*, vol. 19, no. 10, pp. 870-873.
- Sela-Culang, I., Kunik, V. & Ofran, Y. 2013, "The Structural Basis of Antibody-Antigen Recognition", *Frontiers in immunology*, vol. 4, pp. 302.
- Sengupta, N., Rose, S.T. & Morgan, J.A. 2011, "Metabolic flux analysis of CHO cell metabolism in the late non-growth phase", *Biotechnology and bioengineering*, vol. 108, no. 1, pp. 82-92.
- Serino, G., Sallustio, F., Cox, S.N., Pesce, F. & Schena, F.P. 2012, "Abnormal miR-148b expression promotes aberrant glycosylation of IgA1 in IgA nephropathy", *Journal of the American Society of Nephrology: JASN*, vol. 23, no. 5, pp. 814-824.
- Sethupathy, P., Corda, B. & Hatzigeorgiou, A.G. 2006, "TarBase: A comprehensive database of experimentally supported animal microRNA targets", *RNA (New York, N.Y.)*, vol. 12, no. 2, pp. 192-197.
- Shahbazian, M.D. & Grunstein, M. 2007, "Functions of site-specific histone acetylation and deacetylation", *Annual Review of Biochemistry*, vol. 76, pp. 75-100.
- Shan, S.W., Fang, L., Shatseva, T., Rutnam, Z.J., Yang, X., Du, W., Lu, W.Y., Xuan, J.W., Deng, Z. & Yang, B.B. 2013, "Mature miR-17-5p and passenger miR-17-3p induce hepatocellular carcinoma by targeting PTEN, GalNT7 and vimentin in different signal pathways", *Journal of cell science*, vol. 126, no. Pt 6, pp. 1517-1530.
- Shen, D., Kiehl, T.R., Khattak, S.F., Li, Z.J., He, A., Kayne, P.S., Patel, V., Neuhaus, I.M. & Sharfstein, S.T. 2010, "Transcriptomic responses to sodium chloride-induced osmotic stress: a study of industrial fed-batch CHO cell cultures", *Biotechnology progress*, vol. 26, no. 4, pp. 1104-1115.

- Shen, Z., Zhan, G., Ye, D., Ren, Y., Cheng, L., Wu, Z. & Guo, J. 2012, "MicroRNA-34a affects the occurrence of laryngeal squamous cell carcinoma by targeting the antiapoptotic gene survivin", *Medical oncology (Northwood, London, England)*, vol. 29, no. 4, pp. 2473-2480.
- Shibanuma, M., Inoue, A., Ushida, K., Uchida, T., Ishikawa, F., Mori, K. & Nose, K. 2011, "Importance of mitochondrial dysfunction in oxidative stress response: A comparative study of gene expression profiles", *Free radical research*, vol. 45, no. 6, pp. 672-680.
- Shigenaga, M.K., Hagen, T.M. & Ames, B.N. 1994, "Oxidative damage and mitochondrial decay in aging", *Proceedings of the National Academy of Sciences of the United States of America*, vol. 91, no. 23, pp. 10771-10778.
- Shin, A.H., Kil, I.S., Yang, E.S., Huh, T.L., Yang, C.H. & Park, J.W. 2004, "Regulation of high glucose-induced apoptosis by mitochondrial NADP⁺-dependent isocitrate dehydrogenase", *Biochemical and biophysical research communications*, vol. 325, no. 1, pp. 32-38.
- Shukla, G.C., Singh, J. & Barik, S. 2011, "MicroRNAs: Processing, Maturation, Target Recognition and Regulatory Functions", *Molecular and cellular pharmacology*, vol. 3, no. 3, pp. 83-92.
- Siberil, S., Dutertre, C.A., Fridman, W.H. & Teillaud, J.L. 2007, "FcgammaR: The key to optimize therapeutic antibodies?", *Critical reviews in oncology/hematology*, vol. 62, no. 1, pp. 26-33.
- Sibley, C.R., Seow, Y., Saayman, S., Dijkstra, K.K., El Andaloussi, S., Weinberg, M.S. & Wood, M.J. 2012, "The biogenesis and characterization of mammalian microRNAs of mirtron origin", *Nucleic acids research*, vol. 40, no. 1, pp. 438-448.
- Siegel, C., Li, J., Liu, F., Benashski, S.E. & McCullough, L.D. 2011, "miR-23a regulation of X-linked inhibitor of apoptosis (XIAP) contributes to sex differences in the response to cerebral ischemia", *Proceedings of the National Academy of Sciences of the United States of America*, vol. 108, no. 28, pp. 11662-11667.
- Sikand, K., Slane, S.D. & Shukla, G.C. 2009, "Intrinsic expression of host genes and intronic miRNAs in prostate carcinoma cells", *Cancer cell international*, vol. 9, pp. 21-2867-9-21.
- Silber, J., Jacobsen, A., Ozawa, T., Harinath, G., Pedraza, A., Sander, C., Holland, E.C. & Huse, J.T. 2012, "miR-34a repression in proneural malignant gliomas upregulates expression of its target PDGFRA and promotes tumorigenesis", *PloS one*, vol. 7, no. 3, pp. e33844.
- Silva, J.M., Li, M.Z., Chang, K., Ge, W., Golding, M.C., Rickles, R.J., Siolas, D., Hu, G., Paddison, P.J., Schlabach, M.R., Sheth, N., Bradshaw, J., Burchard, J., Kulkarni, A., Cavet, G., Sachidanandam, R., McCombie, W.R., Cleary, M.A., Elledge, S.J. & Hannon, G.J. 2005, "Second-generation shRNA libraries covering the mouse and human genomes", *Nature genetics*, vol. 37, no. 11, pp. 1281-1288.

- Simmen, T., Lynes, E.M., Gesson, K. & Thomas, G. 2010, "Oxidative protein folding in the endoplasmic reticulum: tight links to the mitochondria-associated membrane (MAM)", *Biochimica et biophysica acta*, vol. 1798, no. 8, pp. 1465-1473.
- Sinclair, A.M. & Elliott, S. 2005, "Glycoengineering: the effect of glycosylation on the properties of therapeutic proteins", *Journal of pharmaceutical sciences*, vol. 94, no. 8, pp. 1626-1635.
- Singh, S.K. 2011, "Impact of product-related factors on immunogenicity of biotherapeutics", *Journal of pharmaceutical sciences*, vol. 100, no. 2, pp. 354-387.
- Sleiman, R.J., Gray, P.P., McCall, M.N., Codamo, J. & Sunstrom, N.A. 2008, "Accelerated cell line development using two-color fluorescence activated cell sorting to select highly expressing antibody-producing clones", *Biotechnology and bioengineering*, vol. 99, no. 3, pp. 578-587.
- Smales, C.M., Dinnis, D.M., Stansfield, S.H., Alete, D., Sage, E.A., Birch, J.R., Racher, A.J., Marshall, C.T. & James, D.C. 2004, "Comparative proteomic analysis of GS-NS0 murine myeloma cell lines with varying recombinant monoclonal antibody production rate", *Biotechnology and bioengineering*, vol. 88, no. 4, pp. 474-488.
- Smith, A.L., Iwanaga, R., Drasin, D.J., Micalizzi, D.S., Vartuli, R.L., Tan, A.C. & Ford, H.L. 2012, "The miR-106b-25 cluster targets Smad7, activates TGF-beta signaling, and induces EMT and tumor initiating cell characteristics downstream of Six1 in human breast cancer", *Oncogene*, 31(50), pp. 5162-71.
- Song, E., Lee, S.K., Dykxhoorn, D.M., Novina, C., Zhang, D., Crawford, K., Cerny, J., Sharp, P.A., Lieberman, J., Manjunath, N. & Shankar, P. 2003, "Sustained small interfering RNA-mediated human immunodeficiency virus type 1 inhibition in primary macrophages", *Journal of virology*, vol. 77, no. 13, pp. 7174-7181.
- Song, G., Zhang, Y. & Wang, L. 2009, "MicroRNA-206 targets notch3, activates apoptosis, and inhibits tumor cell migration and focus formation", *The Journal of biological chemistry*, vol. 284, no. 46, pp. 31921-31927.
- Sood, P., Krek, A., Zavolan, M., Macino, G. & Rajewsky, N. 2006, "Cell-type-specific signatures of microRNAs on target mRNA expression", *Proceedings of the National Academy of Sciences of the United States of America*, vol. 103, no. 8, pp. 2746-2751.
- Spanaki, C. & Plaitakis, A. 2012, "The role of glutamate dehydrogenase in mammalian ammonia metabolism", *Neurotoxicity research*, vol. 21, no. 1, pp. 117-127.
- Spenger, A., Ernst, W., Condreay, J.P., Kost, T.A. & Grabherr, R. 2004, "Influence of promoter choice and trichostatin A treatment on expression of baculovirus delivered genes in mammalian cells", *Protein expression and purification*, vol. 38, no. 1, pp. 17-23.
- Steel, L.F. & Sanghvi, V.R. 2012, "Polycistronic expression of interfering RNAs from RNA polymerase III promoters", *Methods in molecular biology (Clifton, N.J.)*, vol. 815, pp. 347-359.

- Stegmeier, F., Hu, G., Rickles, R.J., Hannon, G.J. & Elledge, S.J. 2005, "A lentiviral microRNA-based system for single-copy polymerase II-regulated RNA interference in mammalian cells", *Proceedings of the National Academy of Sciences of the United States of America*, vol. 102, no. 37, pp. 13212-13217.
- Stenvang, J., Petri, A., Lindow, M., Obad, S. & Kauppinen, S. 2012, "Inhibition of microRNA function by antimiR oligonucleotides", *Silence*, vol. 3, no. 1, pp. 1.
- Stiburek, L., Vesela, K., Hansikova, H., Pecina, P., Tesarova, M., Cerna, L., Houstek, J. & Zeman, J. 2005, "Tissue-specific cytochrome c oxidase assembly defects due to mutations in SCO2 and SURF1", *The Biochemical journal*, vol. 392, no. Pt 3, pp. 625-632.
- Stoller, M.L., Chang, H.C. & Fekete, D.M. 2013, "Bicistronic gene transfer tools for delivery of miRNAs and protein coding sequences", *International journal of molecular sciences*, vol. 14, no. 9, pp. 18239-18255.
- Strotbek, M., Florin, L., Koenitzer, J., Tolstrup, A., Kaufmann, H., Hausser, A. & Olayioye, M.A. 2013, "Stable microRNA expression enhances therapeutic antibody productivity of Chinese hamster ovary cells", *Metabolic engineering*, vol. 20, pp. 157-166.
- Su, J., Zhang, A., Shi, Z., Ma, F., Pu, P., Wang, T., Zhang, J., Kang, C. & Zhang, Q. 2012, "MicroRNA-200a suppresses the Wnt/beta-catenin signaling pathway by interacting with beta-catenin", *International journal of oncology*, vol. 40, no. 4, pp. 1162-1170.
- Sun, F., Fu, H., Liu, Q., Tie, Y., Zhu, J., Xing, R., Sun, Z. & Zheng, X. 2008a, "Downregulation of CCND1 and CDK6 by miR-34a induces cell cycle arrest", *FEBS letters*, vol. 582, no. 10, pp. 1564-1568.
- Sun, F., Fu, H., Liu, Q., Tie, Y., Zhu, J., Xing, R., Sun, Z. & Zheng, X. 2008b, "Downregulation of CCND1 and CDK6 by miR-34a induces cell cycle arrest", *FEBS letters*, vol. 582, no. 10, pp. 1564-1568.
- Sun, J., Zhou, M., Mao, Z. & Li, C. 2012, "Characterization and evolution of microRNA genes derived from repetitive elements and duplication events in plants", *PloS one*, vol. 7, no. 4, pp. e34092.
- Sun, Q., Chen, X., Ma, J., Peng, H., Wang, F., Zha, X., Wang, Y., Jing, Y., Yang, H., Chen, R., Chang, L., Zhang, Y., Goto, J., Onda, H., Chen, T., Wang, M.R., Lu, Y., You, H., Kwiatkowski, D. & Zhang, H. 2011, "Mammalian target of rapamycin up-regulation of pyruvate kinase isoenzyme type M2 is critical for aerobic glycolysis and tumor growth", *Proceedings of the National Academy of Sciences of the United States of America*, vol. 108, no. 10, pp. 4129-4134.
- Sun, S., Li, W., Zhang, H., Zha, L., Xue, Y., Wu, X. & Zou, F. 2012a, "Requirement for store-operated calcium entry in sodium butyrate-induced apoptosis in human colon cancer cells", *Bioscience reports*, vol. 32, no. 1, pp. 83-90.

- Sun, Y., Zhao, X., Zhou, Y. & Hu, Y. 2012b, "miR-124, miR-137 and miR-340 regulate colorectal cancer growth via inhibition of the Warburg effect", *Oncology reports*, vol. 28, no. 4, pp. 1346-1352.
- Sung, Y.H. & Lee, G.M. 2005, "Enhanced human thrombopoietin production by sodium butyrate addition to serum-free suspension culture of bcl-2-overexpressing CHO cells", *Biotechnology progress*, vol. 21, no. 1, pp. 50-57.
- Sung, Y.H., Lee, J.S., Park, S.H., Koo, J. & Lee, G.M. 2007, "Influence of co-down-regulation of caspase-3 and caspase-7 by siRNAs on sodium butyrate-induced apoptotic cell death of Chinese hamster ovary cells producing thrombopoietin", *Metabolic engineering*, vol. 9, no. 5-6, pp. 452-464.
- Sunley, K. & Butler, M. 2010, "Strategies for the enhancement of recombinant protein production from mammalian cells by growth arrest", *Biotechnology Advances*, vol. 28, no. 3, pp. 385-394.
- Sunley, K., Tharmalingam, T. & Butler, M. 2008a, "CHO cells adapted to hypothermic growth produce high yields of recombinant beta-interferon", *Biotechnology progress*, vol. 24, no. 4, pp. 898-906.
- Sunley, K., Tharmalingam, T. & Butler, M. 2008b, "CHO cells adapted to hypothermic growth produce high yields of recombinant beta-interferon", *Biotechnology progress*, vol. 24, no. 4, pp. 898-906.
- Suzuki, E., Niwa, R., Saji, S., Muta, M., Hirose, M., Iida, S., Shiotsu, Y., Satoh, M., Shitara, K., Kondo, M. & Toi, M. 2007a, "A nonfucosylated anti-HER2 antibody augments antibody-dependent cellular cytotoxicity in breast cancer patients", *Clinical cancer research : an official journal of the American Association for Cancer Research*, vol. 13, no. 6, pp. 1875-1882.
- Suzuki, E., Niwa, R., Saji, S., Muta, M., Hirose, M., Iida, S., Shiotsu, Y., Satoh, M., Shitara, K., Kondo, M. & Toi, M. 2007b, "A nonfucosylated anti-HER2 antibody augments antibody-dependent cellular cytotoxicity in breast cancer patients", *Clinical cancer research : an official journal of the American Association for Cancer Research*, vol. 13, no. 6, pp. 1875-1882.
- Sylvestre, Y., De Guire, V., Querido, E., Mukhopadhyay, U.K., Bourdeau, V., Major, F., Ferbeyre, G. & Chartrand, P. 2007, "An E2F/miR-20a autoregulatory feedback loop", *The Journal of biological chemistry*, vol. 282, no. 4, pp. 2135-2143.
- Tabuchi, H., Sugiyama, T., Tanaka, S. & Tainaka, S. 2010, "Overexpression of taurine transporter in Chinese hamster ovary cells can enhance cell viability and product yield, while promoting glutamine consumption", *Biotechnology and bioengineering*, vol. 107, no. 6, pp. 998-1003.
- Tagawa, H. & Seto, M. 2005, "A microRNA cluster as a target of genomic amplification in malignant lymphoma", *Leukemia*, vol. 19, no. 11, pp. 2013-2016.

- Tan, Y., Zhang, B., Wu, T., Skogerbo, G., Zhu, X., Guo, X., He, S. & Chen, R. 2009, "Transcriptional inhibition of Hoxd4 expression by miRNA-10a in human breast cancer cells", *BMC molecular biology*, vol. 10, pp. 12-2199-10-12.
- Tang, W., Zhu, J., Su, S., Wu, W., Liu, Q., Su, F. & Yu, F. 2012, "MiR-27 as a prognostic marker for breast cancer progression and patient survival", *PloS one*, vol. 7, no. 12, pp. e51702.
- Tay, Y., Zhang, J., Thomson, A.M., Lim, B. & Rigoutsos, I. 2008, "MicroRNAs to Nanog, Oct4 and Sox2 coding regions modulate embryonic stem cell differentiation", *Nature*, vol. 455, no. 7216, pp. 1124-1128.
- Templeton, N., Dean, J., Reddy, P. & Young, J.D. 2013, "Peak antibody production is associated with increased oxidative metabolism in an industrially relevant fed-batch CHO cell culture", *Biotechnology and bioengineering*, vol. 110, no. 7, pp. 2013-2024.
- Thaisuchat, H., Baumann, M., Pontiller, J., Hesse, F. & Ernst, W. 2011, "Identification of a novel temperature sensitive promoter in CHO cells", *BMC biotechnology*, vol. 11, pp. 51-6750-11-51.
- Tharmalingam, T., Sunley, K. & Butler, M. 2008, "High yields of monomeric recombinant beta-interferon from macroporous microcarrier cultures under hypothermic conditions", *Biotechnology progress*, vol. 24, no. 4, pp. 832-838.
- Thomson, D.W., Bracken, C.P. & Goodall, G.J. 2011, "Experimental strategies for microRNA target identification", *Nucleic acids research*, vol. 39, no. 16, pp. 6845-6853.
- Tigges, M. & Fussenegger, M. 2006, "Xbp1-based engineering of secretory capacity enhances the productivity of Chinese hamster ovary cells", *Metabolic engineering*, vol. 8, no. 3, pp. 264-272.
- Tomasetti, M., Neuzil, J. & Dong, L. 2013, "MicroRNAs as regulators of mitochondrial function: Role in cancer suppression", *Biochimica et biophysica acta*, 1840(4), pp. 1441-51.
- Travers, K.J., Patil, C.K., Wodicka, L., Lockhart, D.J., Weissman, J.S. & Walter, P. 2000, "Functional and genomic analyses reveal an essential coordination between the unfolded protein response and ER-associated degradation", *Cell*, vol. 101, no. 3, pp. 249-258.
- Trigona, W.L., Mullarky, I.K., Cao, Y. & Sordillo, L.M. 2006, "Thioredoxin reductase regulates the induction of haem oxygenase-1 expression in aortic endothelial cells", *The Biochemical journal*, vol. 394, no. Pt 1, pp. 207-216.
- Truettner, J.S., Motti, D. & Dietrich, W.D. 2013, "MicroRNA overexpression increases cortical neuronal vulnerability to injury", *Brain research*, vol. 1533, pp. 122-130.

- Trummer, E., Fauland, K., Seidinger, S., Schriebl, K., Lattenmayer, C., Kunert, R., Vorauer-Uhl, K., Weik, R., Borth, N., Katinger, H. & Muller, D. 2006, "Process parameter shifting: Part I. Effect of DOT, pH, and temperature on the performance of Epo-Fc expressing CHO cells cultivated in controlled batch bioreactors", *Biotechnology and bioengineering*, vol. 94, no. 6, pp. 1033-1044.
- Tsao, Y.S., Cardoso, A.G., Condon, R.G., Voloch, M., Lio, P., Lagos, J.C., Kearns, B.G. & Liu, Z. 2005, "Monitoring Chinese hamster ovary cell culture by the analysis of glucose and lactate metabolism", *Journal of Biotechnology*, vol. 118, no. 3, pp. 316-327.
- Tseng, Y.C., Mozumdar, S. & Huang, L. 2009, "Lipid-based systemic delivery of siRNA", *Advanced Drug Delivery Reviews*, vol. 61, no. 9, pp. 721-731.
- Tsukamoto, Y., Nakada, C., Noguchi, T., Tanigawa, M., Nguyen, L.T., Uchida, T., Hijiya, N., Matsuura, K., Fujioka, T., Seto, M. & Moriyama, M. 2010, "MicroRNA-375 is downregulated in gastric carcinomas and regulates cell survival by targeting PDK1 and 14-3-3zeta", *Cancer research*, vol. 70, no. 6, pp. 2339-2349.
- Ucakturk, E. 2012, "Analysis of glycoforms on the glycosylation site and the glycans in monoclonal antibody biopharmaceuticals", *Journal of separation science*, vol. 35, no. 3, pp. 341-350.
- Uchiumi, T. & Kang, D. 2012, "The role of TFAM-associated proteins in mitochondrial RNA metabolism", *Biochimica et biophysica acta*, vol. 1820, no. 5, pp. 565-570.
- Urbich, C., Kaluza, D., Fromel, T., Knau, A., Bennewitz, K., Boon, R.A., Bonauer, A., Doebele, C., Boeckel, J.N., Hergenreider, E., Zeiher, A.M., Kroll, J., Fleming, I. & Dimmeler, S. 2012, "MicroRNA-27a/b controls endothelial cell repulsion and angiogenesis by targeting semaphorin 6A", *Blood*, vol. 119, no. 6, pp. 1607-1616.
- Vaistij, F.E., Elias, L., George, G.L. & Jones, L. 2010, "Suppression of microRNA accumulation via RNA interference in *Arabidopsis thaliana*", *Plant Molecular Biology*, vol. 73, no. 4-5, pp. 391-397.
- Vander Heiden, M.G., Cantley, L.C. & Thompson, C.B. 2009, "Understanding the Warburg effect: the metabolic requirements of cell proliferation", *Science (New York, N.Y.)*, vol. 324, no. 5930, pp. 1029-1033.
- Vella, M.C., Choi, E.Y., Lin, S.Y., Reinert, K. & Slack, F.J. 2004, "The *C. elegans* microRNA let-7 binds to imperfect let-7 complementary sites from the lin-41 3'UTR", *Genes & development*, vol. 18, no. 2, pp. 132-137.
- Ventura, A., Young, A.G., Winslow, M.M., Lintault, L., Meissner, A., Erkeland, S.J., Newman, J., Bronson, R.T., Crowley, D., Stone, J.R., Jaenisch, R., Sharp, P.A. & Jacks, T. 2008, "Targeted deletion reveals essential and overlapping functions of the miR-17 through 92 family of miRNA clusters", *Cell*, vol. 132, no. 5, pp. 875-886.
- Vergoulis, T., Vlachos, I.S., Alexiou, P., Georgakilas, G., Maragkakis, M., Reczko, M., Gerangelos, S., Koziris, N., Dalamagas, T. & Hatzigeorgiou, A.G. 2012, "TarBase

6.0: capturing the exponential growth of miRNA targets with experimental support", *Nucleic acids research*, vol. 40, no. Database issue, pp. D222-9.

Vogt, M., Munding, J., Gruner, M., Liffers, S.T., Verdoodt, B., Hauk, J., Steinstraesser, L., Tannapfel, A. & Hermeking, H. 2011, "Frequent concomitant inactivation of miR-34a and miR-34b/c by CpG methylation in colorectal, pancreatic, mammary, ovarian, urothelial, and renal cell carcinomas and soft tissue sarcomas", *Virchows Archiv : an international journal of pathology*, vol. 458, no. 3, pp. 313-322.

Walsh, G. 2010, "Biopharmaceutical benchmarks 2010", *Nature biotechnology*, vol. 28, no. 9, pp. 917-924.

Walsh, G. & Jefferis, R. 2006, "Post-translational modifications in the context of therapeutic proteins", *Nature biotechnology*, vol. 24, no. 10, pp. 1241-1252.

Wang, A., Zhang, B., Zhang, J., Wu, W. & Wu, W. 2013, "Embelin-induced brain glioma cell apoptosis and cell cycle arrest via the mitochondrial pathway", *Oncology reports*, vol. 29, no. 6, pp. 2473-2478.

Wang, A.H., Kruhlak, M.J., Wu, J., Bertos, N.R., Vezmar, M., Posner, B.I., Bazett-Jones, D.P. & Yang, X.J. 2000, "Regulation of histone deacetylase 4 by binding of 14-3-3 proteins", *Molecular and cellular biology*, vol. 20, no. 18, pp. 6904-6912.

Wang, D.G., Sun, Y.B., Ye, F., Li, W., Kharbuja, P., Gao, L., Zhang, D.Y. & Suo, J. 2013, "Anti-tumor activity of the X-linked inhibitor of apoptosis (XIAP) inhibitor embelin in gastric cancer cells", *Molecular and cellular biochemistry*, 386(1-2), pp. 143-52.

Wang, I.K., Hsieh, S.Y., Chang, K.M., Wang, Y.C., Chu, A., Shaw, S.Y., Ou, J.J. & Ho, L. 2006, "A novel control scheme for inducing angiostatin-human IgG fusion protein production using recombinant CHO cells in a oscillating bioreactor", *Journal of Biotechnology*, vol. 121, no. 3, pp. 418-428.

Wang, R., Hu, Y., Song, G., Hao, C.J., Cui, Y., Xia, H.F. & Ma, X. 2012, "MiR-206 regulates neural cells proliferation and apoptosis via Otx2", *Cellular physiology and biochemistry : international journal of experimental cellular physiology, biochemistry, and pharmacology*, vol. 29, no. 3-4, pp. 381-390.

Wang, R., Wang, Z.X., Yang, J.S., Pan, X., De, W. & Chen, L.B. 2011a, "MicroRNA-451 functions as a tumor suppressor in human non-small cell lung cancer by targeting ras-related protein 14 (RAB14)", *Oncogene*, vol. 30, no. 23, pp. 2644-2658.

Wang, X., Xu, X., Ma, Z., Huo, Y., Xiao, Z., Li, Y. & Wang, Y. 2011b, "Dynamic mechanisms for pre-miRNA binding and export by Exportin-5", *RNA (New York, N.Y.)*, vol. 17, no. 8, pp. 1511-1528.

Wang, X.F., Shi, Z.M., Wang, X.R., Cao, L., Wang, Y.Y., Zhang, J.X., Yin, Y., Luo, H., Kang, C.S., Liu, N., Jiang, T. & You, Y.P. 2012, "MiR-181d acts as a tumor suppressor in glioma by targeting K-ras and Bcl-2", *Journal of cancer research and clinical oncology*, vol. 138, no. 4, pp. 573-584.

- Watson, W.H., Yang, X., Choi, Y.E., Jones, D.P. & Kehrer, J.P. 2004, "Thioredoxin and its role in toxicology", *Toxicological sciences : an official journal of the Society of Toxicology*, vol. 78, no. 1, pp. 3-14.
- Weber, M., Baker, M.B., Moore, J.P. & Searles, C.D. 2010, "MiR-21 is induced in endothelial cells by shear stress and modulates apoptosis and eNOS activity", *Biochemical and biophysical research communications*, vol. 393, no. 4, pp. 643-648.
- Wei, Y.Y., Naderi, S., Meshram, M., Budman, H., Scharer, J.M., Ingalls, B.P. & McConkey, B.J. 2011, "Proteomics analysis of chinese hamster ovary cells undergoing apoptosis during prolonged cultivation", *Cytotechnology*, vol. 63, no. 6, pp. 663-677.
- Welch, C., Chen, Y. & Stallings, R.L. 2007, "MicroRNA-34a functions as a potential tumor suppressor by inducing apoptosis in neuroblastoma cells", *Oncogene*, vol. 26, no. 34, pp. 5017-5022.
- Wenham, R.M., Landt, M. & Easom, R.A. 1994, "Glucose activates the multifunctional Ca²⁺/calmodulin-dependent protein kinase II in isolated rat pancreatic islets", *The Journal of biological chemistry*, vol. 269, no. 7, pp. 4947-4952.
- Winnard, P., Jr, Glackin, C. & Raman, V. 2006, "Stable integration of an empty vector in MCF-7 cells greatly alters the karyotype", *Cancer genetics and cytogenetics*, vol. 164, no. 2, pp. 174-176.
- Wlaschin, K.F. & Hu, W.S. 2007, "Engineering cell metabolism for high-density cell culture via manipulation of sugar transport", *Journal of Biotechnology*, vol. 131, no. 2, pp. 168-176.
- Wong, D.C., Wong, K.T., Lee, Y.Y., Morin, P.N., Heng, C.K. & Yap, M.G. 2006, "Transcriptional profiling of apoptotic pathways in batch and fed-batch CHO cell cultures", *Biotechnology and bioengineering*, vol. 94, no. 2, pp. 373-382.
- Wu, S.C. 2009a, "RNA interference technology to improve recombinant protein production in Chinese hamster ovary cells", *Biotechnology Advances*, vol. 27, no. 4, pp. 417-422.
- Wu, S.C. 2009b, "RNA interference technology to improve recombinant protein production in Chinese hamster ovary cells", *Biotechnology Advances*, vol. 27, no. 4, pp. 417-422.
- Wu, L., Fan, J. & Belasco, J.G. 2006, "MicroRNAs direct rapid deadenylation of mRNA", *Proceedings of the National Academy of Sciences of the United States of America*, vol. 103, no. 11, pp. 4034-4039.
- Wu, S., Huang, S., Ding, J., Zhao, Y., Liang, L., Liu, T., Zhan, R. & He, X. 2010, "Multiple microRNAs modulate p21Cip1/Waf1 expression by directly targeting its 3' untranslated region", *Oncogene*, vol. 29, no. 15, pp. 2302-2308.

- Wu, S.C. 2009, "RNA interference technology to improve recombinant protein production in Chinese hamster ovary cells", *Biotechnology Advances*, vol. 27, no. 4, pp. 417-422.
- Wurm, F.M. 2004, "Production of recombinant protein therapeutics in cultivated mammalian cells", *Nature biotechnology*, vol. 22, no. 11, pp. 1393-1398.
- Wurm, F.M. & Hacker, D. 2011, "First CHO genome", *Nature biotechnology*, vol. 29, no. 8, pp. 718-720.
- Xia, H.Q., Pan, Y., Peng, J. & Lu, G.X. 2011, "Over-expression of miR375 reduces glucose-induced insulin secretion in Nit-1 cells", *Molecular biology reports*, vol. 38, no. 5, pp. 3061-3065.
- Xie, Y., Tobin, L.A., Camps, J., Wangsa, D., Yang, J., Rao, M., Witasp, E., Awad, K.S., Yoo, N., Ried, T. & Kwong, K.F. 2012, "MicroRNA-24 regulates XIAP to reduce the apoptosis threshold in cancer cells", *Oncogene*, 9(32), pp. 2442-51.
- Xu, C., Lu, Y., Pan, Z., Chu, W., Luo, X., Lin, H., Xiao, J., Shan, H., Wang, Z. & Yang, B. 2007, "The muscle-specific microRNAs miR-1 and miR-133 produce opposing effects on apoptosis by targeting HSP60, HSP70 and caspase-9 in cardiomyocytes", *Journal of cell science*, vol. 120, no. Pt 17, pp. 3045-3052.
- Xu, X., Nagarajan, H., Lewis, N.E., Pan, S., Cai, Z., Liu, X., Chen, W., Xie, M., Wang, W., Hammond, S., Andersen, M.R., Neff, N., Passarelli, B., Koh, W., Fan, H.C., Wang, J., Gui, Y., Lee, K.H., Betenbaugh, M.J., Quake, S.R., Famili, I., Palsson, B.O. & Wang, J. 2011, "The genomic sequence of the Chinese hamster ovary (CHO)-K1 cell line", *Nature biotechnology*, vol. 29, no. 8, pp. 735-741.
- Yamakuchi, M., Ferlito, M. & Lowenstein, C.J. 2008, "miR-34a repression of SIRT1 regulates apoptosis", *Proceedings of the National Academy of Sciences of the United States of America*, vol. 105, no. 36, pp. 13421-13426.
- Yamane-Ohnuki, N., Kinoshita, S., Inoue-Urakubo, M., Kusunoki, M., Iida, S., Nakano, R., Wakitani, M., Niwa, R., Sakurada, M., Uchida, K., Shitara, K. & Satoh, M. 2004, "Establishment of FUT8 knockout Chinese hamster ovary cells: an ideal host cell line for producing completely defucosylated antibodies with enhanced antibody-dependent cellular cytotoxicity", *Biotechnology and bioengineering*, vol. 87, no. 5, pp. 614-622.
- Yan, B., Zhao, L.H., Guo, J.T. & Zhao, J.L. 2012, "miR-429 regulation of osmotic stress transcription factor 1 (OSTF1) in tilapia during osmotic stress", *Biochemical and biophysical research communications*, vol. 426, no. 3, pp. 294-298.
- Yan, D., Dong Xda, E., Chen, X., Wang, L., Lu, C., Wang, J., Qu, J. & Tu, L. 2009a, "MicroRNA-1/206 targets c-Met and inhibits rhabdomyosarcoma development", *The Journal of biological chemistry*, vol. 284, no. 43, pp. 29596-29604.
- Yan, H.L., Xue, G., Mei, Q., Wang, Y.Z., Ding, F.X., Liu, M.F., Lu, M.H., Tang, Y., Yu, H.Y. & Sun, S.H. 2009b, "Repression of the miR-17-92 cluster by p53 has an

- important function in hypoxia-induced apoptosis", *The EMBO journal*, vol. 28, no. 18, pp. 2719-2732.
- Yang, F., Li, Q.J., Gong, Z.B., Zhou, L., You, N., Wang, S., Li, X.L., Li, J.J., An, J.Z., Wang, D.S., He, Y. & Dou, K.F. 2014, "MicroRNA-34a targets Bcl-2 and sensitizes human hepatocellular carcinoma cells to sorafenib treatment", *Technology in cancer research & treatment*, vol. 13, no. 1, pp. 77-86.
- Yang, H., Ye, D., Guan, K.L. & Xiong, Y. 2012, "IDH1 and IDH2 mutations in tumorigenesis: mechanistic insights and clinical perspectives", *Clinical cancer research : an official journal of the American Association for Cancer Research*, vol. 18, no. 20, pp. 5562-5571.
- Yang, J.S., Phillips, M.D., Betel, D., Mu, P., Ventura, A., Siepel, A.C., Chen, K.C. & Lai, E.C. 2011, "Widespread regulatory activity of vertebrate microRNA* species", *RNA (New York, N.Y.)*, vol. 17, no. 2, pp. 312-326.
- Yang, M. & Butler, M. 2000, "Effects of ammonia on CHO cell growth, erythropoietin production, and glycosylation", *Biotechnology and bioengineering*, vol. 68, no. 4, pp. 370-380.
- Yang, W.C., Lu, J., Nguyen, N.B., Zhang, A., Healy, N.V., Kshirsagar, R., Ryll, T. & Huang, Y.M. 2014, "Addition of Valproic Acid to CHO Cell Fed-Batch Cultures Improves Monoclonal Antibody Titers", *Molecular biotechnology*, vol. 56, no. 5, pp. 421-428.
- Yang, X., Du, W.W., Li, H., Liu, F., Khorshidi, A., Rutnam, Z.J. & Yang, B.B. 2013, "Both mature miR-17-5p and passenger strand miR-17-3p target TIMP3 and induce prostate tumor growth and invasion", *Nucleic acids research*, 41(21), pp. 9688-704.
- Yang, X., Rutnam, Z.J., Jiao, C., Wei, D., Xie, Y., Du, J., Zhong, L. & Yang, B.B. 2012, "An anti-let-7 sponge decoys and decays endogenous let-7 functions", *Cell cycle (Georgetown, Tex.)*, vol. 11, no. 16, pp. 3097-3108.
- Yee, J.C., de Leon Gatti, M., Philp, R.J., Yap, M. & Hu, W.S. 2008, "Genomic and proteomic exploration of CHO and hybridoma cells under sodium butyrate treatment", *Biotechnology and bioengineering*, vol. 99, no. 5, pp. 1186-1204.
- Yee, J.C., Gerdtsen, Z.P. & Hu, W.S. 2009, "Comparative transcriptome analysis to unveil genes affecting recombinant protein productivity in mammalian cells", *Biotechnology and bioengineering*, vol. 102, no. 1, pp. 246-263.
- Yeom, K.H., Lee, Y., Han, J., Suh, M.R. & Kim, V.N. 2006, "Characterization of DGCR8/Pasha, the essential cofactor for Drosha in primary miRNA processing", *Nucleic acids research*, vol. 34, no. 16, pp. 4622-4629.
- Yoon, S.K., Song, J.Y. & Lee, G.M. 2003, "Effect of low culture temperature on specific productivity, transcription level, and heterogeneity of erythropoietin in Chinese hamster ovary cells", *Biotechnology and bioengineering*, vol. 82, no. 3, pp. 289-298.

- Yoshikawa, T., Nakanishi, F., Ogura, Y., Oi, D., Omasa, T., Katakura, Y., Kishimoto, M. & Suga, K.I. 2001, "Flow cytometry: an improved method for the selection of highly productive gene-amplified CHO cells using flow cytometry", *Biotechnology and bioengineering*, vol. 74, no. 5, pp. 435-442.
- Young, J.D. 2013, "Metabolic flux rewiring in mammalian cell cultures", *Current opinion in biotechnology*, vol. 24, no. 6, pp. 1108-1115.
- Yuan, J.H., Yang, F., Chen, B.F., Lu, Z., Huo, X.S., Zhou, W.P., Wang, F. & Sun, S.H. 2011, "The histone deacetylase 4/SP1/microrna-200a regulatory network contributes to aberrant histone acetylation in hepatocellular carcinoma", *Hepatology (Baltimore, Md.)*, vol. 54, no. 6, pp. 2025-2035.
- Yun, C.Y., Liu, S., Lim, S.F., Wang, T., Chung, B.Y., Jiat Teo, J., Chuan, K.H., Soon, A.S., Goh, K.S. & Song, Z. 2007, "Specific inhibition of caspase-8 and -9 in CHO cells enhances cell viability in batch and fed-batch cultures", *Metabolic engineering*, vol. 9, no. 5-6, pp. 406-418.
- Zeng, Y. & Cullen, B.R. 2005, "Efficient processing of primary microRNA hairpins by Drosha requires flanking nonstructured RNA sequences", *The Journal of biological chemistry*, vol. 280, no. 30, pp. 27595-27603.
- Zeng, Y. & Cullen, B.R. 2004, "Structural requirements for pre-microRNA binding and nuclear export by Exportin 5", *Nucleic acids research*, vol. 32, no. 16, pp. 4776-4785.
- Zeng, Y. & Cullen, B.R. 2003, "Sequence requirements for micro RNA processing and function in human cells", *RNA (New York, N.Y.)*, vol. 9, no. 1, pp. 112-123.
- Zhang, H., Hao, Y., Yang, J., Zhou, Y., Li, J., Yin, S., Sun, C., Ma, M., Huang, Y. & Xi, J.J. 2011, "Genome-wide functional screening of miR-23b as a pleiotropic modulator suppressing cancer metastasis", *Nature communications*, vol. 2, pp. 554.
- Zhang, L., Liu, X., Jin, H., Guo, X., Xia, L., Chen, Z., Bai, M., Liu, J., Shang, X., Wu, K., Pan, Y. & Fan, D. 2013, "miR-206 inhibits gastric cancer proliferation in part by repressing cyclinD2", *Cancer letters*, vol. 332, no. 1, pp. 94-101.
- Zhang, T. & Brown, J.H. 2004, "Role of Ca²⁺/calmodulin-dependent protein kinase II in cardiac hypertrophy and heart failure", *Cardiovascular research*, vol. 63, no. 3, pp. 476-486.
- Zhang, T., Kohlhaas, M., Backs, J., Mishra, S., Phillips, W., Dybkova, N., Chang, S., Ling, H., Bers, D.M., Maier, L.S., Olson, E.N. & Brown, J.H. 2007, "CaMKII δ isoforms differentially affect calcium handling but similarly regulate HDAC/MEF2 transcriptional responses", *The Journal of biological chemistry*, vol. 282, no. 48, pp. 35078-35087.
- Zhang, T., Liu, M., Wang, C., Lin, C., Sun, Y. & Jin, D. 2011, "Down-regulation of MiR-206 promotes proliferation and invasion of laryngeal cancer by regulating VEGF expression", *Anticancer Research*, vol. 31, no. 11, pp. 3859-3863.

- Zhang, X., Hu, S., Zhang, X., Wang, L., Zhang, X., Yan, B., Zhao, J., Yang, A. & Zhang, R. 2013, "MicroRNA-7 arrests cell cycle in G1 phase by directly targeting CCNE1 in human hepatocellular carcinoma cells", *Biochemical and biophysical research communications*, 443(3), pp. 1078-84.
- Zhao, S., Lin, Y., Xu, W., Jiang, W., Zha, Z., Wang, P., Yu, W., Li, Z., Gong, L., Peng, Y., Ding, J., Lei, Q., Guan, K.L. & Xiong, Y. 2009, "Glioma-derived mutations in IDH1 dominantly inhibit IDH1 catalytic activity and induce HIF-1alpha", *Science (New York, N.Y.)*, vol. 324, no. 5924, pp. 261-265.
- Zheng, X., Baker, H., Hancock, W.S., Fawaz, F., McCaman, M. & Pungor, E., Jr 2006, "Proteomic analysis for the assessment of different lots of fetal bovine serum as a raw material for cell culture. Part IV. Application of proteomics to the manufacture of biological drugs", *Biotechnology progress*, vol. 22, no. 5, pp. 1294-1300.
- Zhou, H., Liu, Z.G., Sun, Z.W., Huang, Y. & Yu, W.Y. 2010, "Generation of stable cell lines by site-specific integration of transgenes into engineered Chinese hamster ovary strains using an FLP-FRT system", *Journal of Biotechnology*, vol. 147, no. 2, pp. 122-129.
- Zhou, J., Li, Y.S., Nguyen, P., Wang, K.C., Weiss, A., Kuo, Y.C., Chiu, J.J., Shyy, J.Y. & Chien, S. 2013, "Regulation of vascular smooth muscle cell turnover by endothelial cell-secreted microRNA-126: role of shear stress", *Circulation research*, vol. 113, no. 1, pp. 40-51.
- Zhou, M., Crawford, Y., Ng, D., Tung, J., Pynn, A.F., Meier, A., Yuk, I.H., Vijayasankaran, N., Leach, K., Joly, J., Snedecor, B. & Shen, A. 2011a, "Decreasing lactate level and increasing antibody production in Chinese Hamster Ovary cells (CHO) by reducing the expression of lactate dehydrogenase and pyruvate dehydrogenase kinases", *Journal of Biotechnology*, vol. 153, no. 1-2, pp. 27-34.
- Zhou, M., Crawford, Y., Ng, D., Tung, J., Pynn, A.F., Meier, A., Yuk, I.H., Vijayasankaran, N., Leach, K., Joly, J., Snedecor, B. & Shen, A. 2011b, "Decreasing lactate level and increasing antibody production in Chinese Hamster Ovary cells (CHO) by reducing the expression of lactate dehydrogenase and pyruvate dehydrogenase kinases", *Journal of Biotechnology*, vol. 153, no. 1-2, pp. 27-34.
- Zhou, S.G., Wang, P., Pi, R.B., Gao, J., Fu, J.J., Fang, J., Qin, J., Zhang, H.J., Li, R.F., Chen, S.R., Tang, F.T. & Liu, P.Q. 2008, "Reduced expression of GSTM2 and increased oxidative stress in spontaneously hypertensive rat", *Molecular and cellular biochemistry*, vol. 309, no. 1-2, pp. 99-107.
- Zhu, X., Santat, L.A., Chang, M.S., Liu, J., Zavzavadjian, J.R., Wall, E.A., Kivork, C., Simon, M.I. & Fraser, I.D. 2007, "A versatile approach to multiple gene RNA interference using microRNA-based short hairpin RNAs", *BMC molecular biology*, vol. 8, pp. 98.

Appendix

Figure A1: microRNAs used in primary screen

microRNA	Pre-miR/Inhibitor (PM/AM)
miR-10a	AM
miR-15a	AM
miR-15b	AM
miR-16-1	AM
miR-18a	PM
miR-23b	PM
miR-23b*	PM
miR-25	AM
miR-27a	AM
miR-29a	AM
miR-34a	PM
miR-34a	AM
miR-34a*	PM
miR-93	AM
miR-106b	AM
miR-126	AM
miR-143	AM
miR-181d	PM
mir-184	AM
miR-200a	PM
miR-206	AM
miR-219	PM
miR-320	PM
miR-320a	PM
miR-320a	AM
miR-338-3p	AM
miR-378	AM
miR-409-3p	AM
miR-450	PM
miR-455-3p	AM
miR-455-5p	AM
miR-532-5p	PM
miR-532-5p	AM
miR-639	PM
miR-874	AM

AM = anti-miR for transient inhibition

PM = pre-miR (mimic) for transient over-expression

Figure A2: Relative data for transient transfection of anti-miR 126, -338-3p, -378 and -409-3p in CHO-K1-SEAP cells

miRNA	Cell numbers/mL			Protein Yield/mL			Cell specific Productivity		
	Day 2	Day 4	Day 7	Day 2	Day 4	Day 7	Day 2	Day 4	Day 7
miR-126	1.03	1.06	0.8	0.95	1.1	0.88	0.92	1.04	1.09
miR-338-3p	1.22	0.86	0.86	1.02	0.97	0.79	0.83	1.11	0.92
	1.06	1.4	1	0.93	1.03	1.07	0.87	0.73	0.99
	0.6	0.47	1.33	0.76	0.82	1.1	1.25	1.43	0.82
	0.57	0.49	1.07	0.69	0.74	1.19	1.19	1.48	1.11
	1.18	1.13	1.59	0.96	0.9	1.03	0.81	0.8	0.64
	0.88	0.9	0.66	0.96	0.92	0.87	1.09	1.02	1.3
miR-378	0.77	0.59	0.83	0.72	0.86	1.21	0.92	1.45	1.12
	0.99	1.05	0.99	0.91	0.95	1.15	0.92	0.9	1.16
miR-409-3p	0.9	0.8	1.18	0.92	0.83	0.93	1.02	1.03	0.78
	1.29	1.97	1.12	0.83	1.16	0.93	0.64	0.59	0.83
	0.87	0.87	1.22	0.89	1.04	1.11	1.02	1.19	0.91
	1.19	0.87	0.83	1.22	1.36	1.44	1.01	1.55	1.71
	1.08	1.27	0.95	1.09	1.09	1.08	1.01	0.85	1.13
	0.99	1.26	1.5	0.92	0.96	1.09	0.89	0.76	0.73
	0.86	0.98	0.6	0.94	0.97	0.95	1.09	1.09	1.57
	0.92	0.9	0.65	0.98	1.16	0.84	1.06	1.28	1.29

Figure A3: High cell density transfection optimisation using siRNA against VCP

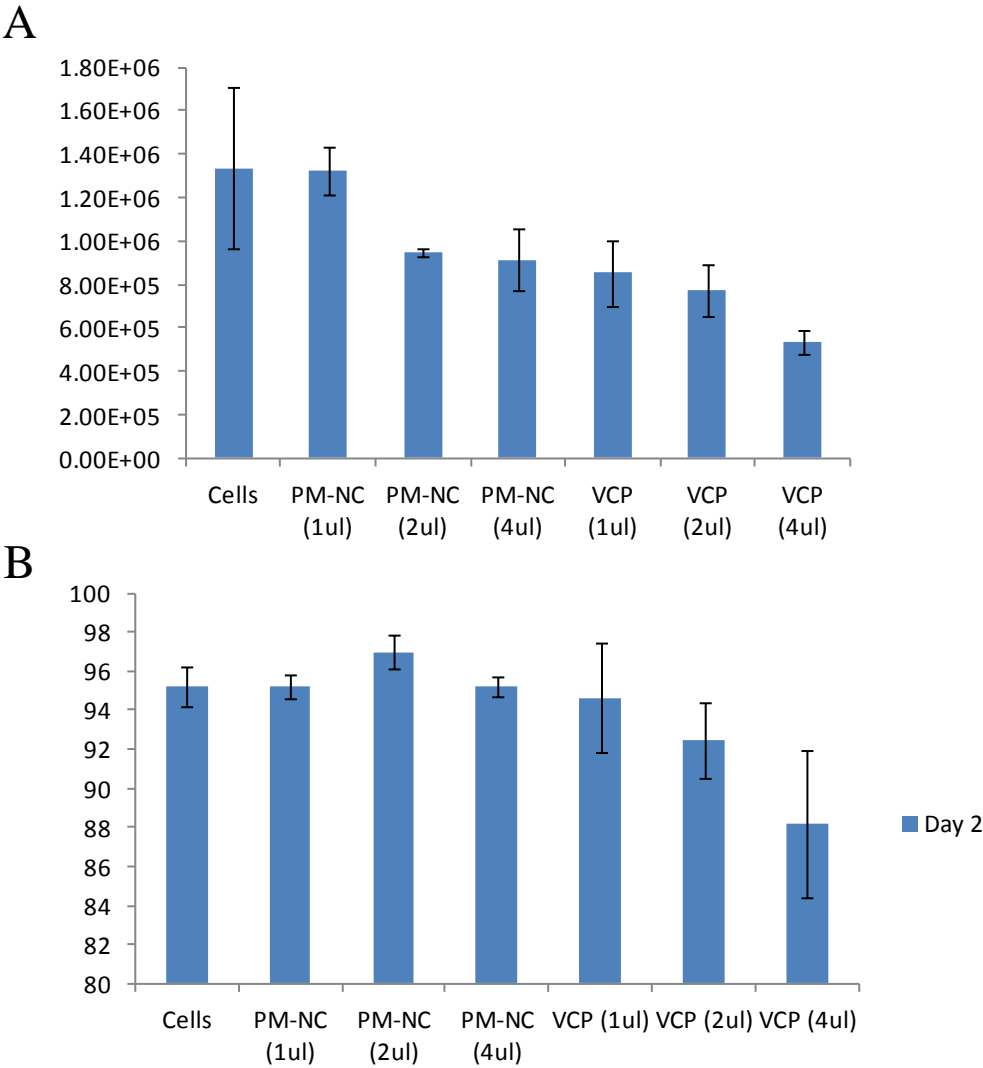


Figure A3: cells were transfected at a density of 4×10^5 cells/mL using 50 nM pre-miR-NC and siRNA designed against VCP using a range of concentrations of INTERFERin™ of 1, 2 and 4 μ l. Part A shows cell numbers/mL while part B shows cell viability.

Figure A4: clustal alignment for miR-34 sponge sequence

CLUSTAL 2.1 multiple sequence alignment

```

seq1      TGTAGGCGGCCGCTCGAGACGCGACAACCAGCTCCAACACTGCCAACGCGACAACCAGCT 60
seq2      TGTAGGCGGCCGCTCGAGACGCGACAACCAGCTCCAACACTGCCAACGCGACAACCAGCT 60
          *****

seq1      CCAACACTGCCAACGAGACAACCAGCTCCAACACTGCCATGACGTACAACCAGCTCCAAC 120
seq2      CCAACACTGCCAACGAGACAACCAGCTCCAACACTGCCATGACGTACAACCAGCTCCAAC 120
          *****

seq1      ACTGCCATCATCGAATTCTCGATGCATGCCTCGAC---- 155
seq2      ACTGCCATCATCGAATTCTCGATGCATGCCTCGACTGTG 159
          *****

```

Figure A4: Clustal alignment to confirm insertion of the miR-34 sponge sequence. Seq1 = template sequence, Seq2 = sequence results from MWG Operon sequencing service. Star denotes a perfect match.

Figure A5: single nucleotide difference between miR-23a and miR-23b

```

miR-23a    5'-aucacauugccagggauuucc-3'
           | | | | | | | | | | | | | | | * | |
miR-23b    5'-aucacauugccagggauuacc-3'

```

Figure A5: Sequence similarity between the mature miR-23a and miR-23b sequences. A single nucleotide difference is indicated by a star (*) with the seed region of both miRNAs being highlighted in a yellow box (nt 2-8).

Figure A6: Diagnostic gels for miR-23b/-23b* sponge vector preparation

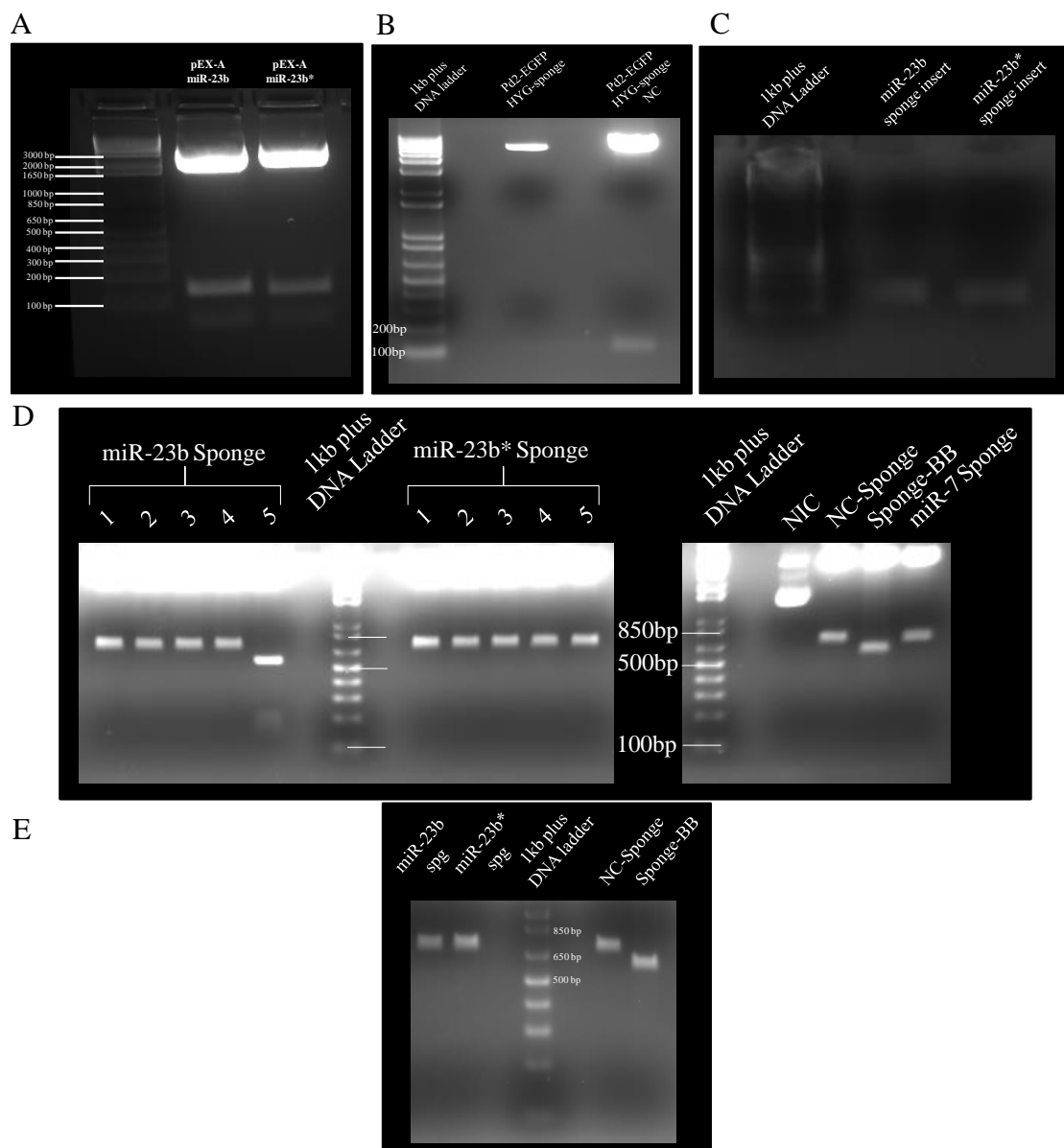


Figure A6: Diagnostic gels for miR-sponge preparation A) stock plasmid containing miR-23b/-23b* (pEX-A) suitable for bacterial culture only B) Digestion of empty and negative control (NC) pd2-EGFP-sponge with *XhoI/EcoRI* C) Extracted miR-23b/-23b* sequence inserts D) Mini-prep diagnostic panel of miR-23b/-23b* sponge vectors E) Final diagnostic of Maxi-prep sponge vectors.

Figure A7: Sequence alignment for miR-23b and miR-23b* sponge vectors

A miR-23b* sponge vector

CLUSTAL 2.1 multiple sequence alignment

```

seq1      GTGTAGGCGGCCGCTCGAGACGCGAAATCAGCCGTACAGGAACCCATCATCAAATCAGCC 60
seq2      GTGTAGGCGGCCGCTCGAGACGCGAAATCAGCCGTACAGGAACCCATCATCAAATCAGCC 60
          *****

seq1      GTACAGGAACCCAACCGTAAATCAGCCGTACAGGAACCCAACGAGAAATCAGCCGTACA 120
seq2      GTACAGGAACCCAACCGTAAATCAGCCGTACAGGAACCCAACGAGAAATCAGCCGTACA 120
          *****

seq1      GGAACCCATCATCGAATTCGATGATGCTCGACTGTGCTTCTAG 168
seq2      GGAACCCATCATCGAATTCGATGATGCTCGACTGTG----- 160
          *****

```

B miR-23b sponge vector

CLUSTAL 2.1 multiple sequence alignment

```

seq1      GGAGCAGGATGATGGCACGCTGCCCATGTCTTGIGCCAGGAGAGCGGGATGGACCGTCA 60
seq2      -----

seq1      CCCTGCAGCCTGTGCTTCTGCTAGGATCAATGTGTAGGCGGCCGCTCGAGACGCGGGTAA 120
seq2      -----ACGCGGGTAA 10
          *****

seq1      TCCGCATCAATGTGATTTCATCGGTAATCCGCATCAATGTGATACCGTAGGTAATCCGCAT 180
seq2      TCCGCATCAATGTGATTTCATCGGTAATCCGCATCAATGTGATACCGTAGGTAATCCGCAT 70
          *****

seq1      CAATGTGATACGAGGGTAATCCGCATCAATGTGATTTCATCGAATTCTCGATGCATGCCTC 240
seq2      CAATGTGATACGAGGGTAATCCGCATCAATGTGATTTCAT----- 110
          *****

```

Figure A7: The Clustal sequence alignments for both miR-23b* (A) and miR-23b (B) sponge sequences referenced against the original sequence designed. Seq1 denotes the original sequence designed while Seq2 denotes the sequence information from MWG Operon. Perfect matches are flagged with stars (*) while just the sponge sequence is highlighted in green.

Figure A8: pre-miR-23b hairpin with base-pair mismatches

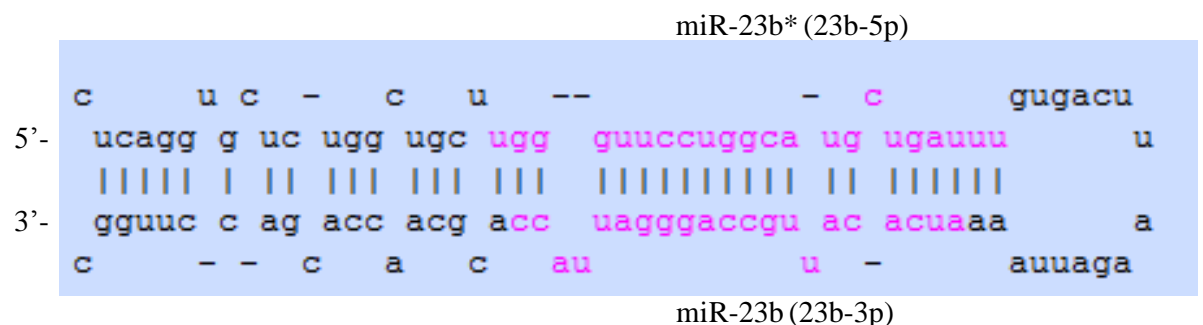


Figure A8: This diagram was sourced from the miRBase database (http://www.mirbase.org/cgi-bin/mirna_entry.pl?acc=MI0000439) and demonstrates the structure of the pre-miR-23b hairpin upon Drosha-mediated processing of the long pri-miRNA. We had specifically requested a tailor designed miRNA (pre-miR-23b* mod) in which instead of an siRNA-like design of complete complementarity, the base-pair mismatches are retained within its structure.

Figure A9: List of differentially expressed proteins when miR-23 and miR-NC samples were randomised



Accession	Peptides	Score	Anova (p)*	Fold	Tags	Description	Average Normalised		FC
							Control	Test	
gi 344243	2	120.07	0.02	1.86		Retinoic acid-induced protein 3 [Cricetulus griseus] [MASS=39746]	8.74E+04	1.62E+05	1.853547
gi 344257	1	53.63	0.03	5.66		Keratin, type II cytoskeletal 1b [Cricetulus griseus] [MASS=93520]	1.22E+04	6.93E+04	
									5.680328

Figure A9: When all clones were randomised and compared for differential protein expression, two proteins were found to be DE. This was a quality control test as a means to determine the likelihood of randomly identifying DE

Figure A10: Differentially Expressed proteins from enriched mitochondrial (miR-23 sponge CHO-SEAP versus miR-NC sponge)

CS	Anova (p)	FC	Gene I.D	Description
65.21	9.61E-09	2.6	KIAA1881	Protein KIAA1881 [Cricetulus griseus] [MASS=39959]
473.97	2.52E-08	3.6	SBSN	Suprabasin [Cricetulus griseus] [MASS=63932]
96.35	6.13E-07	3.7	GRN	Granulins [Cricetulus griseus] [MASS=63924]
158.9	1.41E-06	1.7	LIMA1	LIM domain and actin-binding protein 1 [Cricetulus griseus] [MASS=84545]
76.55	1.52E-06	6.2	AHNAK2	Protein AHNAK2 [Cricetulus griseus] [MASS=81741]
204.15	2.19E-06	2.6	EPRS	Bifunctional aminoacyl-tRNA synthetase [Cricetulus griseus] [MASS=154896]
290.49	2.30E-06	1.9	CALD1	Non-muscle caldesmon [Cricetulus griseus] [MASS=61921]
77.33	2.38E-06	1.5	HTATSF1	HIV Tat-specific factor 1-like [Cricetulus griseus] [MASS=60645]
62.16	2.49E-06	2.5	HSPG	Basement membrane-specific heparan sulfate proteoglycan core protein [Cricetulus griseus] [MASS=334137]
47.16	3.08E-06	2.2	NIP7	60S ribosome subunit biogenesis protein NIP7-like [Cricetulus griseus] [MASS=10402]
42.96	3.50E-06	2.9	ADA	Adenosine deaminase [Cricetulus griseus] [MASS=40940]
110.25	5.57E-06	1.5	HMGB2	High mobility group protein B2 [Cricetulus griseus] [MASS=18197]
216.74	6.04E-06	1.7	NOP2	Putative ribosomal RNA methyltransferase NOP2 [Cricetulus griseus] [MASS=86249]
42.91	6.49E-06	2.2	MCM3	DNA replication licensing factor MCM3 [Cricetulus griseus] [MASS=90790]
83.37	7.49E-06	2.3	DLGAP5	Disks large-associated protein 5 [Cricetulus griseus] [MASS=63127]
60.3	9.07E-06	2.8	ZCCHC3	Zinc finger CCHC domain-containing protein 3 [Cricetulus griseus] [MASS=30279]
112.46	9.29E-06	6.9	AKAP12	A-kinase anchor protein 12 [Cricetulus griseus] [MASS=91046]
499.19	9.69E-06	2.1	RCN1	Reticulocalbin-3 [Cricetulus griseus] [MASS=34399]
172.09	1.06E-05	1.6	SCP2	Non-specific lipid-transfer protein [Cricetulus griseus] [MASS=58892]
528.27	1.09E-05	2.4	GSTM6	Glutathione S-transferase Mu 6 [Cricetulus griseus] [MASS=86559]
85.95	1.19E-05	2.4	KIF2C	Kinesin-like protein KIF2C
107.61	1.97E-05	1.7	P4HA1	Prolyl 4-hydroxylase subunit alpha-1 [Cricetulus griseus] [MASS=58084]
293.89	2.13E-05	2	CALU	Calumenin [Cricetulus griseus] [MASS=87917]
84.54	2.25E-05	1.8	CAPRIN1	Caprin-1 [Cricetulus griseus] [MASS=73689]
40.54	2.28E-05	2.9	PTER	Phosphotriesterase-related protein [Cricetulus griseus] [MASS=39278]

284.33	2.41E-05	2.5	GAA	Lysosomal alpha-glucosidase [Cricetulus griseus] [MASS=105847]
56.39	2.55E-05	1.8	UAP1L1	UDP-N-acetylhexosamine pyrophosphorylase-like protein 1 [Cricetulus griseus] [MASS=58175]
44.26	2.57E-05	23.2	FABP4	Fatty acid-binding protein, adipocyte [Cricetulus griseus] [MASS=14753]
415.32	2.66E-05	1.6	ITGB1	Integrin beta-1 [Cricetulus griseus] [MASS=88342]
96.32	2.70E-05	1.7	CTSB	Cathepsin B [Cricetulus griseus] [MASS=37504]
40.09	2.92E-05	1.8	TXNRD1	Thioredoxin reductase 1, cytoplasmic [Cricetulus griseus] [MASS=61858]
50.25	3.29E-05	2.7	MDH1	Malate dehydrogenase, cytoplasmic [Cricetulus griseus] [MASS=36466]
419.27	3.33E-05	1.6	GP50	GP50 [Cricetulus griseus] [MASS=46598]
152.86	3.40E-05	1.6	IQGAP1	Ras GTPase-activating-like protein IQGAP1 [Cricetulus griseus] [MASS=191377]
160.75	3.46E-05	1.6	SMARCA5	SWI/SNF-related matrix-associated actin-dependent regulator of chromatin subfamily A member 5
57.31	3.49E-05	2.5	DPP2	Dipeptidyl-peptidase 2 [Cricetulus griseus] [MASS=56397]
99.72	4.63E-05	2	IPO5	Importin-5 [Cricetulus griseus] [MASS=89713]
85.75	4.73E-05	2	CLINT1	Clathrin interactor 1 [Cricetulus griseus] [MASS=68215]
576.94	4.78E-05	1.5	HSP90B1	Endoplasmic [Cricetulus griseus] [MASS=92622]
85.86	5.00E-05	1.9	SH3BGR13	SH3 domain-binding glutamic acid-rich-like protein [Cricetulus griseus] [MASS=12747]
134.41	5.03E-05	1.6	RRBP1	Ribosome-binding protein 1 [Cricetulus griseus] [MASS=216696]
42.91	5.12E-05	2.1	SKIV2L2	Superkiller viralicidic activity 2-like 2 [Cricetulus griseus] [MASS=96202]
43.27	5.35E-05	1.4	EIF3H	Eukaryotic translation initiation factor 3 subunit H [Cricetulus griseus] [MASS=34239]
173.71	5.48E-05	1.6	LPH	Lactase-phlorizin hydrolase [Cricetulus griseus] [MASS=301280]
155.61	5.81E-05	1.7	SHMT	Serine hydroxymethyltransferase, mitochondrial [Cricetulus griseus] [MASS=55908]
420.16	5.99E-05	1.7	TOP2A	RecName: Full=DNA topoisomerase 2-alpha; AltName: Full=DNA topoisomerase II, alpha isozyme
48.89	6.04E-05	3.6	GUSB	Beta-glucuronidase [Cricetulus griseus] [MASS=74804]
60.27	6.20E-05	1.9	PRPF8	Pre-mRNA-processing-splicing factor 8 [Cricetulus griseus] [MASS=30142]
287.95	6.33E-05	1.4	STIP1	Stress-induced-phosphoprotein 1
461.22	6.40E-05	1.4	ANXA1	Annexin A1 [Cricetulus griseus] [MASS=38861]
991.99	6.58E-05	1.8	CALR	Calreticulin [Cricetulus griseus] [MASS=48241]
155.37	6.71E-05	1.9	VCP	Transitional endoplasmic reticulum ATPase [Cricetulus griseus] [MASS=237642]
780.39	6.72E-05	1.4	GAPDH	Glyceraldehyde-3-phosphate dehydrogenase
48.83	7.11E-05	3.1	ALCAM	CD166 antigen [Cricetulus griseus] [MASS=65083]

42.71	7.35E-05	1.5	VCL	Vinculin [Cricetulus griseus] [MASS=124877]
534.81	7.65E-05	1.8	PDIA4	Protein disulfide-isomerase A4 [Cricetulus griseus] [MASS=72586]
43.2	8.00E-05	2.5	TWSG1	Twisted gastrulation protein-like 1 [Cricetulus griseus] [MASS=24747]
177.24	8.07E-05	1.7	HP1	heterochromatin protein 1 alpha [Cricetulus griseus]
485.82	8.17E-05	1.5	MYH10	Myosin-10 [Cricetulus griseus] [MASS=229037]
77.41	8.38E-05	1.7	CNN2	Calponin-2 [Cricetulus griseus] [MASS=32507]
42.27	8.41E-05	1.4	EHD3	EH domain-containing protein 3 [Cricetulus griseus] [MASS=60915]
69.02	8.73E-05	6	RPL7	60S ribosomal protein L7 [Cricetulus griseus] [MASS=29237]
998.19	9.15E-05	1.6	NUMA1	Nuclear mitotic apparatus protein 1 [Cricetulus griseus] [MASS=340229]
67.81	0.000104	1.6		Proline synthetase co-transcribed bacterial-like protein [Cricetulus griseus] [MASS=24790]
130.72	0.000106	2	PFDN6	prefoldin subunit 6 [Mus musculus]
106.24	0.000108	1.7	TXNDC5	Thioredoxin domain-containing protein 5 [Cricetulus griseus] [MASS=46354]
86.63	0.00011	1.8	PLAA	Phospholipase A-2-activating protein [Cricetulus griseus] [MASS=87183]
74.08	0.000117	1.5	NCAPH	Condensin complex subunit 2 [Cricetulus griseus] [MASS=81308]
652.03	0.000121	1.6	PDIA3	ERP57 protein [Cricetulus griseus] [MASS=56796]
47.4	0.000122	1.4	GRSF1	G-rich sequence factor 1 [Cricetulus griseus] [MASS=70369]
83.65	0.000128	3	H2AFV	histone H2A.V isoform 1 [Homo sapiens]
40.47	0.000135	1.6	HLAA	MHC class I antigen Hm1-C1 [Cricetulus griseus] [MASS=38752]
154.98	0.000136	2	HMOX1	Heme oxygenase 1 [Cricetulus griseus] [MASS=33023]
313.51	0.00014	2.8	FASN	Fatty acid synthase [Cricetulus griseus] [MASS=271857]
42.21	0.000144	1.9	ZNF593	Zinc finger protein 593 [Cricetulus griseus] [MASS=15247]
113.62	0.00018	2.1	MCM5	DNA replication licensing factor MCM5 [Cricetulus griseus] [MASS=82347]
261.37	0.000194	1.4	CBX3	chromobox protein homolog 3 [Homo sapiens]
94.68	0.000198	1.3	AK2	Adenylate kinase 2, mitochondrial [Cricetulus griseus] [MASS=15424]
135.15	0.000205	2.2	MFGE8	Lactadherin [Cricetulus griseus] [MASS=16152]
40.63	0.000211	2.3	GNGT2	guanine nucleotide-binding protein G(I)/G(S)/G(O) subunit gamma-2 precursor [Mus musculus]
80.18	0.000223	1.8	FUS	RNA-binding protein FUS [Cricetulus griseus] [MASS=21204]
53.68	0.000229	1.2	RPS27L	ribosomal protein S27-like, isoform CRA_a [Homo sapiens]
119.96	0.000234	1.4	SRSF3	Splicing factor, arginine/serine-rich 3 [Cricetulus griseus] [MASS=19310]

60.94	0.000236	3.1	KIF4	Chromosome-associated kinesin KIF4 [Cricetulus griseus] [MASS=185097]
524.15	0.000241	1.6	PDIA3	Protein disulfide-isomerase A3 [Cricetulus griseus] [MASS=50051]
632.16	0.000241	1.7	MYBBP1A	Myb-binding protein 1A [Cricetulus griseus] [MASS=105149]
53.85	0.000255	2	SLC7A1	High affinity cationic amino acid transporter 1 [Cricetulus griseus] [MASS=67614]
62.52	0.000264	2.9	HSPB1	Heat shock protein beta-1 [Cricetulus griseus] [MASS=8903]
106.62	0.000265	1.6	RRP15	RRP15-like protein [Cricetulus griseus] [MASS=42329]
1075.25	0.000265	1.4	GRP78	78 kDa glucose-regulated protein binding
756.55	0.000268	1.3	HSP60	60 kDa heat shock protein, mitochondrial
57.17	0.000269	1.5	COPB1	Coatmer subunit beta' [Cricetulus griseus] [MASS=89506]
105.9	0.000275	1.7	HDAC2	Histone deacetylase 2 [Cricetulus griseus] [MASS=51941]
107.47	0.000316	1.8	MCM2	DNA replication licensing factor MCM2 [Cricetulus griseus] [MASS=102184]
107.76	0.000326	1.5	VAPB	Vesicle-associated membrane protein-associated protein B [Cricetulus griseus] [MASS=27502]
128.89	0.000329	1.4	DNTTIP2	Deoxynucleotidyltransferase terminal-interacting protein 2 [Cricetulus griseus] [MASS=85134]
136.67	0.000342	1.4	NUFIP2	Nuclear fragile X mental retardation-interacting protein 2 [Cricetulus griseus] [MASS=56644]
67.07	0.00035	1.5	NUP93	Nuclear pore complex protein Nup93 [Cricetulus griseus] [MASS=89109]
47.74	0.00035	1.7	KIF15	Kinesin-like protein KIF15 [Cricetulus griseus] [MASS=125621]
123.84	0.000367	1.9	CAD	CAD protein [Cricetulus griseus] [MASS=243029]
145.15	0.000398	1.3	CTTN	Src substrate cortactin [Cricetulus griseus] [MASS=61469]
109.1	0.000407	1.5	OXCT1	Succinyl-CoA:3-ketoacid-coenzyme A transferase 1, mitochondrial [Cricetulus griseus] [MASS=56218]
46.59	0.000411	3.5	PSAP	Sulfated glycoprotein 1 [Cricetulus griseus] [MASS=27374]
319.39	0.000414	1.9	SND1	nuclease domain-containing protein 1 [Cricetulus griseus] [MASS=99748]
96.49	0.000417	1.8	WDR43	WD repeat-containing protein 43 [Cricetulus griseus] [MASS=55890]
180.99	0.000423	1.6	ATP1A1	Sodium/potassium-transporting ATPase subunit alpha-1 [Cricetulus griseus] [MASS=84781]
120.34	0.000436	1.4	MAP4	Microtubule-associated protein 4 [Cricetulus griseus] [MASS=138221]
221.57	0.000439	1.4	NSFL1C	NSFL1 cofactor p47 [Cricetulus griseus] [MASS=41009]
121	0.000454	2.1	PLS3	RecName: Full=Plastin-3; AltName: Full=T-plastin
87.48	0.00046	1.6	CYF1P1	Cytoplasmic FMR1-interacting protein 1 [Cricetulus griseus] [MASS=145275]
71.91	0.00046	1.7	ATP2A3	Sarcoplasmic/endoplasmic reticulum calcium ATPase 3 [Cricetulus griseus] [MASS=103607]
52.46	0.000473	1.8	UHRF1	E3 ubiquitin-protein ligase UHRF1 [Cricetulus griseus] [MASS=88095]

45.14	0.000476	1.6	GMPS	GMP synthase [glutamine-hydrolyzing] [Cricetulus griseus] [MASS=130016]
109.81	0.000483	1.3	NPM1	Nucleophosmin [Cricetulus griseus] [MASS=31052]
97.59	0.000487	1.5	MTHFD2	Bifunctional methylenetetrahydrofolate dehydrogenase/cyclohydrolase, mitochondrial [Cricetulus griseus]
69.28	0.000491	1.4	DDX6	PREDICTED: probable ATP-dependent RNA helicase DDX6 isoform 1 [Sus scrofa]
110.09	0.000492	1.4	PSMD2	26S proteasome non-ATPase regulatory subunit 2 [Cricetulus griseus] [MASS=72983]
197.29	0.000505	1.4	ANXA2	Annexin A2 [Cricetulus griseus] [MASS=27037]
65.4	0.000535	2.3	HSPH1	RecName: Full=Heat shock protein 105 kDa; AltName: Full=Heat shock 110 kDa protein
493.84	0.000553	1.4	SDHA	Succinate dehydrogenase [ubiquinone] flavoprotein subunit, mitochondrial [Cricetulus griseus] [MASS=71658]
56.16	0.000556	1.3	RRM1	Ribonucleoside-diphosphate reductase large subunit [Cricetulus griseus] [MASS=90217]
324.58	0.000565	2.2	MYH11	Myosin-11 [Cricetulus griseus] [MASS=227190]
71.8	0.000572	2.2	GSTA3	Glutathione S-transferase alpha-3 [Cricetulus griseus] [MASS=14752]
93.72	0.000575	2.4	ABCF1	ATP-binding cassette sub-family F member 1 [Cricetulus griseus] [MASS=65859]
121.17	0.000581	1.5	PSME1	Proteasome activator complex subunit 1 [Cricetulus griseus] [MASS=24514]
434.44	0.000603	1.7	DDX1	RNA helicase [Mesocricetus auratus]
269.45	0.000617	1.7	CLTC	Clathrin heavy chain 1 [Cricetulus griseus] [MASS=223961]
80.08	0.000637	1.6	SLC7A8	Large neutral amino acids transporter small subunit 1 [Cricetulus griseus] [MASS=55205]
168.98	0.00067	1.6	HYOU1	Hypoxia up-regulated protein 1
274.94	0.000693	1.6	LRPPRC	Leucine-rich PPR motif-containing protein, mitochondrial [Cricetulus griseus] [MASS=158425]
40.28	0.000698	1.6	HNRNPUL1	Heterogeneous nuclear ribonucleoprotein U-like protein 2 [Cricetulus griseus] [MASS=72420]
294.31	0.000726	1.5	FLNB	Filamin-B [Cricetulus griseus] [MASS=277844]
60.42	0.000737	2.3	BCL9L	B-cell CLL/lymphoma 9-like protein [Cricetulus griseus] [MASS=156723]
77.91	0.000745	1.4	RHOA	transforming protein RhoA precursor [Rattus norvegicus]
103.35	0.000751	1.5	RAB7A	Ras-related protein Rab-7a [Cricetulus griseus] [MASS=23518]
51.97	0.000763	1.9	CETN3	Centrin-3 [Cricetulus griseus] [MASS=19558]
58.48	0.000795	1.3	CCT7	T-complex protein 1 subunit eta [Cricetulus griseus] [MASS=54906]
77.13	0.000817	1.4	PFDN4	Prefoldin subunit 4 [Cricetulus griseus] [MASS=15226]
276.02	0.000827	1.3	KIF27	Kinesin-like protein KIF27 [Cricetulus griseus] [MASS=185707]
183.23	0.000829	1.8	SLC25A3	Phosphate carrier protein, mitochondrial [Cricetulus griseus] [MASS=26018]
113.17	0.000839	2.6	SPRR1A	Cornifin-A [Cricetulus griseus] [MASS=12457]

50.66	0.000873	1.6	EIF1AY	eukaryotic translation initiation factor 1A [Mus musculus]
121.03	0.000876	1.3	LYAR	Cell growth-regulating nucleolar protein [Cricetulus griseus] [MASS=43169]
55.92	0.000896	1.9	PPA1	Inorganic pyrophosphatase [Cricetulus griseus] [MASS=36997]
40.96	0.0009	1.9	CAND1	Cullin-associated NEDD8-dissociated protein 1 [Cricetulus griseus] [MASS=133622]
173.13	0.000923	1.4	RPL6	60S ribosomal protein L6 [Cricetulus griseus] [MASS=32777]
47.96	0.000938	1.9	L7RN6	lethal, Chr 7, Rinchik 6 [Mus musculus]
175.92	0.000989	1.4	YWHAZ	14-3-3 protein zeta/delta [Cricetulus griseus] [MASS=27715]
336.44	0.001001	1.3	ALDOA	Fructose-bisphosphate aldolase A [Cricetulus griseus] [MASS=39382]
160.65	0.001043	1.4	TES	Testin [Cricetulus griseus] [MASS=47209]
249.77	0.001078	1.4	EIF4G1	Eukaryotic translation initiation factor 4 gamma 1 [Cricetulus griseus] [MASS=175081]
211.82	0.001097	1.3	TMPO	Lamina-associated polypeptide 2, isoforms alpha/zeta [Cricetulus griseus] [MASS=34881]
141.92	0.001111	1.6	KPNB1	Importin subunit beta-1 [Cricetulus griseus] [MASS=211197]
42.51	0.001122	1.7	YWHAH	14-3-3 protein eta [Cricetulus griseus] [MASS=27084]
41.01	0.001125	1.7	HDDC2	HD domain-containing protein 3 [Cricetulus griseus] [MASS=20271]
49.9	0.001205	1.8	SLC3A2	putative CD98 protein [Cricetulus griseus] [MASS=58926]
200.38	0.001206	1.3	LDHA	LDH-A [Cricetulus griseus] [MASS=36519]
234.43	0.001211	1.4	HMGCS1	Hydroxymethylglutaryl-CoA synthase, cytoplasmic
48.07	0.001228	1.7	HSPA4	Heat shock 70 kDa protein 4 [Cricetulus griseus] [MASS=62990]
753.03	0.001268	1.4	EEF2	elongation factor 2 [Cricetulus griseus] [MASS=95323]
306.33	0.001271	1.2	TPI	Triosephosphate isomerase [Cricetulus griseus] [MASS=20407]
371.2	0.001338	1.3	HSPA9	Stress-70 protein, mitochondrial
74.66	0.001374	1.5	HGPRT	RecName: Full=Hypoxanthine-guanine phosphoribosyltransferase; Short=HGPRT; Short=HGPRTase
369.15	0.001428	1.4	GSTP1	RecName: Full=Glutathione S-transferase P; AltName: Full=GST class-pi
114.51	0.001441	1.7	MTHFD1	C-1-tetrahydrofolate synthase, cytoplasmic [Cricetulus griseus] [MASS=101286]
146.47	0.001474	1.4	RCN1	Reticulocalbin-1 [Cricetulus griseus] [MASS=29316]
56.71	0.001485	1.4	ANLN	Actin-binding protein anillin [Cricetulus griseus] [MASS=122923]
230.11	0.001584	1.7	NOLC1	Nucleolar phosphoprotein p130 [Cricetulus griseus] [MASS=73455]
61.69	0.001609	1.6	TCOF1	Treacle protein [Cricetulus griseus] [MASS=127813]
263.85	0.001643	1.4	NUDC	Nuclear migration protein nudC [Cricetulus griseus] [MASS=32771]

160.48	0.001645	1.5	MAP1B	Microtubule-associated protein 1B [Cricetulus griseus] [MASS=260385]
152.73	0.001718	1.3	WBP2	WW domain-binding protein 2 [Cricetulus griseus] [MASS=27992]
639.78	0.001771	1.4	PDI	Prolyl 4-hydroxylase subunit beta
117.81	0.00179	1.3	IDH3A	Isocitrate dehydrogenase [NAD] subunit alpha, mitochondrial [Cricetulus griseus] [MASS=39684]
87.63	0.001806	1.5	LGALS1	Galectin-1
188.09	0.001807	1.4	PRKCSH	Glucosidase 2 subunit beta [Cricetulus griseus] [MASS=62353]
177.85	0.001833	1.3	BST2	Bone marrow stromal antigen 2
70.34	0.001869	1.3	TRIM28	Transcription intermediary factor 1-beta [Cricetulus griseus] [MASS=58046]
63.76	0.001889	1.3	DDX10	putative ATP-dependent RNA helicase DDX10 [Cricetulus griseus] [MASS=101337]
69.21	0.001909	2	AIM2	Interferon-inducible protein [Cricetulus griseus] [MASS=14990]
315.2	0.001918	1.2	ACTB	Actin, cytoplasmic 1
84.3	0.001949	1.3	PPP2R1A	Serine/threonine-protein phosphatase 2A 65 kDa regulatory subunit A beta isoform [Cricetulus griseus]
63.6	0.001956	1.6	MATR3	Matrin-3 [Cricetulus griseus] [MASS=94625]
53.37	0.001985	1.3	SMARCC1	SWI/SNF complex subunit SMARCC1 [Cricetulus griseus] [MASS=154765]
143.8	0.001998	1.2	HNRNPAB	Heterogeneous nuclear ribonucleoprotein A/B [Cricetulus griseus] [MASS=23754]
240.68	0.002132	1.5	ACO2	Aconitate hydratase, mitochondrial [Cricetulus griseus] [MASS=85466]
85.16	0.002167	1.5	SNX1	Sorting nexin-1 [Cricetulus griseus] [MASS=58922]
56.33	0.002223	1.8	LEPRE1	Prolyl 3-hydroxylase 1 [Cricetulus griseus] [MASS=73130]
89.12	0.002264	2.3	HMG1	Nucleosome-binding protein 1 [Cricetulus griseus] [MASS=33339]
85	0.002286	1.4	MRPS7	28S ribosomal protein S7, mitochondrial [Cricetulus griseus] [MASS=17257]
53.95	0.002298	1.4	SUCLA2	Succinyl-CoA ligase [ADP-forming] subunit beta, mitochondrial [Cricetulus griseus] [MASS=25797]
59.63	0.002313	1.4	MAGOH	protein mago nashi homolog [Homo sapiens]
94.58	0.002324	1.4	DDX56	putative ATP-dependent RNA helicase DDX56 [Cricetulus griseus] [MASS=61201]
41.04	0.002333	1.5	HAT1	Histone acetyltransferase type B catalytic subunit [Cricetulus griseus] [MASS=21390]
41.44	0.002371	1.4	ERP29	Endoplasmic reticulum protein ERp29 [Cricetulus griseus] [MASS=28603]
215.81	0.002435	1.3	NME2	Nucleoside diphosphate kinase B [Cricetulus griseus] [MASS=17340]
71.77	0.002584	1.5	GB2	growth factor receptor-bound protein 2 isoform 1 [Homo sapiens]
46.64	0.002633	1.6	NUP205	Nuclear pore complex protein Nup205 [Cricetulus griseus] [MASS=223157]
53.37	0.002636	1.4	TALDO1	RecName: Full=Transaldolase

189.83	0.002673	1.3	RPS15	40S ribosomal protein S15 [Cricetulus griseus] [MASS=12990]
164.35	0.00269	1.5	TOP1	DNA topoisomerase I [Cricetulus griseus] [MASS=90837]
146.99	0.002708	1.5	HDGF	Hepatoma-derived growth factor [Cricetulus griseus] [MASS=22716]
48.73	0.002736	1.5	SUMF2	Sulfatase-modifying factor 2 [Cricetulus griseus] [MASS=7750]
46.99	0.002781	1.5	SRSF7	Splicing factor, arginine/serine-rich 7 [Cricetulus griseus] [MASS=26153]
89.77	0.002846	2.3	CMAS	N-acetylneuraminate cytidyltransferase [Cricetulus griseus] [MASS=31274]
96.89	0.002873	6.6	SLC25A5	ADP/ATP translocase 2 [Cricetulus griseus] [MASS=46576]
206.18	0.002913	1.3	RPSA	40S ribosomal protein SA
86.59	0.002921	1.5	RANGAP1	Ran GTPase-activating protein 1 [Cricetulus griseus] [MASS=63142]
263.02	0.003013	1.5	ARHGDI1	Rho GDP-dissociation inhibitor 1 [Cricetulus griseus] [MASS=23423]
231.19	0.003016	1.3	HSD17B10	3-hydroxyacyl-CoA dehydrogenase type-2 [Cricetulus griseus] [MASS=27174]
203.53	0.003086	2.3	RPN1	Dolichyl-diphosphooligosaccharide--protein glycosyltransferase subunit 1 [Cricetulus griseus] [MASS=68577]
832.3	0.003147	1.4	MYH9	Myosin-9 [Cricetulus griseus] [MASS=225794]
203.2	0.003181	1.2	TPR	Nucleoprotein TPR [Cricetulus griseus] [MASS=238753]
57.3	0.003233	1.3	ARD1	hypothetical protein I79_013960 [Cricetulus griseus] [MASS=25829]
108.67	0.00327	1.4	GATAD2B	Transcriptional repressor p66-beta [Cricetulus griseus] [MASS=64918]
136.53	0.003279	2	SF3B3	splicing factor 3B subunit 3 [Mus musculus]
111.74	0.003378	1.3	RPS18	40S ribosomal protein S18 [Cricetulus griseus] [MASS=17763]
58.08	0.003381	1.6	KHDRBS1	KH domain-containing, RNA-binding, signal transduction-associated protein 1 [Cricetulus griseus] [MASS=48326]
75.88	0.003612	1.4	UBXN1	UBX domain-containing protein 1 [Cricetulus griseus] [MASS=23179]
75.04	0.003631	1.7	MFGE8	Lactadherin [Cricetulus griseus] [MASS=22114]
52.21	0.003653	1.6	SDF2L1	Stromal cell-derived factor 2-like protein 1 [Cricetulus griseus] [MASS=19011]
45.27	0.003722	1.8	COX5A	Cytochrome c oxidase subunit 5A, mitochondrial [Cricetulus griseus] [MASS=8603]
171.03	0.003763	1.5	SPTAN1	Spectrin alpha chain, brain [Cricetulus griseus] [MASS=258831]
271.84	0.003789	1.3	SFPQ	splicing factor proline/glutamine rich (polypyrimidine tract binding protein associated) [Rattus norvegicus]
196.86	0.003789	1.4	RBM14	RNA-binding protein 14 [Cricetulus griseus] [MASS=50151]
48.78	0.003814	1.5	LAMC1	Laminin subunit gamma-1 [Cricetulus griseus] [MASS=172121]
47.43	0.003845	1.5	SLC1A5	Neutral amino acid transporter B(0) [Cricetulus griseus] [MASS=17378]
78.34	0.003922	1.3	ADPRH	[Protein ADP-ribosylarginine] hydrolase [Cricetulus griseus] [MASS=38789]

195.07	0.003951	1.5	LRPAP1	Alpha-2-macroglobulin receptor-associated protein [Cricetulus griseus] [MASS=41173]
280.78	0.004029	1.2	HDLBP	Vigilin [Cricetulus griseus] [MASS=141720]
43.14	0.004073	1.9	Cab45	45 kDa calcium-binding protein [Cricetulus griseus] [MASS=41237]
140.74	0.00413	1.9	RPL3	60S ribosomal protein L3 [Cricetulus griseus] [MASS=46152]
87.27	0.004148	1.3	SF3B1	splicing factor 3B subunit 1 isoform 1 [Homo sapiens]
304.02	0.004163	1.3	DDX17	DEAD (Asp-Glu-Ala-Asp) box polypeptide 17, isoform CRA_a [Rattus norvegicus]
140.66	0.004164	1.3	GANAB	Neutral alpha-glucosidase AB [Cricetulus griseus] [MASS=106977]
40.99	0.004195	2.9	LAMP1	Lysosome-associated membrane glycoprotein 1
162.94	0.004226	1.3	BAG3	BAG family molecular chaperone regulator 3 [Cricetulus griseus] [MASS=61111]
101.43	0.00423	1.4	ATX10	Ataxin-10 [Cricetulus griseus] [MASS=34265]
131.59	0.004301	1.3	MDH2	Malate dehydrogenase, mitochondrial [Cricetulus griseus] [MASS=28696]
91.91	0.004348	1.6	ABCG3	ATP-binding cassette sub-family G member 3 [Cricetulus griseus] [MASS=69556]
139.2	0.004449	1.3	HNRNPM	Heterogeneous nuclear ribonucleoprotein M [Cricetulus griseus] [MASS=60304]
80.15	0.004493	1.4	EWSR1	RNA-binding protein EWS [Cricetulus griseus] [MASS=68536]
41.01	0.004497	1.3	RAB1B	ras-related protein Rab-1B [Mus musculus]
65.48	0.00451	1.6	SET	Protein SET [Cricetulus griseus] [MASS=44274]
195.18	0.004615	1.5	FKBP4	FK506-binding protein 4 [Cricetulus griseus] [MASS=46625]
44.57	0.004662	2	IDI1	Isopentenyl-diphosphate Delta-isomerase 1 [Cricetulus griseus] [MASS=32694]
123.1	0.004826	1.5	UQCRC1	Cytochrome b-c1 complex subunit 1, mitochondrial [Cricetulus griseus] [MASS=40615]
199.47	0.004925	1.4	RPL7A	60S ribosomal protein L7a [Cricetulus griseus] [MASS=22240]
43.78	0.005069	1.4	DNAJC8	DnaJ-like subfamily C member 8 [Cricetulus griseus] [MASS=29840]
185.23	0.005078	1.6	EEF1B2	Elongation factor 1-beta [Cricetulus griseus] [MASS=24687]
142.75	0.005097	1.8	PSMD12	26S proteasome non-ATPase regulatory subunit 12 [Cricetulus griseus] [MASS=52978]
56.01	0.005112	1.5	DDB1	DNA damage-binding protein 1 [Cricetulus griseus] [MASS=126926]
150.21	0.005145	1.3	RPS13	RecName: Full=40S ribosomal protein S13
379.43	0.005165	1.5	MKI67	Antigen KI-67 [Cricetulus griseus] [MASS=356150]
59.13	0.005188	1.6	PGAM1	Phosphoglycerate mutase 1 [Cricetulus griseus] [MASS=20205]
57.83	0.005192	1.3	WNK1	Serine/threonine-protein kinase WNK1 [Cricetulus griseus] [MASS=157436]
124.49	0.005193	1.5	GFM1	Elongation factor G, mitochondrial [Cricetulus griseus] [MASS=83298]

1139.28	0.005193	1.5	LMNA	Lamin-A/C [Cricetulus griseus] [MASS=64041]
57.24	0.005195	1.5	CEBPZ	CCAAT/enhancer-binding protein zeta [Cricetulus griseus] [MASS=120496]
112.2	0.005225	1.4	KGD1	2-oxoglutarate dehydrogenase E1 component, mitochondrial [Cricetulus griseus] [MASS=104514]
64.63	0.005231	1.4	SYAP1	Synapse-associated protein 1 [Cricetulus griseus] [MASS=35619]
394.01	0.005336	1.8	PDIA6	Protein disulfide-isomerase A6 [Cricetulus griseus] [MASS=28401]
121.4	0.005428	1.3	CACYBP	Calcyclin-binding protein [Cricetulus griseus] [MASS=21260]
57.72	0.005504	8.6	HIST2H2AA3	histone H2A type 2-A [Homo sapiens]
41.28	0.005535	1.3	RPS16	40S ribosomal protein S16 [Cricetulus griseus] [MASS=15699]
120.44	0.005659	1.3	EIF3G	Eukaryotic translation initiation factor 3 subunit G [Cricetulus griseus] [MASS=35716]
72.63	0.005743	1.2	AIFM1	Apoptosis-inducing factor 1, mitochondrial [Cricetulus griseus] [MASS=66780]
40.65	0.005753	2	SPTBN1	Spectrin beta chain, brain 1 [Cricetulus griseus] [MASS=94523]
251.05	0.005771	1.4	UBA1	Ubiquitin-like modifier-activating enzyme 1 [Cricetulus griseus] [MASS=117697]
95.07	0.005797	1.8	HNRNPU	Heterogeneous nuclear ribonucleoprotein U [Cricetulus griseus] [MASS=57620]
102.32	0.005826	1.8	DDX21	Nucleolar RNA helicase 2 [Cricetulus griseus] [MASS=80626]
94.1	0.005877	1.4	RPL7	60S ribosomal protein L7 [Cricetulus griseus] [MASS=17054]
51.38	0.005887	1.5	RPL29	60S ribosomal protein L29 [Cricetulus griseus] [MASS=12365]
43.74	0.005956	1.4	PMPCB	Mitochondrial-processing peptidase subunit beta [Cricetulus griseus] [MASS=40055]
42.85	0.005957	1.3	ANXA5	Annexin A5 [Cricetulus griseus] [MASS=36065]
398.31	0.005973	1.4	LAML1	Lamin-L(I) [Cricetulus griseus] [MASS=55093]
76.63	0.006009	1.4	TMED9	Transmembrane emp24 domain-containing protein 9 [Cricetulus griseus] [MASS=26765]
48.69	0.006101	13.9	TPM2	Tropomyosin beta chain [Cricetulus griseus] [MASS=30686]
91.36	0.006151	1.3	EBP2	putative rRNA-processing protein EBP2 [Cricetulus griseus] [MASS=35026]
189.08	0.006175	1.3	ATAD3A	ATPase family AAA domain-containing protein 3 [Cricetulus griseus] [MASS=66291]
73.25	0.006177	2.1	SGTA	Small glutamine-rich tetratricopeptide repeat-containing protein alpha [Cricetulus griseus] [MASS=34090]
56.98	0.006188	1.7	EIF2S3	Eukaryotic translation initiation factor 2 subunit 3 [Cricetulus griseus] [MASS=51107]
44.36	0.006279	1.4	DDX39A	ATP-dependent RNA helicase DDX39 [Cricetulus griseus] [MASS=48709]
68.25	0.006284	1.3	RPS2	40S ribosomal protein S2 [Cricetulus griseus] [MASS=8599]
88.54	0.006377	1.5	PSMD6	26S proteasome non-ATPase regulatory subunit 6 [Cricetulus griseus] [MASS=45566]
55.02	0.006636	3.1	HNRNPC	Heterogeneous nuclear ribonucleoproteins C1/C2 [Cricetulus griseus] [MASS=24495]

55.1	0.006649	1.5	UBXN4	UBX domain-containing protein 4 [Cricetulus griseus] [MASS=56719]
107.31	0.006721	1.2	ICAM1	intracellular adhesion molecule 1 [Cricetulus griseus]
73.61	0.006835	1.3	UBE2V1	ubiquitin-conjugating enzyme E2 K isoform 1 [Homo sapiens]
72.75	0.006847	1.3	HEXIM1	Protein HEXIM1 [Cricetulus griseus] [MASS=40208]
81.13	0.006848	1.4	PSAT1	Phosphoserine aminotransferase [Cricetulus griseus] [MASS=33926]
195.33	0.007068	3.5	PABPC1	Polyadenylate-binding protein 1 [Cricetulus griseus] [MASS=62714]
249.85	0.007155	3	HSP90AA1	Heat shock protein HSP 90-alpha [Cricetulus griseus] [MASS=38095]
164.82	0.007238	1.4	NCL	nucleolin, C23 [Cricetulus griseus] [MASS=73289]
86.37	0.007316	1.5	G6PD	RecName: Full=Glucose-6-phosphate 1-dehydrogenase; Short=G6PD
67.1	0.007333	1.2	6PGD	6-phosphogluconate dehydrogenase, decarboxylating [Cricetulus griseus] [MASS=53376]
160.83	0.007423	1.4	TCP1	T-complex protein 1 subunit alpha
135.5	0.007429	1.2	RPL9	60S ribosomal protein L9 [Cricetulus griseus] [MASS=22652]
73.09	0.007567	1.5	MTAP	S-methyl-5'-thioadenosine phosphorylase [Cricetulus griseus] [MASS=35587]
344.42	0.00761	1.4	HSP90AB1	Heat shock protein HSP 90-beta [Cricetulus griseus] [MASS=47807]
48.81	0.007636	1.5	PUR3	phosphoribosylglycinamide transformylase [Cricetulus griseus] [MASS=107446]
136.73	0.007637	1.2	SF3B1	Splicing factor 3 subunit 1 [Cricetulus griseus] [MASS=88710]
79.02	0.007671	1.1	RPL19	60S ribosomal protein L19 [Cricetulus griseus] [MASS=6891]
144.98	0.007927	1.3	SRRM2	Serine/arginine repetitive matrix protein 2 [Cricetulus griseus] [MASS=304044]
40.1	0.00794	7.6	RPL7A	60S ribosomal protein L7a [Cricetulus griseus] [MASS=15698]
46.96	0.008026	1.4	CPSF6	Cleavage and polyadenylation specificity factor subunit 6 [Cricetulus griseus] [MASS=53622]
90.99	0.008104	1.6	ARCN1	coatomer subunit delta [Mus musculus]
110.87	0.008124	1.4	ACTN4	Alpha-actinin-4 [Cricetulus griseus] [MASS=26219]
105.25	0.008335	1.8	HNRNPH2	heterogeneous nuclear ribonucleoprotein H2 [Mus musculus]
61.77	0.008415	1.3	CCT3	T-complex protein 1 subunit gamma [Cricetulus griseus] [MASS=60620]
44.31	0.008612	2.2	DYNC1H1	Cytoplasmic dynein 1 heavy chain 1 [Cricetulus griseus] [MASS=526782]
60.58	0.008695	3	PSMD14	26S proteasome non-ATPase regulatory subunit 14 [Homo sapiens]
145.99	0.008978	1.5	RPS17	40S ribosomal protein S17 [Mus musculus]
137.39	0.009137	1.4	ILF3	Interleukin enhancer-binding factor 3 [Cricetulus griseus] [MASS=97550]
109.8	0.009137	1.4	VAR5	Valyl-tRNA synthetase [Cricetulus griseus] [MASS=166356]

42.45	0.009183	1.5	DTYMK	Thymidylate kinase [Cricetulus griseus] [MASS=8404]
54.54	0.009237	1.4	CCT4	T-complex protein 1 subunit delta [Cricetulus griseus] [MASS=42136]
87.01	0.009261	1.9	CRK	Proto-oncogene C-crk [Cricetulus griseus] [MASS=36171]
87.63	0.009353	1.4	RPS21	40S ribosomal protein S21 [Cricetulus griseus] [MASS=9143]
49.08	0.009364	1.4	PLEKHO2	Pleckstrin-like domain-containing family O member 2 [Cricetulus griseus] [MASS=54045]
468.75	0.009537	1.4	HSP90AA1	RecName: Full=Heat shock protein HSP 90-alpha
45.68	0.009552	1.7	MTA1	Metastasis-associated protein MTA1 [Cricetulus griseus] [MASS=79077]
45.42	0.009559	1.4	RAB14	ras-related protein Rab-14 [Mus musculus]
112.55	0.009801	1.4	PPIB	Peptidyl-prolyl cis-trans isomerase B [Cricetulus griseus] [MASS=23634]
50.37	0.010036	1.4	NACA	Nascent polypeptide-associated complex subunit alpha, muscle-specific form [Cricetulus griseus] [MASS=34787]
47.59	0.010052	1.7	RPL10	60S ribosomal protein L10 [Cricetulus griseus] [MASS=23428]
103	0.010084	1.6	RPL5	60S ribosomal protein L5 [Cricetulus griseus] [MASS=34413]
117.94	0.010379	1.5	HNRNPA1	Putative heterogeneous nuclear ribonucleoprotein A1-like protein 3 [Cricetulus griseus] [MASS=35945]
231.34	0.010501	1.3	MSN	Moesin [Cricetulus griseus] [MASS=34529]
49.53	0.011035	2.2	BCLAF1	Bcl-2-associated transcription factor 1 [Cricetulus griseus] [MASS=47008]
66.36	0.011279	1.2	RPS18	40S ribosomal protein S18 [Cricetulus griseus] [MASS=18872]
72.87	0.011304	1.3	LGALS3	Galectin-3
105.82	0.011314	1.3	RPS26	40S ribosomal protein S26 [Rattus norvegicus]
56.93	0.011323	1.3	KIF5B	Kinesin-1 heavy chain [Cricetulus griseus] [MASS=87850]
62.94	0.011644	1.5	SMC1A	Structural maintenance of chromosomes protein 1A [Cricetulus griseus] [MASS=143220]
79.67	0.011724	2.1	GPRC5A	Retinoic acid-induced protein 3 [Cricetulus griseus] [MASS=39746]
44.13	0.011798	1.3	CTSL	Cathepsin L1 [Cricetulus griseus] [MASS=37248]
54.27	0.011871	1.1	PSMD4	26S proteasome non-ATPase regulatory subunit 4 [Cricetulus griseus] [MASS=41091]
43.31	0.011876	2.8	CAT	Catalase [Cricetulus griseus] [MASS=63099]
53.31	0.01223	1.3	GSR	Glutathione reductase, mitochondrial [Cricetulus griseus] [MASS=44949]
46.24	0.012371	1.5	ACTN4	Alpha-actinin-4 [Cricetulus griseus] [MASS=37673]
243.53	0.012419	1.5	NME1	Nucleoside diphosphate kinase A [Cricetulus griseus] [MASS=17195]
77.74	0.012505	1.4	CHMP4B	Charged multivesicular body protein 4b [Cricetulus griseus] [MASS=21459]
62.52	0.01279	1.4	AGFG1	Arf-GAP domain and FG repeats-containing protein 1 [Cricetulus griseus] [MASS=50397]

250.63	0.012804	1.4	DDX5	probable ATP-dependent RNA helicase DDX5 [Rattus norvegicus]
60.6	0.012926	1.5	ZC3HAV1	Zinc finger CCCH-type antiviral protein 1 [Cricetulus griseus] [MASS=110826]
81.25	0.013009	1.9	EFTUD2	116 kDa U5 small nuclear ribonucleoprotein component [Cricetulus griseus] [MASS=109491]
101.18	0.013245	1.3	PES1	Pescadillo-like [Cricetulus griseus] [MASS=41566]
57.81	0.013468	1.3	RPS14	40S ribosomal protein S14 [Homo sapiens]
47.92	0.013665	2.4	NPTN	Neuroplastin [Cricetulus griseus] [MASS=25086]
51.4	0.013744	1.4	CTNND1	Catenin delta-1 [Cricetulus griseus] [MASS=104051]
522.43	0.014198	2.1	HIST1H2AG	Histone H2A type 1 [Cricetulus griseus] [MASS=34185]
45.77	0.014308	3	TKT	Transketolase [Cricetulus griseus] [MASS=67716]
57.48	0.0145	1.6	LMNB2	Lamin-B2 [Cricetulus griseus] [MASS=67733]
62.86	0.014539	1.5	ADSL	adenylosuccinate lyase [Cricetulus griseus] [MASS=54955]
89.69	0.014654	1.6	CCT8	T-complex protein 1 subunit theta [Cricetulus griseus] [MASS=22223]
75.9	0.014659	1.6	LBR	Lamin-B receptor [Cricetulus griseus] [MASS=70428]
40.42	0.014831	1.3	MCM4	DNA replication licensing factor MCM4 [Cricetulus griseus] [MASS=96542]
100.56	0.015125	1.4	AKR1A1	Alcohol dehydrogenase [NADP+] [Cricetulus griseus] [MASS=36510]
41.99	0.01528	1.4	BOLA2	BolA-like protein 1 [Cricetulus griseus] [MASS=13002]
200.78	0.015326	1.8	SPTBN1	Spectrin beta chain, brain 1 [Cricetulus griseus] [MASS=166268]
40.24	0.015595	2.2	PA2G4	Proliferation-associated protein 2G4 [Cricetulus griseus] [MASS=43715]
43.83	0.015626	1.8	NPC2	Epididymal secretory protein E1 [Cricetulus griseus] [MASS=16471]
54.24	0.015636	1.3	RPL30	60S ribosomal protein L30 [Cricetulus griseus] [MASS=14716]
100.35	0.015764	1.3	STOML2	Stomatin-like protein 2 [Cricetulus griseus] [MASS=38199]
669.08	0.015962	1.4	FLNA	Filamin-A [Cricetulus griseus] [MASS=263654]
65.53	0.016153	1.4	SNAP29	Synaptosomal-associated protein 29 [Cricetulus griseus] [MASS=21734]
171.7	0.016198	1.4	YBX3	DNA-binding protein A [Cricetulus griseus] [MASS=11426]
61.81	0.016287	1.4	UCHL5	Ubiquitin carboxyl-terminal hydrolase isozyme L5 [Cricetulus griseus] [MASS=37660]
65.39	0.016512	1.2	ACTR2	Actin-related protein 2 [Cricetulus griseus] [MASS=20222]
65.72	0.016568	1.4	GPC1	Glypican-1 [Cricetulus griseus] [MASS=86871]
242.47	0.016589	1.4	HNRNPA3	Heterogeneous nuclear ribonucleoprotein A3 [Cricetulus griseus] [MASS=26953]
58.36	0.016636	1.3	EIF3C	Eukaryotic translation initiation factor 3 subunit C [Cricetulus griseus] [MASS=23144]

45.22	0.016895	1.4	PSMD11	26S proteasome non-ATPase regulatory subunit 11 [Cricetulus griseus] [MASS=29618]
44.45	0.01736	1.2	RPA2	Replication protein A 32 kDa subunit [Cricetulus griseus] [MASS=27524]
63.14	0.017467	3.2	TARDBP	TAR DNA-binding protein 43 [Cricetulus griseus] [MASS=22576]
76.47	0.017845	1.4	FXR1	RecName: Full=Fragile X mental retardation syndrome-related protein 1
65.37	0.017889	1.3	BAIAP2	Brain-specific angiogenesis inhibitor 1-associated protein 2
58.73	0.018158	1.5	TBL2	Transducin beta-like protein 2 [Cricetulus griseus] [MASS=39587]
455.92	0.018196	1.2	HNRNPA2B1	Heterogeneous nuclear ribonucleoproteins A2/B1 [Cricetulus griseus] [MASS=29047]
53.28	0.018361	1.1	LMAN2	Vesicular integral-membrane protein VIP36 [Cricetulus griseus] [MASS=40227]
178.72	0.018574	1.9	GSTM5	Glutathione S-transferase Mu 5 [Cricetulus griseus] [MASS=26967]
355.42	0.018585	1.4	HIST1H2AG	Histone H2A type 1 [Cricetulus griseus] [MASS=28463]
69.98	0.018808	1.5	PDLIM1	PDZ and LIM domain protein 1 [Cricetulus griseus] [MASS=35971]
40.29	0.018817	1.3	OPA1	Dynamin-like 120 kDa protein, mitochondrial [Cricetulus griseus] [MASS=117444]
59.2	0.019116	1.5	RRAS2	Ras-related protein R-Ras2 [Cricetulus griseus] [MASS=18078]
42.24	0.019157	1.9	UBA52	PREDICTED: ubiquitin B-like [Rattus norvegicus]
85.81	0.019179	1.2	RPL23A	60S ribosomal protein L23a [Cricetulus griseus] [MASS=17655]
114.63	0.019394	1.5	TUBA1C	tubulin alpha-1C chain [Mus musculus]
426.28	0.019401	1.2	PLEC	Plectin
110.18	0.019683	1.3	PEX19	Peroxisomal biogenesis factor 19
115.43	0.019901	3.4	HNRNPD	Heterogeneous nuclear ribonucleoprotein D0 [Cricetulus griseus] [MASS=29283]
57.01	0.019938	2.4	S100A13	Protein S100-A13 [Cricetulus griseus] [MASS=11241]
46.34	0.020284	1.6	SUCLG1	Succinyl-CoA ligase [GDP-forming] subunit alpha, mitochondrial [Cricetulus griseus] [MASS=34895]
45.85	0.020412	1.2	ERG11	Lanosterol 14-alpha demethylase [Cricetulus griseus] [MASS=56767]
64.37	0.020911	1.2	GPS1	COP9 signalosome complex subunit 1 [Cricetulus griseus] [MASS=53947]
74.72	0.021424	1.4	RNH1	Ribonuclease inhibitor [Cricetulus griseus] [MASS=50022]
77.01	0.021542	1.2	SES1	Seryl-tRNA synthetase, cytoplasmic
60.49	0.021554	1.7	RPL27A	60S ribosomal protein L27a [Bos taurus]
132.1	0.021709	1.4	RPS3A	40S ribosomal protein S3a [Rattus norvegicus]
86.93	0.021721	1.3	SF3B4	splicing factor 3B subunit 4 [Mus musculus]
92.41	0.021732	1.6	SLC25A5	ADP/ATP translocase 2 [Cricetulus griseus] [MASS=29247]

50.91	0.022257	1.4	RBM28	RNA-binding protein 28 [Cricetulus griseus] [MASS=87436]
73.45	0.022335	1.2	TPI	Triosephosphate isomerase [Cricetulus griseus] [MASS=16434]
74.38	0.022832	1.3	CSPG4	Chondroitin sulfate proteoglycan 4 [Cricetulus griseus] [MASS=252010]
135.26	0.022923	1.7	RPL4	60S ribosomal protein L4 [Cricetulus griseus] [MASS=32179]
74.08	0.022936	1.7	NAT10	N-acetyltransferase 10 [Cricetulus griseus] [MASS=115604]
44.37	0.023737	1.4	FKBP10	FK506-binding protein 10 [Cricetulus griseus] [MASS=64718]
58.11	0.023846	1.2	SEPT7	Septin-7 [Cricetulus griseus] [MASS=41218]
56.84	0.024636	1.5	ATP2B3	Plasma membrane calcium-transporting ATPase 3 [Cricetulus griseus] [MASS=130571]
41.35	0.024777	1.7	S100A6	protein S100-A6 [Mus musculus]
99.45	0.024964	1.6	KHSRP	Far upstream element-binding protein 2 [Cricetulus griseus] [MASS=62198]
154.83	0.025369	1.2	YWHAQ	14-3-3 protein theta [Cricetulus griseus] [MASS=27749]
45.84	0.026109	1.6	RCN2	Reticulocalbin-2 [Cricetulus griseus] [MASS=37132]
42.38	0.026185	1.3	SAFB	Scaffold attachment factor B1 [Cricetulus griseus] [MASS=102833]
45.15	0.026507	1.9	HNRNPG	Heterogeneous nuclear ribonucleoprotein G [Cricetulus griseus] [MASS=42131]
99.65	0.026755	1.7	NOMO1	Nodal modulator 1 [Cricetulus griseus] [MASS=32948]
114.55	0.027062	1.5	CSE1L	Exportin-2 [Cricetulus griseus] [MASS=110375]
49.38	0.027317	1.6	RANBP2	E3 SUMO-protein ligase RanBP2 [Cricetulus griseus] [MASS=342142]
40.15	0.027348	1.5	RBBP4	Histone-binding protein RBBP4 [Cricetulus griseus] [MASS=25330]
49.76	0.027401	2.2	HYPK	huntingtin interacting protein K [Oryctolagus cuniculus]
65.08	0.027661	2.7	TMEM43	Transmembrane protein 43 [Cricetulus griseus] [MASS=44797]
56.29	0.027801	1.5	RRP12	RRP12-like protein [Cricetulus griseus] [MASS=153244]
48.66	0.027862	1.2	IMMT	Mitochondrial inner membrane protein [Cricetulus griseus] [MASS=79258]
57.44	0.027871	1.3	EIF4B	Eukaryotic translation initiation factor 4B [Cricetulus griseus] [MASS=69570]
104.08	0.02788	1.2	DSC1	rCG40478, isoform CRA_b [Rattus norvegicus]
43.46	0.028009	1.4	CTB5R3	NADH-cytochrome b5 reductase 3 [Cricetulus griseus] [MASS=34236]
47.77	0.028144	1.5	EZR	Ezrin [Cricetulus griseus] [MASS=69372]
112.09	0.028961	1.2	TAGLN2	Transgelin-2 [Cricetulus griseus] [MASS=22455]
44.03	0.029486	1.4	RFC4	Replication factor C subunit 4 [Cricetulus griseus] [MASS=39938]
104.77	0.029896	1.2	EEF1G	Elongation factor 1-gamma [Cricetulus griseus] [MASS=27155]

52.16	0.029947	1.2	VAPA	Vesicle-associated membrane protein-associated protein A [Cricetulus griseus] [MASS=26075]
69.04	0.030475	1.3	PLOD2	Procollagen-lysine,2-oxoglutarate 5-dioxygenase 2 [Cricetulus griseus] [MASS=67164]
85.07	0.030576	1.5	FKBP9	FK506-binding protein 9 [Cricetulus griseus] [MASS=63008]
76.66	0.030819	1.5	RPL17	60S ribosomal protein L17 [Rattus norvegicus]
105.29	0.032149	1.3	GNB2	Guanine nucleotide-binding protein G(I)/G(S)/G(T) subunit beta-2 [Cricetulus griseus] [MASS=30483]
44.29	0.032227	1.4	PSMD3	26S proteasome non-ATPase regulatory subunit 3 [Cricetulus griseus] [MASS=16842]
57.62	0.032502	1.4	XRCC1	RecName: Full=DNA repair protein XRCC1; AltName: Full=X-ray repair cross-complementing protein 1
42.68	0.032765	1.8	RPLP1	60S acidic ribosomal protein P1 [Cricetulus griseus] [MASS=12230]
132.35	0.033095	1.3	RSL1D11	Ribosomal L1 domain-containing protein 1 [Cricetulus griseus] [MASS=49958]
43.44	0.033786	1.2	VDAC1	Voltage-dependent anion-selective channel protein 1 [Cricetulus griseus] [MASS=53379]
56.84	0.033892	1.2	LAP3	Cytosol aminopeptidase [Cricetulus griseus] [MASS=50275]
56.04	0.034082	1.4	MRPP1	Mitochondrial ribonuclease P protein 1 [Cricetulus griseus] [MASS=59932]
79.82	0.034525	1.4	VAT1	Synaptic vesicle membrane protein VAT-1-like [Cricetulus griseus] [MASS=28523]
108.57	0.034692	1.2	GTF2F1	General transcription factor IIF subunit 1 [Cricetulus griseus] [MASS=57283]
48.77	0.034812	1.7	NDUFA4	NADH dehydrogenase [ubiquinone] 1 alpha subcomplex subunit 4 [Cricetulus griseus] [MASS=14153]
61.52	0.034882	1.2	VDAC2	Voltage-dependent anion-selective channel protein 2 [Cricetulus griseus] [MASS=31739]
57.99	0.035256	1.3	GATAD2A	Transcriptional repressor p66 alpha [Cricetulus griseus] [MASS=51734]
53.22	0.035477	1.2	HMGB1	RecName: Full=High mobility group protein B1; AltName: Full=High mobility group protein 1; Short=HMG-1
59.07	0.035771	1.4	DNAJC10	DnaJ-like subfamily C member 10 [Cricetulus griseus] [MASS=90672]
82.09	0.036085	1.2	IRF2BP2	Interferon regulatory factor 2-binding protein 2 [Cricetulus griseus] [MASS=36160]
46.09	0.036431	1.5	PRPF40A	Pre-mRNA-processing factor 40-like A [Cricetulus griseus] [MASS=81478]
325.97	0.03688	1.9	PKM	Pyruvate kinase isozymes M1/M2 [Cricetulus griseus] [MASS=51559]
62.3	0.036983	1.5	FUBP1	Far upstream element-binding protein 1 [Cricetulus griseus] [MASS=47731]
63.63	0.037078	1.2	SRSF5	serine/arginine-rich splicing factor 5 [Mus musculus]
56.67	0.037201	1.3	RCC1	Regulator of chromosome condensation [Cricetulus griseus] [MASS=48887]
48.38	0.037852	1.5	RPL31	60S ribosomal protein L31 isoform 1 [Homo sapiens]
107.52	0.037926	9.4	NCAM1	Neural cell adhesion molecule 1 [Cricetulus griseus] [MASS=114316]
42.67	0.03809	1.3	SDHB	Succinate dehydrogenase [ubiquinone] iron-sulfur subunit, mitochondrial [Cricetulus griseus] [MASS=25570]
45.23	0.038162	1.4	CBR1	carbonyl reductase 1 [Cricetulus griseus] [MASS=30547]

42.76	0.038599	1.2	TMOD3	Tropomodulin-3 [Cricetulus griseus] [MASS=39388]
127.38	0.039203	1.2	CKAP4	Cytoskeleton-associated protein 4 [Cricetulus griseus] [MASS=36359]
140.2	0.039272	1.3	PARK7	Protein DJ-1 [Cricetulus griseus] [MASS=19929]
45.17	0.039516	1.2	HADHB	Trifunctional enzyme subunit beta, mitochondrial [Cricetulus griseus] [MASS=39535]
78.61	0.039527	1.4	RINL	Ras and Rab interactor-like protein [Cricetulus griseus] [MASS=71795]
59.78	0.039542	1.5	HIST1H2BC	histone H2B type 1-C/E/F/G/I [Homo sapiens]
102.85	0.039719	1.2	DBN1	Drebrin [Cricetulus griseus] [MASS=65309]
43.65	0.040374	1.5	RPS23	40S ribosomal protein S23 [Homo sapiens]
172.46	0.040499	1.3	EEF1A1	elongation factor 1-alpha 1 [Rattus norvegicus]
56.47	0.041029	1.3	CLU	Clusterin [Cricetulus griseus] [MASS=51757]
93.02	0.041185	2	ATIC	Bifunctional purine biosynthesis protein PURH [Cricetulus griseus] [MASS=64651]
50.73	0.041398	1.9	KRT10	Keratin, type I cytoskeletal 10 [Cricetulus griseus] [MASS=27853]
83.8	0.04164	1.2	RAB5C	Ras-related protein Rab-5C [Cricetulus griseus] [MASS=23483]
62.92	0.042015	2.8	RPL28	60S ribosomal protein L28 [Cricetulus griseus] [MASS=13065]
151.51	0.042153	1.2	ENO2	Gamma-enolase [Cricetulus griseus] [MASS=47227]
175.51	0.042683	1.3	CFL1	cofilin-1 [Rattus norvegicus]
88.46	0.042854	1.1	SUMO2	small ubiquitin-related modifier 2 precursor [Mus musculus]
46.05	0.043429	2.7	PRMT1	Protein arginine N-methyltransferase 1 [Cricetulus griseus] [MASS=40522]
42.13	0.043447	1.3	FDPS	Farnesyl pyrophosphate synthetase [Cricetulus griseus] [MASS=43211]
269.53	0.043714	1.2	EEF1D	Elongation factor 1-delta [Cricetulus griseus] [MASS=36598]
41.69	0.044283	2.1	CAV1	Caveolin-1 [Cricetulus griseus] [MASS=17160]
57.47	0.044736	1.2	RTCB	UPF0027 protein C22orf28-like [Cricetulus griseus] [MASS=47794]
53.2	0.045027	1.3	CCT8	T-complex protein 1 subunit theta [Cricetulus griseus] [MASS=24801]
59.64	0.045432	1.9	AHSA1	Activator of 90 kDa heat shock protein ATPase-like 1 [Cricetulus griseus] [MASS=38129]
40.85	0.045875	1.3	IQCE	IQ domain-containing protein E [Cricetulus griseus] [MASS=83194]
45.11	0.045972	1.3	FOSL1	Fos-related antigen 1 [Cricetulus griseus] [MASS=30263]
52.47	0.046094	1.3	PPM1G	Protein phosphatase 1G [Cricetulus griseus] [MASS=54003]
40.31	0.046158	1.6	RARS	RecName: Full=Arginyl-tRNA synthetase, cytoplasmic; AltName: Full=Arginine--tRNA ligase; Short=ArgRS
74.38	0.046454	1.2	CSPR2	Cysteine-rich protein 2 [Cricetulus griseus] [MASS=22944]

58.3	0.047006	1.3	PRPF31	U4/U6 small nuclear ribonucleoprotein Prp31 [Cricetulus griseus] [MASS=49130]
89.3	0.047083	1.5	ALLC	putative allantoicase [Cricetulus griseus] [MASS=80219]
100.86	0.047171	3.5	TUFM	Elongation factor Tu, mitochondrial [Cricetulus griseus] [MASS=49557]
53.53	0.04847	1.2	HM13	Minor histocompatibility antigen H13 [Cricetulus griseus] [MASS=37769]
49.72	0.048702	16.6	MAPRE1	Microtubule-associated protein RP/EB family member 1 [Cricetulus griseus] [MASS=30034]
41.87	0.048822	1.4	ACTR3	actin-related protein 3 [Mus musculus]
82.45	0.049156	1.1	ALDH2	Aldehyde dehydrogenase, mitochondrial [Cricetulus griseus] [MASS=45925]
80.22	0.049456	1.1	GIGYF2	PERQ amino acid-rich with GYF domain-containing protein 2 [Cricetulus griseus] [MASS=150168]
51.01	0.049711	1.2	RPS28	40S ribosomal protein S28 [Homo sapiens]
76.21	0.04984	1.3	PRDX2	RecName: Full=Peroxiredoxin-2

Figure A10: C_T expression patterns for miR-23b/23b* in all CHO clones

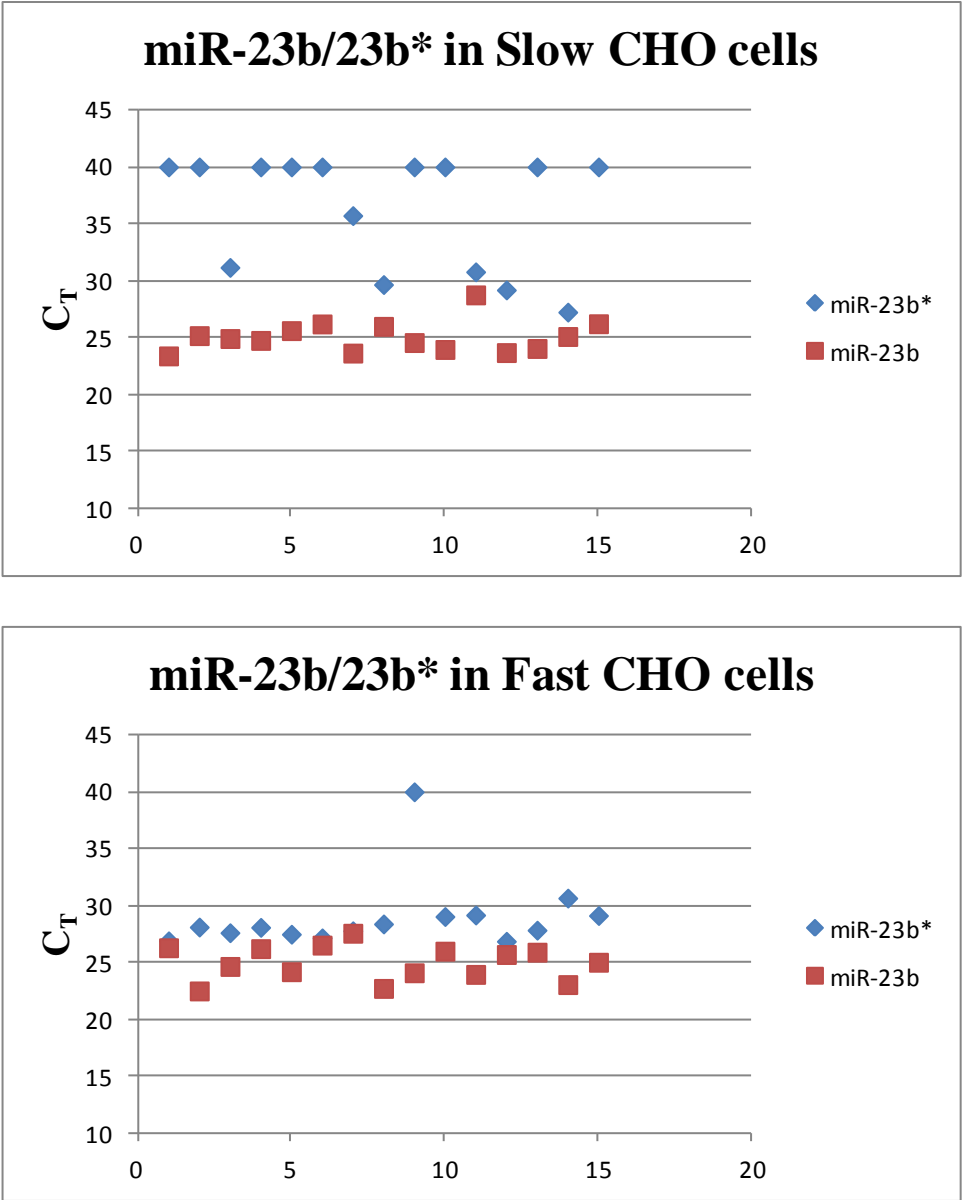


Figure A10: The dogmatic miRNA expression profile of miR-23b (Red) and miR-23b* (Blue) for all clones in the Slow growing panel compared to the Fast growing panel that exhibit an apparent increase in miR-23b* expression with no change in miR-23b expression.

Figure A11: Raw C_T values for miR-532-5p expression in all Fast and Slow CHO clones evaluated using TLDA miRNA microarrays

Clone ID	F/S	Detector ID	Ct	Ave Ct
X5.13F.1.41	F	hsa-miR-532-5p-4380928	40	
X5.13F.2.28	F	hsa-miR-532-5p-4380928	33.34163	
X5.13F.3.31	F	hsa-miR-532-5p-4380928	36.091293	
X5.16F.1.40	F	hsa-miR-532-5p-4380928	35.938572	
X5.16F.2.28	F	hsa-miR-532-5p-4380928	35.28528	
X5.16F.3.33	F	hsa-miR-532-5p-4380928	40	
X5.18F.1.39	F	hsa-miR-532-5p-4380928	32.416298	
X5.18F.2.31	F	hsa-miR-532-5p-4380928	40	
X5.18F.3.35	F	hsa-miR-532-5p-4380928	40	37.96367
X5.22F.1.44	F	hsa-miR-532-5p-4380928	40	
X5.22F.2.33	F	hsa-miR-532-5p-4380928	40	
X5.22F.3.27	F	hsa-miR-532-5p-4380928	40	
X5.2F.1.42	F	hsa-miR-532-5p-4380928	40	
X5.2F.2.31	F	hsa-miR-532-5p-4380928	36.381985	
X5.2F.3.25	F	hsa-miR-532-5p-4380928	40	
X10.2S.1.23	S	hsa-miR-532-5p-4380928	22.911198	
X10.2S.2.16	S	hsa-miR-532-5p-4380928	24.435015	
X10.2S.3.15	S	hsa-miR-532-5p-4380928	23.092752	
X11.1S.1.13	S	hsa-miR-532-5p-4380928	32.94388	
X11.1S.2.16	S	hsa-miR-532-5p-4380928	40	
X11.1S.3.14	S	hsa-miR-532-5p-4380928	35.9087	
X5.11S.1.23	S	hsa-miR-532-5p-4380928	31.040468	
X5.11S.2.14	S	hsa-miR-532-5p-4380928	35.003376	30.99841
X5.11S.3.16	S	hsa-miR-532-5p-4380928	32.213932	
X5.1S.1.11	S	hsa-miR-532-5p-4380928	24.3722	
X5.1S.2.16	S	hsa-miR-532-5p-4380928	26.736874	
X5.1S.3.19	S	hsa-miR-532-5p-4380928	24.942024	
X7.7S.1.17	S	hsa-miR-532-5p-4380928	40	
X7.7S.2.20	S	hsa-miR-532-5p-4380928	36.03121	
X7.7S.3.15	S	hsa-miR-532-5p-4380928	35.344524	

Figure A11: Raw C_T values for the expression of miR-532-5p in all clones within “fast” and “slow” growing groups (highlighted in yellow) including the average expression across each group.

Figure A12: miR-18a expression in a stable miR-17~92 cluster over-expressing CHO-K1 parental cell line

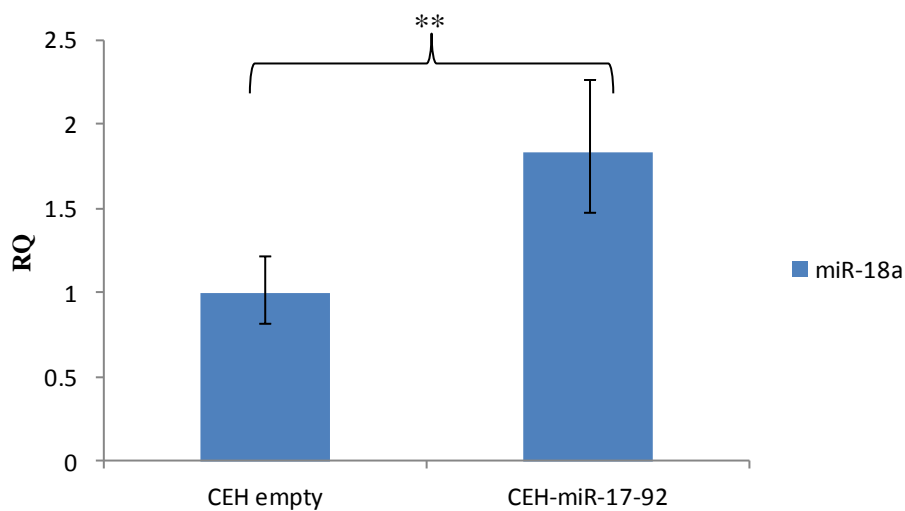


Figure A12: The expression of miR-18a was evaluated in a parental CHO-K1 parental cell line stably expressing the miR-17~92 cluster.

Figure A13: endogenous miR-23b* levels in miR-23b* sponge CHO-SEAP cells

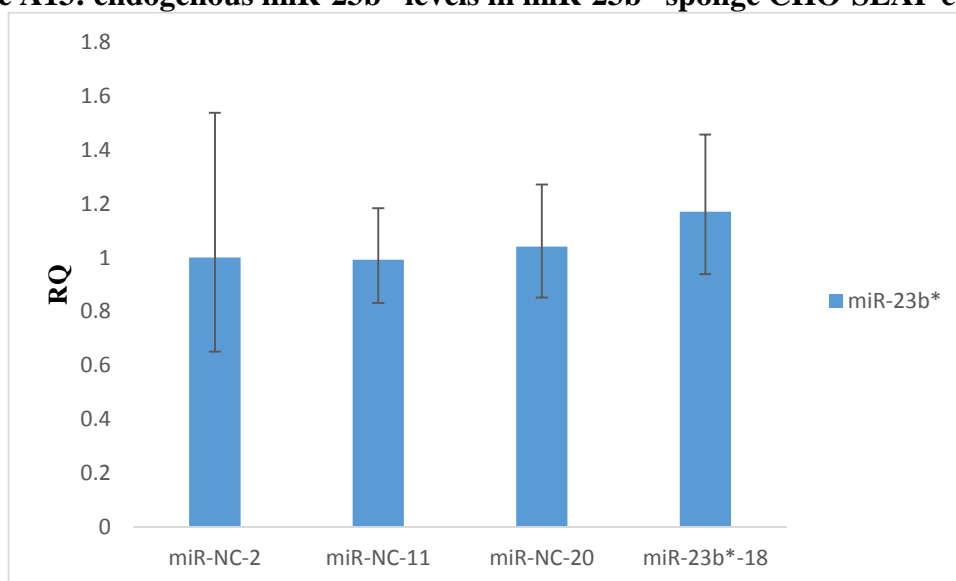


Figure A13: qPCR assessment of the expression of endogenous miR-23b* in CHO-K1-SEAP clones engineered to stably deplete miR-23b*.

Figure A14: CHO-SEAP miR-23 clones 4 and 6 transfected with pre-miR-23

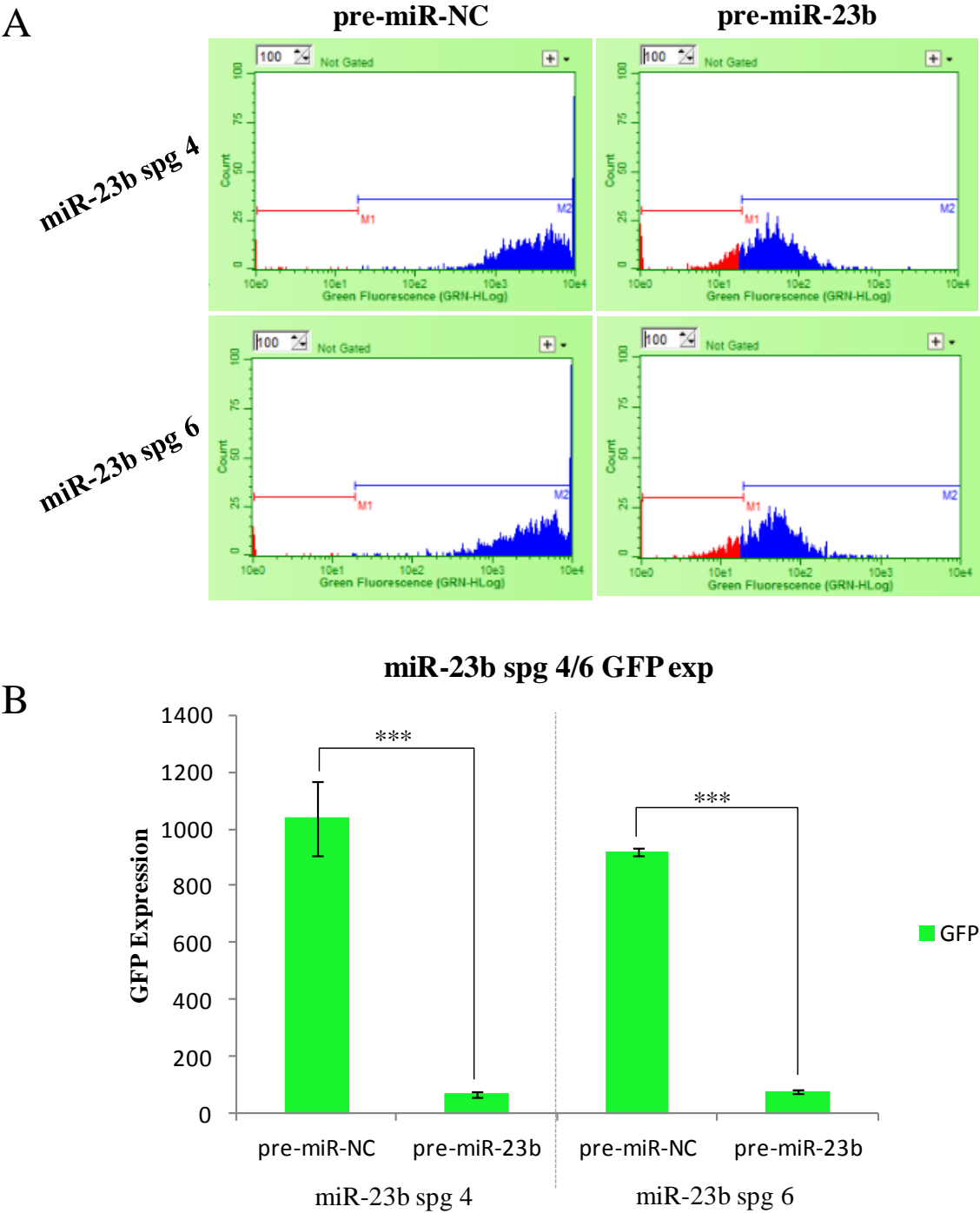


Figure A14: CHO-SEAP clones 4 and 6 stably depleted of miR-23 transfected with pre-miR-23 mimic demonstrating A) the GFP readings from the real-life Guava ExpressPlus programme and B) the average GFP expression within each population.